AD/A-000 449

FIVE POUND BIPROPELLANT ENGINE

L. Schoenman, et al

Aerojet Liquid Rocket Company

Prepared for:

Air Force Rocket Propulsion Laboratory

September 1974

NOTICES

When U.S. Government drawings, specifications, or other data are used for any purpose than a definitely related government procurement operation, the Government thereby incurs no responsibility nor any obligation whatsoever, and the fact that the Government may have formulated, furnished, or in any way supplied the said drawings, specifications or other data, is not to be regarded by implication or otherwise, or in any manner licensing the holder or any other person or corporation, or conveying any rights or permission to manufacture, use or sell any patented invention that may in any way be related thereto.

This report has been reviewed and is approved.

FOR THE COMMANDER
CHARLES E. SIEBER, Lt. Colonel, USAF
Chief, Liquid Rocket Division

ACCESSION for		
NTIS	White Section	☑
D C	Buff Section	☐
UNANNOUNCED		☐
JUSTIFICATION		
BY		
DISTRIBUTION/AVAILABILITY CODES		
Dist.	AVAIL. and/or SPECIAL	
A		

11a

UNCLASSIFIED

SECURITY CLASSIFICATION OF THIS PAGE (When Data Entered)

REPORT DOCUMENTATION PAGE		READ INSTRUCTIONS BEFORE COMPLETING FORM
1. REPORT NUMBER AFRPL-TR-74-51	2. GOVT ACCESSION NO.	3. RECIPIENT'S CATALOG NUMBER AD/A-000449
4. TITLE (and Subtitle) "Five-Pound Bipropellant Engine Final Report"		5. TYPE OF REPORT & PERIOD COVERED Final Report May 73 - July 74
		6. PERFORMING ORG. REPORT NUMBER
7. AUTHOR(s) L. Schoenman R. C. Schindler		8. CONTRACT OR GRANT NUMBER(s) F04611-73-C-0061
9. PERFORMING ORGANIZATION NAME AND ADDRESS Aerojet Liquid Rocket Company P O Box 13222 Sacramento CA 95813		10. PROGRAM ELEMENT, PROJECT, TASK AREA & WORK UNIT NUMBERS P.E. 62302F; Project 3058; Task 11; Work Unit AFRPL-3058-11-VS
11. CONTROLLING OFFICE NAME AND ADDRESS AFRPL/LKDA Edwards CA 93523		12. REPORT DATE September 1974
		13. NUMBER OF PAGES 418
14. MONITORING AGENCY NAME & ADDRESS(if different from Controlling Office)		15. SECURITY CLASS. (of this report) UNCLASSIFIED
		15a. DECLASSIFICATION/DOWNGRADING SCHEDULE

16. DISTRIBUTION STATEMENT (of this Report)

Approved for Public Release; Distribution Unlimited

17. DISTRIBUTION STATEMENT (of the abstract entered in Block 20, if different from Report)

18. SUPPLEMENTARY NOTES

19. KEY WORDS (Continue on reverse side if necessary and identify by block number)

Bipropellant; Attitude Control; Satellite Propulsion; N_2O_4; MMH; Five-Pound Thrust; Blowdown; Radiation-Cooled; Buried Installation.

20. ABSTRACT (Continue on reverse side if necessary and identify by block number)

A fifteen-month program was conducted to develop and demonstrate the technology required to provide a five-pound thrust bipropellant engine capability for attitude control functions typical of future Air Force requirements. Phase I included detailed studies and trade-off analyses of mission/system requirements versus engine parametrics. Phase II developed point designs based upon the Phase I analyses and the results of design verification tests. Phase III consisted of the fabrication and demonstration testing of three variants of a

(see reverse side)

DD FORM 1473, 1 JAN 73 EDITION OF 1 NOV 65 IS OBSOLETE

UNCLASSIFIED

SECURITY CLASSIFICATION OF THIS PAGE (When Data Entered)

Item 20. (continued)

basic engine design (designated AJ10-181) to representative mission requirements. All contract requirements were met or exceeded.

SUMMARY

The objective of the contract described herein was to develop and demonstrate the technology required to provide a high performance, long lived, fast response five-pound-thrust bipropellant engine capability for attitude control functions typical of future Air Force requirements. Specifically, a step function improvement from the characteristics of monopropellant hydrazine thrusters in the same thrust class was desired. The goals of the technical effort were to provide specific impulse values of 240 and 300 sec in pulsing and steady state modes of operation, respectively, minimum impulse bits of 0.050 lb-sec or less, repeatable within $\pm$ 10%, and valve response times of 0.005 sec with the pulse mode characteristics attained equally well on the first and subsequent pulses of a pulse mode duty cycle. In addition, it was intended that the engine would be capable of virtually unlimited quantities of cold starts, operate with propellant temperatures ranging from 20 to 120°F, be suitable for pressure regulated or blowdown pressurization systems and have unlimited duty cycle capability operating in a fully insulated (adiabatic wall) or radiation-cooled configuration.

System studies conducted early in the program verified the need for broad range capabilities as it was found that various spacecraft designs have entirely unlike requirements. Initial analytic studies indicated that low dribble volume multi element injector designs were essential if the pulsing and steady state performance goals were to be achieved with a single engine. Early full scale thruster firings disclosed that the 300 sec steady state and 240 sec specific impulse goals were achieveable using a 100:1 expansion nozzle. Long duration operation of a fully insulated unit, however, would require increased barrier cooling with an attendant performance reduction to insure maintenance of the chamber wall at an acceptable temperature.

The result of this initial work was that three variants of a basic engine design were fabricated for the program's Task III demonstration testing. These engines all utilized silicide coated columbium thrust chambers with multi element transverse platelet injectors which were integral with a torque

Summary (cont.)

motor actuated bipropellant valve, and provided a dribble volume of $\approx$ 0.0003 in.^{3} for each propellant. Specific engine to engine differences in the injector patterns traded performance with maximum feed pressure blowdown capability, the ability to operate with an adiabatic chamber wall, and heat flow to the spacecraft. All engines were successfully tested for extended simulated mission duty cycles accumulating more than 400,000 starts and 17,000 sec of firing without mishap. The demonstrated values of valve response and minimum impulse surpassed the goals by margins approaching 100%. The repeatability of the 0.05 lb impulse bits were $\pm$ 2.4%. In continuous pulsing steady state performance varied with installation and blowdown capability as follows:

Task III Engine	Installation	Blowdown Range	Steady State I_{sp} (ϵ = 100:1)
I	Radiation Cooled	Regulator	300
II	Adiabatic Wall	2:1	290
III	Adiabatic Wall	2.5:1	283

These engines provided a feasibility demonstration of the performance, chamber compatibility and operating advantages which accrue from the integration of the minimum manifold volume multi element platelet injector, bipropellant valve and columbium thrust chamber. These data allow the development of radiation cooled and adiabatic wall thrusters with high steady state and pulse mode performance, good pulse repeatability and virtually unlimited duty cycle capability to proceed from an experimentally verified technical base.

PREFACE

This report covers the work performed under Contract F04611-73-C-0061, "Five-Pound Bipropellant Engine", performed by the Aerojet Liquid Rocket Company at Sacramento, California, and conducted under Air Force Project 3058; Task 11. The performance period covered from 28 March 1973 to 30 June 1974.

The program manager was Dr. S. D. Rosenberg; the project manager was R. C. Schindler; the project engineer was L. Schoenman. The analytical thermal and performance work was conducted by F. H. Miller and J. I. Ito, respectively; J. V. Smith coordinated the valve related activities. The experimental work was conducted by R. S. Gross assisted by P. M. Loyd, test engineer, N. R. Rowett, instrumentation and controls engineer, and H. C. Howard, test data engineer.

The program was administered under the direction of the Air Force Rocket Propulsion Laboratory, M. V. Rogers, project engineer.

TABLE OF CONTENTS

TABLE OF CONTENTS (cont.)

TABLE OF CONTENTS (cont.)

TABLE OF CONTENTS (cont.)

TABLE OF CONTENTS (cont.)

LIST OF TABLES

LIST OF TABLES (cont.)

LIST OF FIGURES

LIST OF FIGURES (cont.)

LIST OF FIGURES (cont.)

LIST OF FIGURES (cont.)

LIST OF FIGURES (cont.)

LIST OF FIGURES (cont.)

LIST OF FIGURES (cont.)

LIST OF FIGURES (cont.)

LIST OF FIGURES (cont.)

SECTION I

INTRODUCTION

1.0 INTRODUCTION

1.1 BACKGROUND

Prior to 1963, few spacecraft missions required the injection of a payload into orbit. Furthermore, there was little need or room for an on-board propulsion system as part of an orbiting package. During the period 1963 to 1968, payload weights increased and a need for station-keeping developed as mission goals became more ambitious. Reaction control systems employed catalytic decomposition of hydrogen peroxide and/or cold gas jets. The instability of the hydrogen peroxide under storage and the need for pressure relief valves made the reliability of this system inherently low. Cold gas systems, although much more reliable, provided very low performance.

Monopropellant reaction control systems utilizing hydrazine were evaluated for station-keeping missions starting in 1967. By 1973, such systems enjoyed an undisputed industry acceptance and had performed well in a wide range of applications. However, the demands being placed on these reaction control systems are becoming more and more stringent and there are indications that the requirements may soon exceed monopropellant system capabilities. Future military space missions, such as space defense and reconnaissance, are likely to have requirements in excess of those of the commercial systems, itemized in Table 1.1-1, which typically illustrates these new demands.

1.1, Background (cont.)

TABLE 1.1-1

COMMUNICATION SATELLITE THRUSTER REQUIREMENTS

Parameter	SYNCOM	ATS-4	INTELSAT IV A	Advanced Spinner	Advanced 3-axis
Start Quantity	100	50	700	4,000	40,000
Total Impulse, lb-sec	6,000	10,000	72,000	75,000	75,000
Predictability % (Total Error)	$\pm$ 40	$\pm$ 30	$\pm$ 20	$\pm$ 15	$\pm$ 15
Life in Orbit, Years	1	3	7	10	10
Propellant System	H_2O_2	N_2H_4	N_2H_4	TBD	TBD

A large number of engine cold starts and very high total impulse have been shown to degrade the response, repeatability and performance of monopropellant thrusters. This is caused by gradual degradation of the catalyst bed. Figure 1.1-1, taken from Reference (1), summarizes the demonstrated capabilities of hydrazine monopropellant engines in 1973. The cold start quantity of less than 700 for 5-lbF class engines is less than adequate and illustrates a need for technology improvement. Efforts to correct this limitation by using bed heaters, improved catalysts and bed designs are in progress and have shown limited success.

A bipropellant system is a logical advance in technology and eliminates the problems associated with catalyst beds and monopropellant systems. Storable bipropellants, such as N_2O_4/MMH, have long been employed in larger engines (greater than 25-lbF), performing reaction control functions with considerable success and a high degree of reliability. In addition to the 25% improvement in steady state specific impulse performance over monopropellant systems, bipropellant systems offer a potential for:

(1) M. E. Ellion, D. P. Frizell and R. A. Meese, "Hydrazine Thrusters - Present Limitations and Possible Solutions AIAA 73-1265 Las Vegas November 1973.

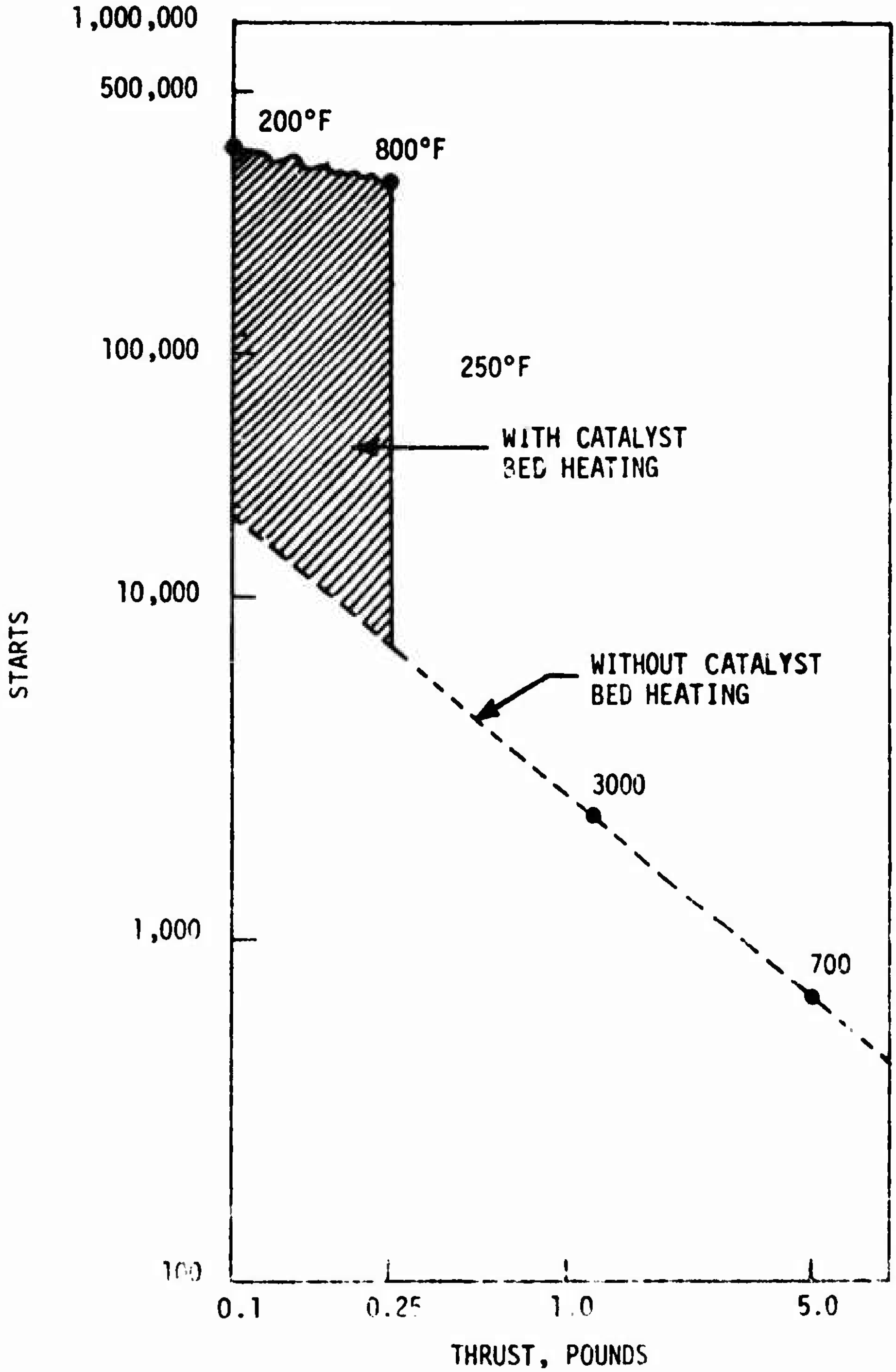

Figure 1.1-1. Demonstrated Monopropellant Thruster Capabilities

- Longer life and nearly unlimited thermal cycling with the performance loss and attendant catalyst bed degradation entirely eliminated;

- Higher pulse mode performance with particular performance advantages obtained on cold starts;

- More predictable response and lower power consumption resulting from an ability to operate without catalyst bed heaters;

- Lower propellant freezing temperatures; and

- Improved handling and reliability resulting from the ability to clean and flush a fully integrated spacecraft control system without fear of catalyst bed contamination or damage.

In some applications, the use of bipropellant engines allows the attitude control system to be integrated with the propellant feed system of the larger bipropellant engines on board the spacecraft. This results in a system weight advantage which is additive to the performance advantage.

Those areas which have historically proved troublesome to small engines were addressed in the new small engine technology work accomplished on this program. These included the following:

- Poor combustion efficiency and performance due to the very low propellant flow rates and limited number of injection elements (usually 2 or 3 orifices);

- Failure to achieve uniform and axisymmetric propellant combustion which is free from wall damaging hot streaks;

1.1, Background (cont.)

- Inadequate nozzle cooling and unacceptable heat soaks over a wide range of duty cycles;

- A relatively high volume of residual propellants within the injector which degrades performance, aggravates ignition spike problems and increases plume contamination levels; and

- Exhaust plume contamination resulting from ejection of propellant droplets due to incomplete combustion.

1.2 OBJECTIVE

The objective of this program was to develop and demonstrate the technology required to provide a high performance, long lived, fast response five-pound-thrust bipropellant engine capability for future Air Force requirements. The propellants employed in the demonstration were nitrogen tetroxide (N_2O_4) and monomethylhydrazine (MMH).

Table 1.2-1 indicates the design goals established for this program. Most noteworthy is the 300 sec steady state and 240 sec specific impulse at impulse bits of 0.05 lb-sec, the 3:1 tank pressure ratio for a blow-down system, the 20 to 120°F range of propellant supply temperatures, and the general life and reliability requirements. A need for buried engine operating capabilities (adiabatic wall) and a limitation on the engine-space craft thermal coupling were added to these goals following an evaluation of mission requirements during the Phase I

1.3 TECHNICAL EFFORT ORGANIZATION

The program structure for this technology development and demonstration consisted of three phases: Phase I - Requirements Definition and Engine Design Analysis; Phase II - Design and Verification Testing; and Phase III - Demonstration Testing. The scope of each phase was as follows.

TABLE 1.2-1

BIPROPELLANT ENGINE DESIGN GOALS

Parameter	Short Duration Blowdown	Short Duration Regulated	Long Duration Blowdown	Long Duration Regulated
Maximum Vacuum Thrust, lbf	5 ± 0.25	5 ± 0.25	5 ± 0.25	5 ± 0.25
Chamber Pressure, psia	TBD ± 5%	TBD ± 5%	TBD ± 5%	TBD ± 5%
Feed System Pressure, psia	300 - 100	500	Blowdown Range TBD	TBD
Expansion Ratio	TBD	TBD	TBD	TBD
Minimum I_{sp} (at max thrust), sec				
Steady State	300	300	300	300
Pulsing	240	240	240	240
Minimum Impulse Bit, lbf-sec	0.05 ± 0.005	0.05 ± 0.005	0.05 ± 0.005	0.05 ± 0.005
Total Impulse Delivery Capability lbf-sec	30,000	30,000	100,000	100,000
Number of Ambient Starts	100	100	1,000	1,000
Total Number of Restarts	175,000	175,000	300,000	300,000
Total Firing Life	2 hr	2 hr	10 hr	10 hr
Total Mission Life	30 days	5 days	7 yr	7 yr
Valve Response, ms				
Signal to full open	<5	<5	<5	<5
Signal to full close	<5	<5	<5	<5
Valve Leakage, scc/hr				
GN_2 at ΔP = Feed System Pressure	<2.5	<2.5	<2.5	<2.5
Propellants				
Oxidizer	Nitrogen Tetroxide (Mon-1) (99% N_2O_4 - 0.8% NO)			
Fuel	Monomethylhydrazine (N_2H_3 CH_3)			
Mixture Ratio	1.6 ± 0.048	1.6 ± 0.048	1.6 ± 0.048	1.6 ± 0.048
Propellant Inlet Temperature, °F	20 to 120	20 to 120	20 to 120	20 to 120
Storage Life Goal, yr	10	10	10	10
Flightweight TCA Reliability Goal	0.999	0.999	0.999	0.999
Flightweight TCA Maintainability Goal	Zero Maintenance Over Storage Life			

1.3, Technical Effort Organization (cont.)

Phase I conducted studies and trade-off analyses of general mission/system requirements versus engine parameters. Typical representative mission duty cycles were identified by literature search, review of current specifications and consultation with space craft manufacturers, users and selected government agencies.

Phase II developed point designs against the selected mission requirements based upon the relationships established in Phase 1. Design verification testing using the N_2O_4/MMH propellant combination was conducted to provide supportive data. Five injector designs and several thermal management systems were evaluated. The best of these approaches became the basis for the design of the demonstration engines.

Phase III consisted of finalizing the selected engine designs and the fabrication and demonstration testing of three engines over three selected simulated mission duty cycles. These duty cycles provided firing durations and quantities of restarts comparable to the goals described in Table 1.2-1. Testing was accomplished under simulated altitude conditions with 50:1 area ratio nozzles. Posttest activities included data and analytic model evaluation, a failure mode and effects analysis and a reliability analyses.

An additional task was added to Phase III in April 1974. This called for a comparative evaluation of the pulse performance forecasting capabilities of the CONTAM[2] and PMPM[3] analytic models. These predictions were then compared with actual pulse mode fire test data to assess the accuracy of the forecasted values.

1.4 REPORT ORGANIZATION

The subject report consists of three parts. The first, titled Introduction provides a background to the program reported herein as well as a description of the program's objectives and its structure. This is followed

(2) R. [illegible] Hoffman, W. [illegible] Webber, et al., Plume Contamination Effects Prediction, The CONTAM Computer Program, Version II, AFRPL-TR-73-46, August 1973.
(3) W. [illegible], [illegible] Pulse Mode Performance [illegible] Final Report, AFRPL-[illegible]

1.4, Report Organization (cont.)

by a summation of the programs accomplishments and a description of Flight Engine Designs which are based on the units tested.

The second portion of the report, Experimental Results and Discussions, is a chronological exposition of the programs three phases with the material arranged in a format similar to the programs three phases described above.

The final section, Conclusions and Recommendations, summarizes the technology improvements and collorary information resulting from the review of the programs data. The recommendations describe the manner in which this data should be utilized to either further develop small thruster technology or to facilitate the application of the technology to current and/or anticipated spacecraft needs.

SECTION II

EXPERIMENTAL RESULTS AND DISCUSSIONS

2.0 PROGRAM ACCOMPLISHMENTS

2.1 ENGINE DESIGN AND OPERATING CHARACTERISTICS

The basic engine developed under this program has demonstrated the feasibility of obtaining the goals itemized in Table 1.2-1. The added requirement for operation in a buried mode was demonstrated using a propellant injection pattern which provided a fuel rich protective barrier along the chamber wall. The barrier cooling, in combination with suitable chamber insulation, allows exterior wall temperatures of less than 200°F to be maintained during and following sustained operation. Although the barrier cooling results in a decrement in the specific impulse delivered with a 100:1 area ratio nozzle from the 300 sec demonstrated with a radiation-cooled engine to 283 sec, this specific impulse is 40 sec greater than the highest reported monopropellant hydrazine engine performance.

In contrast to monopropellant thrusters, the demonstrated 5 lbf thrust bipropellant engines showed no change in pulse shape, response or performance over the duty cycles which comprised more than 300,000 pulses on one unit, 50,000 pulses plus a 6300 sec continuous burn on a second and 50,000 pulses on the third. The adiabatic wall engine, operates in a fully insulated installation and appears to have the broadest application. Data obtained from this engine at duty cycles from 0.3% to 100% on-time, indicate that it has no thermally limiting operating conditions. Structural analysis involving fatigue and creep forecast a useful continuous firing life of 3400 hours with a capability for 50,000 cold starts and more than a million restarts (pulses) with a design margin of 10.

The higher performing radiation-cooled engine design has an unlimited capability for duty cycles from 0.3% to 50% on-time and limited pulse train and burn durations between 50% and 100% duty cycles. Operation of this engine at a slightly reduced chamber pressure would allow virtually unlimited steady state durations.

The valve response times obtained from random samplings of the more than 400,000 firings conducted in Phases II and III showed a response of 0.0023 to 0.0026 sec from signal to start of travel. These data cover a 20 to 120°F propellant temperature and 100 to 400 psia tank pressure operating envelope. Valve closing times ranged from 0.0025 to 0.0028 sec. Valve travel time to open or close under these conditions was approximately 0.0005 sec. The manifold fill, ignition and thrust rise to 90% of steady state requires an additional 0.002 to 0.003 sec, depending on tank pressure. Variations in engine response time under a fixed set of propellant supply temperatures and pressures were too small to be assessed accurately. Other significant response data are provided in Table 2.1-1.

Highly repeatable bit impulses of 0.05 $\pm$ 0.005 lbF-sec were demonstrated at an electrical pulse width of 0.010 sec and maximum tank pressures. In long continuous pulse trains, their reproducibility was $\pm$ 2.4% with a 1 sigma confidence level. The minimum impulse bits demonstrated were 0.02 lb-sec at the same electrical pulse width with the tanks at the lower limits of blow-down mode operation. The reproducibility of these were $\pm$ 3%. Although not demonstrated with hot firings it appears entirely practical to provide impulse bits of 0.01 lbF-sec simply by reducing the electrical pulse width to 0.005 sec.

2.2 IMPROVED CAPABILITIES IN PULSING PERFORMANCE ANALYSES

Analyses were conducted using the CONTAM computer model developed by MDAC-West and AFRPL and pulse mode performance model (PMPM) which

TABLE 2.1-1

TYPICAL ENGINE RESPONSE CHARACTERISTICS

	Propellant Supply Condition			
Tank Pressure, psia	300-400		100-150	
Propellant Temp, °F	22	118	22	18
Start Signal to 90% P_c sec	0.0051	0.0050	0.0061	0.0062
Stop Signal to 10% P_c sec	0.0055	0.0052	0.0075	0.0065
Signal to Valve Open sec	0.0026	0.0025	0.0023	0.0025
Signal to Valve Close sec	0.0025	0.0027	0.0028	0.0025
Valve Travel Open sec	$\approx$0.0005	$\approx$0.0005	$\approx$0.0005	$\approx$0.0005
Valve Travel Close sec	$\approx$0.0005	$\approx$0.0005	$\approx$0.0005	$\approx$0.0005
P_c Decay sec	0.0025	0.0025	0.0047	0.0040

is based on Rocketdyne's distributed energy release (DER) performance model and injector chamber compatibility (ICC) computer programs. Output from these two programs were compared with each other and with experimental data generated by pulse mode firings of two engines. These engines were operated over a specially prepared duty cycle involving 40 pulses of varying fire periods and coast periods to obtain data with different chamber wall temperatures. Comparisons of predicted and measured performance showed that the PMPM model neglects to account for chamber wall film vaporization and therefore is unable to properly account for pulse mode performance variation which occurs as the chamber wall temperature changes. The CONTAM model treats the wall film losses satisfactorily when the wall is hot but underestimates these when the wall is cold. CONTAM also overestimates the persistance of combustion following shutdown. This is especially so for cold chamber walls and results in an overestimation of shutdown impulse. It was found that for a true "a priori" prediction of performance for new design, the CONTAM model was superior. The PMPM model however when "tuned" using empirical data from a particular engine will more economically predict engine pulse mode performance for anticipated duty cycles. Recommendations for model modifications and model usage are provided.

2.3 ANALYTICAL AND EXPERIMENTAL EXPERIENCE WITH EXHAUST PLUME CONTAMINATION

A feature of the CONTAM program is an output of the weight percentages of contaminant generated as a result of incomplete combustion of the propellant. These consist of a wall film component and unreacted droplets entrained in the high velocity exhaust stream with the analyses indicating that improved combustion efficiency and performance result in lower contaminant generation. Thus, it can be inferred that the 300-sec specific impulse engine tested in this program is the cleanest as well as the highest performing engine of its class.

2.3, Analytical and Experimental Experience with Exhaust Plume Contamination (cont.)

The vacuum test facility in which the Phase III life durability testing was conducted contained a window positioned proximate to the engine exhaust plume to allow continuous TV coverage. During the course of testing the first of the adiabatic wall engines for 50,000 pulses, a slight but gradual reduction in window transparency was noted. A major portion of this was due to the flaking of the unprotected Dyna Quartz chamber insulation and its subsequent deposition on the window. Testing of the higher performing radiation-cooled engine (uninsulated) showed no visible change in transparency over a 300,000 pulse duty cycle. An optical sensing device was installed for the final 50,000 pulse engine test series to provide finer resolution and a means of documentation of changes in transparency. This engine was insulated with Dyna Quartz which was encased in metal foil. These measurements showed no change in light intensity and hence window transparency over the entire duty cycle demonstration. These measurements indicate a virtually total absence of radially directed plume contaminants. The high engine performance provides supportive evidence for the minimization of noncombusted exhaust products which are the source of plume contaminants.

3.0 FLIGHT ENGINE DESIGNS

Two of the four engines described in Table 1.2-1 titled "Engine Design Goals", are eliminated if engine life is not a consideration. Since the data obtained on this program shows that there are no design differences between short and long lived engines, the design goals are met with two different engine types. One is a "universal" configuration which can operate in a buried configuration (adiabatic wall), be used with either a blow-down or regulated feed system and provide any desired duty cycle ranging from very short repeatable impulse bits to several hours of continuous firing. The other, which operates only with a regulated feed system and is allowed to radiate, has the same requirement for an unlimited duty cycle capability.

Both engines would provide: high performance for single pulse, continuous pulsing and steady state operation; minimal exhaust plume contamination; no degradation with accumulated operating time in either steady state or pulsing modes; very rapid response; and good pulse repeatability along with high reliability.

The subject program tested a variety of injector configurations and chamber designs and concluded with the successful testing of three different engines for simulated mission duty cycles. These data have been reviewed in light of the Engine Design Goals and two versions of a single engine design formulated to meet these requirements. This basic engine utilizes a silicide coated columbium thrust chamber and a multielement platelet injector which is integrated with a torque motor actuated bipropellant valve to achieve a minimum residual propellant volume. The differences between the two engine versions are that the injector orifice patterns are unlike and one utilizes lightweight insulation to maintain a skin temperature of less than 200°F.

The following chart which summarizes the design characteristics of each identifies the detail design differences.

	MODEL DESIGNATION	
	AJ 10-181-1	AJ 10-181-2
Thrust class, lb	5.0	5.0
Propellant	N_2O_4/MMH	N_2O_4/MMH
Mixture Ratio	1.60	1.60
Installation	Buried, cold back wall required, envelope volume limited	Free to radiate, not volume limited
Injector Type	4-element with low MR at periphery	6-element uniform MR
Valve	Torque motor actuated bipropellant valve with integrated injector	Torque motor actuated bipropellant valve with integrated injector
Residual Propellant Volume	0.0006 in.^{3}	0.0006 in.^{3}
Chamber	Vac Hyd 101 coated FS-85 columbium	Vac Hyd 101 coated FS-85 columbium
Nozzle Area Ratio	100	150
I_{sp}, Steady State, sec	283	298
Skin Temperature	200°F	2750°F
Propellant Feed System	Blowdown	Regulated
Weight, lb	1.3	1.2

The AJ 10-181-1 engine is portrayed in Figure 3.0-1 which includes a tabulation of its full thrust and minimum thrust operating characteristics. Its blowdown feed system operation is summarized in Figures 3.0-2 and 3.0-3 which present performance (I_{sp}) and thrust as a function of tank pressure for steady-state and pulse mode operation, respectively.

Figure 3.0-4 illustrates the AJ 10-181-2 engine and provides a tabulation of its operating characteristics. Although not intended for operation with a blowdown feed system, this unit can safely operate at reduced thrust. Figures 3.0-5 and 3.0-6 present steady state and pulse mode performance and

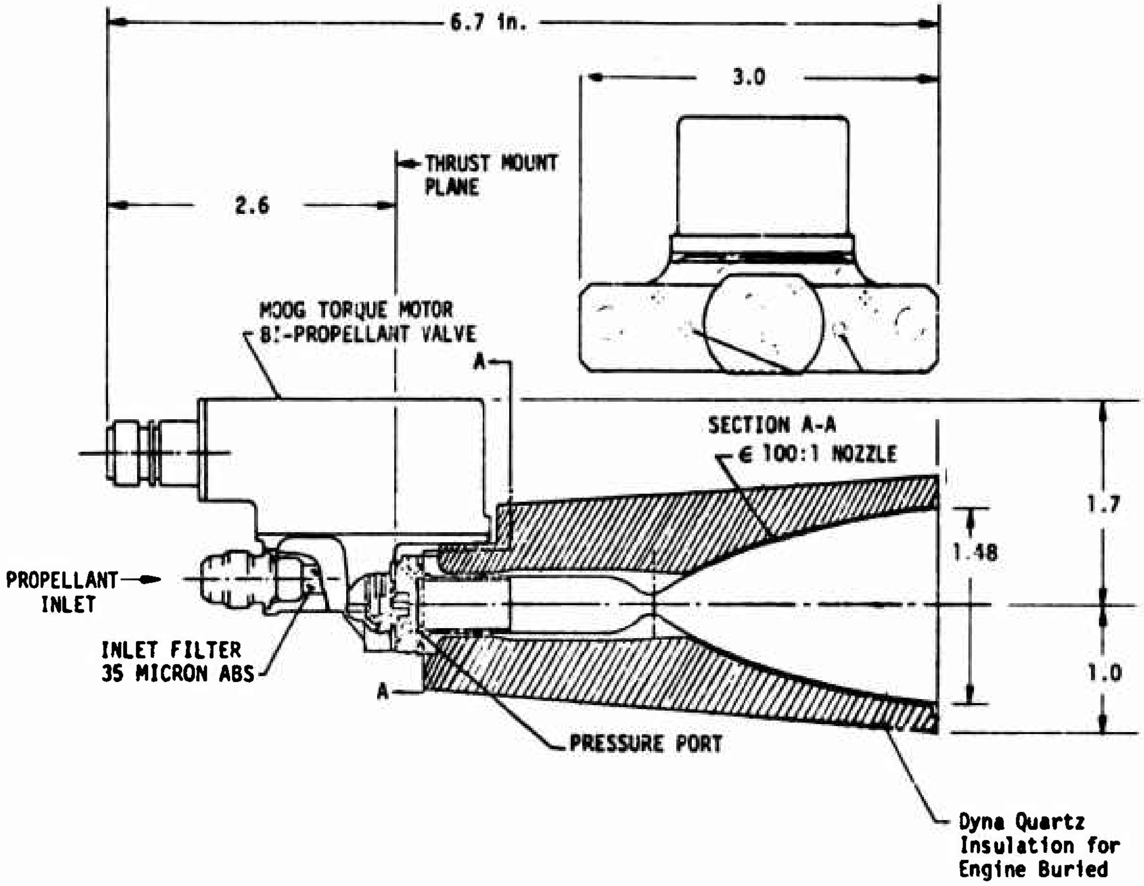

Operating Characteristics

	Full Thrust	Min. Thrust
Thrust, lbf	4.5	2.2
Chamber Pressure, psia	150	75
Feed Pressure, psia	300	125
I_{sp} Steady State, sec	283*	255*
I_{sp} for 0.050 lb-sec Impulse Bit	228	200
Min. Impulse Bit, lb-sec	0.025	0.012
Min. EPW, sec	0.005	0.005
Valve Response Time to Full Open, sec	0.003	0.003
Valve Response Time to Full Shut, sec	0.003	0.003
Sec to 90% of P_c	0.005	0.006

Propellant	N_2O_4/MMH
Mixture Ratio	1.6
Engine Weight, lb	1.3

*A_e/A_t = 100; Add 2.5 sec for A_e/A_t = 150

Figure 3.0-1. AJ10-181-1 Engine

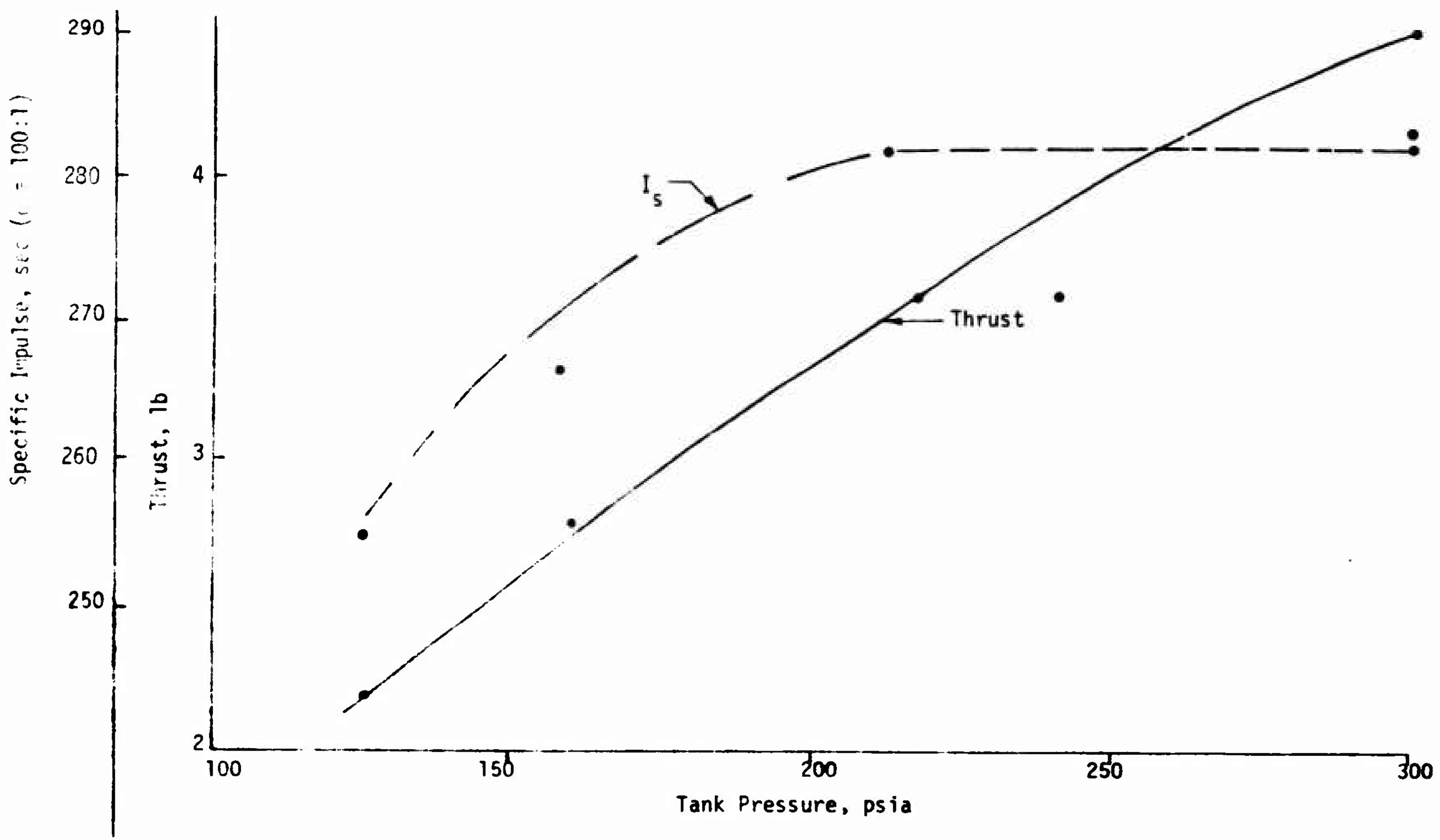

Figure 3.0-2. Steady State Performance AJ10-181-1

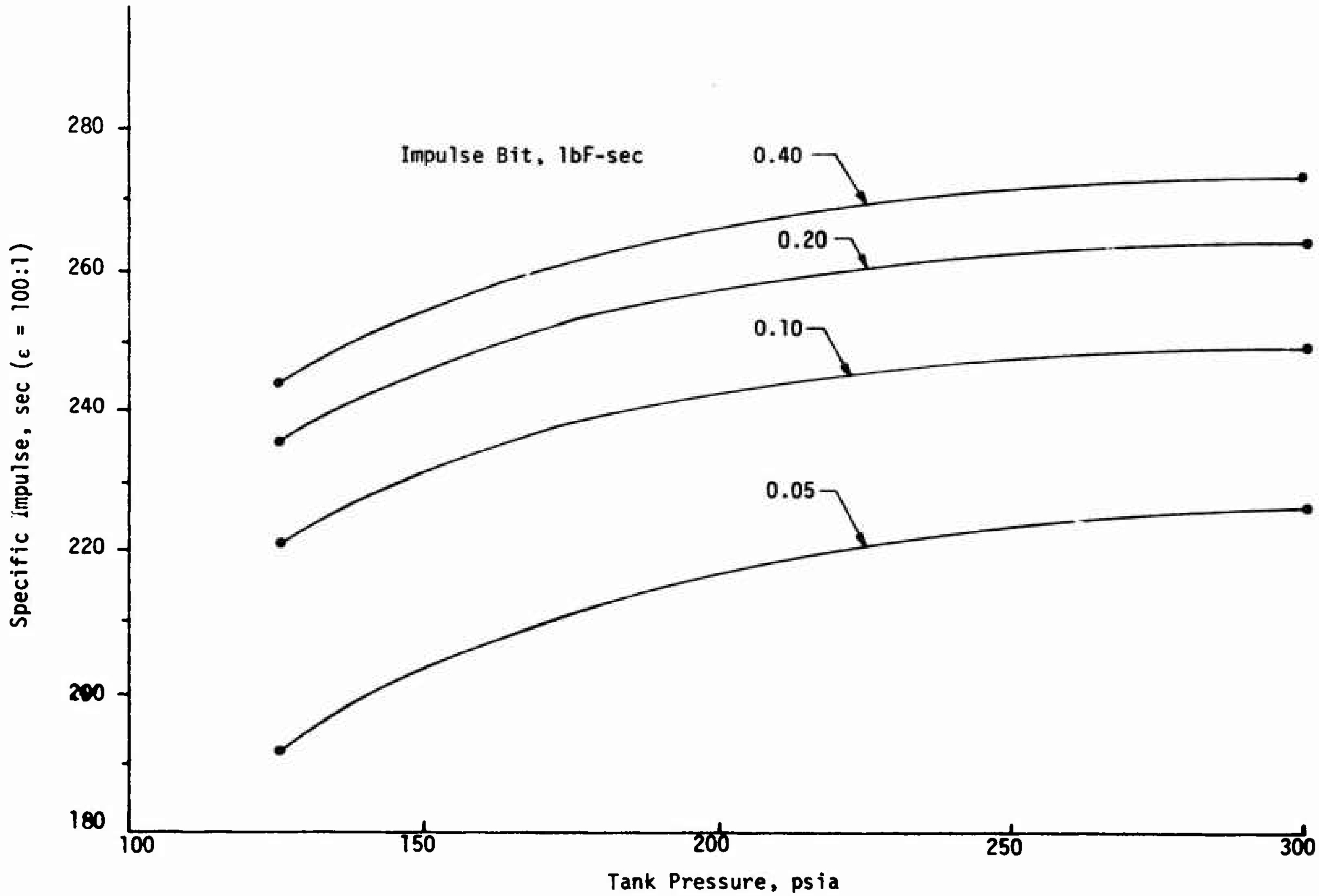

Figure 3.0-3. Pulse Mode Performance AJ10-181-1

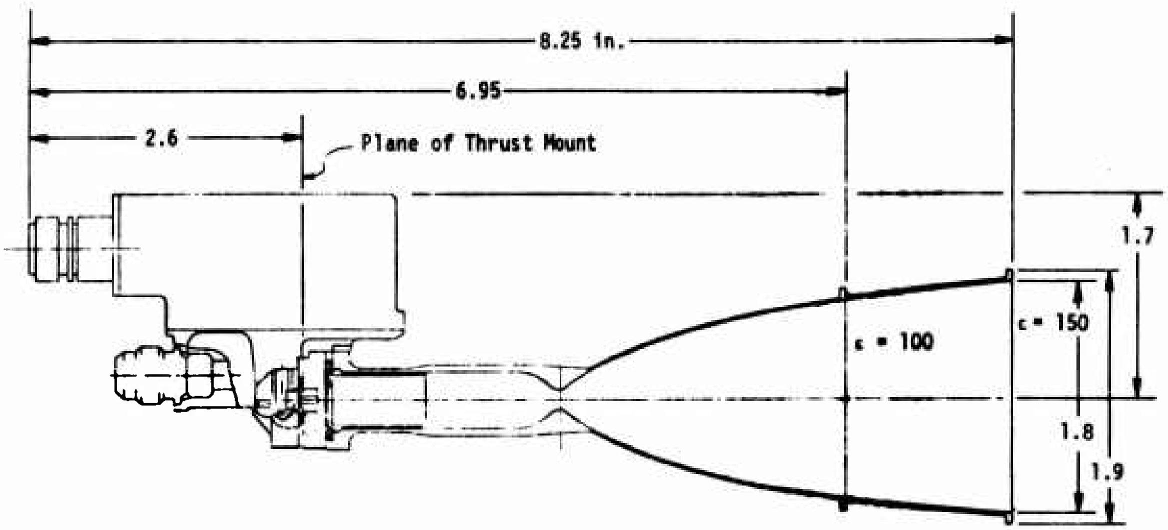

Operating Characteristics AJ10-181-?

Thrust	4.2
Chamber Pressure	120
Feed pressure	345
I_{sp} Steady State	298 (150/1)
I_{sp} for 0.050 lb sec Impulse Bit	245
Min. Impulse Bit at P_c = 120	0.02
Minimum EDW	0.005
Valve Response Time to Full Open, sec	0.003
Valve Response Time to Shut, Sec	0.003
Time to 90% of P_c, sec	0.005
Propellant	N_2O_4/MMH
Mixcure Ratio	1.6
Engine Weight	1.?

Figure 3.0-4. AJ10-181-2 Engine

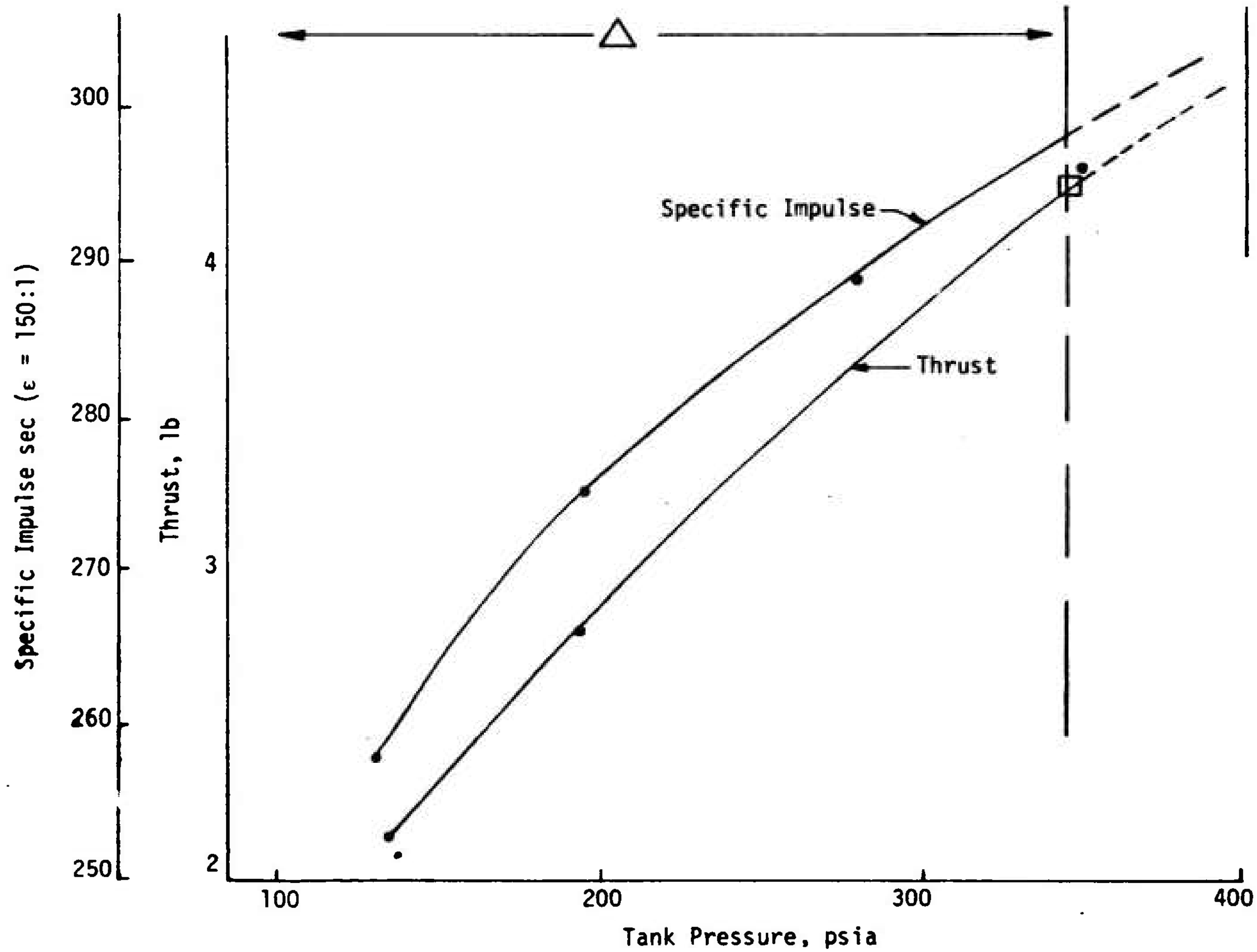

△ Continuous Steady State Operation Apply Only To This Operating Range

Figure 3.0-5. Steady State Performance AJ10-181-2

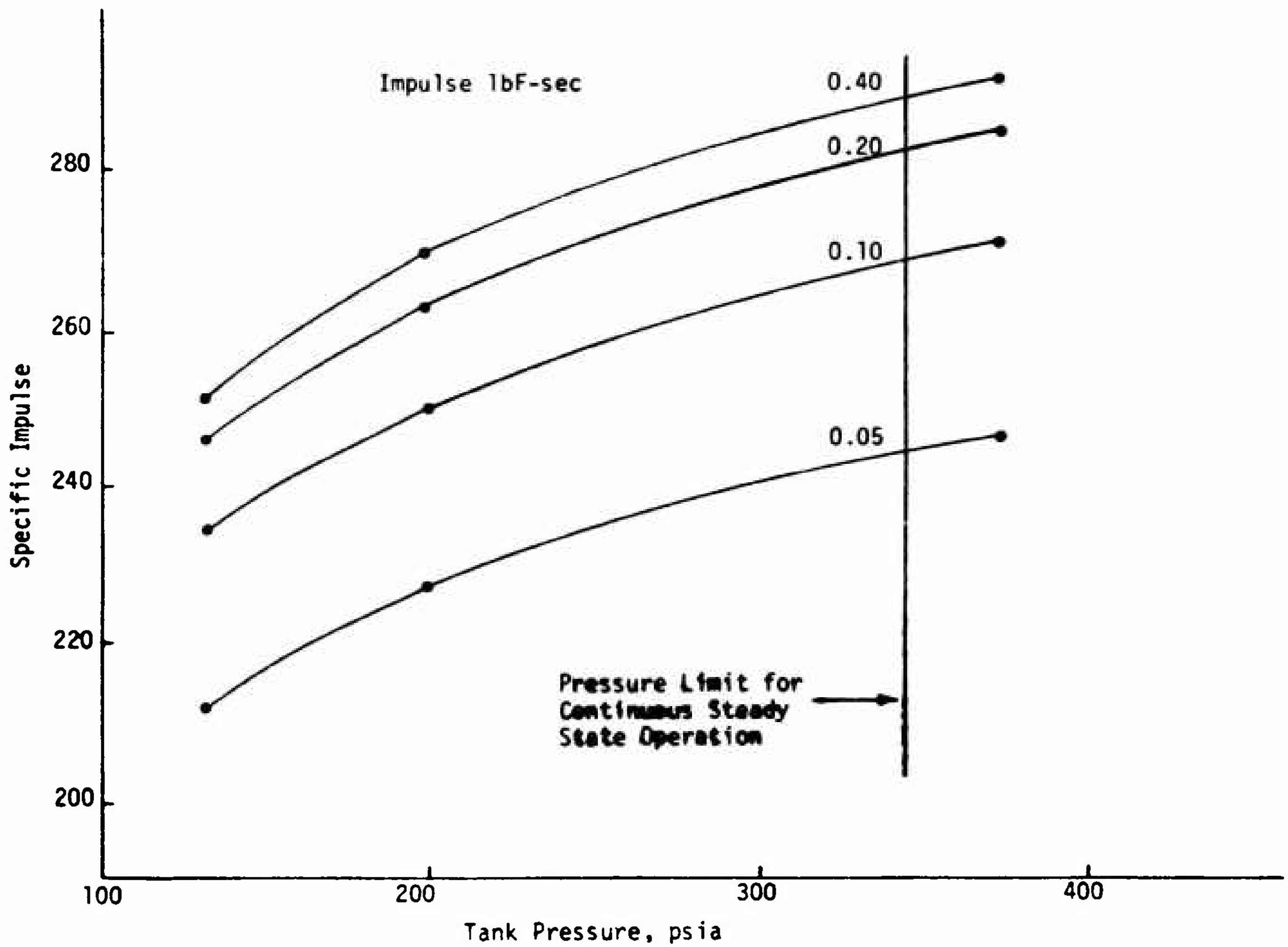

Figure 3.0-6. Pulse Mode Performance AJ10-181-2

thrust as a function of tank pressure. The rapid performance decrement which occurs as tank pressure is reduced results from the design being optimized for full thrust operation.

The AJ 10-181-2 engine can be operated at a chamber pressure (P_c = 132, feed pressure = 400) in excess of its design value. This results in a steady state I_{sp} of over 300 sec (reference Figure 3.0-5) although the percentage duty cycle is limited to less than 50% with single burns not exceeding 30 seconds in duration. This performance improvement-duty cycle curtailment requires that the engine be used for pulse mode operation only.

Although the AJ 10-181-1 and -2 engines have been proven in the duty cycle demonstration testing conducted during Phase III of this program, analyses and test data indicate their performance and operating flexibility could be improved if the injector designs were iterated. These improvements could provide the capability of operation using N_2H_4 in place of the MMH fuel as well as performance increases.

4.0 PHASE I ANALYSIS

The purpose of the program's initial phase was to insure that the engine configuration selected for development was in consonance with the requirements of potential users. The earliest program tasks were therefore to (a) define applications and mission requirements, (b) identify the capabilities of anticipated engine designs, and (c) conduct a system-mission-engine interaction analysis to define those technology areas which required further development.

4.1 MISSION REQUIREMENTS DEFINITION

Mission requirements data was compiled using available literature[4 through 10] and through consultation with industry, NASA and Air Force personnel. These data were compiled into the summaries shown in Figure 4.1-1. The first two categories, Communication and Navigation, and Surveillance and Reconnaissance, represent the major quantity of spacecraft and launchings. It was found that requirements for specific missions within each category, and in some instances, the approach of different spacecraft primes to the same mission were unlike. Thus it was not possible to define a singular set of requirements for a five pound thrust engine. This resulted in the generation of the following requirements for a [illegible] engine.

(4) R. D. [illegible], USAF, [illegible], Satellite Propulsion System Analyses Technical Report [illegible] TR-71-103, dated September 1971

(5) G. J. Nunz and J. [illegible] [illegible] synchronous Satellites, Aerospace Corporation Report [illegible] 0066 (5310)-1, dated 15 May 1970

(6) L. R. Holcomb, Satellite Au[illegible] [illegible] Techniques, NASA-JPL Technical Report 32-[illegible], dated November [illegible]

(7) Launch vehicle estimating factors, NASA [illegible] January 1971 Edition

(8) D. Schnyer, The Space Tug Mission Role [illegible] Program [illegible] AIAA Paper [illegible], [illegible] July [illegible]

(9) Space Tug System [illegible] NASA [illegible]

(10) Leading U.S. and International [illegible] Vehicles Tabulation from Aviation Week Forecast [illegible] dated 19 March 1973

	SHELF LIFE	MISSION LIFE	LAUNCHER	SPACECRAFT WEIGHT, lb	OPERATING ALTITUDE, mi	STABILIZATION	PROPELLANT ACQUISITION	PROPELLANT LOAD, lb	TANK PRESSURE psia	PRESSURIZATION	ENGINE SIZE, lbf & NO.
COMMUNICATION AND NAVIGATION	1 yr	7 years	THOR DELTA ATLAS CENTAUR TITAN III C&D	600 TO 1500 2000 TO 3000 1000 TO 5000	UP TO 23,800	SPIN SPIN &/OR 3 AXIS	DIAPHRAM SCREENS SCREENS	75 300 450	400-80 400-80 400-80	BLOWDOWN BLOWDOWN BLOWDOWN OR REGULATED	5.0 2/4 5/.5 4/12 50/5 2/12
SURVEILLANCE & RECONNAISSANCE	1 yr	3 mo to 7 yr	THOR AGENA TITAN III BC&D	2000 TO 4000 2000 TO 25,000	100-200 100 TO 23,800	3 AXIS 3 AXIS	DIAPHRAM SCREENS	150 300 TO 3000	400-80 400-80	BLOWDOWN BLOWDOWN OR REGULATED	5/.5 4/12 250/5.0 1/12
SPACE DEFENSE	3-5 yr	1 mo to 1 yr	THOR DELTA TITAN III D	1500 TO 5000	100 TO 23,800	3 AXIS	DIAPHRAM	300 TO 1000	≈ 500	REGULATED	1500 & 5.0 1/12
SHUTTLE ORBITER	1 yr	2 mo. 10 yr	SHUTTLE	150,000	100	3 AXIS	SCREENS	-	300	REGULATED	900/10 36/6
SPACE TUG	1 yr	-	SHUTTLE	-	23,800	3 AXIS	SCREENS	-	400-80	BLOWDOWN OR REGULATED	10 TO 50 24
PLANETARY PROBES	1 yr	5 years	THOR DELTA ATLAS CENTAUR TITAN CENTAUR	150 TO 300 500 TO 5000 1500 TO 7500	- - -	SPIN &/OR 3 AXIS	DIAPHRAM	50 100 150	300-80 300 300	BLOWDOWN REGULATED REGULATED	ΔV ENGINES, 5.0 & .5

	LINE SIZE & Lgth, ft	PROPELLANT TANK TEMPERATURE	STABILIZATION	MAX TEMP	MAJOR IMPULSE USAGE	STABILIZATION	PULSE QUANTITY	TOTAL DURATION sec	ALLOWABLE HEAT FLOW watts	PLUME SENSITIVITY
COMMUNICATION AND NAVIGATION	1/4-3/8 6 10 15	20-120 20-120 20-120	SPIN SPIN &/OR 3 AXIS	30 100 100	90%-0.10 sec PULSES (SPIN) 95%-1.0 sec PULSES (3 AXIS) 15%-0.01 sec PULSES	SPIN SPIN &/OR 3 AXIS	50,000 150,000	5,000 20,000 20,000	20 40 40	SLIGHT MODERATE MODERATE
SURVEILLANCE & RECONNAISSANCE	6 10-20	20-120 20-120	3 AXIS 3 AXIS	100 100	75%-1.0 sec PULSES 25%-0.1 to 0.01 sec PULSES	3 AXIS 3 AXIS	20,000 150,000	5,000 25,000	20 40-60	MODERATE TO SEVERE
SPACE DEFENSE	5-20	20-120	3 AXIS	100	75%-1.0 to 10.0 SEC PULSES 25%-0.1 to 0.01 sec PULSES	3 AXIS	10,000 100,000	1,000 20,000	20 40	SLIGHT MODERATE
SHUTTLE ORBITER	60	20-120	3 AXIS	30	75%-0.010 sec PULSES (VERNIER ENG.)	3 AXIS	200,000 (100 MISSIONS)	100,000	-	SLIGHT
SPACE TUG	25	20-120	3 AXIS	50	75%-0.010 sec PULSES(VERNIER ENG.)	3 AXIS	200,000 (100 MISSIONS)	100,000	-	MODERATE
PLANETARY PROBES	5 10 20	20-120 20-120 20-120	SPIN &/OR 3 AXIS	100 100 100	75%-0.10 to 10 sec PULSES	SPIN &/OR 3 AXIS	5,000 TO 20,000	10,000	10	SLIGHT

Figure 4.1-1. Mission Requirements Tabulation

4.1, Mission Requirements Definition (cont.)

- Life - up to 10 years
- Operating Altitude - Vacuum
- Tank Pressure - 400 to 80 psia
- Pressurization - blowdown or regulated
- Propellant Temperature - 20 to 120°F
- Propellant tank Temperature differential - up to 100°F
- Pulse Quantity - up to 500,000
- Allowable Heat Flow to the Spacecraft - 20 to 60 watts
- Plume Contamination - minimum
- Engine Installation - Buried or exposed
- Performance Steady State - maximum (e.g., I_{sp} = 300 sec)
- Performance Pulsing - Maximum
- Minimum Impulse Bit - 0 050 lb-sec or less
- Start up Response Time - <0.010 sec
- Shutdown Response - <0 010 sec
- Pulsing Duty Cycle - unlimited
- Single burn duration - up to 2 hours

The achievement of a 0.010 lbF-sec impulse bit would allow a 5 lbf engine to also assume the function of 1/2 lb thrust class engines on some applications. The engine parameter study described in the following section disclosed that the engine cooling, spacecraft heat flow and pressurization requirements in conjunction with the 300 sec I_{sp} performance goal are too broad to be met with a single engine configuration. Therefore, detail differences in a single basic design were expected to allow performance, duty cycle, wall temperature and heat input to the space craft to be traded.

4.2 ENGINE PARAMETER STUDY

The scope of the engine parameter study is summarized in Figure 4.1-2. The mission requirements study defined parameters, and their range are shown in the two columns to the figure's left. The areas of greatest

PARAMETER	RANGE	COMPONENT			INTERACTION
		INJECTOR	THRUST CHAMBER	VALVE	PERF. & CONTAM.
PULSING & STEADY STATE PERFORMANCE	240, 300 SEC	ERE COMPATABILITY	LENGTH, COOLING	SEQUENCING RESPONSE	X
FEED PRESSURE	100 – 500 PSIA	ΔP		WEIGHT	X
FEED PRESS VARIATION FEED & TANK TEMP VARIATION	± 15 PSIA 20 – 120°F	PATTERN	COOLING	•	X
DUTY CYCLE	NO LIMITS	VOLUME	HEAT SOAK	HEAT SOAK	X
MISSION DURATION	10 YRS. MAX	LIFE	LIFE	LIFE	
VALVE SEQUENCING & RESPONSE	0.005 SEC	VOLUME		REPEATABILITY VOLUME	X
ENGINE WEIGHT & ENVELOPE	MIN.		Pc, AREA RATIO	TYPE	
ENGINE TEMP. STEADY STATE SOAK	2000 – 3000°F < T SAT OX.	BARRIER COOLING	GEOM. WEIGHT	THERMAL STAND OFF	X
ENGINE DEVELOPMENT TIME & COST	MIN.	TYPE & MATERIAL →	→	→	
NUCLEAR HARDENING		MATERIAL & FABRICATION →	→	→	

Figure 4.1-2. Engine Parameter Study Scope

significance with regard to each component are highlighted and the interaction of performance and plume contamination generation is shown to relate to most of the system parameters.

4.2.1 Injector Design

The results of an injector performance study which treated steady state and pulse mode performance are summarized in Figures 4.2-1 and -2. The forecasted injector performance values were in generally good agreement with the subsequent experimental data.

The conclusions drawn from Figure 4.2-1 the steady state portion of the parametric analyses are as follows:

(1) The minimum energy release efficiency required to attain the 300 sec specific impulse goal was ≈ 96%. An injector allowing 4% loss resulting from incomplete vaporization and uncontrolled mixture ratio maldistribution would lead to a 3000°F radiation cooled nozzle wall temperature. Improvement to a 98% ERE; 2% loss due to combined vaporization and uncontrolled MRD in conjunction with a 2% controlled MRD loss in the form of a fuel rich barrier could lead to 2230°F radiation cooled chamber wall temperatures and 2800°F adiabatic wall temperatures at the same 300 sec specific impulse level.

(2) The minimum number of doublet type injection elements required to attain the 300 sec steady state specific impulse was 2. A two element injector would however require a 4 inch chamber length which is unreasonably long for a 5 lb thrust engine. The two element injector would not be expected to provide the uniform axisymmetric gas flow field for good chamber compatibility and long life. Four elements were set as a minimum design value based on attaining uniform chamber wall temperature.

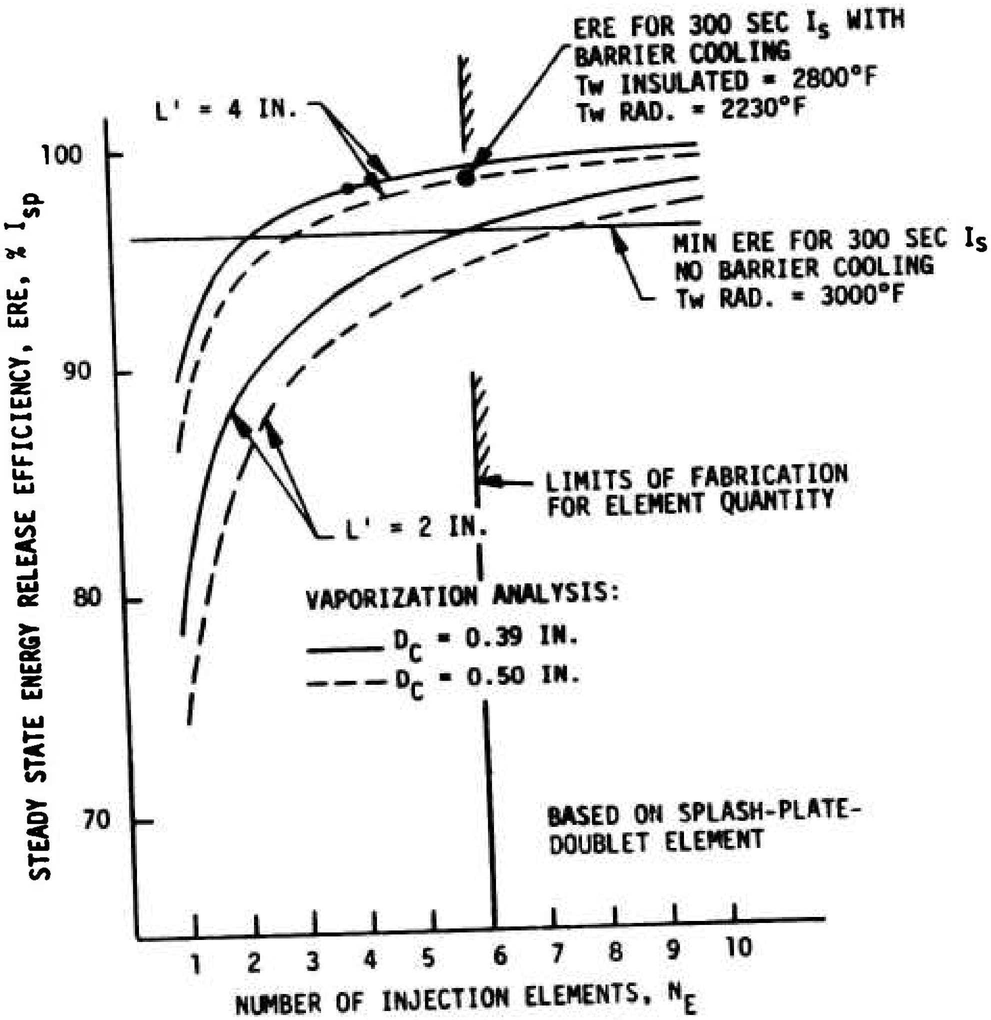

Figure 4.2-1. Element Quantity and Chamber Interaction

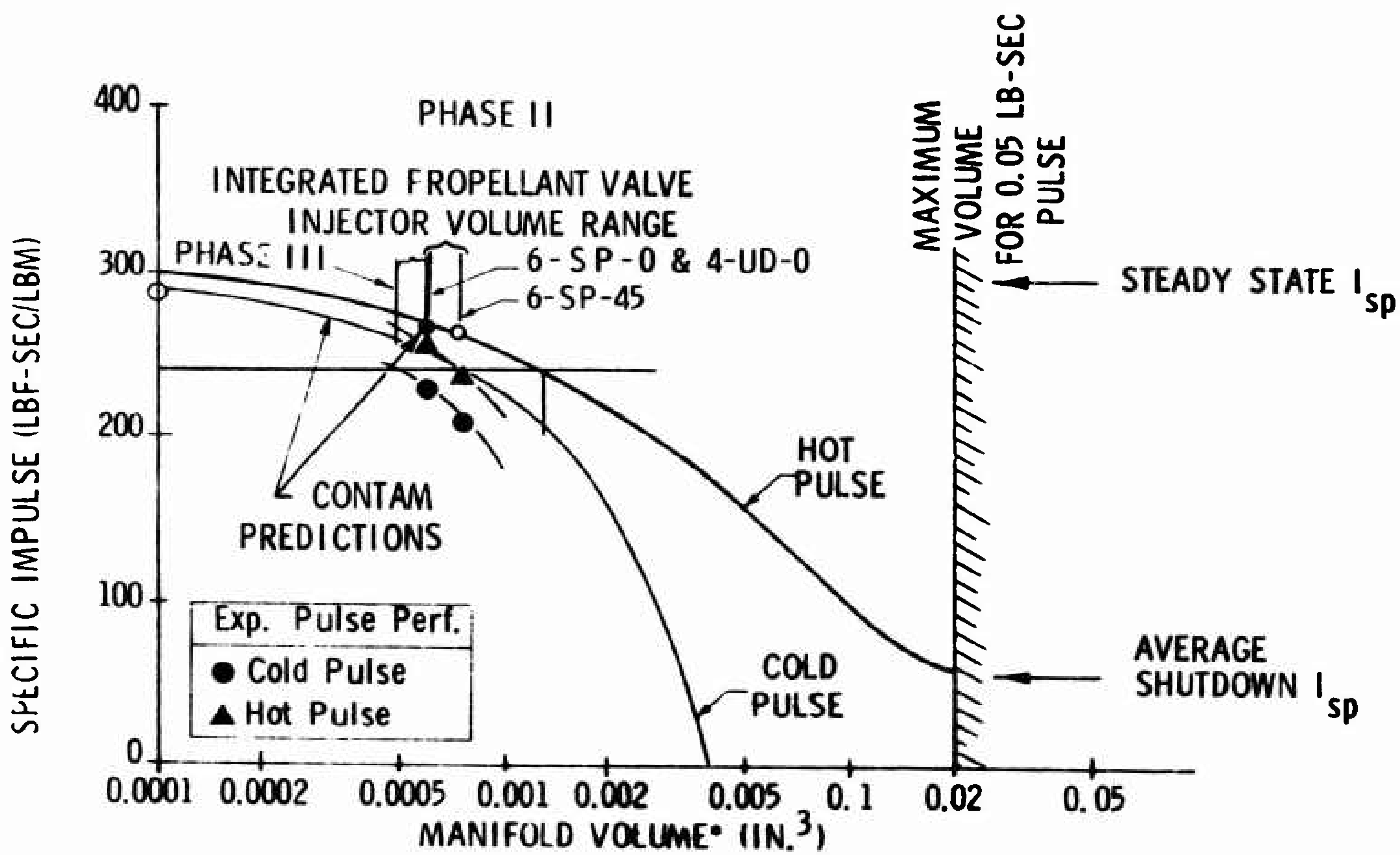

*Includes Total Fuel and Oxidizer Volumes Downstream of Propellant Valve.

Figure 4.2-2. Manifold Volume Versus Pulse Performance for a Minimum 0.05 lbf-sec Pulse

4.2.1, Injector Design (cont.)

(3) The maximum number of injection elements based on a 0.008 inch minimum orifice diameter was 6. Six elements could provide the 300 sec I_{sp} in a 2 in. chamber.

(4) A slight performance advantage for small contraction ratios was shown in the vaporization analyses. The CONTAM program showed no influence of contraction ratio on the pulse mode performance. Subsequent test data showed the contraction ratio to have no influence at full thrust and a small contraction ratio to be beneficial for deep blowdown capabilities.

The predicted effect of manifold volume on pulsing performance is shown in Figure 4.2-2. Performance predictions were obtained using the TCC portion of the CONTAM analysis. This data indicated that the total manifold-volume allowed for the achievement of the pulsing performance goal of 240 sec was 0.0013 cubic inches. Actual pulse mode performance data obtained from Phase II testing (reference Section 5.3) is displayed. These data obtained with injectors having manifold volumes of approximately 0.0007 cubic inches, showed the forecasted performances to be slightly optimistic. Manifold volumes of the subsequent Phase III units were consequently reduced in size.

4.2.2 Thrust Chamber Design

The thrust chamber parameter study was initiated by an examination of the effect of chamber pressure on pulsing and steady state performance, contaminate generation and ignition. These studies, summarized in Figures 4.2-3 through 4.2-5, indicated that higher chamber pressures result in increased performance, reduced contaminates and more assured ignition.

Figure 4.2-3 showed significant theoretical performance improvements up to 200 psia chamber pressure and nozzle expansion ratios to the 100 to 150 range. The use of a Rao nozzle contour which is 25% longer

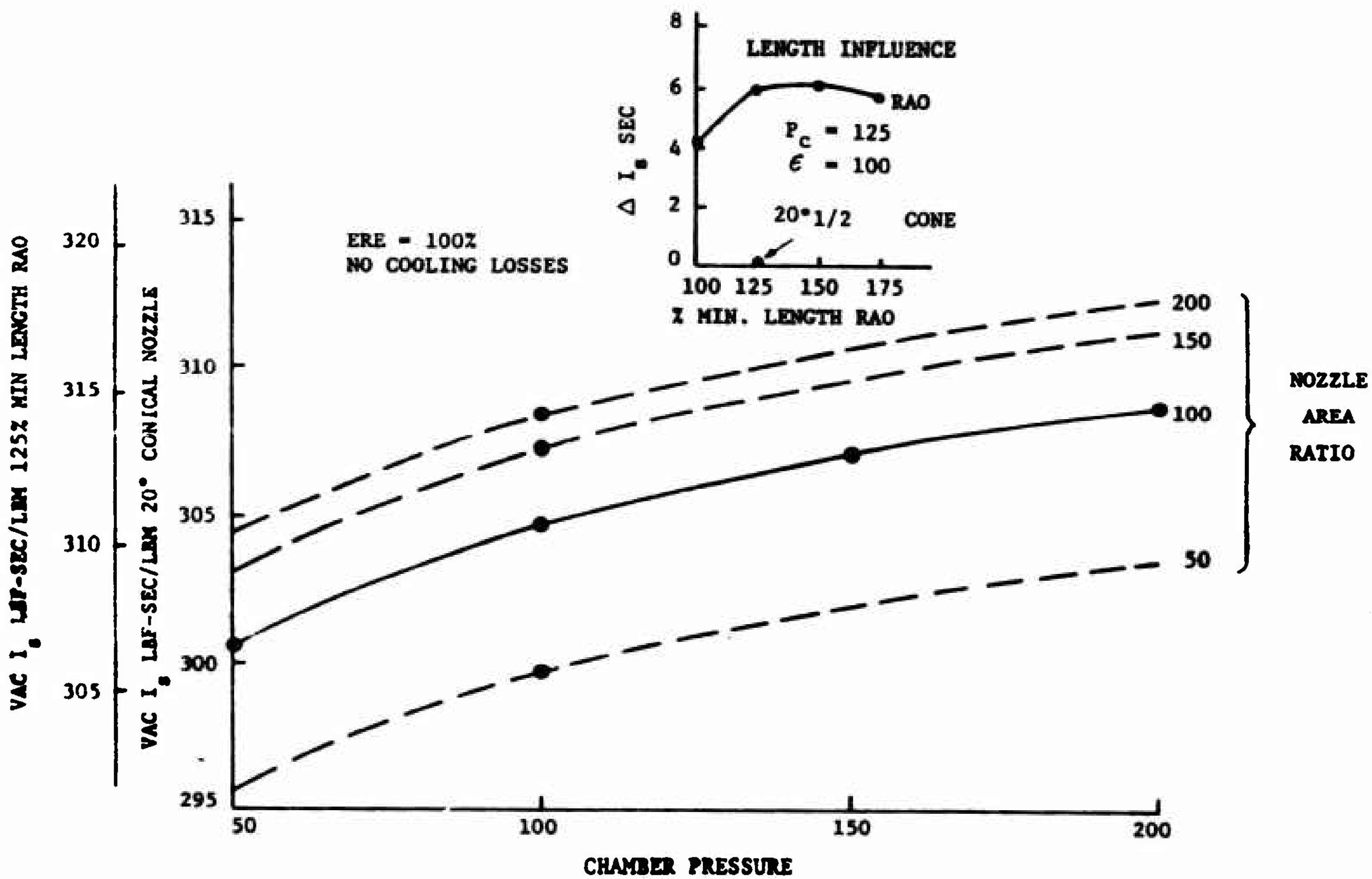

Figure 4.2.3. Theoretical Nozzle Performance Parameters

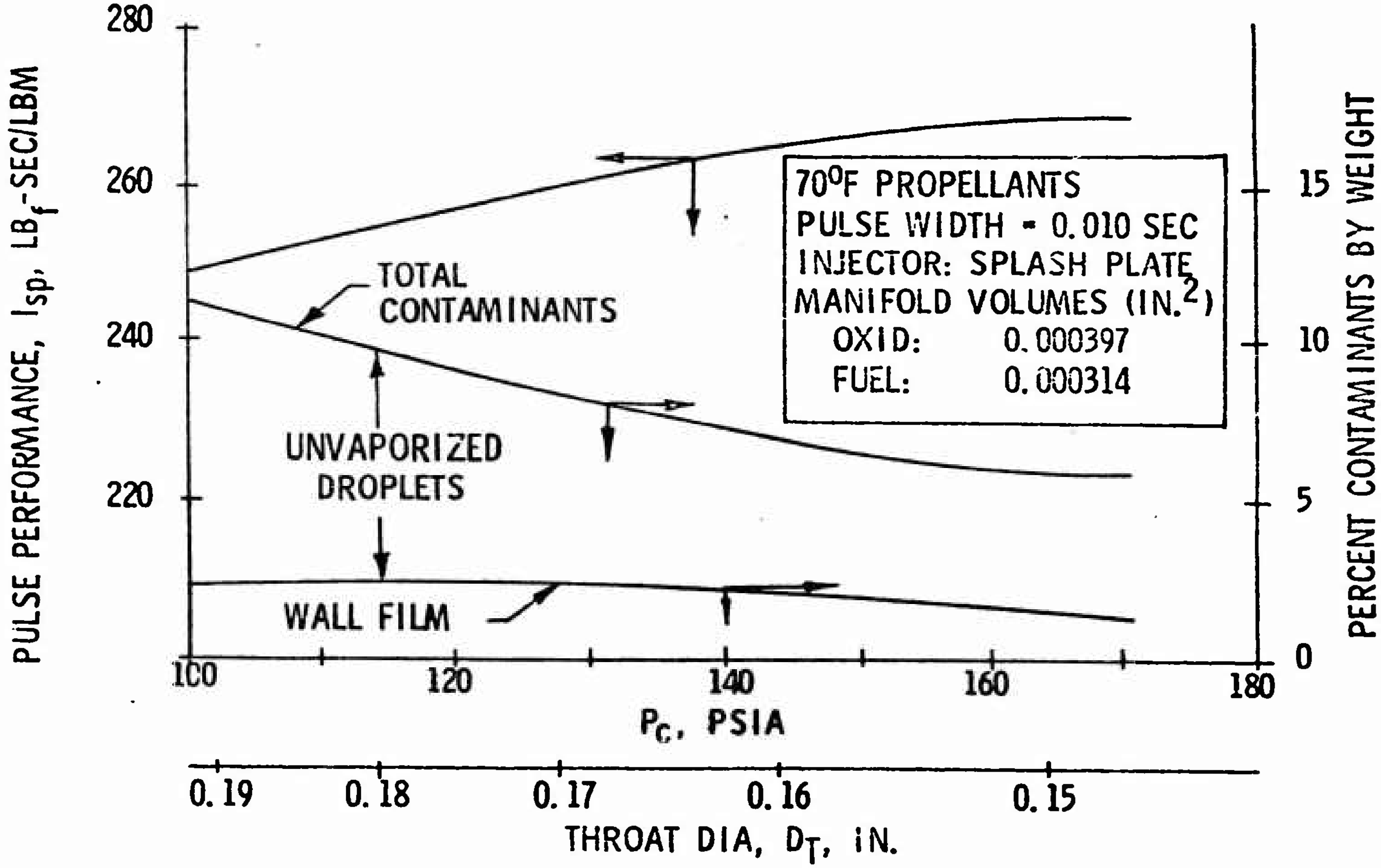

Figure 4.2.4. Nozzle Throat Diameter and Chamber Pressure Effect Upon Pulse Performance and contamination

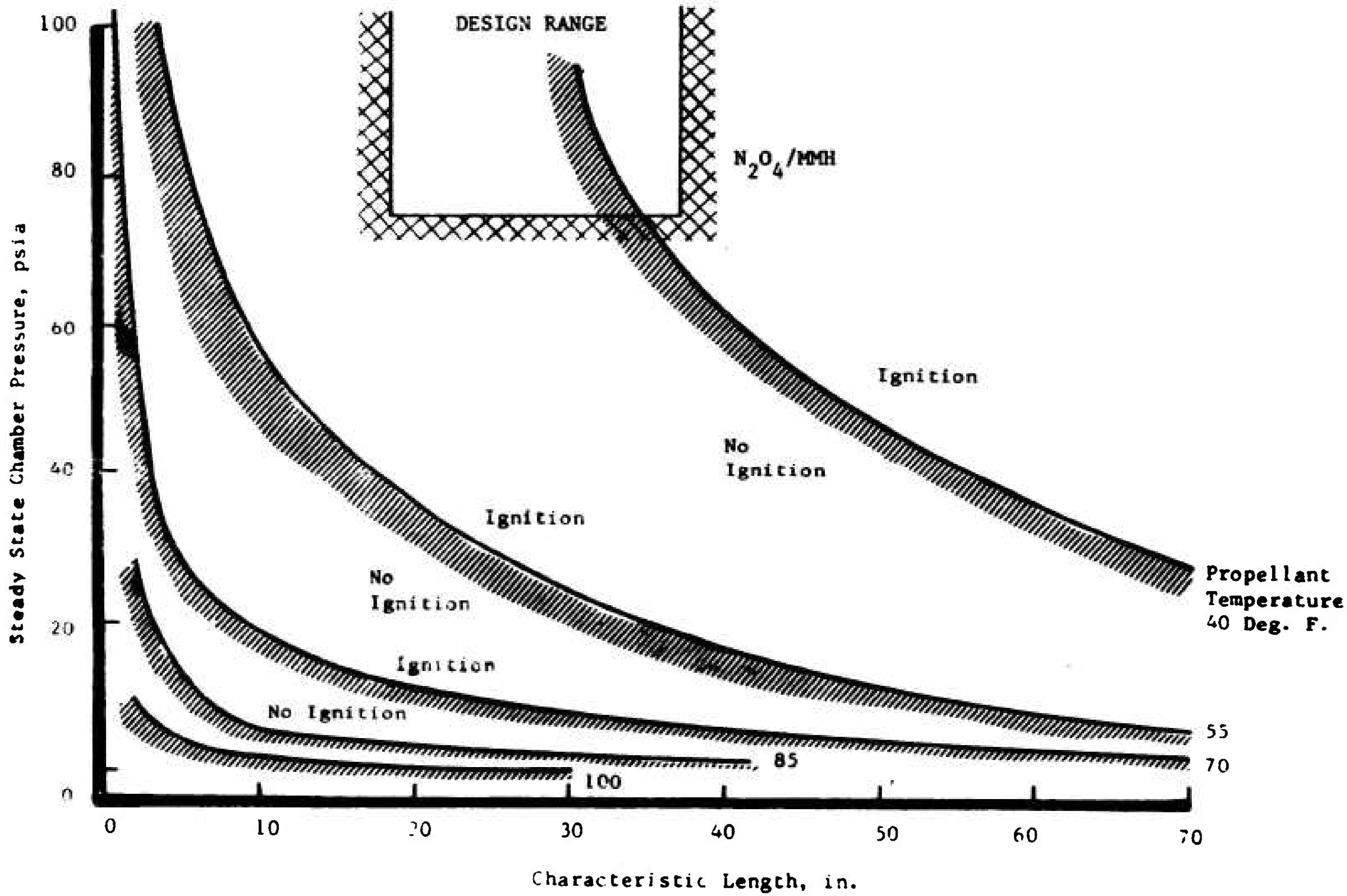

Figure 4.2-5. Ignition Limits at Various Propellant Temperatures

than the minimum length design provides a 2 sec improvement in specific impulse while the Rao contour adds 6 sec over a 20° half angle conical nozzle design.

Figure 4.2-4, prepared from the CONTAM model output assuming a cold chamber wall, shows the advantage of higher chamber pressures for a 0.05 lbF sec impulse. These trends were later verified in Phase II testing although the data showed the model to overstate the performance.

Figure 4.2-5 provided a prediction of the conditions which could result in a failure of the hypergolic propellants to ignite although no such condition was encountered in testing (even down to 20°F). The analyses suggested that the condition could be avoided by employing higher steady state combustion chamber pressures.

Subsequent analysis examined the steady state wall temperature of a radiation cooled chamber as the chamber pressure was varied. These showed (Figure 4.2-6) that gas side wall temperature was only slightly influenced when P_c was increased by reducing the throat diameter and maintaining a fixed chamber OD of 0.62 in. Figure 4.2-7 illustrates the enhancement to radiation cooling as wall thickness at the throat is increased. Figure 4.2-6 includes data from actual fire tests during Phase II (reference Section 5.3). This indicated that the forecasted chamber wall temperatures were slightly low. The analytically forecasted transient and steady state axial temperature gradient at a chamber pressure of 175 psia are shown in Figure 4.2-8. Comparison is made with Phase III test data. Low front end temperatures were forecasted to result from a portion of the unvaporized fuel depositing on the wall. The conceptual design envisioned a free standing internal liner as a means of cooling the front end if the film could not be sustained due to the high rate of axial conduction. The Phase II test data identified a need for such a liner.

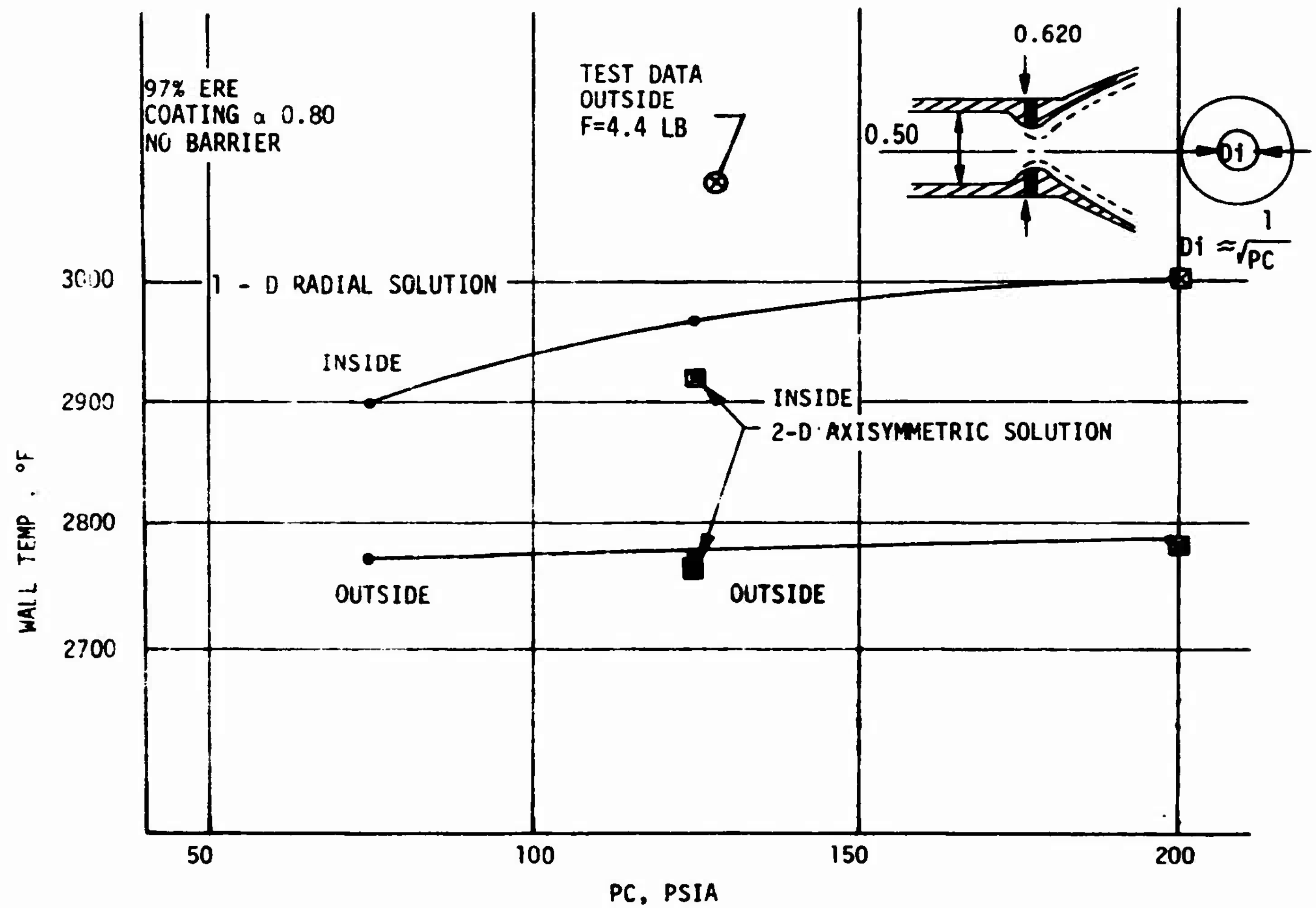

Figure 4.2.6. Maximum Radiation Cooled Nozzle Temperature

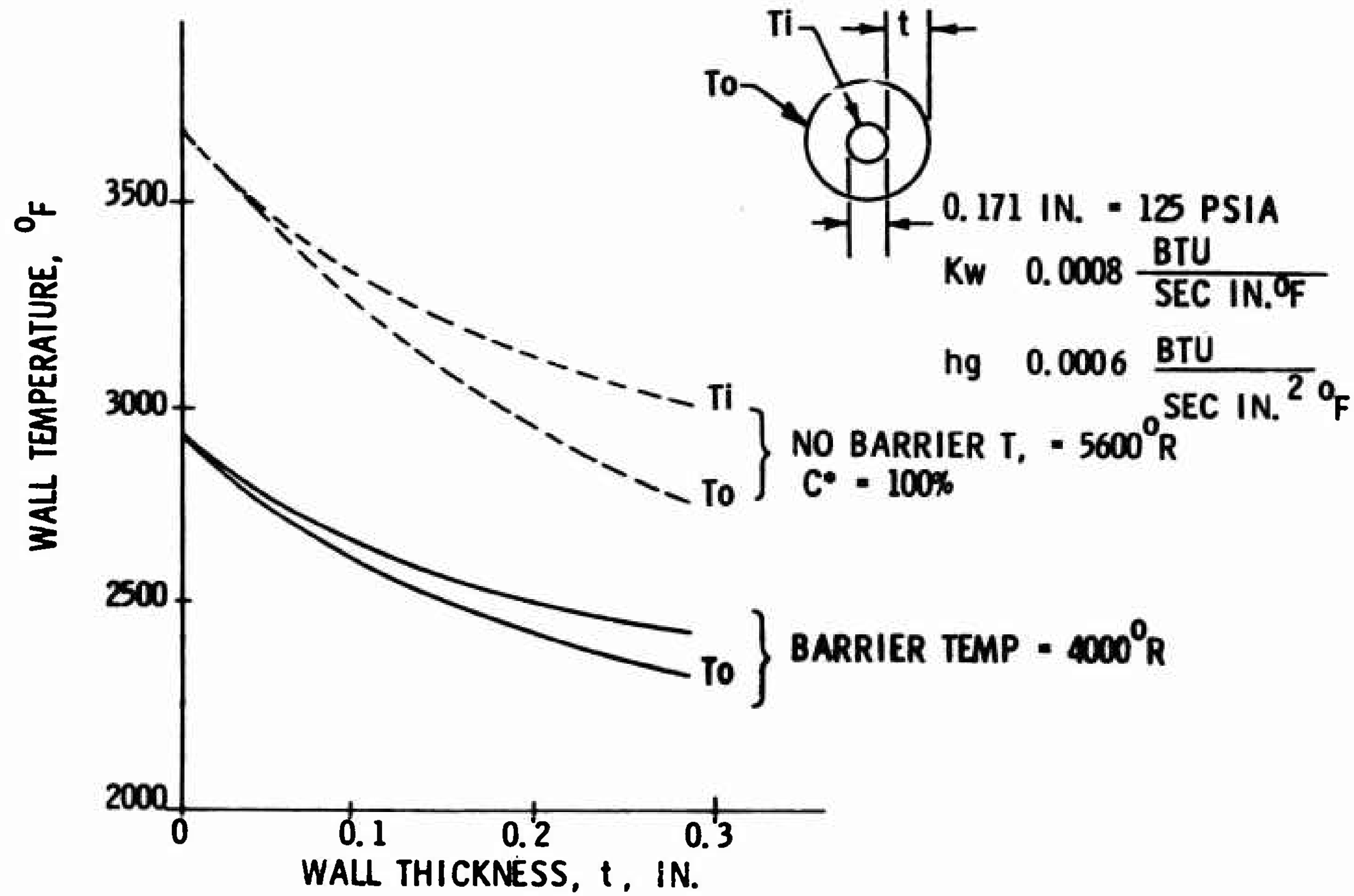

Figure 4.2.7. Nozzle Throat Temperature in Radiation Cooling

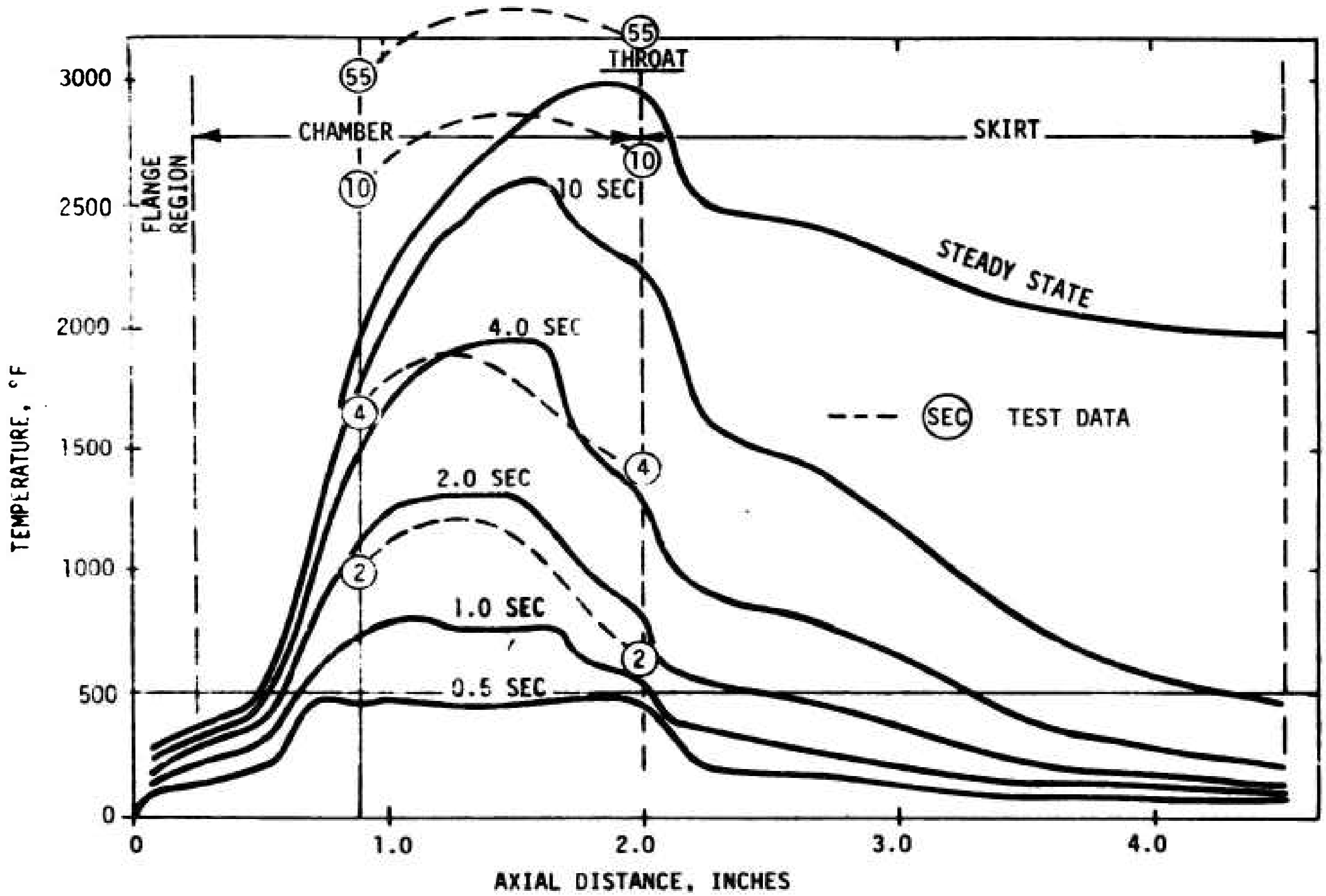

Figure 4.2.8. Transient and Steady State Nozzle Temperature Profiles

Examination of candidate chamber materials resulted in the identification of columbium as the most suitable material with FS-85 because of its high temperature creep properties. Candidate alloys and their properties are shown in Figures 4.2-9 through 4.2-11. Oxidation resistant coatings were examined and the silicide coatings judged to be adequate for the engine duty cycle provided that the wall temperature was held below about 2800°F. Figure 4.2-12 presents temperature versus estimated time to failure for silicide coatings as well as the Phase 3 test results. All engines tested utilized either VacHyd 1o1 or Hitemco R-512E coatings.

The thrust chamber data indicated that barrier cooling was necessary to insure that the chamber temperature did not exceed 2800°F. The performance margin of the multi-element injector (Reference Figure 4.2-1) in combination with its ability to provide barrier cooling was expected to allow the necessary chamber temperature to be achieved. This is shown in Figure 4.2-13 which illustrates the predicted effect of 25% barrier cooling on the wall temperatures of radiation cooled and adiabatic wall thrust chambers. This figure shows that a buried chamber which meets the 300 sec steady state performance goal will have a gas side wall temperature of 2800°F. The same injector operated in a radiation cooled chamber would provide a 2200°F gas side temperature. It was concluded that if optimum performance was desired, different injectors were needed in radiation cooled and adiabatic wall engines. The predictions shown in Figure 4.2-13 were proven qualitatively correct by subsequent testing. The attainment of the requisite barrier cooling proved to be more difficult than the analytic studies indicated. This was due to the fact that the very low propellant flow rates did not allow a separate barrier coolant manifold and distinct orifices. Barrier cooling was achieved by tailoring each element of the multi-element injector to have a defined and repeatable mixture ratio distribution to produce a low MR zone at the chamber wall.

4.2.3 Valves and Flow Control

Eight different valve manufacturers were consulted to determine the development status and availability of valves which could be

COMPOSITION	WC 103	SCb 291	FS 85	WC 129Y
Cb	Bal	Bal	Bal	Bal
Hf	10	-	-	9-11
Tl	1	-	-	-
Zr	0.7	-	0.9	0.5
Ta	0.5	9-11	28	0.5
W	0.5	9-11	10.5	9-11
Yt	-	-	-	0.05-0.3
Weldability	Yes	Yes	Yes	Yes
% Elong. Room Temp.	25-30	25	25	25
UTS 2700 °F	9500	14,000	15,000	17,300

Figure 4.2.9. Candidate Columbium Alloys

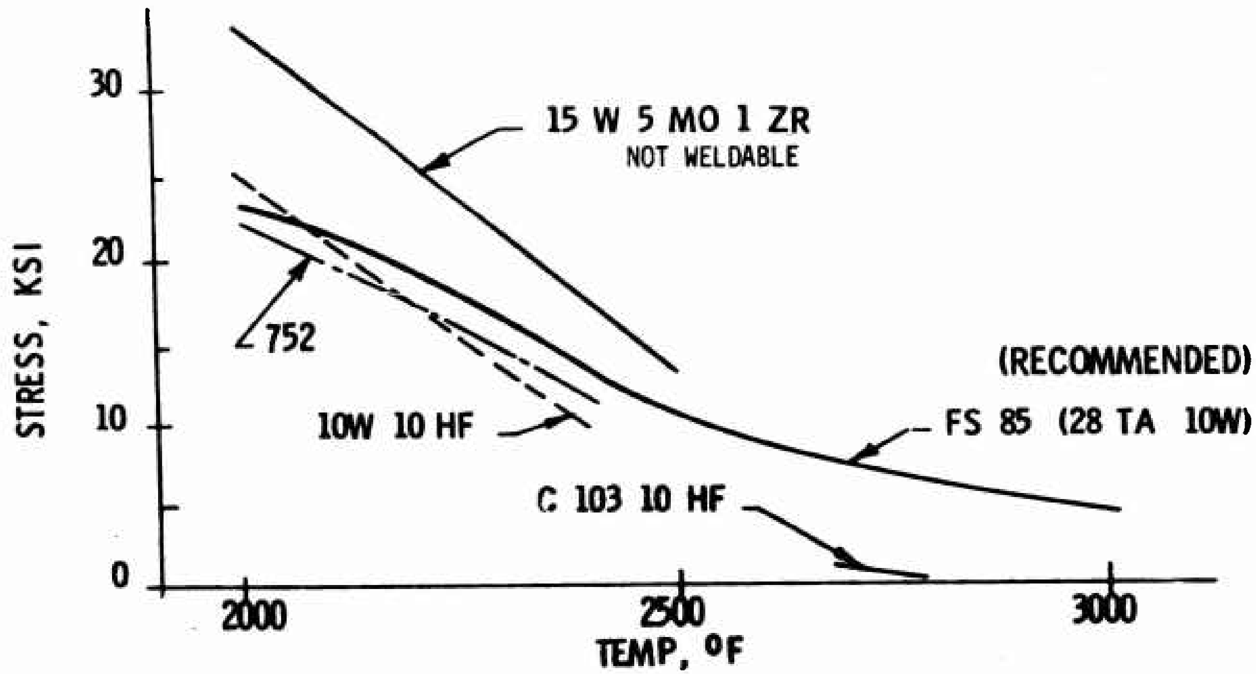

Figure 4.2.10. Ten Hour Creep Rupture Stress for Columbium Alloys

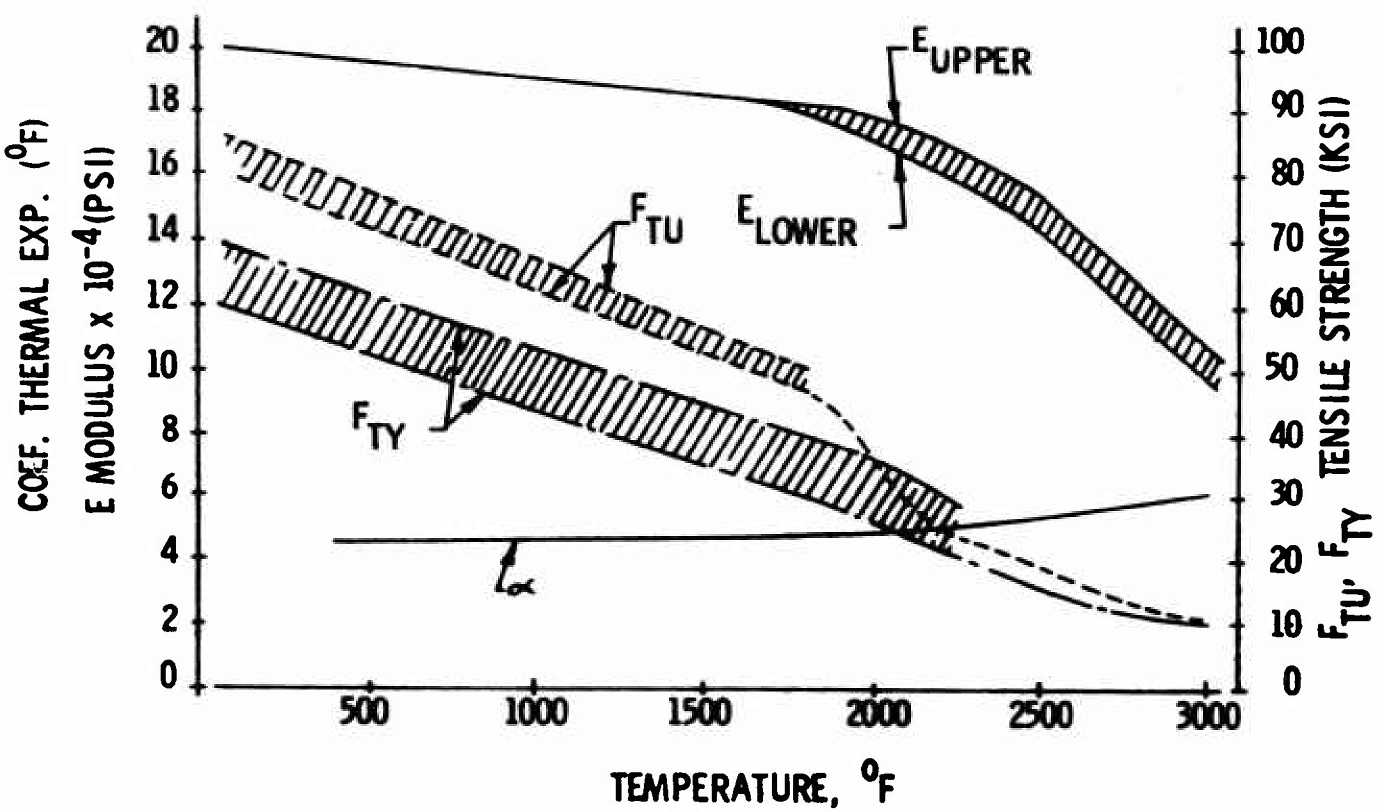

Figure 4.2-11. Material Properties of FS85 Columbium

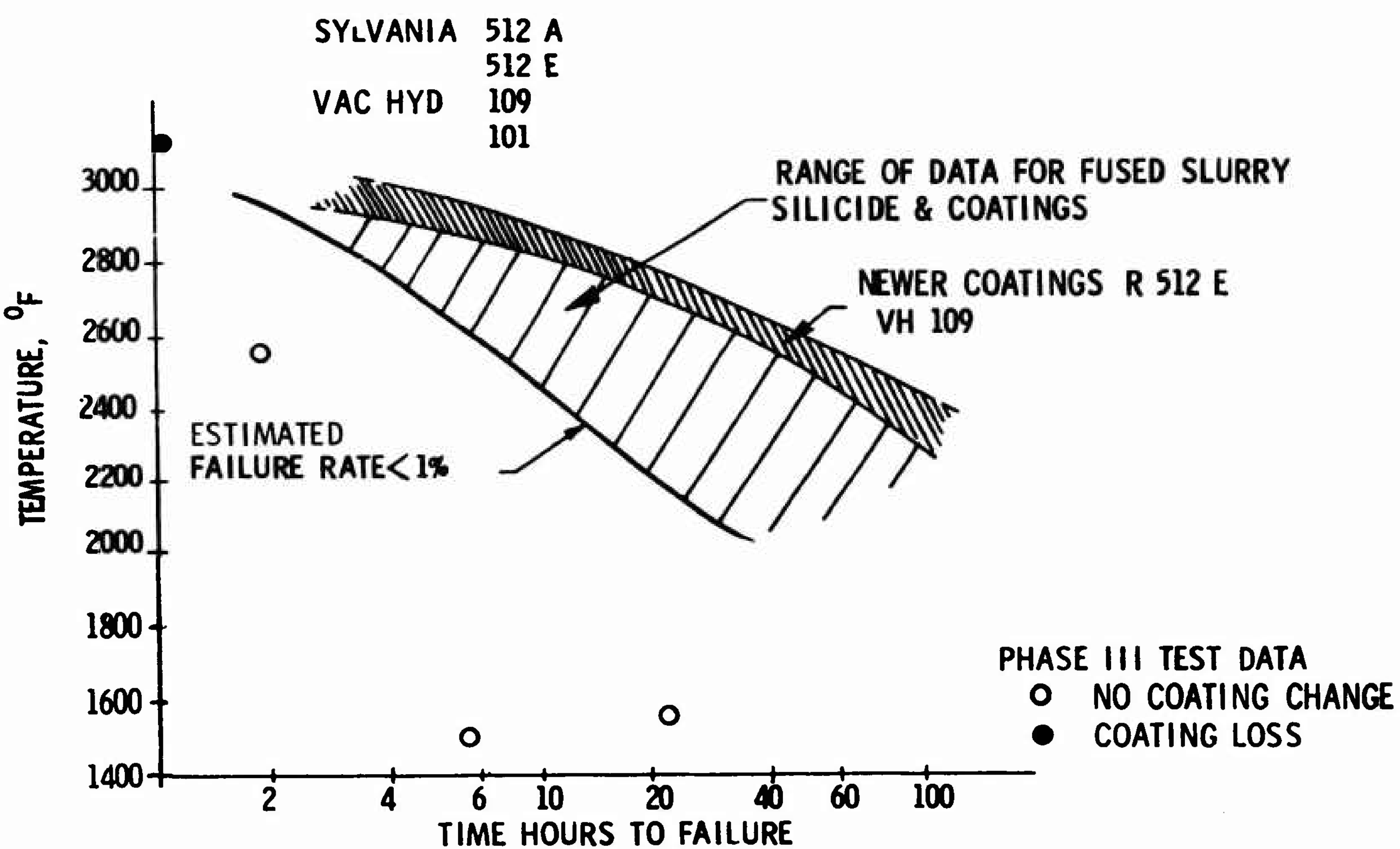

Figure 4.2-12. Protective Coatings Life Versus Steady State Temperature

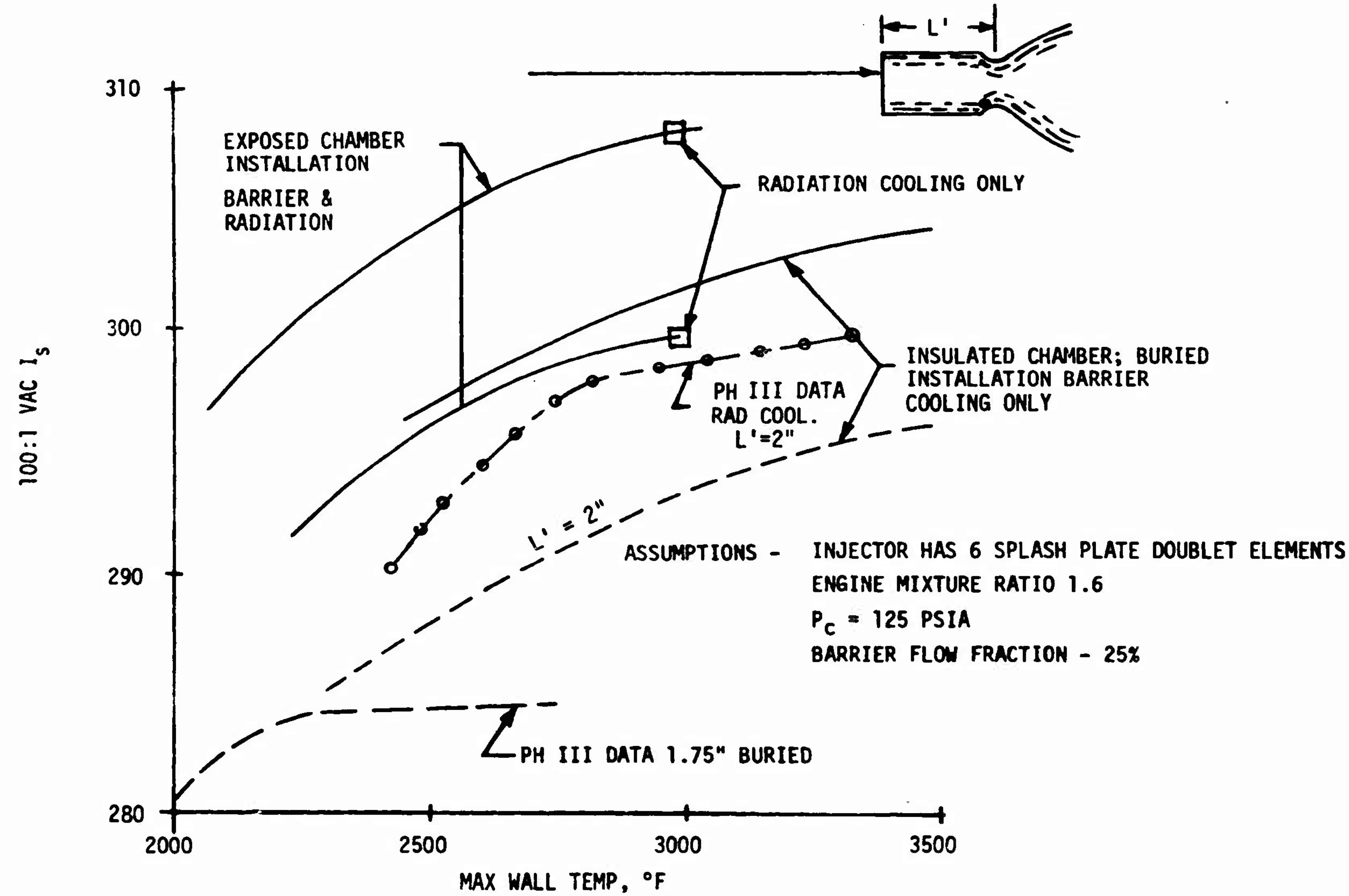

Figure 4.2-13. Nozzle Length Wall Temperature and Performance

4.2.3, Valves and Flow Control (cont.)

best utilized to minimize development costs and risks of an improved 5 lb bipropellant engine. Manufacturers whose product appeared applicable included Hydraulic Research, Marquardt, Moog, Parker Aircraft and Wright Components. Available products included individual monopropellant and linked bipropellant which could be either solenoid (s) or torque motor (TM) actuated. The results of this survey are summarized below:

Manufacturers	Response	Drive and Type	Seat	Weight, lb	Development Status
Hydraulic Research	0.015	S-Mono	Hard	0.47	Flight qual
Marquardt	0.007	S-Mono	Hard	0.31	Flight qual
Moog	<0.005	TM Biprop	Soft	1.0	Flight qual
	0.005	TM S-Mono	Soft	0.4	Unknown
Parker Aircraft	0.005	S-Mono		0.4	Unknown
Wright Components	Detailed data unavailable				

All valves are of the spring loaded normally closed type.

Data generated from this survey indicated that the torque motor drive could provide faster response with lower current drain in trade for some added weight. Other Phase I studies suggested that syncronization of the fuel and oxidizer port opening and closing must be within $\approx$ 0.0002 sec if ignition characteristics and 0.050 lbF-sec impulse bits are to be repeatable over the 10 year life of the engine. The linked bipropellant valve although somewhat less flexible in selecting a specific lead-lag relationship, was considered to be much more repeatable: i.e., not subject to timing drifts due to aging, voltage changes, propellant tank pressure and temperature differentials.

Comparison of hard and soft seats showed valves of both types having been cycled in excess of 10^6 times. Hard seat valves showed a greater sensitivity to contamination induced leakage while less was known about the very long term storability of available soft seat materials in a propellant-vacuum environment.

4.2.3, Valves and Flow Control (cont.)

Preliminary designs were based on the use of a linked-bipropellant torque motor drive valve because of the insured sequencing, faster response and lower current drain. The flight qualified Minuteman III type valve, manufactured by Moog, Inc., appeared to be at the highest state of development, was a production item, had an impressive test history and was thus selected for base line conceptual evaluation. Additional valve analyses are provided in Phase II, Section 5.0.

4.2.4 CONTAM Analysis

CONTAM is a comprehensive computer model of rocket engine operation which has been developed on AFRPL Contracts F04611-70-C-0076 and F04611-72-C-0037. This model is designed to forecast analytically the behavior of the exhaust plume of a bipropellant engine. The subprogram of special interest to the 5 lbf thrust bipropellant engine is the Transient Combustion Chamber Dynamics (TCC) portion which analyzes transient engine operation. The remaining subprograms include MULTRAN, KINCON, and SURFACE which are primarily concerned with deposition of engine contaminants (liquid or solid exhaust particles) upon spacecraft surfaces.

The TCC analysis showed that the least plume contamination would be achieved with the highest performing injector with the smallest propellant manifolds. It also indicated that the wall film produced contaminaants are virtually nonexistent after 300 milliseconds of operation. Axial stream contaminant production due to non-vaporized droplets is not affected by operation duration; it is, however, inversely proportional to chamber length.

The effect of chamber pressure, tank pressure, propellant temperature and pulse duration on engine pulsing characteristics were evaluated as the following design parameters were varied: chamber length and diameter, throat diameter, manifold volumes, injector face and chamber wall temperatures and line lengths. The effect of blowdown pressurization and the use of cavitating venturis was also examined. These effects are shown in Figures 4.2-14 through 4.2-24. They can be summarized as follows:

. Start transient duration is directly proportional to injector manifold volume (Reference Figure 4.2-14).

. Simultaneous oxidizer/fuel fill is desirable. A single propellant lead causes propellant accumulation in the chamber resulting in ignition delay, a performance penalty due to the non-combusted propellant and a higher contamination rate.

. Oxidizer flashing occurs in the injector manifold on vacuum starts due to the high N_2O_4 vapor pressure. This is aggrevated at elevated N_2O_4 temperatures.

. Feed line venturis aid steady state MR control but aggrevate oxidizer flashing and delay oxidizer manifold fill.

. Pulse duration has a first order effect upon both performance and wall film contamination for firing durations of less than 300 millisec (1.5 lb-sec impulse). Beyond 300 ms, the engine operates in a steady state fashion.

. The anticipated injector manifold volumes (0.0003 in.^{3} each) resulted in a predicted 260 sec specific impulse for a single cold start 0.050 lb sec impulse bit.

4.3 SYSTEM-MISSION-ENGINE INTERACTIONS

The previously described studies identified the desired engine parameters which result from the requirements of various missions. The operating ranges of various engine designs resulting from the selection of

	W/O VENTURI'S	WITH VENTURI'S
FUEL FILL:	1.4 MSEC.	1.9 MSEC.
OXID FILL:	1.5 MSEC.	3.1 MSEC.
IGNITION:	1.6 MSEC.	2.2 MSEC
CONTAMINANTS:	4.1%	6.2%
ΔI_{sp}	REFERENCE	-6 SEC.

FEED SYSTEM DESIGN		
	FUEL	OXID
LINE DIA (IN.)	1/4	1/4
LINE LENGTH (IN.)	40	24
MAN.VOL.(IN³)	0.000314	0.000297

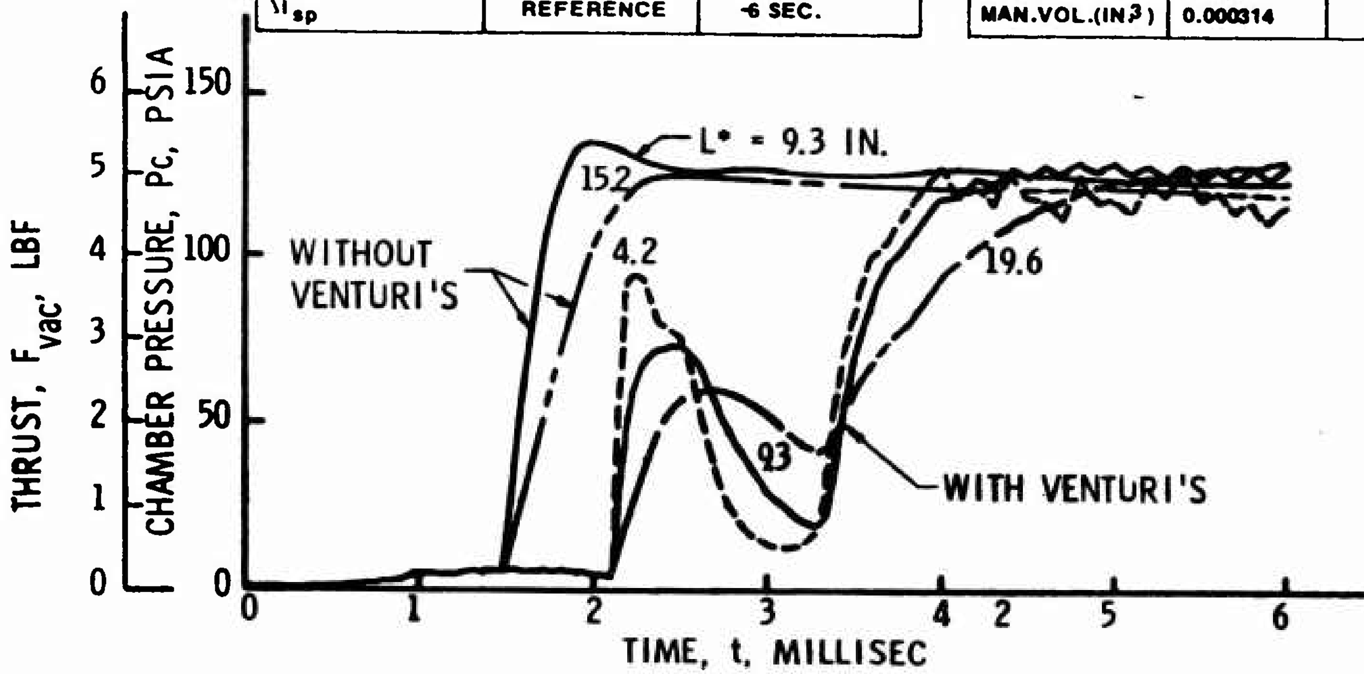

Figure 4.2-14. Effect of Chamber L* and Inlet Line Cavitating Venturis on Engine Start Transient

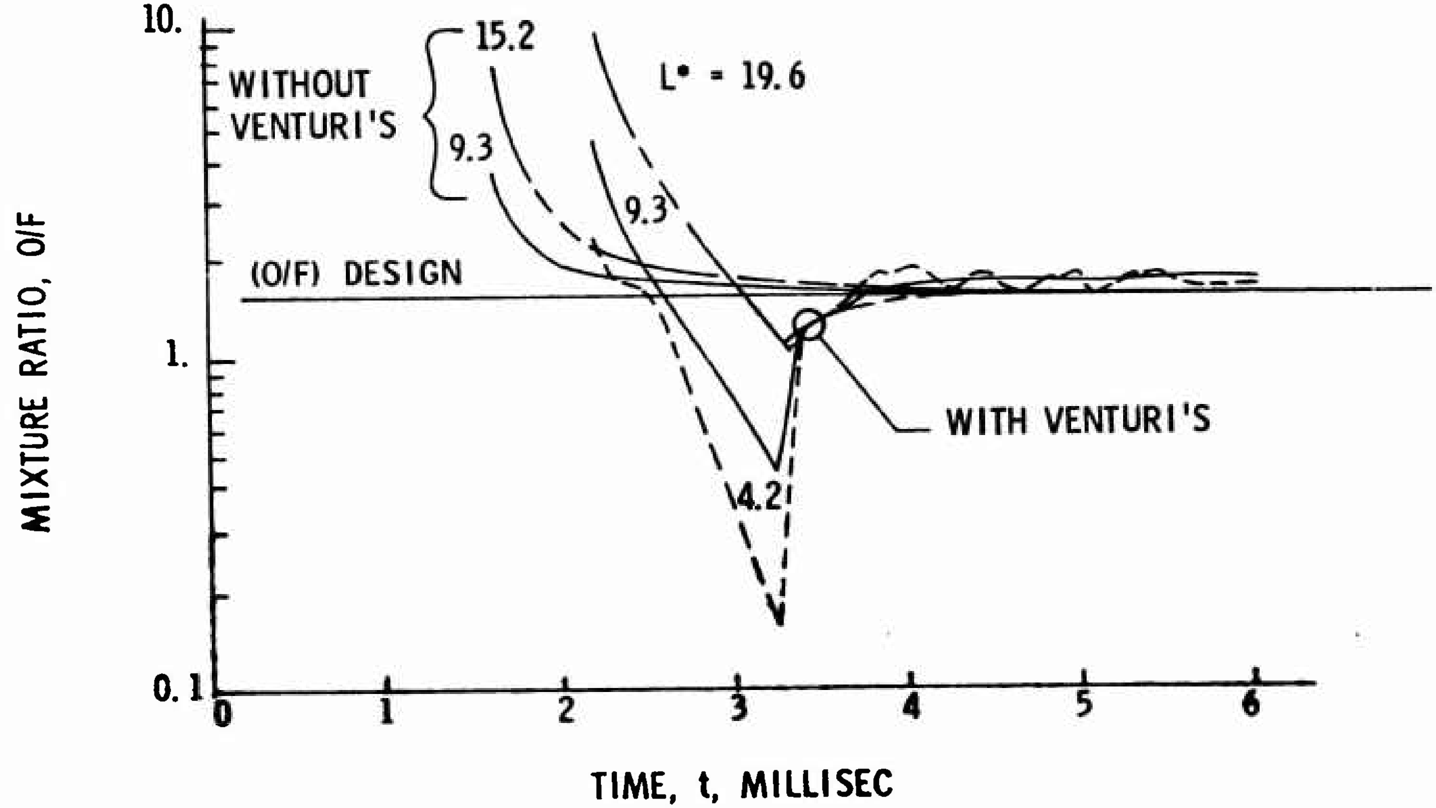

Figure 4.2-15. Effect of Chamber L* and Inlet Line Cavitating Venturis on Start Transient Mixture Ratio

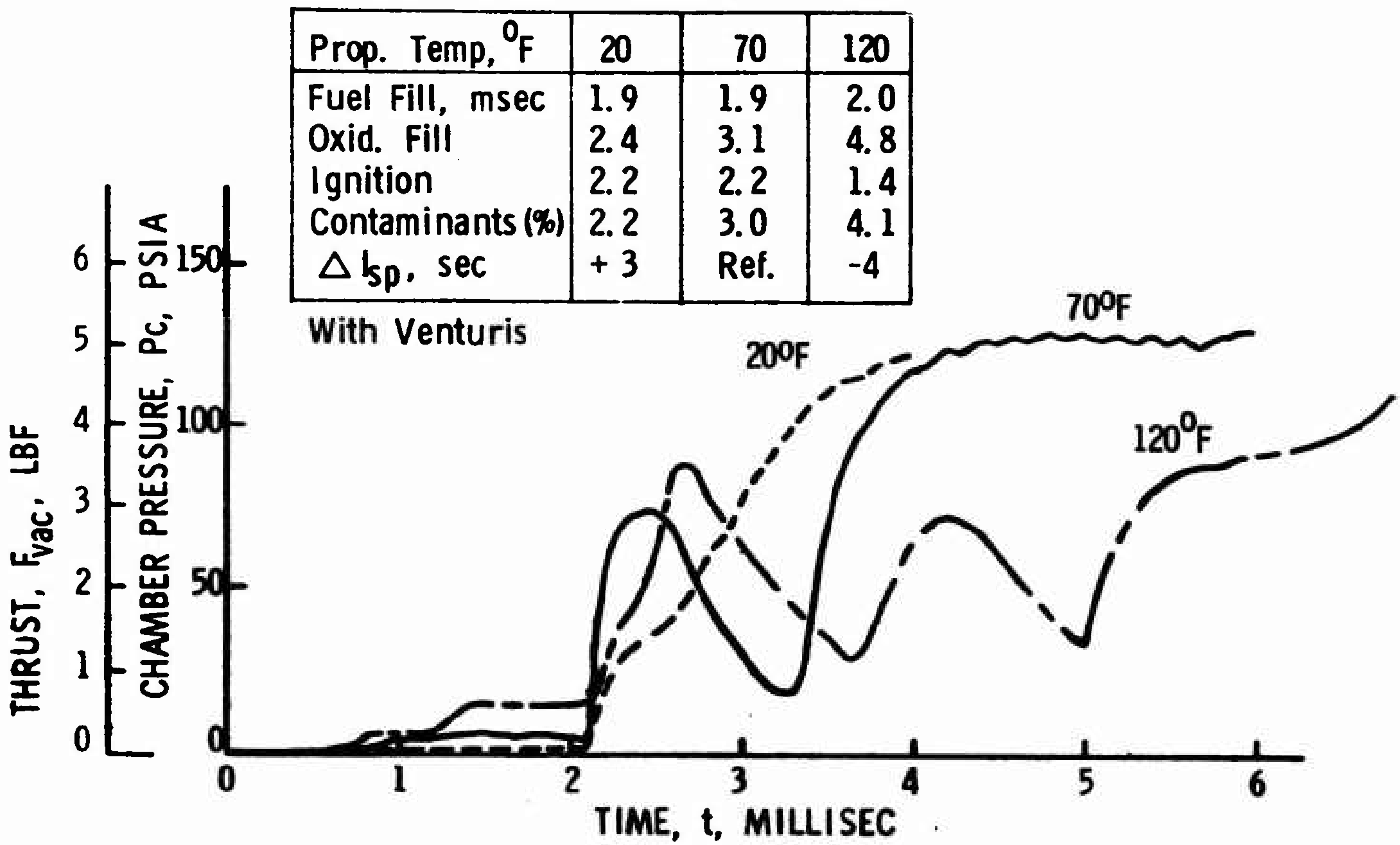

Prop. Temp, °F	20	70	120
Fuel Fill, msec	1.9	1.9	2.0
Oxid. Fill	2.4	3.1	4.8
Ignition	2.2	2.2	1.4
Contaminants (%)	2.2	3.0	4.1
ΔI_{sp}, sec	+ 3	Ref.	-4

Figure 4.2-16. Propellant Inlet Temperature Effect upon Injector Manifold Fill and Ignition Characteristics

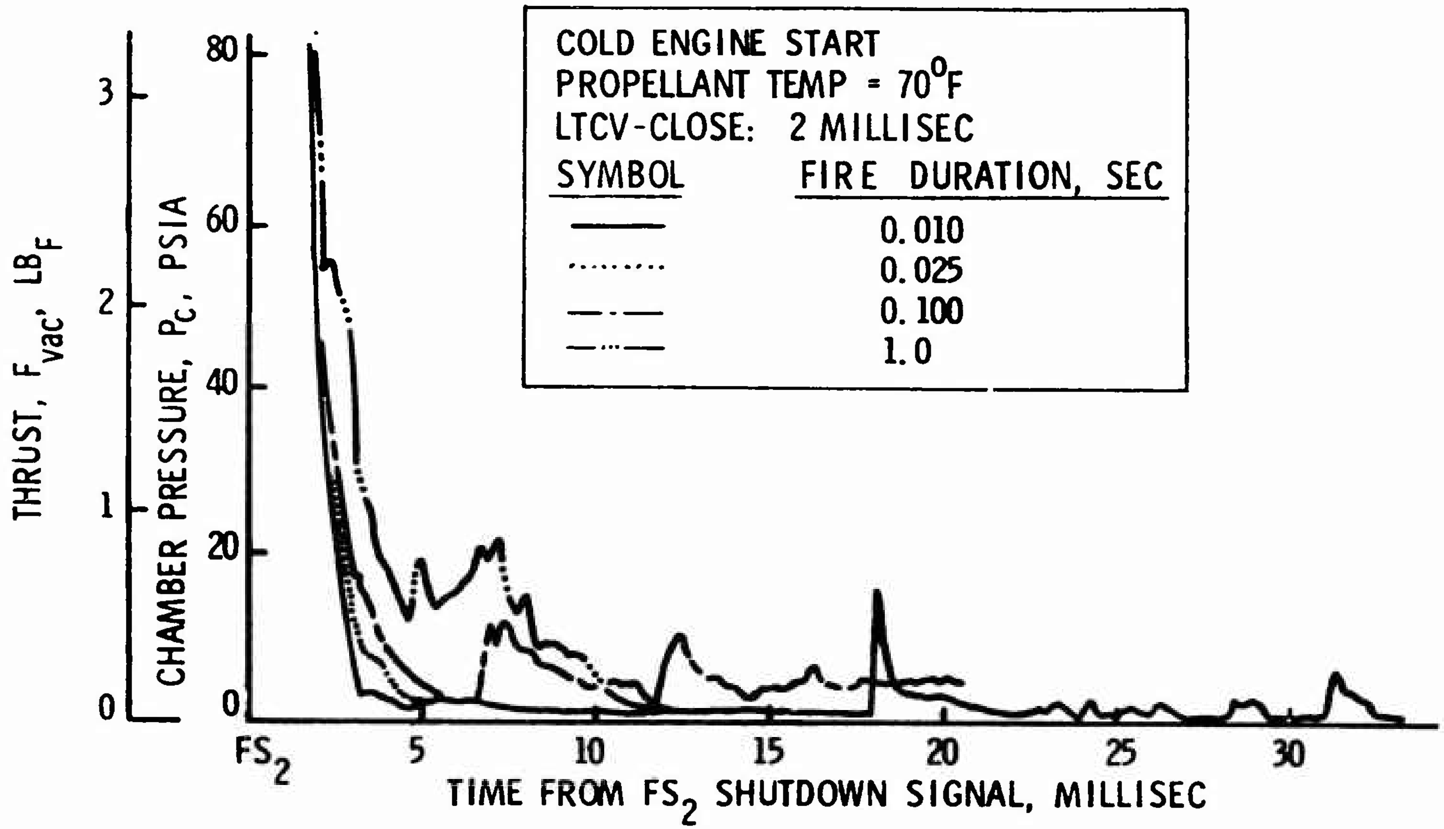

Figure 4.2-17. Firing Duration Effect upon Shutdown Impulse

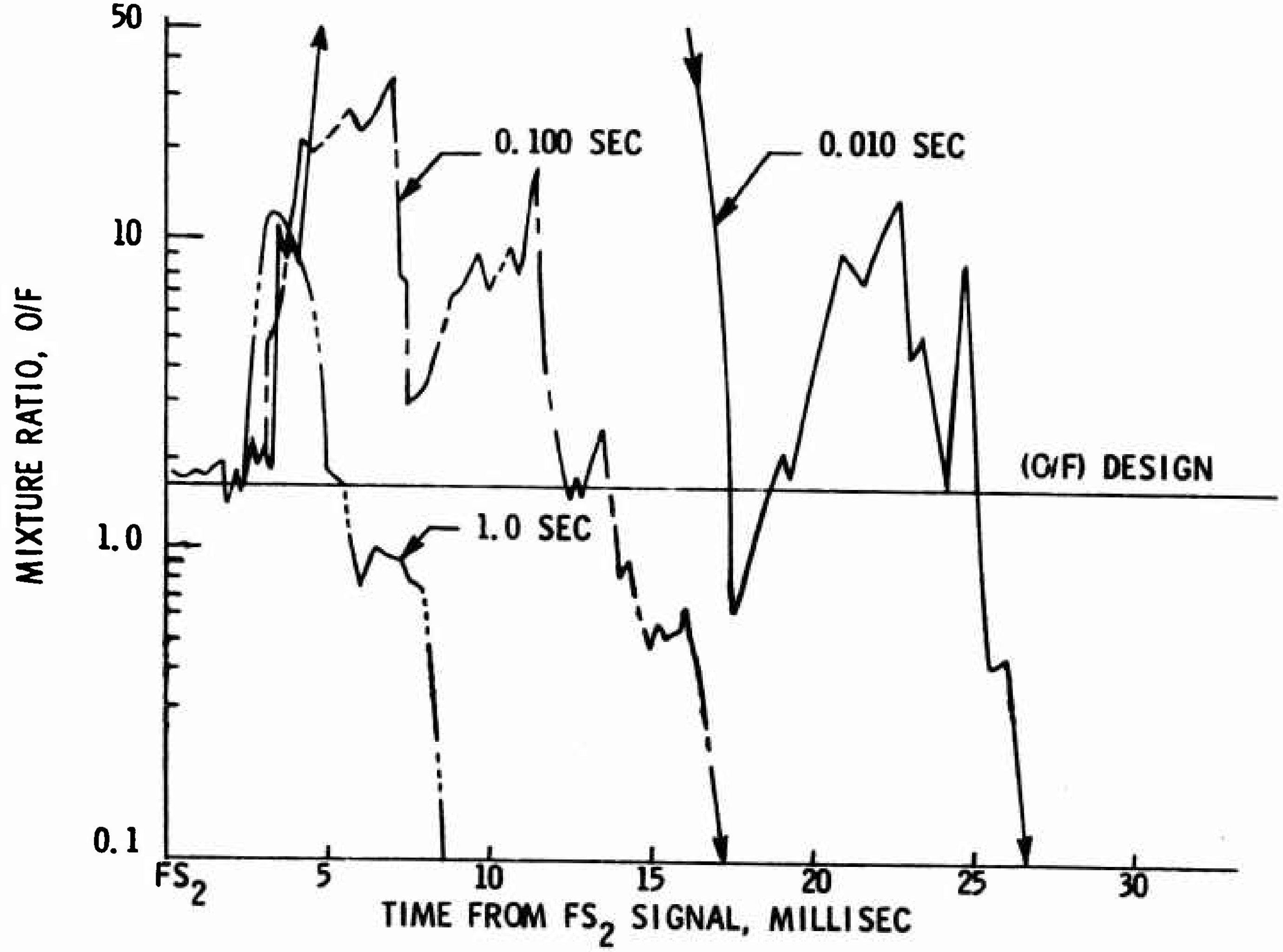

Figure 4.2-18. Effect of Pulse Duration on Shutdown Mixture Ratio

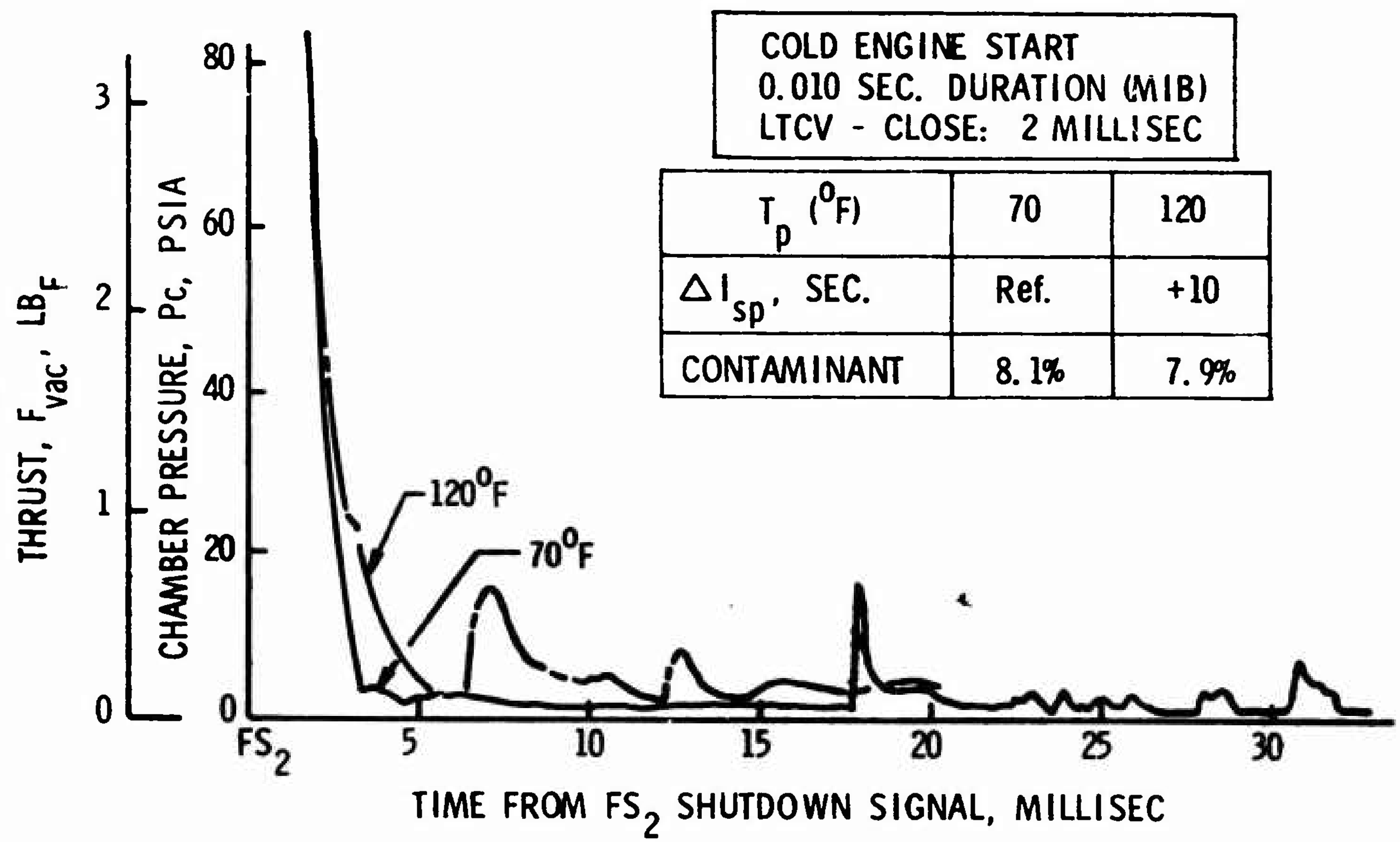

Figure 4.2-19. Propellant Inlet Temperature Effect on Shutdown Impulse

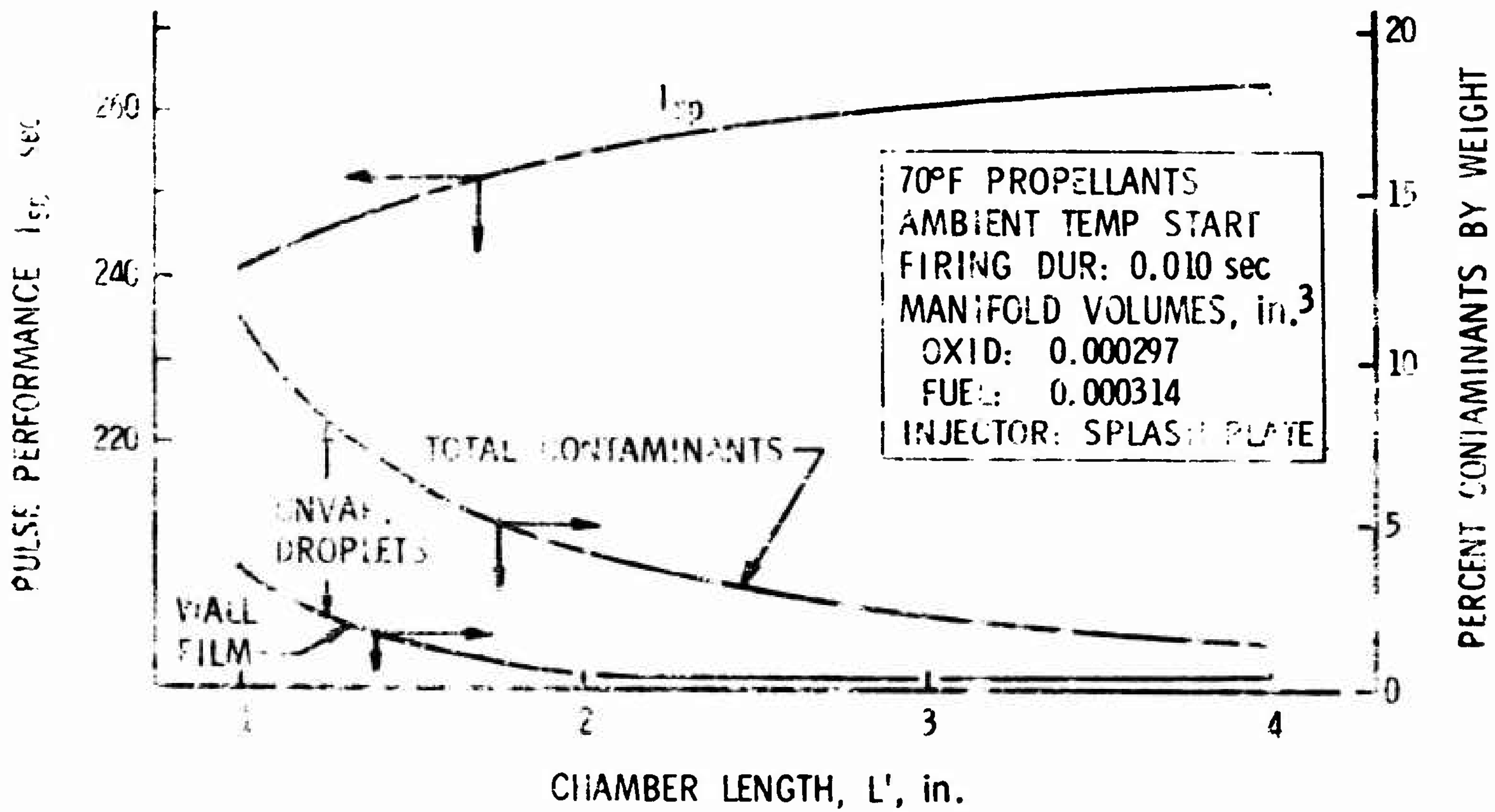

Figure [illegible] Effect of Chamber Length on Pulse Performance and Engine Contaminants

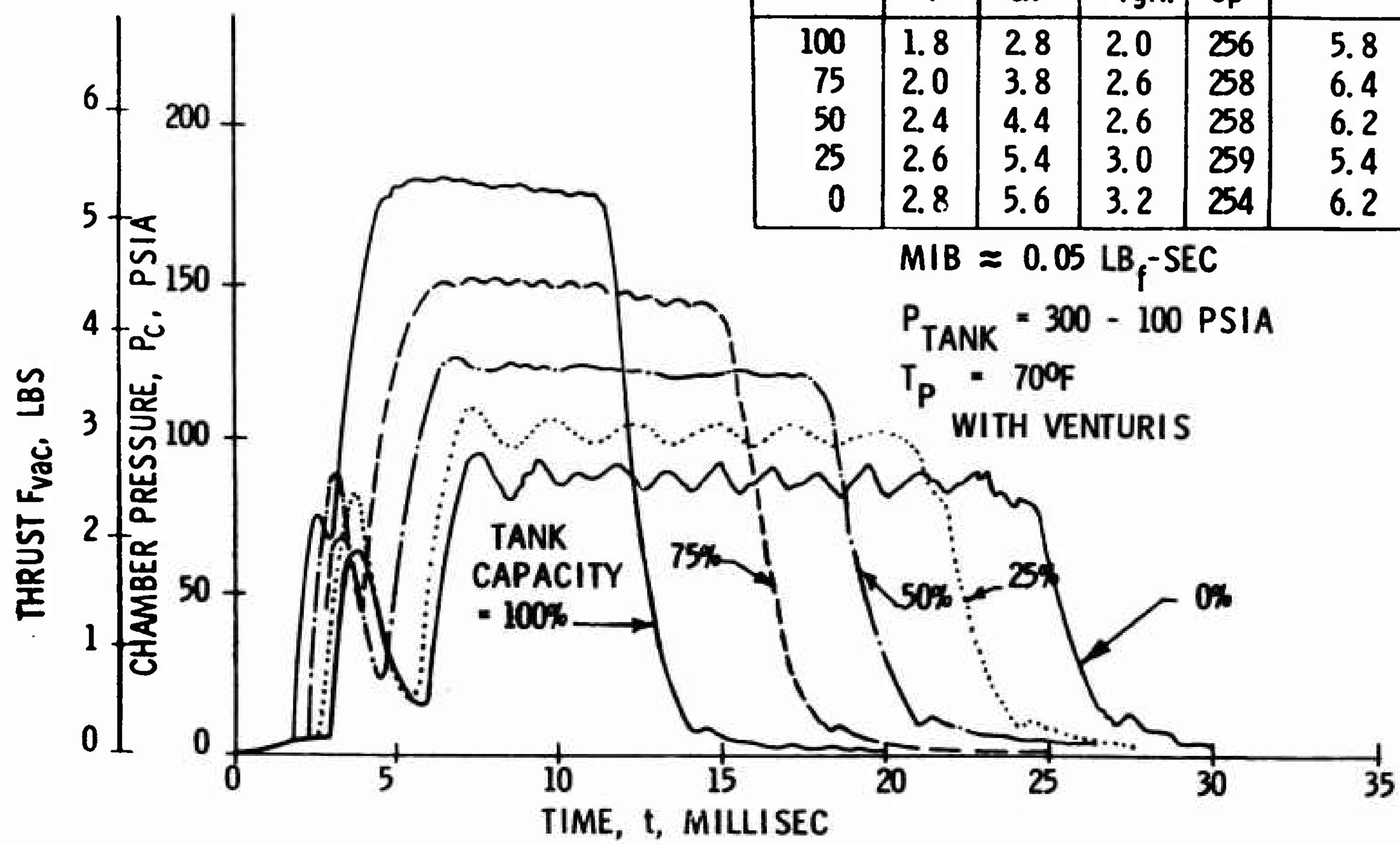

% Tank	τ_f	τ_{ox}	$\tau_{Ign.}$	I_{sp}	% Contam.
100	1.8	2.8	2.0	256	5.8
75	2.0	3.8	2.6	258	6.4
50	2.4	4.4	2.6	258	6.2
25	2.6	5.4	3.0	259	5.4
0	2.8	5.6	3.2	254	6.2

Figure 4.2-21. Tank Blowdown Operating Mode

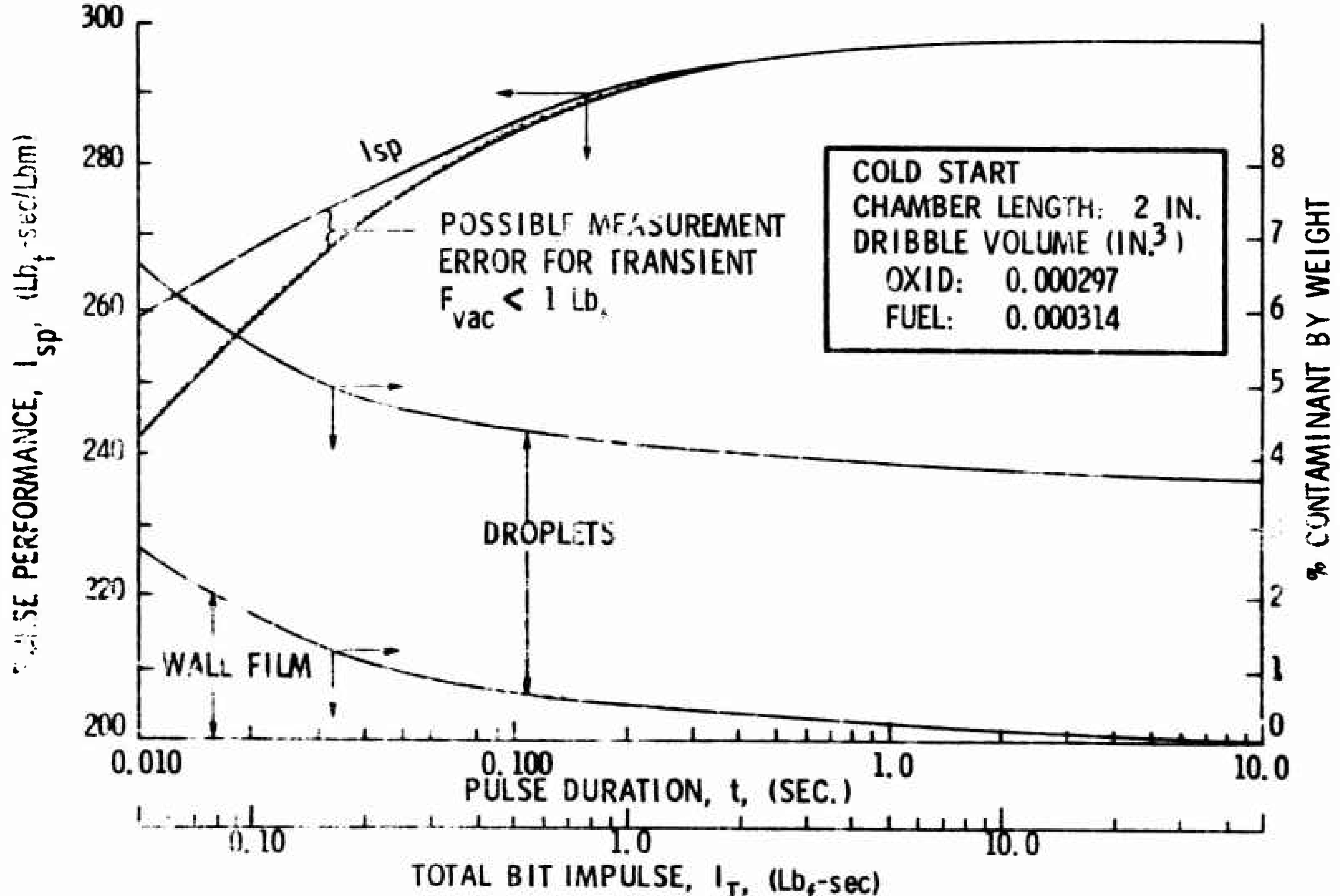

Figure 4.2-22. Firing Duration Effect on Pulse Performance and Engine Contaminants

START NO.	MANIFOLD VOLUME, IN.^{3}		EVENT TIME, MILLISEC			I_{sp}	CONTAMINANTS (%)	
	OXIDIZER	FUEL	OX. FILL	FUEL FILL	IGNITION	SEC	FILM	DROPS
1*	0.000297	0.000314	3.5	2.0	2.6	259	2.5	7.3
2	0.000297	0.000628	4.2	3.4	3.8	254	3.5	6.7
3	0.000594	0.000314	5.0	2.0	2.6	231	4.3	6.2
4	0.000594	0.000628	5.6	3.4	3.8	209	6.4	5.8

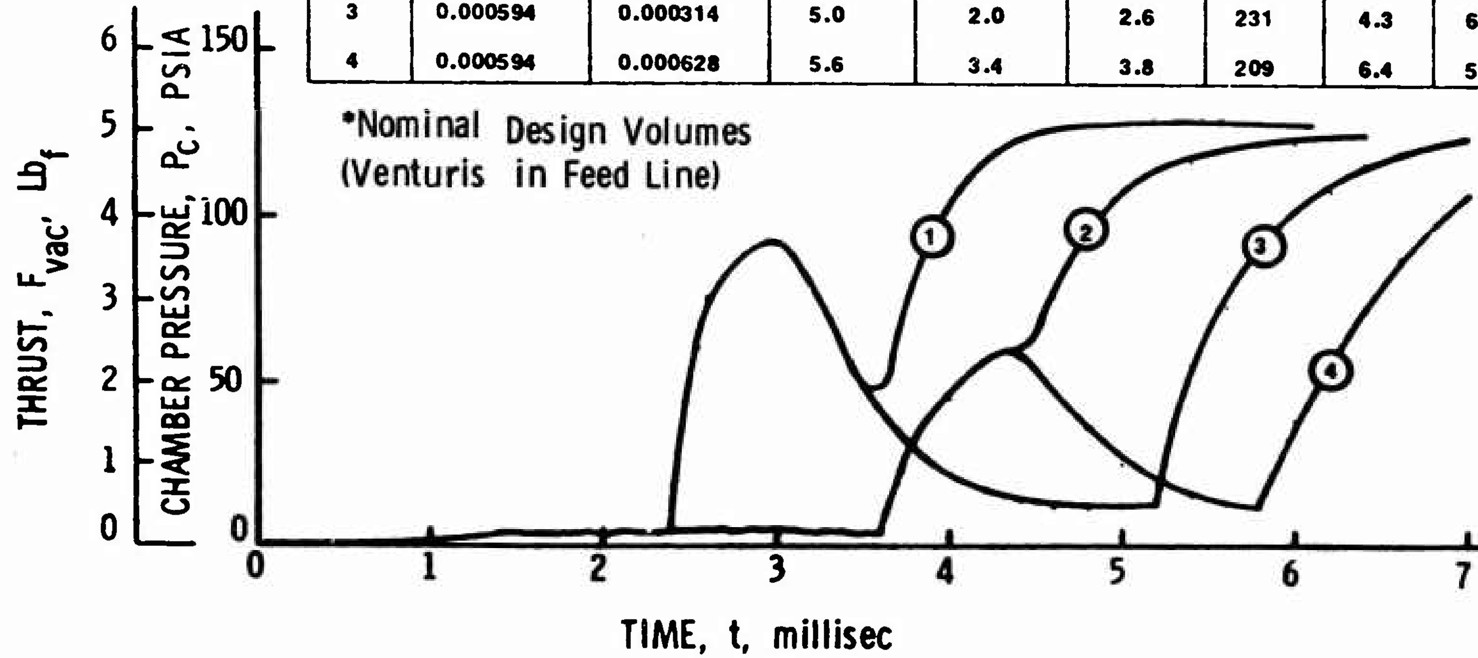

Figure 4.2-23. Injector Manifold Volume Effect on Start Transient

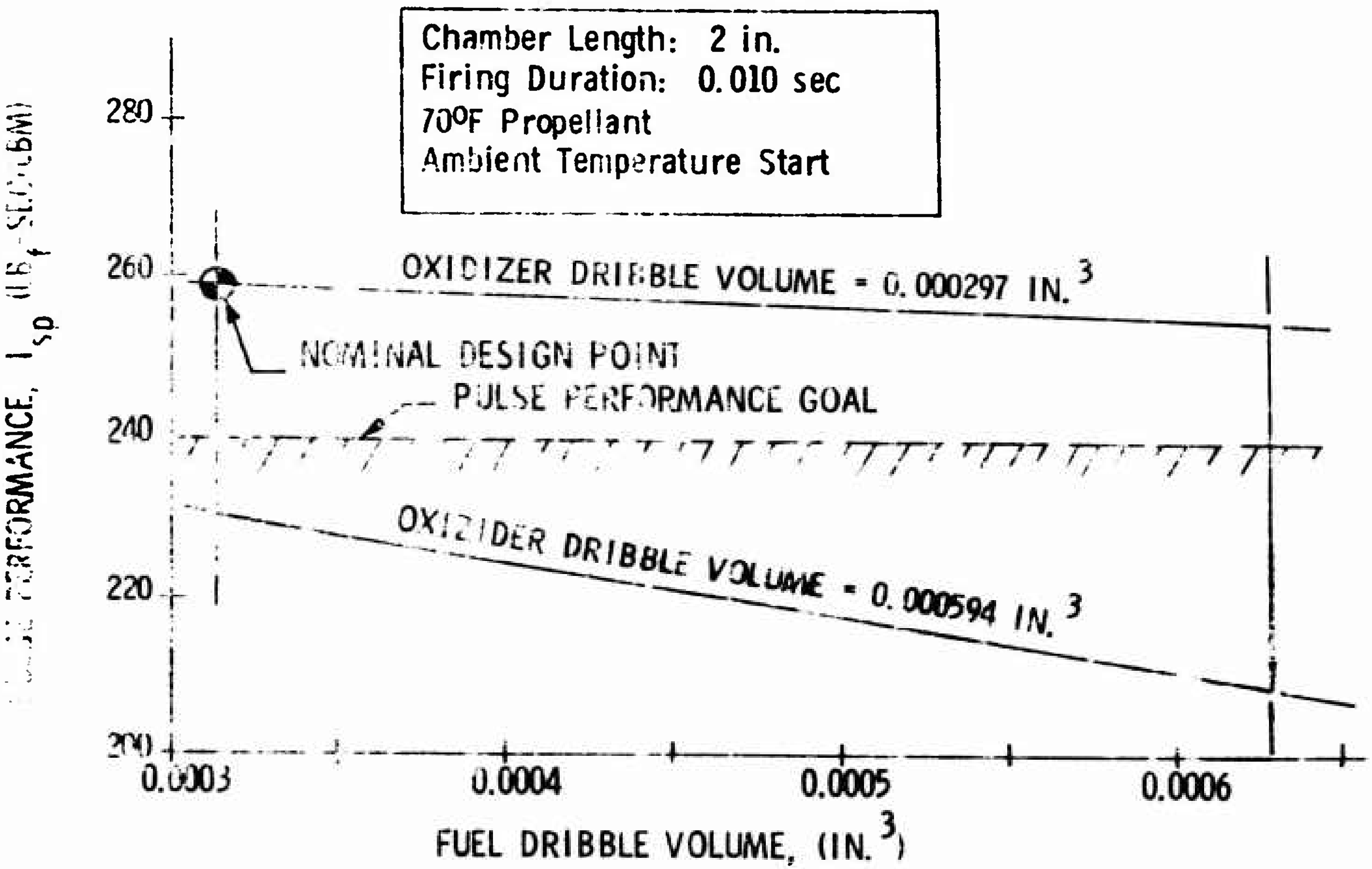

Figure 4.2-24. Pulse Performance Sensitivity to Manifold Dribble Volume

different engine component design configurations and capabilities were also described. The evaluation of the interaction of engine design, system design and mission requirements which is presented below was a logical progression from the earlier studies.

The most significant interaction was found to be in the area thermal design. This is due to the fact that propellant and tank temperatures can substantially influence the tank pressures of a non-regulated blowdown system. The feed pressure variation causes changes of engine P_c and MR which in turn affect thrust, wall temperature, transient operation and plume contaminate generation.

The following were examined to determine their affect on engine operation:

Propellant feed pressure and feed pressure variation
Propellant tank temperature and temperature variation
System and engine weight
Engine thermal environment
Engine envelope

4.3.1 Propellant and Engine Temperature Effects

Examination of the fuel and oxidizer vapor pressure results in the establishment of a temperature limit to insure the high oxidizer vapor pressure will not result in two-phase flow or vapor lock on engine startup. The injector-valve temperature limitations shown in Figure 4.3-1 indicate the minimum temperature to be dictated by the N_2O_4 freezing temperature (12°F). The maximum allowable temperature is that at which the oxidizer vaporizes; this is a function of operating pressure. Although an oxidizer vapor lock condition is non-damaging, it would result in increased plume contamination and/or duty cycle constraints. Hence, the engine-system design was approached with the intent of avoiding a vapor lock on start for any duty cycle. The heat

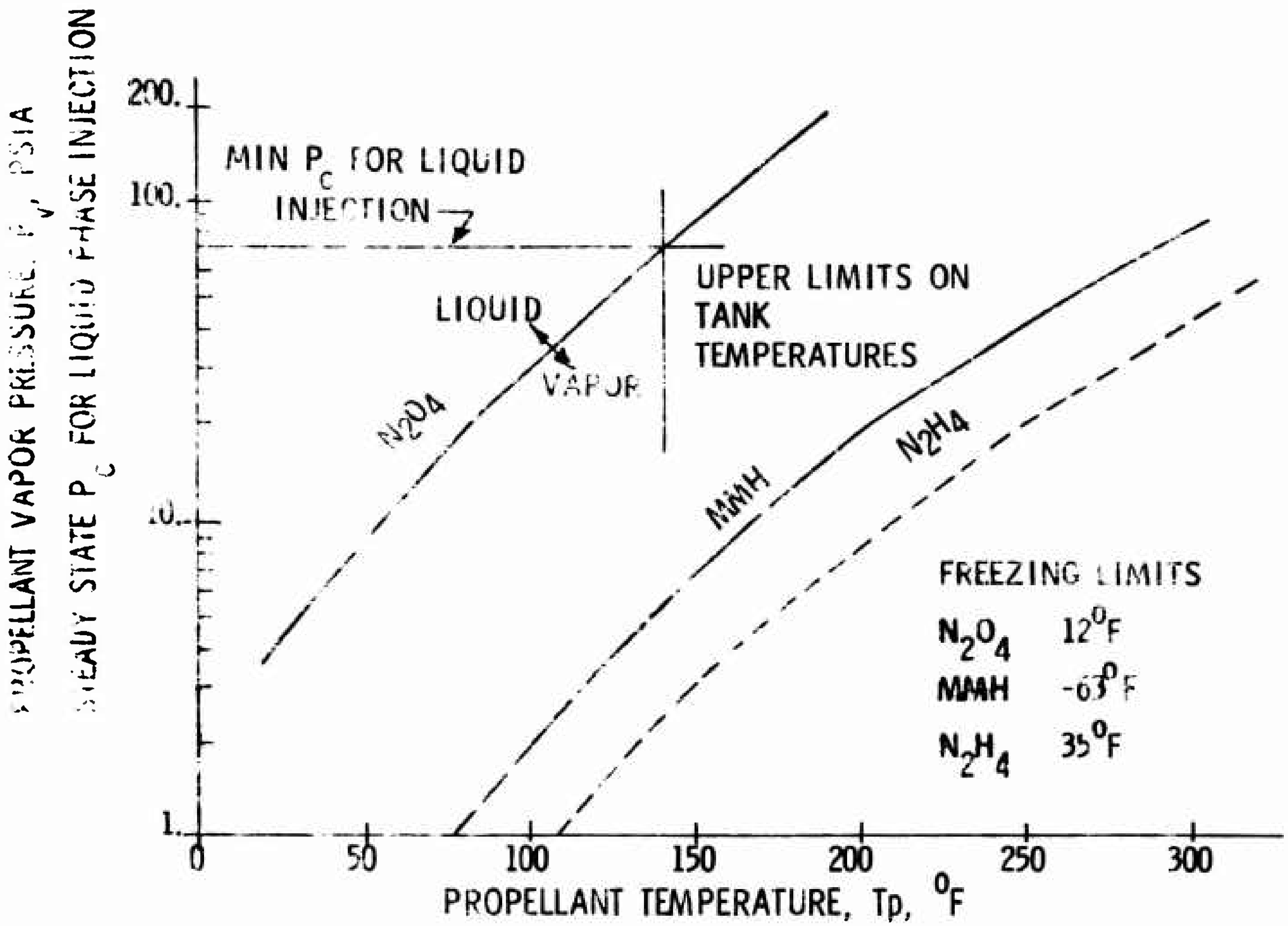

Figure 4.3-1. Injector Heat Sink Limitations

4.3.1, Propellant and Engine Temperature Effects (cont.)

paths used as a radiation cooled engine soaks out following a long duration burn were identified (Figure 4.3-2) and the time-temperature history of each component forecasted as shown in Figure 4.3-3. The injector and valve of the initial engine design are predicted to reach 250°F which is sufficient to vaporize the oxidizer if a restart were to occur. There is a concurrent heat flow of 0.9 watts to the thrust mount. It was found that increasing the conductivity of the stainless steel valve manifold-thrust mount (Figure 4.3-4) by the addition of a 0.030 thick copper facing held the injector-valve temperature to a maximum of 150°F with a total heat flow through the engine mount of 6.4 watts. This was considered acceptable based on the requirements data shown in Figure 4.1-1.

The results of a similar analysis of an adiabatic wall chamber are shown in Figure 4.3-5. In this case the absence of external radiation directs more heat toward the valve and engine mount so that the valve soaks out at nearly 300°F and there is a 6.8 watt heat load through the engine mount. The attainment of a 140°F injector temperature limit requires that either a total of 16.9 watts be conducted through the engine mount or that the thermal resistance at the chamber to injector interface be increased.

Figure 4.3-6 shows the effect of thermal resistance at the chamber to valve-manifold interface for several design options. It is evident that the use of a titanium spacer at the forward end of the chamber significantly reduces heat flow to the mount. Although subsequent testing showed the injector design to considerably influence the heat load to the thrust mount, the following is evident:

. The lowest operating chamber pressure is 75 psia (Reference Figure 4.3-1), based on the delivery of 120°F propellant and an assumed 20°F design margin for heat soak.

. The allowable valve soak temperature increases with P_c; it is 140°F at 75 psia and 190°F at 200 psia.

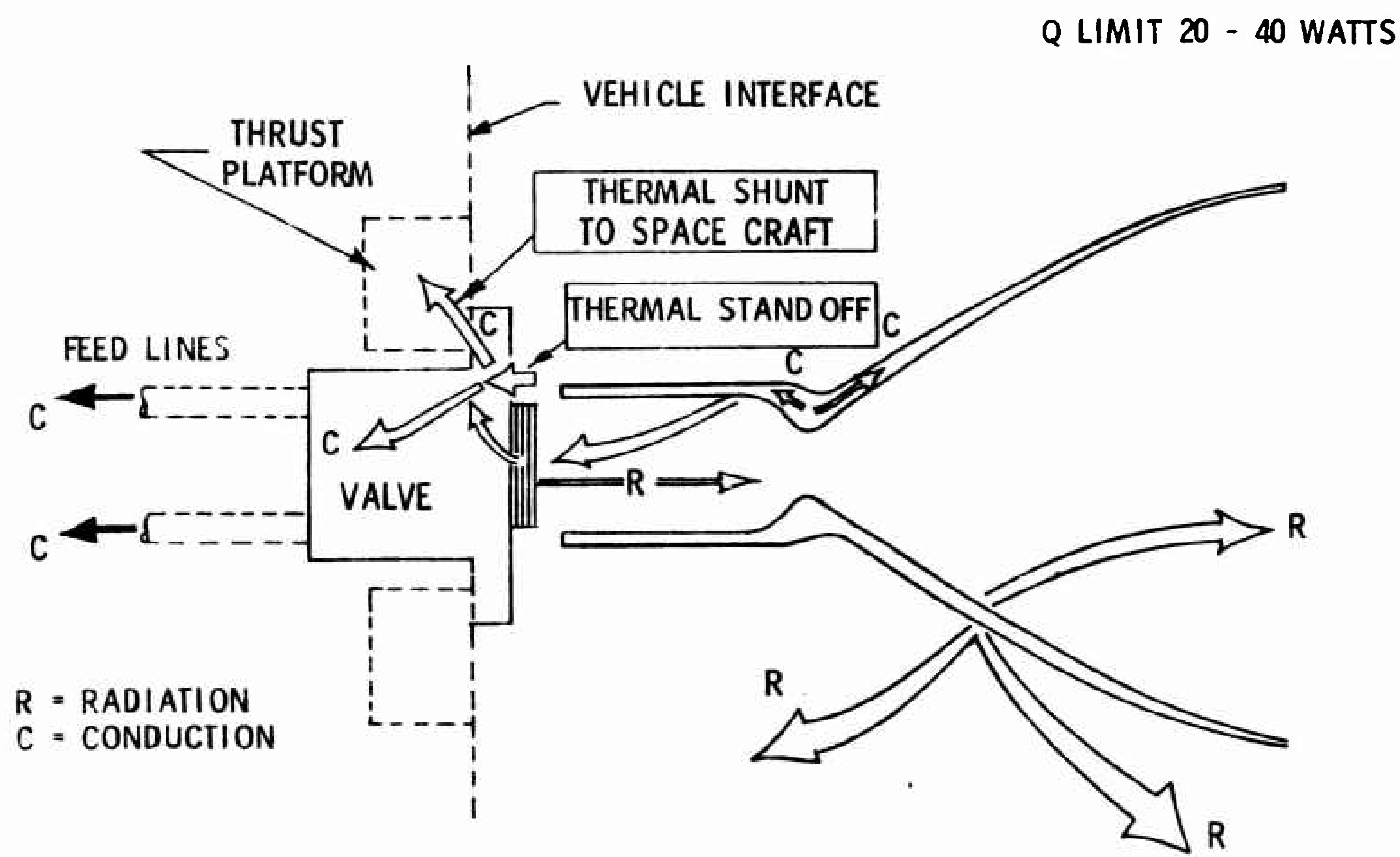

Figure 4.3-2. Spacecraft Thermal Interfaces

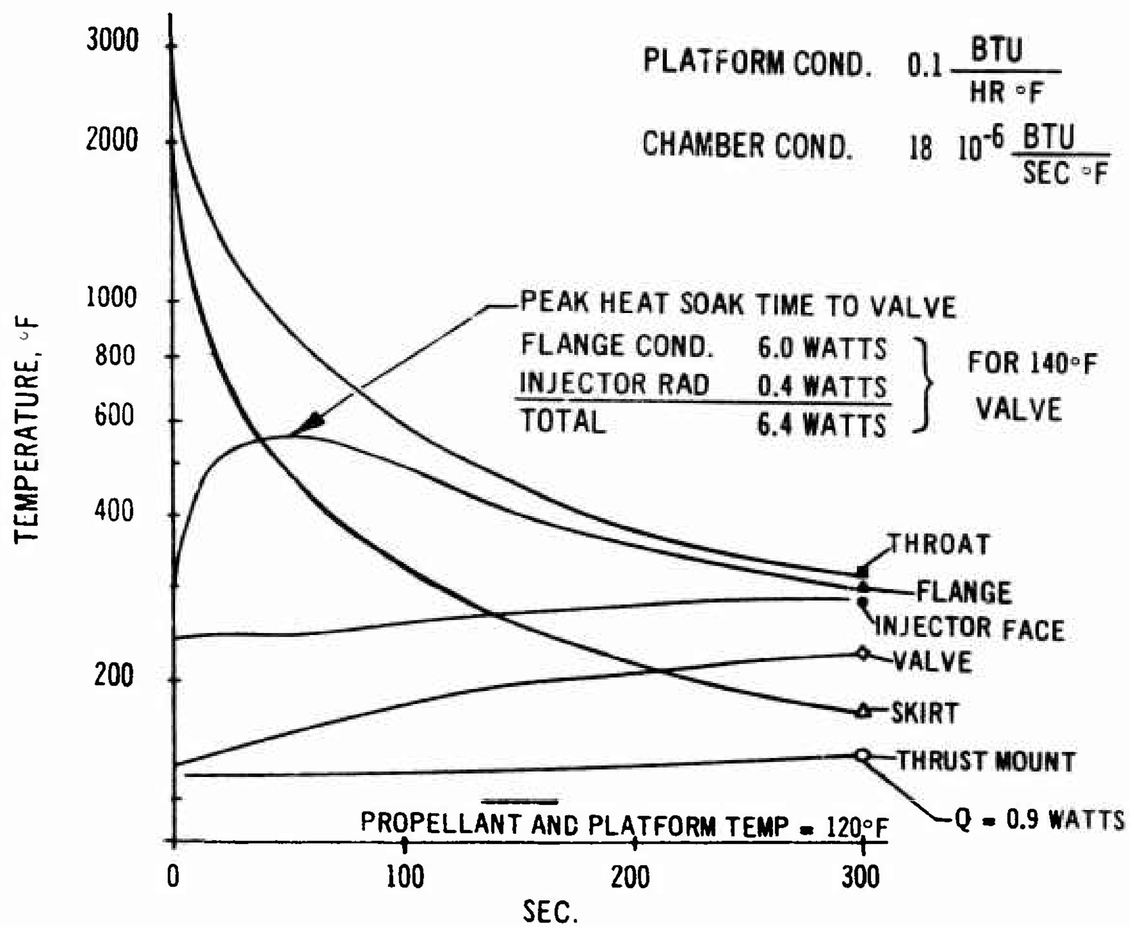

Figure 4.3-3. Postfire Thermal Soak, Radiation Cooled Design

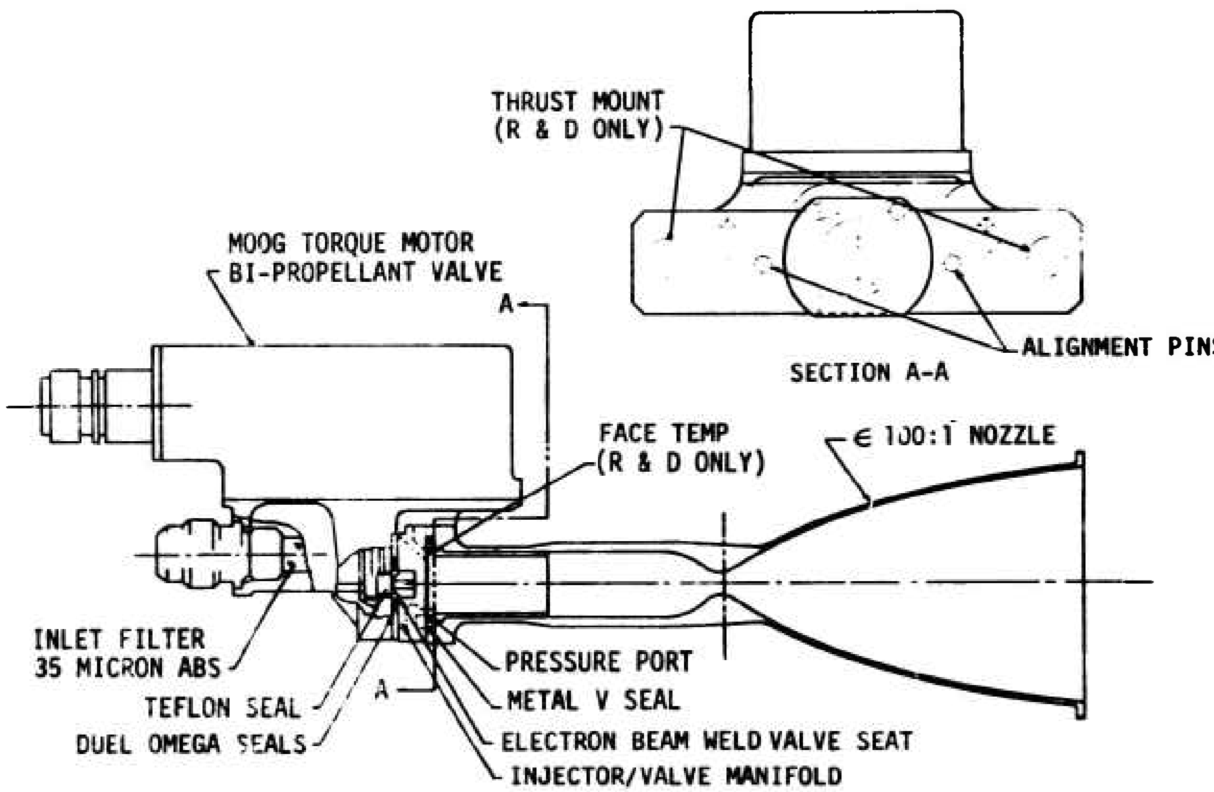

Figure 4.3-4. 5 lb Thrust Bipropellant Engine Thrust Chamber Assembly

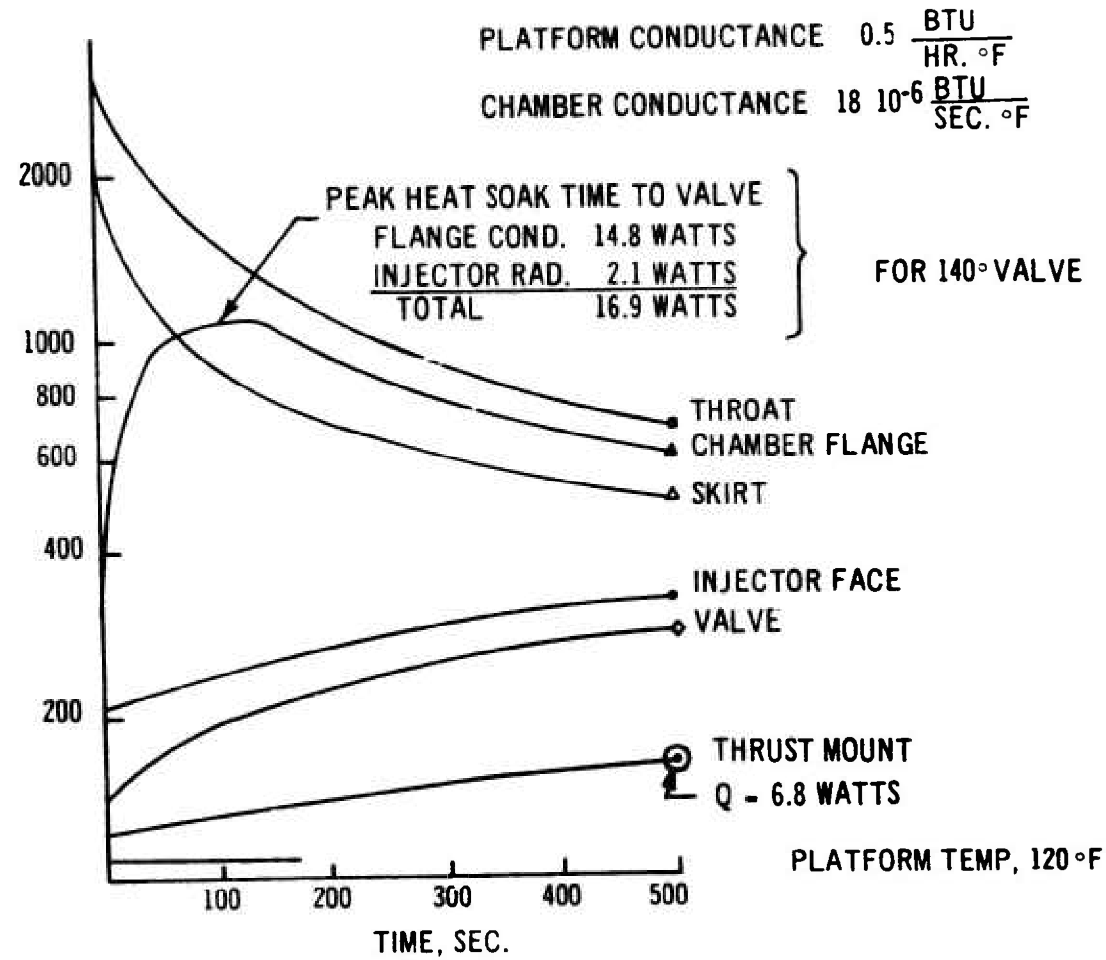

Figure 4.3-5. Postfire Thermal Soak, Buried Design

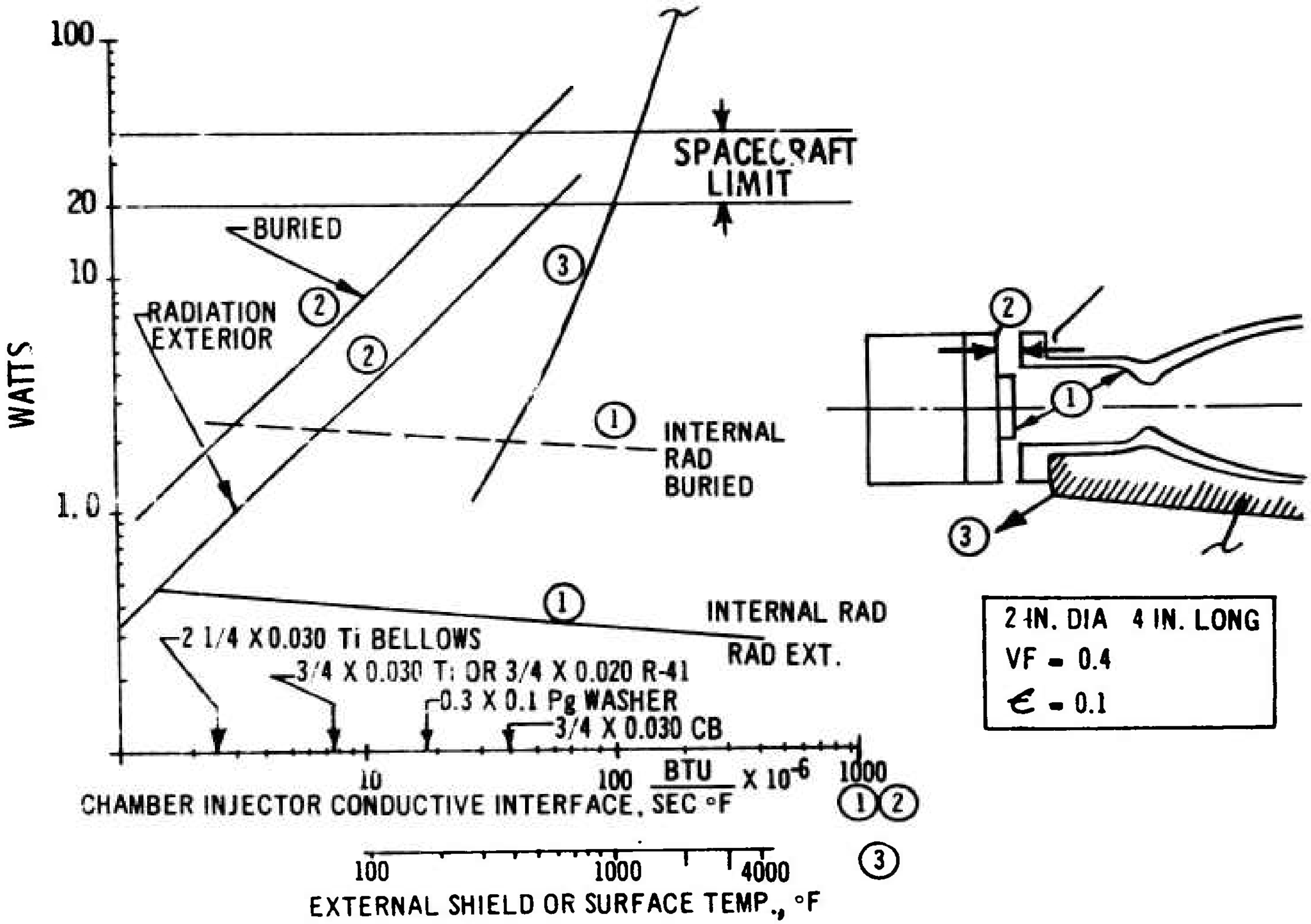

Figure 4.3-6. Postfire Soak Heat Load

. A thermal shunt around the valve is recommended to prevent H_2O_4 vapor lock due to soak out after a long burn. The regenerative cooling capacity of the propellants at 70°F during steady-state operation is in excess of 1000 watts and if proper provisions are made is more than sufficient to cool the valve, injector and thrust mount.

. A non-vapor locking radiation cooled engine can be designed to limit the postfire heat rejection to the spacecraft to less than 6.5 watts; this value is 17.0 watts for an adiabatic wall engine. The deletion of the titanium spacer results in substantially increased heat flow values.

4.3.2 Propellant Tank Temperature and Pressure Effects

The thermal factors which result from off-design operation of the propellant feed system are presented in Figure 4.3-7. The condition most adverse to engine operation results from the combination of a cold fuel tank and hot oxidizer tank with a blowdown feed system. A regulated system, operating from a single source or pressurant, is unaffected by the existance of propellant vapor ullage since the regulation operates to a constant total pressure. Deviations of 15 psi from the nominal tank pressure result in a MR tolerance of $\pm$ 0.06. On a blowdown system, a 100°F tank temperature variation causes over pressurization of one propellant tank and a loss of pressure in the other and results in the mixture ratio shifts shown in Figure 4.3-8. This figure also shows that the addition of cavitating venturis to the engine will suppress the MR excursion. Operation at MR = 2.0 is acceptable to a radiation-cooled chamber since the MR change has little effect on the wall temperature and hence coating life.

The adiabatic wall chamber is dependent upon barrier cooling to maintain an acceptable wall temperature (Reference Figure 4.2-13). High MR operation will result in the core flow being at a higher than stoichiometric MR and reacting with the barrier. This condition can be relieved by over designing the barrier to insure safe operation at the high MR. Subsequent

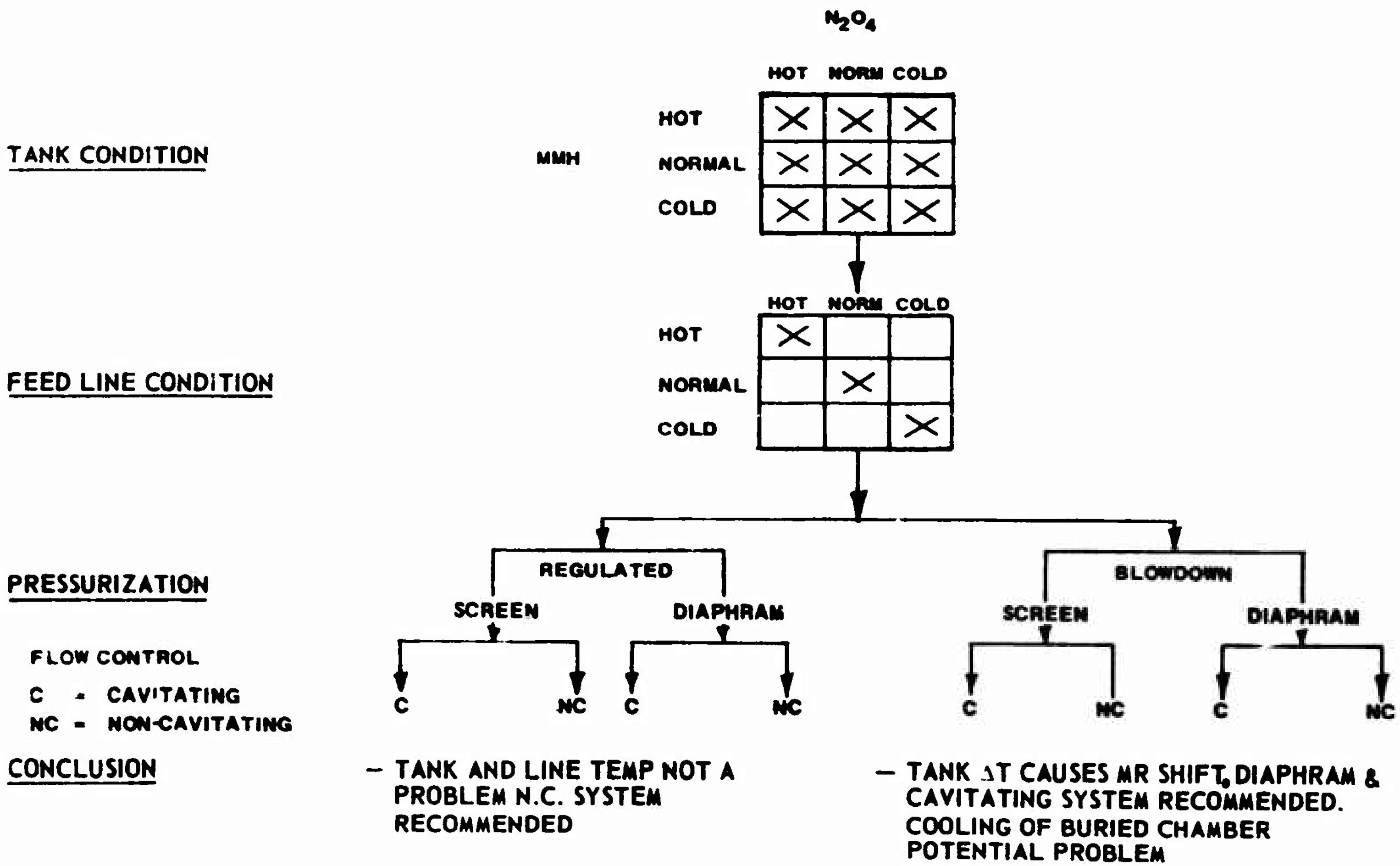

Figure 4.3-7. Feed System Off-Design Thermal Factors

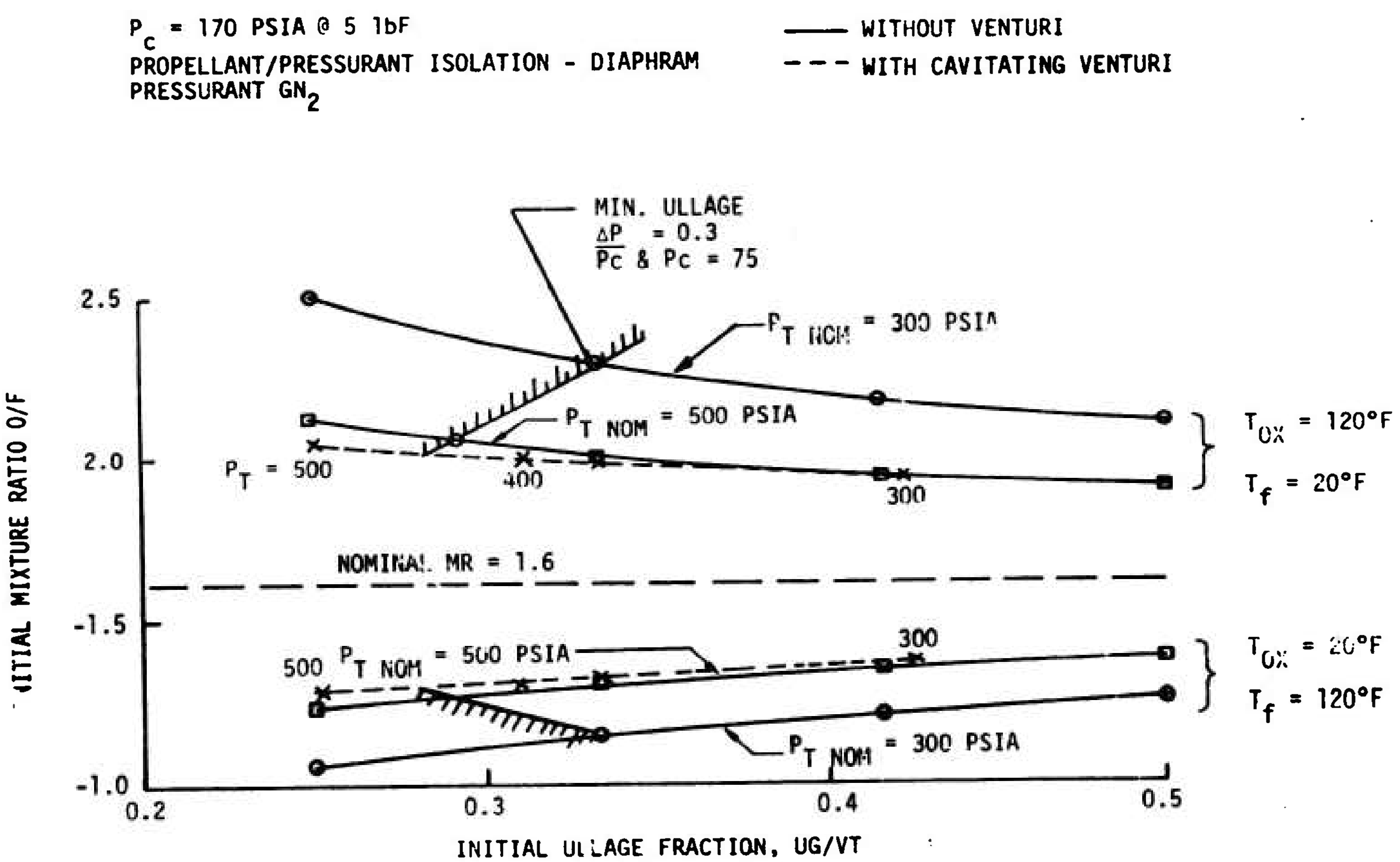

Figure 4.3-8. Effect of Tank Temperature Extremes on Engine Mixture Ratio for a Fixed Design

with various spacecraft fabricators indicates that the high ΔT used is overly conservative. Spacecraft thermal design is generally keyed to minimizing temperature variations which are adverse to electronic equipment.

The effect of local propellant line temperature (nominal tank conditions) on the operation of an engine with cavitating venturis was also examined. As indicated in Figure 4.3-9, the engine will operate over the full range of propellant temperature and blowdown chamber pressure. The MR shifts are less at higher pressures.

It was determined that a single engine could be configured for operation with either a blowdown or regulated feed system and with and without venturis. As shown in Figure 4.3-10, the same engine operating without venturis is suited to either feed system. Using venturis, the unit requires a higher feed pressure and produces slightly less thrust. It will, however, blowdown over a 3 to 1 tank pressure range and have a minimum thrust of 2.2 lbF at the minimum feed pressure. The non-venturi system has the same minimum thrust.

4.3.3 Engine Feed System Limitations

Preliminary analysis showed the engine to be capable of accepting considerable P_c variation. Excessively large MR shifts in the fuel rich direction were expected to be adverse with regard to ignition delays, but not likely to cause damage. The high MR was forecasted to be adverse for an adiabatic wall thrust chamber if there was sufficient firing time. Potential solutions were (1) to limit the engine operation to pulsing only at the high MR, (2) to reduce chamber length to preclude all the barrier coolant from having time to react with the core (this results in a performance decrement at nominal conditions), and (3) to design the blowdown system to limit the oxidizer temperature or more closely match fuel and oxidizer tank temperatures, or (4) add cavitating venturis to reduce the MR shift. Although

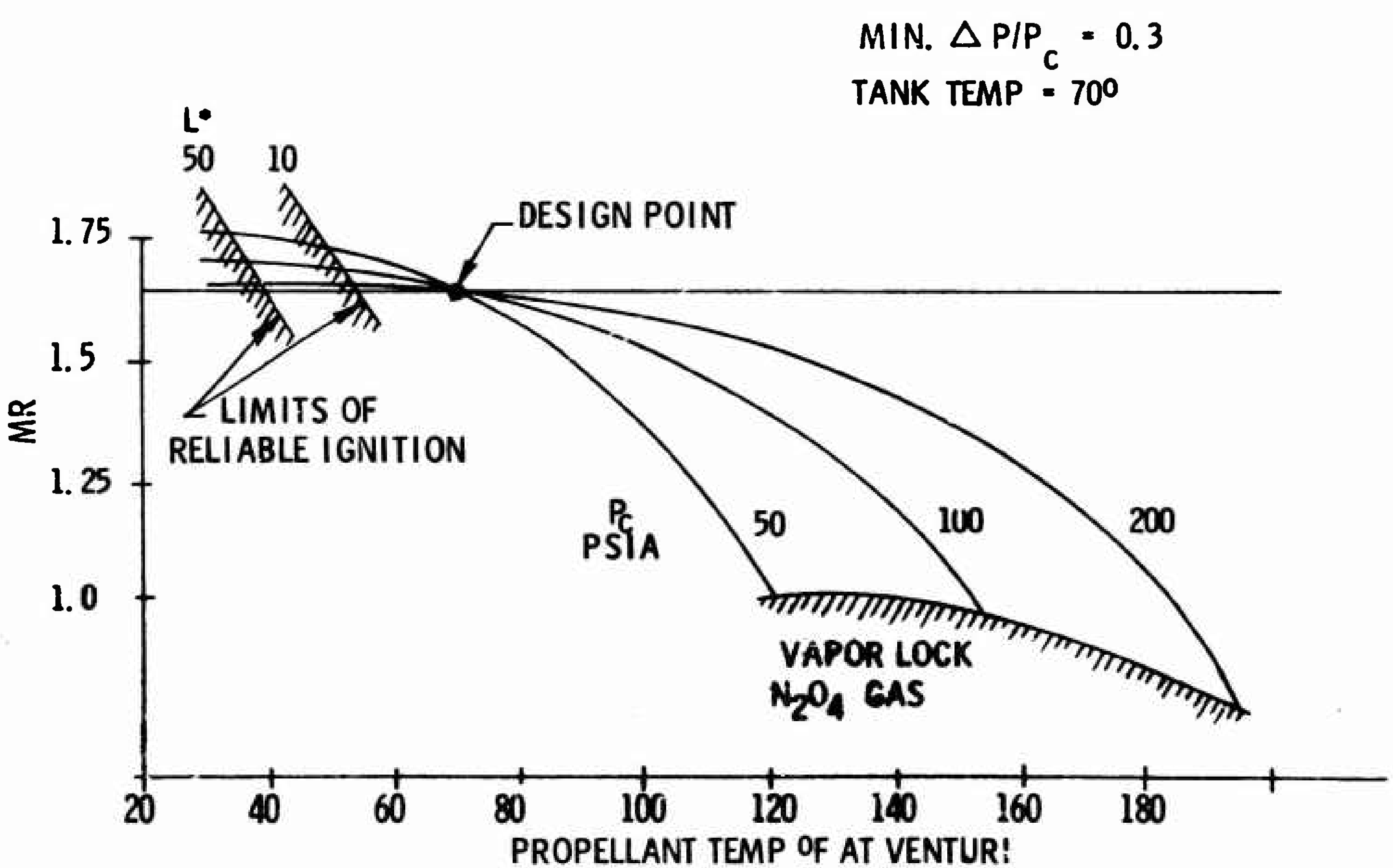

Figure 4.3-9. Effect of Propellant Line Temperature on Mixture Ratio in a Cavitating System

	BLOWDOWN SYSTEM				REGULATED SYSTEM		
	INITIAL		TERMINAL		*		
	*	**	*	**			
TANK PRESSURE	300	384	100	125	100	300	500
INJECTOR ΔP	130	83	25	25	25	130	261
CHAMBER PRESSURE	170	136	75	75	75	170	241
THRUST	5.0	4.0	2.2	2.2	2.2	5.0	7.1
MR	1.6	1.6	1.6	1.5	1.6	1.6	1.6

* NONCAVITATING
** CAVITATING, TANK TEMPERATURE = 70° F

$\frac{\Delta P}{P_c}$ MIN = 0.33

P_c MIN 75 PSIA OX LIQUID TO 140° F

Figure 4.3-10. Common Engine for Blowdown and Regulated Systems

4.3.3, Engine Feed System Limitations (cont.)

cavitating venturis increase system pressure drop and may result in slower start transients their use is recommended if the engine application requires acceptance of large tank temperature differentials.

4.3.4 Engine Weight

Figure 4.3-11 shows engine component weight versus chamber pressure and area ratio. There is virtually no effect as P_c and ε is varied; this is due to the fact that the major weight is in the valve and the valve weight is not sensitive to feed pressure or chamber pressure. Figure 4.3-12 shows the engine envelope as a function of chamber pressure and nozzle area ratio. System studies have not identified particular engine dimensional constraints.

The effect of tank pressure and total impulse on tank weight was studied considering both regulated and blowdown systems using a single spherical tank for each propellant. These studies indicated that the lowest weight system has the lowest tank pressure with minimum pressure defined by the minimum gauge thickness suitable for fabrication. This data, in combination with the engine performance and P_c and injector ΔP constraints indicate that the bipropellant engine's operating pressure range (P_c = 75 to 175) matches the minimum weight tank pressure. The identification of an optimum chamber pressure is complicated by the fact that the space craft may use multiple tanks. This is necessary for mass distribution on a spin stabilized space craft. On three axis stabilized spacecraft multiple tanks may provide more efficient use of space craft volume. Discussion with various space craft primes indicates that their propellant system weight studies usually optimize with a tank pressure of about 300 psia. This is compatible with a chamber pressure ranging from 75 to 175 psia.

4.3.5 Engine Thermal Environment

System review indicates that there are two possible engine installations. One allows the unit to radiate using local radiation shields

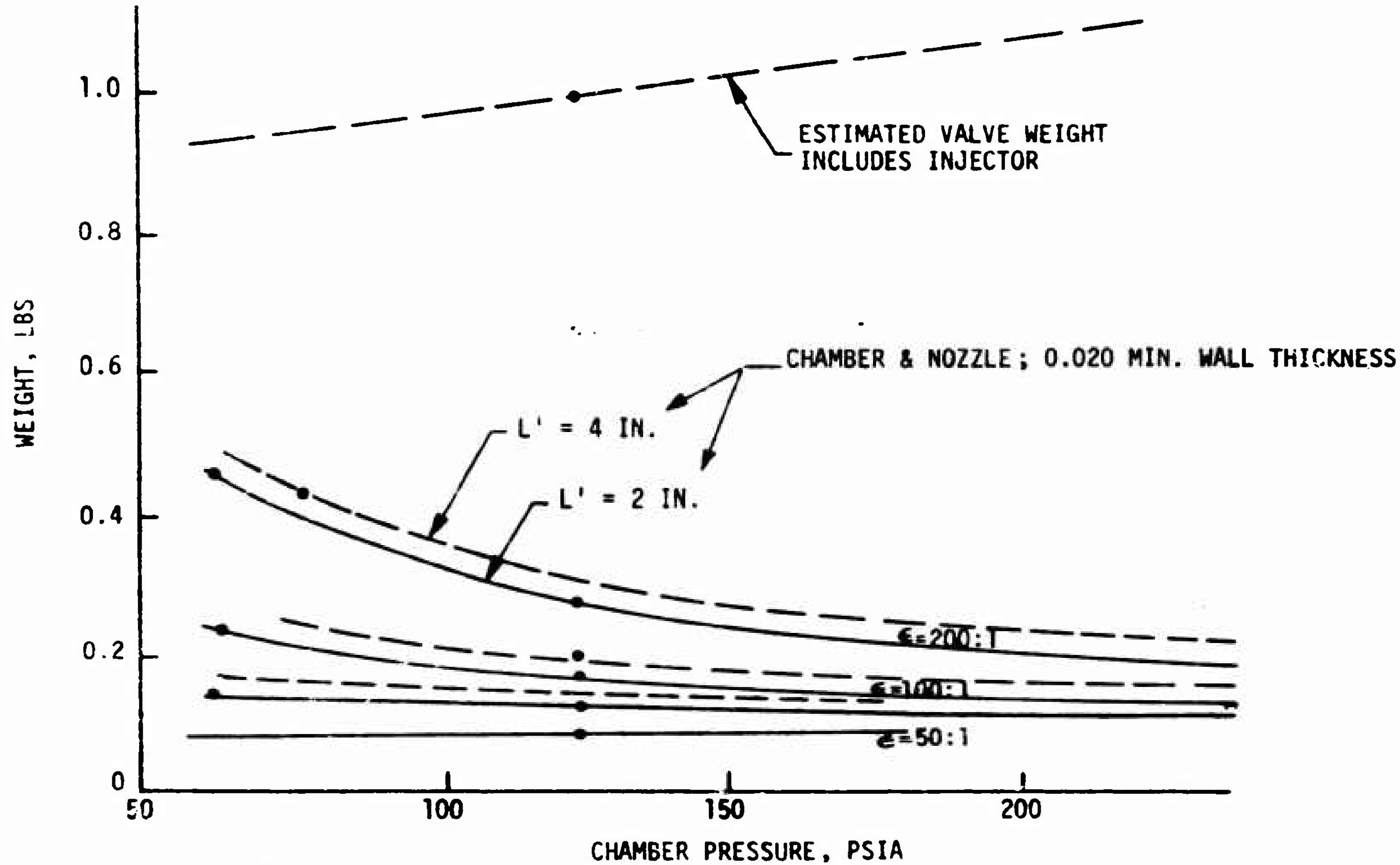

Figure 4.3-11. 5 lb Thrust Bipropellant Engine Component Weights

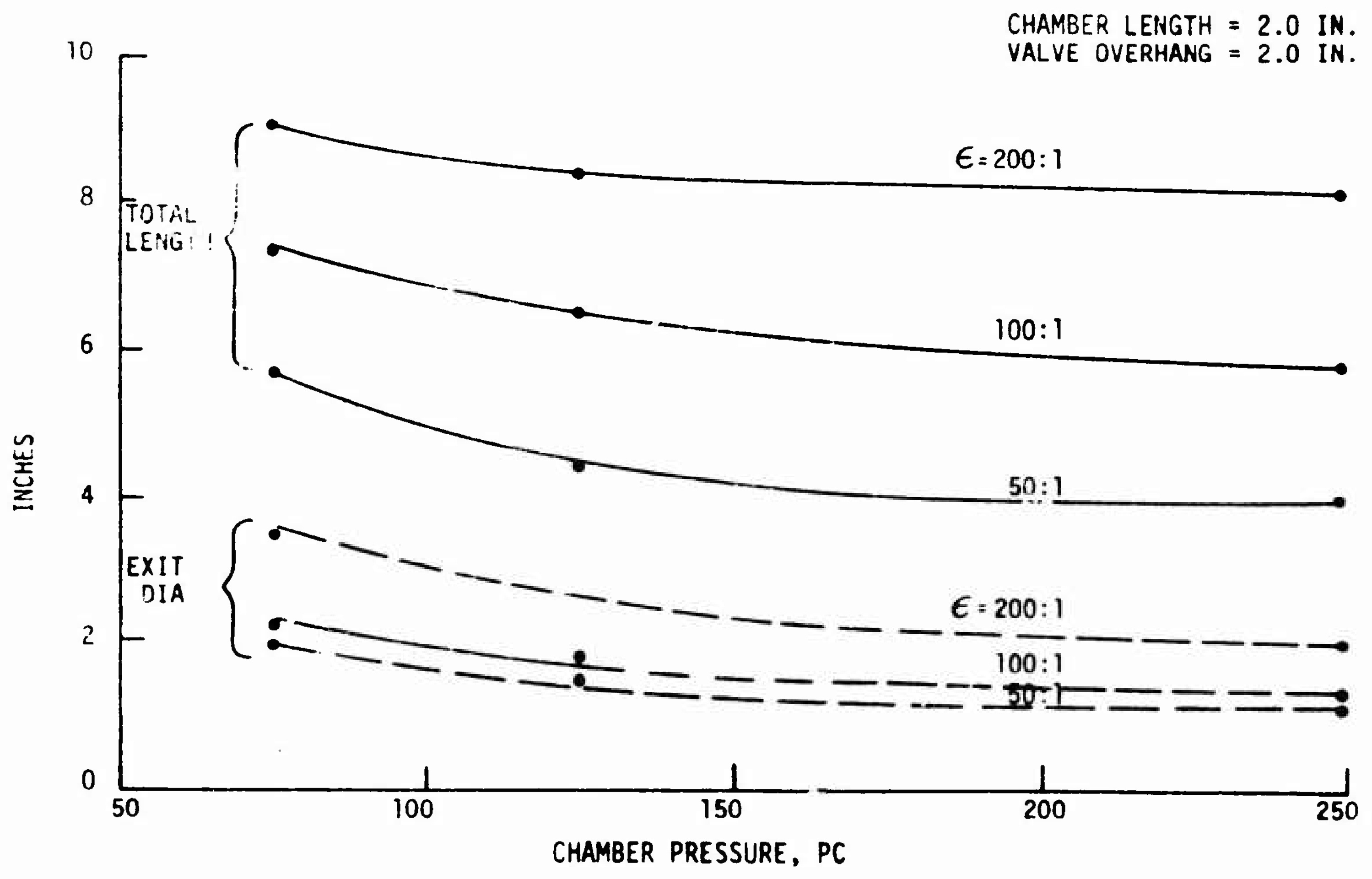

Figure 4.3-12. 5 lb Thrust Bipropellant Engine Envelope

to protect adjacent structure. The other buries the engine in the space craft structure. In this case, either full insulation or a radiation shield can be used to protect the surrounding components. Figure 4.3-13 shows the possible engine thermal shield configurations. The radiation cooled and shielded designs provide the highest performance for a given chamber life. If the same engine is used in a buried configuration (no barrier cooling), the maximum operating duration as a heat sink will be limited to about 5 seconds. An unlimited duration capability in a buried design can be obtained through use of barrier cooling with an attendant performance decrement. Figure 4.2-13 shows the analytically determined relation between performance and steady state throat wall temperatures for chambers which are (1) radiation cooled, (2) radiation and barrier cooled, and (3) barrier cooled only. The longer length chambers run cooler for a given performance level because their higher vaporization efficiency allows the diversion of additional fuel to the barrier. Ideally, a 4 in. long (L') radiation/barrier cooled chamber having a 300 sec steady state vacuum I_{sp} with a 100:1 nozzle will operate with a maximum temperature of 2250°F. The same design would operate at 2900°F in a buried installation.

Parametric analyses were conducted to determine the optimum wall thickness contour for radiation cooled chambers. It was found that thickening the wall in the throat region reduced the maximum wall temperature. This is due to the external surface available for radiation increasing more rapidly than the conduction loss across the thickened wall. There are beneficial effects for wall thicknesses up to 0.3 inches. Increasing chamber pressure by reducing the throat diameter while maintaining a fixed outside diameter resulted in the higher throat heat flux being offset by the higher ratio of cooled to heated surfaces so that little increase in wall temperatures at higher chamber pressures is predicted. The addition of barrier cooling depresses the maximum wall temperatures of radiation cooled nozzles about the same for all combustion pressures.

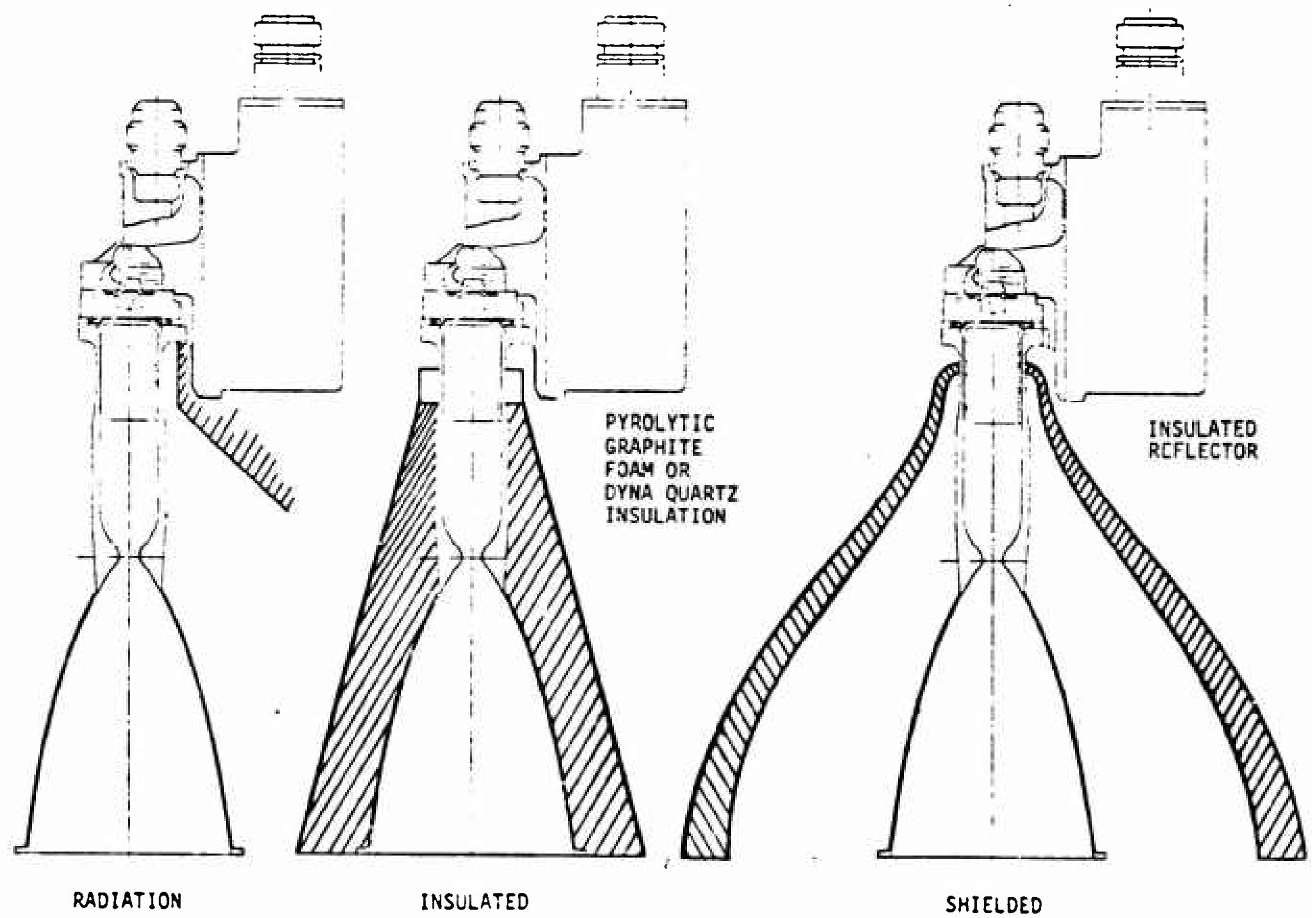

Figure 4.3-13. Installation Options

4.3.5. Engine Thermal Environment (cont.)

. Transient and steady state 2-dimensional axisymmetric thermal analyses were conducted for the selected thrust chamber design (Reference Figure 4.2-8) to determine the nozzle life and identify potential structural failure modes. These analyses were based on the use of Fansteel columbium alloy No. 85, with the assumption that the nozzle would be radiation cooled and the protective fuel barrier fully consumed in the combustion process prior to reaching the throat. The convective boundary conditions were based on available Aerojet data and the method of Reference 11. Analyses were conducted for chamber pressures of 125 and 200 psia. These and other computer data, suggested the following structural failure modes be evaluated:

(1) Flexure of the forward chamber due to the high axial temperature gradient.

(2) Creep in the downstream chamber and throat region at maximum temperature.

(3) Through-the-wall thermal gradients at the thick throat section with cold starts.

(4) Pressure cycling of the chamber wall at maximum temperature at 125 and 200 psia.

(5) Ignition spike capabilities.

A structural analyses was conducted using a finite element plastic flow computer model. The model outputs effective stresses and resulting strains from combined pressure and thermally induced loads. Life was estimated by comparing actual stress or strains to the allowables for the material at temperatures as shown in Figure 4.3-14.

The structural analyses showed all stress to be below the 0.2% yield value. The greatest transient stress occurred on cold start in the throat region, 0.5 sec into the firing. The nozzle cycle capability for cold starts was predicted to be in the order of 10^6-10^7 and the ignition spike capability in the order of 4000 psia. The structurally imposed limits of operation were in Regions [illegible] and [illegible] of Figure 4.3-14. These data indicate the most

(11) Schoenman, L., and Block, P., Laminar Boundary Layer Heat Transfer in Low Thrust Rocket Nozzles, J. of Spacecraft and Rockets, September 1968.

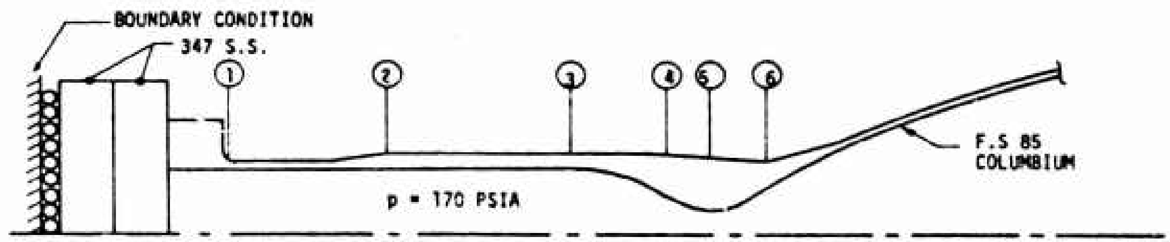

STATION	TIME (SEC)	T_{WG} (°F)	ΔT (°F)	EFFECTIVE STRESS (PSI)	EFFECTIVE STRAIN (%)	ALLOWABLE STRESS FTY KSI	ALLOWABLE STRESS FTU KSI	F.S YIELD	ALLOWABLE LIFE CREEP * (HRS)	ALLOWABLE LIFE FATIGUE** (CYCLES)
1	(PROOF PRESS)	70	-	2,870	0.013	60	80	20.9		
	0.50	154	0	5,400	0.03	60	80	11.1		
	S.S	307	0	1,900	0.01	55	76	-	$>10^6$	$>10^6$
2	(PROOF PRESS)	70	-	1,160	0.005	60	80	-		
	0.50	411	0	7,400	0.03	54	74	7.3		
	S.S.	1,545	0	7,900	0.04	34	52	4.3	$>10^6$	$>10^6$
3	(PROOF PRESS)	70	-	680	0.003	60	80	-		
	0.50	460	84	9,500	0.04	53	73	5.6		
	S.S.	2,828	0	5,700	0.05	11	13.5	1.9	3,400	$>10^6$
4	0	70	-	300	0.001	60	80	-		
	0.50	518	342	24,000	0.11	52	72	2.2		$>10^6$
	S.S.	2,957	127	9,600	0.09	10	11	1.04	10,600	900,000
5	(PROOF PRESS)	70	-	200	0.0001	60	80	-		
	0.50	518	392	21,200	0.10	52	72	2.5		$>10^6$
	S.S.	2,800	86	9,400	0.08	11	12	1.2	50,100	900,000
6	(PROOF PRESS)	70	-	70	0.001	60	80	3.0		
	0.50	223	90	13,600	0.06	60	80	4.5		
	S.S.	2,677	31	10,900	0.07	13	16	1.2	$>10^6$	$>10^6$

*BASED ON PRIMARY STRESS

** $N_F = 10\% \times N_{LIFE}$

Figure 4.3-14. Summary of Stress Analysis, 5 lb Thruster

4.3.5, Engine Thermal Environment (cont.)

likely failure modes to be: creep under steady state firing conditions (3400 hours to rupture at 3000°F) and pressure cycling at high temperature (500,000 cycles with a safety factor of 10).

It was concluded that thrust chamber life was limited not by the structure, but by the previously discussed protective coating for the oxidation sensitive columbium and the ability of the injector to provide a compatible chemical environment along the chamber wall.

5.0 PHASE II - DESIGN AND VERIFICATION TESTING

The design conditions and criteria for the Phase II verification test hardware were based on the Phase I analyses which provided the following engine specifications:

Valve response	less than 0.005 sec
Operating pressure at 5 lb Thrust (P_c)	170 psia
Valve working pressure	500 psia
Minimum P_c and thrust for 3:1 tank blowdown	75 psia, 2.2 lbF
Minimum injector $\Delta P/P_c$	0.33
Number of elements for 300 sec I_s	4 to 6
Chamber length, L'	2-4 inches
Injector + valve dribble volume (total)	0.0007 $in.^3$
Maximum nozzle wall temperatures for sustained firings and buried engine capabilities	2800°F
Heat rejection to space craft	20 - 60 watts

Phase II thus consisted of (1) detailed analyses and the development of design configurations which would satisfy the above requirements, (2) fabrication of the components; valve, injectors and nozzles, required to obtain data, (3) systematic hot fire testing of each of the components over the range of parameters of interest to verify and uprate the analyses and to establish feasibility of the concepts, and (4) the generation of designs for Phase III demonstration testing.

5.1 ENGINE DESIGN AND FABRICATION

This task consisted of (1) the selection of a valve from several available flight qualified designs, (2) the design and fabrication of injectors which could be integrated with the selected valve to provide the 0.0007 $in.^3$ residual volume and (3) design and fabrication of thrust chambers which would allow data on chamber length and thermal characteristics to be obtained for radiation cooled and buried (adiabatic wall) designs.

5.1.1 Valve

5.1.1.1 Selection

The development status of valves suitable for 5 lb thrusters was reviewed during Phase I in (Section 4.2.3). A re-evaluation of the preliminary valve selection along with the valve-injector-chamber integration was made at the start of Phase II. Since mission requirement studies were unable to identify the influence of valve particulars, it was assumed that all candidate valves would meet the defined valve functional criteria. The factors for selection then become those directly related to successful completion of a mission rather than optimization for some not clearly defined mission application.

With this premise, a paired comparison of factors was made to determine the relative importance of each factor. This technique compares each factor with every other factor and requires a decision as to which of the two compared factors is more important. This paired comparison matrix, shown in Figure 5.1-1, provided the weighting factors applied to the evaluation of candidate valves.

The evaluation was limited to two valves; Moog Inc's linked bipropellant valve and Parker's individual solenoid valve; these were selected as the best proven designs for linked and unlinked valves. Each valve design was rated to a 1 to 5 scale for each factor with the highest rating being 5. The ratings were then multiplied by the weighting factors to obtain the final rating values shown in Figure 5.1-2. The Moog bipropellant valve was selected. Figure 5.1-3 is a compilation of operating data for similar type valves and Figure 5.1-4 summarizes the expected operating characteristics of the selected valve and actual data for the valves test-fired in Phases II and III.

Factor	Development Status	Adapt. to Redundancy	Adaptability to Injector Integration	Contamin. Generation	Contamination Sensitivity	Fuel-Ox Repeatability	Packaging Adaptability	Total
Development Status	-	1	0	1	1	1	1	5
Adaptability to Redundancy	0	-	0	0	0	0	1	1
Adaptability to Injector Integration	1	1	-	1	1	0	1	5
Contamination Generation	0	1	0	-	1	0	1	3
Contamination Sensitivity	0	1	0	0	-	0	1	2
Fuel-Ox Repeatability	0	1	1	1	1	-	1	5
Packaging Adaptability	0	0	0	0	0	0	-	0, use 1

Figure 5.1-1. Paired Comparison Matrix

Factor	Factor Weight	Rating		Rating X Weight	
		Moog	Parker	Moog	Parker
Development Status	5	4	3	20	15
Adaptability to Redundancy	1	3	4	3	4
Adaptability to Injector Integration	5	4	2	20	10
Contamination Generation	3	5	4	15	12
Contamination Sensitivity	2	4	4	8	8
Fuel-Ox Repeatability	5	5	4	25	20
Packaging Adaptability	1	3	4	3	4
			Totals	94	73

Figure 5.1-2. Valve Trace Table

Figure 5.1-2. Valve Trade Table

NOVEMBER 1972

MODEL NUMBER	PROGRAM	THRUST LB	FLUIDS	SYSTEM PRESSURE PSIG	RATED FLOW LB/SEC	PRESSURE DROP PSID	WEIGHT LB	VOLTAGE RANGE VDC	COIL RESISTANCE OHMS	INTERNAL LEAKAGE MAXIMUM SCC/HR	MAX RESPONSE TIME MILLISECONDS ON	OFF	SEAT TYPE	FILTRATION NOM	ABS
0050x370	Classified	75	N_2H_4	400	0.40	100	≤ 1.3	24-36	13.5-16.5	5.0	6.0	5.0	Soft Poppet TFE	20μ	35μ
0052-157	MM3	30	N_2O_4 MMH	247	0.0554 0.690	54 68	≤ 0.92	24-30	48-57	5.0	7.5	5	Soft Nozzle	20μ	35μ
0053-105	[illegible]	100	N_2O_4 MMH	240	0.1208 0.1550	35 45	≤ 1.6	27-33	48-57	5.0	15	15	Soft Poppet	20μ	35μ
0054-[illegible]	[illegible]	300	N_2O_4 MMH	247	0.568 0.707	37 29-37	≤ 4.7	24-32	29-35	5.0	40	7	Soft Poppet	25μ	35μ
0053-122	[illegible]	100	HDA UDMH	235	0.263 0.142	35 15	≤ 2.2	27-33	27-33 Per Coil	5.0	35	15	Soft Poppet	20μ	35μ
0050-353	PSD	5	N_2H_4	250	0.025	16	≤ 0.82	24-32	48-57	1.0	5.5	5.5	Soft Poppets	20μ	35μ
0052-151		100	N_2O_4 MMH	500	0.1508 0.1850	37.5 56.5	≤ 20	28-32	48-57	5.0	8.7	1.7	Soft Poppets	None	
0054-105	Mariner	300	N_2O_4 MMH	275	0.536 0.670	27 30	≤ 4.7	26-32	32-35	5.0	40	7	Soft Poppets	[illegible]	35μ
0050-304	CI Engine	100	N_2O_4 MMH	195	0.213 0.133	11 14	≤ 8.4	22-30		5.0	10	10	Soft Nozzle		
0050-147	CI Engine	100	N_2O_4 MMH	310	0.213 0.133	23 23	≤ 1.65	22-30		5.0	9	9	Soft Nozzle		
0050x355	ATS	0.5	N_2H_4	350	0.0025	12	≤ 0.40	18-32	130	5.0	1	1	Soft Nozzle	10μ	25μ
0053-115	Marcus III	100	N_2O_4 MMH	750	0.114 0.184	65 85	≤ 1.65	22-30	13.5-16.5 Per Coil	5.0	8	6	Soft Poppet	10μ	25μ

Figure 5.1-3. Moog TM Bipropellant Valve History

Parameter	Operating Requirements	Actual Data from Phase II and III S/N 1	S/N 2	S/N 3
Weight, lb	1.0	0.98	1.04	0.93
Response at 28 V				
Signal to Open	< 0.005	0.0025	0.0025	0.0025
Travel	0.002	≈ 0.0005	0.0005	0.0005
Power at 28 V (watts)	15	15.2	14.5	14.5
Pull in current MA	-	92	110	99
Dropout Current MA	-	68	75	64
Leakage Internal/ext 250-500 psig GN_2	2.5 scc/hr max 1×10^{-6} sec/sec	0	0	0
Acceleration	150g shock 50 g vibration	Not Tested		
Temperature Range, °F	-65 to 350	Test Range 18-220 sustained (hours) 500°F for 5 minutes		
Pressure Ratings				
Proof, psia (3 min)	1000	1000		
Working, psia	500		500	
ΔP without injector at 5 lbF	40 psi max at 0.01 lb/sec (N_2O_4)	nil		
Filter	35 μ Abs, 20 μ nom	35 μ Abs, 20 μ nom		
Life Cycles	$>10^6$	>300,000	>50,000	>50,000
Total energization time	>10 hr	>2 hr	>.5 hr	>2 hr
Service Life	10 years			

Figure 5.1-4. Moog 52 Series TM Bipropellant Valve Characteristics

5.1.1, Valve (cont.)

5.1.1.2 Valve Design and Interfaces

The valve design work was performed by Moog, Inc. of East Aurora, New York. The subject valve was assigned Model No. 52E163. Its design is based on their Model 52-153 valve modified to meet the requirements shown on Table 1.1-1. The basic valve shown in cross section on Figure 5.1-5 and cutaway-projection in Figure 5.1-6, is a torque motor operated, mechanically linked, bipropellant valve that has no relative sliding parts. The torque motor armature pivots on a flexure tube in response to an electrical signal. This motion lifts a pair of flappers, each with a teflon seal button, off a pair of seats which are located in the outlet manifold. The removable inlet fittings incorporate 35μ absolute filters to remove contaminents from the flowing fluid. Sealing of the outlets is achieved by use of redundant, teflon coated, stainless steel seals at each outlet.

Figure 5.1-7 shows the manifold design and the position of the injector following the bonding assembly. Figure 5.1-8 is a photograph of the valve assembly with an integrated injector. The manifold incorporates the following interface features:

- Two positioning dowels are used to properly locate the valve seats relative to the shutoff seals.
- A recess is located on the downstream side of the manifold plate to accept an injector and allow brazing of the injector to the manifold.
- A positioning hole, which also serves as a P_c tap, is used to assure proper orientation of the injector in the manifold.
- Tapped holes allow mounting of the thrust chamber to the manifold.
- Two holes are provided to mount the thruster to a test stand or vehicle.

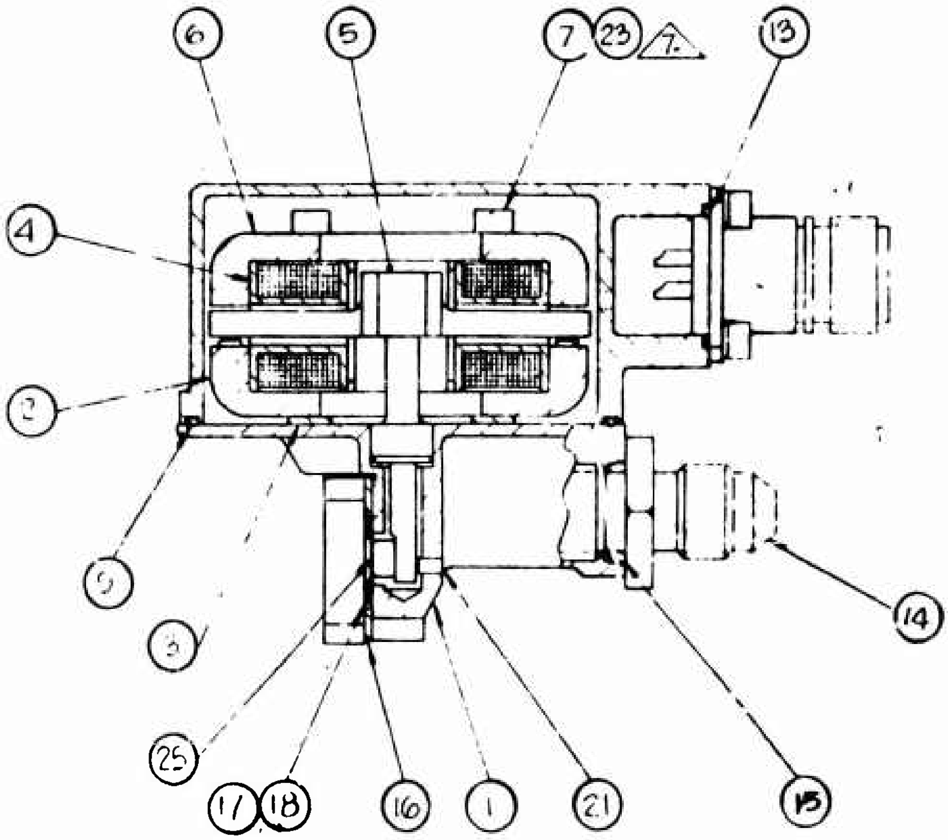

Valve Cross-section

1. Body, arm and flexure assy.
2. Polepiece assy.
3. Spacer, motor
4. Coil assy.
5. Magnet
6. Polepiece, top
7. & 23. Screw
9. Packing
13. Packing
14. Inlet and filter assy.
15. Gasket
16. Seal plate
17 & 18. Seal, metallic
21. Pin, flapper stop
25. Button, flapper

Figure 5.1-5. Cross-Section Basic Valve

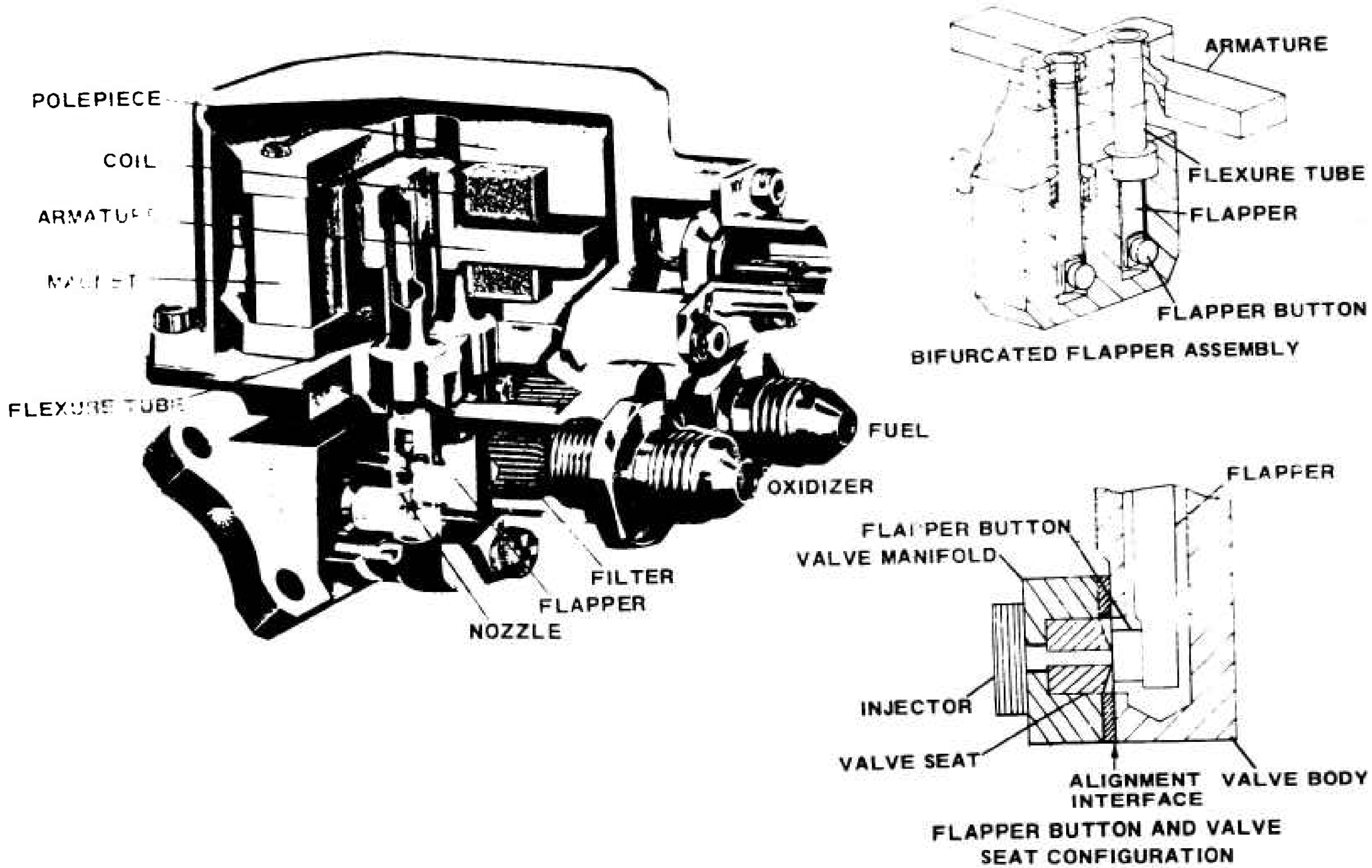

Figure 5.1-6. Bipropellant Control Valve

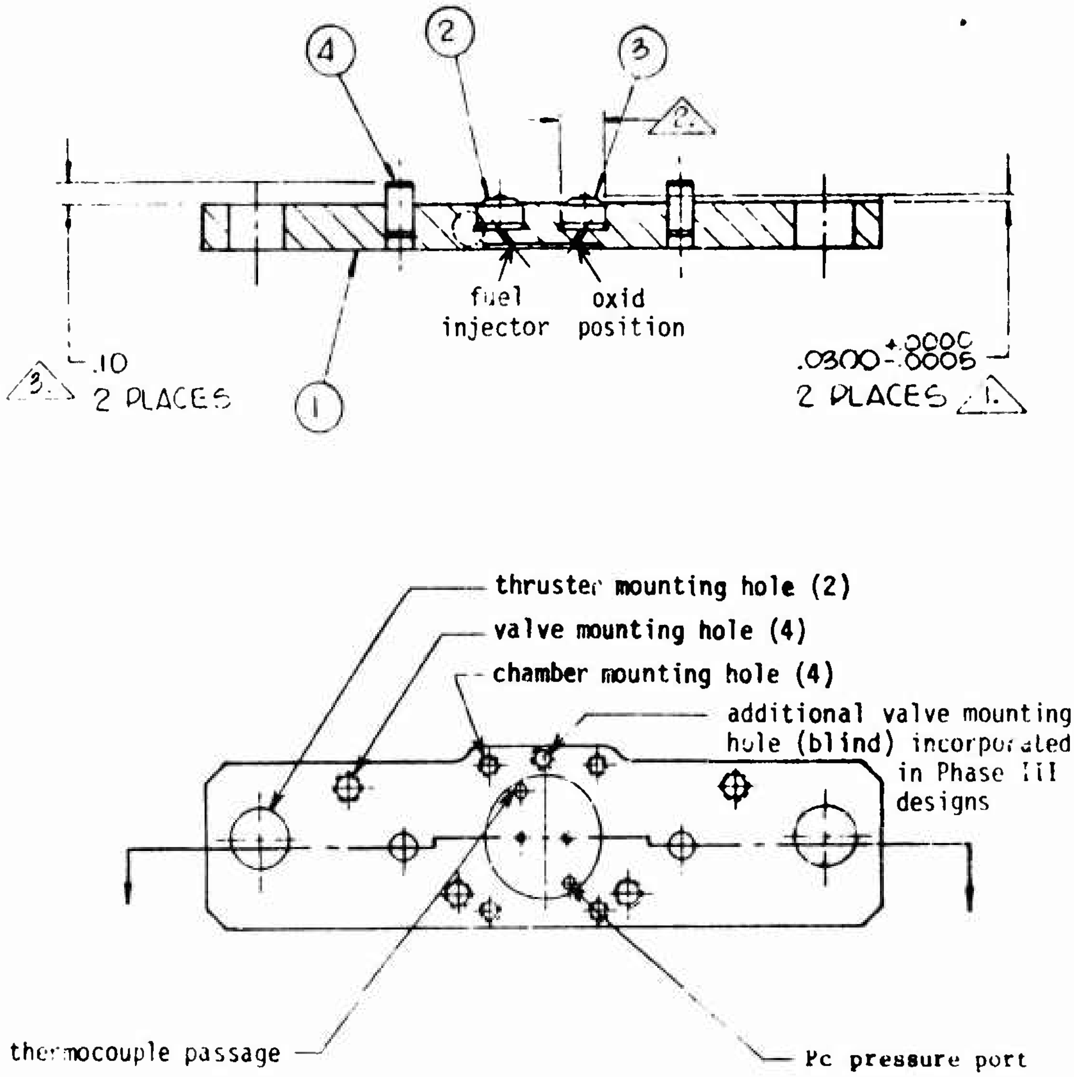

1. Manifold plate
2.&3. Seat nozzles
4. Position pin

generation	Nozzle & Feed Orifice Dia F	C
1st	0.025/0.027	0.032/0.03[illegible]
2nd	0.025/0.027	0.028/0.032
3rd	0.020/0.021	0.026/0.027
	Valve Manifold Volumes in.^{3}	
1st	0.000142	0.0002179
2nd	0.000142	0.0001883
3rd	0.0000888	0.0001486

Figure 5.1-7. Valve Manifold

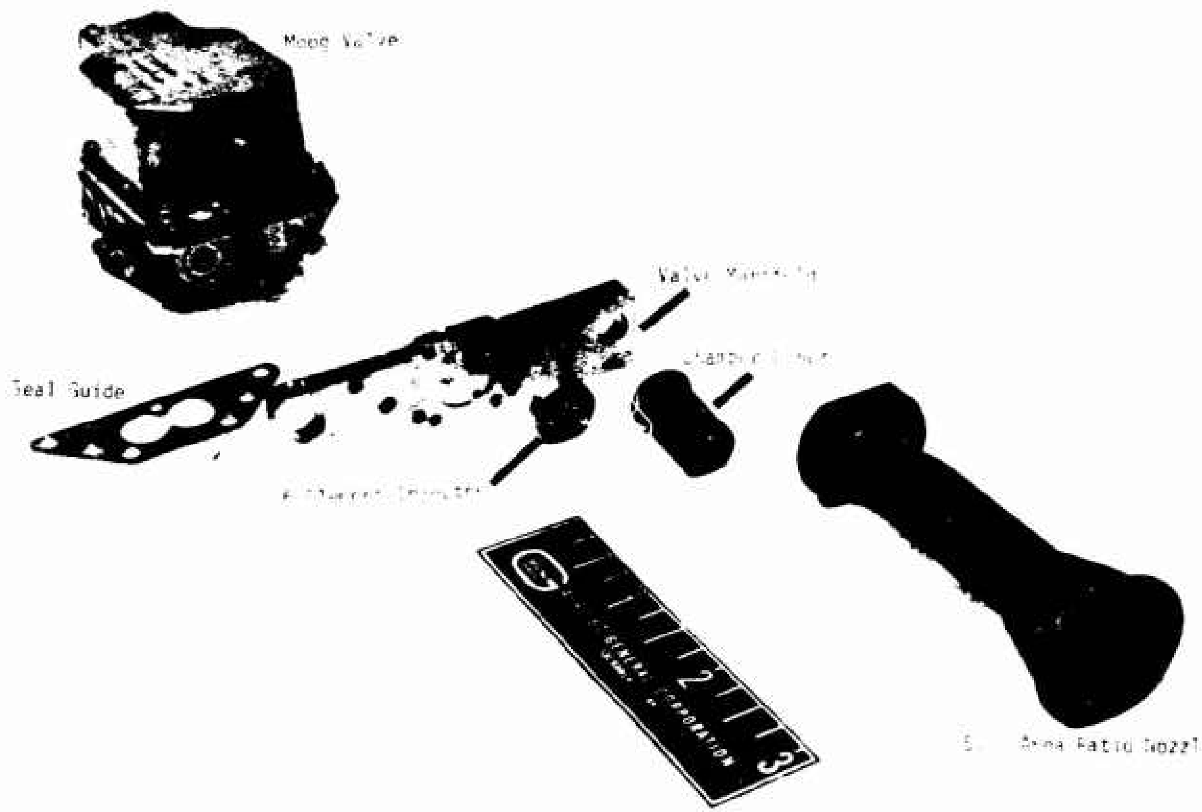

Figure 5.1-8. Valve Assembly with Integrated Injector
(Phase III Test Hardware)

5.1.1, Valve (cont.)

- An access port for thermocouple leads allows monitoring the injector face temperature.
- Four tapped holes are used to mount the manifold to the valve and provide adequate loading to effect an interface seal.

5.1.1.3 Valve Fabrication

Fabrication of the valve was done by Moog using methods and techniques standard to the production of similar torque motor bipropellant valves.

Fabrication of the manifold assembly was accomplished by Moog and ALRC. Two methods of injector-manifold joining were evaluated. One bonded the injector prior to final machining of the valve interface surface, the installation of positioning pins and the installation and electron beam welding of seats. The second bonded the injector into a completely finished and checked out valve assembly. This latter assembly method was preferred because it avoided shipment of components and the possibility of particulates contaminating the injector during final machining. Both techniques were proven satisfactory.

A total of 3 valves, and 8 valve manifolds were utilized on the program. Three 3rd generation, lower volume manifolds (Figure 5.1-7) were obtained for Phase III. The Phase III design provided one additional mounting hole in the manifold and valve body as shown in Figure 5.1-7. Phase II and III values were alike except for the manifold differences.

5.1.2 Injector

5.1.2.1 Design

Injector designs which utilized both conventionally machined and photoetched orifices and manifolds were evaluated. It was found that 0.0003 in.^{3} volume per propellant circuit required for pulsing response and performance in conjunction with the 4 to 6 injection elements required for 300 sec steady state specific impulse, could only be realized using the photoetch fabrication process. This process allowed the design and fabrication of an optimized high velocity, low volume manifolding system which provided uniform flow distribution to all orifices. The design process considered number of element pairs, types of elements and element orientation and manifolding schemes as independent variables. The range of variables are as follows:

Element Quantity	4 and 6
Element Type	90° doublets splash plates triplets shower type mixed elements
Element Orientation	Tangential fans (0 degree) Max spray overlap (45 degree) Intermediate (22 degree)
Manifold	Axisymetric - radial out flow Direct path

The initial injector design analysis established parametric relationships between the number of elements, the passage and orifice sizes and manifolding configuration and volume. Selected designs were then fabricated and cold flowed to determine the resulting element to element flow distribution and spray patterns. This was followed by a redesign effort to further improve the manifolding, prior to the Phase II hot testing. The initial redesigns were provided an A suffix and subsequent modifications a B. All Phase III injection designs were given a C designation.

5.1.2.1 Element Selection

The configuration (orifice sizes, impingement lengths and angles, etc.) of splash plate and doublet elements shown schematically in

5.1.2, Injector (cont.)

Figures 5.1-9 and 5.1-10 were based on unielement cold flow and hot fire test data obtained in company sponsored activities and also from data in Reference (12). A FOF triplet element similar to the doublet with the addition of a second fuel leg positioned 180 degrees was also evaluated. The fuel passages of this configuration had smaller dimensions than the one-on-one O-F element and thus were rejected.

The mixed element patterns were a second generation design which resulted from the initial Phase II test data showing a need for additional wall cooling for the buried engine design.

5.1.2.1.2 Element Quantity Orientation

All designs utilized an even number of elements in order to maintain a symmetrical manifolding system and spray pattern. The minimum element quantity of four was based on the requirement for an axisymmetric flow field and high performance. The maximum of six was established by precluding orifices smaller than 0.008 inch and manifold passage dimensions less than 0.005 inch. The four element designs had higher injection velocities and thus provided extended throttling capabilities required for the blowdown mode of operation.

In a multi element injector, elements can be oriented as shown in Figures 5.1-11 and 5.1-12, to provide various degrees of spray overlap. This, influences mixing efficiency and the amount of liquid phase fuel and oxidizer which is deposited on the chamber wall. The wall film deposit in turn is related to pulsing performance efficiency and contaminant generation. Element orientations of 0 degrees (fans tangent to the wall), 30 degrees and 45 degrees were evaluated. All designs located fuel orifices

(12) L. B. Bassham, Orbit Maneuvering Engine Platelet Injector Evaluation Report 13133 M-3, 12 January 1973, Contract NAS 913133.

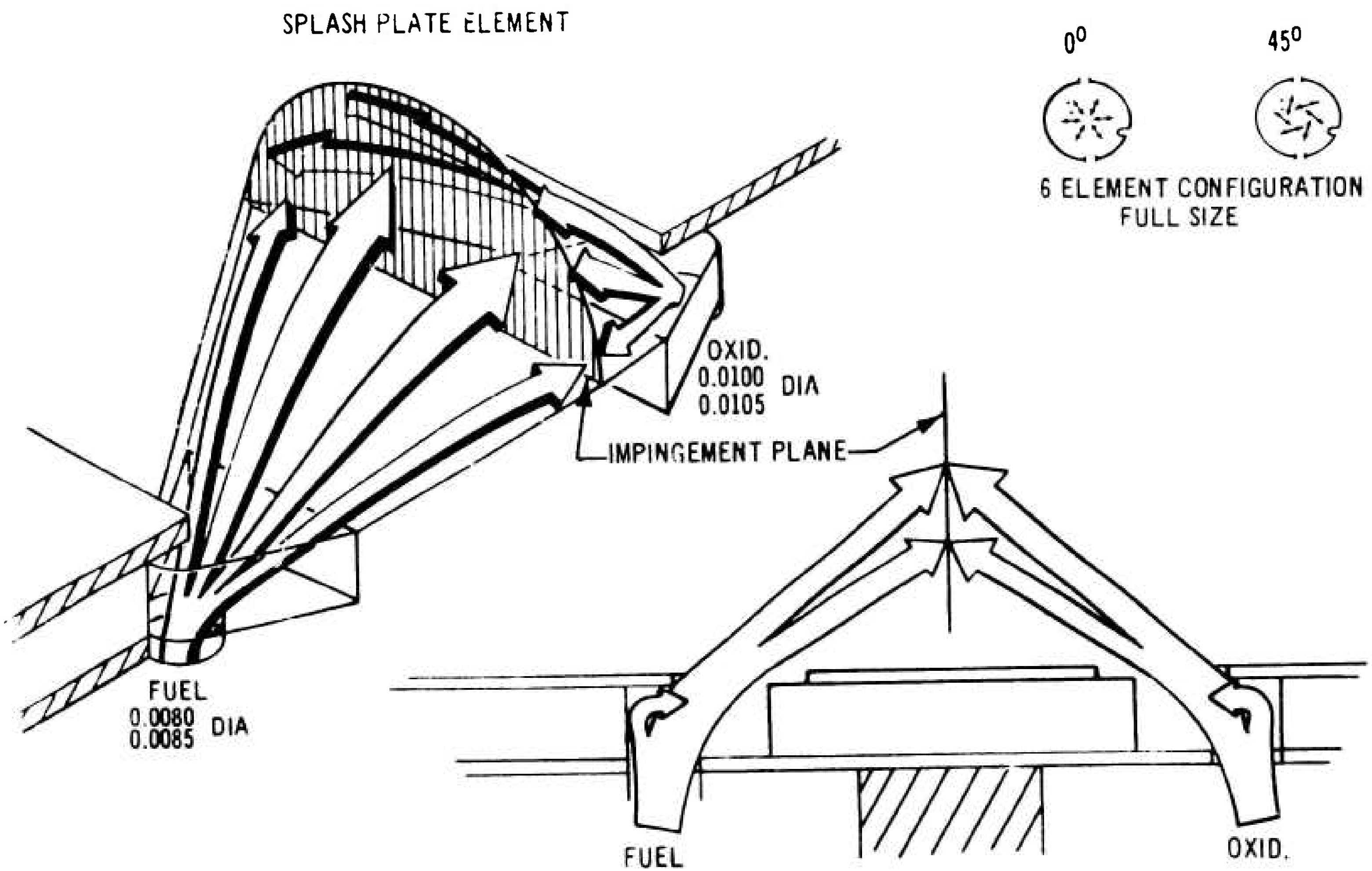

Figure 5.1-9. 5 lb Thrust Bipropellant Engine Injector Element

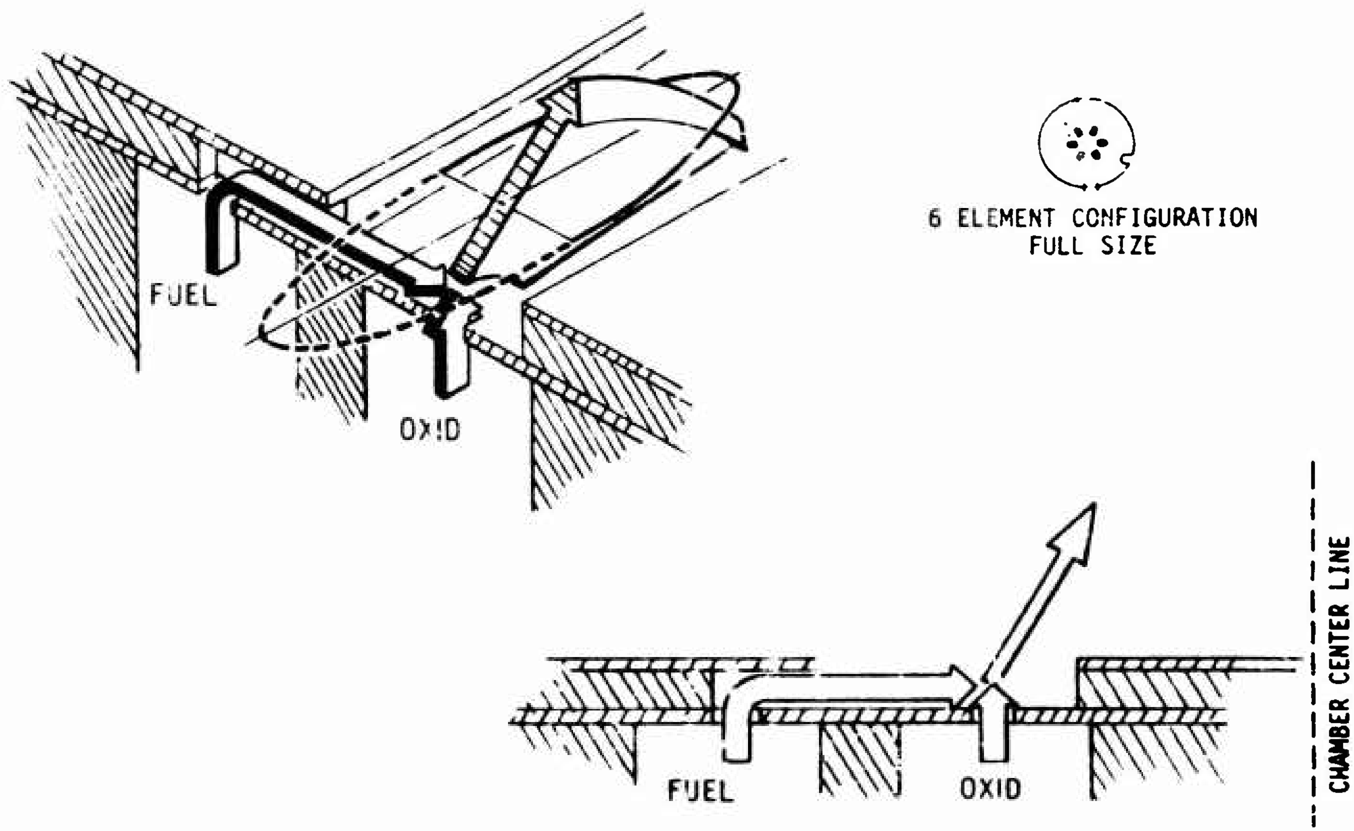

Figure 5.1-10. Unlike Doublet Element Configuration

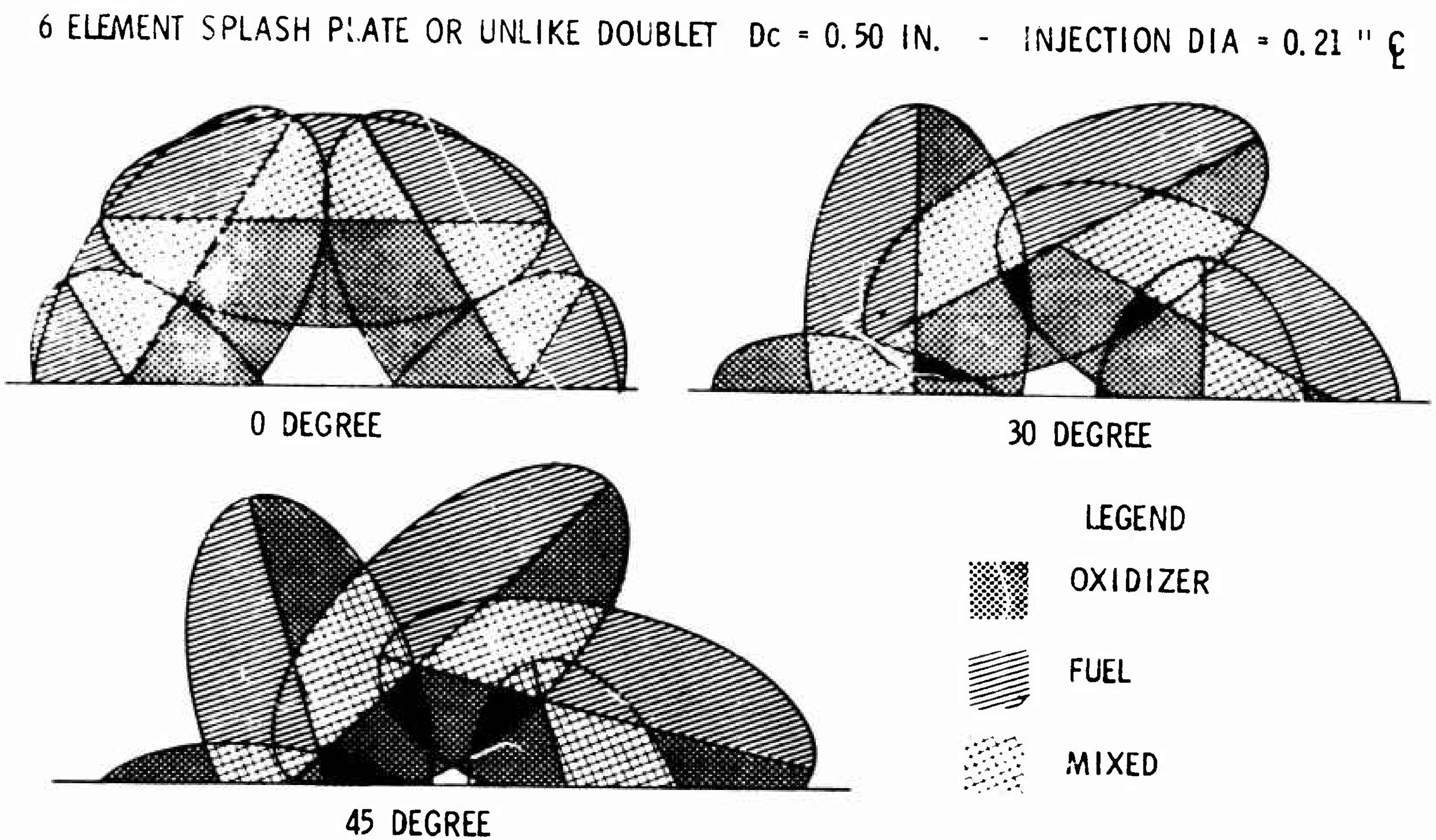

Figure 5.1-11. Wall MR Control by Element Orientation

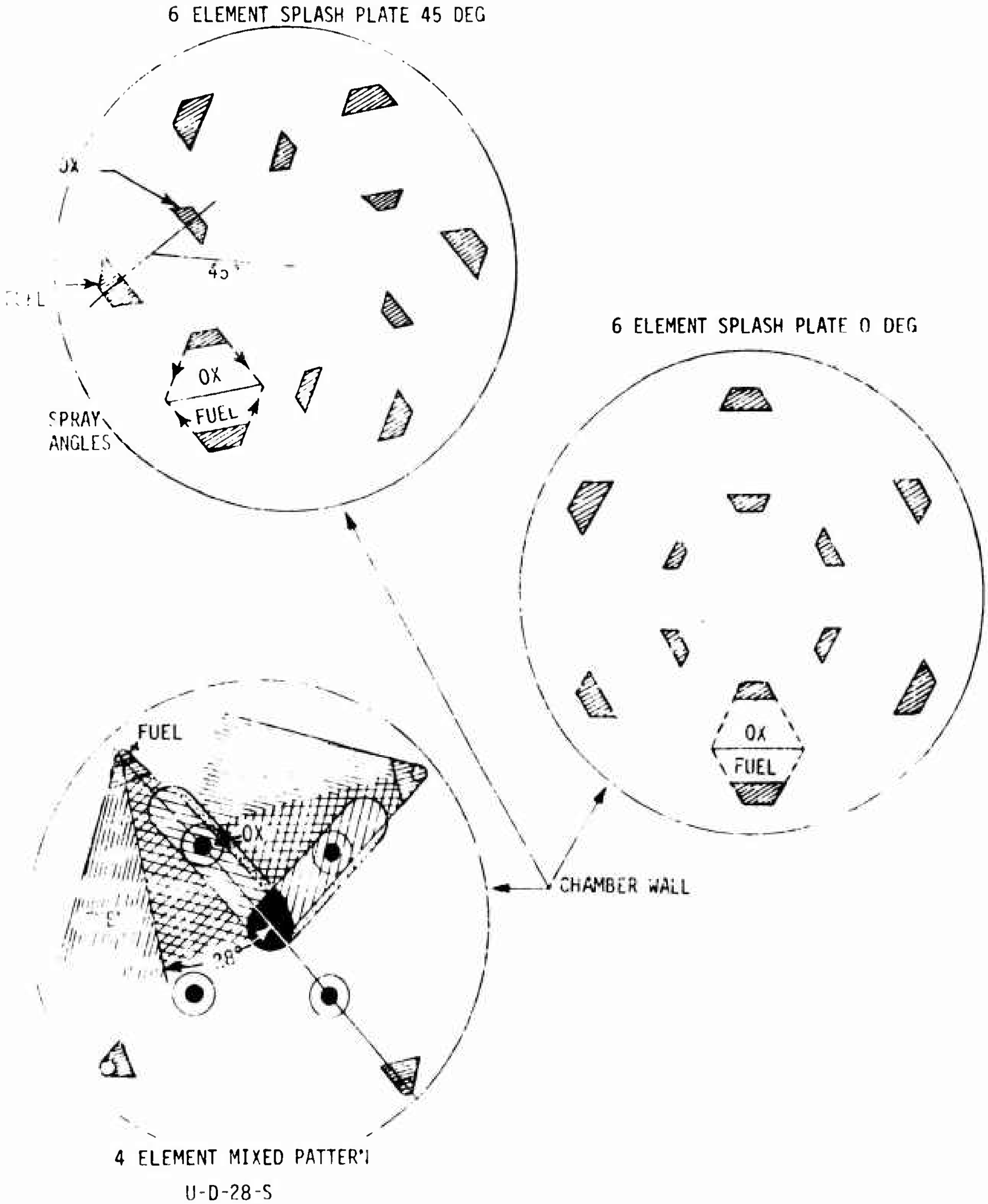

Figure 5.1-12. Injection Element Configuration

at the periphery to provide a fuel rich environment at the chamber wall as shown in Figure 5.1-11. The shading in Figure 5.1-11 indicates the expected fuel rich, mixed and oxidizer rich zones. The very black zones represent regions of highest unreacted oxidizer concentration. The 0 degree pattern was projected to provide the most fuel rich environment at the wall and thus to be the most compatible design; the 45 degree pattern the most well mixed and thus highest performing. Test data showed both pattern arrangements to be very high performing with little difference in compatibility.

Several mixed element pattern designs (4-UD-28 series shown in Figure 5.1-12) were subsequently configured in which approximately 25% of the fuel was directed around the oxidizer fan and towards the wall, in a swirling manner, to provide a higher degree of barrier cooling. The two versions of this pattern had designations based on the angle of the fuel spray relative to the plane of the injector face. A shallow angle (30°) resulted in a short impingement length "S" and a larger angle (50°) design designated "SL" resulted in moving both the bipropellant and the fuel wall impingement distances away from the injector face.

5.1.2.1.3 Manifolding

The two manifolding techniques shown in Figure 5.1-13 were evaluated. In the first, propellants were transferred from a side by side position at the valve seats as (Ref. Figure 5.1-14) to central redistribution plenums at two levels within the injector. Each injection orifice was then supplied from this central source by an equal length leg providing uniform propellant heating paths as well as flow resistance. Over 50% of the injector pressure drop was taken in the manifold "legs" to provide face cooling, low volume, and good distribution. The design shown in Figure 5.1-13 places the oxidizer nearest the heated face. Designs which reversed the levels of fuel and oxidizer manifolds were also evaluated. These were rejected because of their larger oxidizer manifold volume and more complex fuel distribution system.

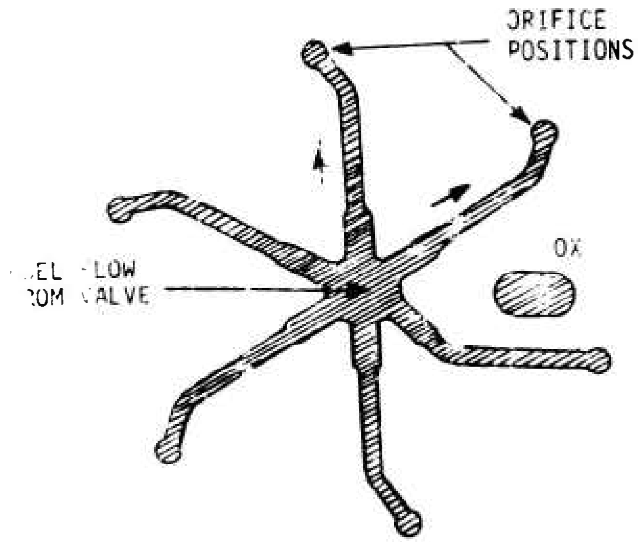

6 ELEMENT

AXISYMMETRIC RADIAL OUT-FLOW MANIFOLD
TYPE A

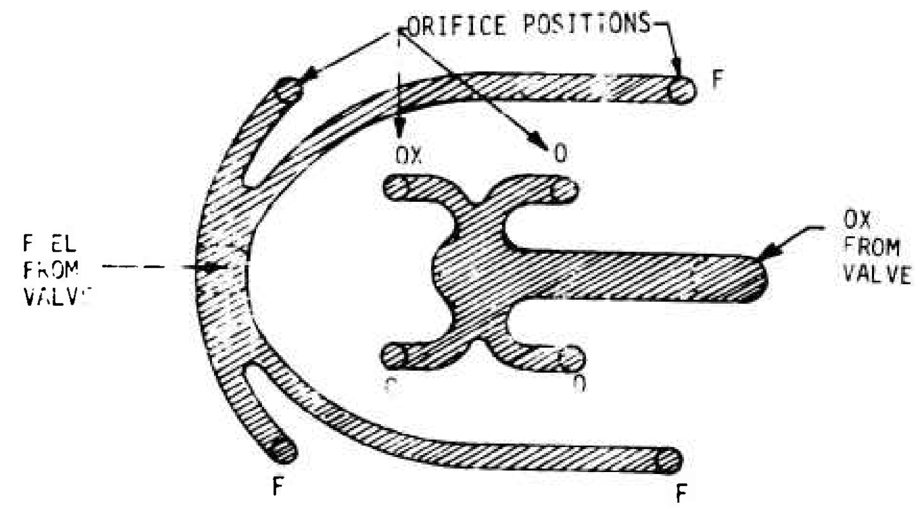

4 ELEMENT

DIRECT PATH
TYPE D

Figure 5.1-13. Manifolding Techniques

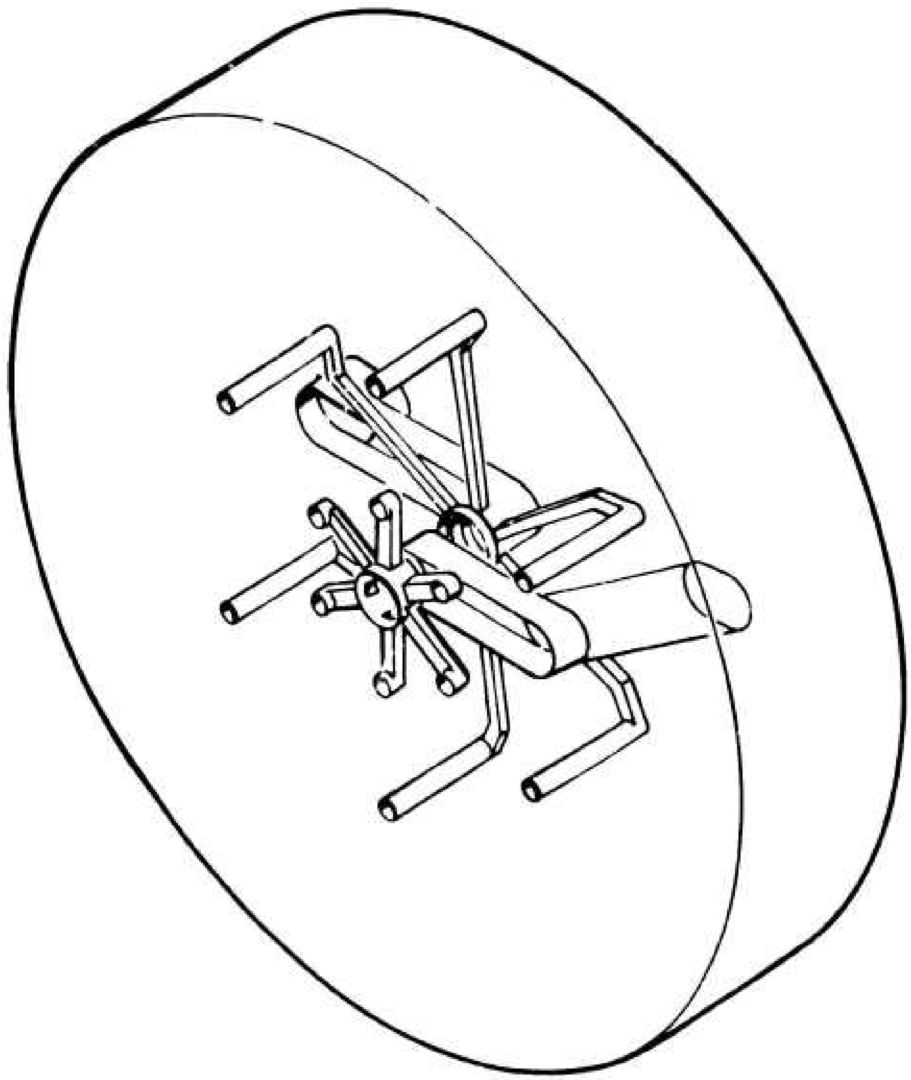

Figure 5.1-14. 6-SP Series Injector Manifold Schematic

5.1.2, Injector (cont.)

The second manifolding scheme shown in Figure 5.1-13 had direct paths from the valve inlet locations to the injection orifices. Both propellants are transported in a common plane by the shortest practical route. This shortens the flow paths and simplifies the design and number of levels of stacking. However; in order to insure uniform flow distribution, manifolds were more conservatively designed (lower velocity) and flow regulators and heat dams installed to balance the longer and shorter paths.

5.1.2.1.4 Injector Assemblies

The injector nomenclatures (e.g., 6-SP-45-A) used related to configuration and generation as follows:

6 - Number of elements

SP - Splash plate type element and corresponding manifold

45 - Rotational position of pattern

A - first modification

The following detailed designs were prepared in the first injector design iteration.

Splash plates with the following element quantity and orientation:

6 elements, fans parallel to the chamber wall	6-SP-0
4 elements, fan parallel to the chamber wall	4-SP-0
6 elements, fans 20 degrees to the chamber wall	6-SP-20
6 elements, fans 45 degrees to the chamber wall	6-SP-45

5.1.2, Injector (cont.)

Doublet elements with the following element quantity and orientations:

6 elements, fans parallel to the chamber wall	6-UD-0
4 elements, fans parallel to the chamber wall	4-UD-0
6 elements, fans 20 degrees to the chamber wall	6-UD-20
6 elements, fans 45 degrees to the chamber wall	6-UD-45

Triplet FOF elements with the following element orientations:

4 elements, fans parallel to the wall (unbalanced)	4-UT-0

All injector designs are summarized in Table 5.1-1. Each was configured to provide a nominal 130 psid at the design flow rate. The 6-SP-45 manifolding was redesigned following cold flow to improve the flow distribution. The modified design was designated 6-SP-45-A. The design modification involved reducing primary cross flow manifold velocities, increasing velocities in the legs feeding the individual orifices and general improvement of entrance and turn configurations. The computed residual volume for each of the designs is provided in Table 5.1-1, along with the injection orifice dimensions and minimum passage sizes. The 4-UT-0 design was not considered because of its large fuel volume. The 6-UD-0 design was rejected following cold flow in favor of 4-UD-0 due to its less than optimum flow distribution, and the undesirability of the 0.004 in. orifice dimension.

The second generation Phase II injector designs indicated in Table 5.1-1 were completed following cold flow and hot fire testing of the 6-SP-0 and 6-SP-45 A units. The second generation designs were directed towards improved compatibility (the first design fire tested exceeded the 300 sec steady state specific impulse goal at full thrust) and

TABLE 5.1-1

SUMMARY OF INJECTOR DESIGNS

Designation	10^{-4} in.^{3} Volume F/O	Manifold Passage Size (in.) F/O	Orifice Passage F/O		No. Platelets	Impingement Length F/O	Quantity Fabricated	Valve** Manifold	Injector Manifold*** Type
*6-SP-0	.14/3.10	0.008/0.010	0.008 x 0.012	0.006/0. 12	13	Short/Short	6	1	A
6-SP-45	.14/3.24	0.008/0.010	0.008 x 0.012	0.006/0. 12	13	Short/Short	5	1	A
6-UD 0	.04/3.65	0.004 x 0.008/0.009	0.004 x 0.009	0.006 x 0.012	1[illegible]	0	[illegible]	1	A
4 LT (	4.87/3.2[illegible]	0.004 x 0.006/0.012	0.004 x 0.006	0.0[illegible] x 0.012	13	C	0	1	D
*6-SP-45A	3.39/3.86	0.008/0.010	0.005 x 0.010	0.0[illegible] x 0.012	15	Short/Short	6	1	A
Second Generation									
6-S[illegible] B-1	3.39/3.86	0.008/0.009	.005 x 0.010	0.006 x [illegible]012	18	Long/Short	2	1	A
B-2	3.39/3.86	0.008/0.010	0.005 x 0.010	0.006 x 0.012	1[illegible]	Long/Short	2	1	A
B-3	3.39/3.86	0.00[illegible]/0.010	0.005 x 0.010	0. 6 x 0.012	1[illegible]	Long/Long	[illegible]	1	A
*4 UDO	2.93/3.4[illegible]	0.005 x 0.009/0.010	0.005 x 0.009	0.006 x 0.015	[illegible]	0/Axial	6	2	[illegible]
4 UDA	2.93/3.4[illegible]	0.005/0.010	0.006 x 0.014	0.[illegible] x 0.01[illegible]		Axial/Axial	[illegible]	2	[illegible]
*4 [illegible] 28 S	.93/3.76 .93/3.46	0.008/0.010	0.006 x 0.014	0.006 x 0.015		Short/Axial	[illegible] 0	1 2	D
*4 OD 28 S	2.93/3.46	0.008/0.010	0.006 x 0.014	0.006 x 0.01		Long/Axial	3	2	D
Total Fabricated							[illegible]		

*

**

	Valve Manifold Vol in^3 F	O
1 - 1st Generation	0.0001[illegible]	0.0002174
2 - 2nd Generation	0.0001[illegible]	0.0001883

(Ref. Figure 5.1-7)

***Ref. Figure [illegible]1-[illegible]

improved performance at lower flow rates for blowdown mode operation. The attempt to improve compatibility was made by (1) increasing the oxidizer injection angle from 20 to 50 degrees thus increasing the impingement distance and moving the oxidizer fan away from the wall and (2) employing the mixed element patterns shown in Figure 5.1-12. Design improvement for blowdown mode performance resulted in increased injection velocities via a reduction in the quantity of elements from 6 to 4 and/or reduction in orifice diameter.

5.1.2.2 Injector Fabrication

All injector components were fabricated in sets of 6, as shown in Figure 5.1-15, from 304 stainless steel, using ALRC's standard photo-etching methods and specifications. Each component was inspected as follows: the platelet thickness was measured with a micrometer and the results recorded to 1/10,000 in. These measurements were within 0.0002 in. of specific values. Significant etched dimensions such as manifold widths or diameters were measured by an optical comparator having a digital readout accurate to ± 0.001 in. Critical dimensions such as flow controlling passages and injection orifices were measured using a calibrated tool makers microscope and dimensions recorded by the project engineer to 1/10,000 in.

Following inspection, the individual platelets were stacked on a bonding fixture using the 3 alignment holes shown in Figure 5.1-15 to maintain position. Each plate contains a code number which is compared with a stacking sequence check list. The project engineer verified that the sequence was correct for each injector set fabricated on the program.

In most cases multiple designs were fabricated simultaneously. Small modifications such as the change of orifice diameters are achieved by altering the master negative for one or more of the 6 units in the frame. This was done for the 6-SP-45-B-1, -2 and -3 (2 each) and

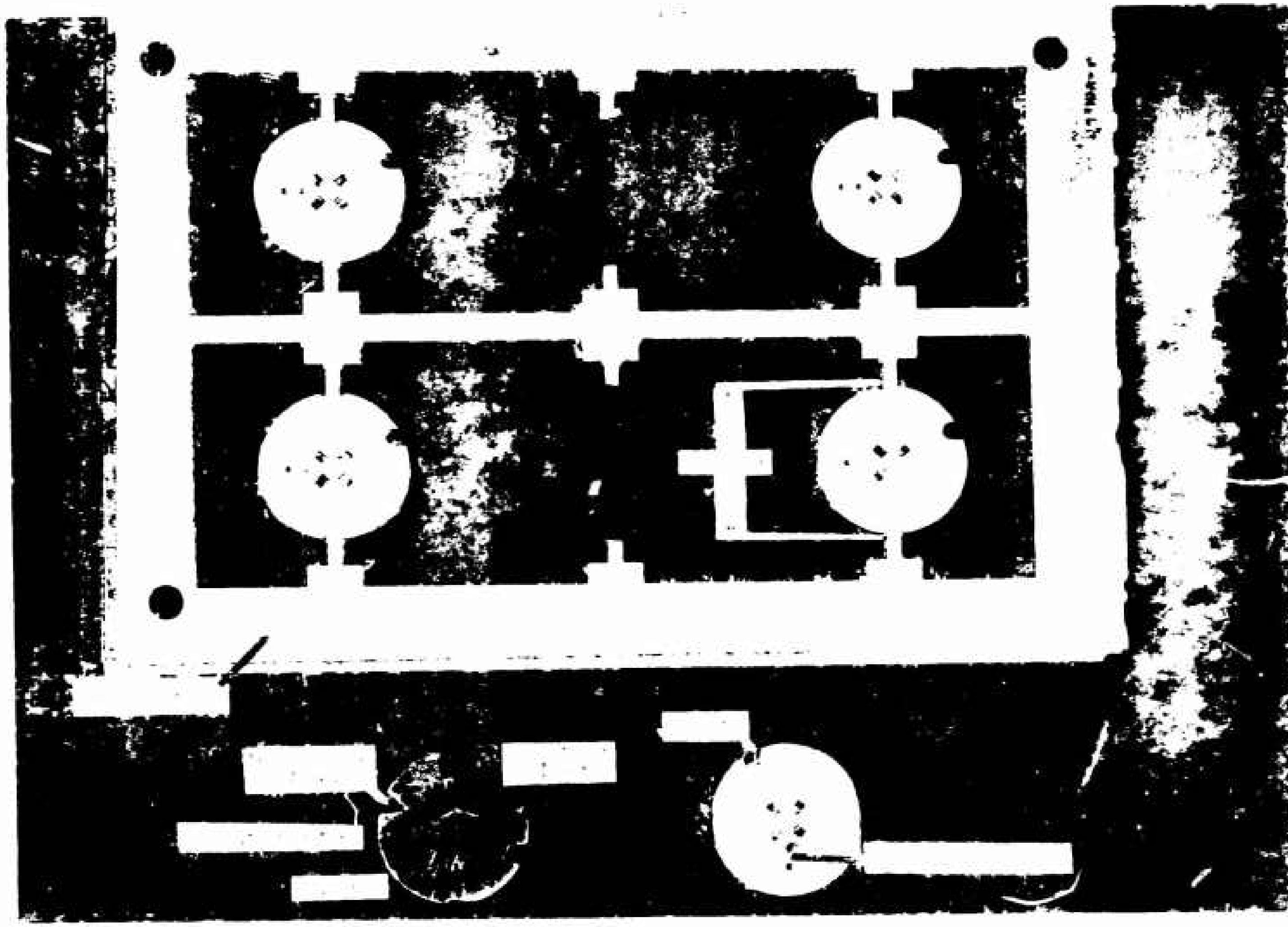

Figure [illegible] Fabric[illegible] x [illegible]

4-UD-28-S and -SL (3 each) injector series. Two or more completely different injector sets were bonded in each operation by placing a specially prepared separator over the top platelet of the assembly and stacking the second and third injector sets series with the first. The injectors are assembled using standard ALRC diffusion bonding schedules for stainless steel materials.

Following the bonding operation, selected injectors are cut from the frame identified by a S/N, and pattern checked. Inspections are made for pressure drop reproducibility, flow maldistribution due either to improper manifold design or plugging, and also for interpropellant leakage using GN_2. The cold flow procedures are described in the following section. In production, one or more of the injectors from each frame could be subjected to destructive testing to assess the quality of the bond of the remaining units in each set.

Injector designs selected as having the most favorable spray and uniform flow pattern were subsequently brazed into the valve manifold as shown in Figures 5.1-8 and 5.1-16. The injectors preceded by a * in Table 5.1-1 are those selected for integration with the valve manifolds. The injector P_c port provided the index to align the propellant manifolds on the two components.

Installation of the fitting for the through-the-face P_c measurement and thermocouples for injector face temperature measurements were accomplished at this point in fabrication. Each injector design incorporated passages for two 0.020 in. dia thermocouples.

Each integrated injector-valve manifold assembly was again cold flow and leak checked with water and GN_2 following this final assembly operation. As indicated in Table 5.1-1, a total of 48 injectors representing 13 design variations were built through Phase II of the program. Of these, five were selected for integration into the valve manifold and hot

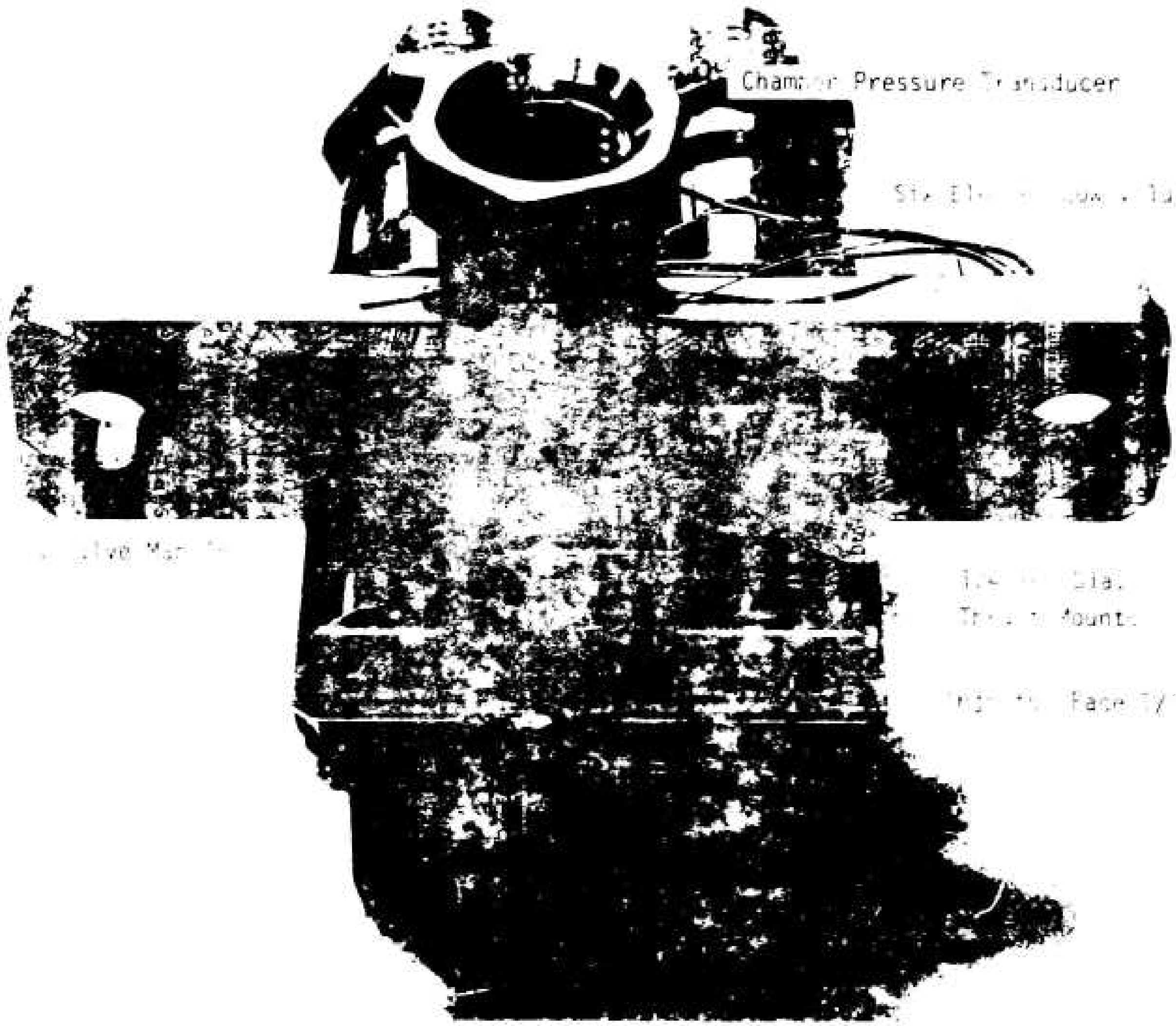

Figure [illegible] Manifold

5.1.2, Injector (cont.)

fire testing. No significant fabrication difficulties were encountered in the program.

5.1.3 Thrust Chamber Design and Fabrication

5.1.3.1 Design

Phase II thrust chambers were designed, on the basis of Phase I analyses, for a nominal 5 lbF thrust at a chamber pressure of 170 psia with an assumed 97% energy release efficiency. The minimum chamber length considered was 2 in. Spacer designs were prepared to extend the injector to throat length from 2 in. to 2-3/4 and 4 in. Detailed drawings are provided in Figures 5.1-17 and 5.1-18. A 50:1 nozzle area ratio was selected for the altitude verification tests based on the need for testing at pressures down to 75 psia without nozzle flow separation. The estimated separation pressure was 0.64 psia compared to a facility capability of ≈ 0.3 psia for firings up to approximately 15 minutes and 0.5 - 1.0 psia for unlimited duration.

The Rao nozzle contour selected for the 50:1 area ratio verification tests was based on matching the optimum 34 degree initial divergence angle of a 125% minimum length 100:1 expansion nozzle which had a 99.56% divergence efficiency. The matched expansion angle was required in order to properly simulate the throat region thermal characteristics. The use of the 125% length nozzle design provides an additional 2 sec of specific impulse at 100:1 while the Rao contour provides a 6 sec margin over a 20 degree half angle conical nozzle of the same length. The 50:1 nozzle results in the engine having an approximately 7 sec lower specific impulse than can be realized with the 100:1 expansion ratio.

Two upstream and two external chamber contours were selected for evaluation. One was considered to be superior for barrier cooling and buried operation with the second more desirable for radiation cooling.

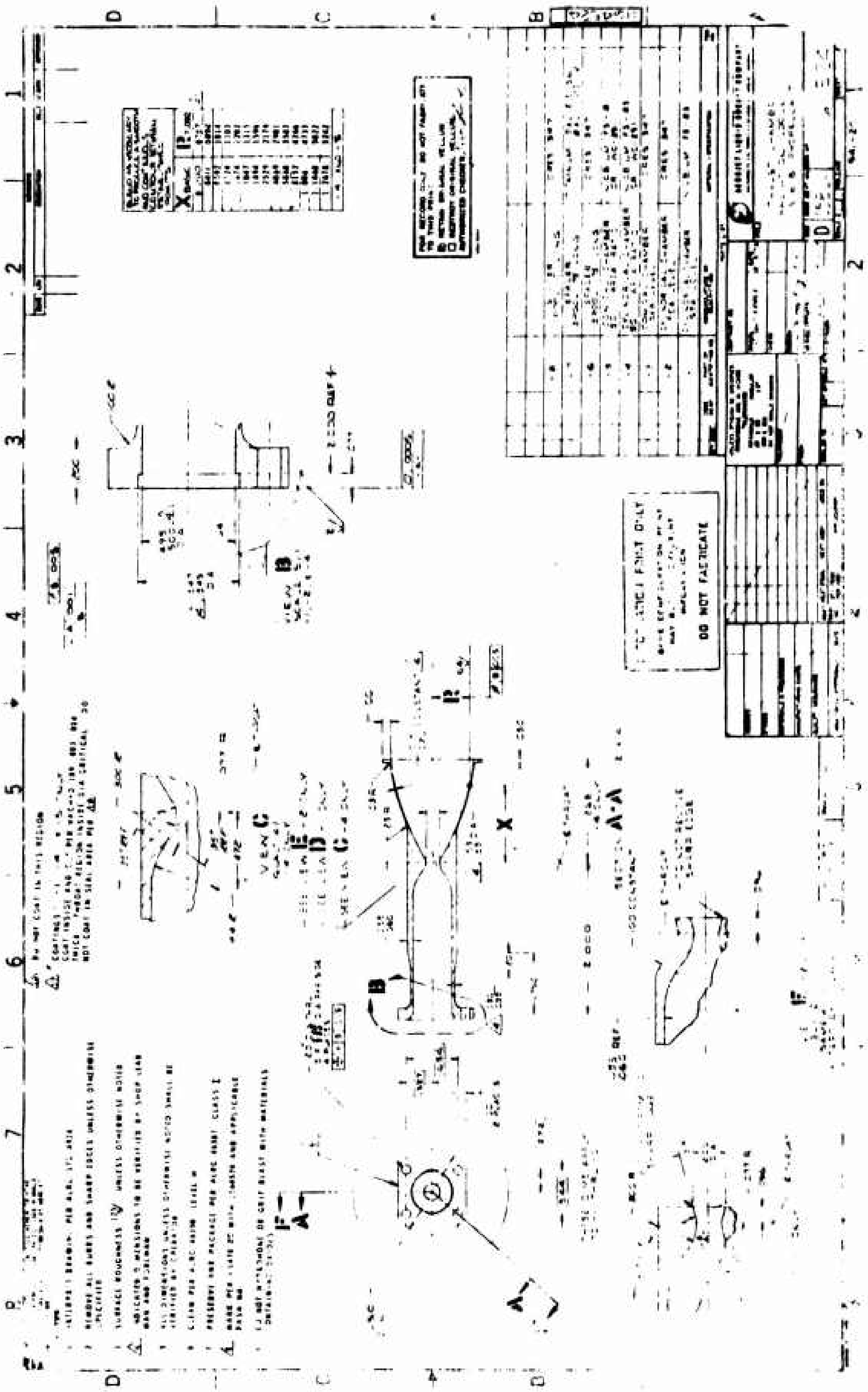

Figure 5.1.17. Detailed Drawing, Radiation Cooled Thrust Chamber

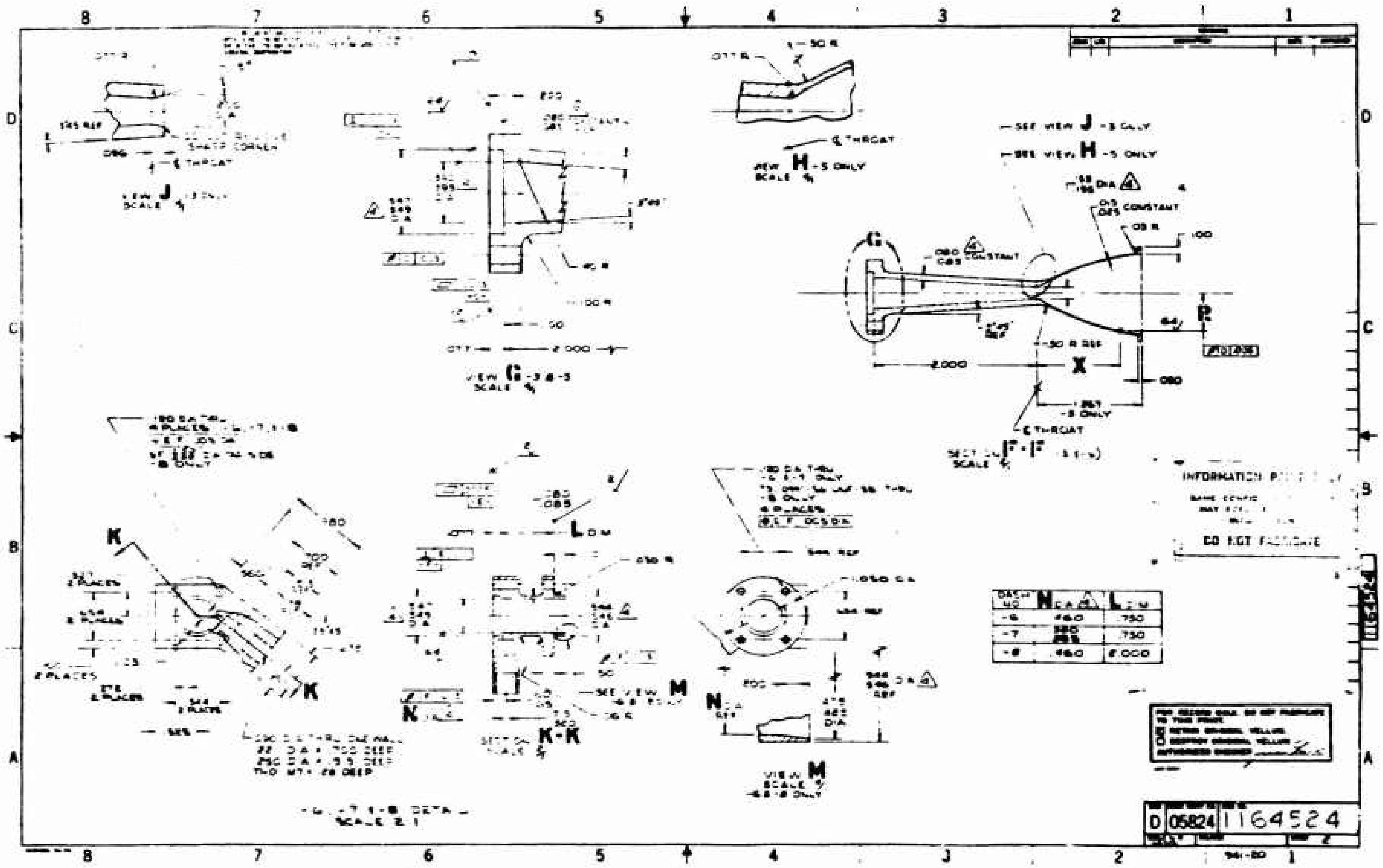

Figure 5.1-18. Detailed Drawing, Radiation Cooled Thrust Chamber

5.1.3. Design (cont.)

The external wall contour for the barrier cooled buried design resulted in a thin wall conical configuration, (Reference dash 5 design in Figure 5.1-17). The thin wall minimized the chamber mass and thus the stored energy which could soak to the valve following a long burn. The conical shape was expected to improve the effectiveness of the barrier cooling by eliminating mixing losses normally associated with turning of a gas stream. The weight of this chamber was 0.14 lb.

The radiation cooled chamber (Reference dash 4 design in Figure 5.1-17) provided a thick wall at the throat. As indicated in Figure 4.2.7 of the Phase I analyses this maximizes the heat rejection capabilities via radiation relative to the convective heat input. A very thin wall (0.030 in.) at the forward end restricted heat flow to the flange region. The internal contour was selected to minimize the convective heat load based on the analytical procedures of References 13 and 14. The cylindrical external contour was influenced by the wall thickness optimization and fabrication considerations. The aft flange on the 0.020 in. wall divergent nozzle provided structural rigidity and facilitated handling. This configuration weighed 0.173 lb when fabricated from FS 85 material.

The forward flange of all designs was configured to mate with the valve manifold using four NAS 1351-03-10 screws as shown schematically in Figure 5.1-19. Sealing was accomplished by use of a gold plated Inconel V type seal (HVG 2-11). The V seal compression was regulated by the copper and stainless steel spacers shown in Figure 5.1-20 which also acted as a thermal shunt and heat dam to move the heat rejected from the engine

(13) L. H. Back, A. B. Witte, Prediction of Heat Transfer from Laminar Boundary Layers, with Emphasis on Large Free Stream Velocity Gradients and Highly Cooled Walls, J. of Heat Transfer, August 1965.
(14) L. Schoenman, J. Block, Laminar Boundary Heat Transfer in Low Thrust Rocket Nozzles, J. Spacecraft and Rockets, September 1968.

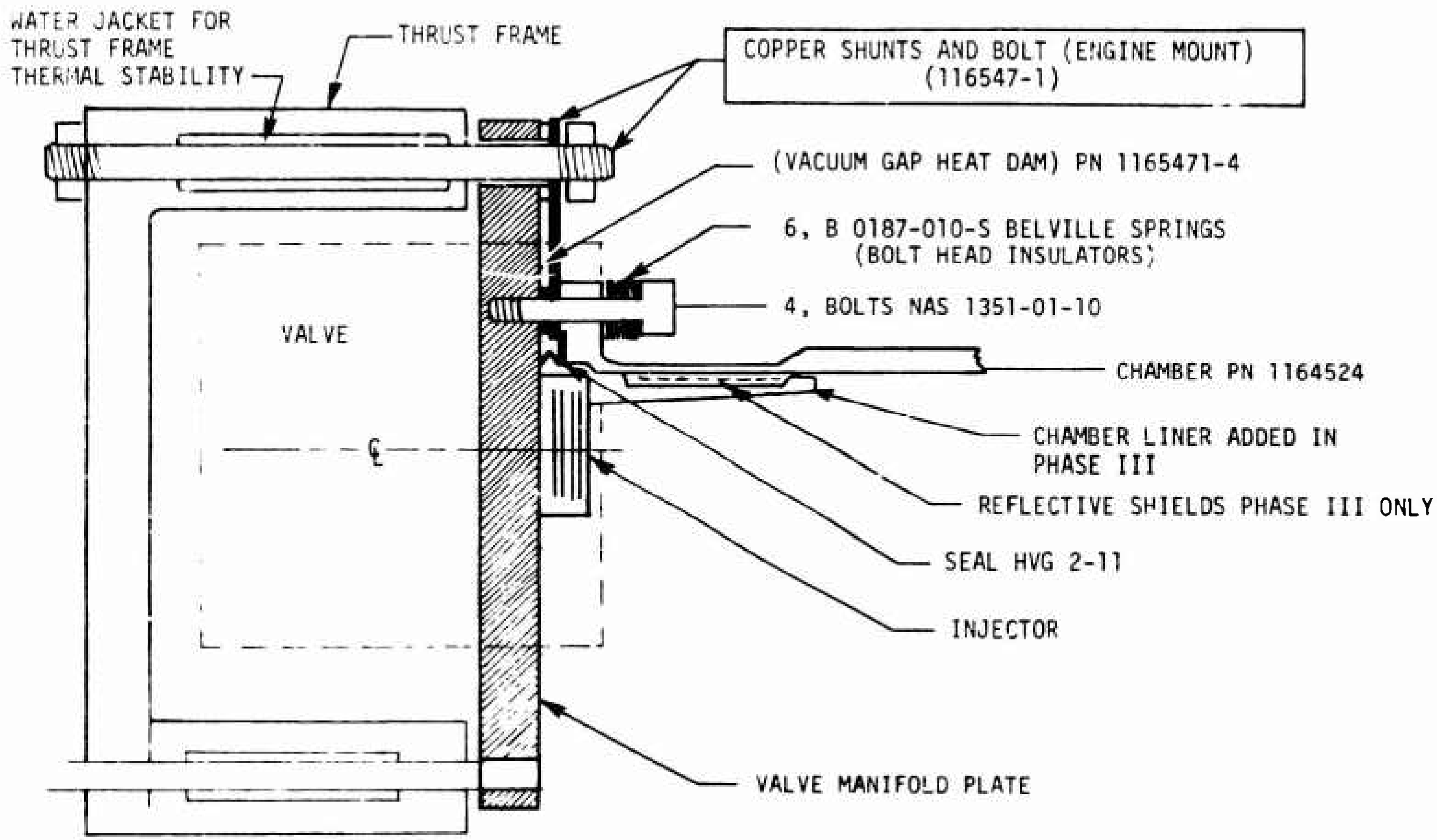

Figure 5.1-19. Flange, Thrust Mount and Heat Dams Schematic

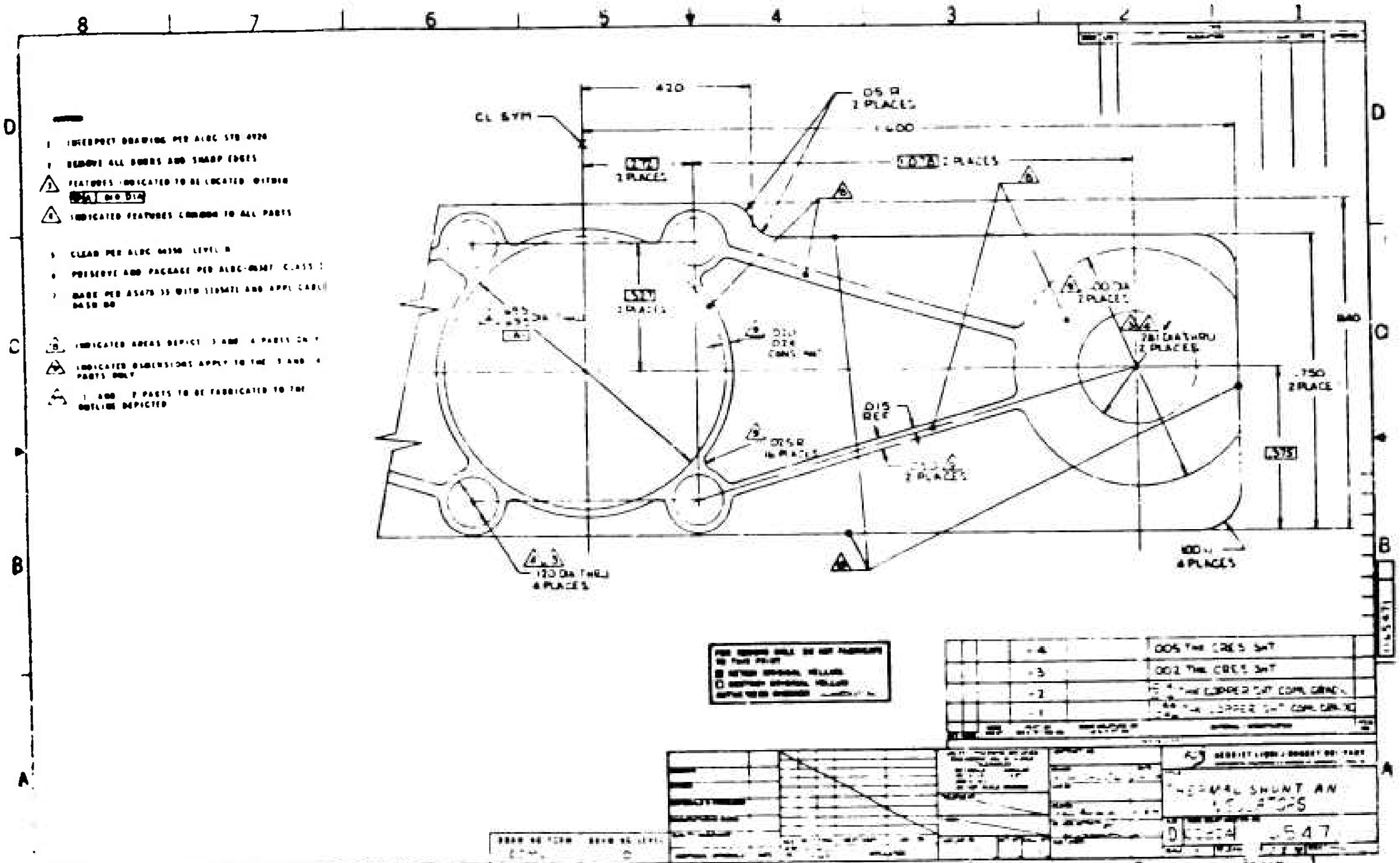

Figure 5.1(c) Thermal Shunt and Insulators Drawing

5.1.3, Design (cont.)

around the injector ard valve. The bolt heads were also insulated from the chamber flange by six stainless steel belleville spring washers in a 3-nested 2-series configuration as shown in Figure 5.1-19.

Other chamber components designed for Phase II testing included 15 degree half angle exit nozzle thrust chambers for sea level checkout testing and 3/4 inch and 2 inch long cylindrical spacers which interface with the valve manifold on one end and the thrust chamber on the other. These spacers incorporated a port for a Kistler 601 AL transducer to monitor response and ignition spikes.

5.1.3.2 Chamber Fabrication

Nine chamber components were fabricated as indicated in Table 5.1-2. Eight of the components were built to the dimensions shown in Figures 5.1-17 and 5.1-18. The -9 chamber, having a 1-1/4 in. injector-to-throat length and integral kistler port, was assembled by rework of the -2 chamber and -8 extension after testing on those components had been completed.

The -1, -4, -5 and -5A columbium chamber/nozzle components were fabricated from WC 291 and FS 85 alloys based on the results of Phase I studies. Some 291 material was employed because of faster delivery schedules.

Final machining of the OD and ID of the 50:1 divergent nozzles was accomplished on a tracer lathe using a nozzle contour template formed to the X, R dimensions in Figure 5.1-17. The upstream nozzle contour and throat for the conical design were final machined with a tapered ream. A special form tool having a larger radius of curvature in the convergent nozzle and throat was used for the cylindrical chamber. The only manufacturing problems encountered were those of holding the very tight throat dimension on the first of the fabricated parts. This resulted in a 0.011 inch over size throat on the -5A part. A second -5 part manufactured as a replacement was to tolerance.

TABLE 5.1-2

DESCRIPTION OF NOZZLES AND SPACERS FABRICATED

PN 1164524		Material	Approximate No. of Restarts
-1	Sea Level Radiation Cooled (Cylindrical)	Cb WC 291	60
-2*	Sea Level (cylindrical) 2 in. L'	CRES 347	0
-3	Sea Level (conical) 2 ft L'	CRES 347	6
-4	50:1 Radiation Cooled (cylindrical)	Cb WC 291	1400
-5	50:1 Barrier Cooled (conical VacHyd 101 Coating	Cb FS-85	800
-5A	50:1 Barrier Cooled (conical) Hitemco R512E	Cb FS-85	0
-6	2/4 in. L' Extension Large ID	CRES 347	800
-7	/34 in. L' Extension Small ID	Titanium 6 Al-4V	800
-7A	3/4 in. L' Extension Small ID	Titanium	0
-8*	2 in. L' Extension Large ID	CRES 347	10
-9*	1-1/4 L' nozzle made from -2 and -8	CRES 347	2100
Total number of chamber parts = 11			
		Approximate Total Starts	4360

* -9 made from -2 and -8.

5.1.3, Design (cont.)

Oxidation resistant silicide coatings were applied via the VacHyd 101 and HiTemco R512E processes to the components indicated in Table 5.1-2. Both processes require a 1 hour vacuum diffusion cycle at 2550°F. The VacHyd process requires two coating applications with a 1/2 hour furnace cycle following each application. The R 512E process is accomplished in one step. The internal dimensions on the thrust chambers were selected to allow a 0.003 inch radius reduction due to coating application. The actual throat inside-diameter dimensions before and after coating are provided in the following table.

SUMMARY OF THROAT DIMENSIONS
Inside Diameter

Part No.	-1	-4	-5	-5A
Coating	VH 101	VH 101	VH 101	RS12E
Precoated	0.157	0.158	0.152	0.165
Postcoating	0.151	0.151	0.146	0.159
Dia Change	0.006	0.007	0.006	0.006

Figure 5.1-21 shows the -4 and -5 chambers after final machining and prior to coating. Figure 5.1-22 shows the inside of the nozzle after coating as follows; left FS 85/VH 101, right VC, 291/VH 101, and center FS 85/R512E. The photographs of left and right were prefire, the center was following 50,000 pulses. There was no noticeable change in surface finish as a result of the firing. The VacHyd process resulted in a large glass-like fractured crystal structure which was more pronounced on the 291 material than on the FS 85 alloy. The R512E coating had the appearance of fine grain gray sand. A subsequent recoating of the FS 85 nozzle by VacHyd following Phase II testing resulted in chamber having an appearance similar to the 512E processed unit. The VacHyd coated Phase III chambers also had the same appearance as the 512E coating.

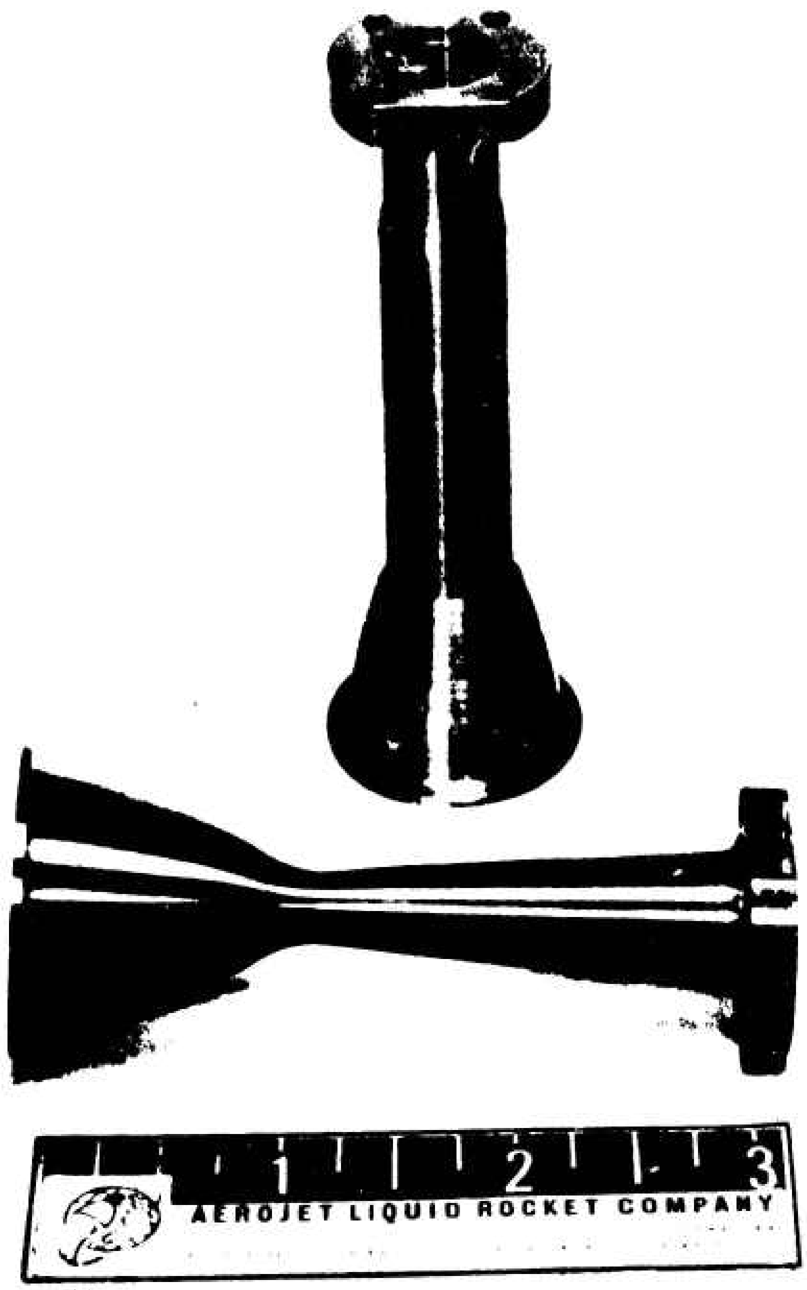

Figure 5.1-21. 50:1 Area Ratio Columbium Thrusters

F585/VH101 WC291/VH101

Figure 5.1-22 Thrust Chamber after Final Machining and Silicide Coating

5.1.3, Design (cont.)

Other sea level checkout chambers were built from CRES 347. Spacers were built from CRES 347 and 6 Al-4V titanium to evaluate the suitability and compatibility of these materials as heat dams between the hot nozzle and the valve.

5.2 VERIFICATION TESTING

This task consisted of valve bench testing, injector cold flow testing and hot fire testing.

5.2.1 Valve Bench Testing

Moog, Inc. valve assembly P/N 010-72049, S/N 001 was received with manifold S/N 01 and 6-SP-0 injector which was earlier installed by ALRC. This assembly had been subjected to acceptance tests, Table 5.2-1, by the valve supplier prior to shipment.

Additional testing was performed in Bay 4 of the ALRC Research Physics Laboratory using the test set-up, shown schematically on Figure 5.2-1. The primary tests and objectives were as follows:

Test	Objective
Proof	Demonstrate structural integrity
Leak	Demonstrate conformance to requirements
Response	Demonstrate conformance to requirements
Flow	Establish flow characteristics of integrated assembly
Response Sensitivity	Determine effects of pressure voltage and energization time on response
Manifold Change	Determine whether manifolds can be successfully changed and seals reused
Electrical Characteristics	Determine current drain, pull-in and drop-out voltages

TABLE 5.2-1

ACCEPTANCE TEST DATA SHEET

MODEL 52E163 DATE 9-7-73

SERIAL NO. 001

1.	Proof pressure, 1000 psi 3 min	OK	
2.	Pull in current	300 psi	500 psi
		99 ma	105 ma
3.	Drop out current at 25 psi	64 ma	
4.	Response time (see attached curves)		
5.	Internal leakage (total) at	25 psi	0.0 cc/hr
		300 psi	0.0 cc/hr
		500 psi	0.0 cc/hr
6.	Insulation resistance at 500 vdc		>300,000 megohms
7.	Dielectric strength at 500 vdc		<2.0 μ amps
8.	Coil resistance		52.0 Ω
9.	Unit weight		0.975 lb

E. Smith 9-7-73

Inlet Pressure psig	Voltage, VDC	Response time, millisec Open	Close
300	20	4.1	2.6
500	20	4.3	2.6
300	24	3.4	2.7
500	24	3.5	2.7
300	28	2.9	3.0
500	28	3.1	3 0
300	32	2.6	3.3
500	32	2.8	3.3

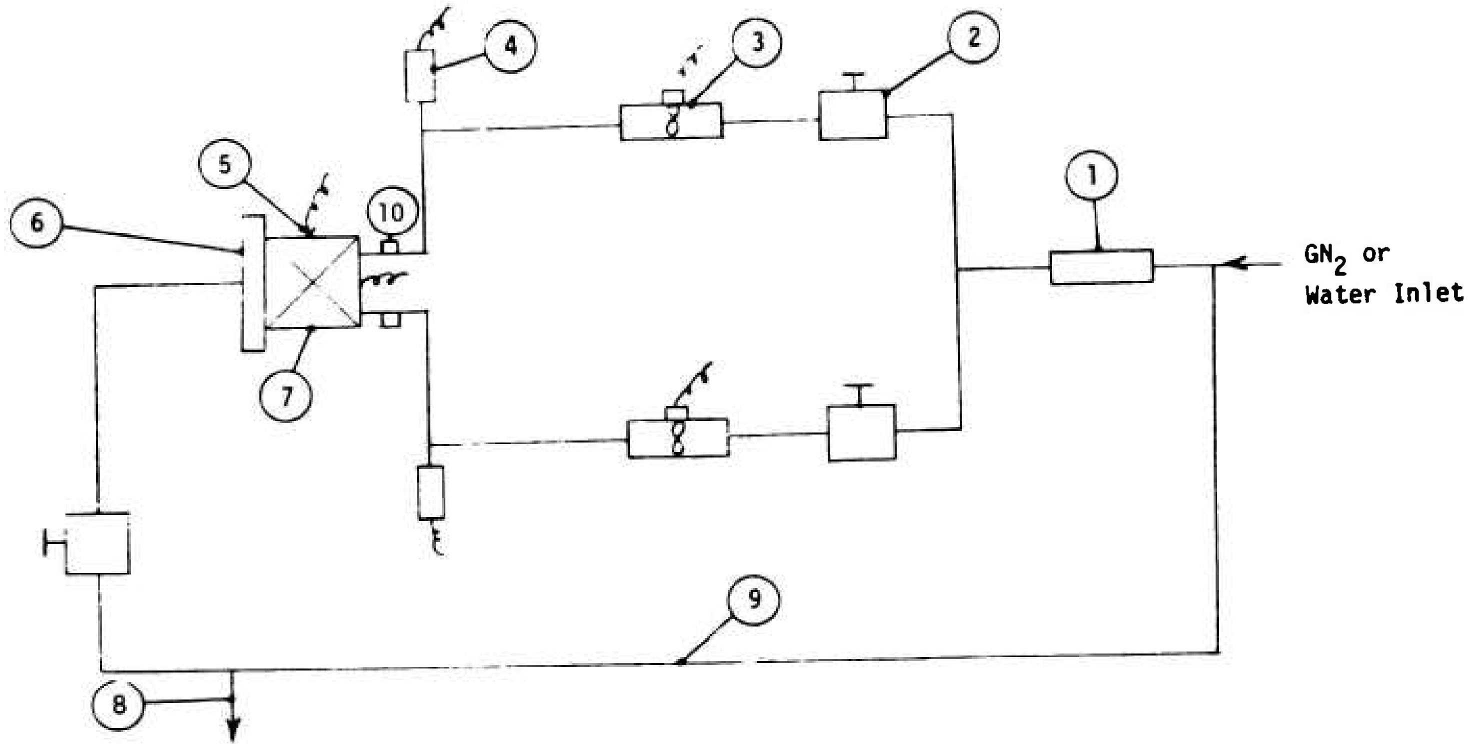

1. Filter, 5μ, Fluid Dynamics P/N 002263-0405
2. Shutoff valve, 1/4", Control Components Inc.
3. Flowmeter, Flow Technology P/N FT-1-5
4. Transducer, 500 psig, Teledyne Model 206-5A
5. Thermocouple, chromel-alumel
6. Outlet adapter
7. Test unit, Moog Model 52E163, P/N 010-72049, S/N 001
8. Vent line to atmosphere
9. Pressure line, used only for proof test
10. Kistler 601 A1 pressure transducer (added for Phase III postfire response evaluation)

Figure 5.2-1. Test Set-Up Schematic

5.2.1, Valve Bench Testing (cont.)

5.2.1.1 Proof

Inlet and outlet ports of the valve were manifolded and subjected to 750 psig GN_2 for 2 minutes. The valve was examined and there was no evidence of permanent deformation or damage.

5.2.1.2 Leak

Internal and external leak tests were performed using GN_2 at 50, 300 and 500 psig. External leakage was checked using Leaktec solution. Internal leakage was checked using the water displacement method. There was no evidence of bubble leakage, either internally or externally at any of the test pressures.

5.2.1.3 Response

The valve was operated with 23 VDC under a no flow, no inlet pressure condition. Response time from signal to full open based on the current trace was 3.38 millisec and from signal to full closed was 2.86 millisec. These times compared favorably with the vendor test data which showed times of 3.4 millisec open and 2.7 millisec closing at 24 VDC.

5.2.1.4 Flow

This flow test was performed with S/N 01 manifold installed on the valve. Demineralized water was supplied to the valve at various inlet pressures from 50 to 300 psig and the test assembly flow tested to determine the *K_w of the fuel and oxidizer circuits. The resultant K_w factors were 0.000655 for the fuel circuit and 0.000781 for the oxidizer circuit. This compares with 0.00651 and 0.000763 for the fuel and oxidizer of the injector prior to being installed in the valve.

$$*K = \frac{\dot{w}}{\sqrt{\Delta P\ s.g.}}$$

5.2.1, Valve Bench Testing (cont.)

5.2.1.5 Response Sensitivity

With the test valve in the flow test setup, the flow rate was adjusted to obtain a flow approximately equivalent to nominal propellant flow with an inlet pressure of 300 psig. The valve was then functioned 3 cycles under varied conditions to evaluate the effects of inlet pressure, voltage and energization time on valve response. These tests were all performed without any back EMF suppression in the electrical circuit.

Table 5.2-2 presents the results of these tests. The valve response is insensitive to inlet pressure up to 300 psig where the opening response, again based on the current trace, is about 3 millisec. At 500 psig, the opening response increases to 3.33 millisec. Closing response appeared to be independent of the test parameters. The range of closing response times was from 2.46 to 3.20 millisec.

Voltage had some effect on opening response as expected. Opening response was 4.87 millisec at 18 VDC and got faster as voltage was increased to 32 VDC where response was 2.85 millisec. This trend is shown in Figure 5.2-2. Closing response did not show a similar trend and varied randomly from 2.27 to 2.69 millisec over the voltage range. The response band includes data from the two additional valves bench tested in Phase III. These are consistent within $\pm$ 0.00035 sec.

Energization frequency and duration did not have a significant affect on either opening or closing response. The tests covered a range of valve energization times at 28 VDC from 1 to 240 sec. The response time ranges were from 3.03 to 3.31 millisec for opening and 2.56 to 3.2 for closing. No trend was evident. During the energization time tests, the torque motor cover temperature was monitored. The greatest temperature variation noted was less than 3°F.

TABLE 5.2-2

RESPONSE TEST DATA

Inlet Pressure, psig	Voltage vdc	Energization Time, sec	Response Time, millisec	
			Open	Close
125	28	<1	2.91	2.69
182	28	<1	2.91	2.91
229	28	<1	2.91	2.46
310	28	<1	3.12	2.73
405	28	<1	3.17	2.78
507	28	<1	3.33	2.72
300	18	<1	4.87	2.50
300	24	<1	3.42	2.27
300	28	<1	3.12	2.69
300	32	<1	2.85	2.59
300	28	20	3.04	2.82
300	28	40	3.03	2.56
300	28	60	3.21	2.65
300	28	90	3.31	2.69
300	28	120	3.16	3.20
300	28	240	3.25	2.94

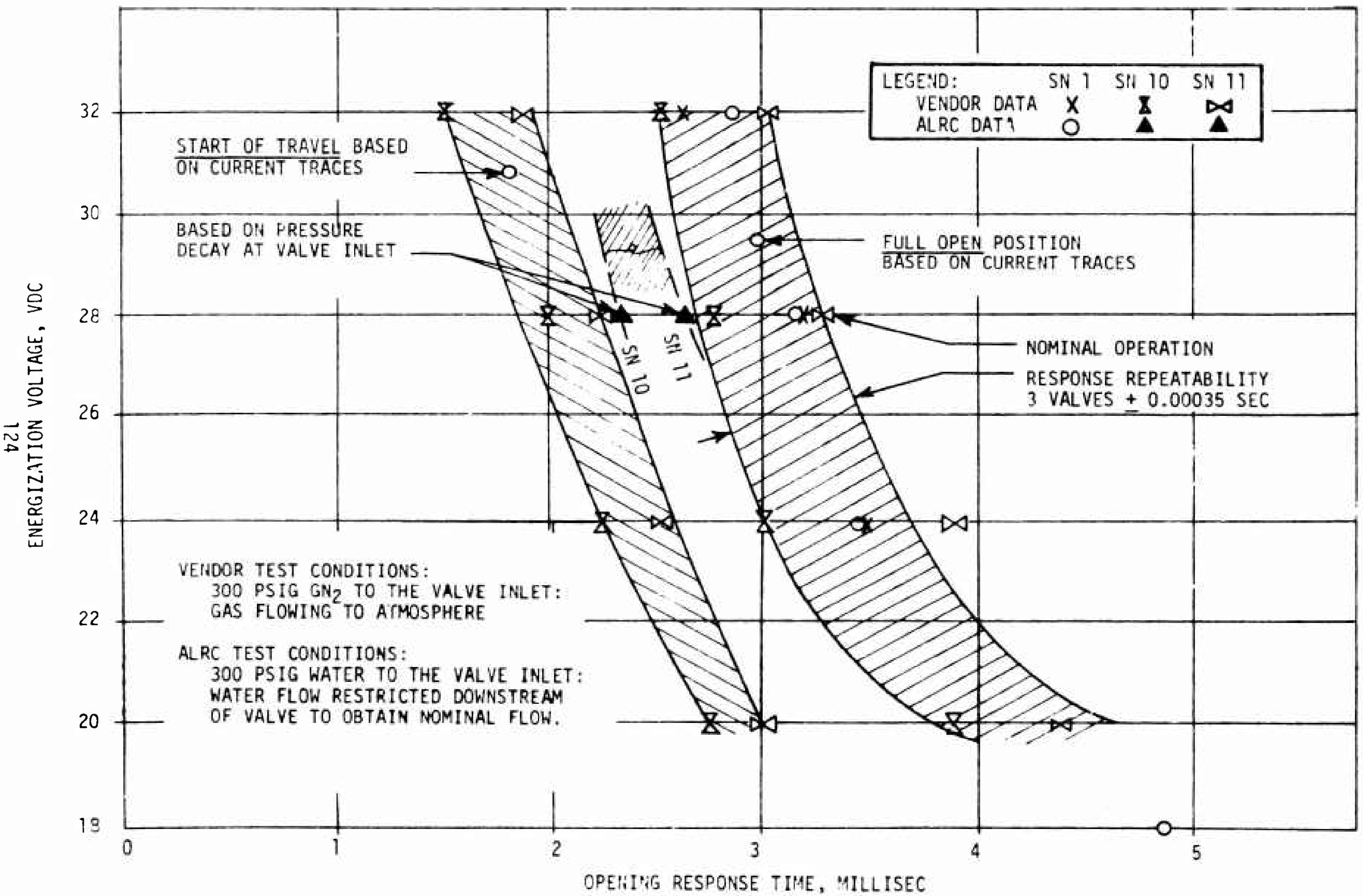

Figure 5.2-2. Effect of Voltage on Response Time

Open and closing response was faster than the 5 millisec requirement over the full operating range.

5.2.1.6 Electrical Characteristics

A series of tests were performed to determine pull-in and drop-out voltage over a range of inlet pressures and to define the current drain at nominal voltage. Current drain was 0.54 amps at 28 VDC. Pull-in and drop-out voltages are tabulated in Table 5.2-3.

TABLE 5.2-3

PULL-IN AND DROP-OUT VOLTAGES

Inlet Pressure, psig	Voltage, VDC	
	Pull-in	Drop-out
46	6.2	3.0
198	6.0	3.0
304	5.8	3.0
506	6.1	2.9

5.2.1.7 Manifold Change

The manifold change test involved a series of leak, flow and cycle tests.

Manifold S/N 03 was installed on the valve using the original valve to manifold interface seals. Since this manifold did not have an injector P_c pressure fitting or thermocouple wires installed; these openings were blocked manually for the leak tests. Two 500 psig leak checks indicated that the shut-off seals were not leaking.

The assembly was flow tested with water following the procedure used for the prior flow test, but at lower inlet pressures. Reduced inlet pressures were required to keep the flow rate within the range of the flow meters. A low range pressure transducer was installed to monitor inlet pressures in the range of about 2 to 10 psig. The flow tests indicated K_w values of 0.00211 and 0.00311 for the fuel and oxidizer sides respectively.

This assembly was then cycled 500 times without pressure or flow and checked for response time and leakage. Response time was 2.9 millisec opening and 2.26 millisec closing. There was no indication of shut-off seal leakage. Two additional manifold changes were accomplished without experiencing leakage.

5.2.1.8 Discussion and Conclusions

The shutoff seals demonstrated bubble tight sealing throughout the program with 3 different manifolds. This indicated that manifold changes could be achieved on a single valve. Examination of the teflon shutoff seal after valve cycling did not reveal any seal indentation. A determination of seal indentation occurrence after propellant exposure, high temperature exposure and extended cycling was made following Phase III testing.

Response time on ALRC tests, based on current traces, were nearly identical to vendor test results on opening but were generally about 1/2 millisec faster on closing. This difference is probably the result of back EMF suppression. The vendor used a suppression network to limit the voltage spike on closing to a maximum of 56 volts. The ALRC tests were performed without back EMF suppression and voltage spikes were about 70 volts when the valve was deenergized. Suppression at lower values results in slower closing; therefore, the vendor closing times should be slower than those obtained at ALRC. The ▲ data point shown in Figure 5.2-2 was obtained at a later date based on line pressure decay recorded by a close coupled

Kistler transducer. These data are shown in Figure 5.2-3 and provide a more accurate indication of effective response. This method shows that the valve can respond to an electrical pulse as short as 0.0025 sec. Figure 5.2-4 shows the response of a valve following 300,000 engine firings for comparison.

Response time was essentially unaffected by any of the variables tested except voltage. Temperature effects were not fully explored; it is expected that as temperature increases, valve opening response will be slower. Although this may be a concern with regard to combined effects of heat soakback and a vacuum environment the valve performance obtained with variable voltage indicates valve response should still be less than 5 millisec at elevated temperature. The energization time test was intended to provide some indication of the temperature effect but the conductive cooling from water flow and the convective cooling to atmosphere limited the temperature rise. Vacuum, hot fire testing later in the program showed no change in response at temperature up to 220°F.

5.2.2 Injector Flow Testing

The purpose of injector flow testing was four fold.

(1) Verify the predicted pressure drop.

(2) Establish the pressure drop reproducibility for different units of the same design.

(3) Determine the element to element flow uniformity (i.e., manifold distribution efficiency).

(4) Visually inspect the spray pattern for flow uniformity, wall impingement covering etc. and document the pattern photographically using shadowgraph techniques.

5.2.2.1 Pressure Drop Reproducibility

The pressure drop and flow distribution were established by collecting the effluent first from each circuit flowing independently and

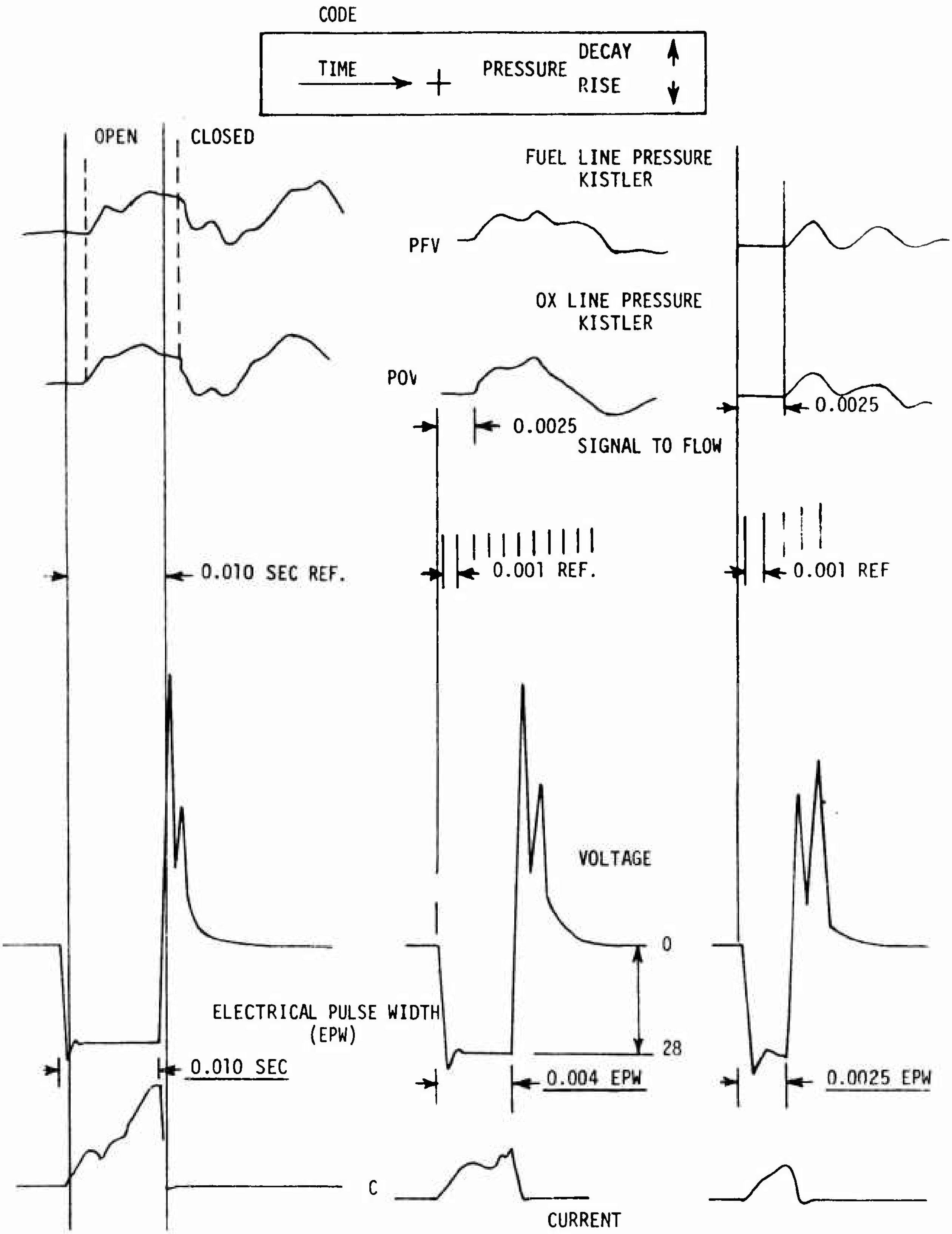

Figure 5.2-3. Valve Response

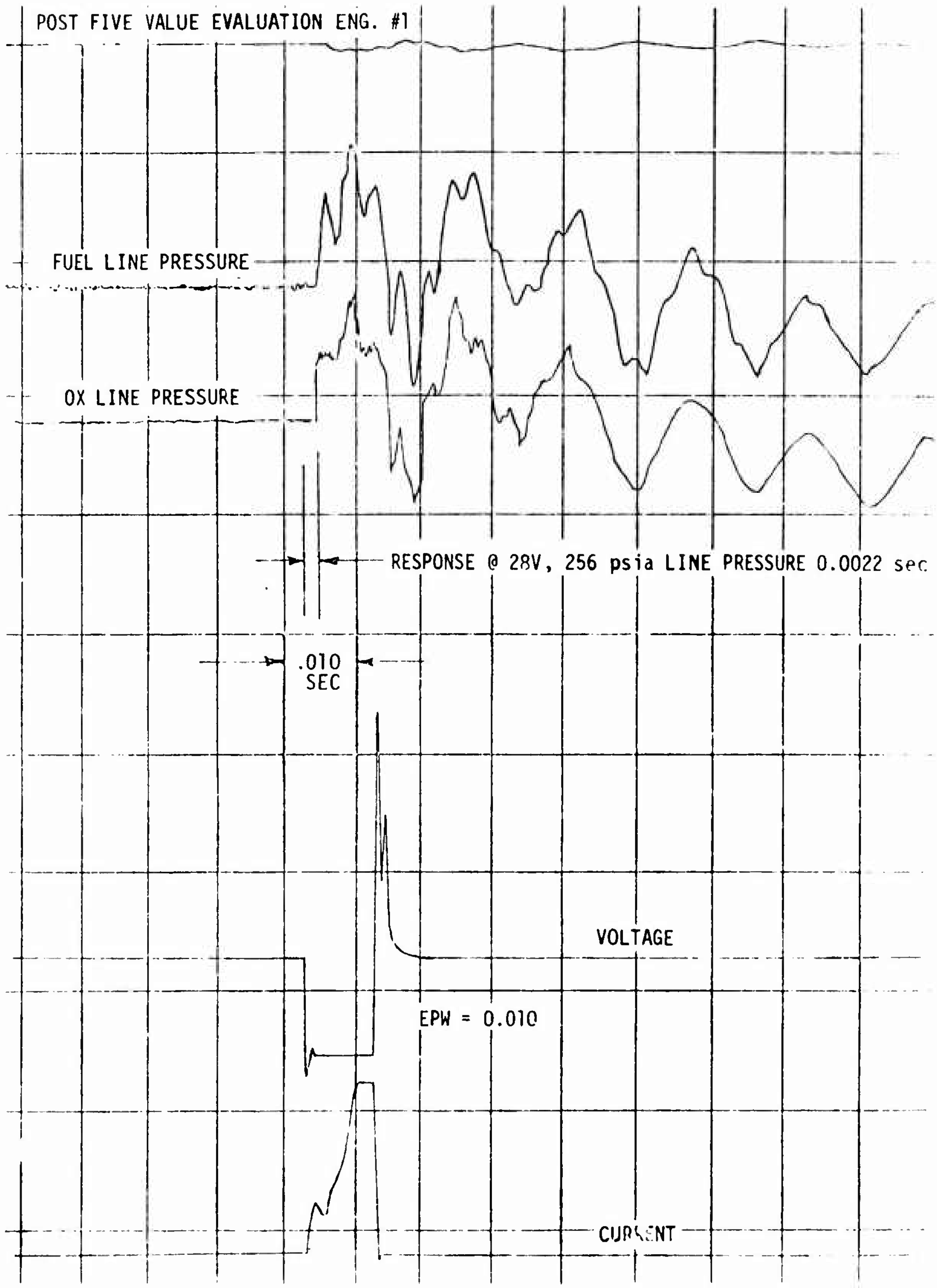

Figure 5.2-4. Postfire Valve Evaluation, Engine SN 1

5.2.2, Injector Flow Testing (cont.)

secondly from each of the orifices with a specially prepared probe. Injector flow coefficients are expressed as

$$K_W = \frac{\dot{W}}{\sqrt{\Delta P \ sG}}$$

where: K_W = flow coefficient

$\dot{W}$ = flow rate lb/sec

ΔP = pressure differential psi

sG = specific gravity

Values for K_W were obtained at 3 ΔP values in the 25 to 150 psi range with 2 samples at each flow condition. The collection period was 50 sec for individual orifices; 100 sec for a full circuit.

Table 5.2-4 provides a summary of the flow characteristics for 19 injectors of 9 designs which were evaluated in Phase II cold flow testing. The data indicated a unit to unit flow (K_W) reproducibility of 5% or better where 2 or more injectors of the same design were flowed. In the case of the 6-SP-45-A and 4-UD-28-S, the reproducibility of 3 assemblies was better than $\pm$ 2%.

The lower part of Table 5.2-4 showed that the injector valve manifold integration (Figures 5.1-8 vs 5.1-16) resulted in no significant changes in the K_W values. This indicates that proper alignment was attained in all assemblies manufactured and that the bonding process did not alter the flow characteristics. The last set of data provided are the hot fire test values and postfire cold flow re-evaluation. The % change shown represents the pre- to postfire water flow K_W values. These were reproducible within 2 percent.

TABLE 5.2-4

HISTORY OF INJECTOR FLOW COEFFICIENTS

	6 ELEMENT DESIGNS										4 ELEMENT DESIGNS							
INJECTOR TYPE	SP-45-A		SP-0		SP-45-B1		SP-45-B2		SP-45-B3		UD-0		UD-A		UD-28-S		UD-28-SL	
	OX	FUEL	OX	FUEL	OX	FUEL	OX	FUEL	OX	FUEL	OX	FUEL	OX	FUEL	OX	FUEL	OX	FUEL
INJECTOR ONLY																		
COLD FLOW																		
SN-1			781	663	569	640	647	601	630	634	808	560	760	657	800	686	760	633
SN-2	625	614			594	635	686	633	602	650	802	563			815	695	780	680
SN-3	617	633													780	680	783	628
SN-4	624	629																
% DEV	0.5	1.7			4.3	1.0	5.8	5.0	4.5	2.5	0.8	0.6			2.0	1.0	2.0	5.0
INTEGRAL/INJECTOR - VALVE																		
MANIFOLD SN	2		1		INJECTORS NOT TESTED						2				1		3	
COLD FLOW	627	602	770	670							835	550			840	671	784	667
HOT FIRE K_w	590	600	780	660							930	601			815	671	740	*
POST TEST K_w	634	585									—		—		840	660	770	663
% CHANGE	+1	-2.8													0	-1.6	-1.8	-0.6

$K_w = \frac{w}{\sqrt{\Delta P\ SG}}$ (VALUES TABULATED = ($K \times 10^6$))

*LEAK IN VALVE MANIFOLD - VALVE BODY SEAL

5.2.2, Injector Flow Testing (cont.)

5.2.2.2 Manifold Flow Distribution

Data from the first generation six element design showed the following mass and mixture ratio distributions.

Element	1	2	3	4	5	6
6 SP-0						
Fuel Mass*	0.99	0.76	0.97	0.98	1.05	1.22
Ox Mass	1.05	0.85	1.00	1.00	1.02	1.07
MR (Elem.)**	1.69	1.77	1.64	1.63	1.55	1.39
6-SP-45						
Fuel Mass	1.01	0.90	0.60	0.92	1.23	1.37
Ox Mass	1.10	1.05	1.08	0.72	91	1.13
MR (Elem.)	1.74	1.86	2.88	1.25	1.18	1.32
6-UD-0						
Fuel Mass	1.19	1.10	0.50	1.07	1.13	1.10
Ox Mass	1.03	1.14	0.99	1.05	0.94	0.86
MR	1.38	1.66	3.16	1.57	1.34	1.25

The flow and mixture ratio uniformity for the 6-SP-0 was considered acceptable since all elements generated a mixture ratio very close to the nominal 1.60 value. The 6-SP-45 and 6 UD-0 injectors were not acceptable because of the high MR on the No. 3 element. This condition was reproducible for each of the injectors indicating a design deficiency rather than a fabrication problem.

The (6-SP-45-A) unit incorporated an improved manifolding system obtained by: (1) lowering velocities prior to splitting the flow into 6 streams, (2) providing a plenum and a low velocity approach plus rounded

$$*\text{Mass} = \frac{\text{Element flow rate}}{\text{Avg of all elements}}$$

$$**\ \frac{\text{ox flow}}{\text{fuel flow}}$$

entrances to the flow splitting region, and (3) increasing the velocity in the legs (Figure 5.1-13) connecting the central plenum to the injection orifices. This was accomplished with only a minor increase in overall volume. Flow distribution for the improved manifolding was recorded as follows:

6-SP-0, -45-B and -C Type Manifolding (% Flow Deviation)

Element No.	1	2	3	4	5	6
F Mass	-1.4	+9.1	-11.3	-5.4	-1.4	+10.3
O Mass	-0.5	-6.7	+2.9	-5	-5.2	+10.3
MR Element	1.6	1.4	1.8	1.7	1.5	1.5

The flow for the four element designs were:

4-UD-0

Element	1	2	3	4
F Mass	+11.0	+3.5	-9.4	-5.1
O Mass	+8.2	-4.7	-8.5	+5.0
MR	1.6	1.5	1.6	1.8

4-UD-28-SL

Element	1	2	3	4
F Mass	+0.5	-2.1	-1.7	+3.4
O Mass	-3.6	-5.5	+1.6	+7.5
MR	1.5	1.5	1.7	1.7

This level of flow uniformity was considered very good in view of the very small flow quantities and the premium being placed on manifold volume.

5.2.2.3 Pattern Documentation and Shadow Photography

Spray pattern angles and density distribution were documented by shadow photography. The propellant circuits were flowed individually and are in concert at maximum and minimum flowrates. Photographs were taken at various angles to record the axisymmetric pattern.

Figure 5.2-5 shows a typical photographic record for a particular injector design. This photo technique has been very effective in understanding and evaluating wall impingement and blow-apart phenomena. Since fine spray and drop size details which are clearly visible in the original photos are lost in the resolution available for commercial publication, only a token of the photographic results are included in this report.

The apparent absence of a distinct spray pattern for the individual circuits of the 4-UD-0 injector in Figure 5.2-5 at the high flow condition is a result of the spray being finer than the resolution of the printing process.

Since each stream of the 4-UD-0 injector is self atomizing, precise alignment of very small diameter streams is not a requirement. The dark bar in the center photograph of Figure 5.2-1 is a 1 in. long reference. The photos show that atomization starts at the injector face. The fact that the pattern is more visible with both circuits flowing is due to the higher (combined) flow rates but mostly to agglomeration of fine fuel and oxidizer droplets. When translated to hypergolic propellants this means the propellants have reacted.

Figure 5.2-6 shows the spray characteristics of the 4-UD-28 series injectors with both circuits at the high flow condition. The upper photograph is that of the shallow angle short impinging fuel (S). This results in a fuel spray half angle of 65°. A portion of this fuel bypasses the ox fan and impinges upon the chamber wall approximately 1/4 in. downstream of the injector; providing a fuel rich environment at the wall.

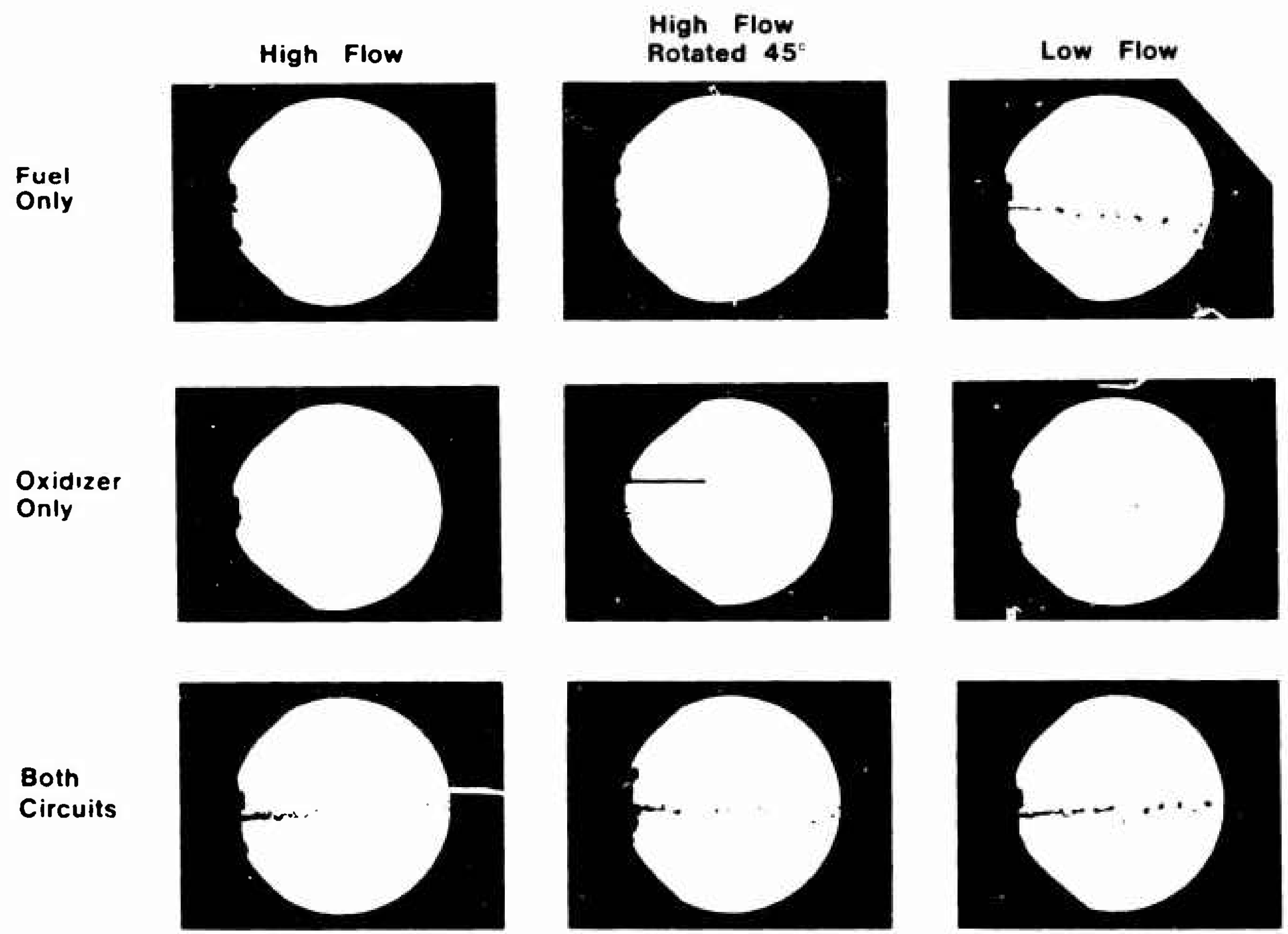

Figure 5.2-5 [illegible] Doublet Cold Flow

SHORT FUEL IMPINGEMENT

LONG FUEL IMPINGEMENT

Figure 5.2-6. Cold Flow Spray Characteristics, 4-UD-28 Series Injector, Both Circuits ΔP = 130 psi

5.2.2, Injector Flow Testing (cont.)

The lower photograph of the long impingement (SL) configuration, shows the spray half angle to be 20 degrees. The fuel which bypasses the oxidizer in this design contacts the wall about 1 in. downstream thus providing less front end cooling and more throat region cooling.

Both of these designs were selected for hot fire test evaluation on the basis of cold flow results which indicated good compatibility and good propellant atomization over the full blowdown range. The hot fire test data verified these conclusions.

Figure 5.2-7 provides a similar display for the 6-SP-45-B-2 and -B-3 injectors; short fuel impingement distance (top) versus a longer impingement distance (bottom). Fuel impingement closer to the face results in more propellant on the wall thus more wall cooling at the forward end.

Neither of these two designs were selected for hot fire testing. The short fuel, long ox (top) was very similar to the already tested 6-SP-45-A which was a short design and provided over 300 sec of specific impulse. The long impingement design appeared to offer even higher performance and less compatibility.

5.2.3 Hot Fire Testing

5.2.3.1 Test Objectives

The objective of this test activity was to verify (1) forecasted steady state and pulsing mode performance, (2) dynamic and response characteristics, and (3) thermal characteristics of components for a 5 lbF Thrust Bipropellant Engine.

B2 LONG OX, 0.010 DIA ORIFICE
SHORT FUEL, 0.008 DIA ORIFICE

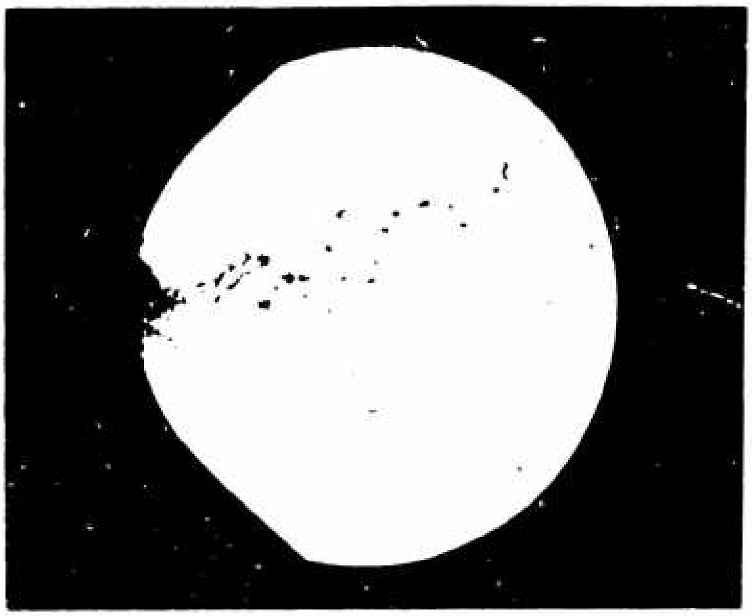

B3 LONG OX, 0.010 DIA ORIFICE
LONG FUEL, 0.008 DIA ORIFICE

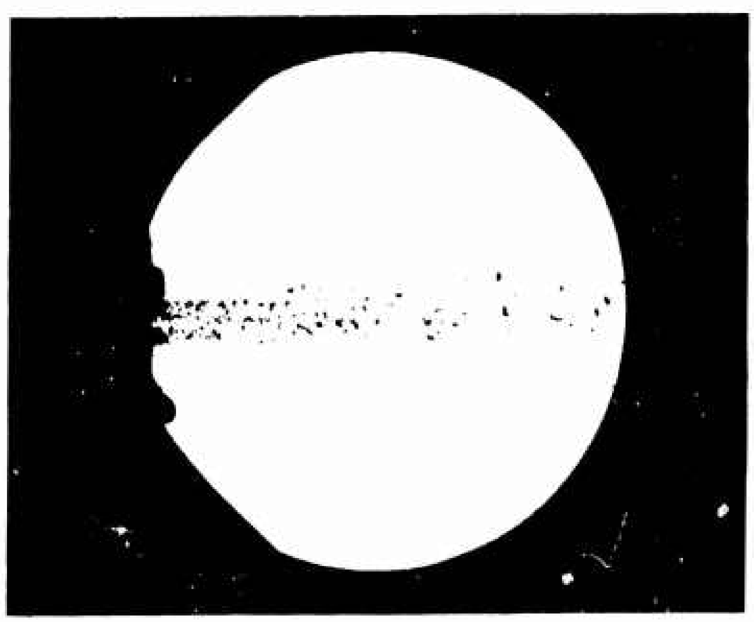

Figure 5.2-7. Cold Flow Spray Characteristics, 6-SP-45 Series Injector

5.2.3, Hot Fire Testing (cont.)

5.2.3.2 Test Specifications and Goals

The program goal was to demonstrate a steady state specific impulse of 300 sec and a bit impulse capability of 0.05 lb sec ($\approx$ 0.01 sec pulse) for which the pulse performance was 240 sec. The Phase II testing was intended to verify the capabilities of the anticipated Phase III designs. Testing was conducted over the following range of conditions:

P_c	72 - 170 psia
Thrust	2 - 5 lb
MR	1.6 nom. Range 1.2 - 2.0
Prop. Temp	20 - 120°F

The propellants employed in testing were <u>Green</u> N_2O_4 (99.0 + % N_2O_4, 0.8% NO) per MIL-P-26539 and MMH ($CH_3N_2H_3$) (98% purity) per MIL-P-27404. Certification of all propellants was provided.

5.2.3.3 Test Hardware

The test hardware employed in Phase II testing included the following:

One (1) Moog bipropellant valve

Five (5) injector-valve manifold assemblies

Two (2) 50:1 Columbium thrust chambers; one conical chamber and one cylindrical combustion chamber

Three (3) sea-level thrust chambers; two stainless and one Columbium

Three (3) L* extensions, two 3/4 in. long; one 2 in. long, stainless and titanium versions available

Chamber bolts - 0.099 - 56 UNJF-3A bolts 5/8 in. long and 1.5 in. long

Haskel V seals HVG 2-11. Bellville springs

Positioning plates and thermal shunts

5.2.3, Hot Fire Testing (cont.)

5.2.3.4 Test Facility

Testing was accomplished in Bay 1 of the Research Physics Laboratory. Figure 5.2.8 provides a test facility flow schematic. Important features of the facility include:

1. A low deflection (4.95×10^{-5} in. at 5 lbF) low mass (4 lb including thruster and instrumentation) test stand (frequency $\approx$ 575 Hz).
2. A dual bridge thrust measuring cell (100 lbF) and 10 lb standard cell for in-place calibration of the measurement cell before and following each test series.
3. A water cooled thrust mount to prevent thermal distortion during sustained fire periods.
4. Thin wall 1/4 in. dia feed lines with lengths tuned to prevent shifts in engine MR due to feed system oscillations. Fuel line length = 46.5 in., ox line length = 28 in.
5. A precisely calibrated positive displacement flow measurement (PDFM) system having a 20 sec duration capability at full thrust.

The facility also contained two large ($\approx$ 50 gal) propellant tanks located 30 ft (fuel) and 20 feet (ox) from the test stand. These were used for PDFM fill and for sustained firing. A 10 micron (absolute) facility filter was located between the large tanks and the positive displacement tanks. The 35 micron absolute filter within the valve was the only on-line filter during firings fed from the PDFM system.

Figure 5.2-9 provides a photograph of the test facility following the first sea level checkout tests. The following stand modifications were made following the checkout tests: (1) the forward flexure stiffness was reduced by milling 4 transverse slots, (2) an additional flexure loop was added to the feed lines (visable in Figure 5.2-10), and (3) the feed line lengths were increased to 33 in. for the ox and 60 in. for the fuel as a result of the added loop.

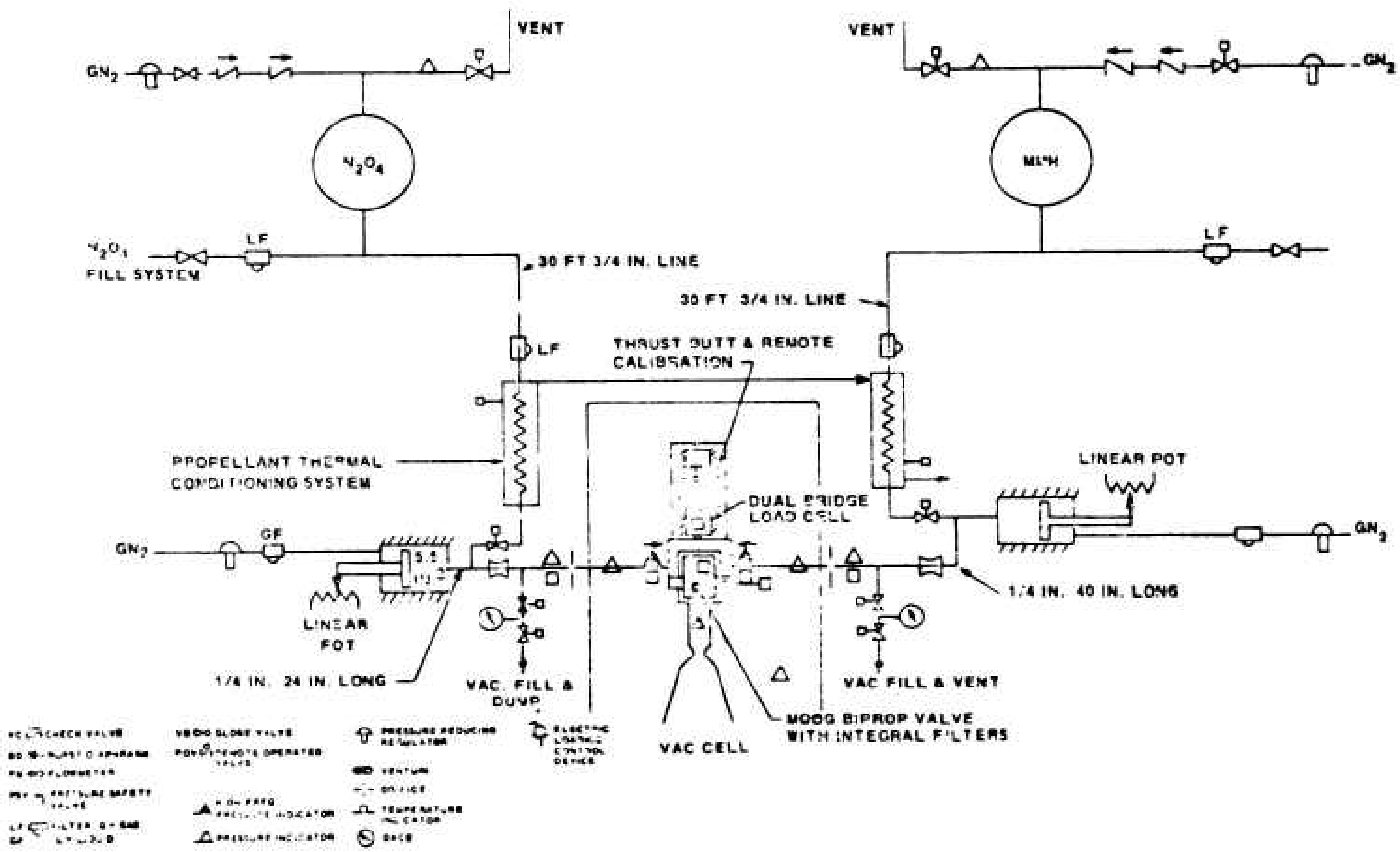

Figure 5.2-8. Test Facility Schematic

1. 100 lb DUAL BRIDGE LOAD CELL
2. 10 lb STANDARD LOAD CELL
3. THRUST BUTT
4. ALIBRATION RODS
5. EXURES
6. NGINE MOUNT (WATER COOLED)
7. ENGINE WITH (SL) NOZZLE
8. PDFM FEED SYSTEM
9. LINE PRESSURES
10. CHAMBER PRESSURE
11. FEED LINE KISTLER

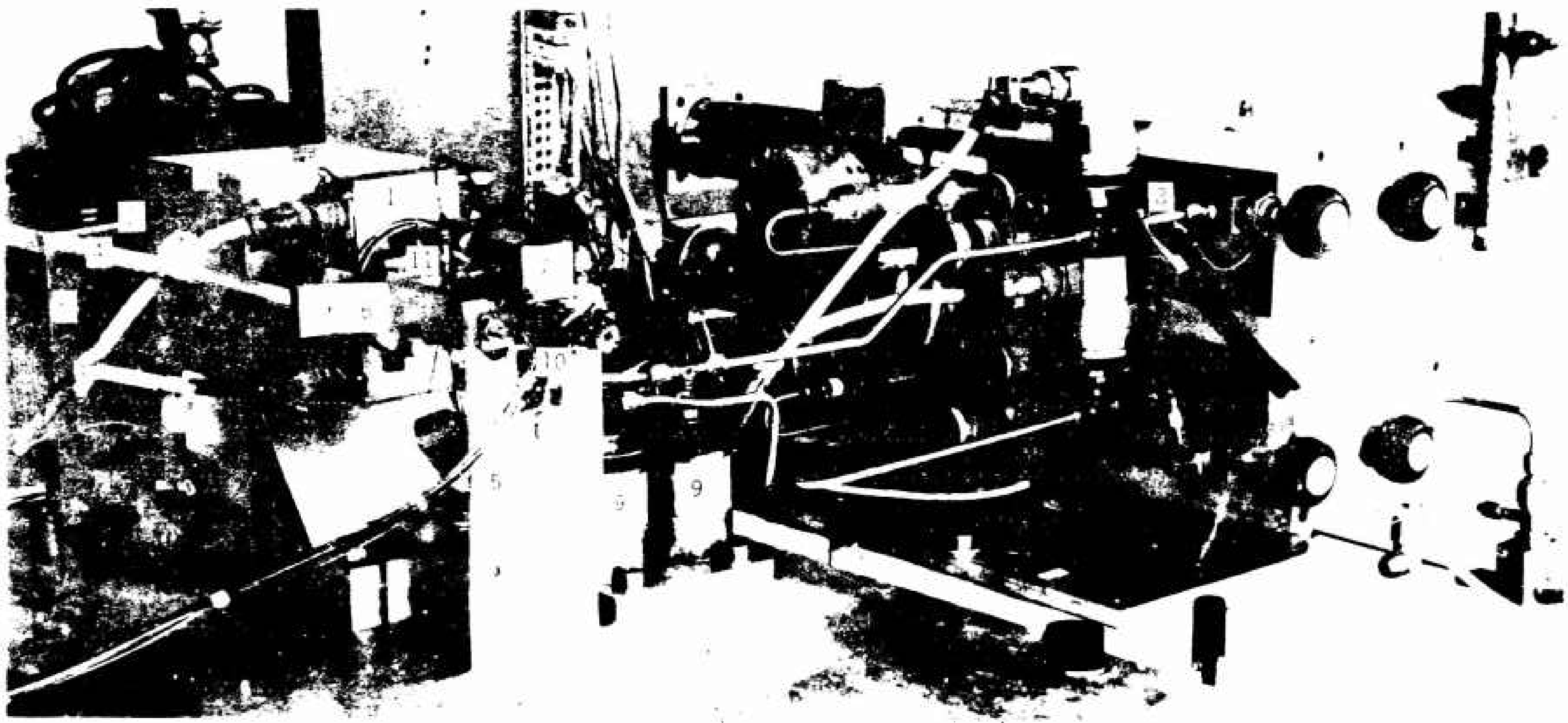

Figure 5.2-9. Bay 1 Test Facility - Sea Level Configuration

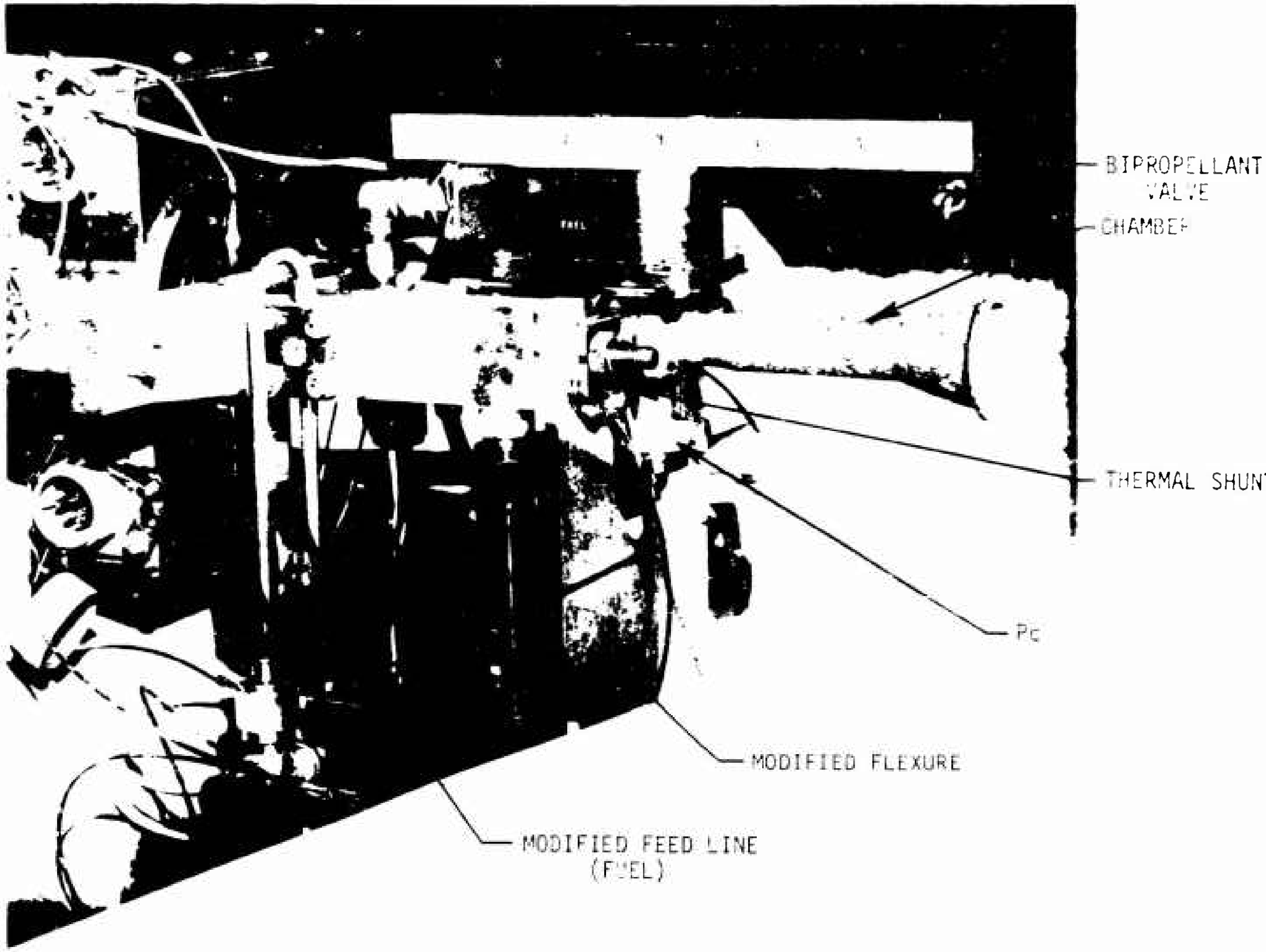

Figure 5.2-10   Thrust Stand and Engine Assembly with 50:1 Area Ratio Chamber, Vacuum Configuration

5.2.3, Hot Fire Testing (cont.)

5.2.3.5 Measurements and Data Recording

Table 5.2-5 provides a tabulation of the facility instrumentation, nomenclature employed, and the modes of data recording.

Continuous records of thrust, P_c, feed line and high frequency chamber pressure measurements were available from a Model 3500, 14 channel Sagamo FM recorder. The response capability of the recorder is in excess of 20 KHz. Digital thrust data was recorded at intervals of 0.000768 sec in all pulse tests. Sampling rates on other parameters are itemized in Table 5.2-5.

Performance parameters were computed for each pulse as follows:

Bit impulse, $FT = \Sigma$ thrust x time $= \Sigma\ (Fa + Fb)\ \Delta T$
($\Delta T = 0.000768$ sec)

Total fuel flow, $W_f = K_1\ [V_2 - V_1]$ PDFM's volume change per pulse.

Total ox flow, $W_o = K_2\ [V_2 - V_1]$

Total propellant flow, $W_t = W_f + W_o$

$$MR = \frac{W_o}{W_f}$$

Bit Specific Impulse, $BSI = FT/W_T$

The thrust measuring portion of the test stand was calibrated immediately before and after each test. This calibration was accomplished by the pneumatic application of 4 force levels to the stand on the axis of thrust such that the dual bridge measuring cell was loaded in series with a 10 lb standard cell. This was accomplished with the engine and all instrumentation in position, lines pressurized, and at vacuum conditions when applicable. The tare forces ranged from 2 to 5% depending on the amount of

TABLE 5.2-5

FIVE-POUND BIPROPELLANT ENGINE TEST INSTRUMENTATION

Parameter Performance	Symbol	Transducer or TC Type	Range	Digital sec	No. Channels	Direct Writing Oscillograph	FM Tape	Visual
				Recording System				
Thrust lb	Fa		100	0.00153	3	X	X	
	Fb	BLH PN 402433		0.00153	3			
	Fa + Fb			0.000768	6			
Chamber Press psia	P_c	Whittaker SP 66	1000	0.00115	4	X	X	X
Chamber Press Hi Freq	P_cHf	Kistler 601A	2000				X	
Fuel Flow lb/sec	LF	Positive Disp.	0-0.012	0.0023	4		X	X
Fuel Flow lb/sec	ẇF	Turbine	0 0.012	0.0046	1	X		
Ox Flow lb/sec	LO	Positive Disp.	0-0.020	0.0023	4		X	X
Ox Flow lb/sec	ẇo	Turbine	0-0.020	0.0046	1	X		
Fuel Feed Pressures								
Tank psig	PFT	Taber-206	500					X
Orifice up psia	PFV	Taber-206	500	0.00231	2	X		X
Valve inlet psia	PFTCV	Taber-206	500	0.00231	2	X		
Valve inlet Hi Freq	PFHF	Kistler 601A	1000				X	
Fuel Feed Temp								
Fuel orifice up °F	TFV	CC	0-200	0.0046	1			
Valve inlet °F	TFTCV	CC	0-200	0.0046	1	X		X
Conditioning fluid	TFB	Thermometer	0-200					X
Ox Feed System Press								
Tank psig	PoT	Taber-206	500					X
Orifice up psia	PoV	Taber-206	500	0.00231	2	X		X
Valve inlet psia	POTCV	Taber-206	500	0.00231	2	X		
Valve inlet Hi Freq	POHF	Kistler 601A	1000				X	
Ox Feed Temp								
Orifice up °F	TOV	CC	0-200	0.0046	1			
Valve inlet °F	TOTCV	CC	0-200	0.0046	1		X	X
Conditioning fluid °F	TFB	CC	0-200					X
Cell Pressure psia	Pa	Taber-206	0-10.7	0.0046	1			X
Load Cell Temp °F	TLC	CA	0-200	0.0046	1			
Valve Signal Volts	EV			0.00231	2	X	X	
Valve Current Amps	IV					X	X	
B-Bit				0.000025			X	
Narration							X	
Injector Face °F	TFJ1	CA	0-1000	0.0046	1	X		
	TFJ2	CA	0-1000	0.0046	1			
Valve Body	TVb	CA	0-500	0.0046	1			
Valve Manifold	TVm	CA	0-500	0.0046	1			
Chamber								
Wall Temp	TCTR 1-6	W-RE	0-3200	0.0046	6	(2)		
Wall Temp	TCCA	Ca	0-2200	0.0046	6	(2)		
Thermal Shunt	TTSH1	Ca	0-1000	0.0046	1			
	TTSH2	Ca	0-1000	0.0046	1			
Total Channels					48	16	12	14
Capabilities					48	36	14	

Digital = Consolidated Systems Corp. 10,400 ch/sec 48 ch.

FM Tape Sagamo Model 3500 14 ch.

Direct reading CEC 5-133 36 ch

5.2.3, Hot Fire Testing (cont.)

instrumentation being employed in the test setup. The calibration data for the standard cell is contained in the following table. Recalibration at the conclusions of Phase II testing showed repeatability of 0.05% full scale.

Ten pound standard cell calibration data - linearity under load, full load ≈ 10,000 counts.

% Load	Date	0	20	40	60	80	100	80	60	40	20	0
% of Full Scale	7-13-73 4-19-74	0 0	+.15 +.17	+.27 +.30	+.29 +.31	+.21 +.26	0 .04	+.24	+.34	+.30	+.21	+.4
% Repeat		0	.02	.03	.02	.05	.04					
% Repeat Unloading								.03	.05	.03	.06	.04

Temperature Sensitivity

	Room	30°F	130°F	R.R.
Zero	+20	+32	+2	+23
Exit	9369	9470	9276	9366
50%	-1	+15	-10	-2
75%	-2	+25	-16	-3
Date	12 Jul 73	13 Jul 73	13 Jul 73	13 Jul 73

Compensation for the slight nonlinearity and cell temperature was made in data reduction. Load cell temperatures were monitored (TLC) during precal, firings, and posttest calibrations for this purpose.

Figure 5.2-11 provides data for the reproducibility of the dual bridge measuring cell on 4 typical tests. These data represent the pre-to-post test percent change in thrust of each leg as compared to the 10 lb standard cell. At 5 lbF, this is noted to about 0.5 percent.

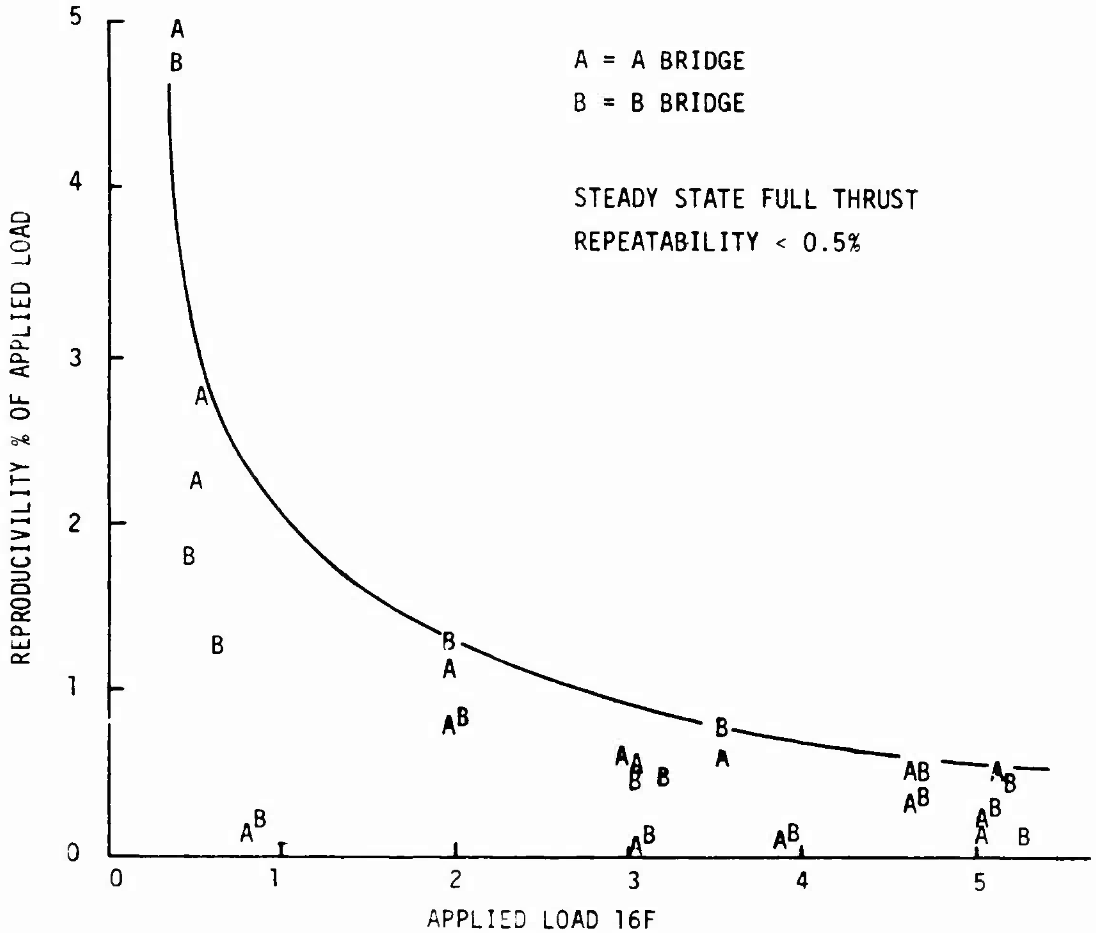

Figure 5.2-11. Pre versus Post Test, Thrust Measurement Repeatability, Four-Test Sample

5.2.3, Hot Fire Testing (cont.)

5.2.3.6 Test Conditions

Figure 5.2-12 illustrates the Phase II firing modes. Initial steady state tests were conducted for 5 to 20 sec fire periods. A thrust stand "0" shift of up to 10% was noted for firings longer than about 8 sec in duration in the first checkout test series. This was reduced to 2% (0.1 lb max) following the test stand modifications described earlier. The steady state firing mode was modified to include a 0.3 sec coast period after each 5 sec of steady firing. This allowed a new stand zero, which was employed to further refine the thrust measurement to be obtained periodically in the course of firing. This also provided hot restart experience.

The duty cycle involving 4 pulses, a long burn, soak and 4 pulse repeat, shown in Figure 5.2-12, allowed comparisons of cold and hot chamber pulsing performance, and steady state values to be obtained. The 20-40 sec coast following the long burn also provided heat soak and hot restart data. The pulsing-only series involved the quantity of pulses, the fire duration and coast time, and % duty cycle indicated in Figure 5.2-12.

5.2.3.7 Test Summary and History

Phase II testing involved a total of 4360 hot firings or engine pulses using 5 different injectors (Ref. Figure 5.2-13) with the 1.6:1 and 50:1 nozzles and 3/4 in. L' extensions shown in Figure 5.2-11. A 2 in. long spacer is not shown. All components had a common flange design and were thus fully interchangeable.

Table 5.2-6 provides a chronological documentation of the test conditions and hardware. The 6-SP-45-A injector was test fired and was expected to provide the highest performance of all the designs. Its initial firings with a 2 in. long chamber were facility and test stand check-outs. The first valid tests at full thrust showed that the 300 sec specific

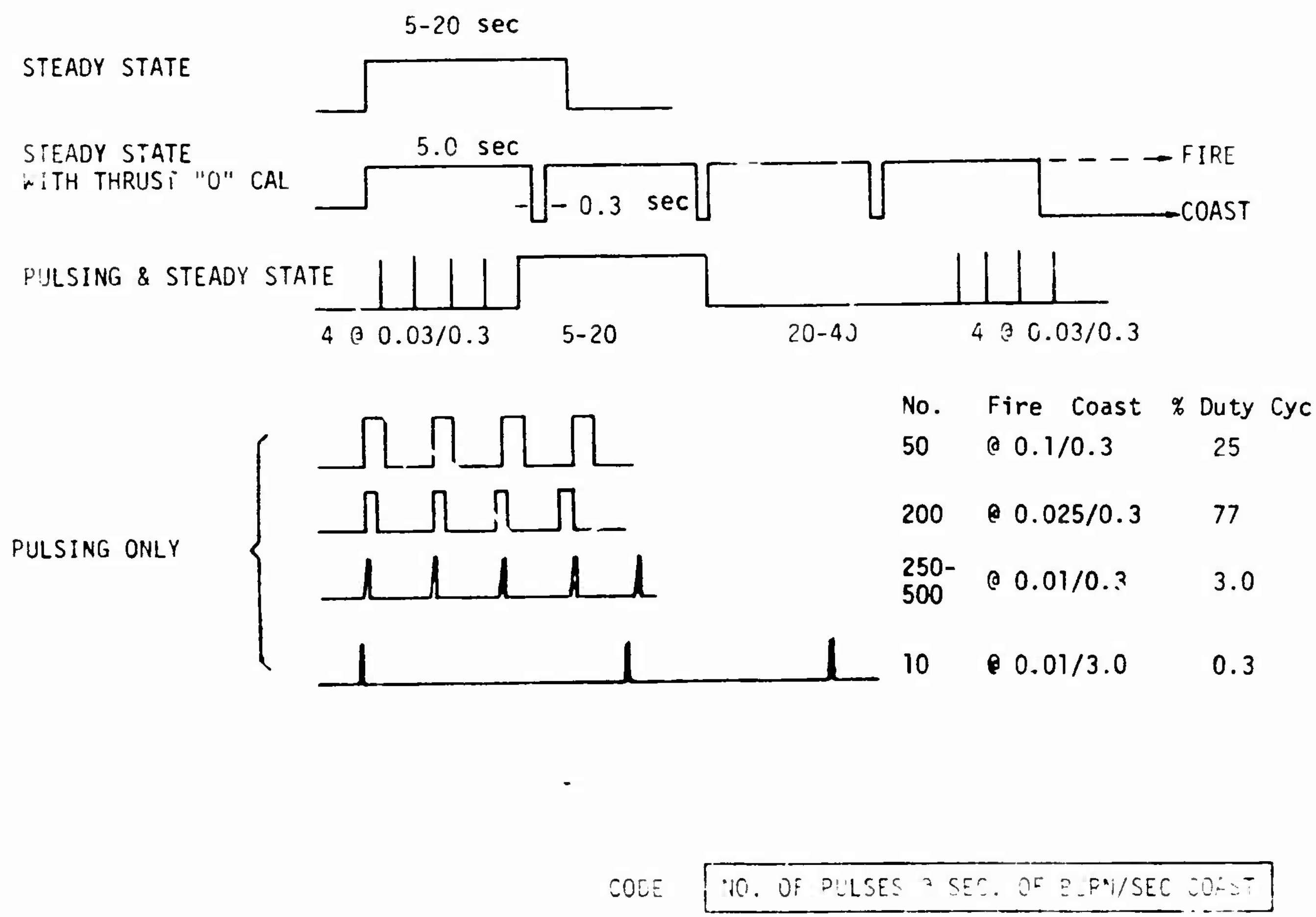

Figure 5.2-12 Duty Cycles Employed in Phase II Testing

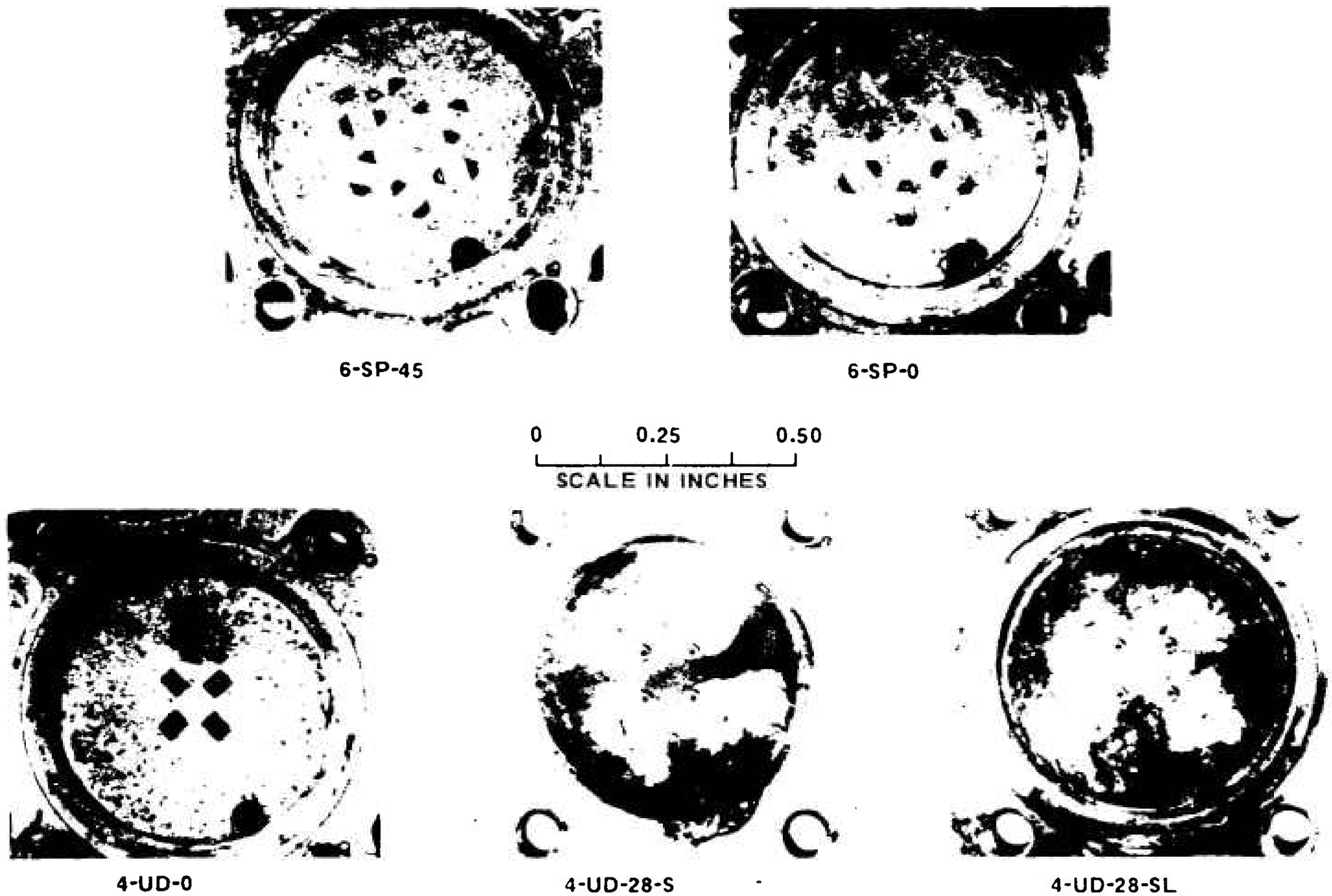

Figure 5.2-13. Postfire Injector Photographs

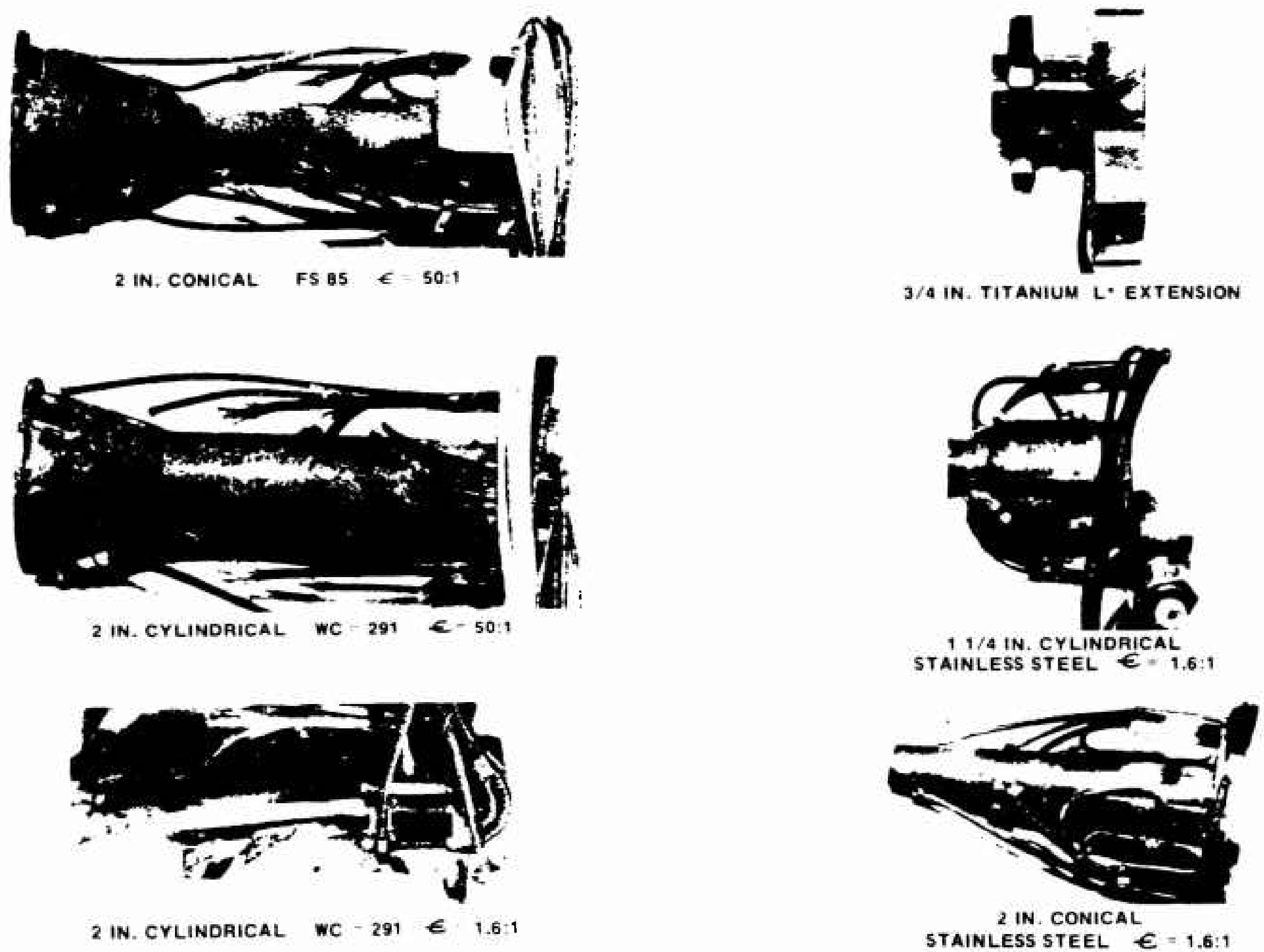

Figure 5.2-14. Combustion Chamber (Postfire)

TABLE 5.2-6

PHASE II TEST SUMMARY

Test No.	Date	L' in.	Environment	Duty Cycle: No. Cold Pulses 0.030 sec	Duty Cycle: S.S. Duration sec	Duty Cycle: No. Hot Pulses 0.030 sec	P_c psia	MR	Notes
Injector 6-SP-45									
OC-26-100 -103	10-15								Facil·ty calibration.
OC-26-104	10-16	2	SL	-	4.5	-	150	1.18	Thrust shift.
OC-26-105	10-22	2	SL	-	5	-	154	1.62	Stand modified and problem corrected.
OC-26-106	10-22	No digital data							
-107		2	SL	-	5	-	153	2.07	
OC-26-108	10-22	2	SL	4	10	4	67	1.61	
OC-26-109	10-23	4	SL	4	5	4	155	1.65	Photo coverage. Slight leak in ox PDM.
OC-26-110	10-23	4	SL	-	5	-	156	1.90	
OC-26-111	11-15	2-3/4	Vac	4	10	4	65	1.61	
OC-26-112	11-15	2-3/4	Vac	4	7	-	150	1.17	Open T/C junction on thermal kill.
OC-26-113	11-15	2-3/4	Vac	4	9.7	-	108	1.59	
OC-26-114	11-15	2-3/4	Vac	4	5	4	155	1.56	
OC-26-115	11-15	2-3/4	Vac	4	5	4	155	1.92	
OC-26-116	11-15	2-3/4	Vac		(Pulsing)		155	1.60	No. Pulses / EPW sec / Duty Cycle: 50 / 0.1 / 25% 200 / 0.025 / 7.7% 500 / 0.010 / 3.2%
OC-26-117	11-15	2	SL	-	1.5	-	154	1.6	Conical SL chamber.
Injector 6-SP-0									
OC-26-118	11-19	2	SL		19.5		86	1.60	No digital data.
-119		2	SL		4.9		86	1.64	
-120		2	SL		5.0		158	1.29	
-121		2	SL		5.0		152	1.63	
-122		2	SL		5.0		94	1.60	
OC-26-123	11-21	2-3/4	Vac	4	10	4	75	1.48	
-124		2-3/4	Vac	4	3.2	-	159	1.26	Thermal shutdown.
-125		2-3/4	Vac	4	3.5	-	170	1.20	No performance data.
-126		2-3/4	Vac	4	3.6	-	159	1.63	
-127				4 (Pulsing)			160	1.60	
				No.	EPW	Duty Cycle			
				50	0.1	25%			
				200	0.025	7.7%			
				500	0.010	3.2%			
OC-26-128	11-27	2 Cyl	SL	-	11	-	160	1.63	
-129					20	-	158	2.02	
Injector 4-UD-0									
OC-26-130	12-3	2	SL		1.2	-	170	1.60	Thermal shutdown T_f = 600°F
OC-26-131	12-4	2	Vac	-	5.0	-	77	1.52	
-132		2	Vac	4	9.0	-	94	1.49	
-133		2	Vac	4	0.6	-	162	1.84	Hot face.
-134		2	Vac	4	9.0	-	76	1.97	
-135		2	Vac	4	9.0	-	77	1.50	
-136		2	Vac		(Pulsing)		170	1.6	No. Pulses / EPW sec / Duty Cycle: 50 / 0.1 / 25% 200 / 0.25 / 7.7% 250 / 0.01 / 3.2% 10 / 0.010 / 0.3%

Tests 100-116 used cylindrical high contraction ratio chamber.

NS = Not scheduled.

TABLE 5.2-6 (cont.)

Test No.	Date	L' in.	Chamber	P_c psia	MR	Duration sec	Notes
Injector 4-UD-28 S (Sea Level Tests)							
OC-26-137	12-18	2	Cyl Cb	170	1.56	7	
-138		2	Cyl Cb	153	1.52	15	Zero shift.
-139		2	Cyl Cb	152	1.58	3 x 5 = 15	0.3 coast for "F" 0.
-140		2	Cyl Cb	56	1.63	4 x 5 = 20	0.3 coast for "F" 0 chugging.
-141		2	Cyl Cb	73	1.59	4 x 5 = 20	
-142		2	Cyl Cb	82	1.68	4 x 5 = 20	0.3 coast for "F" 0.
-143		2	Cyl Cb	145	1.82	3 x 5 = 15	
OC-26-144	12-18	1.25	Cyl SS	144	1.54	2 x 5 + 2 = 12	Thermal shutdown at 2100°F.
-145		1.25	(with sleeve)	140	1.77	2 x 5 + 2 = 12	Thermal shutdown at 2100°F.
-146		1.25	(with sleeve)	152	1.20	2 x 5 + 2 = 12	Thermal shutdown at 2100°F.
Injector 4-UD-28 SL (Sea Level Tests)							
OC-26-147	12-19	2	Cyl Cb	170	1.6	2 x 5 + 2 = 12	Open TC.
-148		2	Cyl Cb	170	1.2	15	Out of fuel; leak in feed line.
OC-26-149	12-20	2	Cyl Cb	170	1.2	3 x 5 = 15	Performance data valid for first 5 sec burn only. Some valve leakage at end of high pressure tests due to thermal distortion of manifold plate.
-150		2	Cyl Cb	75	1.6	4 x 5 = 20	
-151		2	Cyl Cb	125	1.6	4 x 5 = 20	
-152		2	Cyl Cb	170	2.0	3 x 5 = 15	
Injector 6-SP-45-A Sea Level Tests							
OC-26-153	12-21	1.25	Cyl SS	70	1.6	3 x 5 = 15	0.3 sec coast between burns.
-154		1.25	Cyl SS	90	1.6	3 x 5 = 15	
-155		1.25	Cyl SS	170	1.2	5 + 4.6 = 9.6	Thermal shutdown at 2100°F.
-156		1.25	Cyl SS	170	1.6	5 + 2.3 = 7.3	Thermal shutdown at 2100°F.
-157		1.25	Cyl SS	170	2.0	5 + 3.4 = 8.4	Thermal shutdown at 2100 F.

Test No.	Date	L'	ε	Environment	Duty Cycle	P_c	MR	Notes
Injector 6-SP-45								
OC-26-153	12-21-73	1-1/4	1.6	SL	3 x 5 = 15	65	1.57	Stainless Steel chamber.
-154					3 x 5 = 15	78	1.65	
-155					5 + 4.6 = 9.6	149	1.25	
-156					5 + 2.8 = 7.8	149	1.65	
-157					5 + 3.4 = 8.4	148	2.02	
					Pulsing			
OC-26-158a	1-3-74	1-1/4	1.6	Vac	10 at 0.01/3.0 250 at 0.01/0.3 200 at 0.025/0.3	75	1.6	Propellant temperature 22°F
OC-26-159				Vac	Same as -158	155	1.6	28°F Propellant max P_c spike $\approx$ 450 psia
					Pulsing			
OC-26-160				Vac	10 at 0.01/3.0 250 at 0.01/0.3 200 at 0.025/0.3 50 at 0.100/0.3	80	1.6	118°F propellant
OC-26-161				Vac		155	1.6	118°F propellant

impulse could be achieved with a 2 in. chamber length and 100:1 nozzle. Subsequent tests with a 4 in. length provided an additional ≈ 11 sec improvement in performance (I_s = 311), high wall temperatures and slight evidence of longitudinal mode combustion instability (1L; 5,600 Hz). This was the only instability noted during the entire program. All subsequent testing in this series was accomplished with a 2-3/4 in. L', 50:1 expansion nozzle. All critical temperatures were monitored and provided the basis of run durations; no hardware damage was encountered.

The second test series employed the 6-SP-0 injector and a conical thin wall chamber which was expected to be lower performing and more compatible, thus allowing longer test durations. This design also provided specific impulse values slightly in excess of 300 sec and conflicting data concerning chamber compatibility. The thermal data uncertainty was related to the poor durability of the spot welded thermocouples. All testing was completed without damage to the hardware. Postfire inspection of the nozzle following Test 127 showed minor local coating spalling and cracking downstream of the throat. This was determined to be a result of excessive coating thickness (evaluation made by VacHyde). Additional factors which may have influenced the coating deterioration were operation above 3000°F and abrupt thinning of the nozzle wall downstream of the throat. It was later determined (Phase III) that the throat radius of curvature selected for the conical chamber may have been too sharp resulting in a trip of the laminar boundary layer at the throat. Subsequent tests in cylindrical chamber provided comparative data.

The next injector evaluated was a 4-UD-0) four-element design which provided higher injection velocities and was expected to provide extended blowdown capabilities. Sustained firings at full thrust were precluded by high injector face temperature (>700°F). No thermal limitations were encountered in pulsing operation.

5.2.3, Hot Fire Testing (cont.)

The 4-UD-28-S and 4-UD-28-SL designs were completed following the review of thermal and performance data from the previous tests, which showed an excess of performance and a lack of wall cooling capabilities. Testing on these designs was directed at achieving maximum sustained firing durations. Testing of the "S" version was conducted with a 2 in. and 1-1/4 in. chamber. The ability of the barrier cooling flow to reach the throat was considered superior in the short chamber. A stainless steel thermal liner (0.5 in. long 0.020 in. wall) was evaluated in some of these tests as indicated in Table 5.2-6. The purpose of the liner was to keep the forward chamber region cool. Testing was limited to 2100°F in the stainless steel chambers.

Simulated blowdown testing on the 4-UD-28-S design showed an ability to operate between 73 and 170 psia without chugging with the 2 in. chamber length. Chugging was first noted when P_c dropped to 56 psia. No damage was encountered in this series.

Testing of the 4-UD-28-SL design was also completed without damage. Propellant leakage believed to be at the valve-valve manifold interface was experienced in the longer duration higher pressure tests; thus reliable performance data for this design is lacking. The leak was later traced to a scratched seal surface which became marginal when the manifold was heated.

The final test set up employed the highest performing injector, 6-SP-45-A in the shortest chamber length, 1-1/4 in. Testing with hot and cold propellants was also conducted in this configuration at a cell pressure of 0.39 psia.

The history of the 5 injectors shown in Figure 5.2-13 at the time of photography; is as follows:

	No. Starts	Total Firing Time sec
6-SP-45-A	[illegible]10	38
6-SP-0	800	105
4-UD-0	600	48
4-UD-28-S	26	148
4-UD-28-SL	17	96

An additional 2117 pulses were executed on 6-SP-45-A following the photograph. The 6-SP-45-A injector experienced minor deformation of the face following a sustained period of pulsing with 22 and 28°F propellants. No changes in performance or flow characteristics were noted as a result of the platelet deflection. The 4-UD-0 was the only injector that experienced face temperatures which were considered to be excessive. No damage was encountered as the engine was shutdown when temperatures in excess of 700°F were observed. The dark area of the 4 element 4-UD-28 series injectors is the result of deposition from the fuel rich environment and not an indication of overheating. The 700°F injector temperature occurred at a low mixture ratio high chamber pressure test conditions.

Figure 5.2-14 provides photographic documentation of the 1.6:1 and the 50:1 area ratio thrust chambers and the L* extension employed in Phase II evaluation. The large rectangular boss on the titanium spacer and 1-1/4 in. long chamber contained the high response Kistler 601 pressure transducer. The total number of starts for these components was 4360, maximum duration accumulated on a single chamber was about 100 sec.

Figure 5.2-15 provides a reproduction of a typical oscillograph trace (Test 143) showing the last 0.6 sec of a 5 sec continuous burn, a 0.3 sec coast and a subsequent hot restart. This rate of response was typical of all restarts on all of the engines tested. Analyses of these data are provided in a subsequent section.

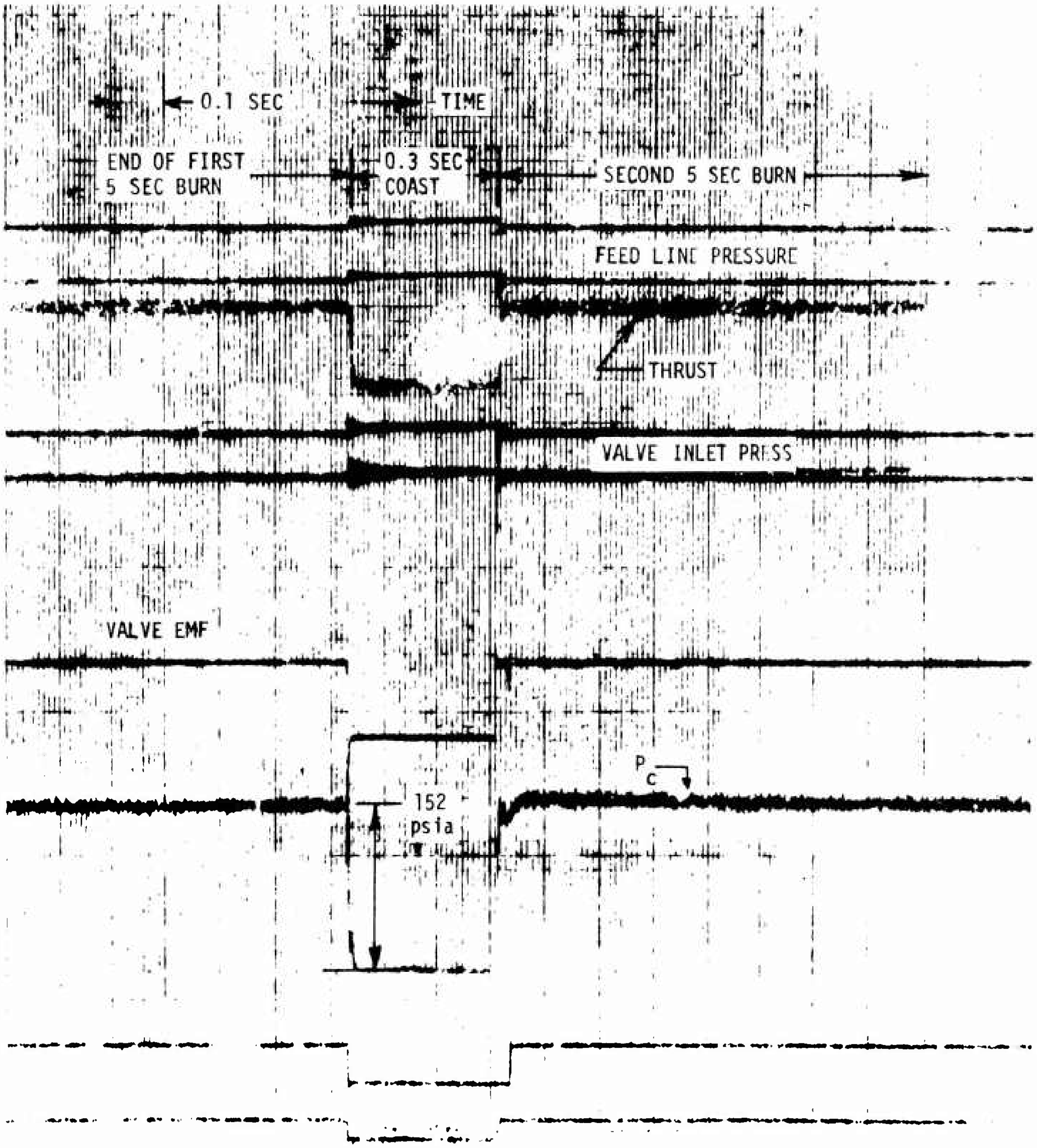

Figure 5.2-15. Typical Oscillograph Trace (Test 143)

Figure 5.2-16 provides a record of 0.03 sec electrical pulses before and after a long burn (Test 109). High response feed system and chamber pressure traces are shown in comparison to the normal low response chamber pressure measurement. This data record was obtained via playback from the FM recording system. Items to be noted include:

(1) The P_c rise rate measured by both chamber pressure transducers is very rapid and repeatable as is the P_c decay rate.

(2) The maximum spike pressure of 250 psia represents a 60% overpressure which is well within the engine's design limits.

(3) The cold chamber and hot chamber pulses have the same response and shape.

(4) A 0.0034 sec period of unstable operation, which was self attenuating, was the only incident of high frequency instability noted in the entire test program. The 5600 Hz corresponded to a first longitudinal mode in a 4 in. chamber length which was the longest length tested. This length provided a 99% energy release efficiency which converts to a 311 sec specific impulse at $\epsilon = 100$. All subsequent testing was conducted at lengths of 2-3/4 in. or less. The short period of unstable operation on the first pulse following the soak is attributed to the warmed propellant at the valve inlet in conjunction with the excessively long chamber.

Figure 5.2-17 provides a comparison of the first and second 0.010 sec electrical pulses for 3 different injector designs relative to a common valve voltage trace. The response is noted to be independent of injector design. It is related to the manifold volumes which were comparable and the close coupled relationship to the valve seats. The first and second pulses are noted to be identical in each case. The relative delay of thrust and rounding of the shape are due to the use of a 300 Hz filter to remove the stand ringing at 575 Hz from the trace.

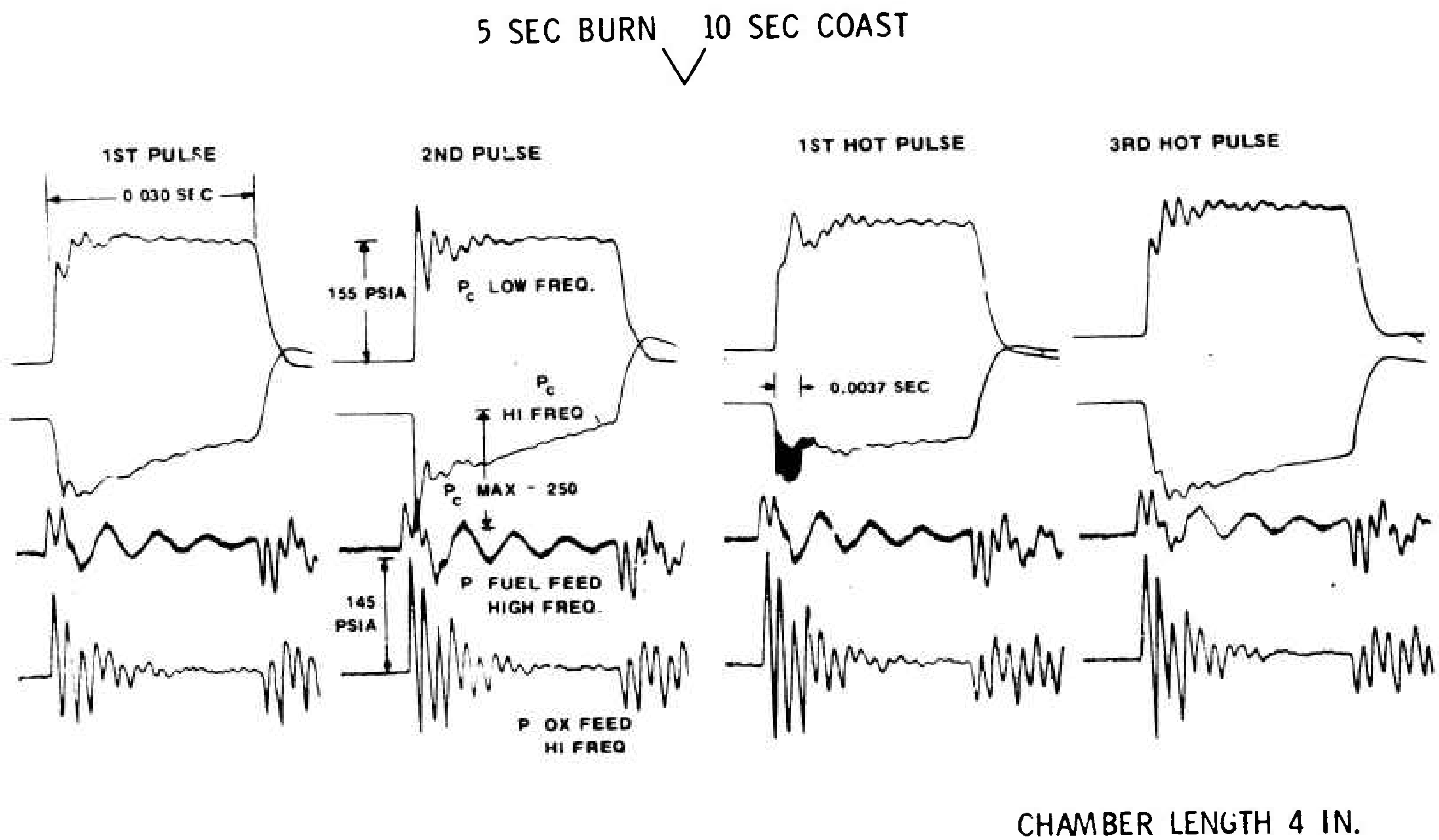

Figure 5.2-16. Comparison of Cold Chamber Pulses with Pulses after Long Burns

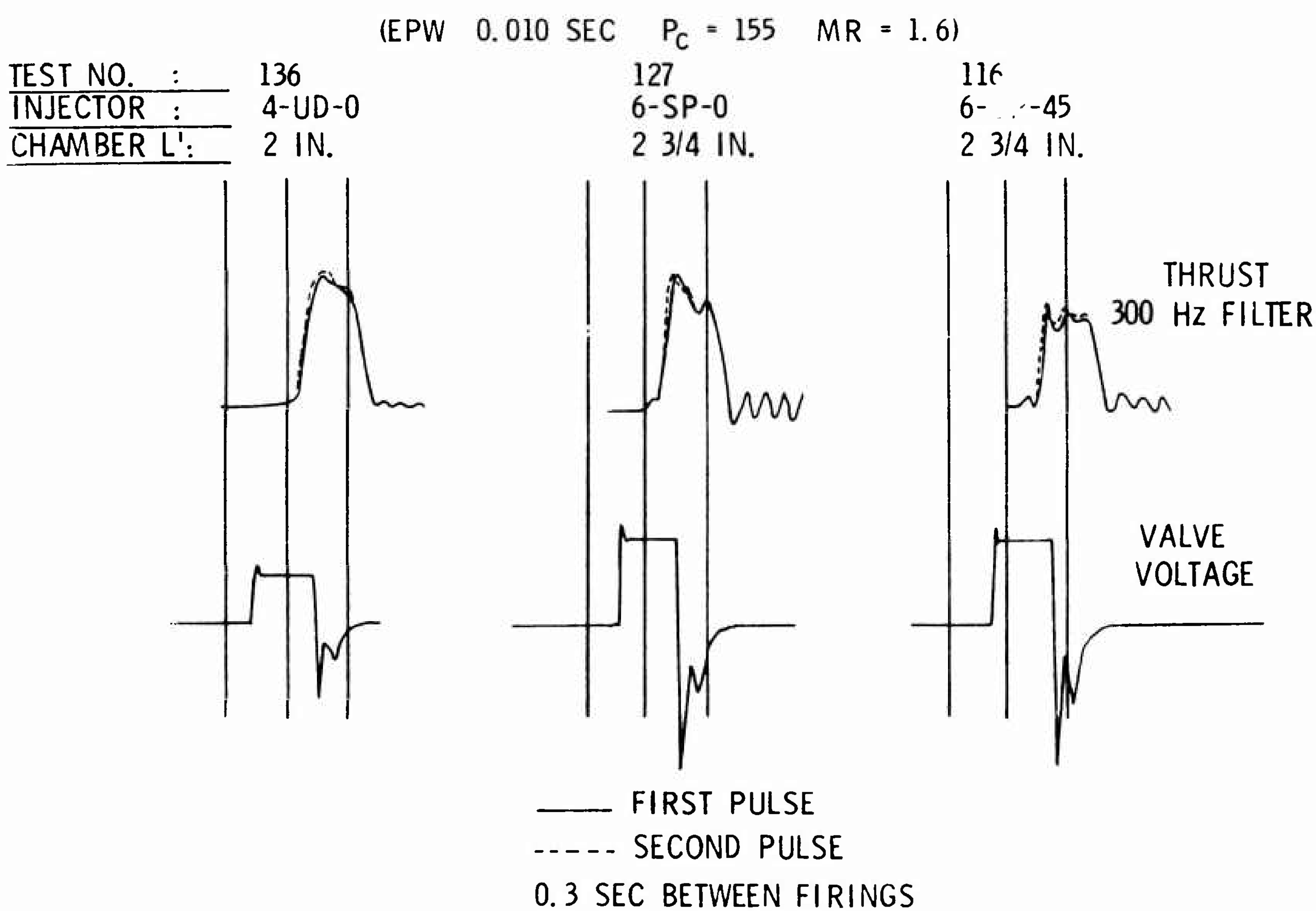

Figure 5.2-17. Comparison of Vacuum Thrust Response with Various Injectors

5.2.3, Hot Fire Testing (cont.)

Figure 5.2-18 provides a comparison of the chamber pressure and thrust level relative to a common valve electrical signal at 3 tank pressure levels. This corresponds to various levels of blowdown. Reduced tank pressure is noted to result in slightly longer fill times, longer ignition delay times and slightly harder starts as indicated by greater thrust and P_c over shoots. All these, however, are trends rather than significant effects and the general square wave pulse is retained over a 3:1 blowdown range. The failure of the P_c trace to return to "0" in many of these pulses is due to thermal effects on the transducer diaphram located about 1/4 in. from the combustion zone.

Figure 5.2-19 provides typical response data obtained by playback from the FM recording system at a highly expanded scale. The data in this test correspond to a 0.010 sec pulse at vacuum conditions (P amb 0.39 psia) with 22° propellant in a 1-1/4 in. chamber length. The cold propellant and very short chamber length represent the worst condition for low level propellant reactions which lead to ignition delay and large ignition spikes. The response, pressure decay and ignition spike data were obtained at the four corners of the feed system temperature-pressure operating box at the following test conditions.

Tank Pressure	Temp, °F: 22	118
	Duty cycle at each of 4 conditions	
100 psia	0.01/3.0	0.3% DC
	0.01/0.3	3%
300 psia	0.025/0.3	7.7%
	0.100/0.3	25%

Ignition spikes which were obtained directly from high response graphic data are displayed in Figure 5.2-20. These data indicated a peak pressure of 460 psia in the first few pulses with cold hardware and

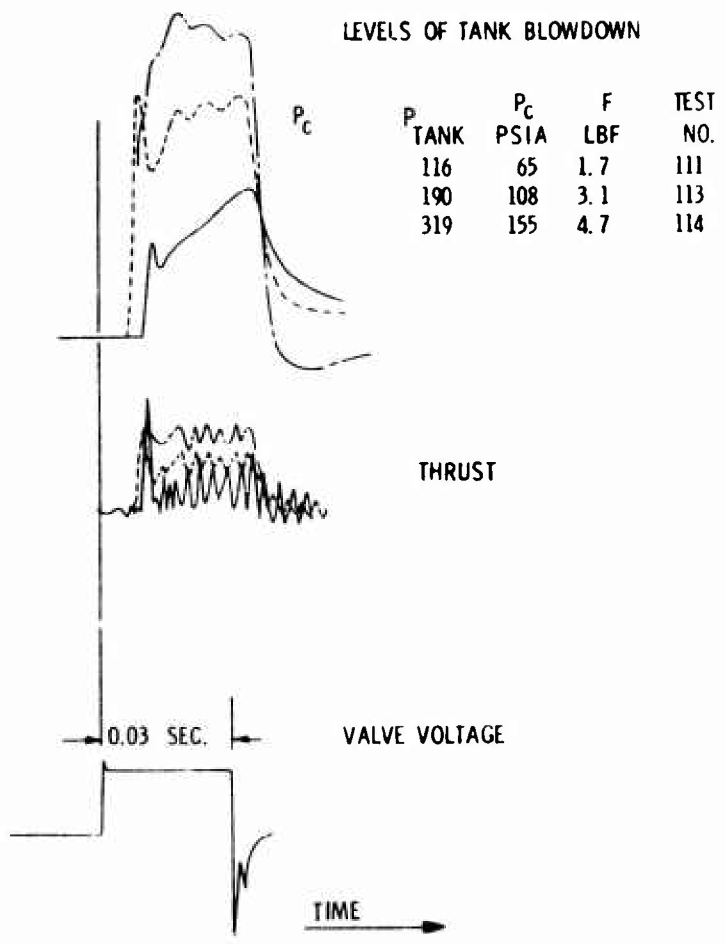

Figure 5.2-18. Comparison of Chamber Pressure and Thrust Level Relative to a Common Valve Electrical Signal at Three Tank Pressure Levels

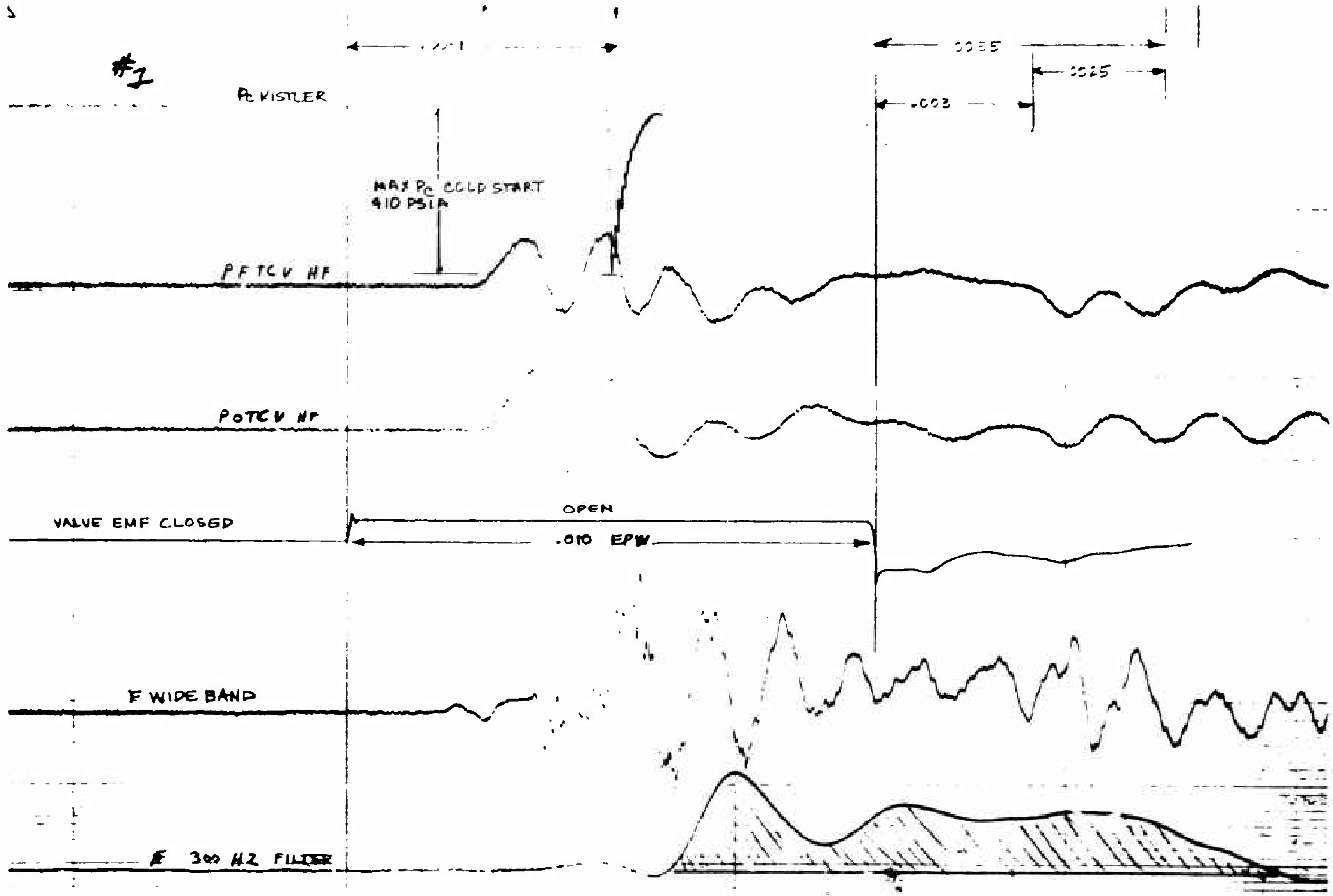

Figure 5.2-19. Engine Response, 150 psia, 22°F Propellants, First Pulse

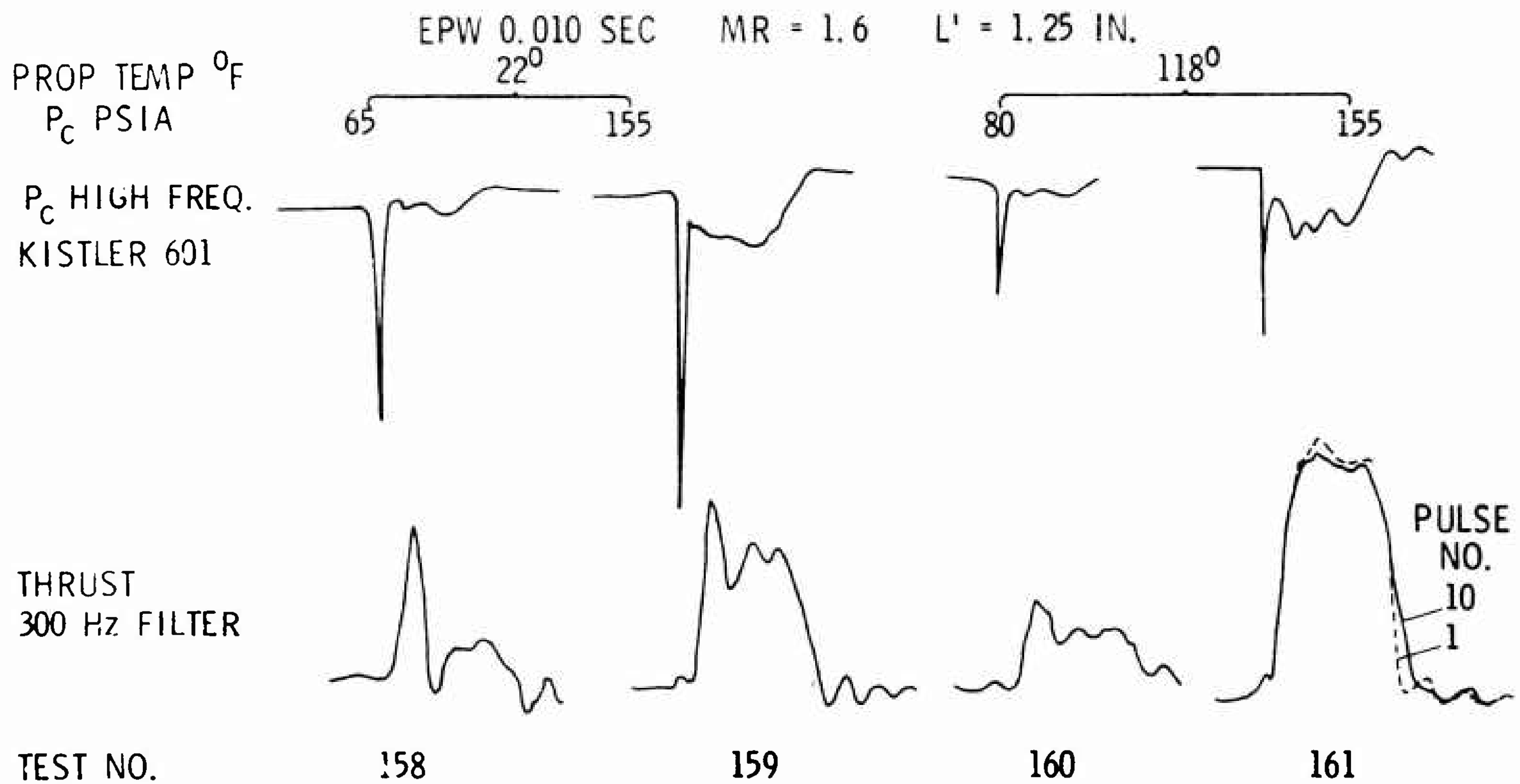

P_C PEAK VALUES (PSIA)

	DUTY CYCLE	3%	0.3%	3%	0.3%	3%	0.3%	3%	0.3%
PULSE NO.	1	160	180	416	380	184	144	240	210
	2	384	260	460	440	230	180	350	320
	3	450	160	420	300	240	180	360	-
	10	-	140	-	260	-	200	-	320
	≈200	200	-	260	-	170	-	250	-

Figure 5.2-20. Engine Start Characteristics and Pulse Shape at Extreme Operating Conditions

cold propellants. This was nearly independent of tank supply pressure and duty cycles from 0.3 to 3%. The magnitude of these spikes were about 100 psia less with heated propellants; these compare with a 2000 psi allowable spike pressure based on the yield point strength of the chamber materials. Minor deformation of the 6-SP-45-A injector face platelet which occurred in the process of conducting 1020 pulses at the low temperature conditions led to a platelet thickness increase which strengthened the Phase III injector faces by a factor of four.

5.3 DATA EVALUATION

5.3.1 Test Data Evaluation

5.3.1.1 Response

Table 2.1-1 provides a summary of the engine response at limiting propellant-hardware temperatures and tank supply pressures. Engine response (electrical signal to 90% P_c) is noted to be 0.0056 sec $\pm$ 0.0006 sec at all anticipated operating conditions. Valve response (activation period at 28 volts) is 0.0023-0.0026 sec to open and 0.0025-0.0028 sec to close under all anticipated operating conditions. Valve travel time is estimated to be 0.0005 sec providing a nominal signal to full mechanically open or fully closed of 0.003 sec. The valve is hydraulically open in about 0.0026 sec. These response data were found to be independent of duty cycle and were the same for all pulses including the first of the series. The valve response of 0.0026 sec is highly favorable in comparison to the contract goal of 0.005 sec.

5.3.1, Test Data Evaluation (cont.)

5.3.1.2 Repeatability of Pulses

The pulse repeatability was evaluated by computing the force time integral using a force sampling rate of 1302 measurement per sec. The accuracy of when applied to a 0.010 sec square wave input signal pulse was determined to be within 2%. Table 5.3-1 provides some typical data for a nominal 0.05 lbF-sec pulse train series. The first pulses are noted to be slightly lower than the average of the data. This is due to the rapid pulsing frequency (3/sec) which does not allow the propellant on the wall and within the manifold to exhaust completely on the first pulses when the chamber is cold. Data from Pulse No. 5 through 402 are completely repeatable within the 2% accuracy allowed by the sampling rate. This can be observed by comparing the 0.0498, 0.0500 and 0.0500 lbF-sec impulse average obtained from pulse Nos. 11-20, 21-30 and 393-492, respectively. These data are well within the 0.05 ± 0.005 lbF-sec goal of the program.

Figure 5.3-1 graphically displays the impulse data for 6-SP-45-A and 4-UD-0 injectors. The ability to attain the goal of 0.05 ± 0.005 lbF sec repeatability is noted to be independent of injector pattern design. The triangular data points on the lower half of the plot illustrates that an order of magnitude change in pulsing frequency (3 pulses per sec to 1 pulse per 3 sec) has no influence on measured impulse.

The impulse reproducibility of electrical pulse with of 0.025 sec was 0.125 lbF-sec ± 1%, as shown in Figure 5.3-2.

5.3.1.3 Performance

During Phase II, performance data from 46 steady state and 7 pulse test series were analyzed. These tests were conducted with five different injector patterns, chamber lengths ranging between 1.25 and 4.0 inches, and sea level and vacuum area ratios of 1.6:1 and 50:1, respectively.

TABLE 5.3-1

IMPULSE REPEATABILITY FOR 0.010 SEC ELECTRICAL PULSES, TEST NO. 116

Pulse No.	Impulse lbF-sec	Pulse No.	Impulse lbF-sec	Pulse No.	Impulse lbF-sec	
1	0.0436	11	0.0488	21	0.0507	
2	0.0469	12	0.0508	22	0.0507	
3	0.0465	13	0.0491	23	0.0490	
4	0.0475	14	0.0518	24	0.0488	
5	0.0484	15	0.0480	25	0.0501	
6	0.0490	16	0.0504	26	0.0497	
7	0.0499	17	0.0501	27	0.0499	
8	0.0483	18	0.0493	28	0.0496	
9	0.0481	19	0.0492	29	0.0509	
10	0.0489	20	0.0502	30	0.0501	Average 1-30
Avg.	0.0477		0.0498		0.0500	0.0492 lbF-sec
Std Dev	3.4%		2.2%		1.4%	
Dev. from 30 pulse avg.						
	-3.0		+1.3		+1.6	
Avg. of Pulse Nos. 393 - 402					0.0500	

MR = 1.6, P_c = 150

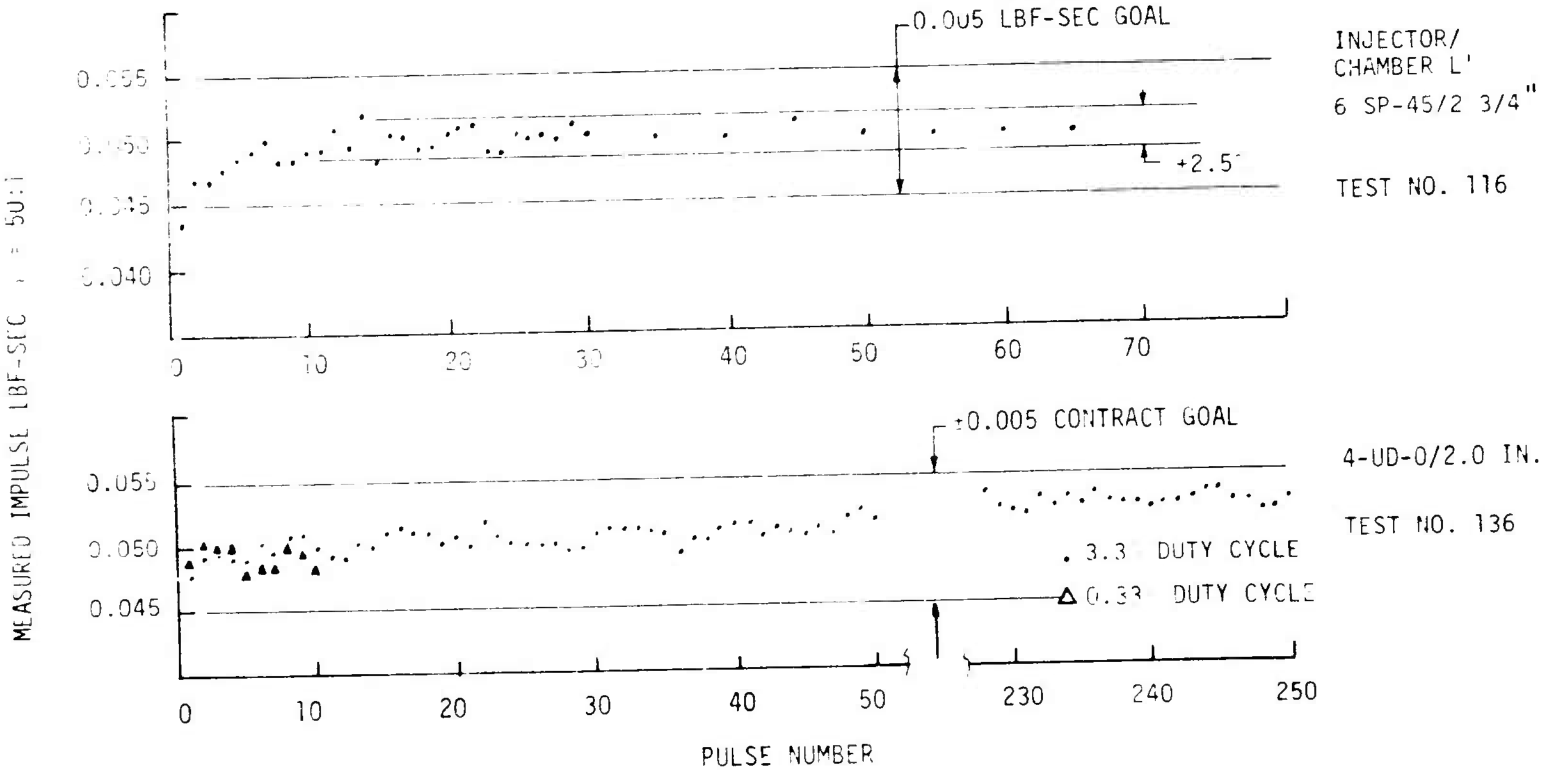

Figure 5.3-1. Bit Impulse Repeatability at 0.010 sec EPW, 0.05 lbf-sec

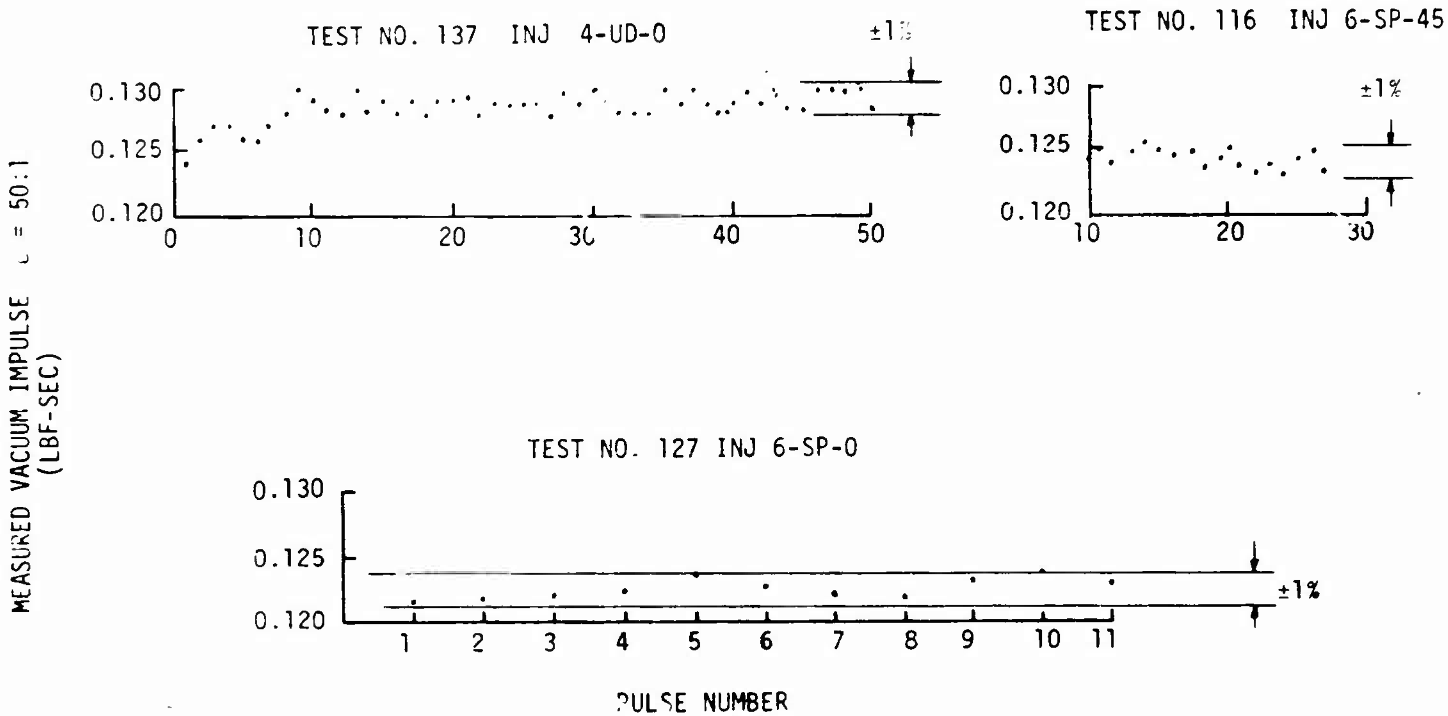

Figure 5.3-2 Bit Impulse Repeatability at 0.025 sec Electrical Pulse Widths from Series of 200 Firings

These data indicate that the ϵ = 100:1 vacuum performance extrapolations are in excess of the 300 sec steady state and 240 sec pulsing performance goals specified in the contract goals. The Phase II performance data verify the steady state Priem vaporization analysis and the pulsing performance trends predicted via the CONTAM analysis documented in Phase I.

5.3.1.3.1 Steady State Performance at Full Thrust

The steady state performance data are summarized in Table 5.3-2. To simplify testing, $\approx$ 2/3 of all testing was conducted at sea level. The ϵ = 1.6 nozzle exit area ratio was selected to preclude nozzle flow separation at all P_c's. The simplified JANNAF performance methodology was used to allocate the total engine losses into (1) nozzle divergence, (2) nozzle kinetic, (3) chamber/nozzle boundary layer, (4) transient thermal heat loss, and (5) combined energy release and mixture ratio maldistribution performance losses. These sea level performance losses were then extrapolated to the nominal ϵ = 100:1 vacuum nozzle design point. The ϵ = 1.6 to ϵ = 100 extrapolation resulted in an approximately 70 sec I_{sp} increase. Although the nominal vacuum engine design is based upon an ϵ = 100 nozzle exit area ratio, the Phase II vacuum tests were conducted at ϵ = 50 to preclude nozzle flow separation at the low ($P_c \leq$ 70 psia) end of the blowdown cycle because of test facility vacuum limitations. The ϵ = 50 to ϵ = 100 extrapolation is only 7 sec ΔI_{sp}. Because of the small vacuum extrapolation and the excellent correlation between sea level and vacuum extrapolations to ϵ = 100 shown herein, a high degree of confidence was placed upon the steady state data.

The 6-SP-45 injector was tested at sea level at chamber lengths (L') of 1.25, 2.0, and 4.0 in. as well as at vacuum in 2.75-in. L'. The performance extrapolations to ϵ = 100 steady state conditions are shown in Figure 5.3-3. The I_{sp} after $\approx$ 5 seconds firing duration is also shown. The initial I_{sp} is lower due to transient thermal heat loss. The maximum steady state I_{sp} is indicated to be 310 sec at L' = 4 in. Interpolation

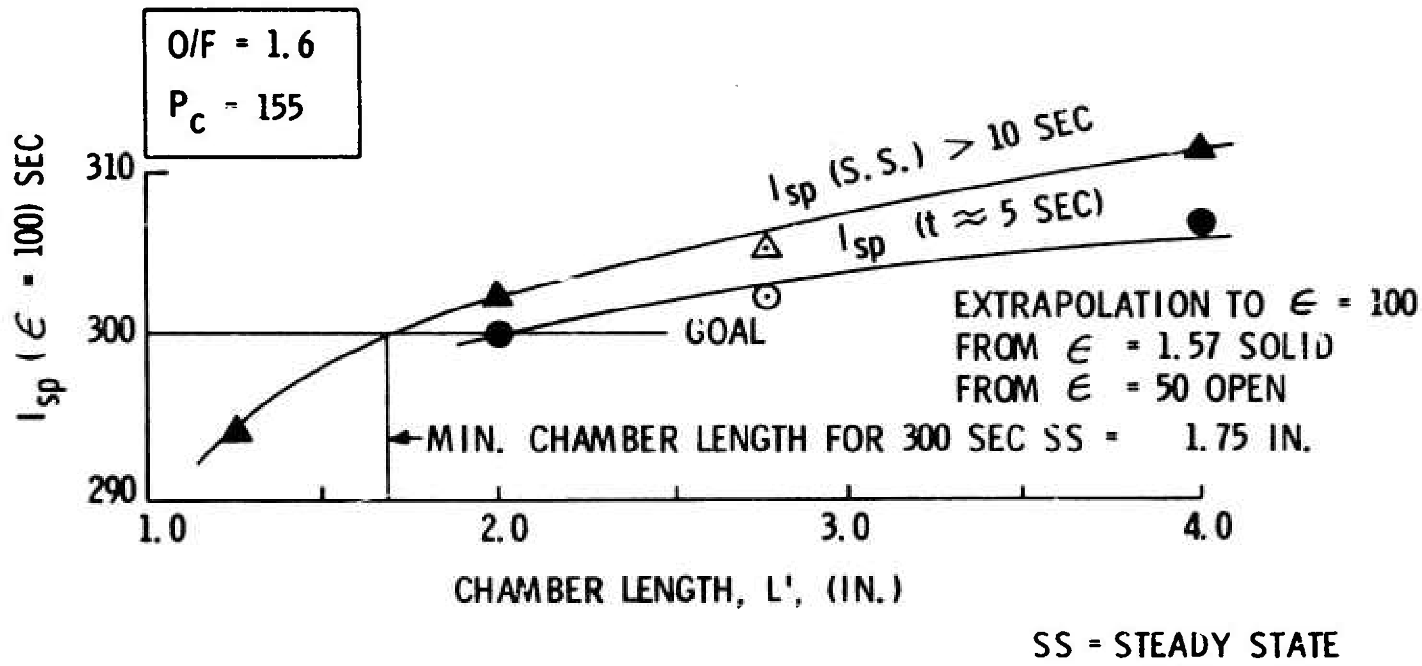

Figure 5.3-3. 6-SP-45 Injector Long Burn Performance Summary at 5 lb Thrust (Chamber Length Effects)

shows it is possible to achieve the 300 sec steady state performance goal with this injector in a minimum chamber L' ≈ 1.75 in. Figure 5.3-4 shows a more extensive map of steady state performance of the 6-SP-45-A injector versus mixture ratio and chamber length. These data and the 100% ERE dotted line show that the % ERE is nearly constant at any value of L' and maximum performance is attainable at the peak one dimensional kinetic (ODK) I_{sp} which occurs at O/F ≈ 1.9 rather than the nominal design engine O/F = 1.6. Another observation is that a 4 in. L', the demonstrated I_{sp} approaches the perfect injector (100% ERE) I_{sp} limit.

The 6-SP-0 injector performance versus O/F at L' of 2.0 and 2.75 in. is shown on Figure 5.3-5. The injector also indicates the potential of exceeding 300 sec steady state I_{sp} for L' $\geq$ 2 in.

Due to its high injector face temperatur , the 4-UD-0 injector was not capable of being tested at nominal P_c = 160 psia. However, at P_c = 94 psia and O/F = 1.49, it too indicated a capability of exceeding 300 sec I_{sp} (see Test 132 of Table 5.3-2).

Fuel leakage of the 4-UD-28-SL injector at high pressure due to a faulty seal surface, precluded an accurate determination of this injector's steady state performance. It was estimated that this injector operated in the 290-300 sec performance range. It was discarded from further development due to its high operating temperatures along the forward chamber wall.

The 4-UD-28-S injector provided a relatively cool chamber wall due to use of barrier fuel cooling supporting the conclusions drawn from cold flow evaluation. Steady state performance was ≈ 283 sec (extrapolated from sea level to 100:1). This injector was later selected for the long duration firing in an adiabatic wall engine configuration. Additional data on all the injectors is provided in the discussion on Blowdown Performance which follows.

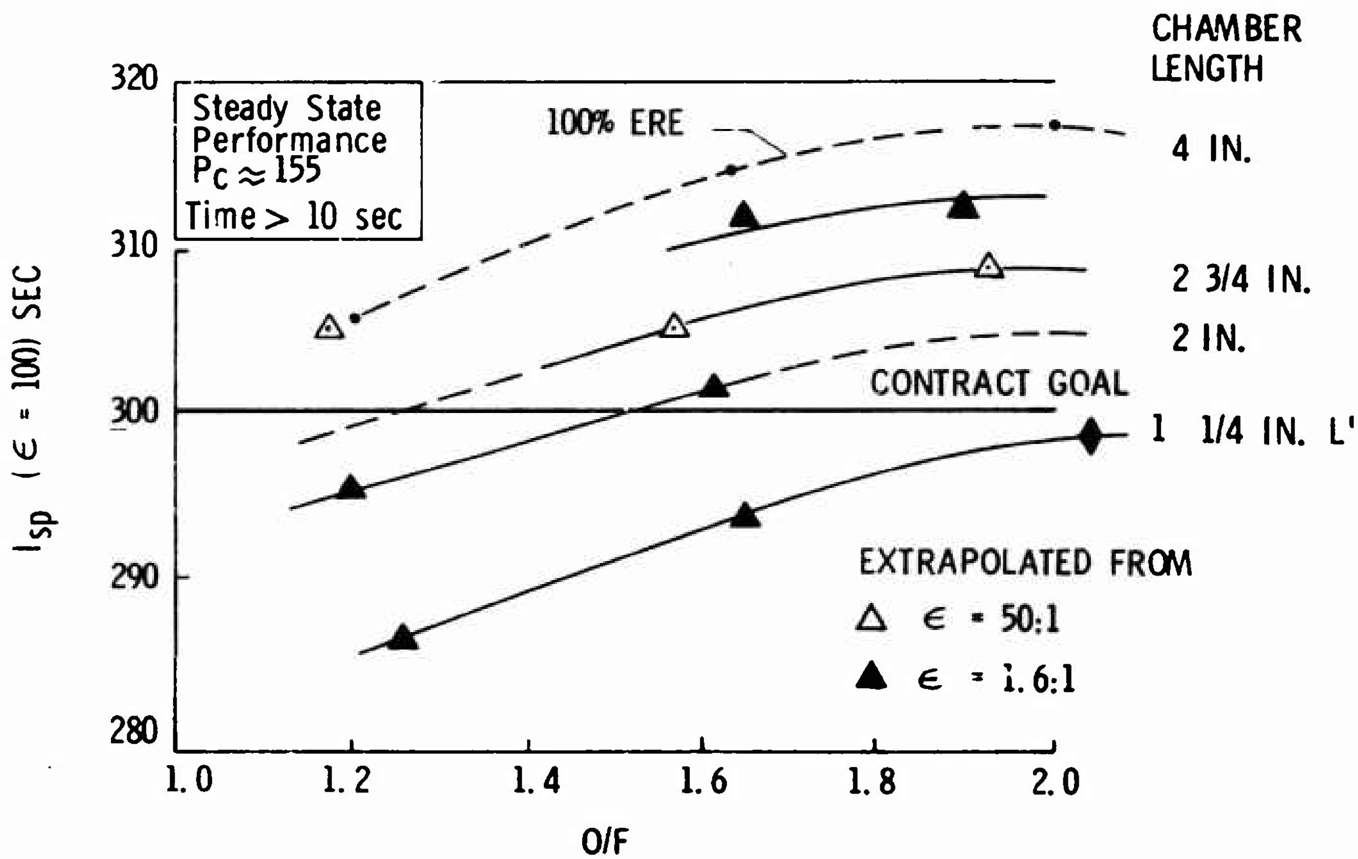

Figure 5.3-4. 6-SP-45 Injector Long Burn Performance Summary at 5 lb Thrust (Mixture Ratio Effects)

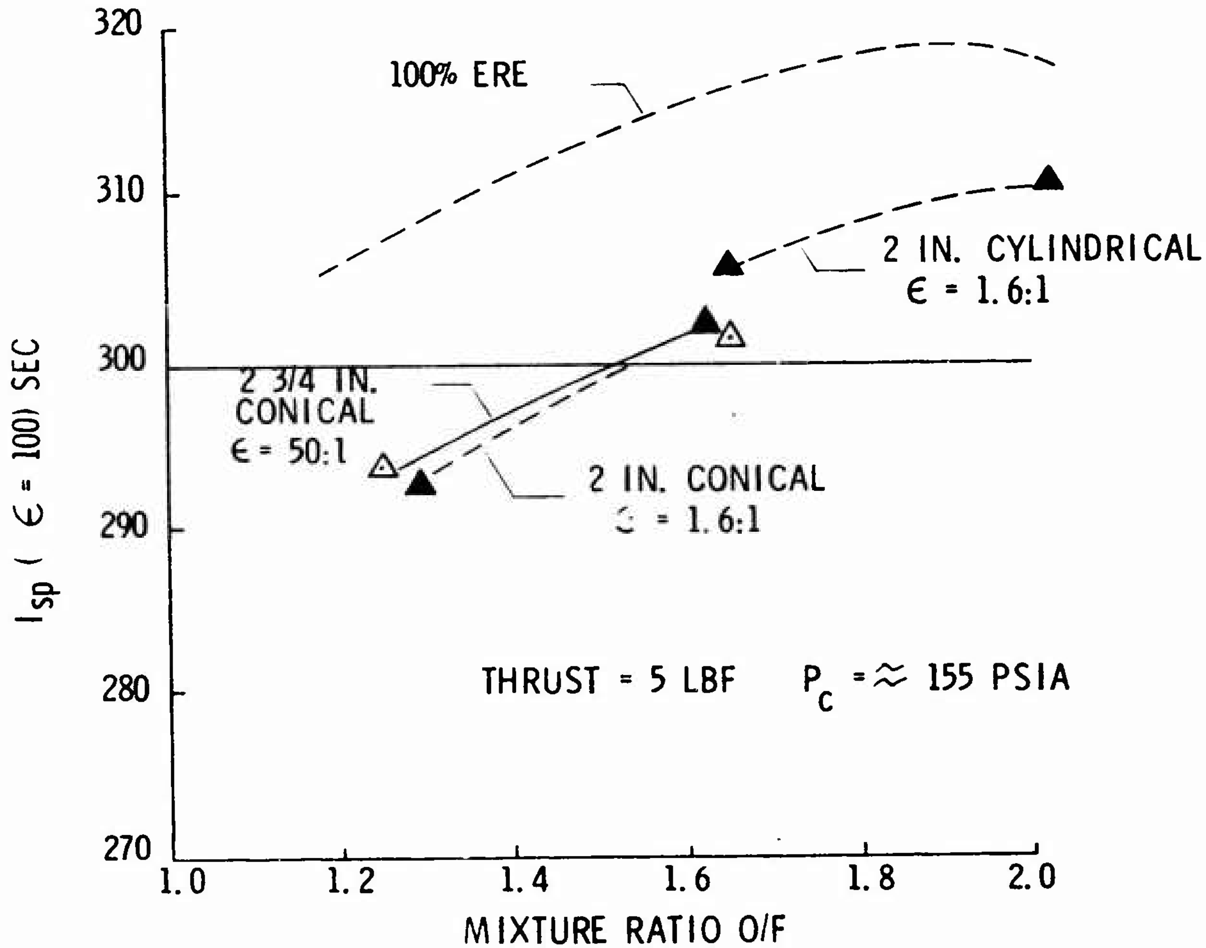

Figure 5.3-5. 6-SP-0 Injector Long Burn Performance Summary

TABLE 5.3-2

STEADY STATE PERFORMANCE SUMMARY FOR VARIOUS INJECTORS

Test No.	104	105	107	108	109	110	111	112	113	114	115	117
Injector	6SP-45 →											
Chamber Length	2-in. →				4-in. →		2.75 →					2-in. Conical
Nozzle Exit	1.6 →						50 →					1.7
Sea Level or Vacuum	SL →						Vac →					SL
Summary Period												
Chamber Pressure	150	154	153	67	155	156	65	150	108	155	155	154
Mixture Ratio	1.18	1.62	2.07	1.61	1.65	1.90	1.61	1.17	1.59	1.56	1.92	1.60
Thrust							2.10	4.85	3.51	4.99	5.02	3.95
Delivered I_{sp}	222	225	226	199	227	227	259	292	289	296	300	228
% ERE	96.9	97.1	97.7	87.5	98.0	99.0	86.7	98.0	95.[illegible]	96.3	96.1	96.7
$I_{sp_{ss}}$ $(\epsilon = 100)_{Extra}$	295	306	309	266	308	311	268	300	298	305	309	305

Test No.	119	120	121	122	123	124	126	128	129
Injector	6SP-0 →								
Chamber Length	2-in. Conical →				2.75 Conical →			2-in. Cyl →	
Nozzle Exit	1.7 →				53 →			1.6 →	
Sea Level or Vacuum	SL →				Vac →			SL →	
Summary Period									
Chamber Pressure	86	158	152	94	75	159	159	160	158
Mixture Ratio	1.64	1.29	1.63	1.60	1.48	1.26	1.63	1.63	2.02
Thrust	1.73	3.91	3.92	2.18	2.10	4.82	4.96	4.17	3.93
Delivered I_{sp}	201	220	223	207	266	284		224	222
% ERE	88.0	95.2	96.0	90.5	89.4	96.1		96.1	97.1
$I_{sp_{ss}}$ $(\epsilon = 100)_{Extra}$	270	292	302	280	273	294		303	310

Test No.	131	132	133	134	135
Injector	4UD-0 →				
Chamber Length	2-in. Cylindrical →				
Nozzle Exit	50 →				
Sea Level or Vacuum	Vac →				
Summary Period					
Chamber Pressure	77	94	162	76	77
Mixture Ratio	1.52	1.49	1.84	1.97	1.50
Thrust	2.51	3.03	5.20	2.46	2.47
Delivered I_{sp}	284	295	285	275	284
% ERE	95.2	97.9	93.5	91.2	94.8
$I_{sp_{ss}}$ $(\epsilon = 100)$	292	302	294	278	290

TABLE 5.3-2 (cont.)

Test No.	137	138	139	140	141	142	143	144	145	146
Injector	4UD-28-S →									
Chamber Length	2 in. Cyl →							1.25 Cyl →		
Nozzle Exit	1.6 →							1.7 →		
Sea Level or Vacuum	SL →									
Summary Period										
Chamber Pressure	152	153	152	56	73	82	145	144	141	152
Mixture Ratio	1.56	1.52	1.58	1.63	1.59	1.68	1.82	1.54	1.77	1.20
Thrust	3.63	3.54	3.66	1.33	1.73	2.01	3.46	3.71	3.62	3.83
Delivered I_{sp}	210	205	204	187	196	206	195	208	203	205
% ERE	90.4	88.3	88.7	83.9	87.1	91.1	85.6	88.2	86.3	88.6
$I_{sp_{ss}}$ (ϵ = 100)	283	275	277	254	265	281	267	274	269	268

Test No.	147	148	150	151	152	153	154	155	156	157
Injector	4UD-28-SL →					6-SP-45 →				
Chamber Length	2 in. Cyl →					1.25 Cyl →				
Nozzle Exit	1.6 →					1.7 →				
Sea Level or Vacuum	SL →					SL →				
Summary Period										
Chamber Pressure	159	157	77	118	156	65	78	149	149	148
Mixture Ratio	1.43	1.09	1.50	1.53	1.73	1.57	1.62	1.25	1.65	2.02
Thrust	3.76									
Delivered I_{sp}	203	198	202	215	201	179	199	218	221	218
% ERE	68.4	87.8	89.9	94.4	87.5	78.1	85.7	93.8	94.1	93.7
$I_{sp_{ss}}$ (ϵ = 100)	274	263	274	294	274	234	261	287	296	294

The Phase II experimental energy release efficiencies of the 4 and 6 element injectors tested at 1.25, 2.0, and 4.0 in. chamber lengths are plotted on Figure 5.3-6 in comparison with the Phase I Priem vaporization analysis results. The effects of chamber length and element quantity were in general agreement with analytical predictions. The effect of chamber contraction ratio (CR), however, was not discernible to the extent analytically predicted. This is attributed to the influence of the propellant film upon the chamber wall which is not accounted for by the steady state Priem analysis. The data showed little difference between 6.7 CR conical and 10.9 CR cylindrical chamber performance.

5.3.1.3.2 Blowdown Performance Characteristic

Many 5 lbF engine applications for spacecraft require a blowdown capability to simplify propellant pressurization requirements. A typical blowdown may start at a 300 psia tank pressure and conclude at 100 psia. Consistent with these tank pressure requirements, an initial or maximum P_c of 170 psia was selected. This results in a terminal P_c value of 75 psia. The corresponding engine thrust ranges from 5 lbF maximum to $\approx$ 2.2 lbF minimum. To simulate these requirements during Phase II, all prospective engine designs were tested at 160 and 70 psia; some designs were tested at intermediate $P_c \approx 100$ psia.

The steady state blowdown performance characterization of the 6-SP-45-A injector is shown in Figure 5.3-7 for both 1.25 and 2.75 in. chamber lengths. Also shown is the approximate propellant tank level during a 3:1 tank pressure blowdown mode. It can be seen that as the tanks blowdown and empty, the steady state performance is degraded. The magnitude of performance degradation with decreasing P_c is steeper than analytically forcasted considering reduced droplet heat flux and a decreasing vaporization rate. The test data suggests that at least part of the performance degradation is due to reduced atomization efficiency.

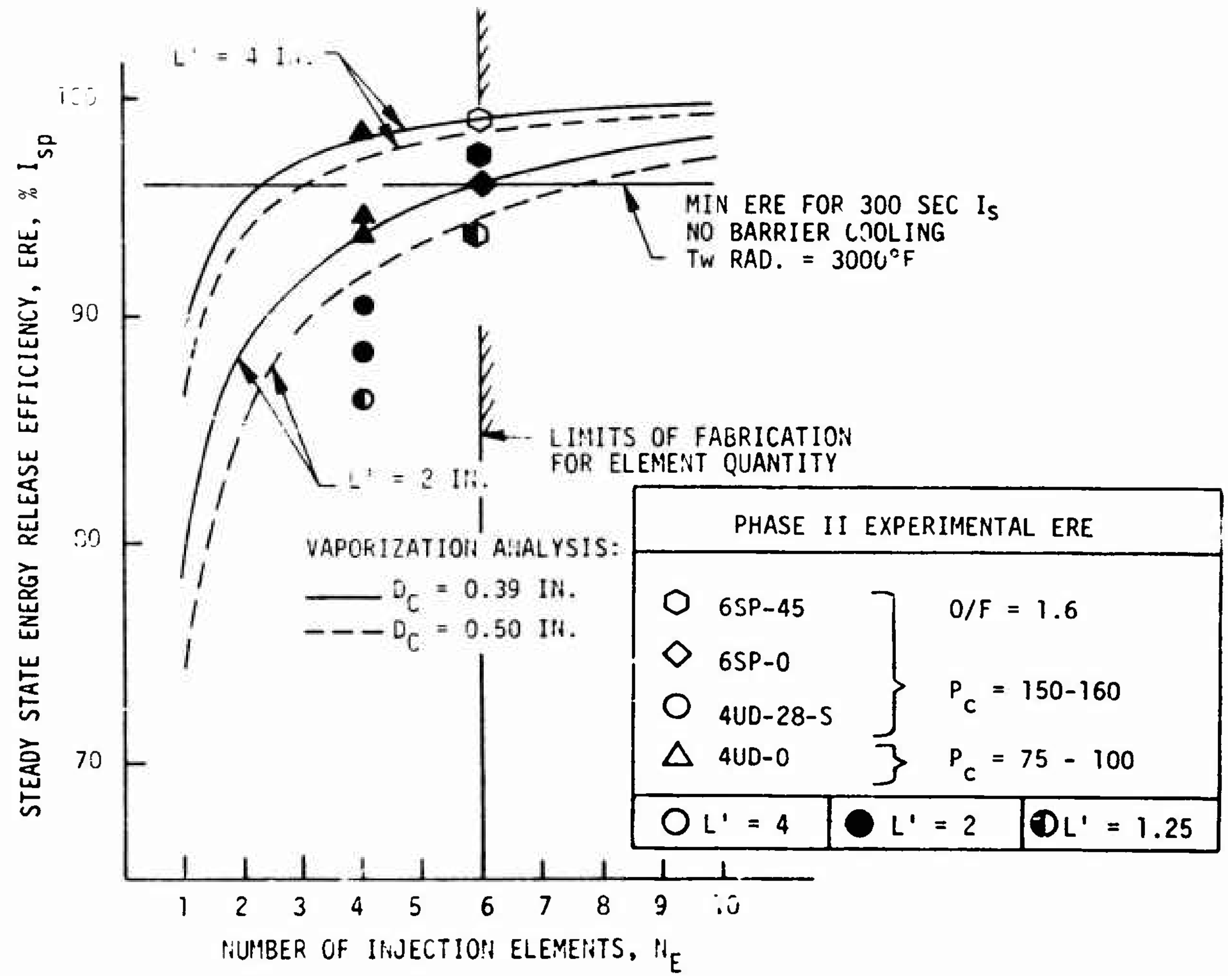

Figure 5.3-6. Element Quantity and Chamber Interaction

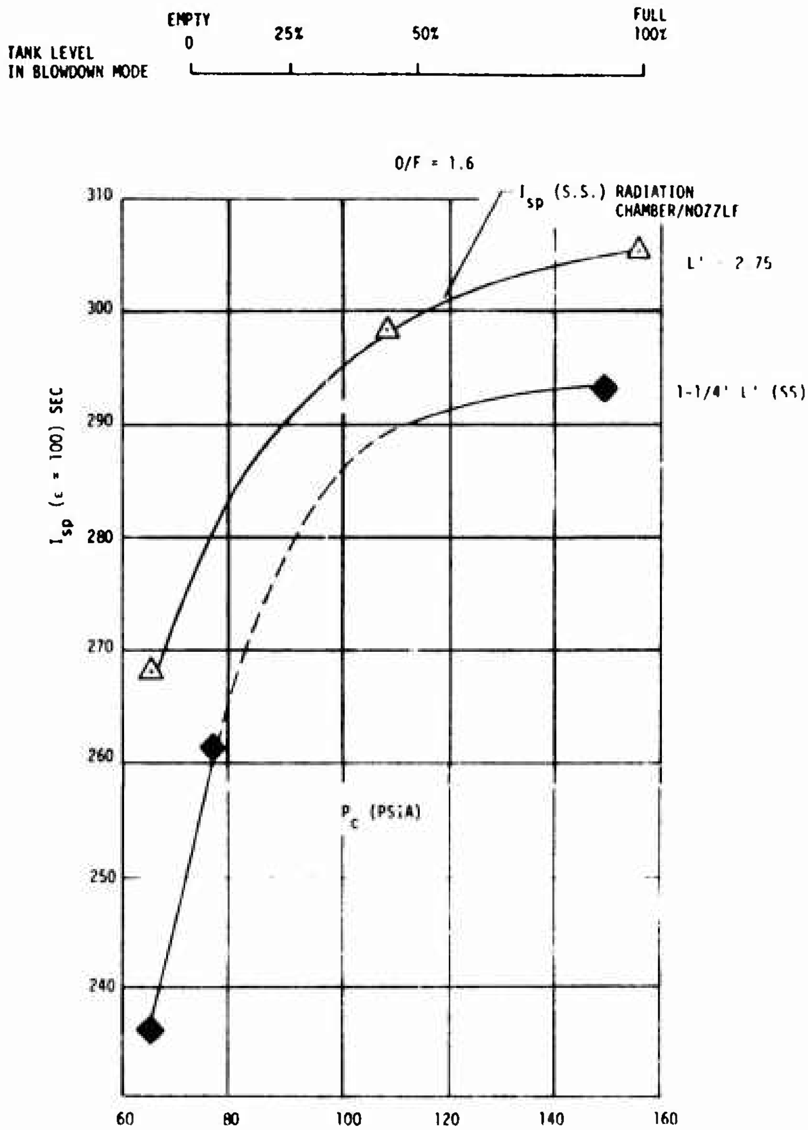

Figure 5.3-7. 6-SP-45 Injector Long Burn Performance for Simulated Blowdown Mode Operation

5.3.1, Test Data Evaluation (cont.)

Similarly, the 6-SP-0 blowdown performance is depicted in Figure 5.3-8. Negligible differences between the 2.0 and 2.75 in. L' chamber performance are noted at nominal P_c = 160 psia. A significant difference is measured, however, at the low end of the blowdown; since injection atomization efficiency is poor, added chamber length improves performance. If atomization is effective and steady state performance is high (as at maximum P_c) the vaporization improvement with length may be largely offset by the steady state radiant heat/boundary layer performance loss. Both of the aforementioned 6-element injectors have similar blowdown performance characteristics.

The 4-UD-0 blowdown performance is substantially higher as shown in Figure 5.3-9. This is attributed to the higher injection velocities of the 4-element injector at minimum flow rates and P_c. Unlike the 6-element splash plate injectors, the unlike doublet maximum steady state performance occurs at a relatively low O/F rather than at the peak $I_{sp_{ODK}}$ at 1.9 O/F. This occurs because the unlike doublet atomization distribution is extremely injection momentum ratio sensitive. Maximum ERE was found to occur at O/F ≈ 1.3.

The blowdown performance characteristics of the 4-UD-28-S injector is provided in Figure 5.3-10. This is the coolest operating but also lowest performing injector at all steady state operating conditions. It likewise shows a performance reduction at the lowest operating P_c's.

At the minimum blowdown P_c ≈ 70 psia, the 6 element injectors have steady state fuel injection velocities ≈ 40 fps; but their minimum oxidizer injection velocities are only ≈ 25 fps. Numerous cold flow literature data, as well as hot fire test data, indicate that atomization efficiency is significantly degraded below 40 fps. This prior experience suggested that although the fuel injection velocities were sufficiently high

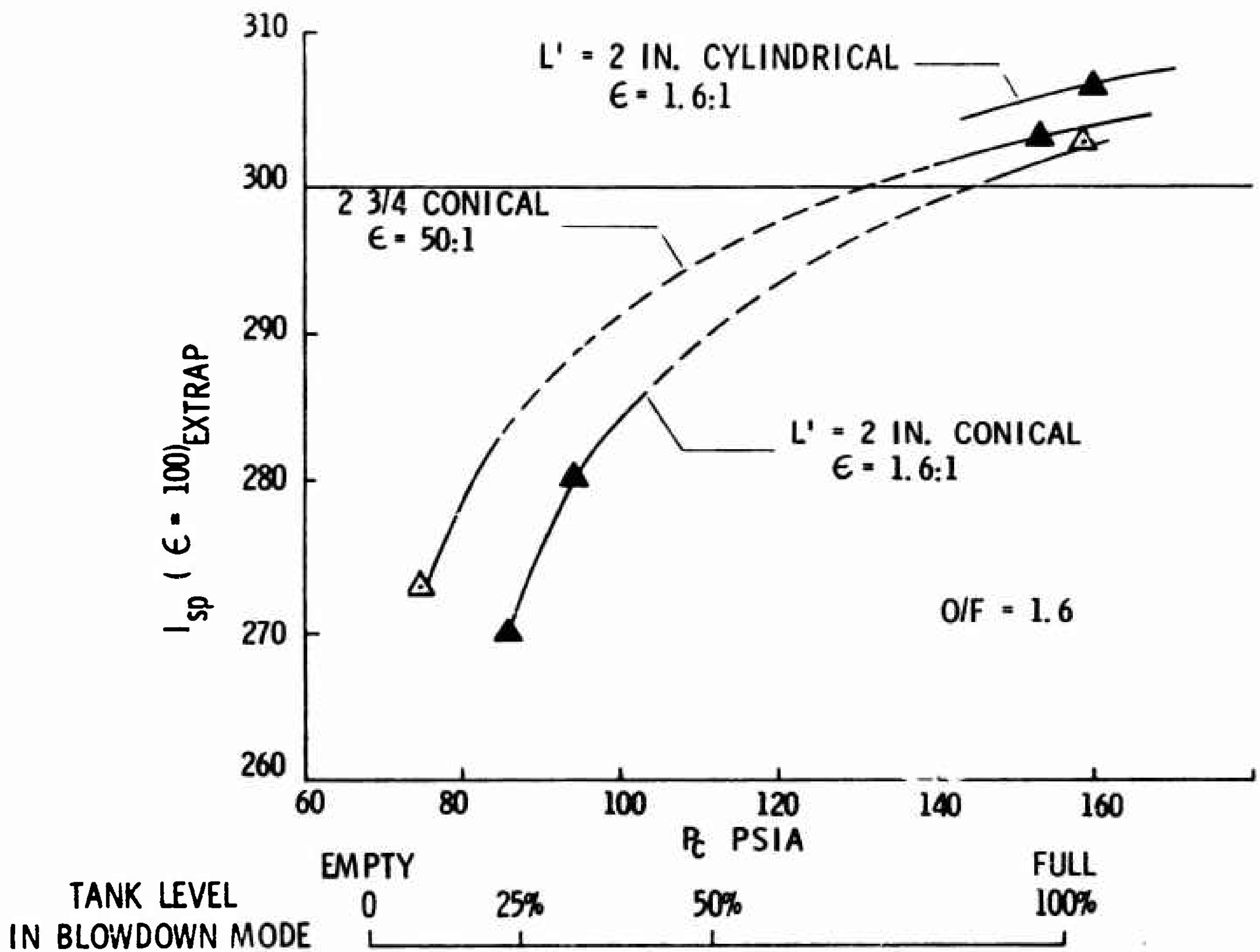

Figure 5.3-8. 6-SP-0 Injector Long Burn Performance for Simulated Blowdown Mode Operation

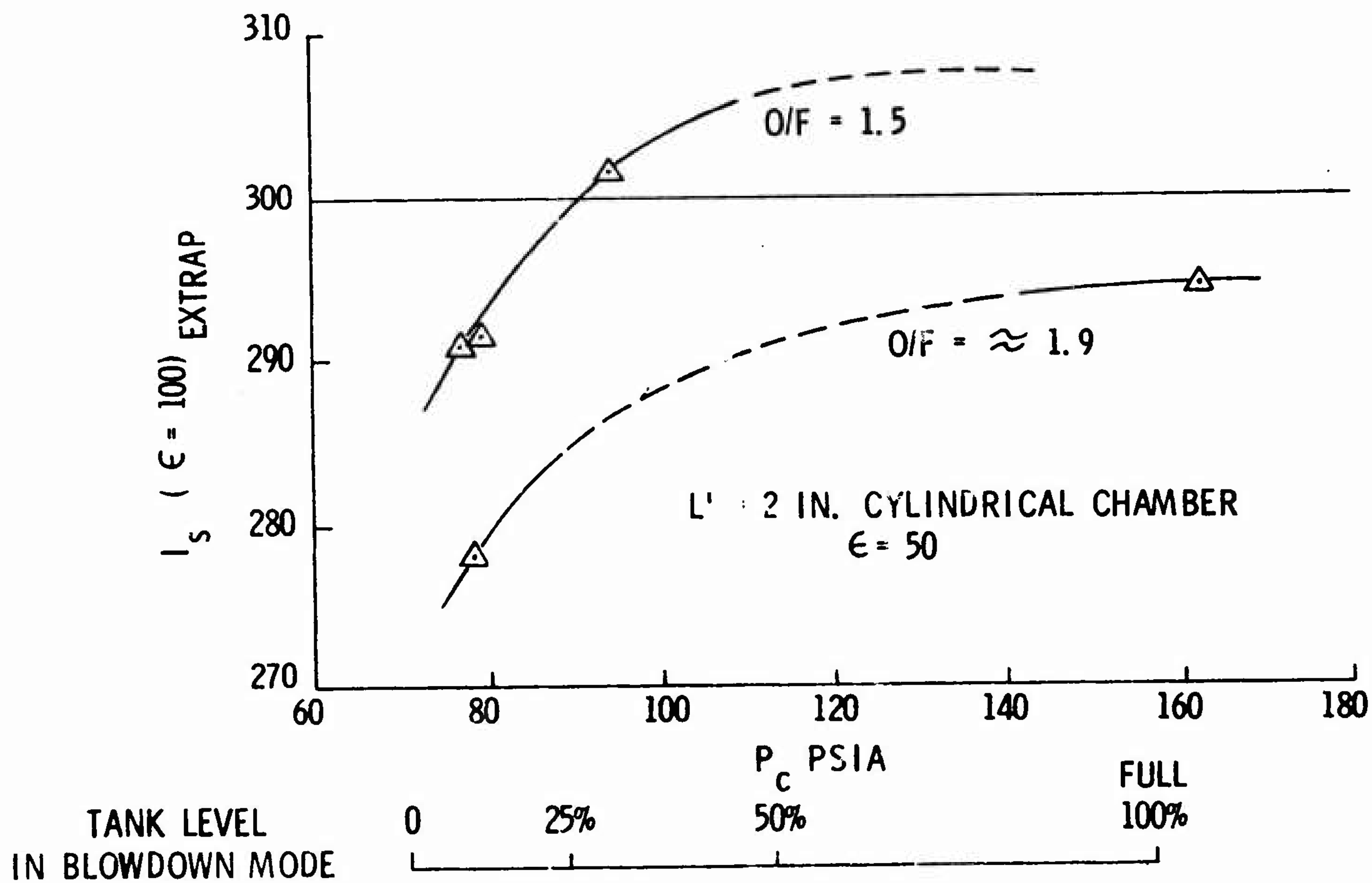

Figure 5.3-9. 4-UD-0 Injector Long Burn Performance for Simulated Blowdown Mode Operation

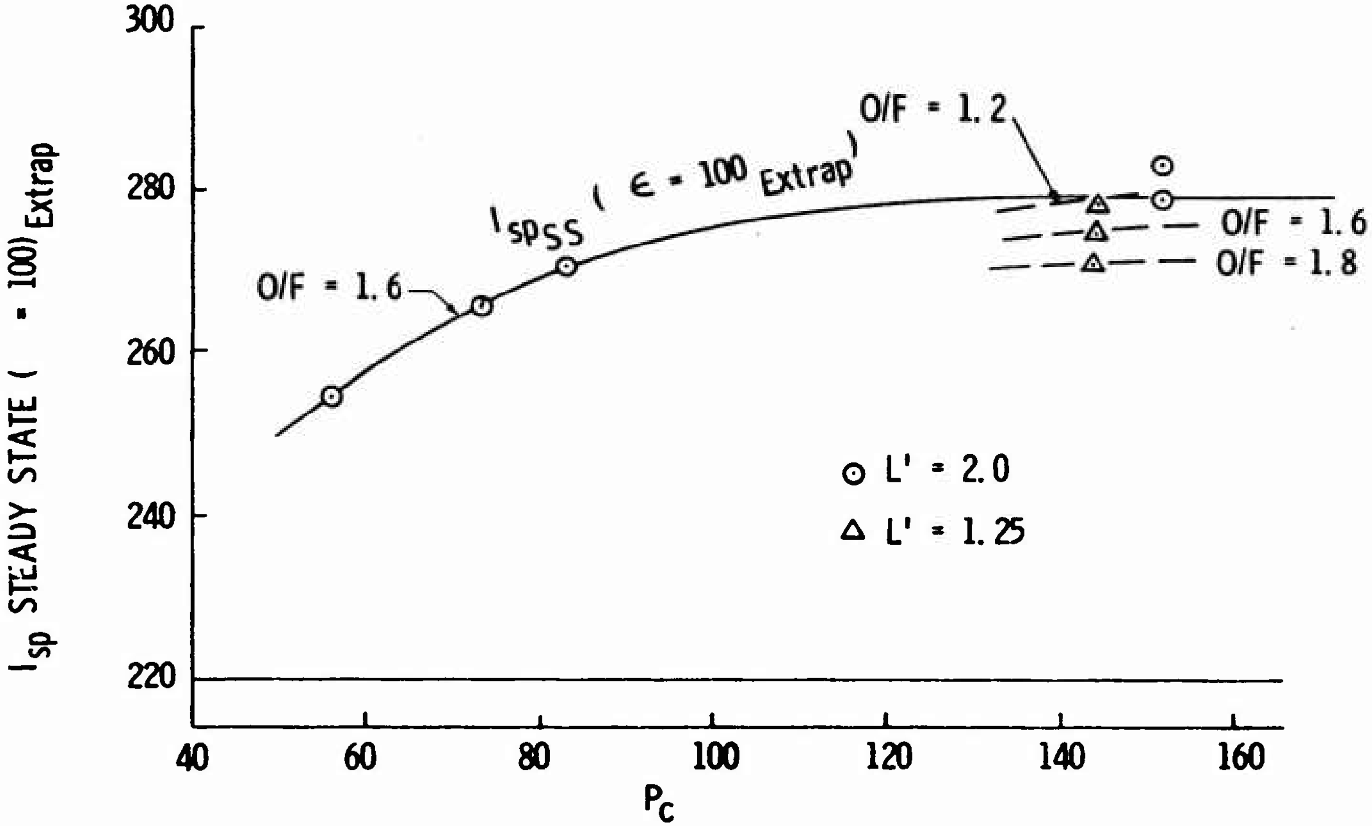

Figure 5.3-10. 4 UD-28-S Injector Long Burn Performance

to produce efficient fuel atomization, the low oxidizer velocity might be a problem. The 40 fps critical oxidizer injection velocity was calculated to occur at P_c = 100 psia for the 6-element injector designs. The 4-UD-0 injector, on the other hand, had a 40 fps minimum oxidizer injection velocity at minimum blowdown $P_c \approx 70$ psia. Thus, this mechanism accounts for the significantly higher blowdown performance of the 4-element design as shown on Figures 5.3-11 and 5.3-12. When either delivered I_{sp} or % ERE is plotted vs oxidizer injection velocity, the blowdown data of both 6-element splash plate and the 4-element unlike doublet injectors become consistent. Furthermore, the "knee" occurs at 40 fps as analytically forcasted. Figures 5.3-11 and 5.3-12 suggest that the 6-element blowdown performance will be comparable to that of the 4-element design if 40 fps minimum oxidizer injection velocity is maintained. This requires reducing the 6-element injector's oxidizer injection metering orifice diameters from 0.010 in. to 0.008 in. This modification was one of several incorporated on the Phase III injector designs, however the test data showed no blowdown performance improvement.

5.3.1.3.3 Pulsing Performance

Three injectors were subjected to an extensive series of pulse tests involving a minimum of 510 firings per injector. A summary of the types and quantity of pulse tests conducted is presented in Figure 5.2-12 and Table 5.2-6. Table 5.3-3 contains a performance digest of a portion of these data. All tests were made with a 50:1 area ratio nozzle at vacuum conditions (cell pressure $\approx$ 0.3 psia). The measured vacuum performance data [accumulated thrust/accumulated total flow] are shown in Figure 5.3-13 for the 0.010 sec electrical pulses. The data shown presents the effective specific impulse for pulse trains consisting of N pulses with each pulse providing a bit impulse of $\approx$ 0.05 lbf-sec. The data scatter for the first few pulses results from the flow measurement accuracy for single pulses. The flow rates for each propellant for the individual pulse (approximately 0.0001 lb propellant per pulse) results in very small movements of the positive

TABLE 5.3-3

PULSE TEST PERFORMANCE SUMMARY

	Units													
Test No.	-	112	113	114	115	116A	116B	116C	123	124	126	127A	127B	127C
Injector	-	6-SP-45							6-SP-0					
L'	in.	2.75							2.75					
ϵ	-	50							53.5					
EPW	sec	0.030	0.030	0.030	0.030	0.100	0.025	0.010	0.030	0.030	0.030	0.100	0.025	0.010
Coast Time	sec	0.30							0.30					
Steady State:														
P_c	psia	150	108	155	155	160			75	159	159	160		
O/F	-	1.17	1.59	1.56	1.92	1.6			1.57	1.26	1.63	1.6		
F_{vac} (ϵ)	lb_f	4.85	3.51	4.99	5.02	5.0			2.10	4.82	4.96	5.0		
$T_{prop.}$	°F	Ambient							Ambient					
Cold Start:														
Pulse Nos.	-	1-4	1-4	1-4	1-4	1-4	N.A.	1-4	1-4	1-4	1-4	1-4	1-4	1-4
I_{TOT} (ϵ)	lb_f-sec	0.1397	0.0987	0.1420	0.1449	0.4903	N.A.	0.0462	0.0650	0.1398	0.1433	0.4768	0.1221	0.0486
I_{sp} (ϵ)	sec	250.9	229.5	252.7	257.8	277.5	N.A.	193.1	203.2	254.3	253.1	267.2	252.7	220.6
I_{sp} (ϵ = 100) extrap.	sec	Add 7 sec to above value												
Hot Restart:														
Pulse Nos.	-	N.A.	N.A.	6-9	6-9	21-24	47-50	61-64	6-9	N.A.	N.A.	21-24	47-50	491-494
I_{TOT} (ϵ)	lb_f-sec	N.A.	N.A.	0.1525	0.1536	0.4979	0.1235	0.0498	0.0677	N.A.	N.A.	0.4866	0.1230	0.0517
I_{sp} (ϵ)	sec	N.A.	N.A.	272.1	273.0	288.1	266.7	231.1	214.6	N.A.	N.A.	277.5	264.6	248.3
I_{sp} (ϵ = 100) extrap.		Add 7 sec to above value												

TABLE 5.3-3 (cont.)

Test No.	132	133	134	135	136A	136B	136C	136C'
Injector	4-UD-0 →							
L'	2.0 →							
ε	50 →							
EPW	0.030	0.030	0.030	0.030	0.100	0.025	0.010	0.010
Coast	0.30 →							3.0
Steady State:								
P_c	94	162	76	77	160 →			
O/F	1.49	1.34	1.97	1.50	1.5 →			
F_v (ε)	3.03	5.20	2.46	2.47	5.0 →			
T_{ox}/T_f	Ambient →							
Cold Start:								
Pulse Nos.	1-4	1-4	1-4	1-4	1-4	1-4	1-4	1-4
I_T (ε)	0.0868	0.1535	0.0721	0.0719	0.5154	0.1264	0.0490	0.0498
I_{sp} (ε)	232.8	263.9	223.4	233.9	279 5	248.9	221.2	217.4
I_T (ε = 100)								
I_{sp} $(\epsilon = 100)_{extrap}$	Add 7 sec to above value →							
Hot Restart:								
Pulse Nos.	N.A. →				21-24	196-199	247-250	7-10
I_T (ε)	↓				0.5266	0.1251	0.0534	0.0492
I_{sp} (ε)					288.2	269.5	251.7	232.6
I_T $(\epsilon = 100)_{extrap}$								
I_{sp} $(\epsilon = 100)_{extrap}$	Add 7 sec to above value →							

Test No.	158'	158A	158B	159A'	159A	159B	160A'	160A	160B	160C	161A'	161A	161B	161C
Injector	6-SP-45 →													
L'	1.25 →													
ε	1.7 →													
EPW	0.010	0.010	0.025	0.010	0.010	0.025	0.010	0.010	0.025	0.100	0.010	0.010	0.025	0.100
Coast	3.0	0.30	0.30	3.0	0.30	0.30	3.0	0.30	0.30	0.30	3.0	0.30	0.30	0.30
Steady State:														
P_c	70 →			160 →			70 →				160 →			
O/F	1.6 →			1.6 →			1.6 →				1.6 →			
F_v (ε)	1.65 →			3.7 →			1.65 →				3.7 →			
T_{ox}/T_f	22 →						118 →							
Cold Start:														
Pulse Nos.	1-4	1-4	1-4	1-4	1-4	1-4	1-4	1-4	1-4	1-4	1-4	1-4	1-4	1-4
I_T (ε)	0.0115	0.0128	0.0308	0.0313	0.0346	0.0896	0.0177	0.0176	0.0436	0.1555	0.0363	0.0370	0.0938	0.3653
I_{sp} (ε)	86.8	105.0	106.0	147.6	165.2	182.6	128.0	117.9	138.9	143.0	165.0	166.5	180.2	190.6
I_T (ε = 100)	0.0152	0.0169	0.0407	0.0414	0.0457	0.1185	0.0234	0.0233	0.0576	0.2056	0.0480	0.0489	0.1240	0.4830
I_{sp} $(\epsilon = 100)_{extrap}$	114.8	138.8	140.2	195.2	218.4	241.4	169.2	155.9	183.7	189.1	218.2	220.1	238.3	252.0
Hot Restart:														
Pulse Nos.	5-9	240-243	184-187	7-10	247-250	194-197	5-8	242-245	195-198	45-48	7-10	243-246	197-200	47-50
I_T (ε)	0.0103	0.0160	0.0352	0.0338	0.0363	0.0900	0.0184	0.0195	0.0428	0.1549	0.0379	0.0367	0.0930	0.3658
I_{sp} (ε)	83.1	117.7	121.2	160.4	166.6	187.7	130.8	138.2	146.1	150.3	171.6	168.5	191.3	200.4
I_T $(\epsilon = 100)_{extrap}$	0.0136	0.0212	0.0465	0.0447	0.0480	0.1190	0.0243	0.0258	0.0566	0.2048	0.0501	0.0485	0.1230	0.4837
I_{sp} $(\epsilon = 100)_{extrap}$	109.9	155.6	160.3	212.1	220.3	248.2	172.9	182.7	193.2	198.7	226.9	222.8	252.9	265.0

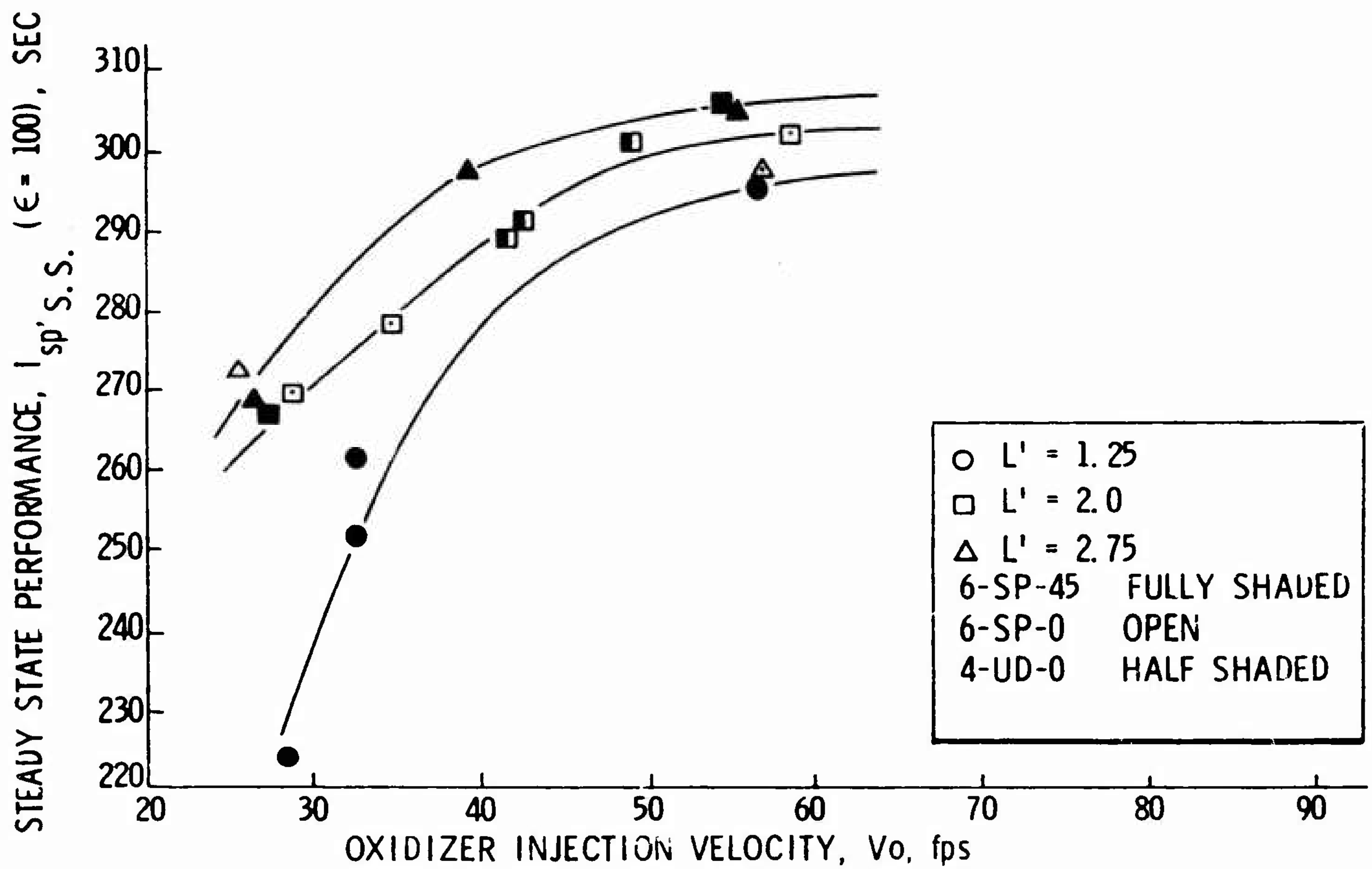

Figure 5.3-11. Effect of Oxidizer Injection Velocity upon Steady State Performance

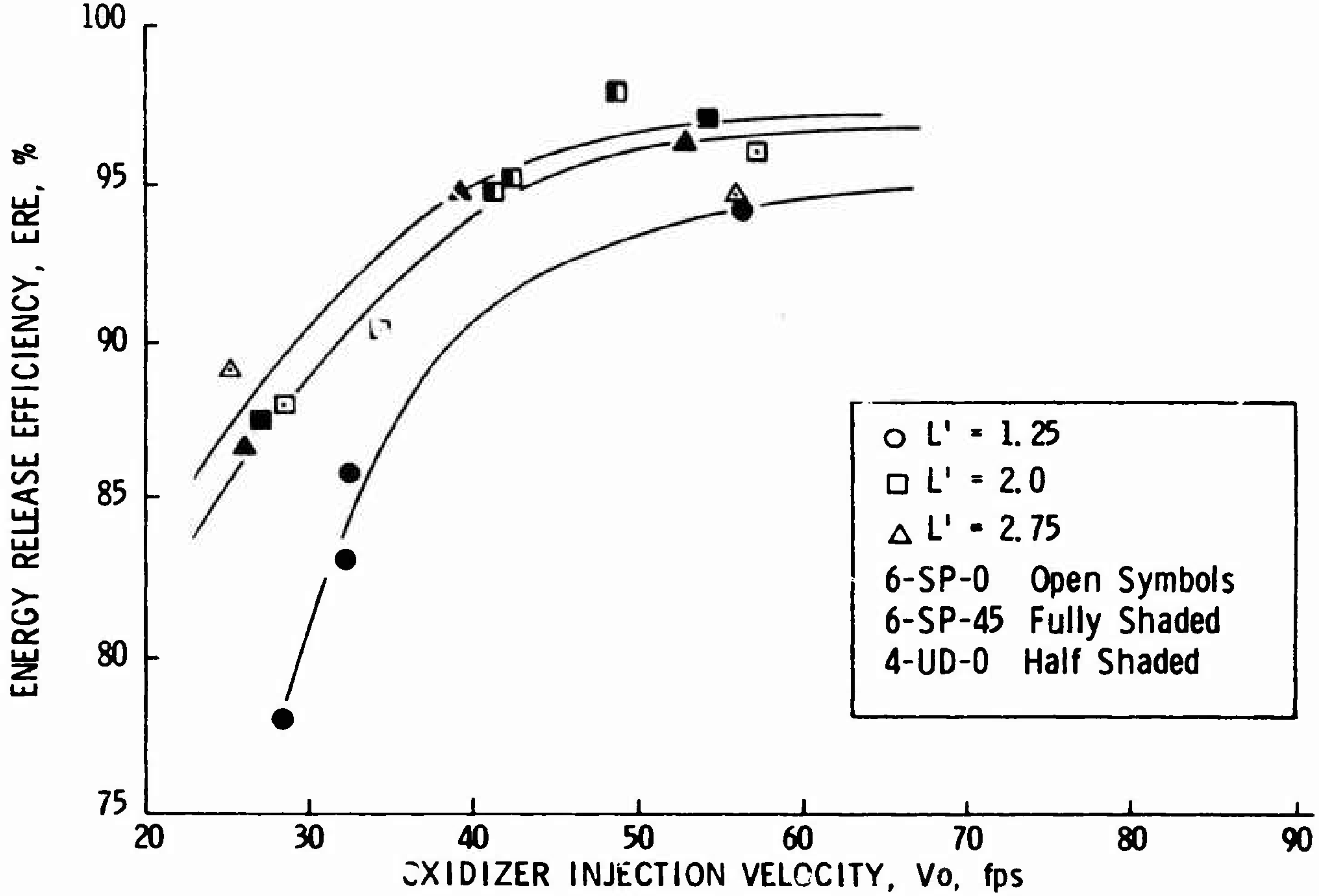

Figure 5.3-12. Effect of Oxidizer Injection Velocity upon Energy Release Efficiency

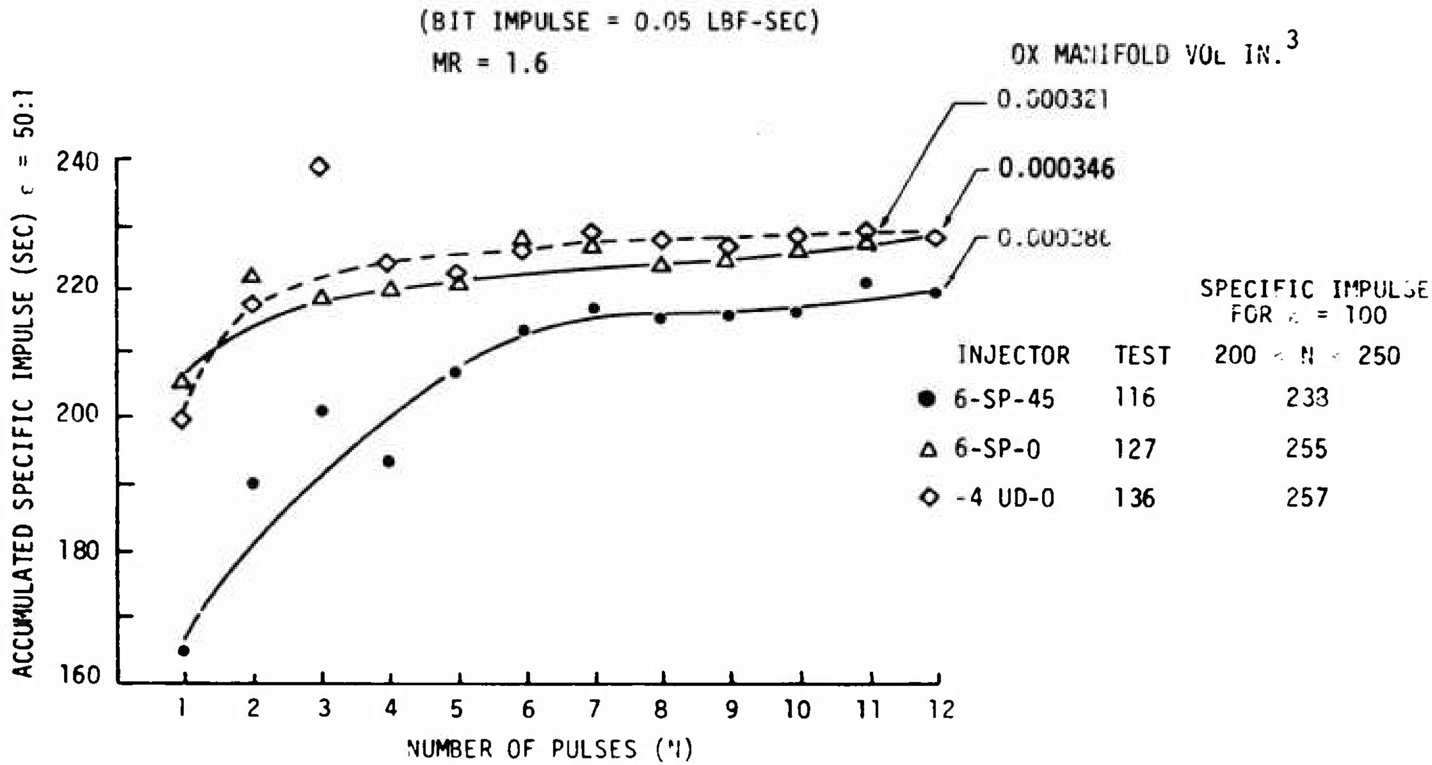

Figure 5.3-13. Measured Accumulated Specific Impulse for 0.010 sec Electrical Pulses

displacement flow meters. The accuracy of measurement improves with the number of pulses fired. The minimum sample size for 0.010 sec pulses is 4.

Figures 5.3-13 and 5.3-14 provide a comparison of the 3 designs tested to 0.010 and 0.10 sec EPW. The total bit impulses of the initial pulses are somewhat lower than average due to cold chamber walls contributing to chamber wall film accumulation and reduced pulsing efficiency. After the first few pulses the data becomes highly repeatable. Likewise, the accumulated I_{sp} (total impulse of all pulses/total propellant utilization of all pulses) improves rapidly during the first few pulses. The accuracy of a single pulse performance is questionable because of the minute quantity of propellants utilized and the difficulty of accurate flow measurement. The accumulated performance from several consecutive pulses minimizes the flow measurement inaccuracy and results in more reliable data. Since the first few pulses are especially affected by manifold volume minimizing the dribble volume significantly improves the initial cold pulse performance. The asymptotic pulse performance for hot restarts are also tabulated for each injector in Figures 5.3-13 and 5.3-14. The cold first pulse performance drop off is not nearly as severe, nor so strongly dependent upon manifold volume for these same injectors at 0.100 sec EPW pulses.

The overall pulsing characteristics of the 6-SP-45-A injector is plotted versus total impulse in Figure 5.3-15. The difference between the cold start (first 4 pulse average) performance and the asymptotic hot restart pulse performance at nominal P_c = 160 psia is indicated. In addition, the effect of reduced P_c cold chamber performance is indicated for blowdown applications. The lower blowdown pulse performance is attributed to its reduced steady state I_{sp}.

Similar cold chamber versus hot restart and nominal versus blowdown pulse performance for the 6-SP-0 injector is shown in Figure 5.3-16. This figure also provides a comparison of the cold wall pulsing

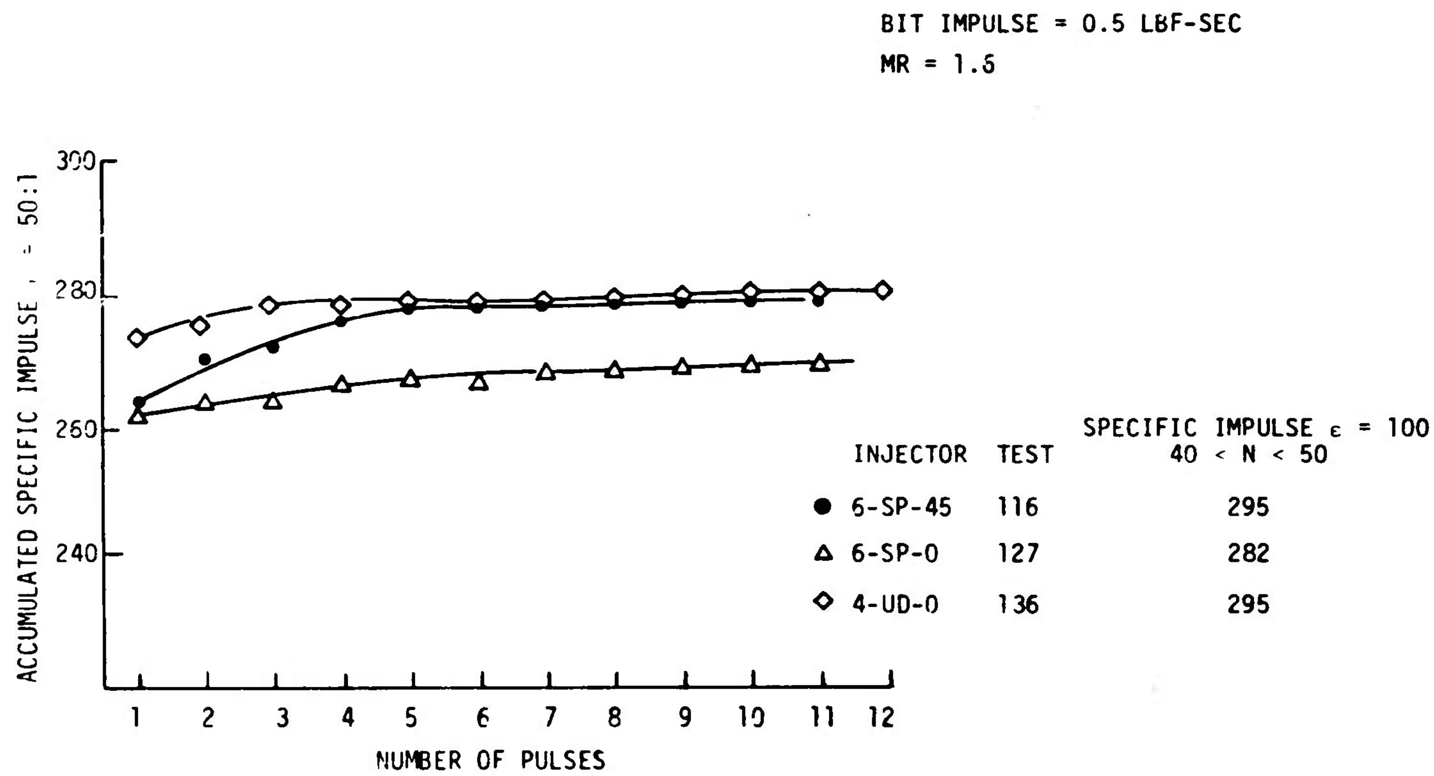

Figure 5.3-14. Measured Accumulated Specific Impulse for 0.10 sec Electrical Pulses

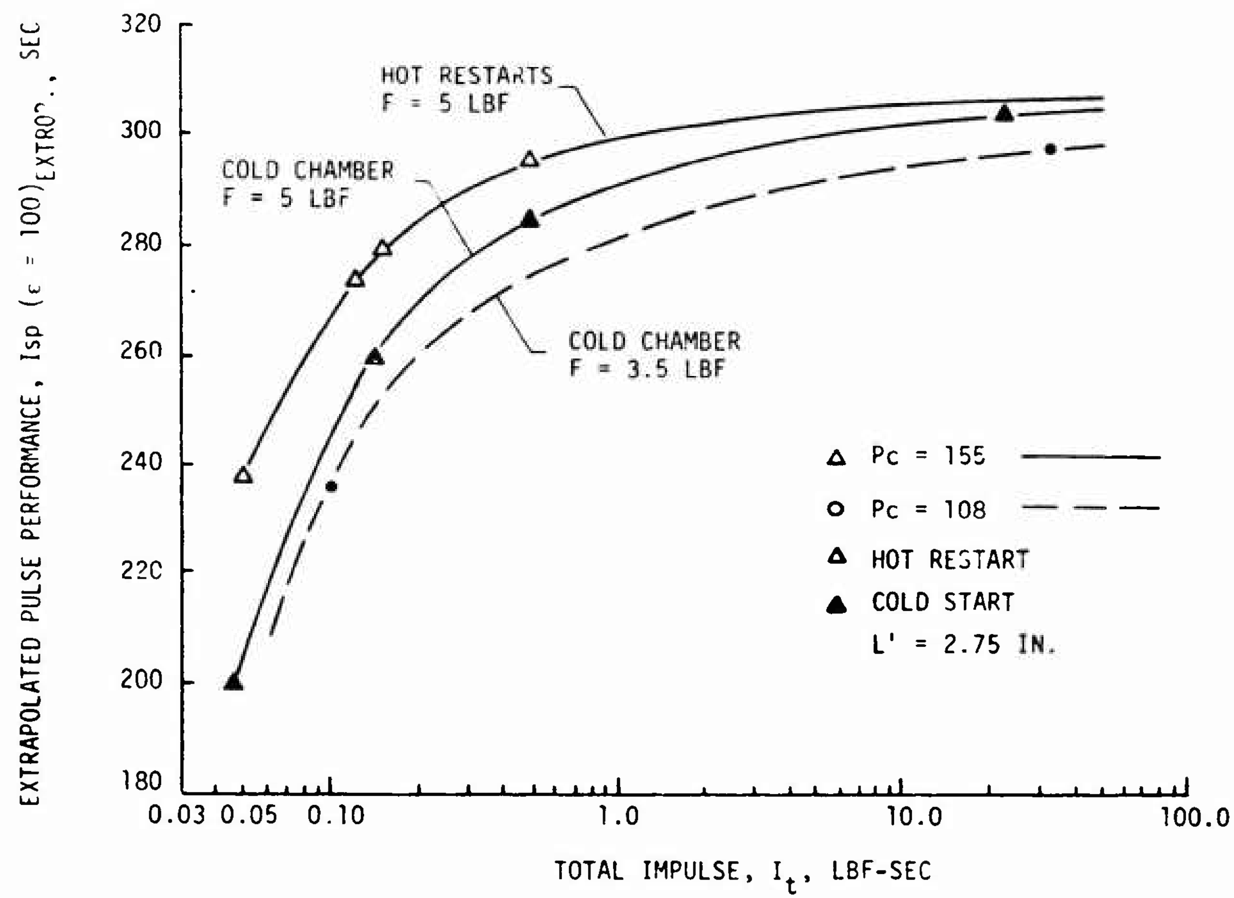

Figure 5.3-15. 6-SP-45 Injector Pulsing Performance

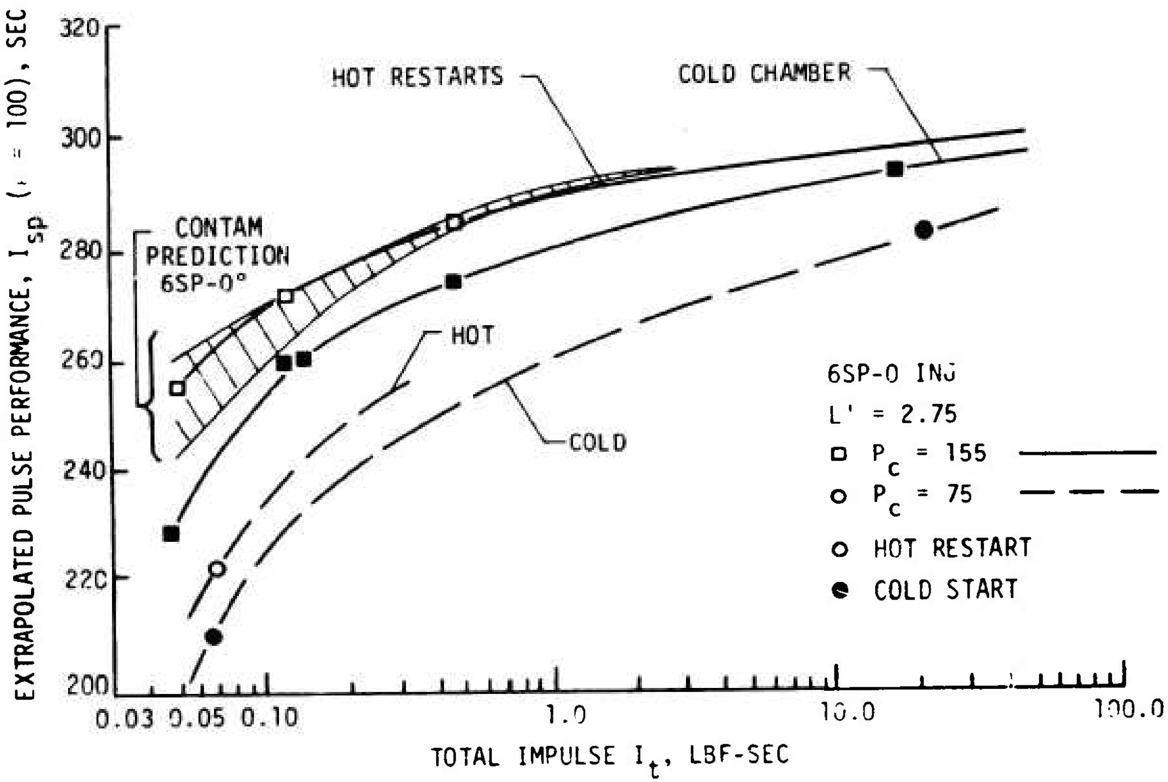

Figure 5.3-16. 6-SP-0 Injector Pulsing Performance

performance predicted by the CONTAM computer program with the experimental data. The analysis is noted to over-predict the measured cold chamber performance by about 10 sec or about 3%. When one considers all of the input options and assumptions required, it is concluded that 3% is quite good for a prediction made prior to the testing. It is anticipated that the data can be more precisely matched by modifying the appropriate input parameters and assumptions concerning the fuel monopropellant reactions during the blowdown period. Further analyses and discussion are provided in Section 6.5.

The 4-UD-0 injector data plotted in Figure 5.3-17 indicates little influence of blowdown upon cold chamber pulse performance. This is considered to be due to higher injection velocities.

A comparison of the 3 injectors pulsed with ambient temperature propellants is shown in Figure 5.3-18 which plots specific impulse versus bit impulse after the initial chamber heat-up. Only at the 0.010 sec EPW (0.05 lbf-sec impulse) is the 6-SP-45 pulse performance lower than the other injectors. This is due to its larger manifold volume. At 0.020 sec EPW (0.10 lbf-sec impulse) all 3 injectors yield equivalent pulsing $I_{sp} \approx 275$ sec. Between 0.020 sec and 5 sec EPW the 6-SP-0 injector delivers lowest pulse performance.

Throughout Phase II testing, it was observed that hot chamber walls resulted in higher ERE's for both steady state and pulsing performance. The chamber wall temperature versus number of pulses for pulse duration, duty cycle and injector configuration is shown in Figure 5.3-19. A plot of pulse performance vs chamber wall temperature is shown in Figure 5.3-20 for EPW's of 0.010, 0.025, 0.030, and 0.100 sec. The data conclusively shows higher pulse performance with hotter chamber walls. This is consistent with the CONTAM wall film evaporation model. At 305°F wall temperature, the MMH vapor pressure equals 160 psia or nominal P_c. Once the wall temperature exceeds the fuel saturation temperature, the wall film is

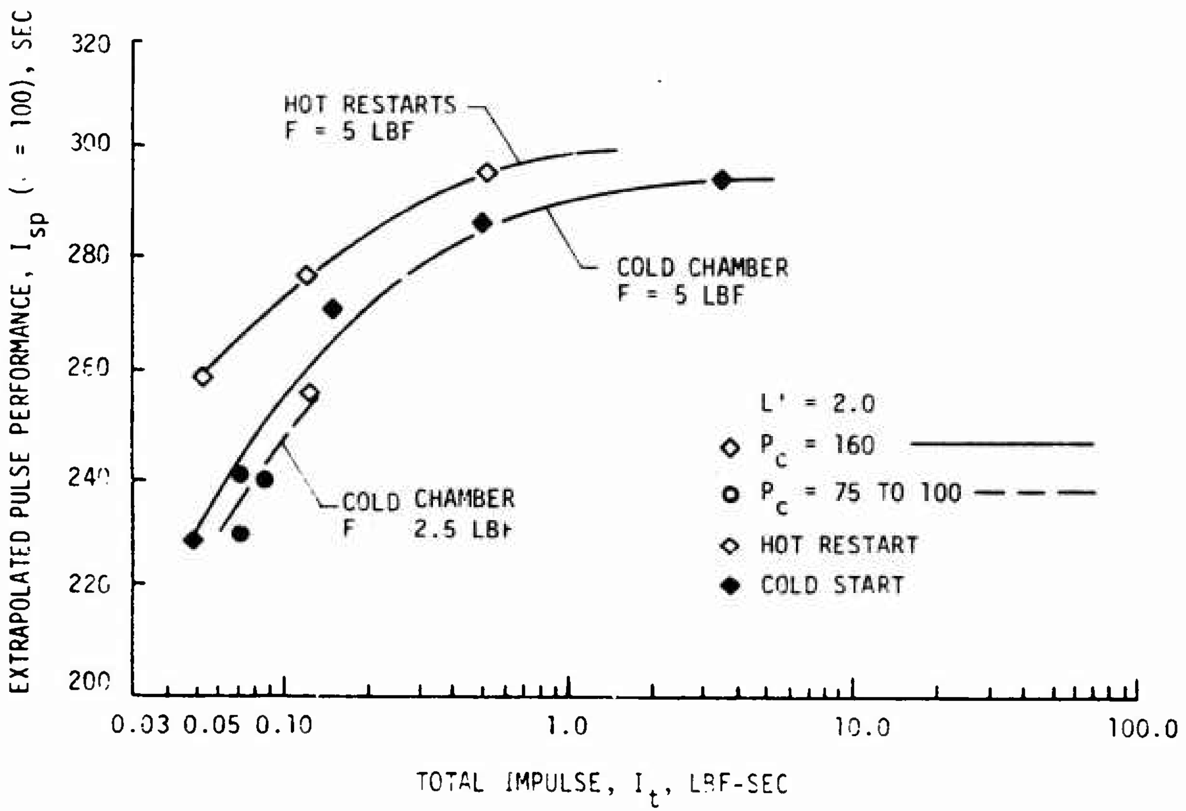

Figure 5.3-17. 4-UD-0 Injector Pulsing Performance

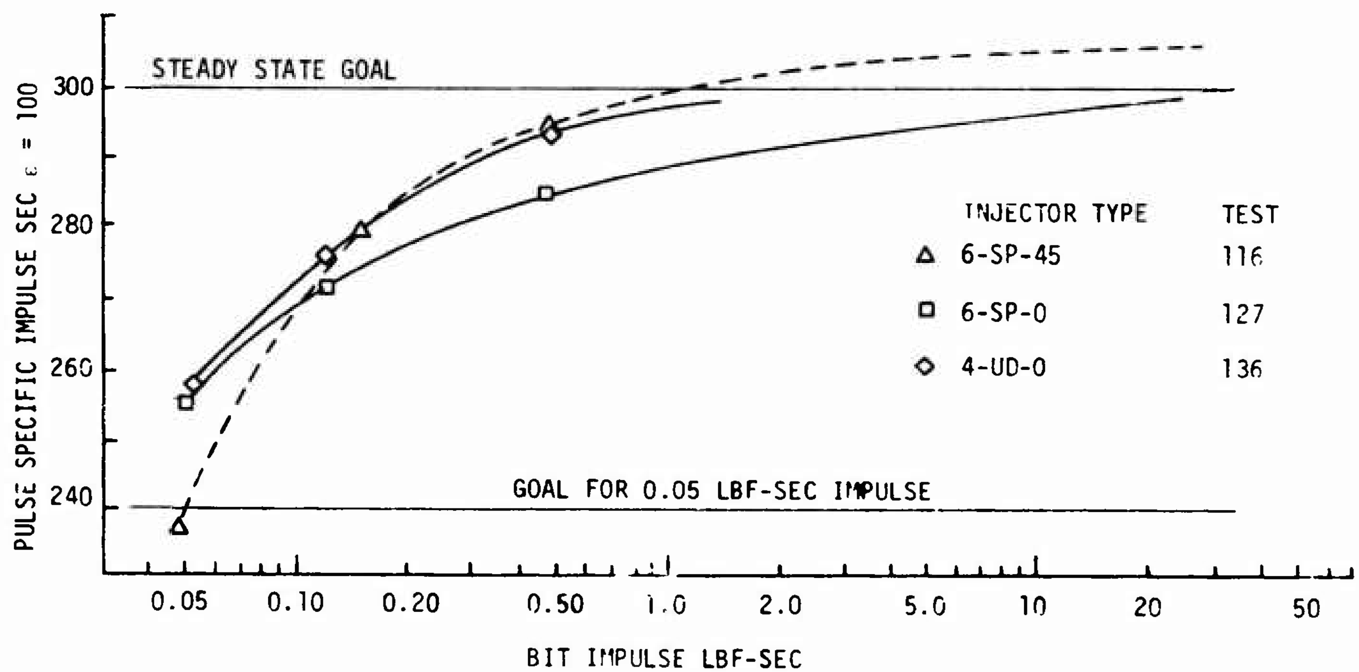

Figure 5.3-18. Specific Impulse Versus Bit Impulse for Long Pulse Trains

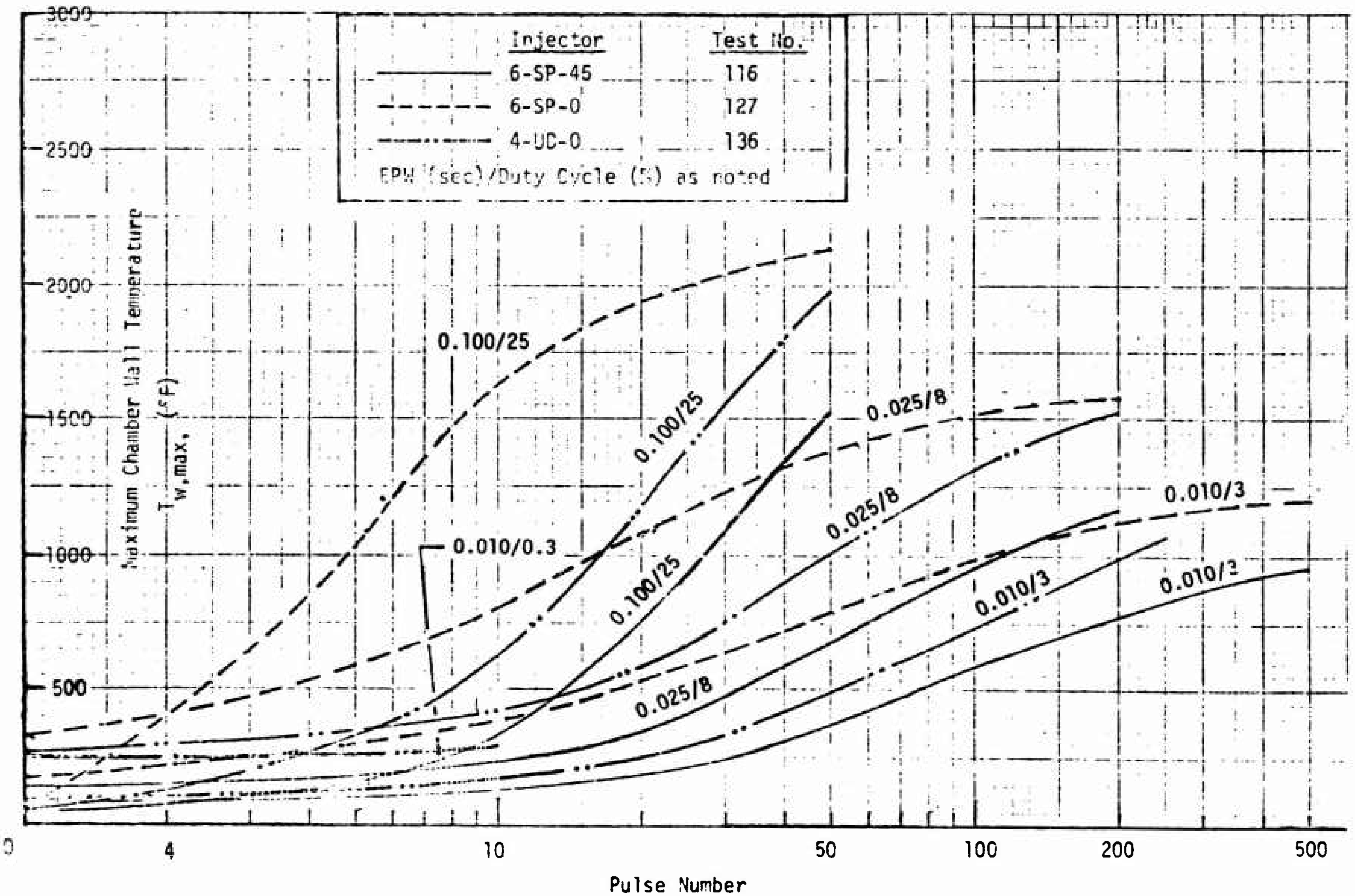

Figure 5 3-19. Chamber Wall Temperature Rise versus Pulse Number

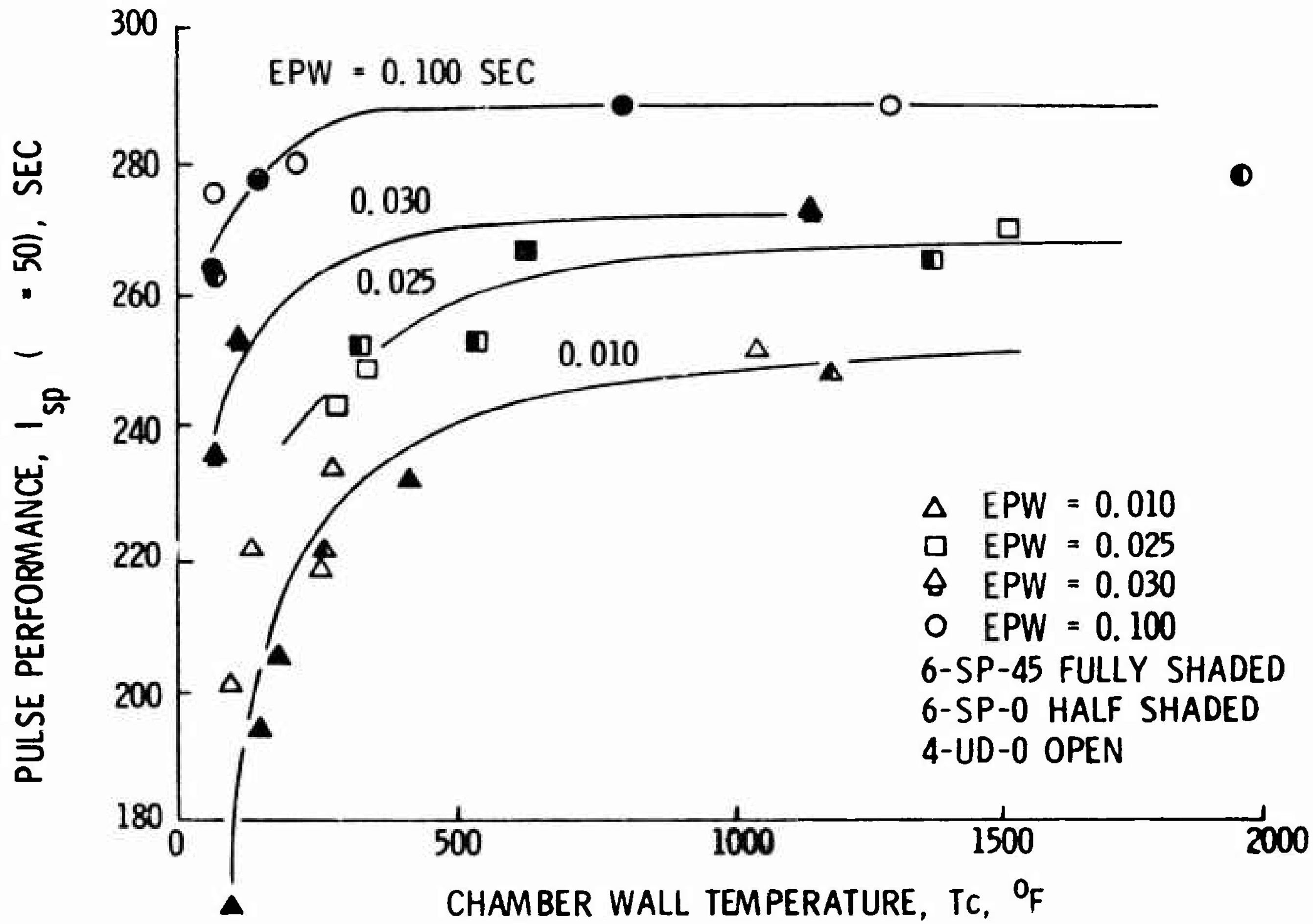

Figure 5.3-20. Effect of Chamber Wall Temperature upon Pulsing Performance

eliminated. No further influence of wall temperature is to be expected above 609°F since that value corresponds to the MMH critical temperature. For thin wall columbium chambers, the wall is heated from ambient temperature to 350°F in approximately 0.3 sec of firing duration. This implies pulsing performance will approach the hot restart pulse performance shown in Figure 5.3-18 after approximately 30 pulses at 0.010 sec EPW, 10 pulses at 0.030 sec EPW, or 3 pulses at 0.100 sec EPW. The above offers a reasonable "rule of thumb".

All of the previous pulsing data was obtained with ambient (≈ 50 to 60°F) propellant temperatures. Pulsing tests were also conducted for nominal and blowdown P_c's at cold (22°F) and hot (118°F) propellant temperature limits called out on the contract specifications. These conditioned propellant temperature tests were conducted with the 6-SP-45 injector in the vacuum test facility, with the 1.25 in. chamber length and ϵ = 1.6:1 nozzle. The cold and hot temperature data are shown in Figure 5.3-21, respectively. At the blowdown P_c operational conditions the pulse performance increased ≈ 40 sec I_{sp}/100°F increase in propellant inlet temperature. At nominal P_c the pulse performance increase was ≈ 10 sec I_{sp}/100°F increase in temperature. These data cannot be compared directly with the ambient temperature pulsing data because the latter data were obtained in a 2.75 in. length chamber which operates at a high performance level.

5.3.1.3.4 Performance Conclusions and Recommendations

The Phase II test results indicated that the 300 sec steady state specific impulse goal could be attained with either 6-SP-45-A, 6-SP-0 or 4-UD-0 injectors in a 2 in. long thrust chamber with a 100:1 expansion nozzle.

It was also concluded that the performance of the 6-element injectors could be derated from 5 to 10 sec in order to obtain additional wall cooling and still meet the 300 sec goal. The three designs

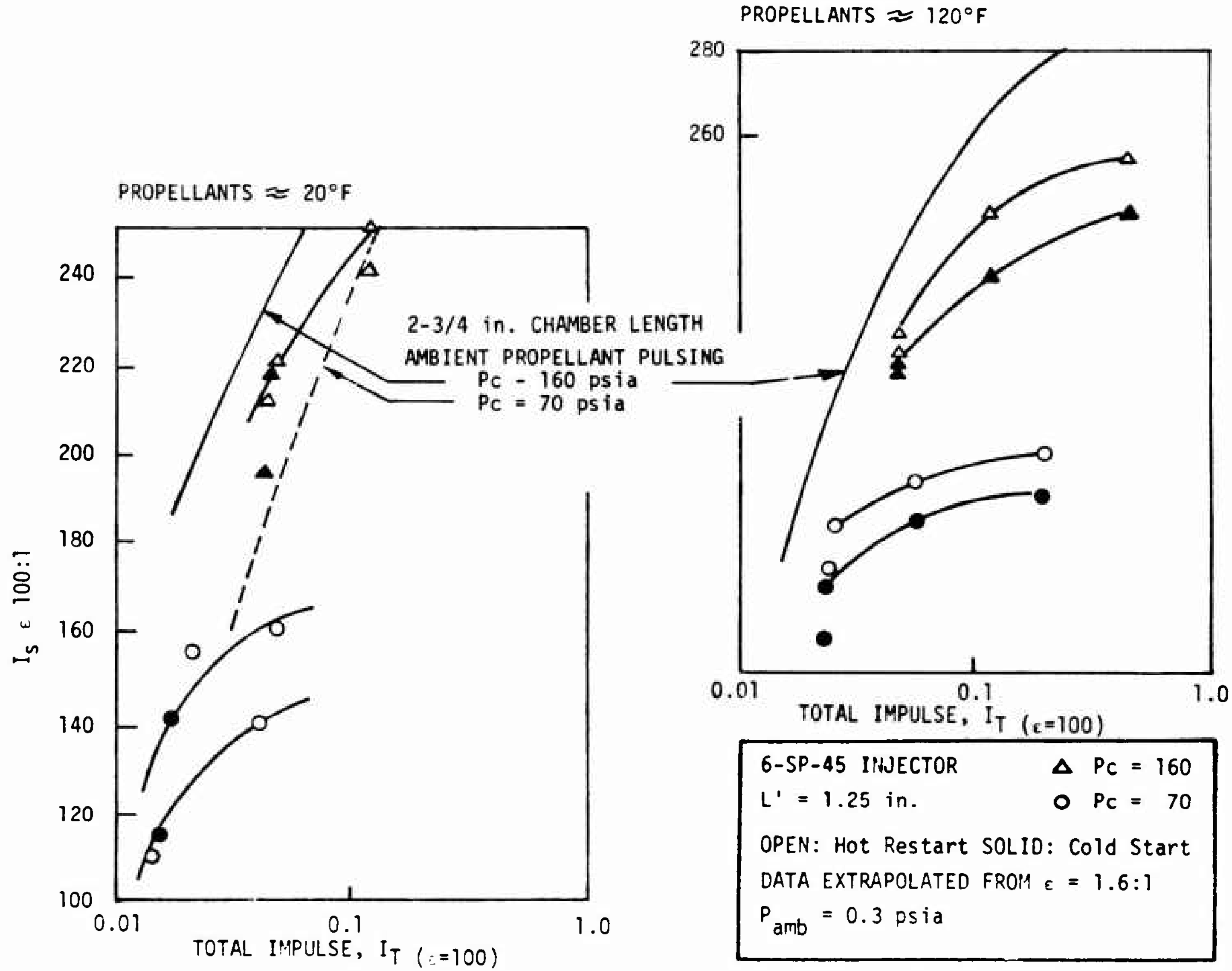

Figure 5.3-21. Pulsing Performance - Experimental Temperature Effects

for which pulsing performance data was available all indicated the capability of providing pulsing performance of 240 sec or greater at 0.05 lbF-sec when the chamber wall was warm. The Phase III designs should have a total manifold volume approaching 0.0005 in.^{3} for the 240 goal to be attained with a cold chamber wall as shown in Figure 4.2-2. It appeared that the performance decrement experienced at the blowdown condition could be corrected by increasing the minimum propellant injection velocity of 40 fps.

The two 6-element designs were recommended for use in Phase III with the following modifications:

(1) Reduce the oxidizer orifice dia from 0.010 to 0.008° to obtain an injection velocity of 40 fps at the lowest thrust level.

(2) Adjust the oxidizer spray angle to obtain the same resultant spray vector with higher injection velocity.

(3) Strengthen the face plate to withstand ignition over pressures with 20°F propellant.

(4) Reduce the manifold volume as much as possible without reintroducing flow distribution problems.

The 4-UD-28-S design was recommended for Phase III buried engine demonstration because of the low chamber wall temperatures and the ability to maintain moderate performance levels (280 sec I_{sp}) over a wide blowdown range.

The 4-UD-0 and 4-UD-28-SL injectors were not recommended due to high injector face and forward chamber region temperatures, respectively. The 4-UD-0 injector was considered suitable for operation at reduced thrust or in pulse mode only.

5.3.1, Test Data Evaluation (cont.)

5.3.1.4 CONTAM Analysis Update

5.3.1.4.1 Performance

A comparison of experimental cold and hot pulse performance data with the hot and cold pulse CONTAM model prediction is shown in Figure 4.2-2. This figure which illustrates the effect of total injector manifold volume for the minimum 0.010 sec EPW, shows the experimental data to be somewhat lower in absolute magnitude than the CONTAM predictions. Never the less, the CONTAM model appears to be very good for predicting performance trends.

5.3.1.4.2 Engine Contamination

Spacecraft contractors are concerned about liquid or solid phase engine plume contaminants which could potentially degrade spacecraft components such as solar panels and optics. Although engine contamination data were not experimentally measured during Phase II the extensive parametric analyses conducted using the CONTAM computer model during Phase I show that low performance aggravates the contamination problem.

The pulsing performance characteristics analytically predicted by CONTAM as a function of engine design parameters and operating conditions were verified by Phase II performance data; thus there is indication that the contamination forcasts are likewise valid. This presumption in conjunction with the model's inverse relation between performance and contamination generation allows the probable pulsing and steady state engine contamination levels to be inferred. The performance data discussed in the prior section is shown in Figure 5.3-22 which relates I_{sp} to contaminate %. The worst condition is for the initial cold pulses at the minimum impulse bit. The highest performing designs are noted to result in the lowest predicted contaminate level. The inserted data bands indicate the inferred contamination levels for each of the operating conditions demonstrated.

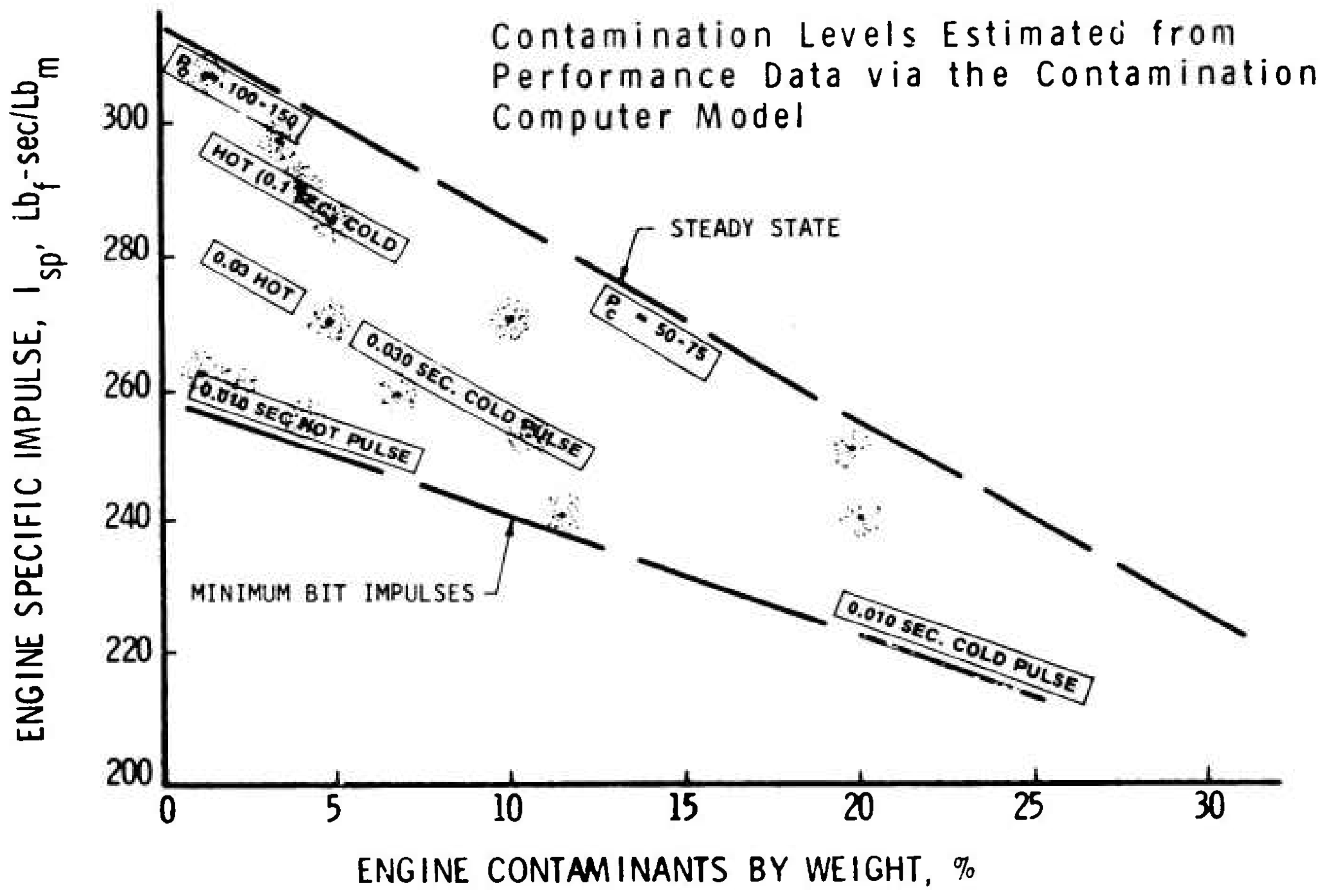

Figure 5.3-22. Engine Specific Impulse versus Engine Contaminants by Weight

5.3.1.5 Thermal Characteristics

5.3.1.5.1 Test Data

Figures 5.3-23, -24, -25 and -26 provide measured thermal transients for the 6-SP-45-A injector for 25, 7.7 and 3.2% duty cycles. Figure 5.3-23 shows no significant postfire heat soak. This is attributed to the 3/4 in. long, low conductivity titanium spacer located between the columbium nozzle and the valve. Figures 5.3-24 through -26 provide greater detail of the individual fire periods and show the asymptotic temperature values used in subsequent parametric data presentation. No thermal limitations were encountered in pulse mode operation of any assemblies tested ($T_{max} < 2500°F$).

Figure 5.3-27 provides similar data for the 6-SP-0 injector with a thin wall columbium chamber (50 pulses at 0.5 lbf-sec impulse 25% duty cycle). The nozzle wall is noted to heat and cool faster than the previous engine tested due to its lower heat storage capability. This improves pulsing performance and minimizes heat soak problems.

Figure 5.3-28 provides the time temperature history of a continuous firing with the 4-UD-28-S injector which was designed for buried operation. This injector was tested at chamber lengths of 1-1/4 in. (stainless steel) and 2 in. (Columbium). The shorter length chamber contained a thermal liner 1/2 in. in length to shield the forward chamber region from the hot gas and thus reduce the heat rejection through the thrust mount. This thin wall liner is also expected to improve pulsing performance. The wall temperatures indicated are well within operating the limits of columbium and its coatings. The shorter chamber ran slightly cooler. The heat rejection rates (watts) through the copper thermal shunt were calculated from the measured temperature gradient ($\frac{\Delta T}{\Delta X}$) obtained from two thermocouples spaced at 0.4 in. along the heat flow path via the following equation:

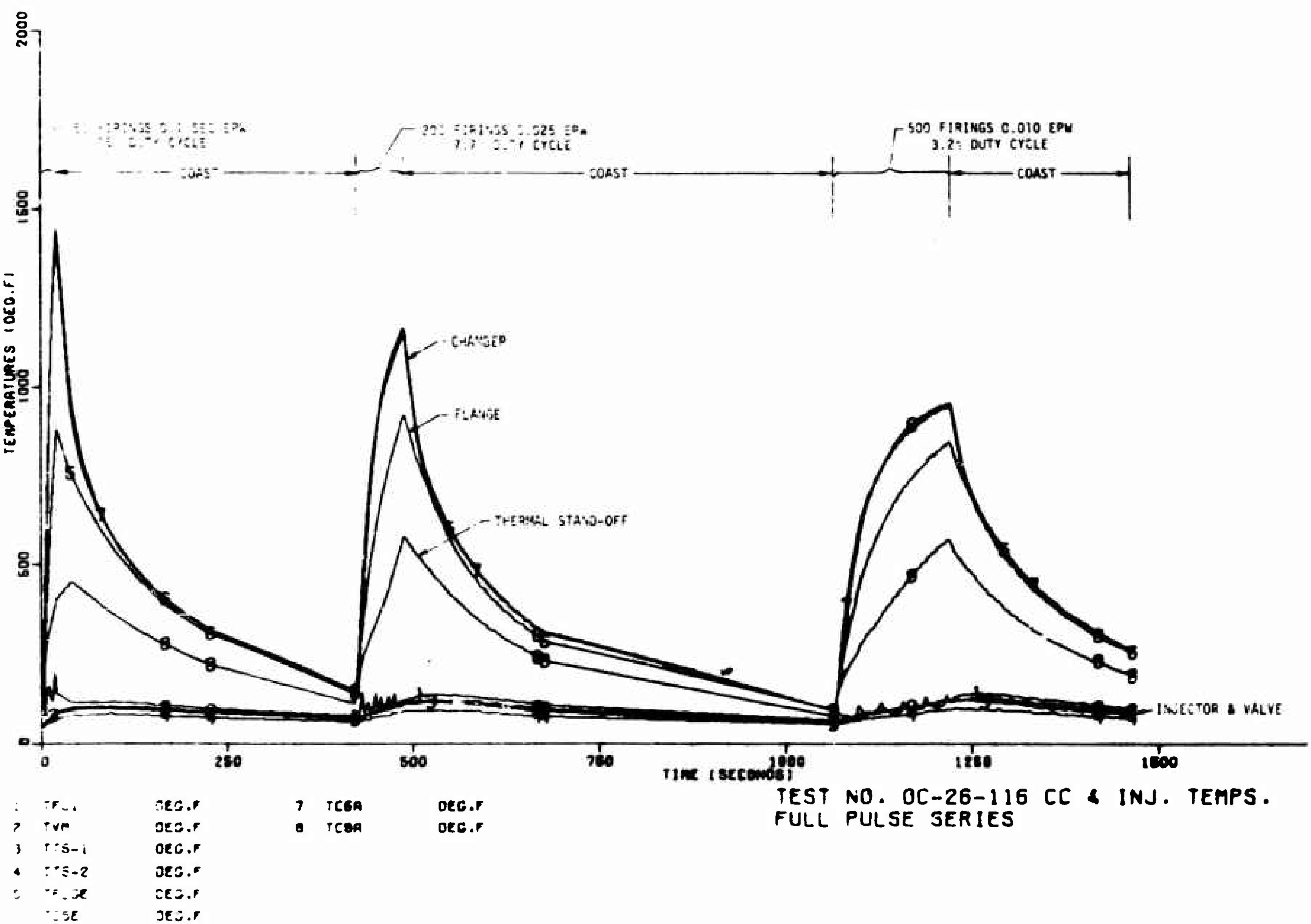

Figure 5.3-23. 6-SP-45 Injector, Pulse Testing Thermal and Postfire Soak Data

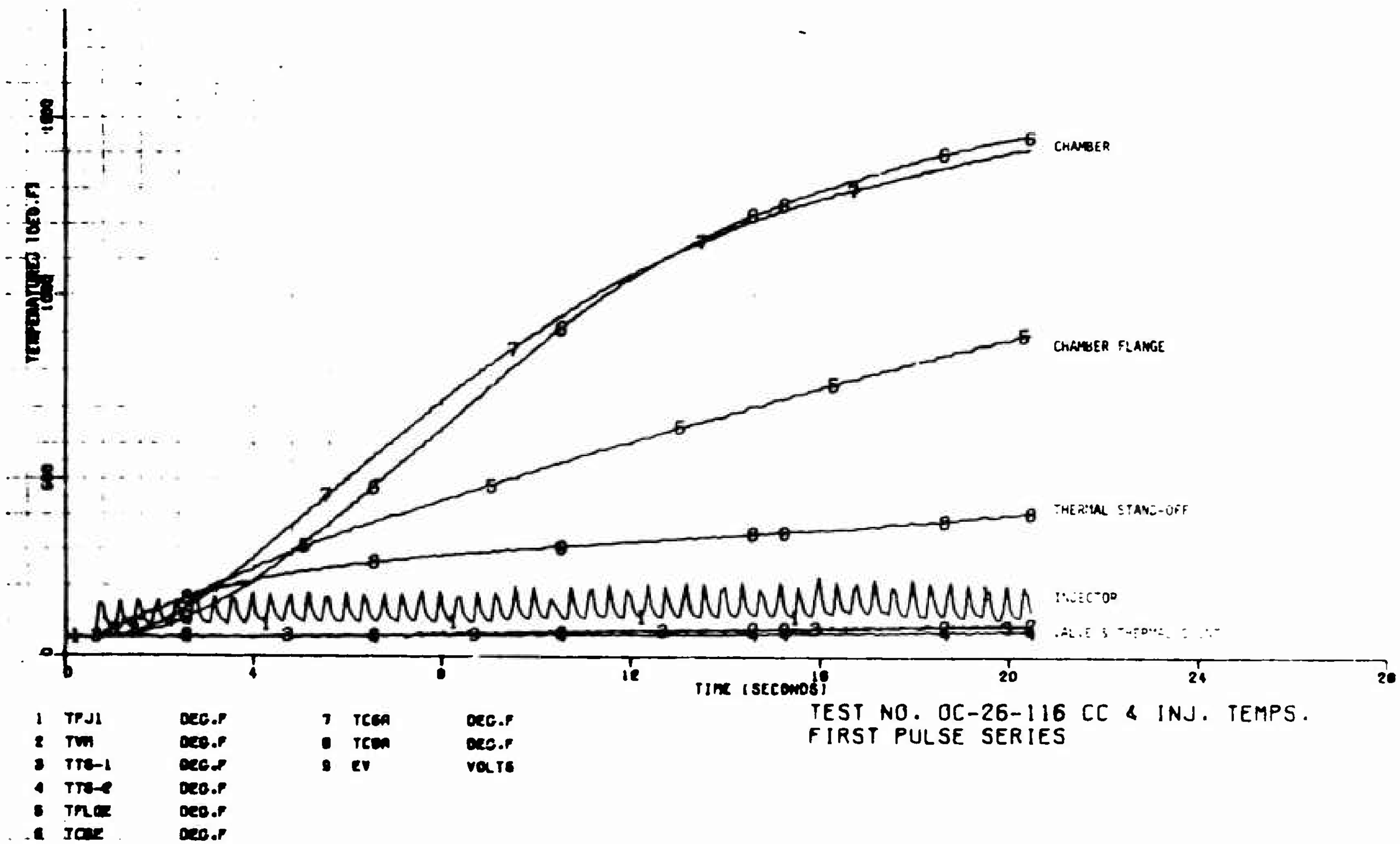

Figure 5.3-24. 6-SP-45 Injector, Pulse Testing Thermal Data, 50 Pulses, 0.10 sec EPW, 0.3 sec Coast

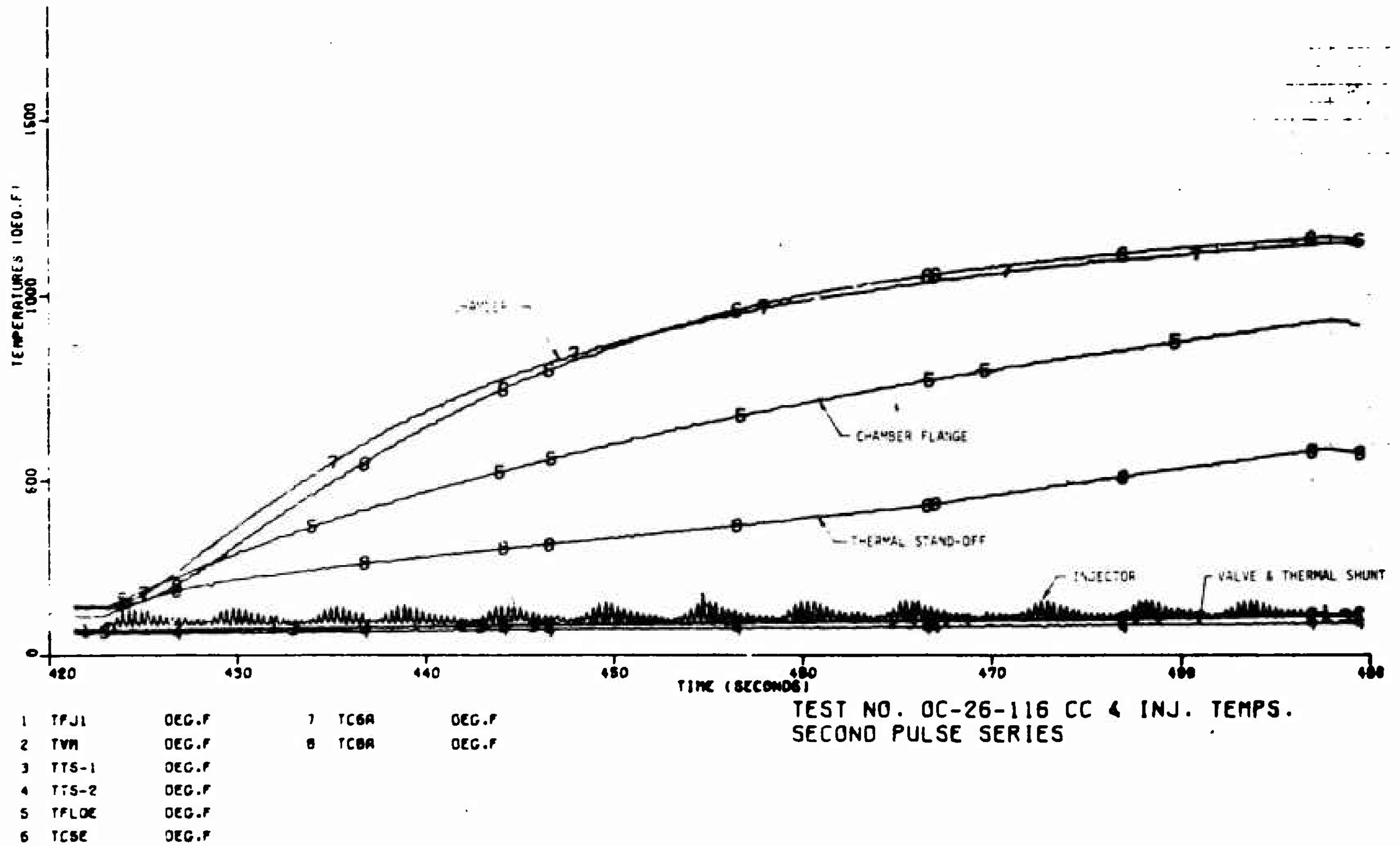

Figure 5.3-25. 6-SP-45 Injector, Pulse Testing Thermal Data, 200 Pulses, 0.025 sec EPW, 0.3 sec Coast

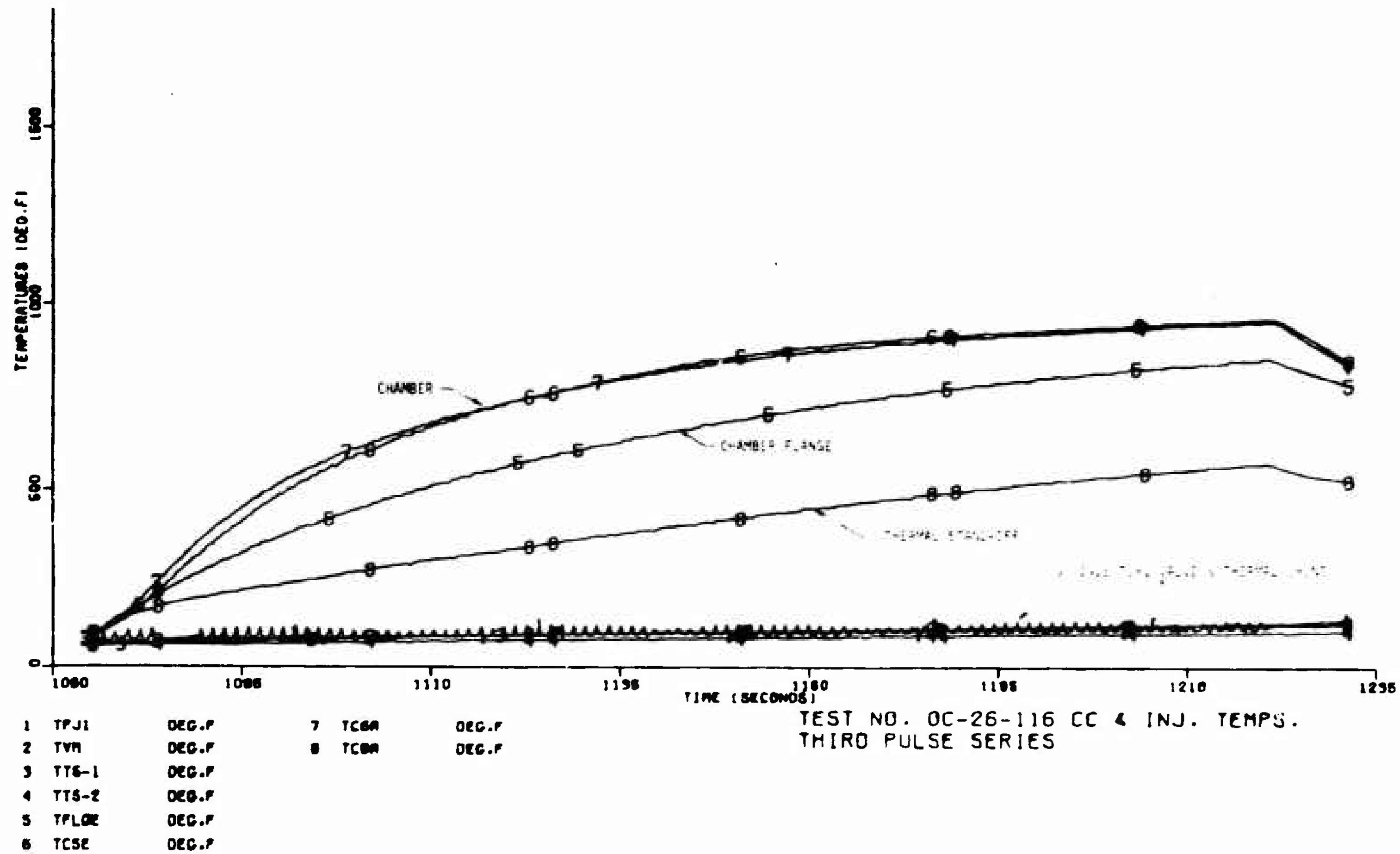

Figure 5.3-26. 6-SP-45 Injector, Pulse Testing Thermal Data, 500 Pulses, 0.010 sec EPW, 0.3 sec Coast

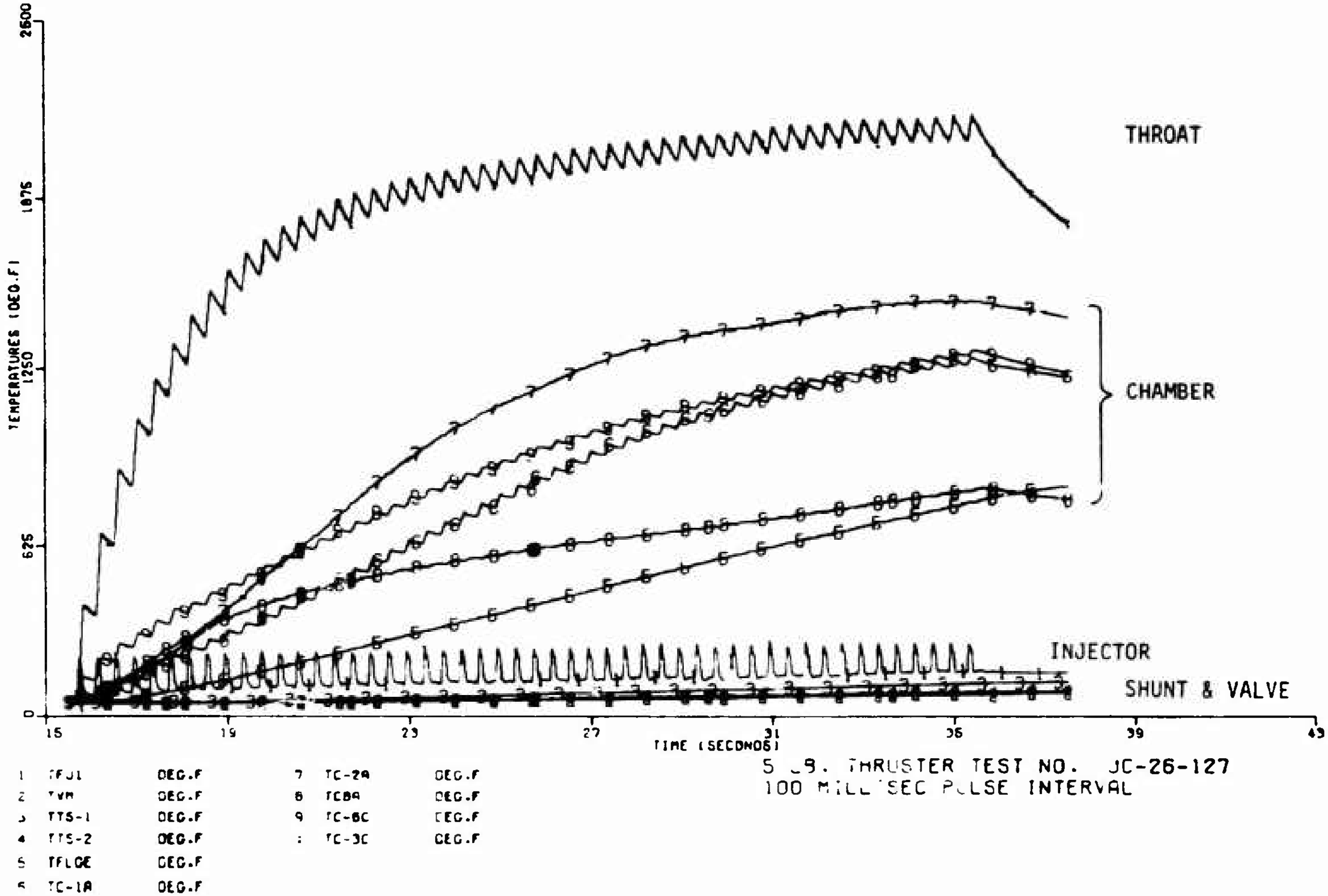

Figure 5.3-27. 6-SP-0 Injector, Pulse Testing Thermal Data, 50 Pulses, 0.10 sec FPW, 0.3 sec Coast

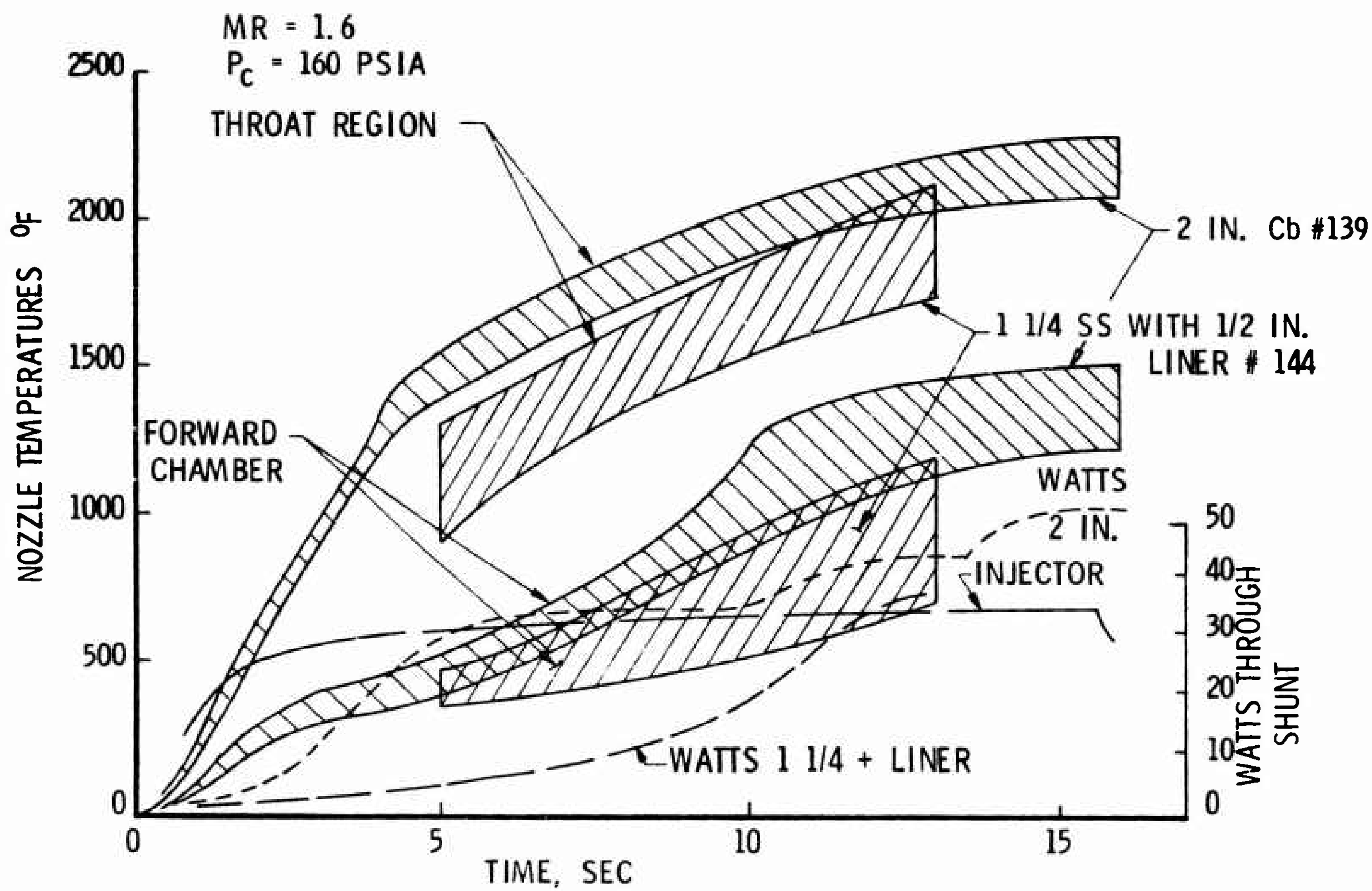

Figure 5.3-28. 4-UD-28-S Injector, Measured Thermal Transients

$$W = 1055\ K\ A\ \frac{\Delta T}{\Delta X} = 0.74\ \Delta T$$

where: K = thermal conductivity

A = area for conduction in.^{2}

ΔX = 0.4 in.

The heat load through the shunt stabilized at 50 watts in the columbium chamber without the liner and about 10 watts lower with the stainless chamber and liner. The chamber wall of the latter test chamber, however, was not optimized to restrict the heat flow. Neither test configuration was able to sustain the ≈ 300-400°F forward end temperature normally expected when fuel film cooling is employed as shown in Figure 5.3-28. This is because the heat conduction rate along the chamber wall exceeded the heat removal capabilities of the fuel film. The net effect of the 1500°F rather than 400°F front end temperature was a higher heat load through the thermal shunt and higher performance. It was concluded that additional insulation between the flange and shunt plus an improved liner are required for the Phase III designs rather than additional cooling. This would allow a reduction in the heat rejection and possibly higher performance.

The 600°F injector face temperature obtained with the 4-UD-28-S design, although structurally acceptable, was 200°F higher than desired. Phase III designs were successfully configured to improve this condition.

Figure 5.3-29 provides similar data for the 4-UD-28-SL injector which was designed to impinge a portion of the fuel spray on the wall further down the chamber. The temperature measurements show a much cooler throat ≈ 2100°F vs 2500 for the 4-UD-28-S. This, however was at the expense of a much hotter front end, 2600°F. The hot front end, in turn, drove the shunt heat flow up to 210 watts which was unacceptable. The short impingement fuel configuration with modification was recommended for the Phase III blowdown mode because of the more favorable axial temperature distributions.

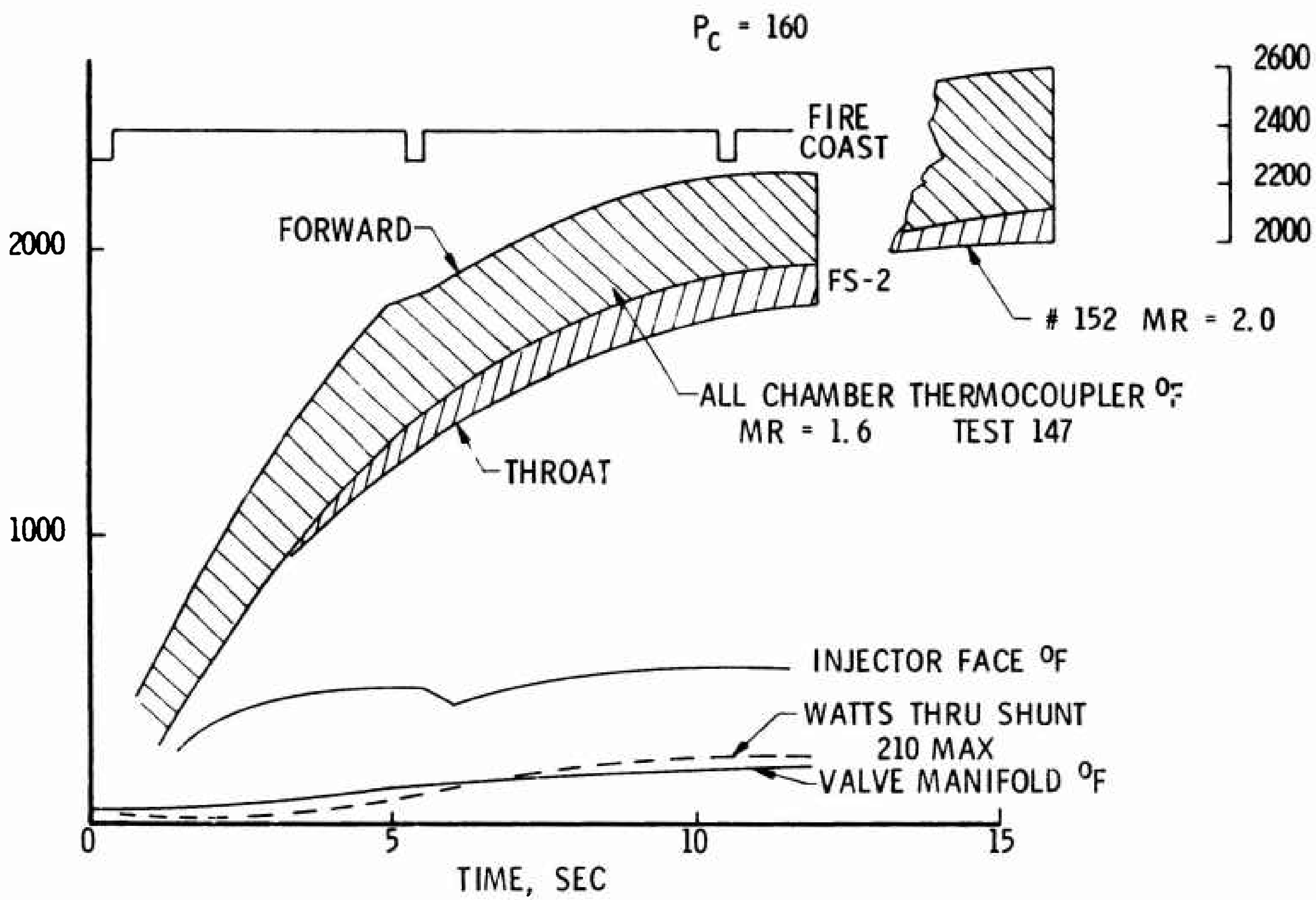

Figure 5.3-29. 4-UD-28-SL Injector, 2-in. Radiation Cooled Cb Nozzle, Measured Thermal Transients

5.3.1, Test Data Evaluation (cont.)

5.3.1.5.2 Injector Thermal Characteristics

Figure 5.3-30 provides parametric data on the steady state injector face temperature with mixture ratio and chamber pressure as parameters. Analysis of these and other data indicated that the injector face temperatures could be reduced by reducing the head end chamber diameter.

Figure 5.3-31 demonstrates that the maximum head end injector temperatures occur during steady state firing 100% duty cycle, and that pulsing operation is less critical. The 4-UD-0 injector was ruled out from further consideration because of the high face temperatures.

5.3.1.5.3 Heat Rejection Loads

Figure 5.3-32 shows the heat rejection rate through the copper shunt which bypasses the injector and valve, as a function of time and % duty cycle. The 3/4 in. titanium forward end insulator provided a significant reduction of heat flow. A thermal dam of some form located between the chamber and shunt is recommended for the Phase III designs.

5.3.1.5.4 Chamber Thermal Characteristics

Figure 5.3-33 provides the nozzle wall temperature inferred from the thermal data obtained with radiation cooled nozzles. The adiabatic wall temperatures were computed by eliminating the effects of radiation. Some inconsistencies exist in the data due to the poor service life of the thermocouples located in the throat region. The temperatures at the full thrust (P_c = 140-160 psia) approach the useful limit of the coatings available for columbium alloys (2500-3000°F). These data indicate that engines must either operate at lower pressures or contain some additional degree of cooling (film or otherwise) if extended firing life is to be obtained. The designs selected for Phase III should operate at pressures in the 100-120 psia range and contain slight modification to the injector pattern to provide additional wall film cooling.

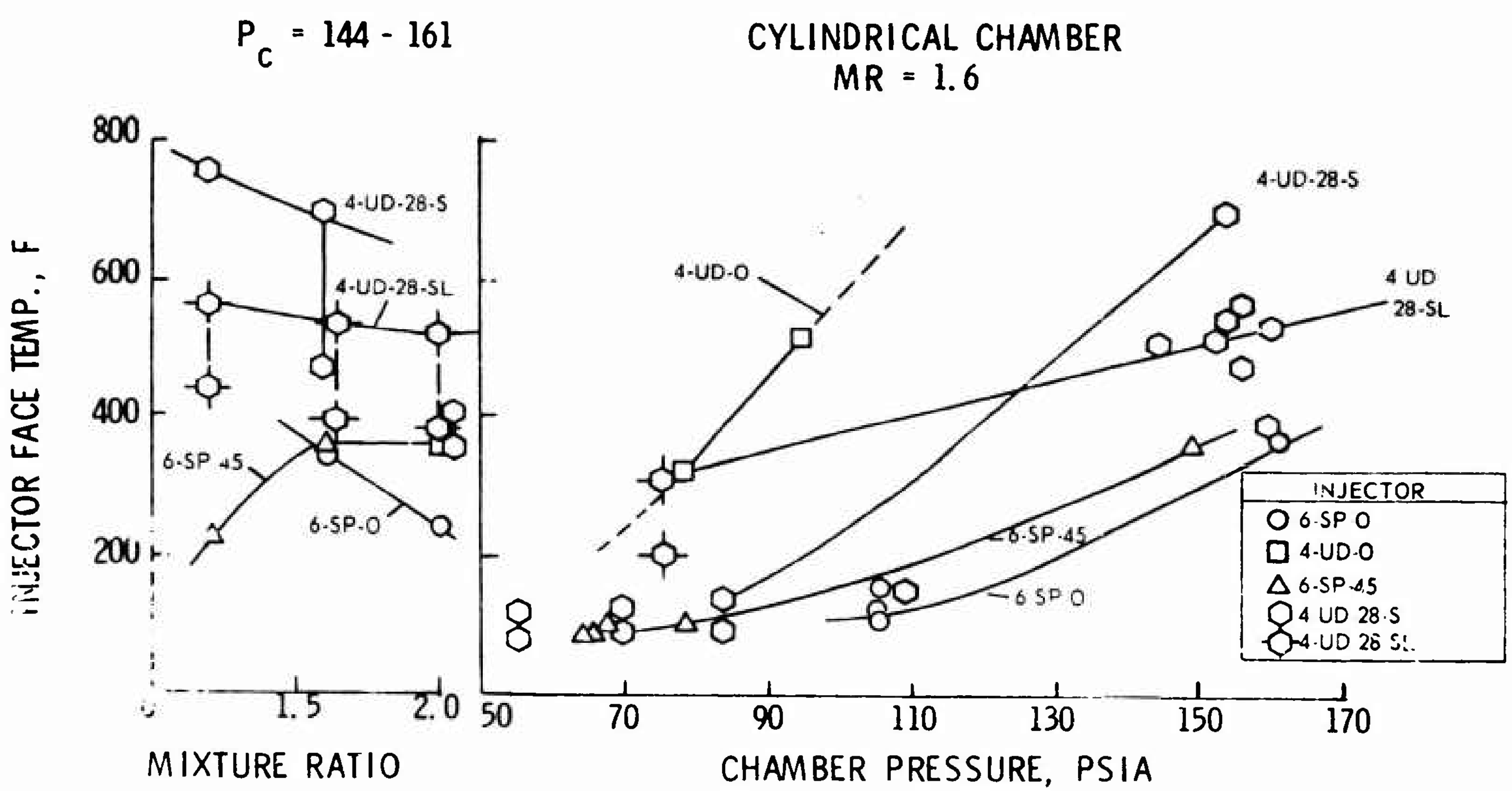

Figure 5.3-30. Steady-State Injector Face Temperature

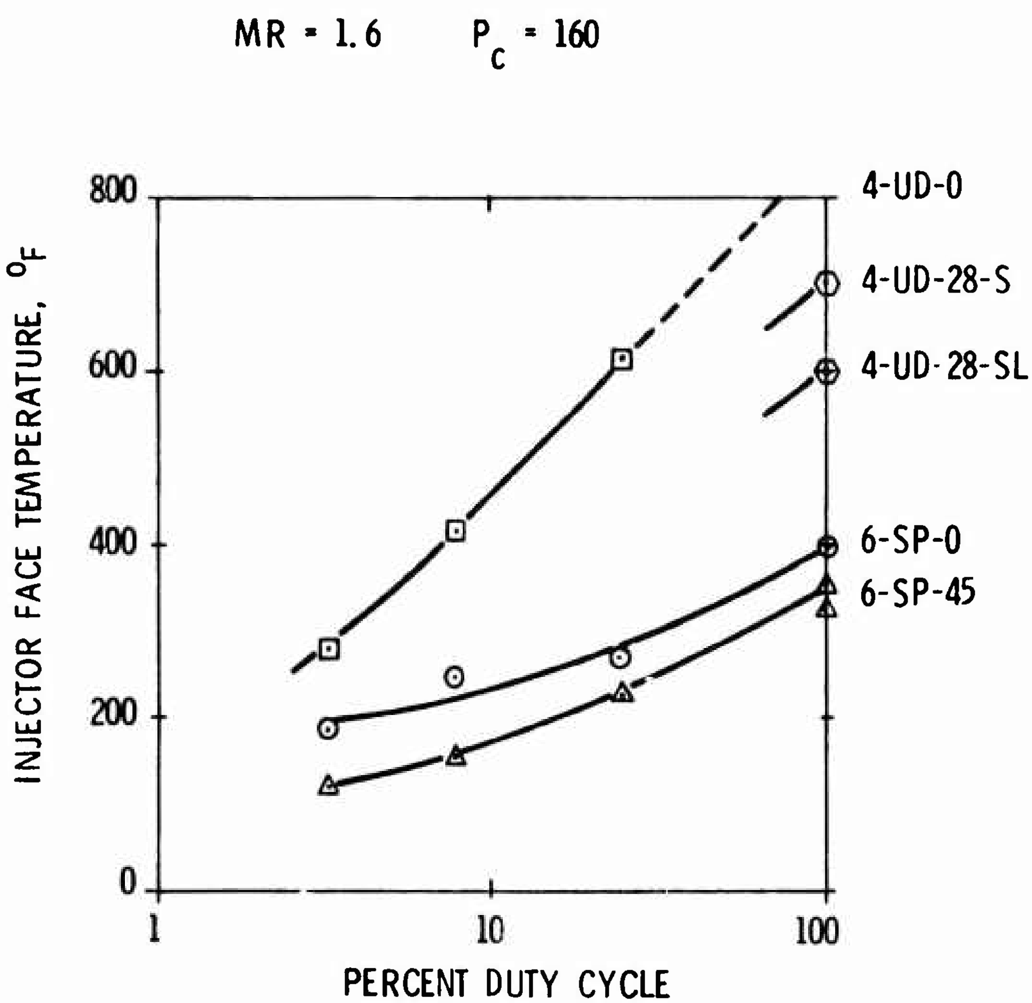

Figure 5.3-31. Injector Face Temperatures

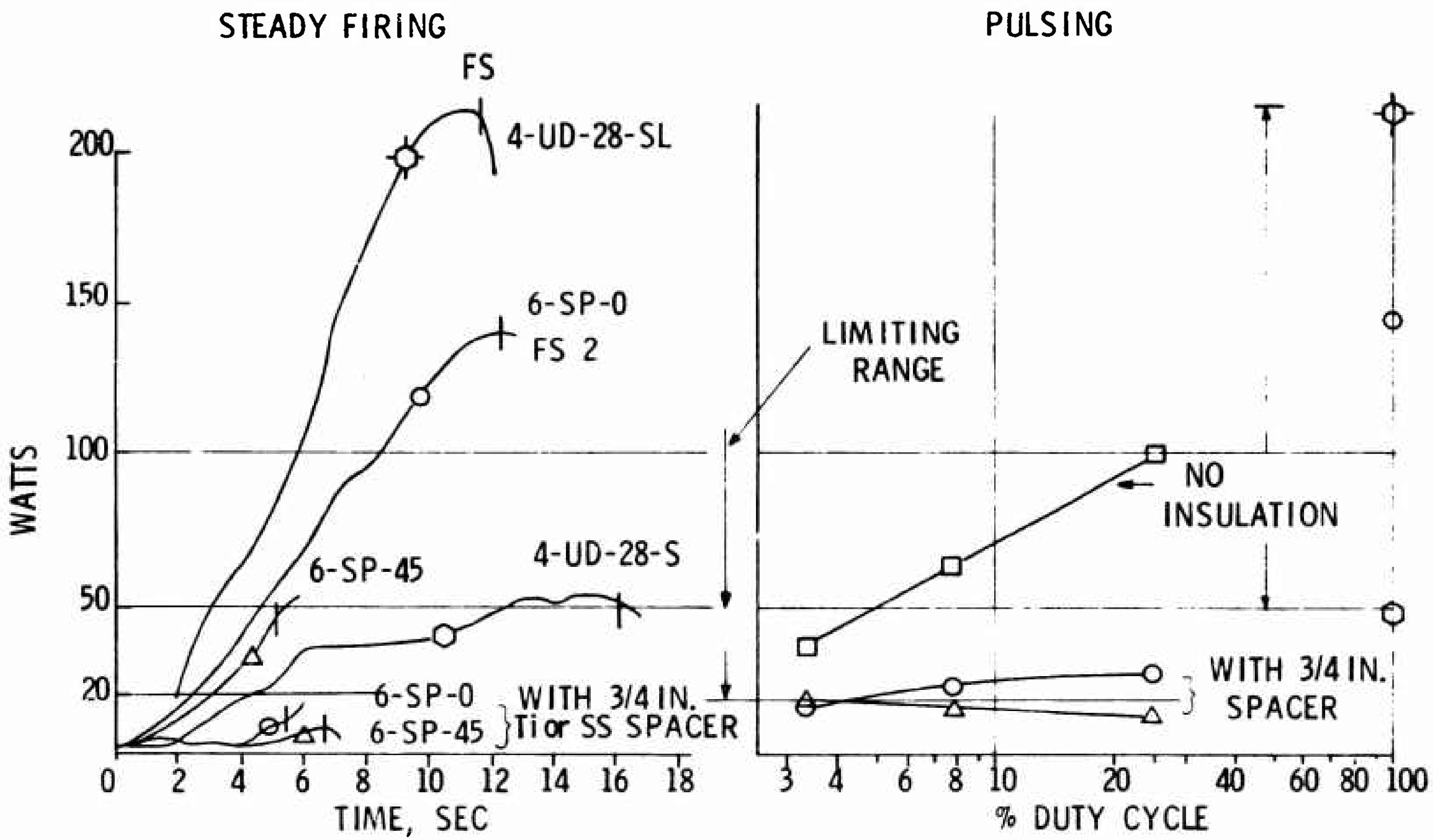

Figure 5.3-32. Thermal Shunt Heat Flow

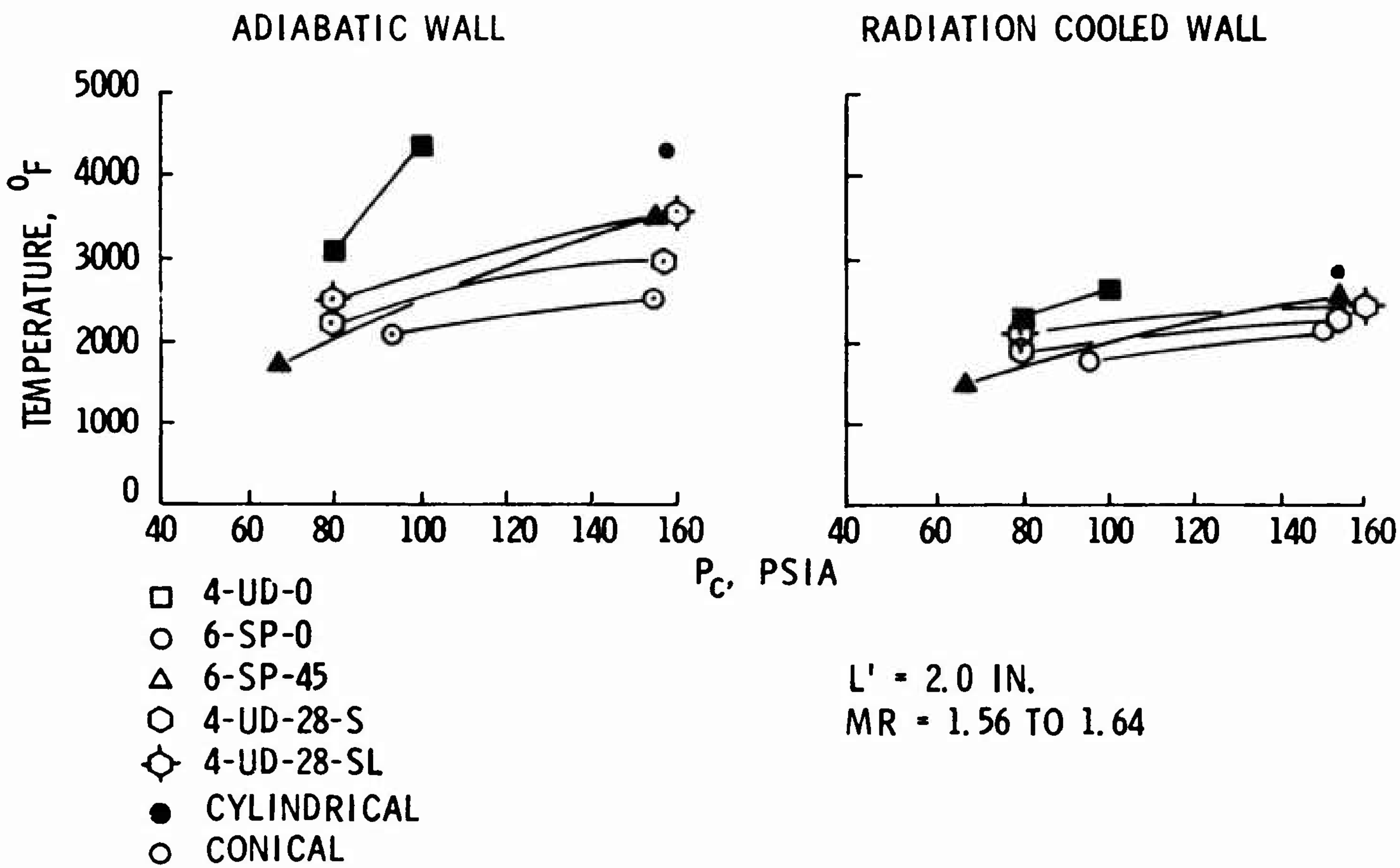

Figure 5.3-33. Pressure Effects on Wall Temperature, Location 0.5-in. Upstream of Throat

5.3.1, Test Data Evaluation (cont.)

Figure 5.3-34 shows a comparison of the maximum chamber wall temperatures as a function of the % duty cycle fired for all the configurations tested. Steady state firing is noted to be the most adverse operating condition. The right hand column provides a ranking of maximum temperatures and resulting performance values. The 4-UD-28-S design was the most conservative while the two 6-element designs provided the highest performance potential.

Figure 5.3-35 provides a map of the circumferential temperature variations 0.5 in. upstream of the throat for four of the injector designs tested. The good propellant distribution resulting from the manifold design in conjunction with the multi-element patterns results in a very uniform circumferential temperature distribution.

5.3.1.5.5 Thermal Conclusions

(1) The multi-element injectors provide a uniform axisymmetric flow field which is essentially streak free.

(2) The face temperatures of the two 6-element designs are sufficiently low to allow at least 10^6 full thermal cycles. The higher face temperatures encountered with the 4-element designs are caused by hot gas recirculation and can be reduced by decreasing the contraction ratio at the head end.

(3) The axial temperature profiles provided by the 4-UD-28-S injector are satisfactory for long duration adiabatic wall chamber operation. Some derating of the 6-element designs is required to achieve additional wall cooling.

(4) A thermal dam is required between the chamber and thermal shunt to limit the heat flow to the spacecraft.

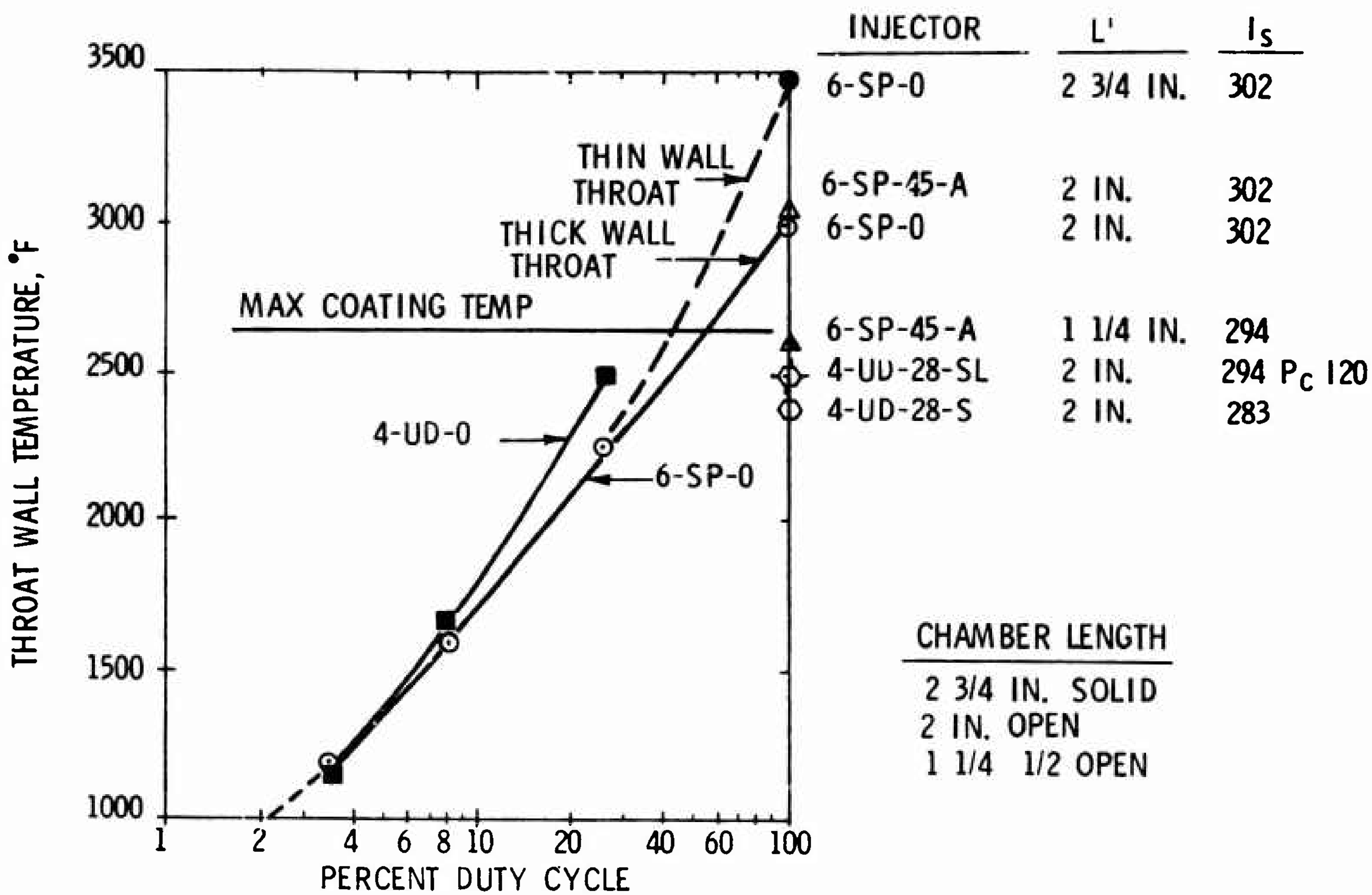

Figure 5.3-34. Maximum Chamber Temperatures, Radiation Cooled

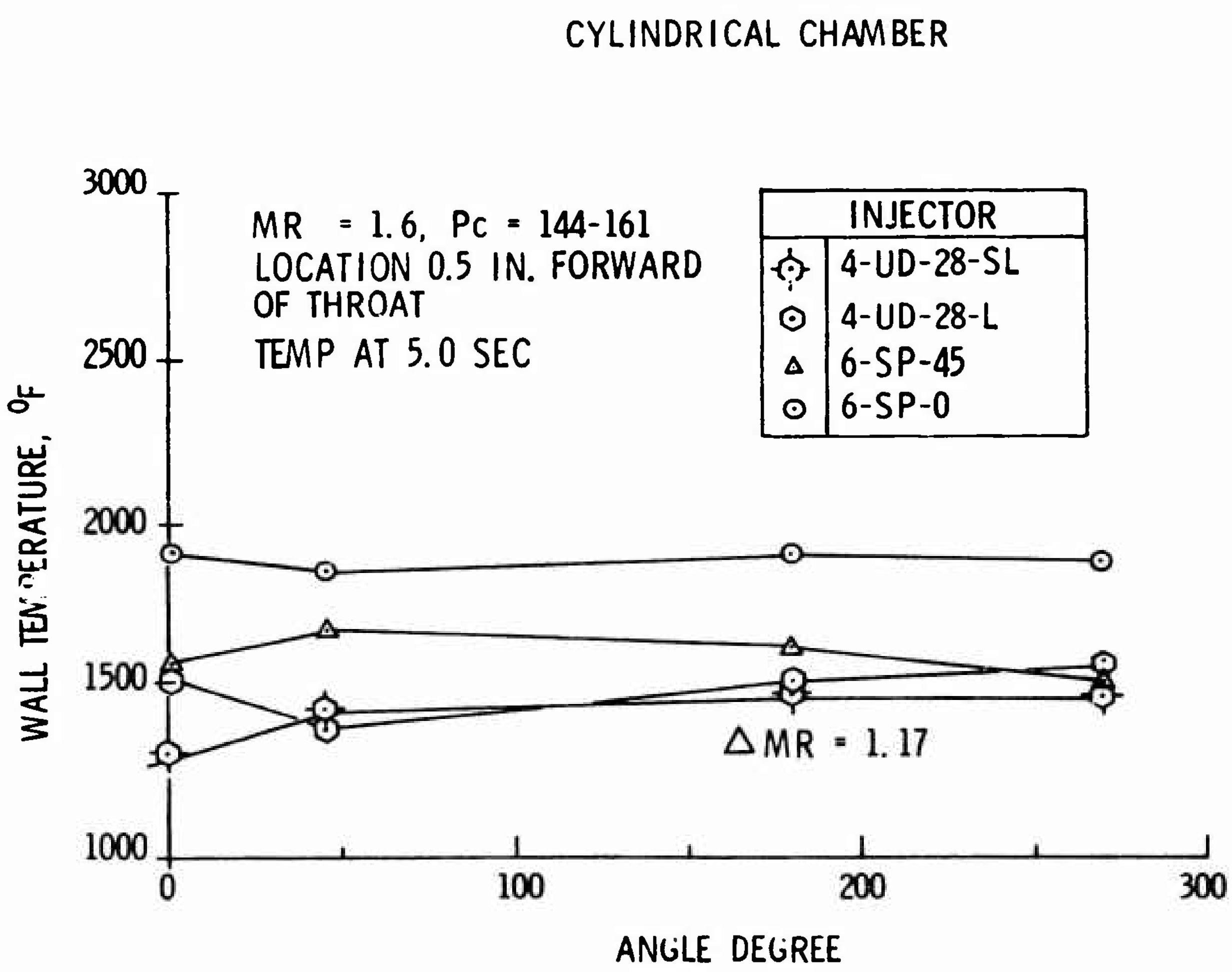

Figure 5.3-35. Circumferential Temperature Variation

5.4 PHASE II - CONCLUSIONS AND RECOMMENDATIONS

At the conclusion of Phase II data evaluation, the demonstrated engine capabilities were compared to the contract goals and to the updated mission requirements. Figure 5.4-1 summarizes this comparison of goals and achievements. The data shown represent the capabilities of all engine designs tested, not that of a single engine. These data indicate that a single engine which meets all of the contract goals and exceeds some (such as minimum bit impulse of 0.02 lbF-sec vs 0.05 required and > 0.003 sec valve response vs 0.005 required) by wide margins can be configured for Phase III. The requirements for a buried engine, established in the mission analyses, was not a stated contract goal. This design required a modified injector configuration which was also demonstrated in Phase III.

Areas requiring additional design optimization related to (1) chamber cooling and heat rejection rates, and (2) blowdown performance capabilities.

Figure 5.4-2 provides a summary of the operational capabilities of each of the Phase II engine assemblies tested. The lower "application" portion of the figure indicates the maximum allowable chamber pressure each engine could run at without exceeding a 2700°F wall temperature. Engines can operate at a higher pressure and provide a higher performance and blowdown ratio when allowed to radiate.

Figure 5.4-3 provides a summary of the mission and engine requirements for three axis stabilized, small spin stabilized and large spin stabilized spacecraft. These were considered typical satellite systems. Three engines which best match the requirements were identified from the Phase II results. Engine SN 3, which is the most conservative design, could actually meet the life requirements of all anticipated missions. Recommended modifications to the injector thermal shunt, standoff and chamber length are

CONTRACT DEFINED GOALS	END OF PHASE II ACHIEVEMENTS
Thrust 5 ± 0.25 LBF	5 ± 0.25 lbf
Chamber Pressure TBD	165 to 56 psia
Feed System Pressure 500 to 100	400 to 100 psia
Expansion Ratio TBD	100/1 Design Point; 50/1 Tested
I_{sp} (Full Thrust)	
Steady State 300 sec	310 sec
Pulsing 240 sec	257 sec
Minimum Impulse Bit 0.05 ± 0.005 lbf-sec	$\approx 0.05 \pm 0.00125$ lbf-sec, ≈ 0.02 min
Total Impulse Capability 30,000 to 100,000 lbf-sec	Not Demonstrated
Ambient Starts 100 and 1,000	≈ 100
Number of Restarts 175,000 & 300,000	2900 (Single Inject .)
Total Firing Life 2 hr to 10 hr	Not Demonstrated
Valve Response <5 ms	<3 ms
Propellants N_2O_4/MMH	N_2O_4/MMH
MR 1.6 ± 0.048	1.2 to 2.0 Tested
Propellant Inlet Temperature 20 to 120°F	22, Ambient & 118 Demonstrated
Storage Life 10 Years	Not Demonstrated
Reliability Goal 0.999	Not Demonstrated
Maintainability Goal Zero During Storage Life	Not Demonstrated
Thrust Chamber Assy Weight TBD lbs	≈ 1.2 lbs

Figure 5.4-1. Thrust Chamber Technology Status

INJECTOR	6-SP-45	6-SP-0	4-UD-0	4-UD-28-S	4-UD-SL
I_{sp} STEADY STATE (RAD)	302	302	302	280	294
MAX SS P_c TESTED	160	160	94	160	118
I_{sp} PULSING AT 0.05 LBF-SEC	238	255	257	-	-
FACE TEMP	350	400	550	700	550
CHAMBER TEMP	3000	2700	2700	2500	2600
APPLICATION					
RADIATION COOLED					
CHAMBER TEMP	2700	2700	2700	2500	2600
CHAMBER PRESSURE	125	160	94	160	118
I_{sp} STEADY STATE	302	302	302	280	294
ADIABATIC WALL					
CHAMBER TEMP	2700	2700	2700	2700	2700
CHAMBER PRESSURE	< 75	120	< 70	90	< 70
I_{sp} STEADY STATE	-	300	-	270	-

Figure 5.4-2. Phase II Engine - Operational Capabilities Summary

DEMO ENGINE NO.		
I	3 AXIS STABILIZED	FREE TO RADIATE REGULATED PRESSURIZATION SYSTEM PULSE MODE FIRING, 1% TO 10% DUTY CYCLE 300,000 PULSES STEADY STATE FIRING 10 HRS TOTAL BURN 10 YR LIFE
	INJECTOR 6-SP-45-C	INCREASED OX INJECTION VELOCITY 0.008 IN. ORIFICE INCREASE FACE THICKNESS FROM 0.008 TO 0.020 ELIMINATE INJECTOR FACE THERMOCOUPLES
	CHAMBER	2 IN. CYLINDRICAL CHAMBER WITH FORWARD END THICKNESS REDUCED
	THERMAL SHUNT	REQUIRED THICKNESS REDUCED TO 0.020 IN.
	THERMAL STANDOFF	LAMINATED STAINLESS SHIM COLUMBIUM LINER + LAMINATED REFLECTORS
	EXPECTED I_s	0.03 SEC EPW $\approx$ 275, 300 SEC STEADY STATE
II	SMALL SPIN STABILIZED	ADIABATIC WALL BLOWDOWN PRESSURIZATION PULSE MODE 10 - 15% D.C. AND 30 SEC STEADY STATE 50,000 PULSES 20 WATTS HEAT REJECTION TOTAL LIFE 10 YEARS 10 HRS BURN TOTAL
	INJECTOR 6-SP-0-C	THICKER FACE AND 0.008 IN. OX ORIFICE, LONGER OX IMPINGEMENT ANGLE MODIFY MANIFOLDING TO IMPROVE FLOW DISTRIBUTION ELIMINATE INJECTOR FACE THERMOCOUPLES
	CHAMBER	2" L" CONICAL USE RESIDUAL HARDWARE FROM PHASE II
	THERMAL SHUNT REQUIRED	.020 THICKNESS THERMAL STAND OFF LAMINATED STAINLESS STEEL
	EXPECTED I_s	290 - 295 STEADY STATE 280 PULSING AT 0.1 SEC EPW
III	LARGE SPIN STABILIZED	ADIABATIC WALL BLOWDOWN PRESSURIZATION PULSE MODE AND VERY LONG DURATIONS FIRINGS 25,000 PULSES: 60 - 70 WATT LIMIT
	INJECTOR 4 UD 28-SC	THICKEN FACE PLATE MODIFY FUEL SPLASH PLATE TO PROVIDE MORE WALL COOLING
	CHAMBER	(1) 1 3/4 IN. L' CONICAL WITH LINER & REFLECTORS (2) SAME + TITANIUM FORWARD END
	THERMAL SHUNT	REQUIRED THERMAL STANDOFF RECOMMENDED TO LIMIT HEAT REJECTION ON LONG BURNS
	EXPECTED I_s	$\approx$ 280 STEADY STATE, MIN. EPW 0.040 SEC $I_{sp} \approx$ 265 SEC

Figure 5.4-3. Spacecraft Missions and Engine Requirements

provided for each design. The expected steady state and pulsing performance at the MIB required for each mission is also indicated.

Figure 5.4-4 provides an assembly drawing of a flightweight engine design with a 100:1 area ratio nozzle. This engine applies to all systems. Detail injector differences are not discernible in the figure.

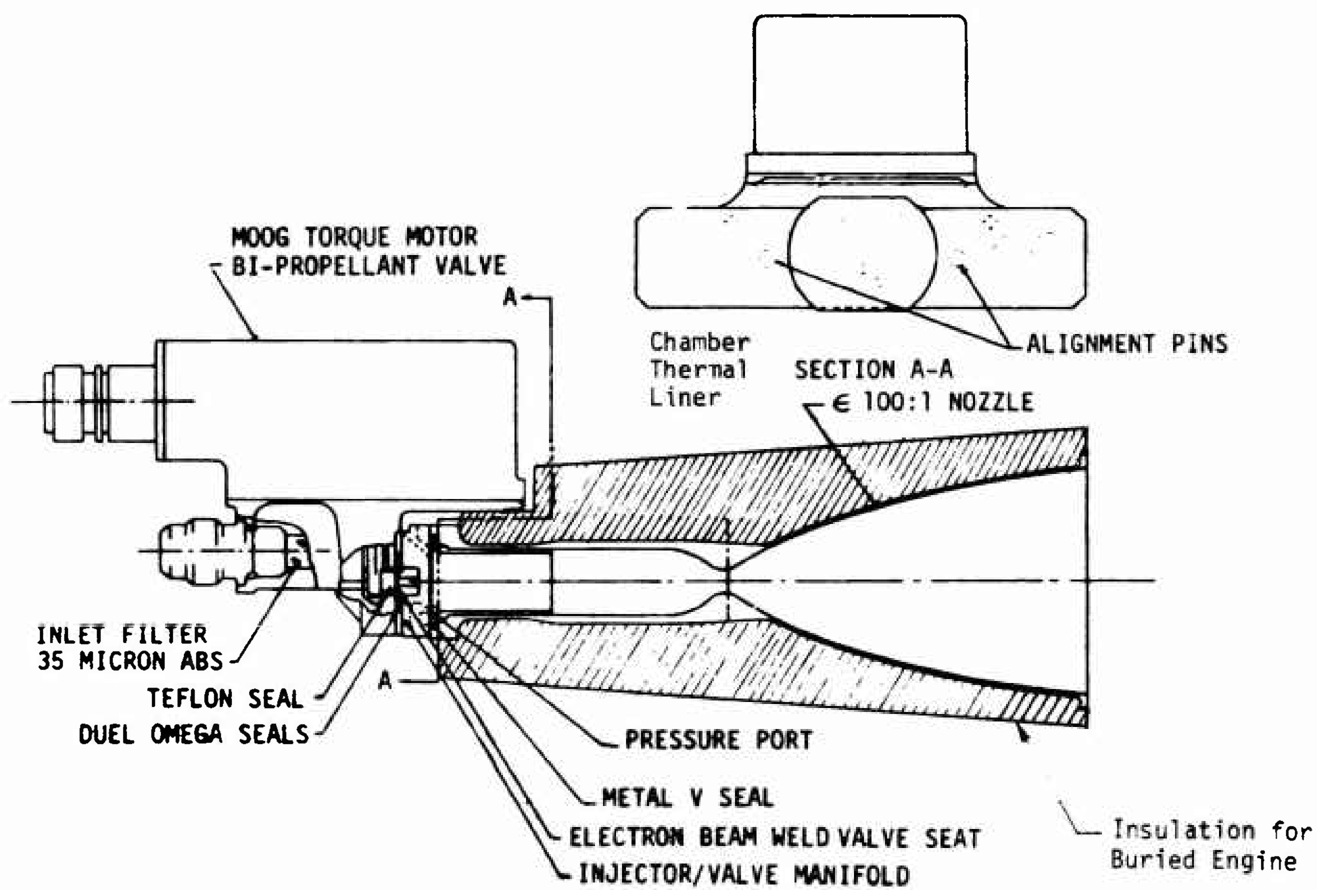

Figure 5.4-4. Five Pound Bipropellant Thrust Chamber Assembly

6.0 PHASE III - ENGINE DEMONSTRATION

This phase of the program included the following tasks: (1) an update of the engine designs generated during Phase II which was based on the results of the evaluation of Phase II test data and review of the mission analysis, (2) component fabrication, (3) hot fire performance and durability testing, (4) test data evaluation, (5) pulse performance modeling using CONTAM and PMPM computer programs, and (6) reliability analyses.

6.1 DEMONSTRATION ENGINE DESIGN UPDATE

The design update resulted in the incorporation of the changes (see Table 6.1-1) to the designs of the three engines programed for fabrication and testing. These detail modifications do not result in a significant departure from the initial design selection shown in Figure 5.4-4.

The design changes summarized in Table 6.1-1 were intended to improve blowdown and pulsing performance, trade excess performance at full thrust for added wall cooling, and to reduce heat flow from chamber to injector. They are discussed in detail in the following sections of this report.

6.1.1 Injector-Valve Assembly

There were no changes made to the Phase III valve seats and actuator system designs. The changes made to the valve manifold which were really injector changes were minor. The bore diameters of the pressed-in valve seats and the adjacent manifold plate were changed to reduce the manifold volume. The fuel bores were changed from 0.025/0.026 inch diameter to 0.020/0.021 and the oxidizer bores changed from 0.032/0.033 to 0.026/0.027. A blind, tapped hole was added to the manifold plate and a through hole added to the valve body. This allowed the addition of a bolt to reduce manifold deflection and possible seal leakage under the most adverse thermal conditions.

TABLE 6.1-1

SUMMARY OF PHASE III DESIGN UPDATE

ENGINE NO.

Component	1	2	3
Valve (All Engines)	Nozzle and valve manifold volumes ($in.^3$) in all engines were reduced from 0.000142 to 0.0000888 (fuel) and 0.000188 to 0.000149 (ox). One additional mounting hole (see Figure 5.1-7) was added to improve seal loading.		
Injector Design	6-SP-45-C	6-SP-0-C	4-UD-28-C
	Effective face plate thickness (in.) increased from /to).		
Face Thickness	0.006/0.021	0.006/0.021	0.006/0.010
Orifices	Ox orifice dia reduced from 0.010 to 0.008 in. and angle change to provide same resultant vector.		No change.
Manifold	No change.	Manifold like 6-SP-45-A.	No change.
Chamber Length	2.0 inches	2.0 inches	1-3/4 inches
Chamber Contour	Cylindrical	Conical	Cylindrical
Forward End	Thermal Liner	No Liner	Thermal Liner
Shunt and Insulator - all engines (see Figure 5.1-19).	Copper shunt thickness was reduced from 0.040 in. to 0.030. The single 0.005 in. thick stainless steel insulator used to reduce heat rejection was replaced by 6 laminates as follows: Injector Manifold 1 - SS 0.005 in. 1 - SS 0.002 in. 2 - CU 0.015 in. each 4 - SS 0.002 in. each Chamber flange	9 interface contacts to reduce heat flow.	

6.1.1, Injector-Valve Assembly (cont.)

The injector face plates were thickened to withstand the peak pressures (460 psia) experienced in the cold propellant pulse tests. Oxidizer orifice diameters on the 6-element injectors were reduced to provide a injection velocity of 40 fps at the minimum tank pressure condition. The manifold of the 6 SP-0-C design was modified to include the flow distribution improvements first incorporated on the A modification of the 6-SP-45. Thermal isolation rings were incorporated at the injector periphery to reduce heat flow from the chamber to the face. Thermal instrumentation was deleted from the 6-SP series injectors on the basis of the very low face temperatures (400°F max; Figure 5.3-30) experienced in Phase II.

Figure 6.1-1, -2 and -3 illustrate the platelets for the three injector designs employed in the Phase III testing. The total residual propellant volume of each of these injector-valve assemblies is as follows:

	6-SP-45-C	6-SP-0-C	4-UD-28-SC
Fuel (in.^{3})	0.000305	0.000276	0.000245
Ox (in.^{3})	0.000344	0.000315	0.000299
Total	0.000649	0.000591	0.000544

6.1.2 Thrust Chambers

The thrust chamber injector to throat lengths (L') described in Table 6.1-1 are less than those used for the bulk of the Phase II vacuum pulsing and steady state fire testing. The reduced lengths resulted from trading the 2 to 10 second specific impulse margins realized in Phase II, Figures 5.3-4 and 5.3-5 for improved cooling margin. Figure 6.1-4 is a detailed drawing of the chamber used for the -1 engine. This chamber differs from the Phase II cylindrical chamber in two areas:

(1) The wall thickness of the forward end thermal dam was reduced from a nominal 0.030 in. to 0.017 in. to restrict the heat flow to the thermal shunt located between the valve manifold and chamber flange.

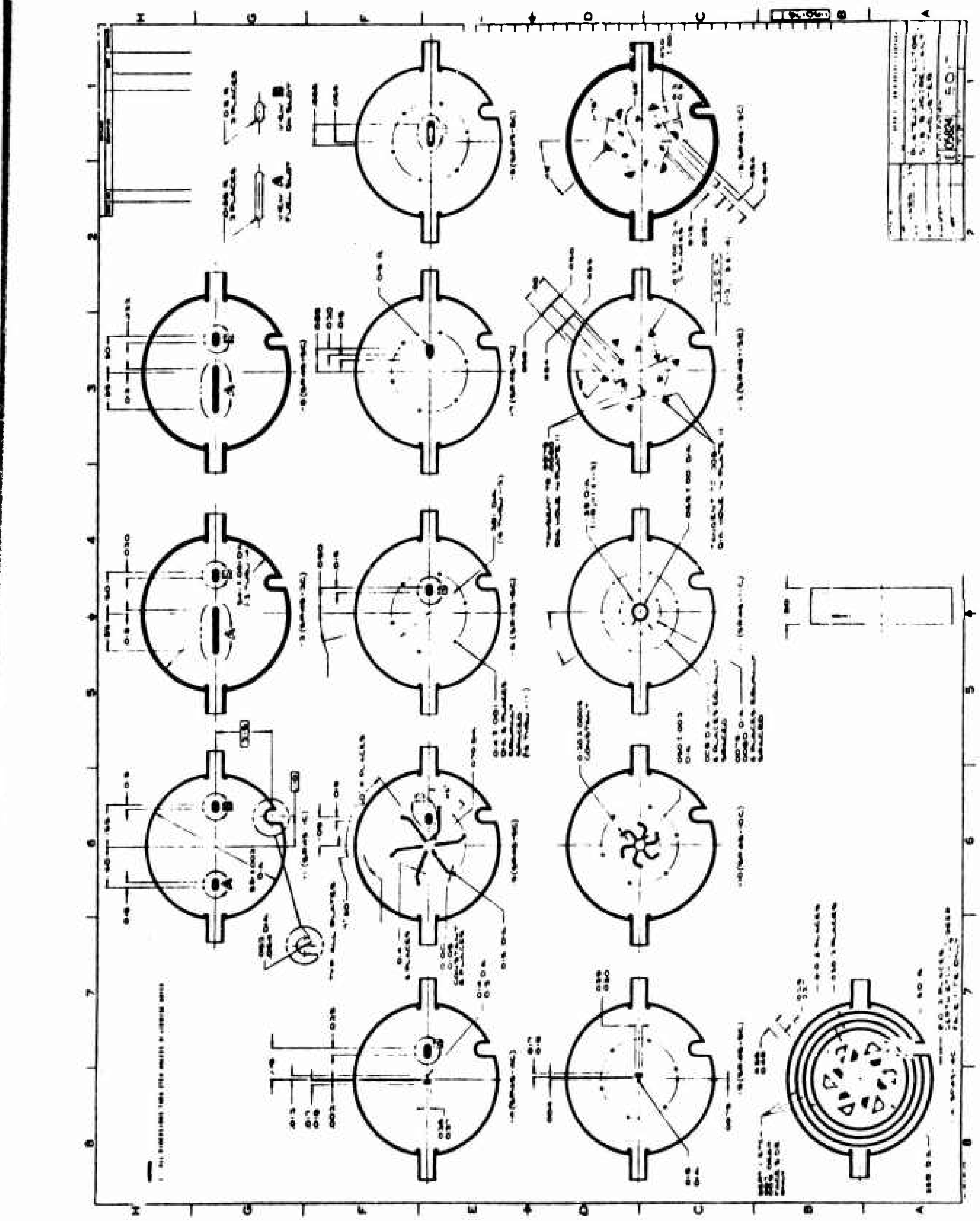

Figure 6.1-1. 6-SP-45-C Platelet Injector

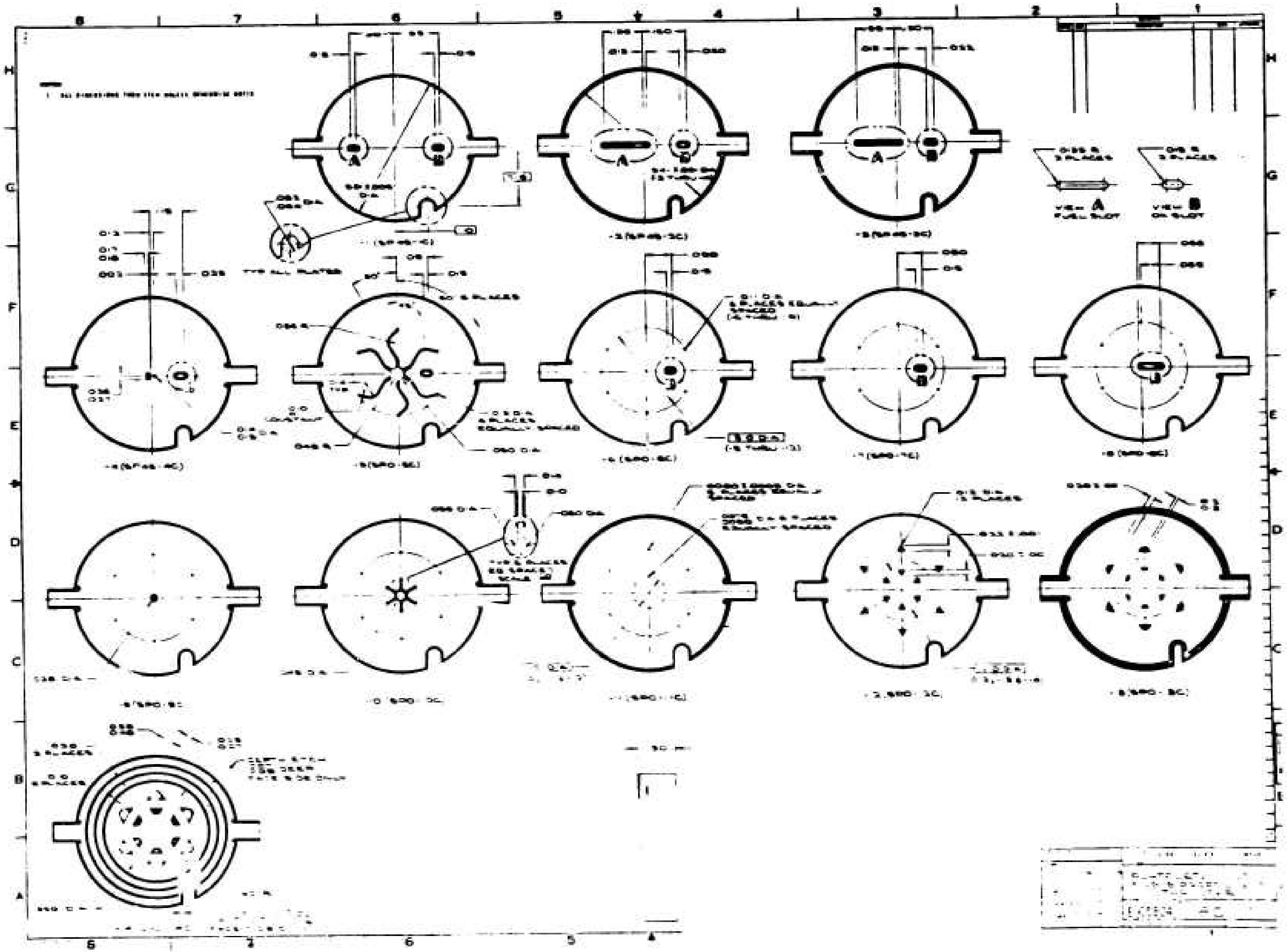

Figure 6.1-2. 6-SP-O-C Platelet Injector

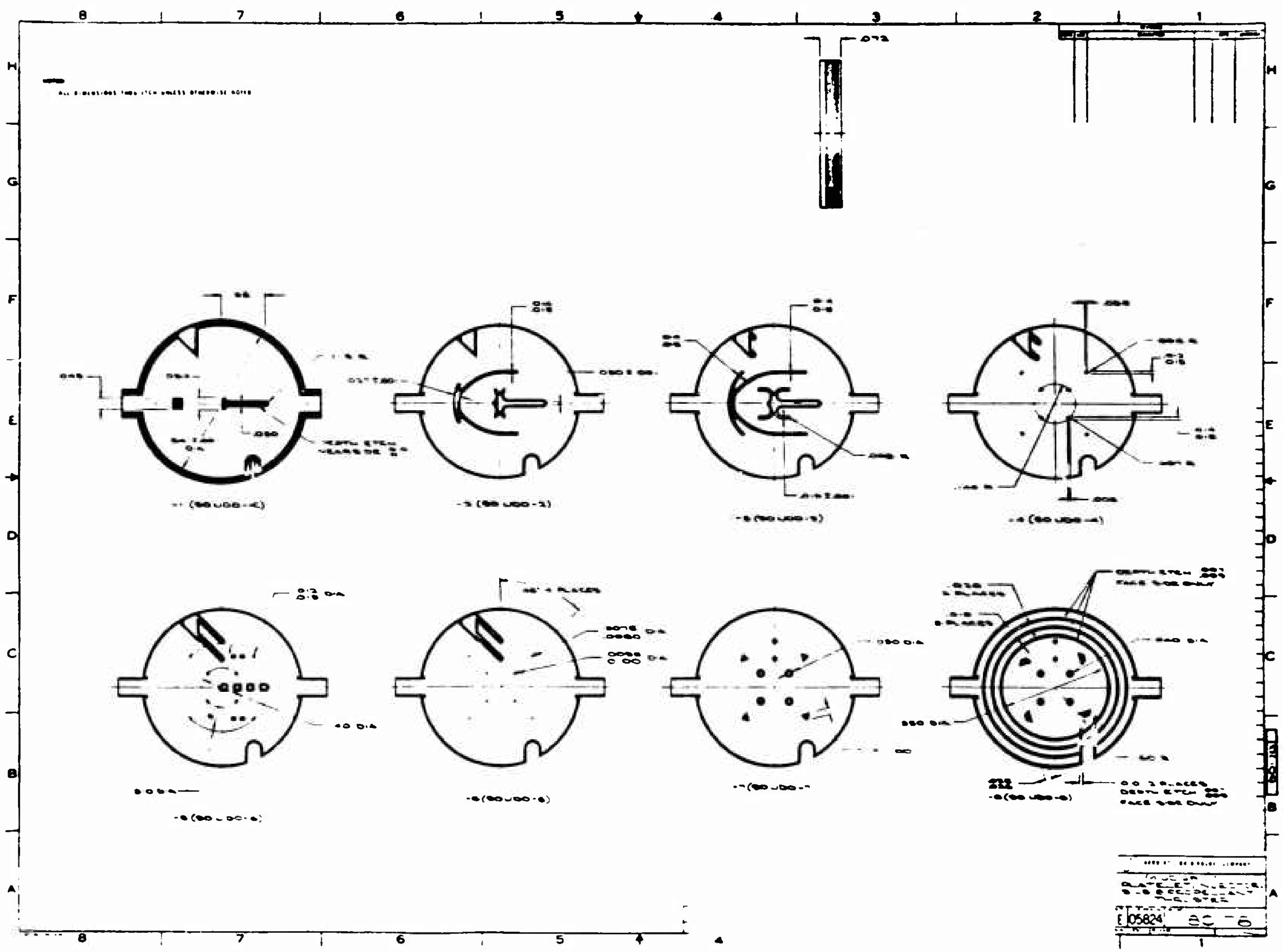

Figure 6.1-3. 4-UD-28-SC Platelet Injector

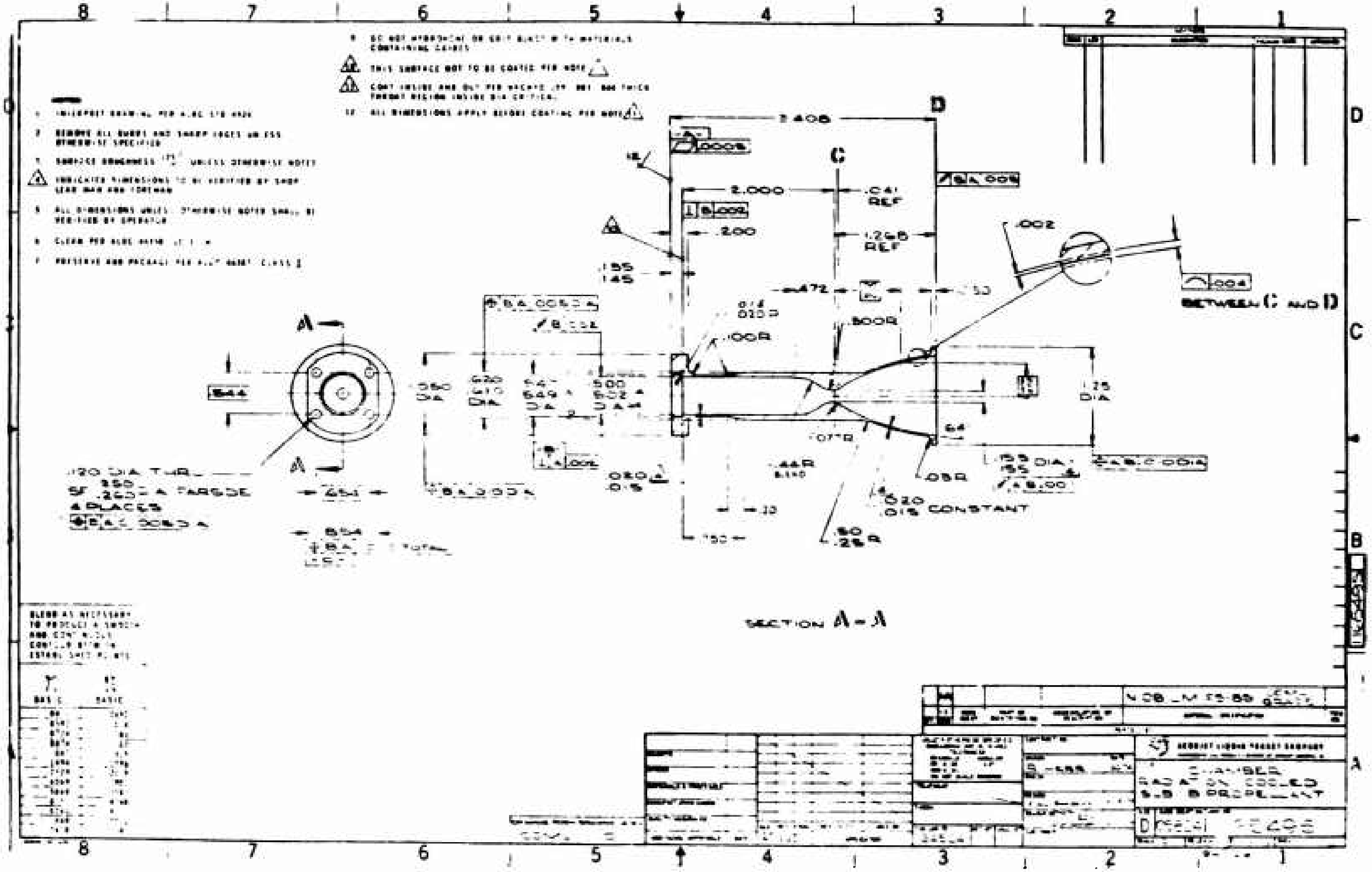

Figure 6.1-4. Detailed Drawing, A Radiation Cooled Chamber used for the -1 Engine

6.1.2, Thrust Chambers (cont.)

(2) The chamber was modified at the forward end to accept the thermal liner shown in Figure 6.1-5. This sleeve shields the thin wall and aids in reducing the heat flow to the injector. Its installation is shown in Figure 5.1-19. The conical design thrust chamber employed for Engine SN 2 is shown in Figure 5.1-18.

The thrust chamber utilized on Engine SN 3 is illustrated in Figure 6.1-6. This chamber differs from that of Engine SN 1 by having an L' of 1.75 inches and a convergent nozzle modified to enhance film cooling effectiveness. This design also incorporates the chamber liner shown in Figure 6.1-5. Since this chamber is required to operate in a buried mode the 0.429 in. ID of the downstream end of the liner is matched to the 0.460 in. chamber ID to minimize breakup of the wall film. This is in contrast to the intentionally larger step employed with the radiation cooled Engine SN 1 to promote breakup of the wall film and thus improve performance.

The 0.450 OD of the chamber liner was overwrapped with six and nine layer radiation shields for Engines SNs 3 and 1, respectively. Each shield was formed from a 0.60 in. wide strip of 0.001 inch thick stainless steel, coated with 0.0005 in. of aluminum oxide on one surface. This selection was based on the analysis shown in Figure 6.1-7 which, utilized heat rejection rate data obtained in the Phase II testing. The analysis shown accounts for radiation from the liner to the chamber wall through four to ten reflectors plus conduction along the 0.017 in. thick columbium section between the exposed chamber and the flange. The effect of employing a lower conductivity titanium flange and thermal dam to reduce the heat rejection rates is also shown. The selection of the all columbium chamber design was based on the ability to limit the heat rejection to 50 watts without introducing a columbium to titanium weld joint, thus improving both fabricability and reliability.

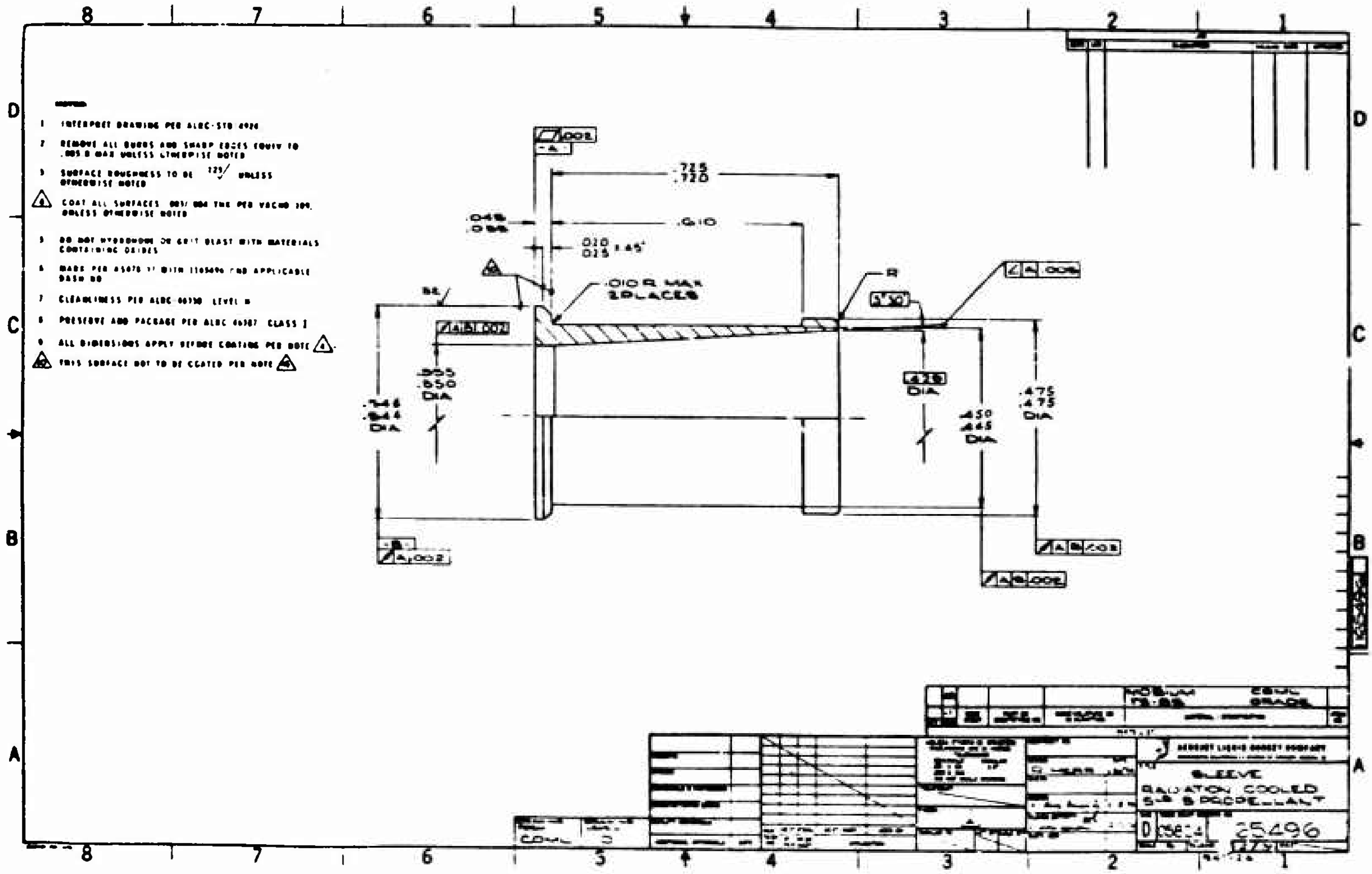

Figure 6.1-5. Detailed Drawing, Sleeve, Radiation Cooled Chamber

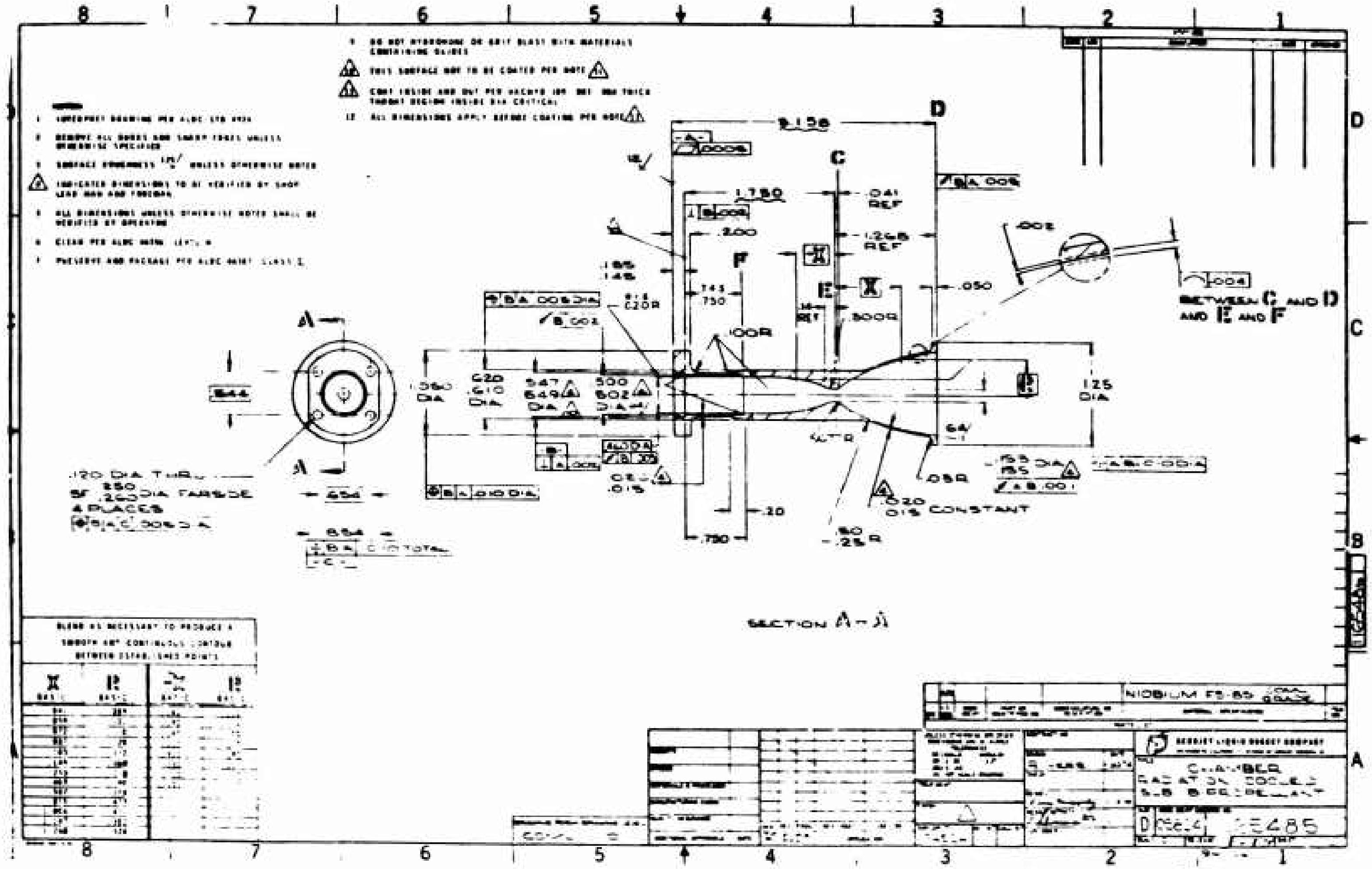

Figure 6.1-6. Detailed Drawing, Radiation Cooled Chamber used for the -6 Engine

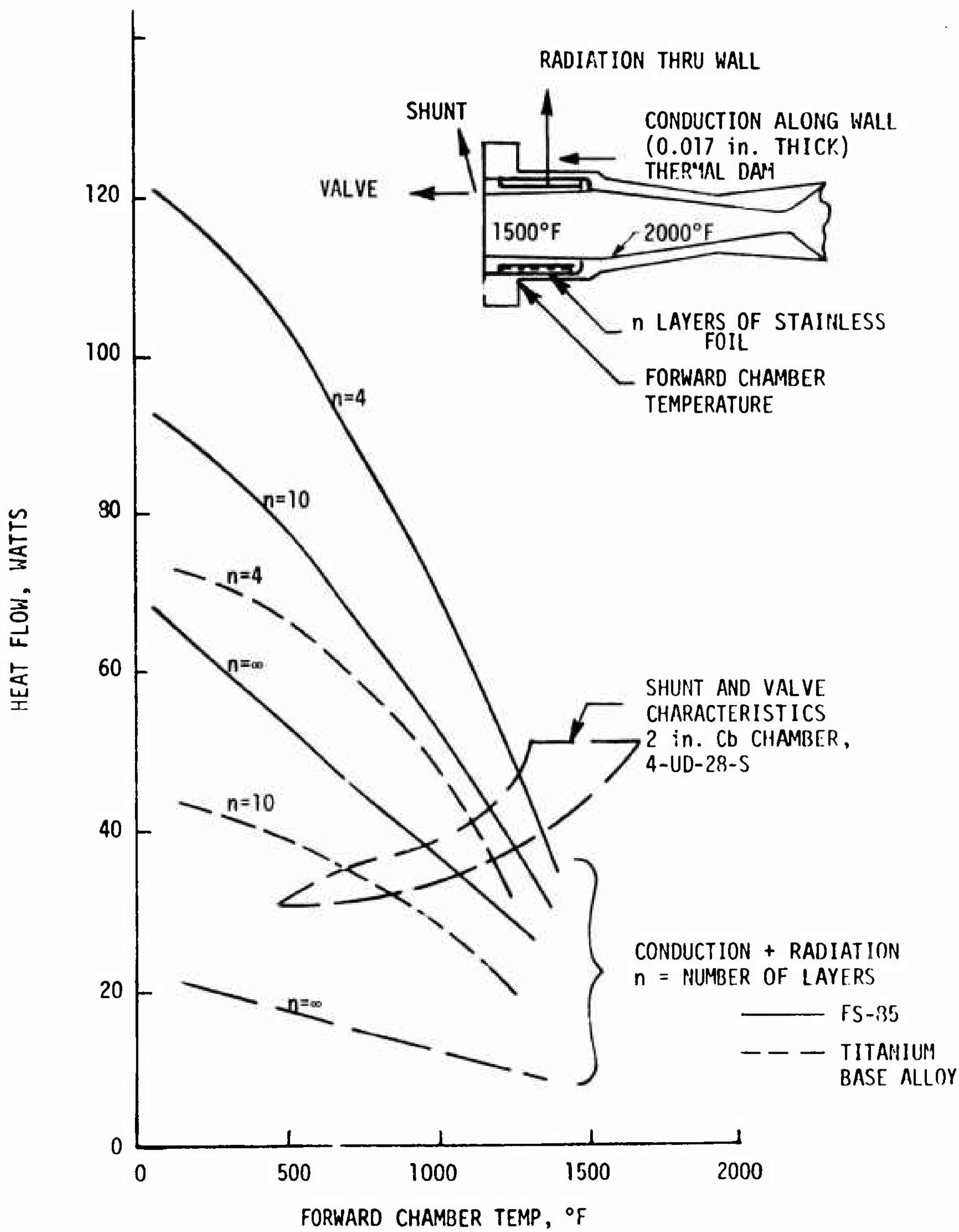

Figure 6.1-7. Heat Flow Characteristics of Phase III Buried Engine

6.1.2, Thrust Chambers (cont.)

The 0.350 inch ID at the sleeve's forward end, was based on the data of Figure 6.1-8, which shows lower contraction ratios reduce the injector face temperature; this, in turn, reduces the heat rejection rate to the valve manifold plate.

The use of multiple interface contacts as a means of further restricting heat flow from the chamber flange to the shunt and valve manifold body was based on Phase II results obtained with a single contact design. Measured contact resistances ranged from 0.00785 to 0.025 hr-°F-ft^2/Btu for the various assemblies. These compare with a calculated contact resistance of 0.003 hr-°F-ft^2/Btu based on data involving material properties, surface conditions and contact pressures. A contact resistance of 0.014 hr-°F-ft^2/Btu was selected for design purposes. This resulted in an effective resistance of 10°F/watt per contact when applied to the surface area of the insulator platelet, PN 1165471-3 (Figure 5.1-20).

Five contacts were selected to separate the chamber flange from the shunt thus providing a heat rejection of 2 watts per 100°F rise in flange temperature. Flange temperatures of 500 to 1500°F were expected. Multiply material was used at the chamber to valve manifold to achieve this in series multi contact design. The multiple spacer separates chamber and manifold body; the seal at this interface is provided by a Haskel V seal.

6.1.2.1 External Insulation

A review of available lightweight insulations suitable for buried chamber designs indicated "Dyna Quartz" (John Manville Company) to be most effective to temperatures of 2700°F. Analyses showed a 1.2 in. thickness of 6.2 lb/ft^3 insulation block K = 0.9 Btu-in./sq ft-hr-°F to be sufficient to maintain external temperatures below 300°F for all operating modes and unlimited firing durations.

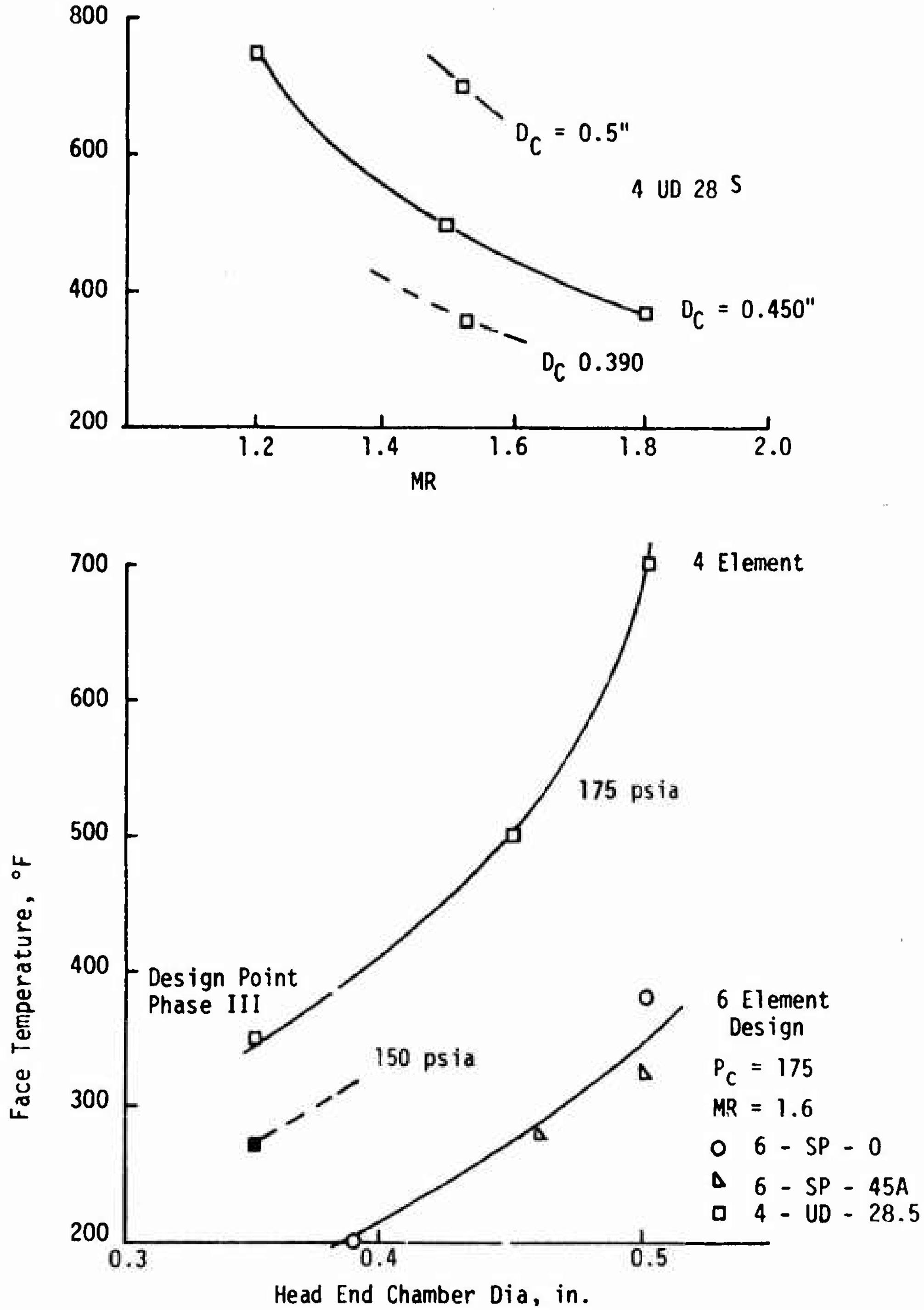

Figure 6.1-8. Chamber Diameter Versus Injector Temperature

6.1.2, Thrust Chamber (cont.)

An engine assembly drawing is provided in Figure 6.1-9 and the insulation configuration is shown in Figure 6.1-10. All other components, i.e., seals, etc., were the same as Phase II designs.

6.2 ENGINE FABRICATION

6.2.1 Valves

Two valves, identified as Moog, Inc. Model 52E163A, and three manifolds (P/N 100-73074) were procured for Phase III work (Figure 5.1-8). The manifolds were completely machined by Moog, Inc. and seat nozzles installed and electron beam welded before shipment to ALRC. Each valve was also acceptance tested (proof, response and leak) with a manifold using O-ring seals for the interface joint prior to shipment. Aerojet brazed the injectors into the manifold, and installed the metal seals at the valve to manifold interface to complete the valve assembly prior to valve functional testing and engine fire testing. Both valves performed satisfactorily as shown by the data of Figures 5.1-4 and 5.2-3.

The valves were checked for flow, pressure drop and leakage after completion of the brazing operations on the manifold. The leak check of valve S/N 011 with manifold S/N 002 revealed leakage past the fuel shutoff seal. Visual examination of the manifold revealed the seating area of the nozzle to be locally deformed. Since this discrepancy had not been seen prior to manifold brazing, the damage occurred during processing or handling at ALRC. The manifold was reworked by Moog, Inc. and returned. There were no leaks on pretest leak checks.

6.2.2 Injectors

Six each of 6-SP-45-C, 6-SP-OC and 4-UD-28-SC injector designs were fabricated for the Phase III testing using the procedure

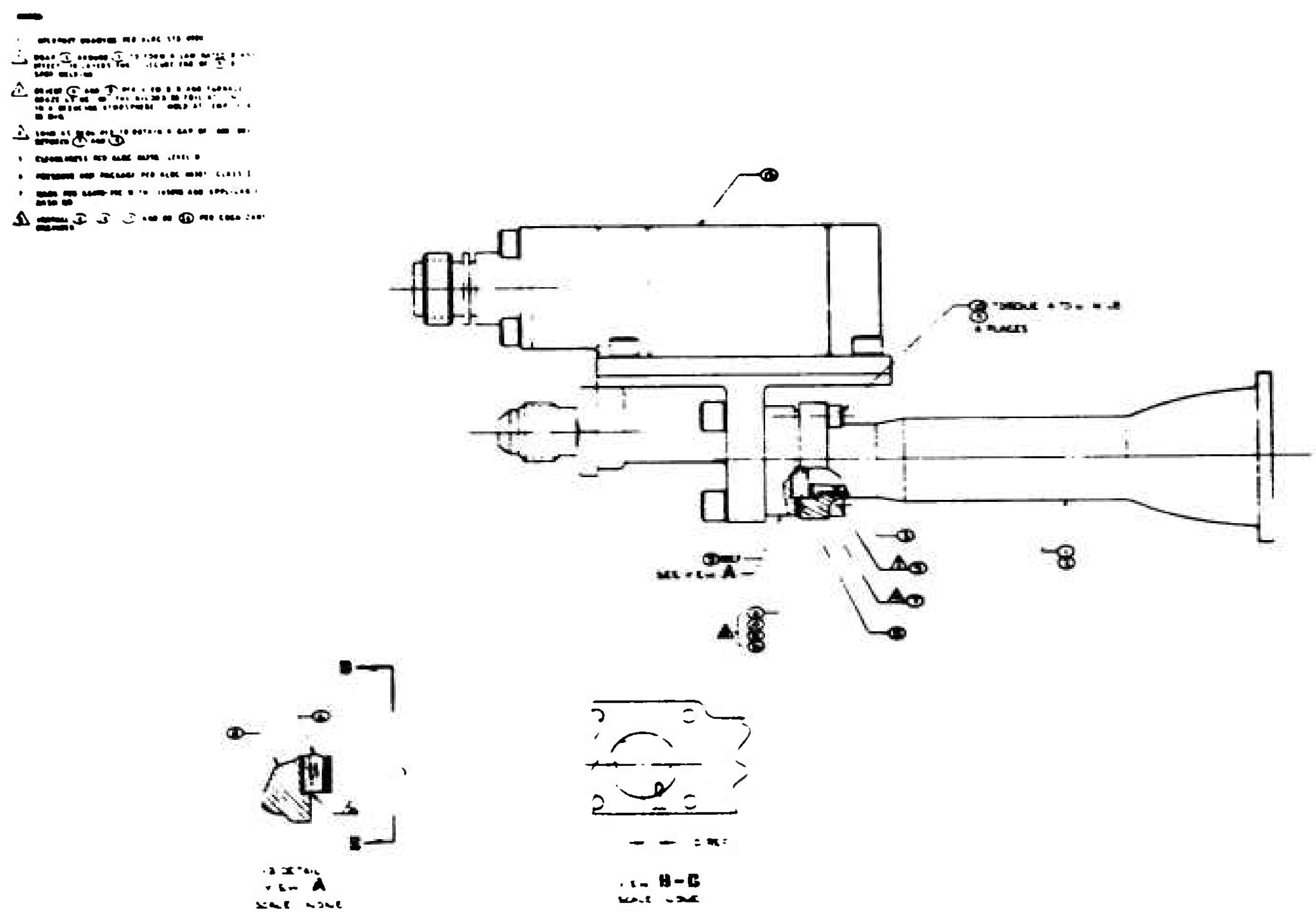

Figure 6.1-9. Five Pound Thrust Chamber Assembly

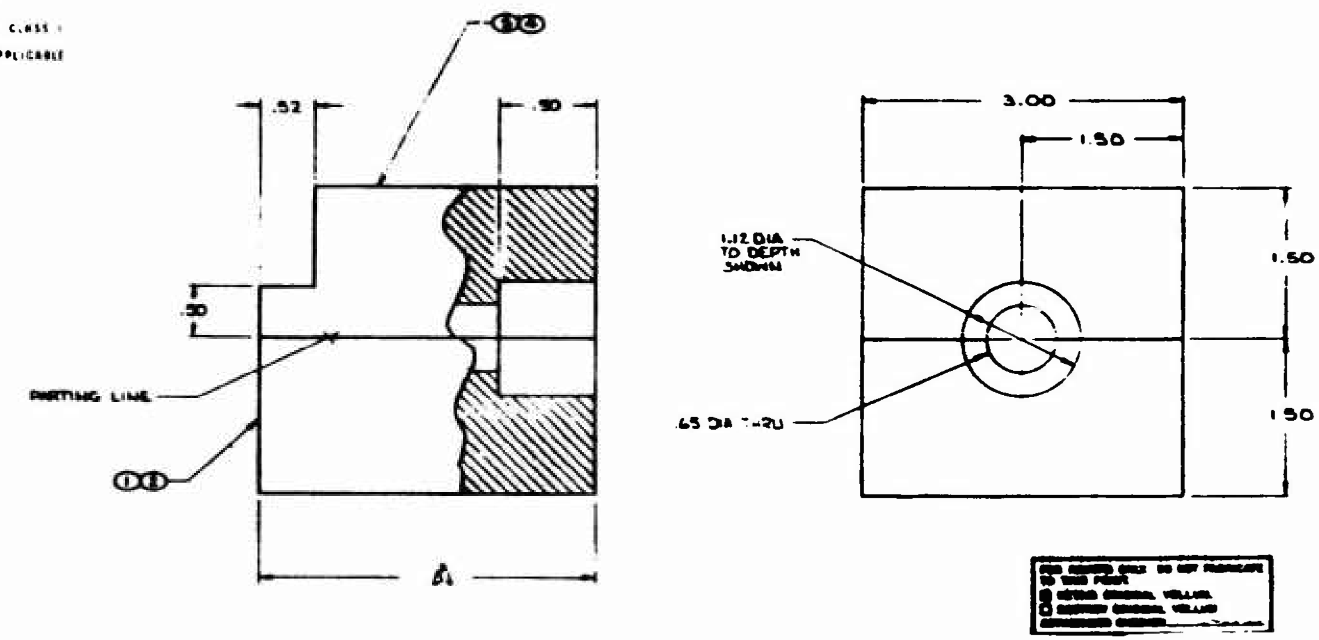

TAB BLOCK	
PART NO.	DIM A
-1	3.15
-2	2.90
-3	3.15
-4	2.90

Figure 6.1-10. Chamber Insulator

described in 5.1.2.2 and shown typically in Figure 5.1-15. The Phase III injectors, shown in Figure 6.2-1, were fabricated using the platelet designs shown in Figures 6.1-1, -2 and -3.

Cold flow of the 6-SP-OC and 6-SP-45-C designs indicated good spray patterns and flow uniformity. Cold flow of the 4-UD-28-C injectors, however, showed improper atomization of one of the 4 oxidizer fans in the 4-element patterns and fuel impingement lengths which were more like the SL pattern of Phase II. All six of the injectors experienced identical flow characteristics. The oxidizer problem was attributed to poor alignment during the stacking operation which was subsequently traced to the use of undersized stacking pins. The differences in the fuel fan angles were traced to the design changes associated with the thickening of the face plate for improved structural margin. Replacement injectors were manufactured, however, in order to maintain schedule the phase II 4-UD-28-S design was employed for the Phase III durability testing. The only difference between the phase II and III injector designs of this type were the thickened face plate. The nozzles of the Phase III manifolds were slightly larger but this was not expected to affect the durability testing.

Table 6.2-1 provides a summary of the flow coefficients of these designs showing the reproducibility in fabrication. These data also indicate no change in flow characteristics when installed in the manifold and no more than ≈ 2% change over the 50,000-300,000 cycle life of the engines.

6.2.3 Chamber Fabrication and Instrumentation

One each of the chamber designs shown in Figure 6.1-4 and -5 and two of liner design shown in Figure 6.1-5 were fabricated from Fansteel Alloy No. 85. These were subsequently coated with a slurry Hafnium Silicide coating (Vac-Hyd 101) per Vac-Hyd processing specification 110A. A third chamber which had experienced minor coating spalling downstream of the throat

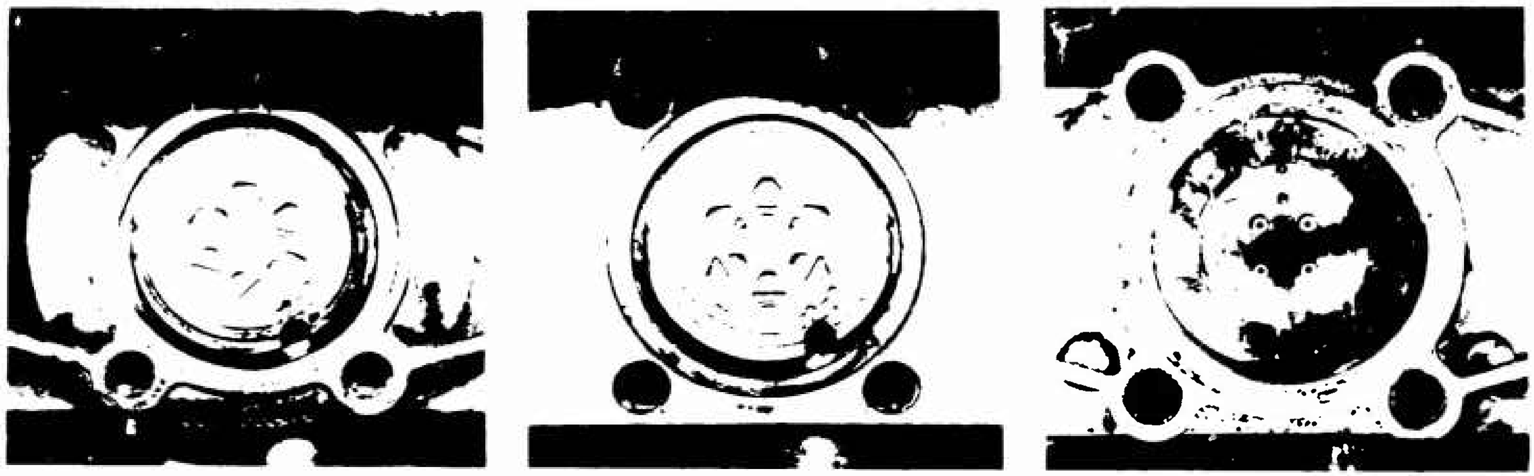

3000,000 PULSES SN 1 | 50,000 PULSES SN 2 | 50,000 PULSES SN 3

Fgiure 6.2-1. Phase III Injector (Postfire)

TABLE 6.2-1

FLOW COEFFICIENTS* FOR PHASE III INJECTORS

	Unit	6-SP-45-C Fuel	6-SP-45-C Ox	6SP-0 Fuel	6SP-0 Ox	4-UD28-SC Fuel	4-UD28-SC OX
Injector as Fabricated	1	618	533	592	664	710	820
	2	576	492	579	655	710	820
	3	575	499	570	650	704	858
	4	621	506	579	643	725	847
	5	600	515	573	700	728	847
	6	593	519	579	679	730	845
Selected Unit Injector in Manifold		C-1		C-6		4-UD28S from Phase II See Table 5.2-3.	
Prefire Kw		582	530	526	679	671	840
No. Pulses (hot fire)		>300,000		>50,000		>50,000	
Post Durability Kw		588	519	523	666	677	821
% Change in Life Testing		1.0%	2.1%	0.6%	1.9%	0.9%	2.3%

*Times 10^6

6.2.3, Chamber Fabrication and Instrumentation (cont.)

during the Phase II testing was also returned to the coating subcontractor for evaluation of the failure. It was found that there was excessive coating thickness in the spalled area. This was due to runoff during processing. The unit was stripped, recoated and returned with the Phase III hardware. An unused conical chamber with a R512E coating was also available from Phase II. A photograph of a chamber after coating but before instrumentation is shown in Figure 5.1-8.

The poor thermocouple durability experienced in Phase II resulted in the modification of instrumentation procedures as indicated in the following table:

TC Type and Temp Range	Parameter	Phase II	Phase III
W - 5% Re vs W - 26% Re	Wire dia (in.)	0.003	0.010
0 - 3200°F	Installation	Remove coating and spot weld	Remove coating - drill and stake
	Expansion	1 loop	Multicoil
Chromel vs Alumel			
0 - 2200°F	Wire dia	0.003	0.005
	Installation	Remove coating and spot weld	Remove coating and spot weld in inert atmosphere
	Expansion	1 loop	Fix near junction

Figure 6.2-2 is a photograph of an instrumented columbium thrust chamber before the Dyna Quartz insulation was applied. The larger diameter coiled wires are the 0.010-in.-dia Tungsten-Rhenium wires which are staked in. The coil allows for thermal expansion and vibration loads. The smaller, darker wires are the chromel vs alumel TC's located in the regions which were expected to operate below 2200°F. Figure 6.2-3 shows a cross section of the -1 and -3 chamber contours and the thermocouple locations.

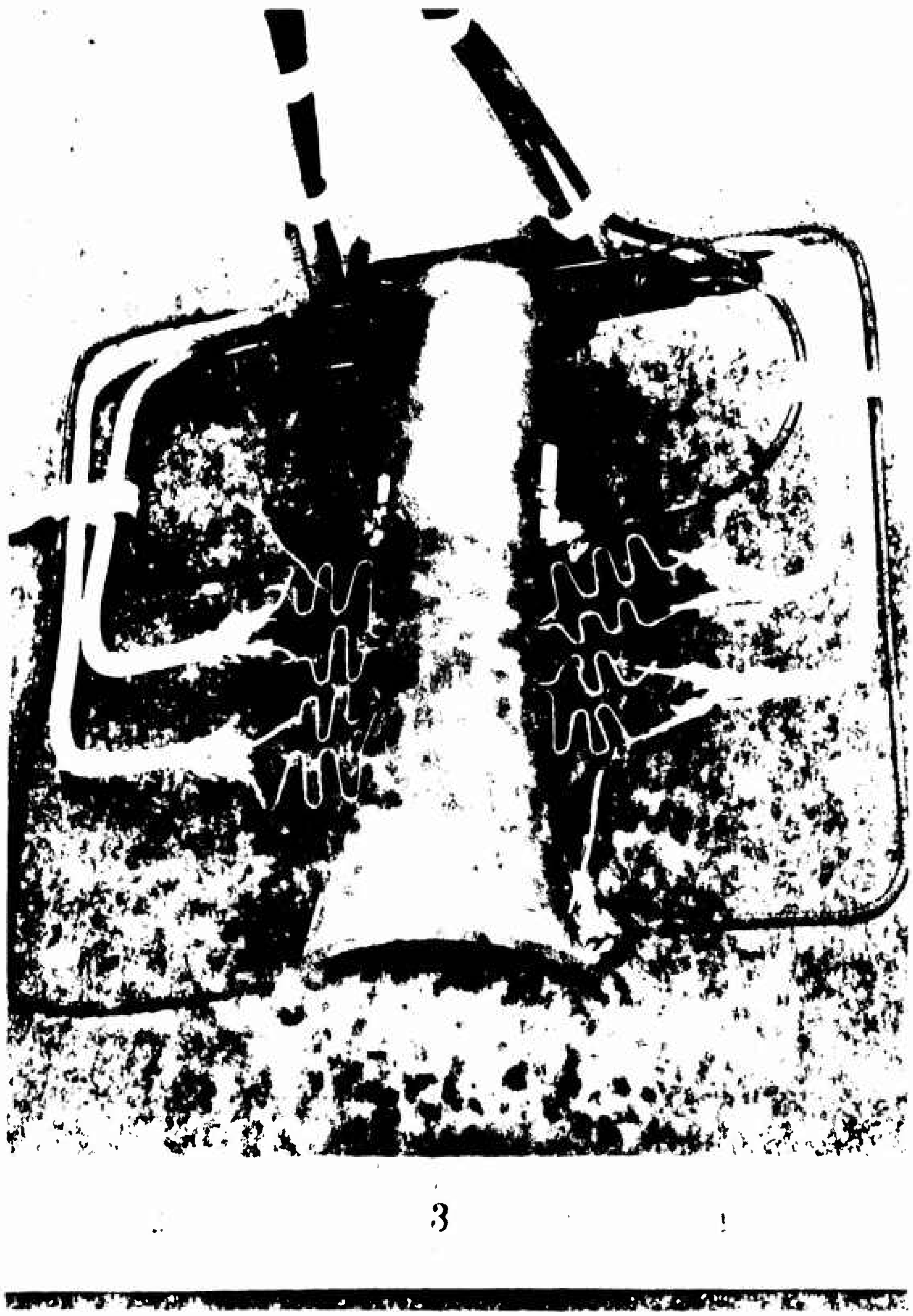

Figure 6.2-2. Typical Instrumentation of 50:1 Area Ratio Phase III Thrust Chamber (Prefire)

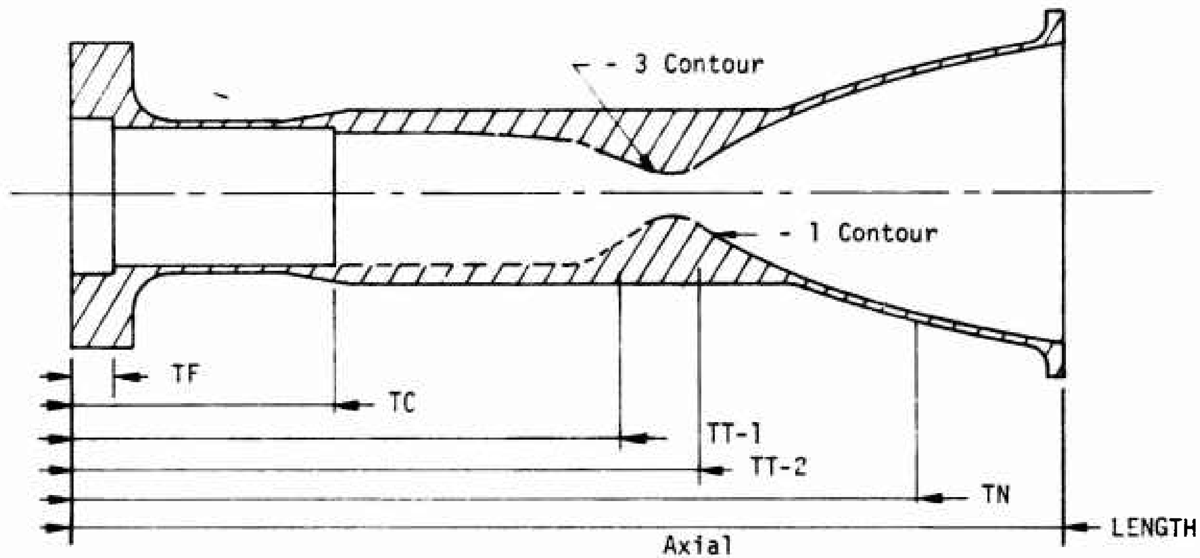

LOCATION	NAME	TYPE	INSTALL	Axial Position, in. SN 1	SN 3	Range, °F
Flange	TFL TFR	0.005 CA 0.005 CA	Spot Weld Spot Weld	0.10 0.10	0.10 0.10	0 - 2400
Chamber	TCL TCR	0.005 CA 0.005 CA	Spot Weld Spot Weld	0.90 0.90	0.90 0.90	
Throat	TT1L,2L TT1R,2R TTB	0.010 T-R 0.010 T-R 0.003 T-R	Stake Stake Spot Weld	1.94 2.18 2.18	1.69 1.94 -	0 - 3000
Nozzle	TNL TNR	0.005 CA 0.005 CA	Spot Weld Spot Weld	2.89 2.89	2.64 2.64	0 - 2400
Length R.F.				3.408	3.158	

Peripheral Location

B = Bottom
L = Left Side
R = Right Side

Figure 6.2-3. Cross Section of the -1 and -3 Chamber Contours and Thermocouple Locations

The durability of the thermal instrumentation used in the Phase III testing was very good, lasting through tens of thousands of pulses and many hours at temperature. The eventual failure of the instrumentation was not due to the thermocouples but the columbium wall where the silicide coating had been removed to drill and stake the wires in place. Local oxidation in the non-protected areas on the external surface of the chamber resulted in material regression up to 0.050 in. deep after several hours of testing.

6.2.4 Engine Assembly

Figure 5.1-8 is a photograph of all major engine components with the exception of the shunt and head end thermal dam. Photographs of the shunt, insulator platelets and seals are provided in Figure 6.2-4. Post-fire photographs of the SN 1 radiation cooled and SN 2 and SN 3 buried engine assemblies are shown in Figures 6.2-5, -6 and -7.

6.3 DEMONSTRATION TESTING

The performance, thermal characteristics and durability of three engine designs were evaluated in this phase of the program. The accumulated fire time for the three engines was approximately 17,000 sec, involved over 400,000 engine starts and a continuous single burn of 1 hr and 45 minutes on one of the engines. Each engine was tested per the test plan logic described below. Tables 6.3-1, -2 and -3 summarize the fire testing accomplished with each engine.

Series A - Steady state performance was evaluated at [illegible] levels of tank pressure. Testing was initiated at a P_c of 75 psia and increased in increments of 25 psi to characterize each engine at stages of simulated blowdown and to simultaneously determine the thermal limits of operation with successively increasing tank pressures. The maximum tank pressure levels compatible with life and missions requirements were selected as a base point for all subsequent pulsing, durability and post-durability evaluations.

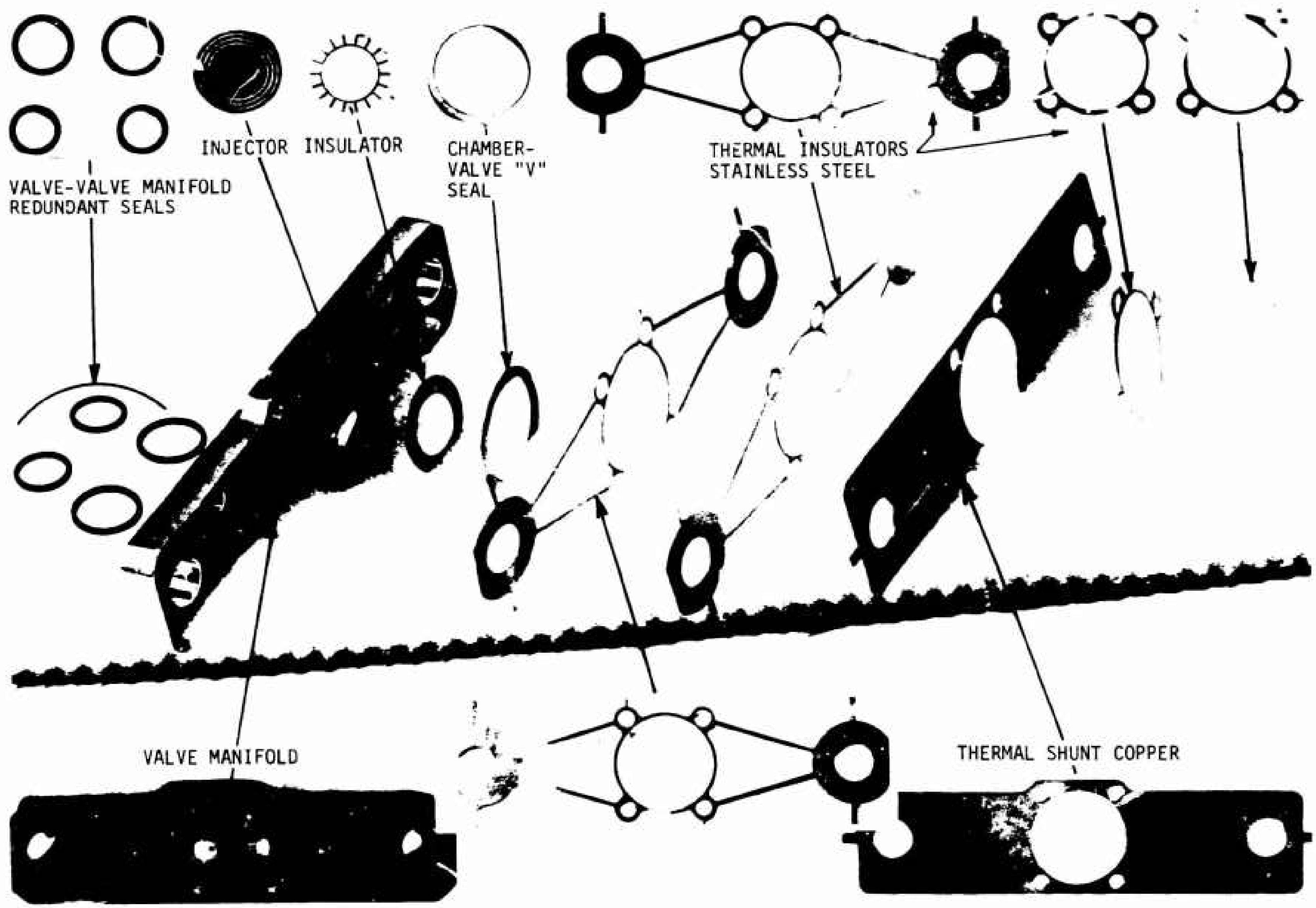

Figure 6.2-4. Shunt and Insulator Platelets and Seals

TEST HISTORY

≈ 305,000 PULSES

≈ 7,650 SEC TOTAL FIRING TIME

PROPELLANT TEMP 18°F - 122 °F

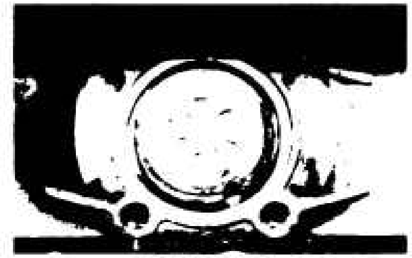

INJECTOR

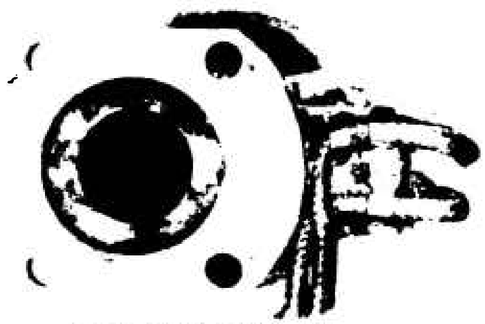

CHAMBER FORWARD END

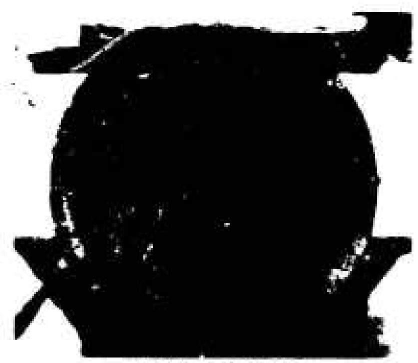

NOZZLE EXIT

Figure 6.2-5. Engine SN 1 Radiation Cooled Posttest

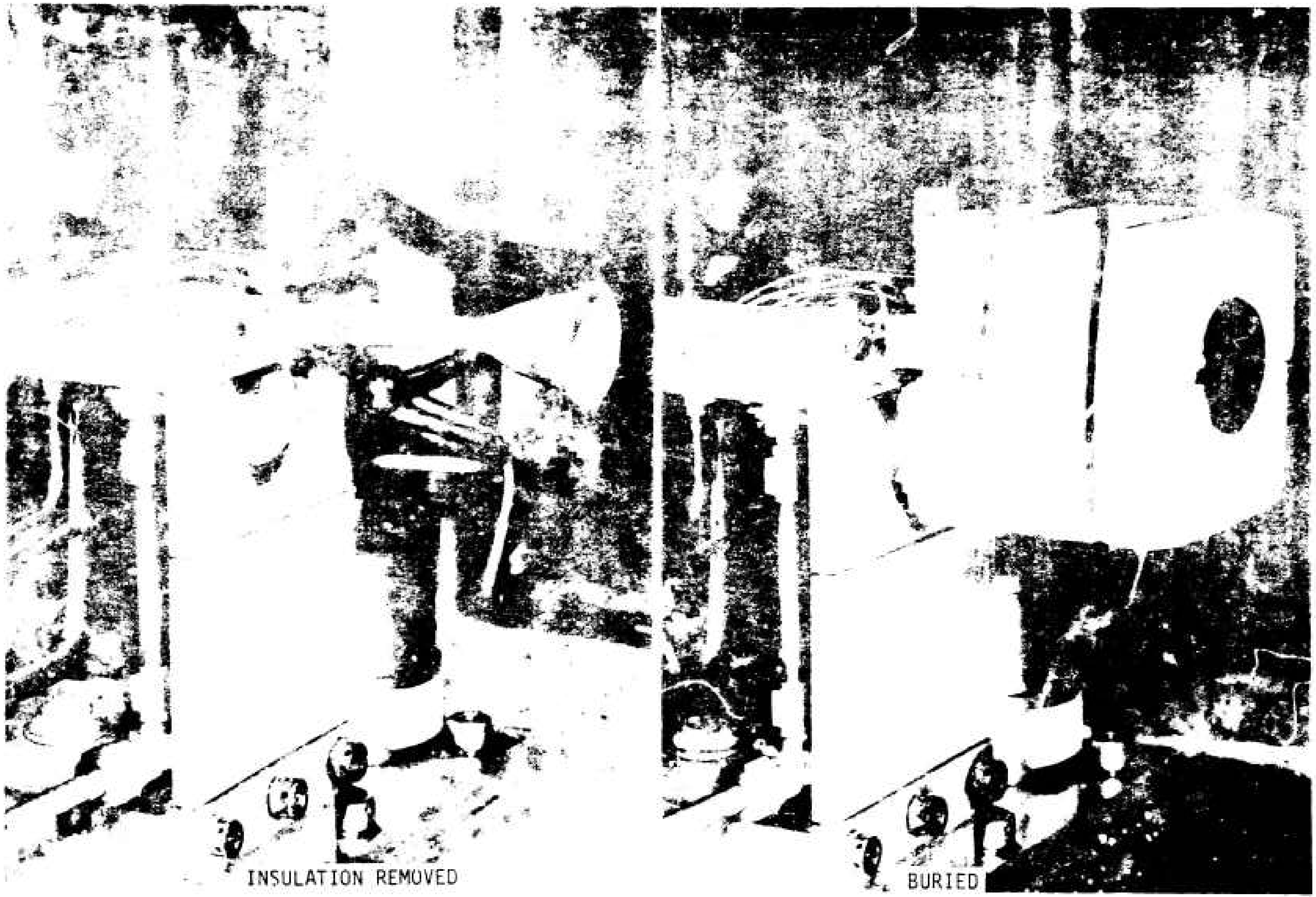

Figure 6.2-6. Engine SN 2 Post Fire 50,000 Pulses

BURIED (TESTED CONFIGURATION)

INSULATION REMOVED (DYNA QUARTZ)

Figure 6.2-7. Engine SN 3 after 55,268 Firings, 7791 sec Total Burn Time

TABLE 6.3-1

TEST SUMMARY, ENGINE SN 1 RADIATION COOLED AND REGULATED (FIXED P_c)
INTENDED FOR UNLIMITED PULSING AND LIMITED STEADY STATE OPERATION

Series	No.	Bit Impulse or F	MR	P_c	Pulses Duration, sec	Total Fire Duration	% Duty Cycle	Objectives
	184	2.2	1.6	75	1 at 5	5	100	Checkout.
A	185	2.2	1.7	75	4 at 5	20	100	Determine operating pressure vs performance and maximum pressure for 2700°F wall.
	186	2.9	1.6	100	4 at 5	20		
	187	3.7	1.6	125	3 at 5	15		
	188	3.7	1.4	125	1 at 5	5		
	189	3.7	1.8	125	3 at 5	15		
	190	3.7	1.8	125	3 at 5	15		All test durations achieved.
	191	4.4	1.2	150	2 at 5	10		No overheating encountered.
	197	4.4	1.6	150	2 at 5	10		
		Cost period between pulses 0.5 sec for thrust "0" evaluation.						
B	192	0.0928	1.47	150	600 at 0.025(1)	15	7.5	MR = 1.6
	193	0.4363	1.49	150	150 at 0.100(1) 3 per sec	15	30	Pulse performance and thermal evaluation.
	194	0.2176	1.55	150	300 at 0.050	15	15	No limiting conditions encountered.
	195	0.0458	1.45	150	1000 at 0.010	10	3.0	Data log at 1 record per sec
	196	0.0450	1.30	150	100 at 0.010 3 sec	1	0.3	after 50 sec.
C	198		1.6	150	3×10^5 0.025 4 per sec	7500	10	Life durability test. Stopped firing at 70,007 due to pitting of chamber in area of thermocouples. Chamber recoated locally, testing resumed for 230,000 pulses to accumulate 300,006.
C	199	0.4229	1.43	150	150 at 100	15	30	Pulse performance re-evaluation.
	200	0.1097	1.42	150	150 at 0.025	3.7	7.5	MR = 1.6.
	201	Variable	1.6	40	PMPM Evaluation	1.6	Variable	Special cycle for PMPM and CONTAM evaluation.
E	202	4.4	1.33	150	4 at 5	20	100	Steady state performance re-evaluation.
	203	4.4	1.54	150	4 at 5	20	100	Steady state performance re-evaluation.
D	204	4.4	1.68	150	4 at 5	20	100	Steady state performance re-evaluation.
	205	4.4	1.65	150	1	283	100	Programmed 300 sec to evaluation chamber duration capability. Shutdown at 283 sec due to overheating of cylindrical portion of chamber.
F	206	0.1024	1.6	150	100 at 0.025 3 per sec	2.5	7.5	Cold propellant 19°F, Engine 24°F.
	207	0.1066	1.6	150	100 at 0.025 3 per sec	2.5	7.5	Hot propellant 123°F, Engine 119°F. No limiting conditions encountered in environmental tests.

(1) Duration ± 0.0001 sec.

TABLE 6.3-2

PHASE III TEST PLAN ENGINE SN 2 ADIABATIC WALL BLOWDOWN, LIMITED STEADY STATE OPERATION

Series	No.	Bit Impulse or Thrust	P_c	Pulses Duration, sec	Total Fire Duration	% Duty Cycle	Comments
	208	2.2	75	1 at 5	5		Checkout test normal.
	209	2.2	75	6 at 5	30	100	Test normal.
A	210	2.9	100	6 at 5	30		Thermal shutdown 2900°F at 24 sec.
	211	3.7	125	4 at 5	20		Thermal shutdown 3000°F at 14 sec.
	212	4.4	150	3 at 5	15		Thermal shutdown 3000°F at 7 sec.
		5.0	175	3 at 5	15		No test at this condition - overheating chamber.
		Coast period between pulses 0.5 sec for thrust "0" evaluation.					
	213	3.7	125	PMPM and CONTAM evaluation cycle. Replaced chamber with R512E coated unit.			
	217		125	150 at 0.100* 3 per	15	30	Pulse performance and thermal evaluation.
B	214			600 at 0.025 sec	15	7.5	(No chamber thermocouples).
	215			1000 at 0.010	10	3.0	
	216			100 at 0.010 3 sec	1	0.3	All testing completed without overheating.
	218		125	0 - 600 } Perf.			Data invalid to pulse 8513 due to control room electrical problem.
	219		75	601 - 1200 } Perf.			
	220		125	1201 - 8513			
C	221	0.0913	125	8514 - 9114 } Perf.			50,000 pulse durability test with periodic performance evaluations 0.025 sec pulses 4/sec duty cycle. No change in hardware condition, no limiting conditions encountered. No change in performance noted.
	222	0.0541	75	9115 9715 } Perf.			
	220		125	9716 - 48376			
	223	0.0913	125	48377 - 48979 } Perf.			
	224	0.0529	75	48980 - 50000 } Perf.			
	225	0.2044	75	150 at 0.100 3 per	15	30	Replaced conical chamber with 1-3/4 in. cylindrical chamber, to establish influence of chamber contour on temperatures.
	226	0.3579	125	150 at 0.100 sec	15	30	
B	227	0.0865	125	150 at 0.025	3.7	7.5	
	228	0.0339	125	150 at 0.010	1.5	3.0	
	229	0.0187	75	750 at 0.010	1.5	3.0	
A	230	3.7	125	Steady State			MR = 1.6 thermal trip 12 sec at 2700°F.
	231	2.9	100	Steady State			MR = 1.6 thermal trip 20 sec at 2700°F.

*Duration ± 0.0001 sec. Tests 208 - 216 conical chamber 2 in. L'. Tests 225 - 231 1-3/4 in. cylindrical chamber.

TABLE 6.3-3

TEST SUMMARY, ENGINE SN 3 ADIABATIC WALL BLOWDOWN,
UNLIMITED STEADY STATE OPERATION

Injector from Phase II, 148 sec duration, 26 starts

Series	No.	Bit Impulse or Thrust	MR	P_c	Pulses Duration, sec	Total Fire Duration	% Duty Cycle	Objectives and Comments
	162	2.2	1.4	75	1 at 5	5		Checkout.
	163, 164	2.1	0.8, 2.0	52 73	6 at 5	30	100	Determine (1) maximum operating pressure for 2700°F wall and (2) steady state performance at 5 levels of blowdown. All testing at MR = 1.6. All test durations achieved before reaching 2700°F.
A	165	2.7	1.75	97	6 at 5	30		
	166	3.5	1.65	121	4 at 5	20		
	167	4.1	1.61	140	4 at 5	20		
	168	4.8	1.53	160	4 at 5	20		
		Coast period between pulses 0.5 sec for thrust "0" evaluation						
	169	0.4133		150	150 at 0.100 3 per sec	15	30	Pulse performance and thermal evaluation. MR = 1.6. All test normal.
	170	0.2096			300 at 0.050 sec	15	15	
B	171	0.1043			600 at 0.025	15	7.5	
	172	0.0413			1000 at 0.010	10	3.0	
	173	0.0423			100 at 0.010 3 sec	1	0.3	
C	Not assigned			150	(50,842) 0.025 4/sec	1250	10%	Pulse durability. Simulated blowdown. Tank 230 psia 0-25K, reduced to 190 psia 25-42K, 130 psia 42 to 50.8K. External surface oxidized at thermocouple. Attach points. All other parameters normal.
	174	0.[illegible]4196		150	150 at 0.1 3 per sec	15	30	Performance re-evaluation. Test conducted without chamber insulation.
	17[illegible] [illegible]5	0.[illegible]54			150 at 0.025	3.7	7.5	
B		0.2038			and 0.050			
	177	0.0418			150 at 0.010	1.5	3.0	
	17[illegible],179	4.1		141	Steady State	5	100	MR 1.4, 1.6, 5 sec each.
D	180	3.7-2.9		125-100	Steady State	6301	100%	MR = 1.6 1 hour and 45 minute burn achieved.
E	181	3.7	1.57		Perf. Re-evaluation.	5	100%	No change in hardware condition noted.
F	182	0.1026		150	100 0.025 3 per sec	2.5	7.5	Cold propellant 20°F, Engine temperature 32°F.
	183	0.1083			100 0.025	2.5	7.5	Hot propellant 121°F, Engine temperature 115°F.

*All tests achieved full duration planned without thermal trips.
Tests IIIC and IIIE were run in series to provide 6300 sec. Tank pressures were incremental during test.

6.3, Demonstration Testing (cont.)

Series B - Pulsing performance was evaluated at the maximum allowable propellant supply pressures selected from series "A" at electrical pulse widths of 0.010, 0.025, 0.050 and 0.100 sec; duty cycles ranged from 0.3 to 30% on time.

Series C - Each engine was durability tested per the contract goals.

Engine SN 1	300,000 pulses
Engine SN 2	50,000 pulses
Engine SN 3	50,000 pulses

Series B Repeat - This was to allow pulse performance to be reevaluated following the durability testing so that the predurability and post durability data could be directly compared.

Series D - The durability under continuous firing conditions was evaluated for each engine.

Series E - Steady state performance was re-evaluated and compared to the A series data.

Series F - Two of the engines were tested at environmental temperatures of 20°F and 120°F per the contract requirements. Hardware and propellants were conditioned to these temperatures. Engine SN 1 and 3 were selected for environmental testing.

All testing was conducted with 50:1 area ratios nozzles at simulated altitude. The environmental pressures ranged from 0.3 psia for short tests (< 10 minutes), to approximately 1.0 psia for test firings in excess of an hour. Operation at the higher back pressures occurred during the durability testing only. No performance from these tests is provided since the possibility of flow separation in the nozzle exists at the lower P_c levels tested. All steady state performance tests longer than 5 sec in duration employed a 5 sec burn-0.5 sec coast -5 sec burn sequence (discussed in Phase II testing) to account for a potential zero shift in thrust measurement due to test cell heating. Steady state durability tests (Series D) were continuous firings.

The test facility was the same as that used for Phase II testing (described in Section 5.2.2 of this report) except that the P_c transducer employed for Engines SN 1 and 2 was a Taber Model 2210 (weight 2.5 oz). Engine SN 3 was the first unit tested; it was followed by SN 1 and SN 2.

Data acquisition on the 50,000 and 300,000 pulse test series included the following parameters which were recorded on digital printout for each 20th pulse.

FT	Bit impulse lbF-sec
V	Valve temperature
M	Injector manifold temperature
S	Shunt heat flow
*T	Maximum chamber temperature
*F	Chamber flange temperature
*O	Oxidizer tank pressure
*F	Fuel tank pressure
*P	Vacuum cell pressure

*The parameters were also on visual display. Oscillograph records of the line pressures, valve response and thrust response were recorded at 30 minute intervals.

6.3, Demonstration Testing (cont.)

6.3.1 Demonstration Testing of Engine SN 1

This engine was designed to operate in the radiation cooled mode with a regulated feed system.

Testing of this radiation-cooled, regulated feed system engine shown in Figure 6.2-5 was initiated 1 April 1974 and completed 17 April 1974. The test conditions are summarized in Table 6.1-1 and are discussed below.

Test Series A, Steady State - 23 starts; 115 sec total duration

Steady state performance was evaluated at four levels of tank pressure, testing was initiated at 2.2 lbF (60 psia) and increased in 25 psi increments until limiting conditions were reached. All tests achieved their planned durations without exceeding the limiting operational temperatures.

The 300-sec specific impulse goal at an extrapolated area ratio of 100.1 was demonstrated at the 4.4 lbf level. All further testing on this engine was conducted with fixed tank pressures which corresponded to this maximum performance operating condition. Figure 6.3-1 provides an oscillograph record of Test 197 (max thrust) showing: a cold start, the final portion of the first 5 sec burn shutdown, and a hot restart. The slow rise in P_c is due to the use of the larger volume Taber Model 2210 transducer.

Test Series B, Pulsing - 2150 starts; 55 sec total burn

Pulsing performance was evaluated at electrical pulse widths of 0.10 to 0.01 sec and duty cycles ranging from 30% to 0.3% on-time. No limiting operational conditions were encountered. Figure 6.3-2 provides a

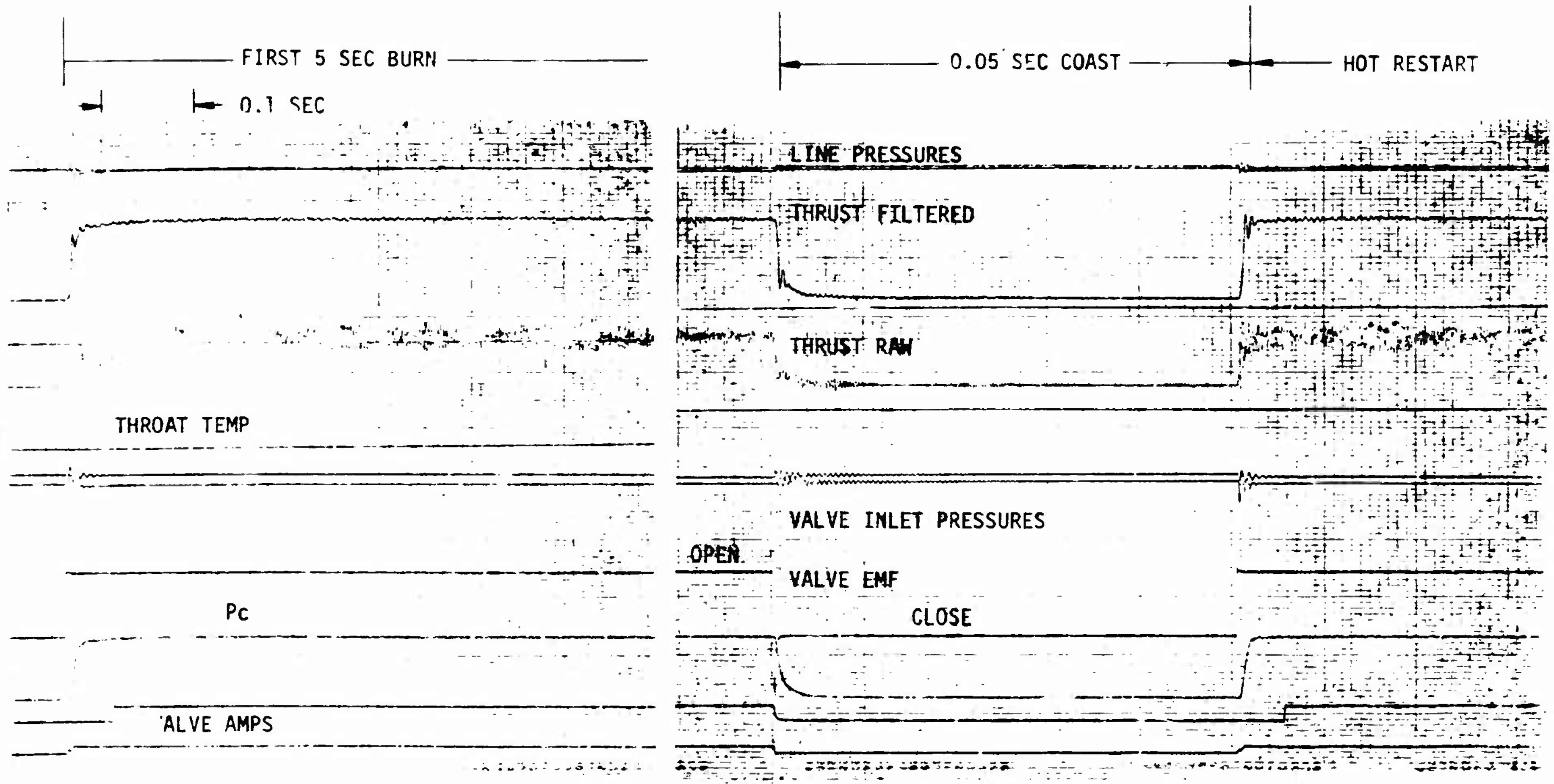

Figure 6.3-1. Steady State Firing Radiation Cooled Engine, Test 197

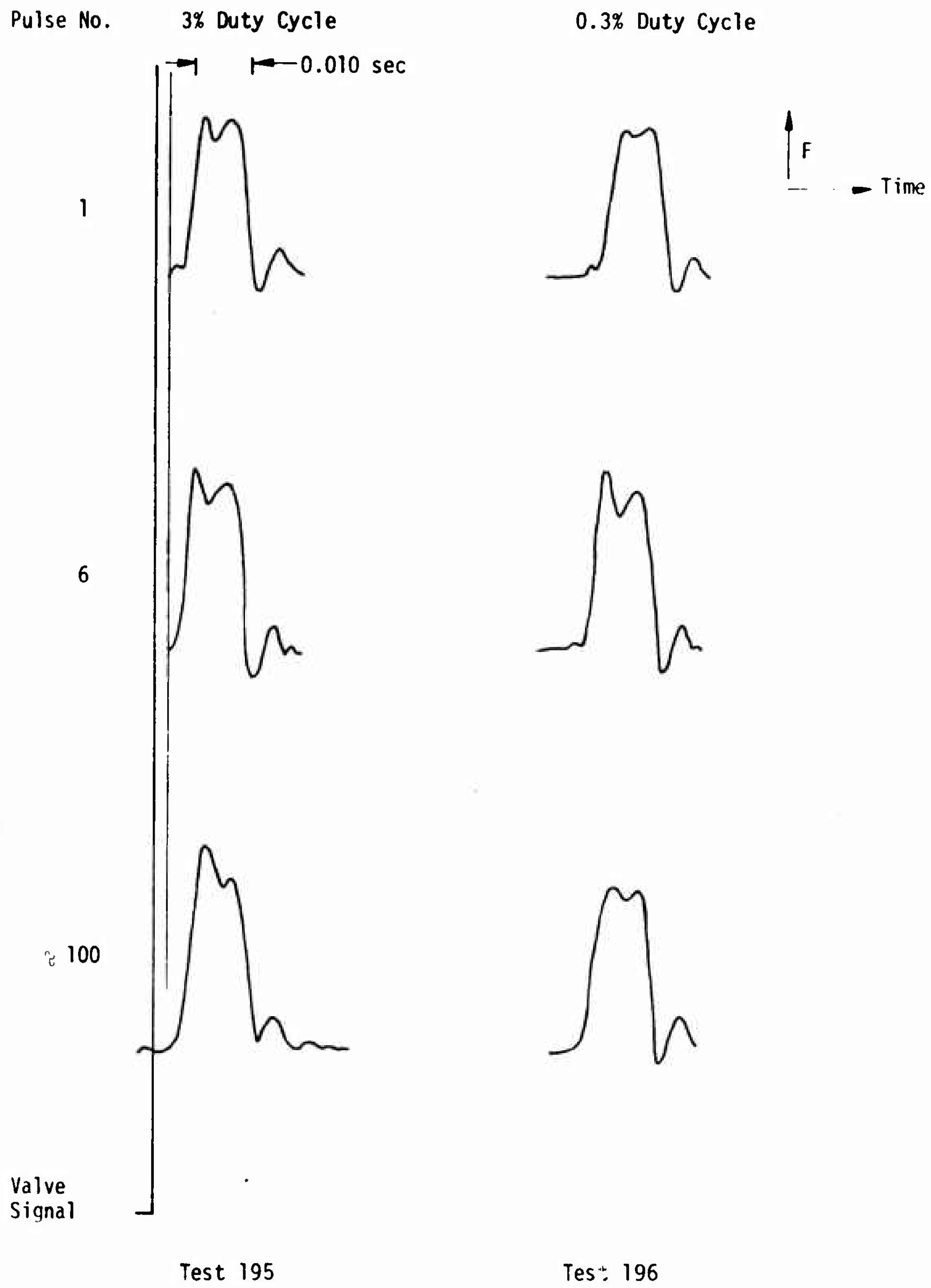

Figure 6.3-2. Thrust Trace Engine SN 1, 0.044 lbf-sec Impulse

6.3.1, Demonstration Testing on Engine SN 1 (cont.)

reproduction of thrust traces at the 0.044 lbF-sec impulse level at a 0.3 and 3% duty cycle. Data for these pulses are provided in a later section.

Test Series C, Durability - 300,007 starts, 7500 sec total burn

The history of this 3 day test is summarized in Figure 6.3-3. Testing was initiated at a 9% duty cycle. Periodic termination of pulsing was necessary for paper servicing of the on-line computer terminal. All parameters functioned normally during the first 5 hours of testing. Minor deterioration of the chamber wall at the thermocouple attachments where the silicide coating was removed was noted upon routine inspection after pulse 62,621. Testing was interrupted for the removal of the instrumentation and local recoating of the chamber after 6 hr (70,007 pulses) of firing. Testing was resumed on the following day at a 10% duty cycle and proceeded for 16 continuous hours until the 300,000 pulse goal was attained. During this period, all parameters were normal and there was no further deterioration of the chamber wall. As indicated in Figure 6.3-3, there was no change in engine response, impulse or other operating characteristics during this period. Figure 6.2-5 provides photographs of the engine assembly and both ends of the chamber following this test. The throat diameter was within 0.001 in. of its original dimension. The engine temperatures recorded on the durability demonstration are shown in Figure 6.3-4.

Test Series B Repeat, Pulsing Performance Re-evaluation - 340 starts, 20 sec total burn

Pulsing performance was re-evaluated following life durability testing. No significant change in performance was noted. Figure 6.3-5 shows the excellent impulse repeatability for a typical test and some of the performance parameters. The data scatter in mixture ratio and I_{sp} reflects the inability to measure flow rates for individual pulses. The following

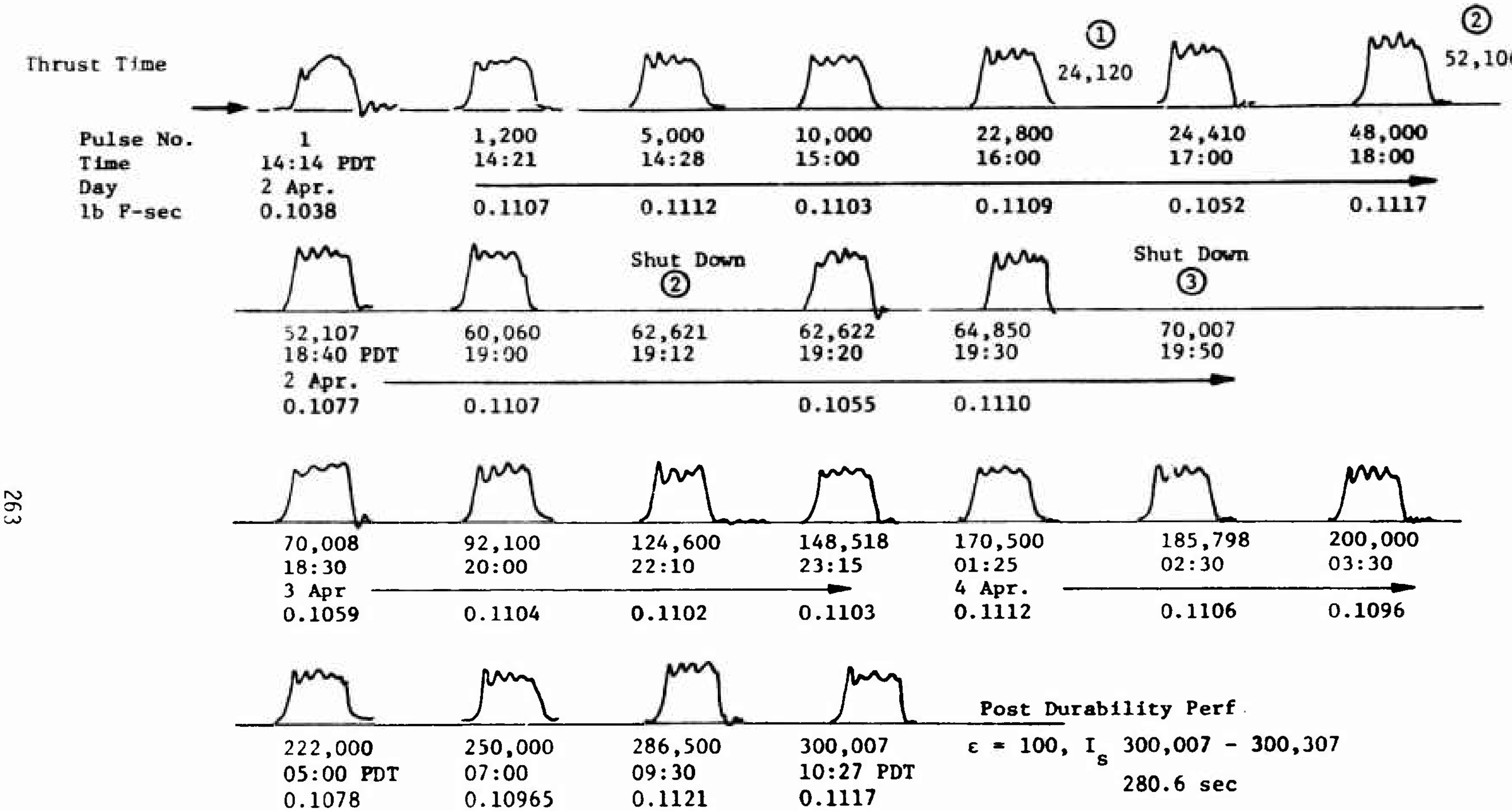

① Computer Malfunction

② Change or Adjust Recording Paper & Hardware Inspection (External Only)

③ Remove Chamber Thermal Instrumentation & Hardware Inspection (Internal & External)

Figure 6.3-3 Engine SN 1 Radiation Cooled 300,000 Pulse Thrust Time History

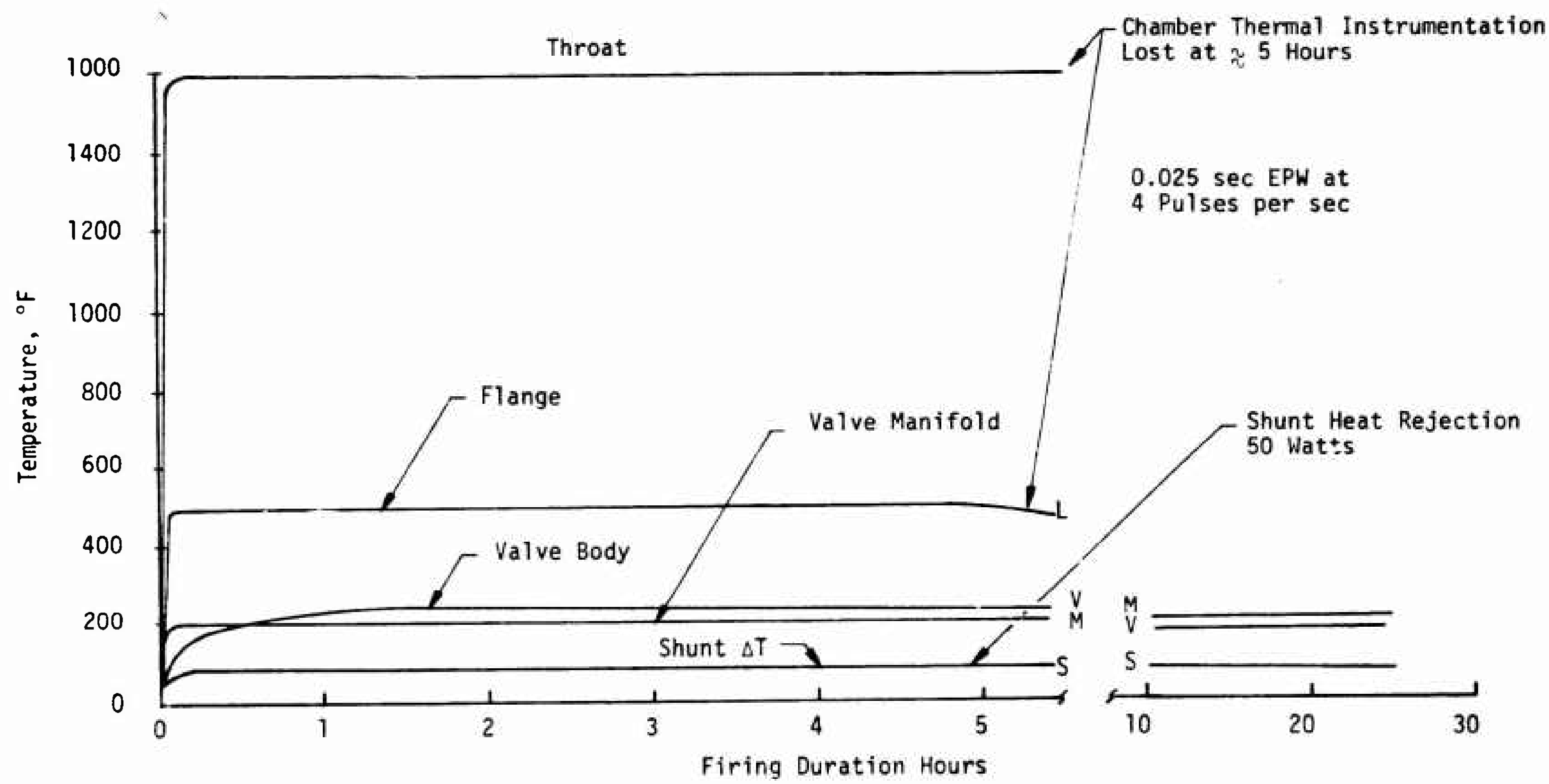

Figure 6.3-4. SN 1 Engine Temperatures - [illegible] Durability Testing

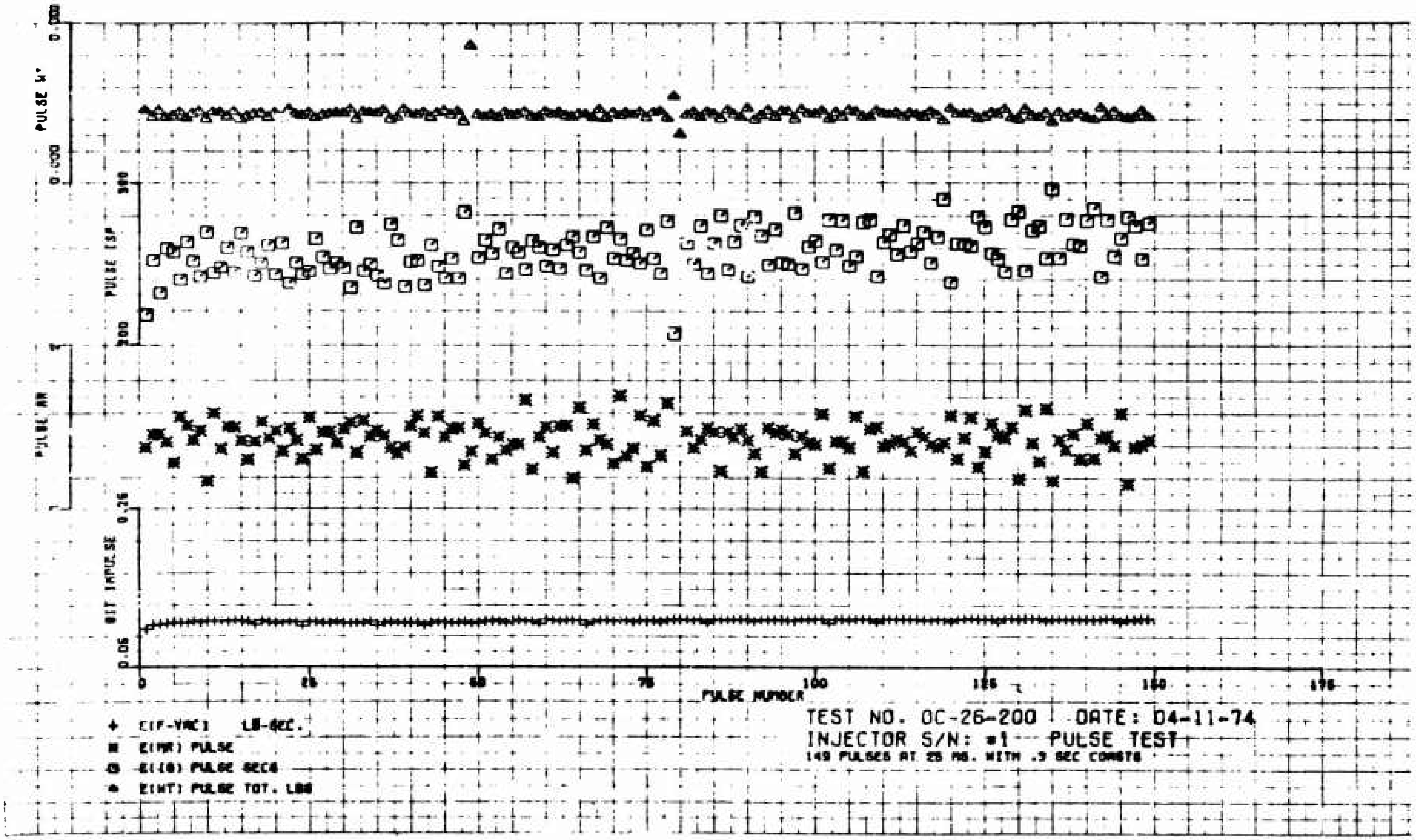

Figure 5.3-5. Impulse and Performance Summary, 0.025 sec Pulses, Engine SN I

6.3.1, Demonstration Testing on Engine SN 1 (cont.)

special duty cycle test was added to obtain data to be used in evaluating the PMPM and CONTAM computer program.

No. Pulses	On Time sec	Interval 1 sec	Coast Following Last Pulse sec
4	0.010	3.0	3.0
4	0.010	0.33	3.0
4	0.025	0.30	3.0
4	0.050	0.28	3.0
8	0.100	0.23	0.3
4	0.050	0.28	0.3
4	0.025	0.30	0.3
4	0.010	0.33	2.7
4	0.010	3.0	3.0

Figure 6.3-6 provides summarized impulse and performance parameters for this special cycle. The analyses of data from this cycle is presented in Section 6.5.

Test Series D and E - Steady State Performance and Durability - 13 starts, 343 sec total burn

Steady state performance was re-evaluated following the durability tests. No change was observed. A single 300 sec continuous burn was undertaken to determine the steady state capabilities of this design. Local overheating of the chamber a short distance downstream from the chamber liner was noted at 283 sec at which time the testing was terminated. Inspection of the hardware showed local damage to this area. It is believed that the use of the stepped insert configuration which was incorporated to promote secondary mixing during pulsing operation resulted in the local overheating. The use of an insert which blends with the contour of the chamber wall is expected to result in unlimited firing capability with some compromise of specific impulse when the chamber is cold such as during low % duty cycle pulse mode operation.

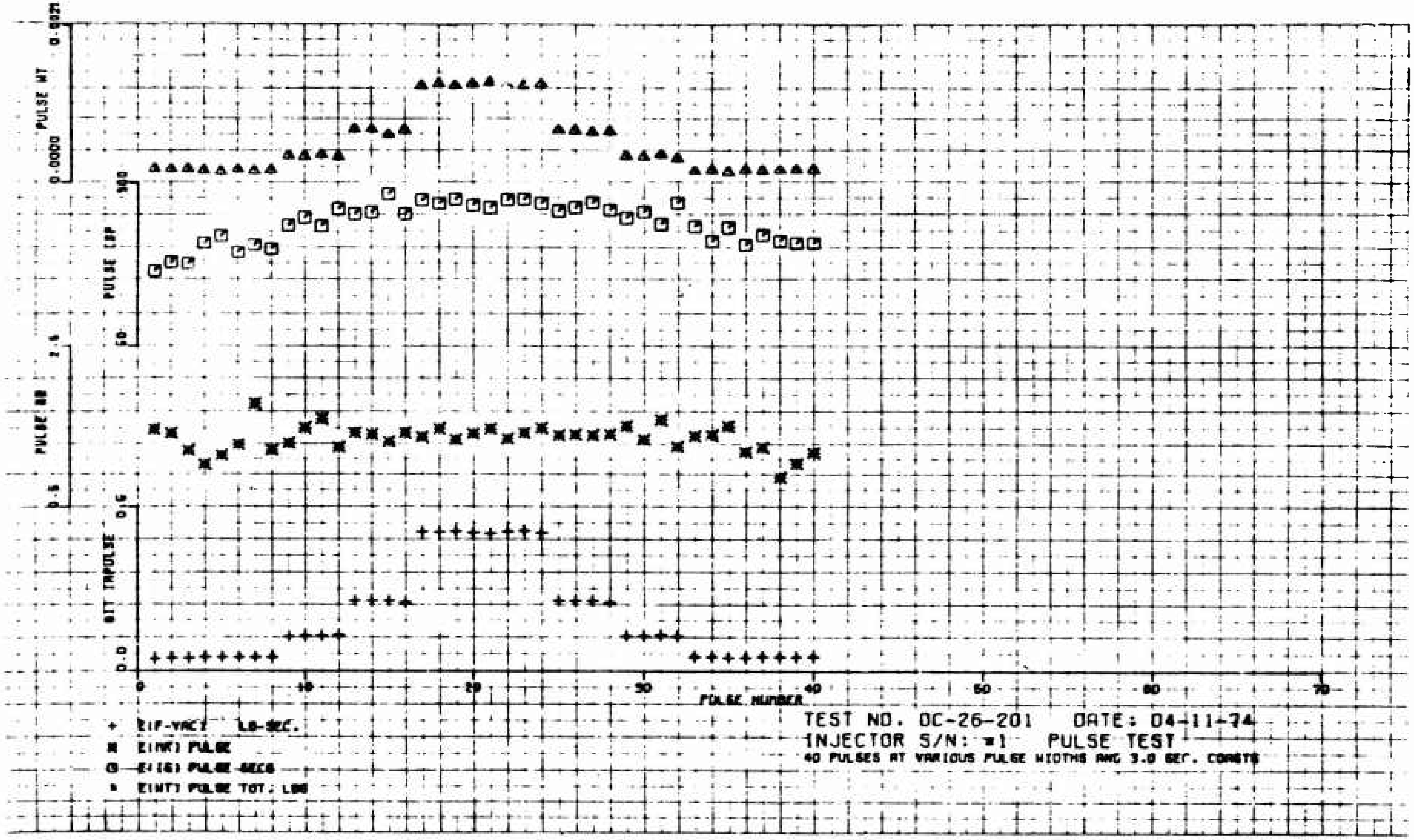

Figure 6.3-6. Impulse and Performance Summary, CONTAM-PMPM Duty Cycle, Engine SN 1

6.3.1, Demonstration Testing on Engine SN 1 (cont.)

Series F Cold and Hot Environmental Tests - 200 starts, 5 sec total burn

These hot and cold propellant and hardware tests were conducted with a Phase II residual chamber having the same length and internal contour with the exception of the forward end chamber liner which was not employed. Engine response was not influenced by propellant temperatures (0.005 sec from signal to 90% thrust). The first few pulses with 19°F propellant showed harder than normal starts with P_c over pressures of 200 to 300%. These are well within the design limitations of the engine and no damage was experienced. The photograph of the injector in Figure 6.2-5 was taken at the conclusion of testing. Figure 6.3-7 provides a summary of the pulsing performance and repeatability in the hot (120°F) environmental test series at a pulse width of 0.025 sec. Impulse repeatability was excellent even under the most adverse environmental conditions. Figure 6.3-8 shows the summation of the impulse data of Figure 6.3-7 indicating the linearity with time.

Re-evaluation of the injector flow characteristics at the conclusion of testing (Table 6.2-1) showed the fuel and oxidizer flow coefficients Kw to be within 1.0 and 2.1% of the as-fabricated values. The valve response was unchanged and there was no internal or external leakage when pressurized with GN_2 at 500 psia. Table 6.3-4 summarizes the test history of this engine.

6.3.2 Engine SN 2

Engine SN 2 was designed for limited steady state firing duration, a buried installation and a blowdown propellant supply. Its chamber internal contour differed from Engine SN 1 in that the chamber was conical rather than cylindrical. Its performance was lower than that of SN 1 due to the barrier cooling needed for the adiabatic wall operation. The absence of

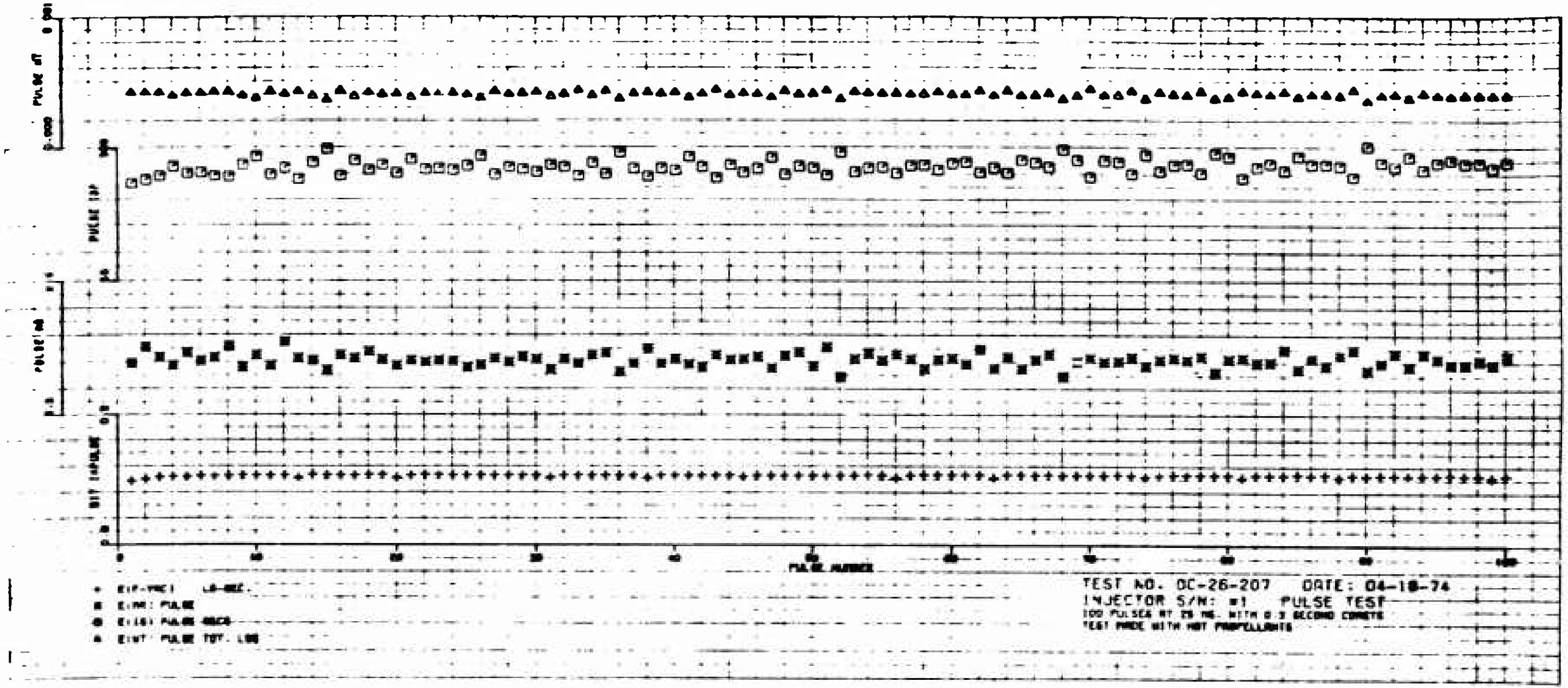

Figure 6.3-7. Impulse and Performance - Environmental Tests (T_{amb} = 120°F, P_{amb} = 0.39 psia

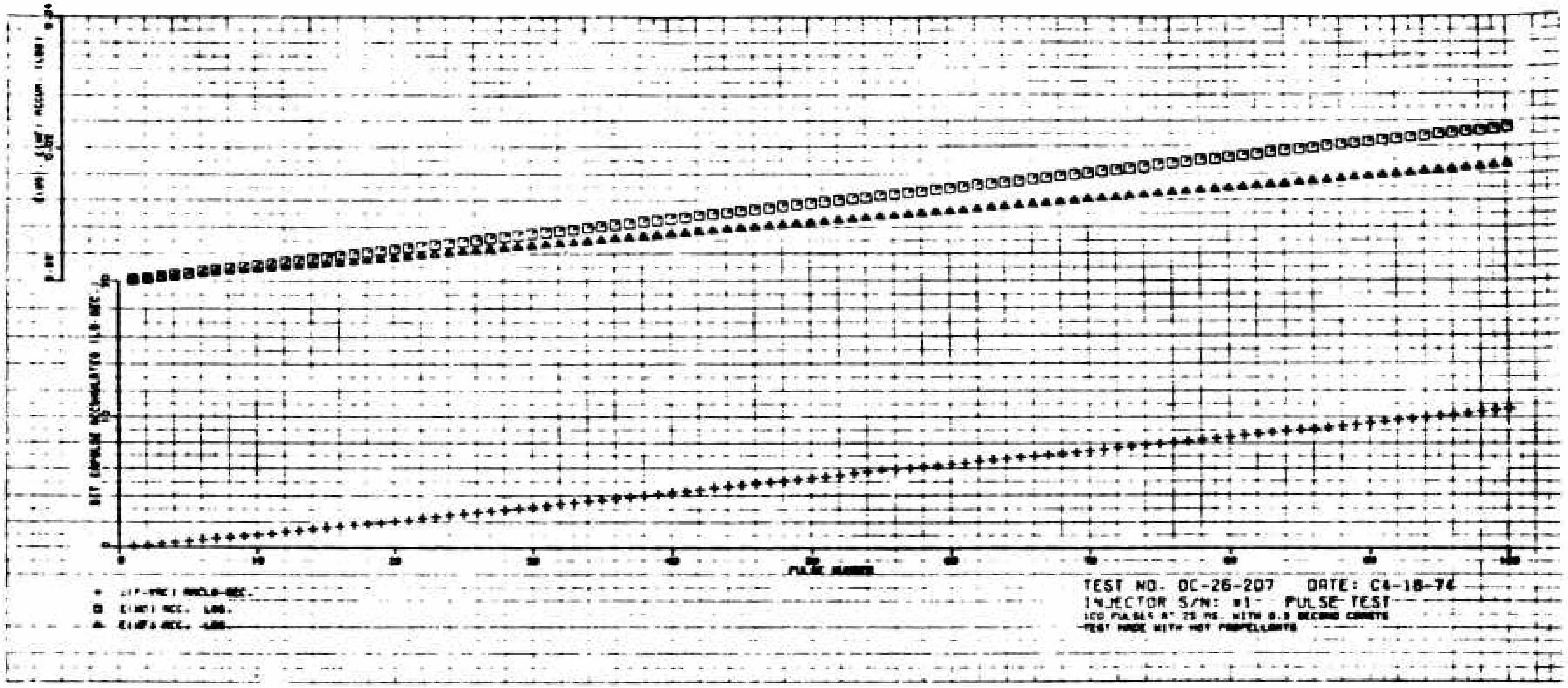

Figure 6.3-8. Pulse Train Linearity at an Environmental Temperature of 120°F, Engine SN 1, 0.025 sec EPW

TABLE 6.3-4

TEST HISTORY, ENGINE SN 1

Test No.	P_c psia	Test Type	No. Press Cycles	Total Burn Time sec	Temp Max Throat °F	Temp Max Chamber °F	Time of Max Temp
184	75	SS	1	5	700	750	5
185	75		4	20	1800	1650	20
186	100		4	20	2100	2200	20
187	125		3	15	2250	2150	15
188	125		1	5	No data		
189	125		3	15	2250	2000	15
190	125		3	15	2100	2000	15
191	150		2	10	2000	1600	10
192	150		600	15	1400	1200	200
193	150	Pulse	150	15	2300	1900	50
194	150		300	15	1800	1500	50
195	150		1000	10	1100	1000	325
196	150		100	1	--	--	--
197	150		2	10			
198	150		70,007	7500 (Total Time at Temp 75,000 sec)			
	150		230,000		1600	1350	
199	150		150	15	2300	1900	50
200	150		150	3.7	--	--	--
201			40	1.6	--	--	--
202	150	SS	4	20	>3000°F	No data	20
203			4	20	3050	2800	20
204			4	20	3100	2800	20
205			1	283 - Limiting operating temperatures at mid chamber reg. at 283 sec into run.	3250	3000	15-283 sec

6.3.2, Engine SN 2 (cont.)

a requirement for continuous burn durations exceeding 30 sec, however, allows its performance to be superior to SN 3 which was intended for unlimited steady state firing capability.

Figure 6.2-6 shows this engine mounted on the test stand buried and also with the Dyna-Quartz insulation removed. Table 6.3-2 summarizes its test history.

Test Series A, Steady State Performance - 23 starts, 115 sec total burn

Testing was initiated at 2.2 lbF and a P_c of 75 psia and P_c increased in increments of 25 psia until a limiting thermal condition was attained. A reinstrumented Phase II chamber (-5) was employed for this purpose. The thermal data showed that the anticipated low adiabatic wall temperatures which had been inferred from the Phase II data shown in Figure 5.3-33 were not obtained. Temperatures at and downstream of the throat station were much higher than expected. The maximum safe operating condition for this engine was judged to be about 100 psia in steady state and 125 psia in pulsing mode operation.

Test Series B, Pulsing Performance - 1890 starts, 42 sec total burn

Pulse testing including the PMPM-CONTAM cycle was conducted with a second Phase II chamber (-5A) which was coated with R512E silicide. This chamber unlike that used for the Series A testing contained no thermal instrumentation. It was visually noted, however, that the skirt was much hotter out to a 50:1 area ratio with the conical chamber design than was observed with the Engine SN 1 cylindrical chamber. The test series was completed without mishap.

Test Series C, Pulsing Durability Testing - 50,000 starts, 1250 sec burn over a 5 hour period

The -5A uninstrumented chamber used for Series B testing was also used for these tests. Pulsing testing was conducted at 125 and 75 psia to simulate the upper and lower limits of blowdown. Performance was evaluated periodically during this series by switching from tank supply to the positive displacement flowmeters. No change in performance was noted. Temperatures measured during this 10% duty cycle pulse series were as follows:

Valve Temperature, °F	190
Manifold Temperature, °F	300
Heat Flow Watts	38

The uninstrumented chamber avoided oxidation problems encountered with the other engines on long duty cycles. Figure 6.3-9 provides a summary of the pulse shape and impulse bit repeatability over the test duration. Figures 6.2-6 and 5.1-22 show this engine following the completion of this test series.

Test Series B Repeat, Re-evaluation of Pulsing Performance - 1350 pulses, 73.5 sec fire duration

A departure from the test plan was made at this point to determine if a change from the conical to cylindrical contour could correct the high throat temperatures encountered in the A series. Pulsing performance was first re-evaluated using a partially reinstrumented 1-3/4 in. L' chamber which had experienced 2 hr of firing with Engine SN 3. Testing for pulse repeatability was conducted at 75 P_c and a pulse width of 0.010 sec. Response data from this test series at 125 and 75 psia are shown in Figures 6.3-10 and -11. The slower rised fall in P_c is due to the use of the larger volume model 2210 transducer. Data from the low pressure MIB test, shown in Table 6.3-5, demonstrates a 0.018 lbF-sec $\pm$ 0.0006 lbF-sec capability for this type of engine.

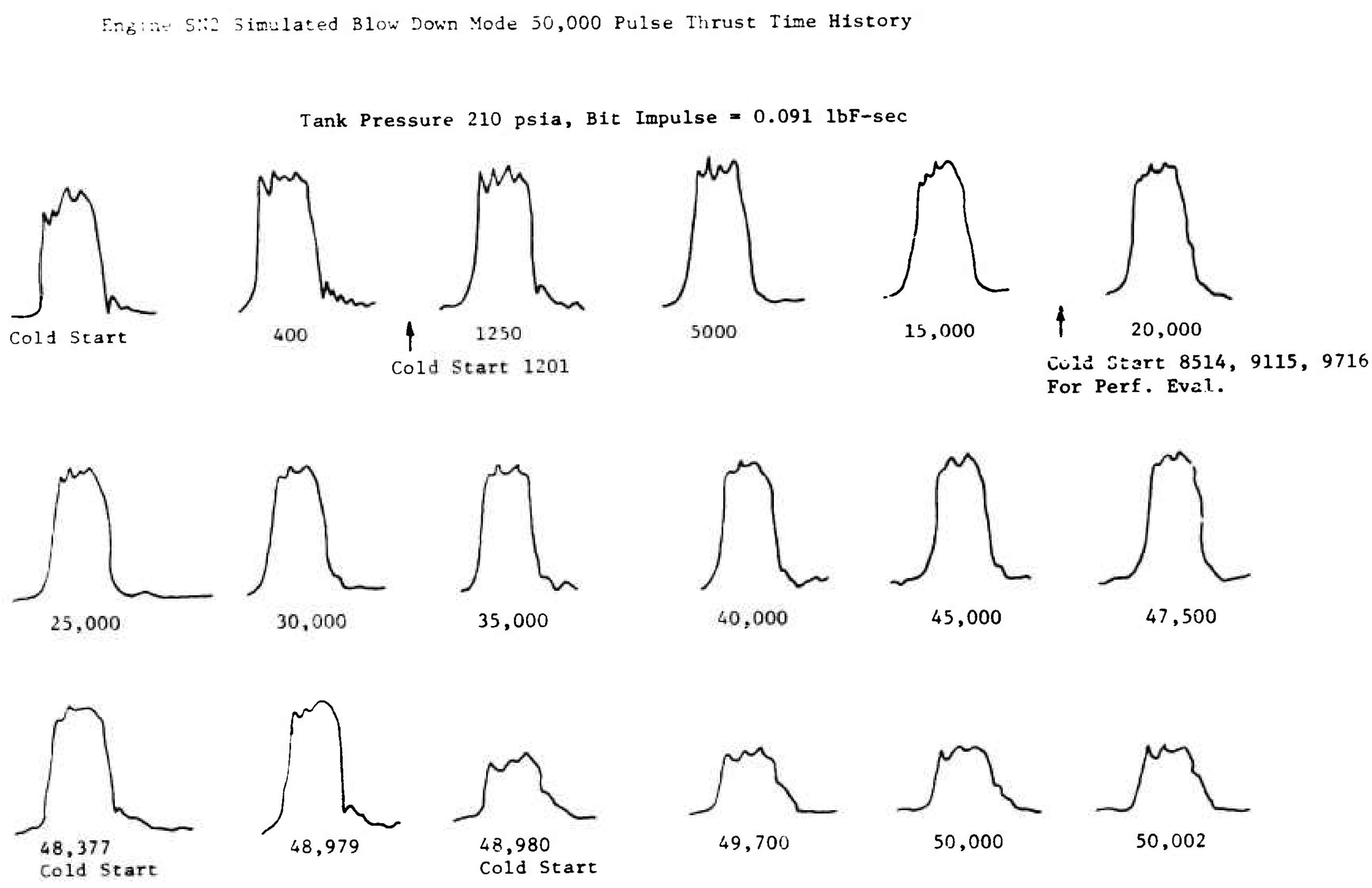

Figure 6.3-9. Summary of Pulse Shape and Impulse Bit Repeatability

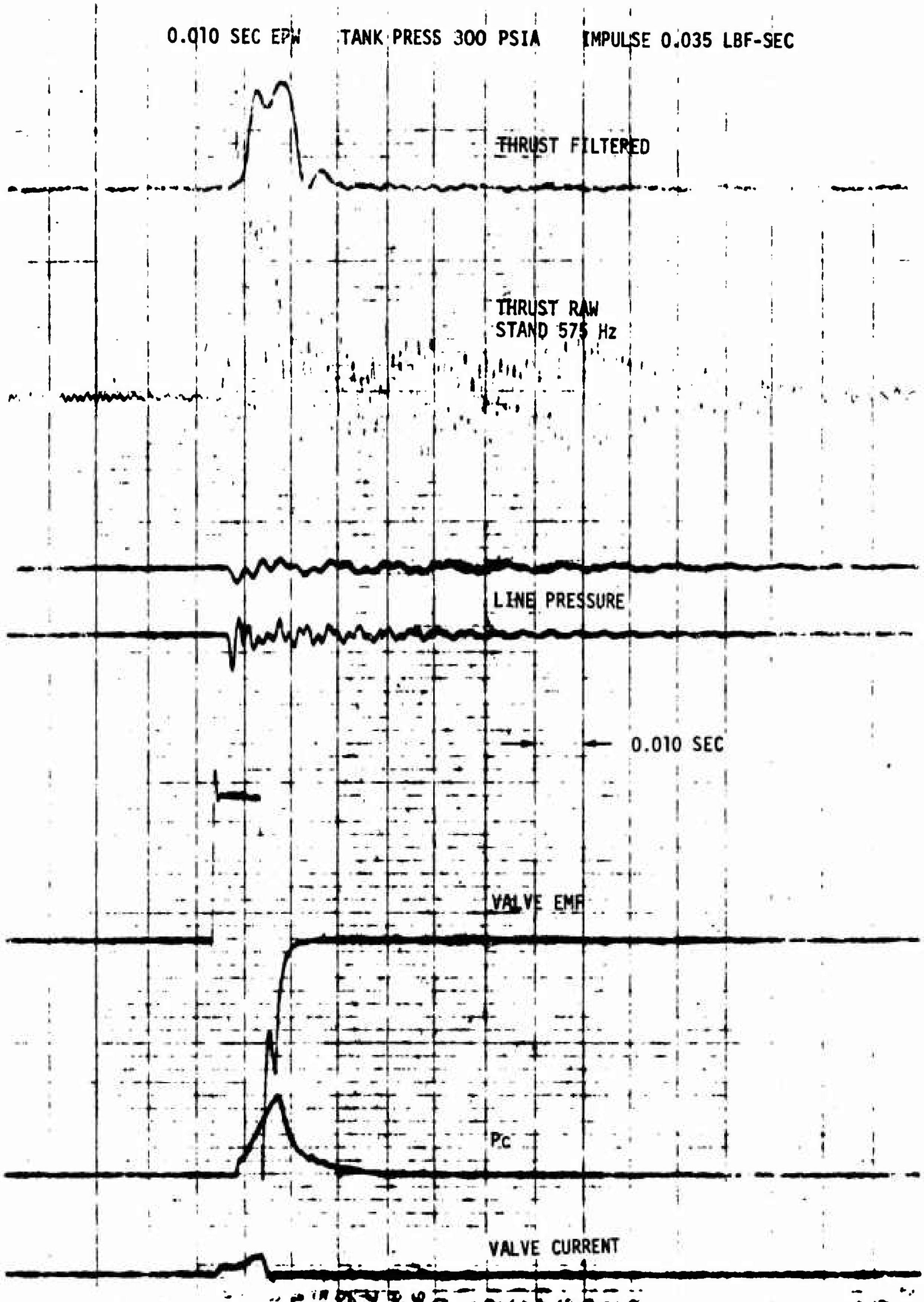

Figure 6.3-10. Response Data From Pulse Repeatability Test P_c = 125 psia

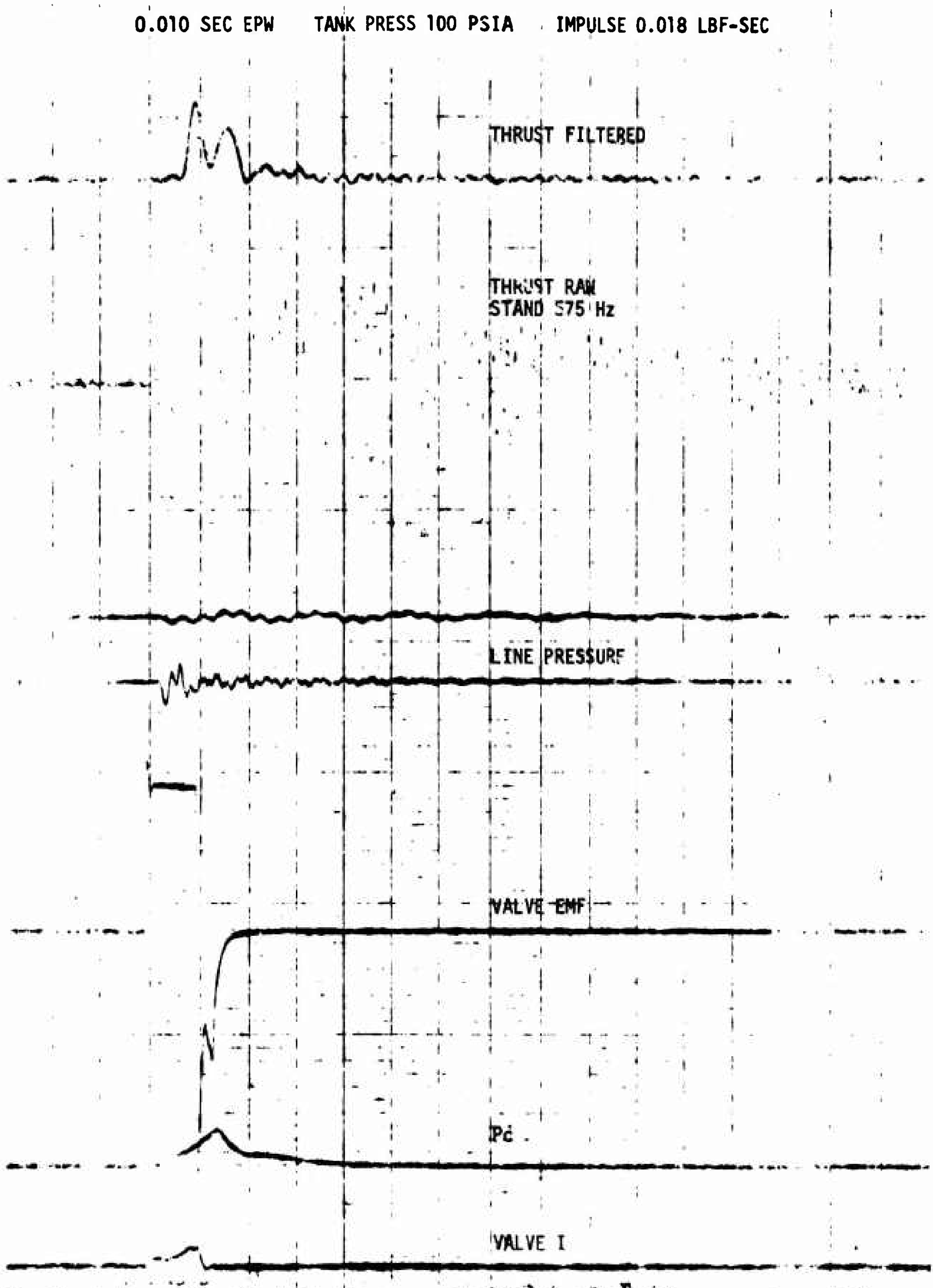

Figure 6.3-11. Response Data from Pulse Repeatability Test P_c = 75 psia

TABLE 6.3-5

RCS PROPULSION - ENGINE SN 2 MIB REPEATABILITY

Demonstrated Minimum Impulse Performance (lbf-sec)

Contract Defined Goal 0.050 ± 0.005 lbf-sec

Pulse No.	Bit Impulse								
1	0.0174	11	0.0172	21	0.0177	91	0.0188	101	0.0189
2	0.0184	12	0.0177	22	0.0171	92	0.0186	102	0.0184
3	0.0211	13	0.0186	23	0.0177	93	0.0189	103	0.0194
4	0.0159	14	0.0171	24	0.0177	94	0.0189	104	0.0185
5	0.0180	15	0.0177	25	0.0178	95	0.0187	105	0.0193
6	0.0155	16	0.0179	26	0.0180	96	0.0186	106	0.0192
7	0.0203	17	0.0178	27	0.0175	97	0.0187	107	0.0191
8	0.0179	18	0.0174	28	0.0180	98	0.0186	108	0.0195
9	0.0169	19	0.0172	29	0.0176	99	0.0191	109	0.0178
10	0.0190	20	0.0180	30	0.0181	100	0.0190	110	0.0186
Mean	0.01804		0.01766		0.01772		0.01879		0.01887

Mean of 50 Pulses 0.0182 lbf-sec ± 0.0006 lbf-sec (± 3%)

Operating Condition:
Tank Pressure 100 psia
MR 1.6
Electrical Pulse Width 0.010 sec
Duty Cycle 3%

6.3.2, Engine SN 2 (cont.)

Series A Repeat, Steady State Performance and Thermal Characteristics - 2 starts, 32 sec total burn

The final test series with this engine was conducted with the 1-3/4 in. long cylindrical chamber design to obtain comparative data on the influence of chamber contour at steady state thermal characteristics. These tests showed chamber contour did not significantly influence the wall temperature at the throat station. Further data is presented in Section 6.4.4 of this report. Figure 6.2-6 shows the injector at the completion of testing. Postfire valve leak and cold flow tests showed no leakage when pressurized with GN_2 at 500 psia and no change in response or flow characteristics.

6.3.3 Engine SN 3

The engine shown in Figure 6.3-7 was subjected to the test series summarized in Table 6.3-3. This engine design was configured for unlimited firing capability (both steady state and pulsing) in a buried installation supplied by a blowdown pressurized propellant feed system.

Test Series A, Steady State Performance - 7 tests; 23 starts; 115 sec total duration

Steady-state performance was evaluated at five levels of blowdown. All tests achieved the full planned duration. The predicted 280-sec specific impulse at high thrust was exceeded by about 3 sec. It was determined that this engine could provide unlimited steady state burn capability between 2.2 lbf (75 psia) and approximately 4.4 lbf (150 psia). Feed line coupled combustion roughness (30 psi peak-to-peak, 350 Hz) was noted at the lowest (75 psia) chamber pressure level.

Test Series B, Pulsing Performance - 5 tests; 2150 starts; 55 sec total burn

Pulsing performance was evaluated at electrical pulse widths of 0.10 to 0.010 sec and with duty cycles ranging from 30% on-time to 0.3% on-time. No limiting operational conditions were encountered. The left column of Figure 6.3-12 provides photographs showing the hardware condition following this test.

Test Series C, Pulsing Durability Testing - 1 test; 50,842 starts; 1270 sec of burn over a 5-1/2 hour period

Engine pulse durability tests were successfully completed. The center column of Figure 6.3-12 documents the hardware condition following this test series. The measured throat dimensional increase was less than 0.001 inch. The maximum temperatures and heat loads measured were as follows:

Throat Max	1500°F
Flange	600°F
Manifold	300°F
Valve Body	180
Shunt Heat Load	44 watts

Figure 6.3-13 provides a record of the thrust-time traces for randomly selected pulses. Blowdown was simulated by reducing tank pressure from 230 psi to 190 psi after 25,000 pulses and to 130 psi after 42,000 pulses.

External coating in thermocouple region was touched up and chamber reinstrumented following this test.

Test Series B Repeat, Pulsing Performance Evaluation - 6 tests; 2052 starts; 65 sec total burn

Pulsing and steady-state performance were re-evaluated following the 50,000-pulse demonstration. Inadvertently the chamber insulation which had been removed for chamber thermocouple installation was not reinstalled. Performance was within 1% of the as-new performance value when corrections for the additional chamber heat losses were applied.

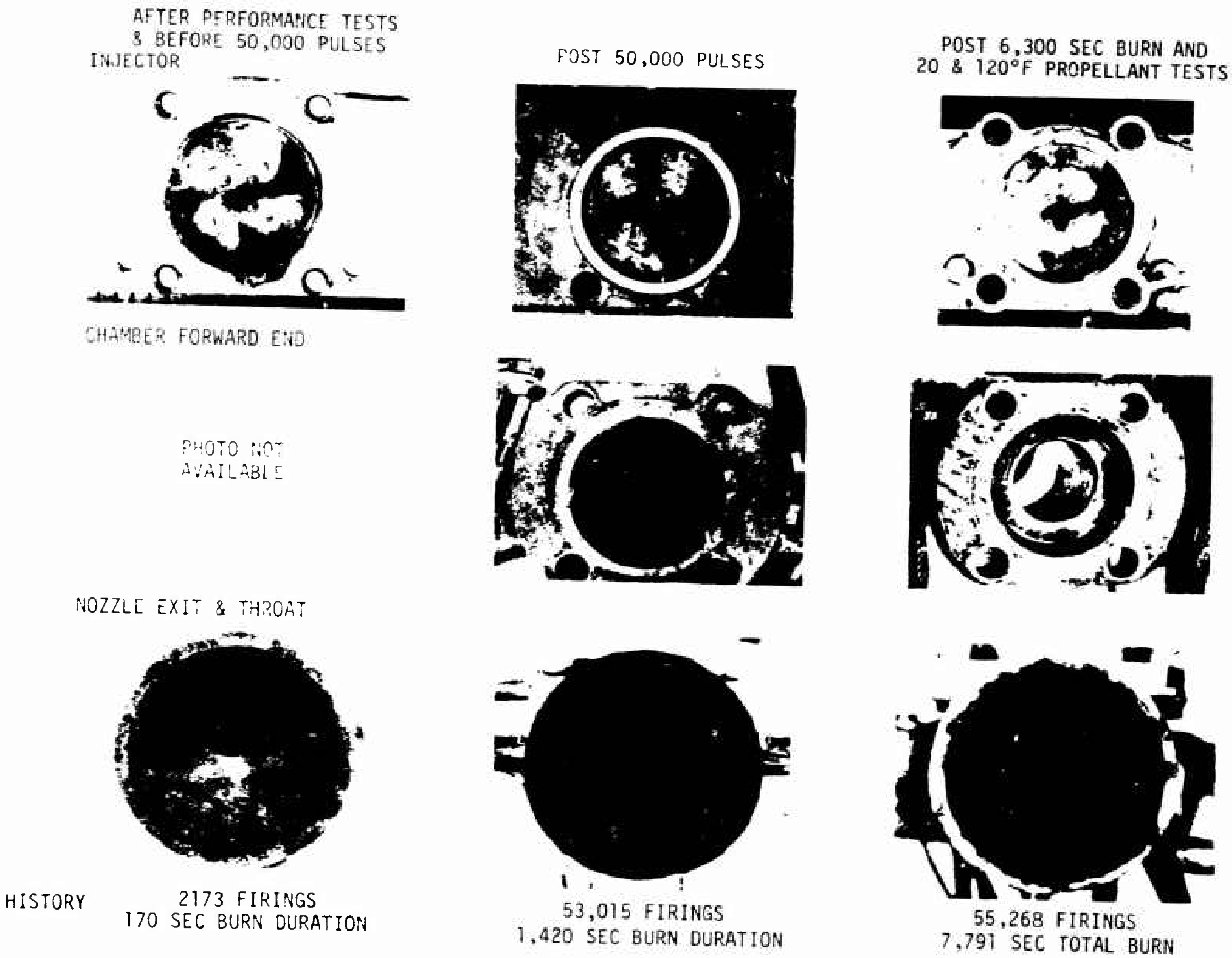

Figure 6.3-12. Engine SN 3 (Buried Blowdown Mode) Life History

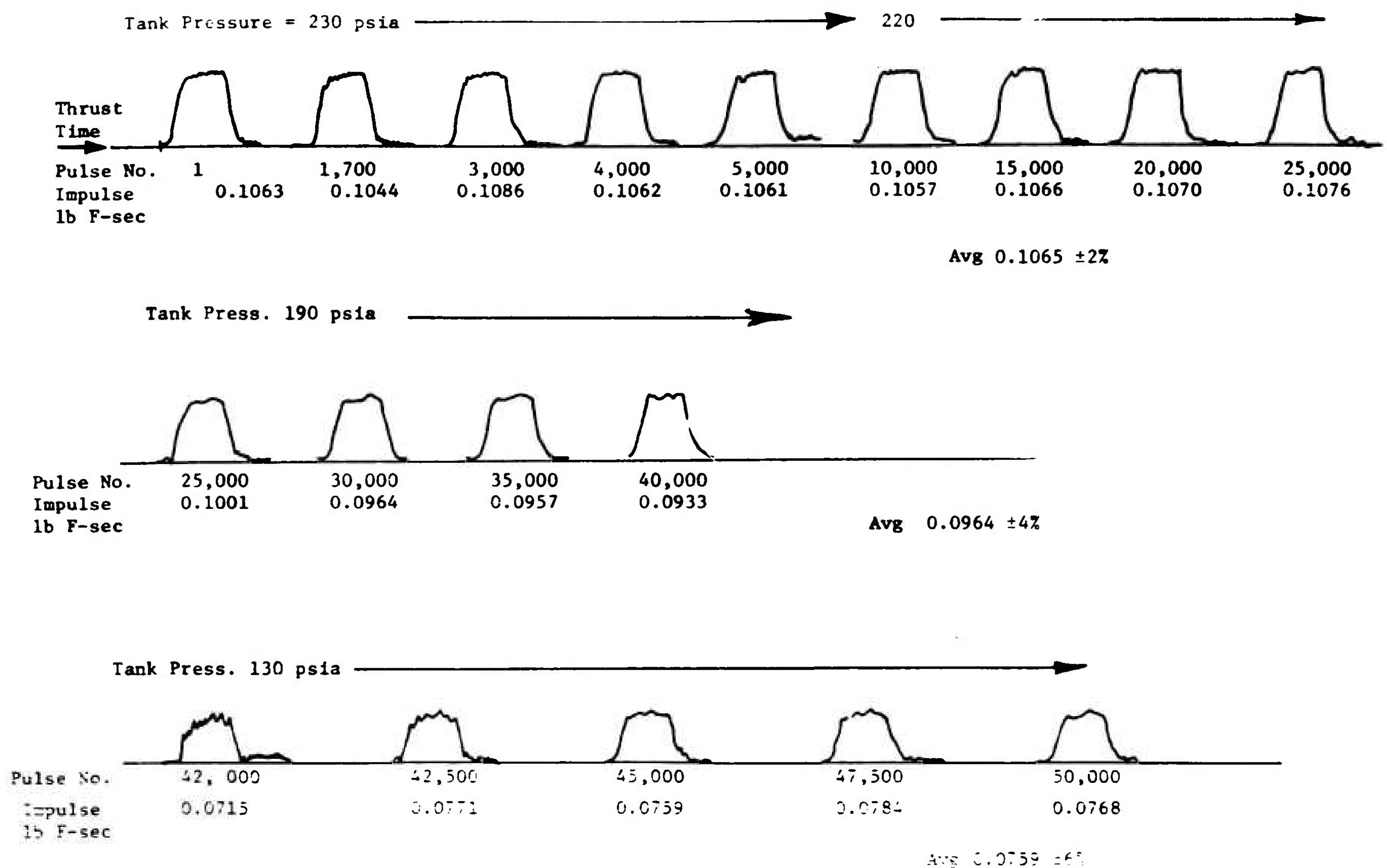

Figure 6.3-13. Engine SN 3 Simulated Blowdown Mode, 50,000 Pulse Thrust-Time History

6.3.3, Engine SN 3 (cont.)

Test Series D and E, Steady State Durability and Performance - 1 test; 1 start; 6301 sec total burn

The long burn (1 hour and 45 minutes) durability test was successfully completed over various tank pressure levels which simulated blowdown operation. This test was followed by (5 sec) steady state performance re-evaluation. Temperature data at the low and high tank supply pressures for the 6300 sec continuous burn are shown in Figure 6.3-14. Maximum temperatures on all components occurred at full thrust conditions. The only component which heats following shutdown is the injector which increases from 270°F during the firing to 400°F 20 sec after shutdown. The throat diameter (0.148 in.) was within 0.001 in. of the as-fabricated dimension. The maximum nozzle temperature of 2550°F should allow a firing life of 20 to 40 hours at full thrust based on the data of Figure 4.2-12. The maximum shunt thermal load was 66 watts. The five second performance re-evaluation, accomplished using the positive displacement flowmeters showed that there was no performance change following the 6300 sec firing.

Test Series F, Cold and Hot Propellants - 2 tests; 200 starts; 15 sec total duration

The engine showed no adverse effects from operation with 20°F and 121°F propellants. Postfire photographs of Engine SN 3 at the conclusion of testing are shown in the right column of Figure 6.3-12 and in Figure 6.2-7.

Posttest valve response, leakage and cold flow tests showed no changes from the pretest condition.

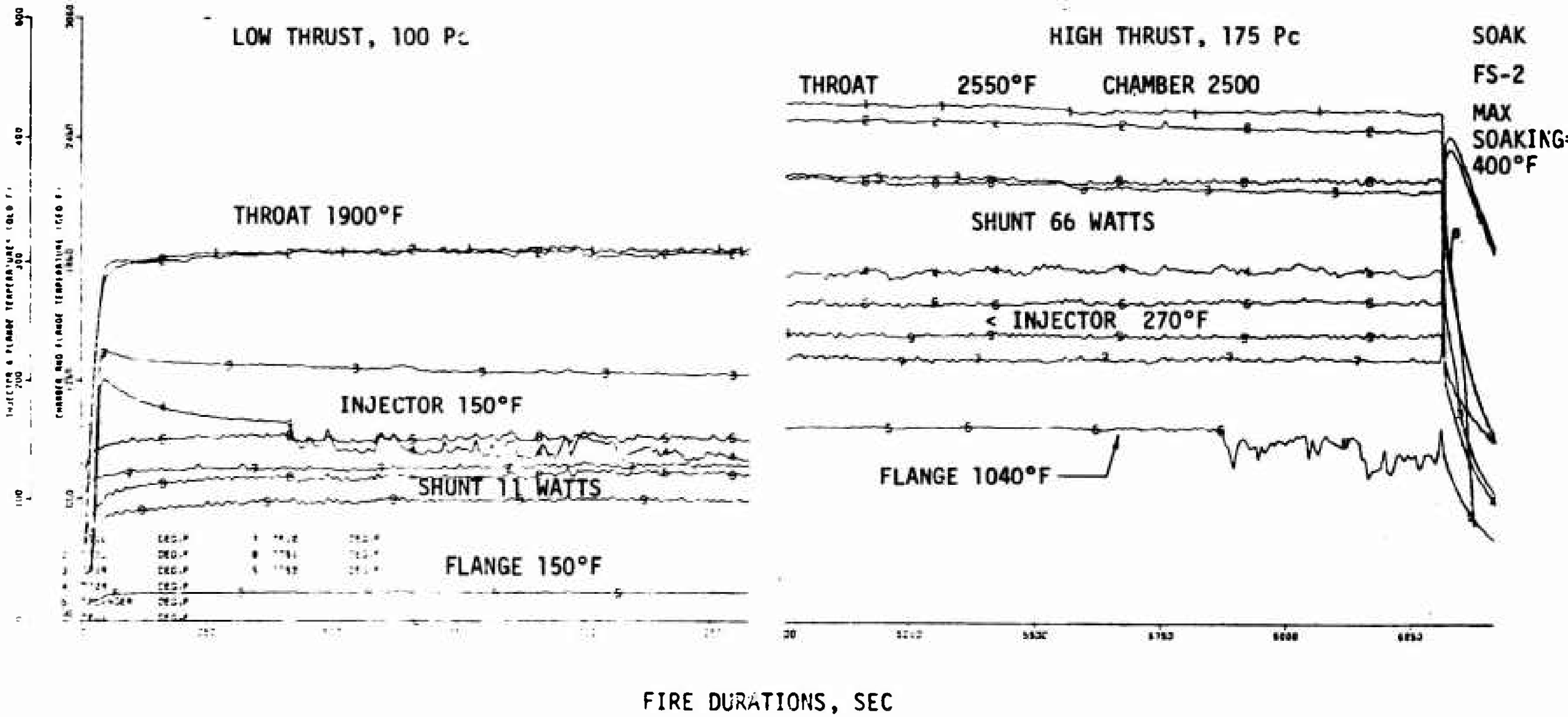

Figure 6.3-14. Engine SN 3 Thermal Data, 6300 sec Continuous Burn

6.4 TEST DATA EVALUATION

6.4.1 Response

The engine response times measured in the Phase III testing were essentially unchanged from those obtained in the Phase II testing. These results reported in Table 2.1-1, show a valve response of 0.0023 to 0.0026 sec from signal to start of valve travel at 28 watts and 0.0056 $\pm$ 0.0006 sec from signal to 90% thrust at all operating conditions. The $\pm$ 0.0006 sec variance is due mainly to the tank supply pressures in the blowdown system. Thus, with full tanks and the accompanying high supply pressure (300 psia), response is 0.005 sec. This increases to 0.0062 sec when the tank pressure is decreased to 100 psia. The pulse-to-pulse repeatability of these data are within ≈ $\pm$ 0.0002 sec for a given set of operating conditions. This time period approximates the limits of resolution of time. Response data obtained for the three valves revealed a variance between valves of less than $\pm$ 0.00035 sec as indicated from the valve inlet pressure decay data of Figure 5.2-3.

6.4.2 Repeatability at MIB

The ability of each engine to provide repeatable impulse bits was evaluated at electrical pulse durations of 0.100, 0.050, 0.025 and 0.010 sec. This evaluation was made before, throughout and after the durability testing in order that the impulse degradation, if any, could be assessed.

The influence of environmental and propellant temperature was assessed at the 0.025 sec electrical pulse duration using test data obtained from the fire testing engine SN's 1 and 3 at 20°F and 120°F. Impulse bit repeatability was directly comparable to that obtained at room temperature conditions. Additional data were obtained with engines SN 2 and 3 at several levels of tank pressure simulating the influence of tank blowdown.

6.4.2, Repeatability at MIB (cont.)

Figure 6.4-1 shows the impulse repeatability of engine SN 1 at the design point supply pressures for a regulated feed system. The upper portion of the curve contains data from five test series involving an electrical pulse of 0.025 sec. The general trend of increasing impulse with pulse number is typical of all engines and is a result of improved vaporization and combustion efficiency as the chamber wall is heated. The first pulses are typically 10% lower in impulse than those obtained with a hot chamber wall.

Data from four of the five test series conducted at 0.025 sec EPW and nominal tank pressures fall within a narrow, highly reproducible band. This data band indicates an insensitivity to propellant temperatures from 50 to 120°F and no degradation over the 300,000 pulse durability tests. The lower curve for 18°F propellants shows a significant influence when the environment approaches the freezing point of the oxidizer. However, the condition is self correcting, and after 10 pulses the chamber has warmed to a level where the impulse is once more highly predictable. This effect was not noted in the Phase II testing but did not repeat on Engine SN 3 low temperature tests.

The MIB data on the bottom half of Figure 6.4-1 were obtained at the same tank pressure settings but with an electrical pulse of 0.010 sec. The 0.3% and 3.0% duty cycle data show that varying pulsing frequency from 0.3 to 3.0 pulses/sec does not influence impulse repeatability. Figure 6.4-1 shows the pulses to be highly repeatable down to an MIB of ≈ 0.04 lbF-sec and that the tolerance goal of $\pm$ 0.005 lbF sec has been demonstrated.

Figure 6.4-2 provides similar data for Engine SN 2 obtained at two different tank supply pressure levels. Environmental temperatures effects were not evaluated with this engine. The upper data set shows measured impulse before and after the durability testing at tank

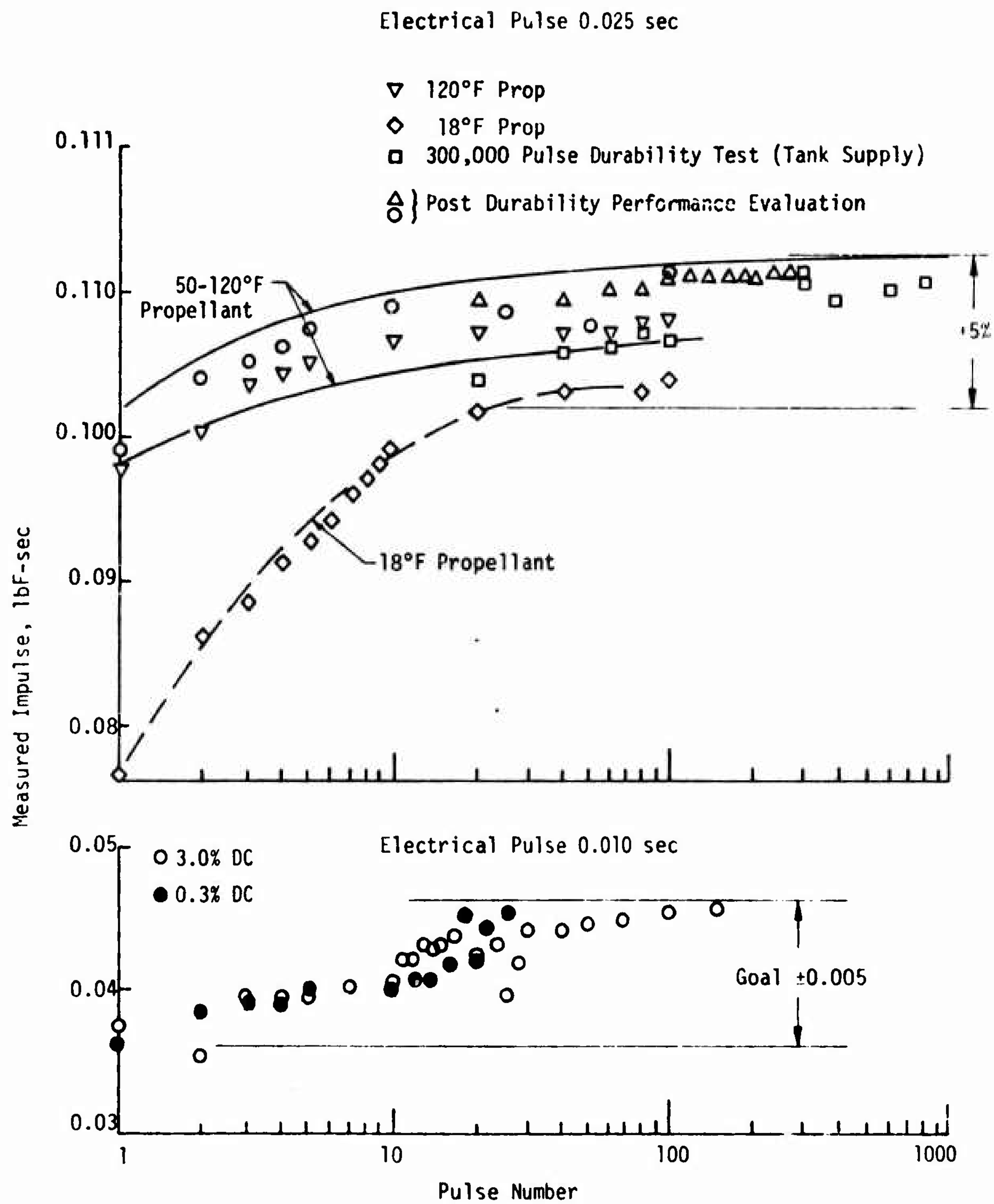

Figure 6.4-1. Impulse Repeatability, Engine SN 1

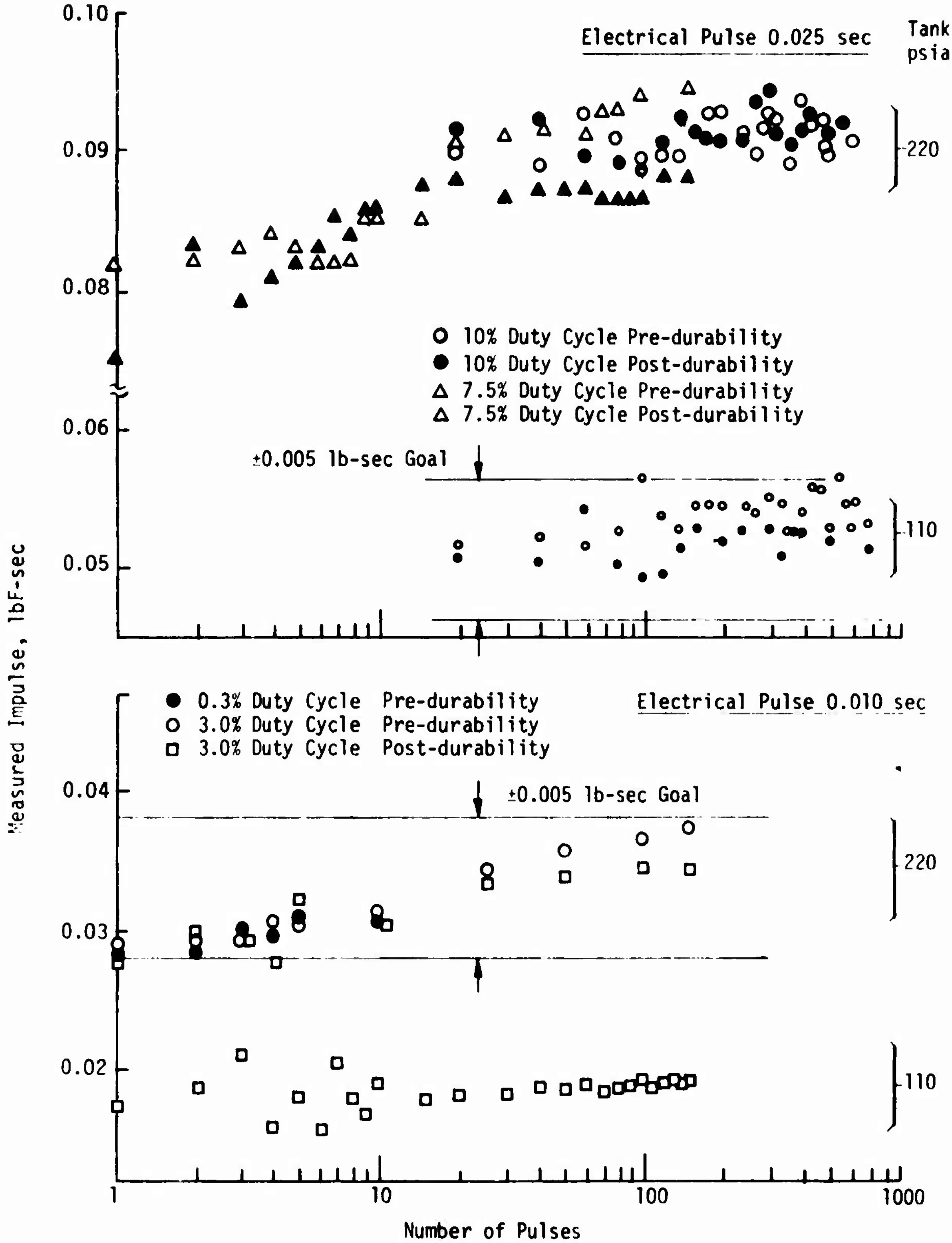

Figure 6.4-2. Impulse Repeatability, Engine SN 2

6.4.2. Repeatability at MIB (cont.)

pressures of 220 and 110 psia (2:1 blowdown). Transient effects are again noted to stabilize after about 20 pulses. No data were obtained for the first 20 pulses at the low pressure condition due to one sample per 20 firings data acquisition mode used on this test series.

The pre- versus post durability impulse data are virtually identical at both high and low tank pressure. This demonstrates the capability of a highly predictable long life engine for use in a blowdown system. It should be noted that the contract goal of 0.05 lbF-sec ± 0.005 lbF-sec was demonstrated in two operating modes:

(1) High tank pressure - short pulses
(2) Low tank pressure - longer pulses

The data presented in the lower portion of Figure 6.4-2 are for 220 and 110 psia tank pressures at an electrical pulse of 0.010 sec. The influence of an order of magnitude change in % duty cycle is again noted to have virtually no influence on MIB repeatability. A series of low pressure short pulses provided a highly repeatable MIB capability of 0.018 lbF-sec. The chamber thermal transients have a much smaller influence on impulse at these very low impulse bits because the temperature rise rate per pulse is very small. A tabulation of impulse bits of pulses 1 through 30 and 91 through 110 is provided in Table 6.3-5. In order to eliminate the influence of random measurement errors resulting from the thrust sampling rate, which is in the order of 2%, a comparison was made of ten pulse groupings. This method provided a mean impulse of 0.0182 ± 0.0006 lbF sec when 5 groups are compared.

Figure 6.4-3 provides similar data for Engine SN 3. Here data are presented for all of the pulses evaluated. The upper set of data compare pre- and post durability at a 0.100 sec pulse width. These are reproducibly within ± 1%. Similar results are found for the 0.050 sec pulse. The third data set for 0.025 sec pulses compares pre versus post durability

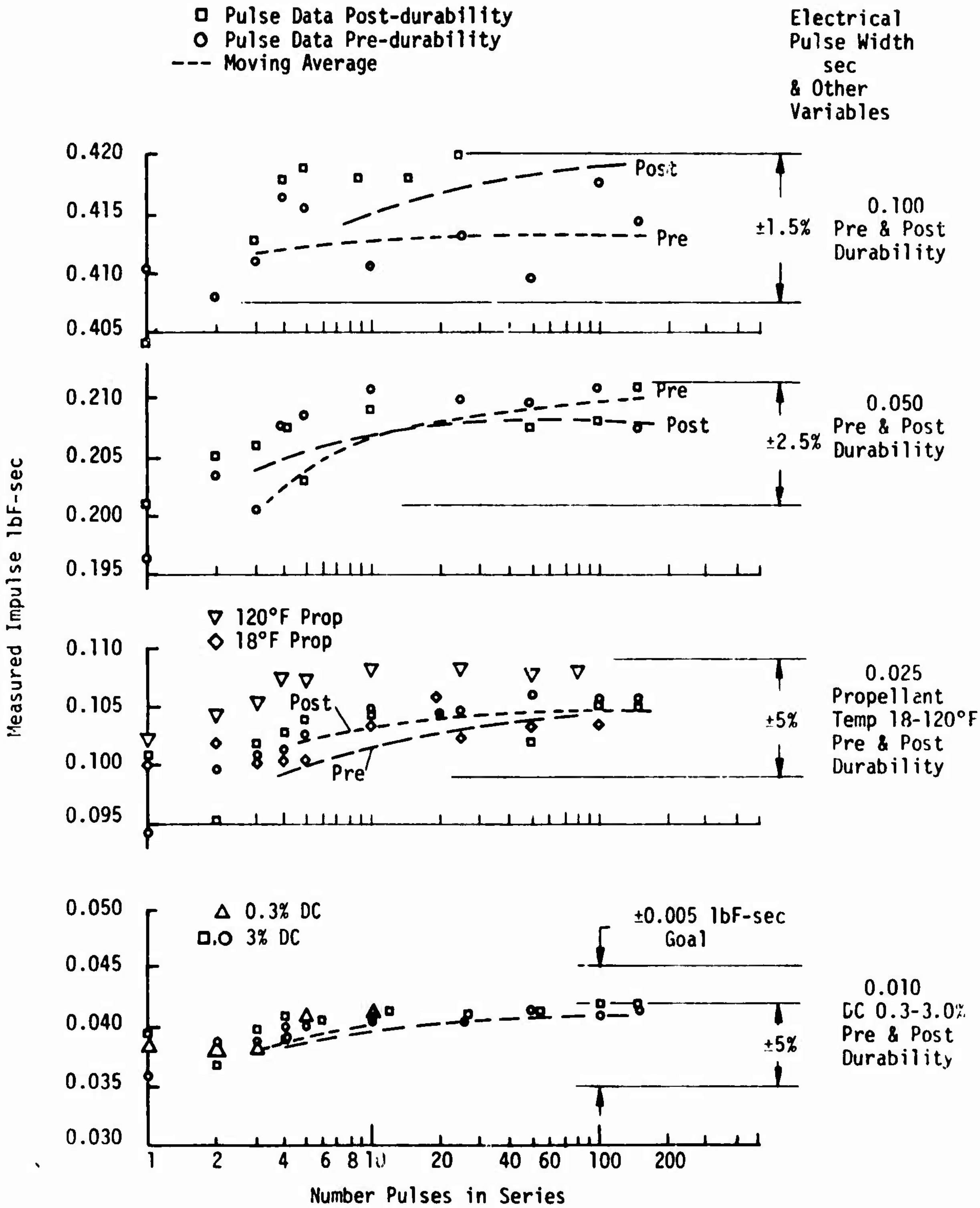

Figure 6.4-3. Bit Impulse Repeatability, Engine SN 3

6.4.2, Repeatability at MIB (cont.)

data at ≈ 60°F environmental temperatures with data obtained at 18°F and 120°F. These data are noted to be highly repeatable with the hot environment providing only 3% higher impulse than the normal 60°F data. These results differ from testing with Engine SN 1 in that there is no impulse decrement associated with 18°F environmental tests.

The lower data provides the MIB obtained with the engine at a 0.3 and 3.0% duty cycle and comparing pre- and post durability impulse at a common tank pressure setting. These data are all very repeatable, providing an impulse of 0.04 ± 0.002 lbF-sec including the influence of chamber wall heating.

Figure 6.4-4 provides random samples of data obtained from the more than 400,000 pulses accumulated on the durability tests of the three engines. These data shown no aging effect on any of the engines. The 3 levels of impulse shown for Engine SN 3 are a result of tank blowdown at selected intervals in the firing.

Figure 6.4-5 provides the 1 sigma pulse repeatability as a function of impulse and quantity of pulses in a pulse train. The more repeatable data obtained with longer pulse trains is due to the chamber reaching an equilibrium thermal condition. All three engines provide approximately the same level of impulse repeatability for trains longer than 10 pulses. The asympotic values at 100 pulses are as follows:

Impulse Bit lbF-sec	Sigma Repeatability N = 100
0.400	1%
0.100	2%
0.04	2.4%

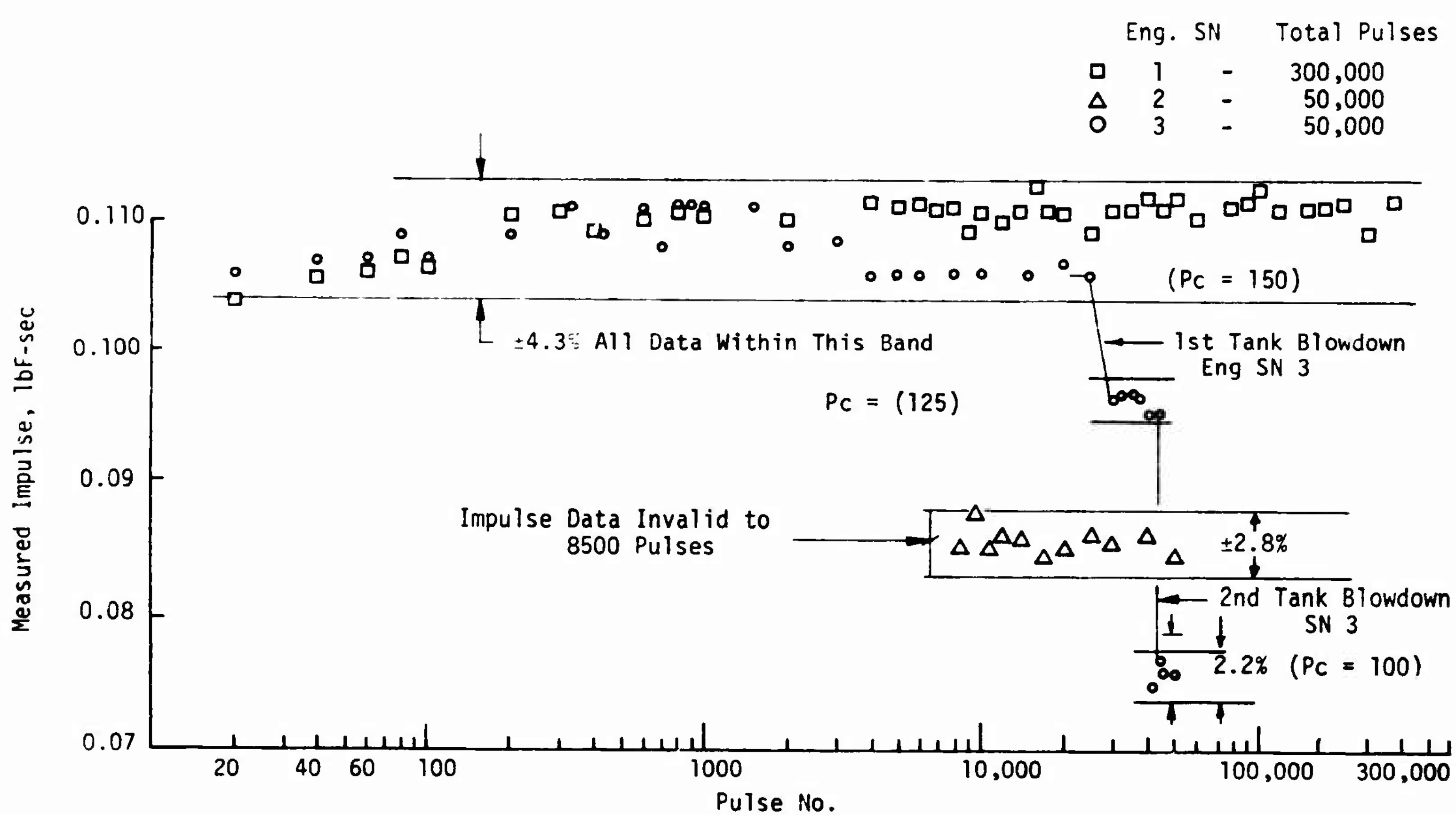

Figure 6.4-4. Impulse Repeatability, Three Engines, 400,000 Pulse Endurance Test, Electrical Pulse 0.025 sec, 10% Duty Cycle

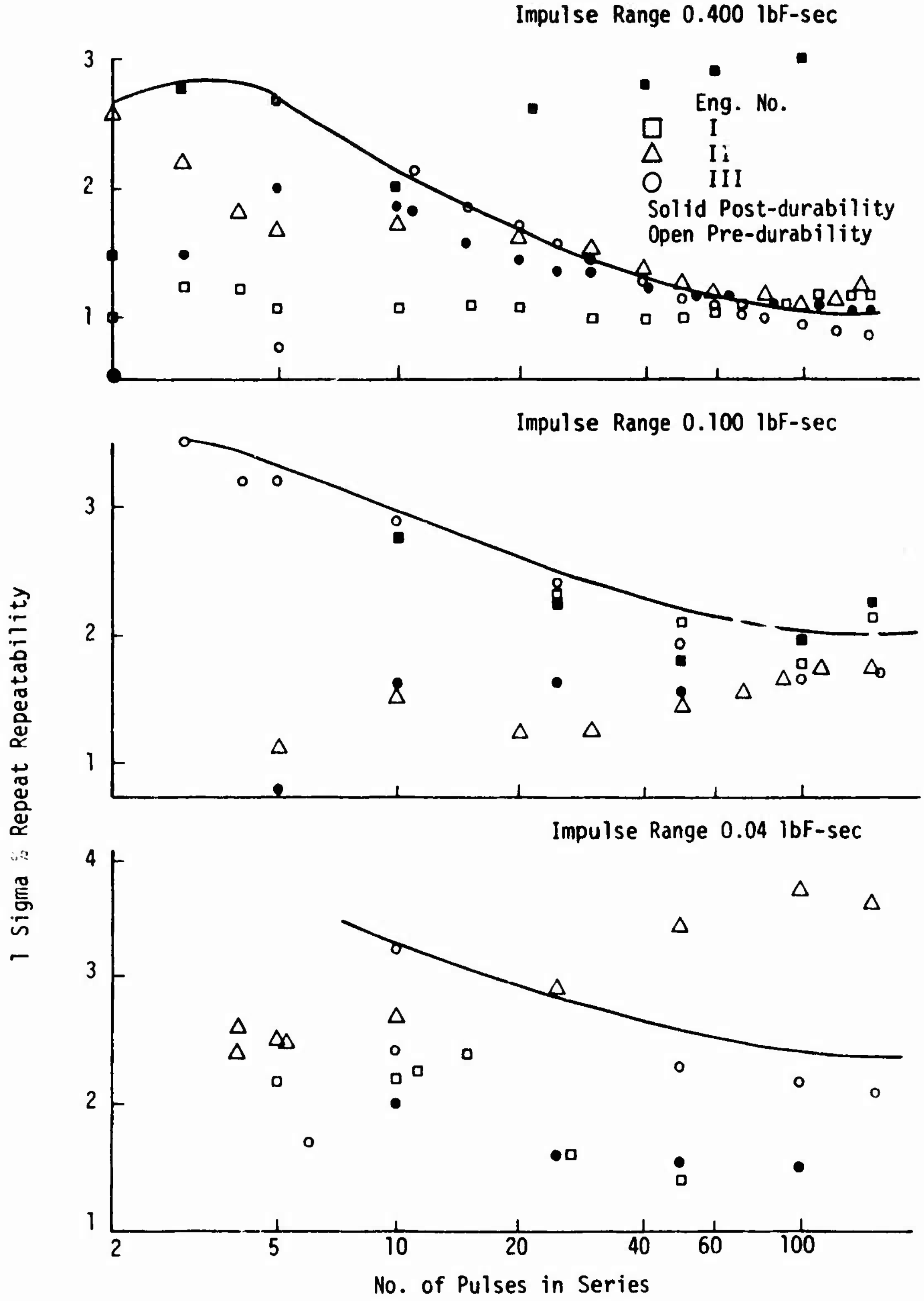

Figure 6.4-5. One Sigma Pulse Repeatability as a Function of Impulse and Quantity of Pulses in a Pulse Train

6.4.2, Repeatability at MIB (cont.)

The linearity and repeatability of the three engines and test facility, including all variables, are shown in Figure 6.4-6. The three curves on the lower portion of the figure show the relationship between bit impulse and the time period voltage is applied to the valve. The parameters which in addition to the engine influence the linearity and repeatability include: feed system pressures, environmental temperatures, the supply voltage and electrical system commanding the pulses and the thrust measurement and data reduction. All data are closely fit by a line through the origin. The slope of each of these lines is determined by the tank pressure and hydraulic resistance of each engine. The linearity of the complete system was calculated by dividing impulse by time, which should be a constant ($\overline{X}$). These data are shown graphically on the upper set of curves and are summarized as follows:

Engine SN	Linearity Constant at max Tank Pressure	Standard Deviation of Data %
1	4.345	3.5
2	3.551	5.4
3	4.188	1.5

Most of the variance in data is believed to be due to limitations on returning to the same pressure setting for the positive displacement flowmeters on successive firing days. The linearity of the actual engine is believed to be better than 1% over its entire life and range of operation.

6.4.3 Performance

This section summarizes the Phase III data including; steady state performance at maximum engine thrust, effect of blowdown upon performance and effect of firing duration or impulse upon pulsing performance.

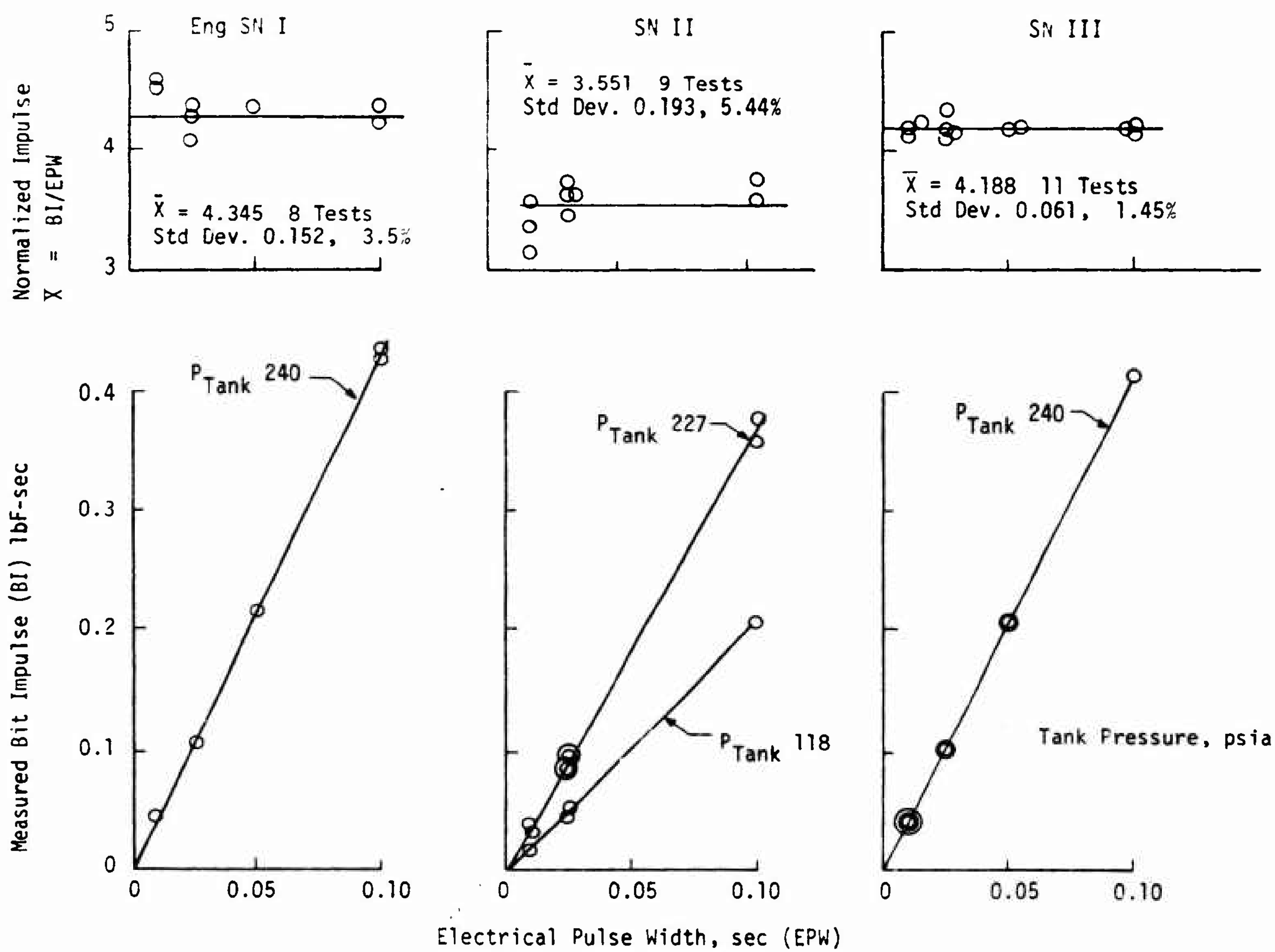

Figure 6.4-6. Linearity and Repeatability of Engine and Test Facility

6.4.3, Performance (cont.)

6.4.3.1 Steady State

Phase III steady state and blowdown performance data for the three engines tested is listed in Table 6.4-1.

Engine SN 1 (6-SP-45-C injector) was selected to be used for a radiation cooled chamber with a regulated feed pressurization system. At the 5 lbf thrust level, the Phase II data indicated a performance capability between 302-305 sec I_{sp} with chamber lengths of 2.0-2.75 in. and with nozzle exit area ratio, ϵ = 100.1. Chamber wall temperatures exceeding 3000°F were measured within ≈ 20 sec firing duration in Phase II. In order to improve chamber thermal compatibility and extend duration capability, the oxidizer spray angle was made more axial to reduce oxidizer spray upon the chamber wall. This modification resulted in a slightly more fuel rich barrier as indicated by the improved chamber compatibility and extended duration capability achieved during Phase III. The compatibility improvement resulted in a corresponding 2 to 5 sec sacrifice in steady state performance. The specific impulse for Engine SN 1 in the Phase III testing was 300 sec at a nominal chamber pressure of 125 psia. As shown in Figures 6.4-7 and 6.4-8, the 300,000 firings on 6-SP-45-C resulted in no perceptible change in steady state performance.

The energy release efficiency (ERE) characteristics vs engine mixture ratio (O/F) of the Phase III injector differed slightly from the Phase II unit (6-SP-45-A) whose ERE was constant with O/F in the range from 1.2 to 2.0 as shown in Figure 6.4-7. The Phase III injector's ERE decreased with increasing O/F and I_{sp} maximized near the nominal engine O/F = 1.6 as shown in Figure 6.4-8. This maxima at 1.6 O/F results from the product of increasing kinetic I_{sp} and decreasing ERE with increasing O/F; the maximum Phase II performance occurred at O/F = 1.9 which corresponded to the peak kinetic I_{sp} mixture ratio.

TABLE 6.4-1

PHASE III STEADY STATE AND BLOWDOWN PERFORMANCE DATA FOR THREE ENGINES TESTED

Engine SN-1

Phase III Test Series: ØC-26-XXX

Test No. (Pulse)*	184(1)	185(1)	185(4)	186(1)	186(4)	187(1)	187(3)	188(1)	189(1)	189(3)	190(1)	190(2)	191(1)	191(2)	197(1)	197(2)	203(1)**	203 (4)**	204(1)**	204(4)**
Injector	6-SP-45C →																			
Chamber Length, L', (in)	2.0 →																			
Nozzle Exit Area Ratio, ε	45.3 →																			
Sea Level or Vacuum	Vacuum →																			
Chamber Pressure, Pc, (psia)	60	60	60	82	82	105	104	102	102	102	100	100	106	106	123	124	123	123	124	124
Mixture Ratio, O/F	1.50	1.55	1.72	1.53	1.65	1.53	1.56	1.38	1.49	1.51	1.83	1.89	1.22	1.23	1.55	1.56	1.54	1.51	1.67	1.65
Vacuum Thrust, F_{vac} (ε), (lb_f)	2.15	2.09	2.00	2.81	2.78	3.58	3.65	3.55	N.A.	N.A.	3.52	3.52	3.65	3.74	4.29	4.42	4.28	4.35	4.32	4.36
Delivered Isp (ε), (sec.)	250	247	240	265	264	278	284	276	↓	↓	276	279	276	282	283	292	284	292	288	292
Energy Release Eff. ERE, (%)	85.4	83.9	80.8	89.5	86.8	92.9	93.9	93.1	↓	↓	91.4	92.1	94.5	95.8	93.6	96.1	93.7	95.6	94.5	95.2
Isp_{ss} (ε = 100)$_{Extrap}$, (sec)	258	255	248	273	271	286	292	283	↓	↓	284	287	284	230	290	300	292	300	295	300

*Each pulse is 5.0 sec. Firing duration followed by 0.5 sec. Coast period between pulses

**Post demonstration performance re-verification following 300,000 firings.

(1) First 5 sec burn
(2) Second 5 sec burn
(3) Third 5 sec burn
(4) Fourth 5 sec burn

TABLE 6.4-1 (cont.)

Engine SN-2

Test No. (Pulse)*	208(1)	209(1)	209(6)	210(1)	210(5)	211(1)	211(3)	212(1)	230(1)**	230(3)**	231(1)**	231(4)**
Injector	6-SP-OC											
Chamber Length, L', (in)	2.0								1.75			
Nozzle Exit Area Ratio, ε	49.3								50.6			
Sea Level or Vacuum	Vacuum											
Chamber Pressure, Pc, (psia)	69	70	68	91	91	121	120	131	114	112	91	8[illegible]
Mixture Ratio, O/F	1.65	1.67	1.78	1.47	1.52	1.42	1.43	1.53	1.67	1.69	1.70	1.78
Vacuum Thrust, F_{vac} (ε), (lb_f)	2.10	2.12	2.10	2.78	2.84	3.72	3.78	4.29	3.50	3.50	2.76	2.73
Delivered Isp (ε), (sec)	262	262	258	271	277	283	287	283	275	274	261	258
Energy Release Eff. ERE, (%)	87.9	87.8	85.9	90.6	91.4	94.1	94.6	93.4	91.1	90.2	87.1	84.7
Isp_{SS} (ε = 100)$_{extrap}$ (sec)	269	269	265	278	285	290	295	290	282	281	268	265

TABLE 6.4-1 (cont.)

Engine SN-3

Test No. (Pulse)*	162(1)	163(1)	163(6)	164(1)	164(6)	165(1)	165(6)	166(1)	166(4)	167(1)	167(3)	168(1)	168(3)	178(1)**	179(1)**
Injector	4-UD-28S →														
Chamber Length, L', (in)	1.75 →														
Nozzle Exit Area Ratio, ϵ	51.3 →														
Sea Level or Vacuum	Vacuum →														
Chamber Pressure, Pc, (psia)	75	52	52	73	72	97	94	121	121	140	142	159	166	142	141
Mixture Ratio, O/F	1.41	0.84	0.88	1.91	2.02	1.61	1.79	1.55	1.65	1.60	1.61	1.53	1.54	1.50	1.43
Vacuum Thrust, F_{vac} (ϵ), (lb_f)	2.12	1.52	1.51	2.07	2.04	2.76	2.71	3.48	3.53	4.04	4.14	4.70	4.83	4.11	4.08
Delivered Isp (ϵ), (sec)	236	198	202	239	238	259	261	266	275	266	275	267	276	264	267
Energy Release Eff., ERE, (%)	81.0	71.5	72.4	81.4	81.5	86.6	86.2	88.3	90.1	88.2	89.9	86.1	90.5	87.2	88.6
Isp_{ss} (ϵ= 100)$_{Extrap.}$, (sec)	243	205	209	246	245	266	268	273	282	273	282	274	283	271	274

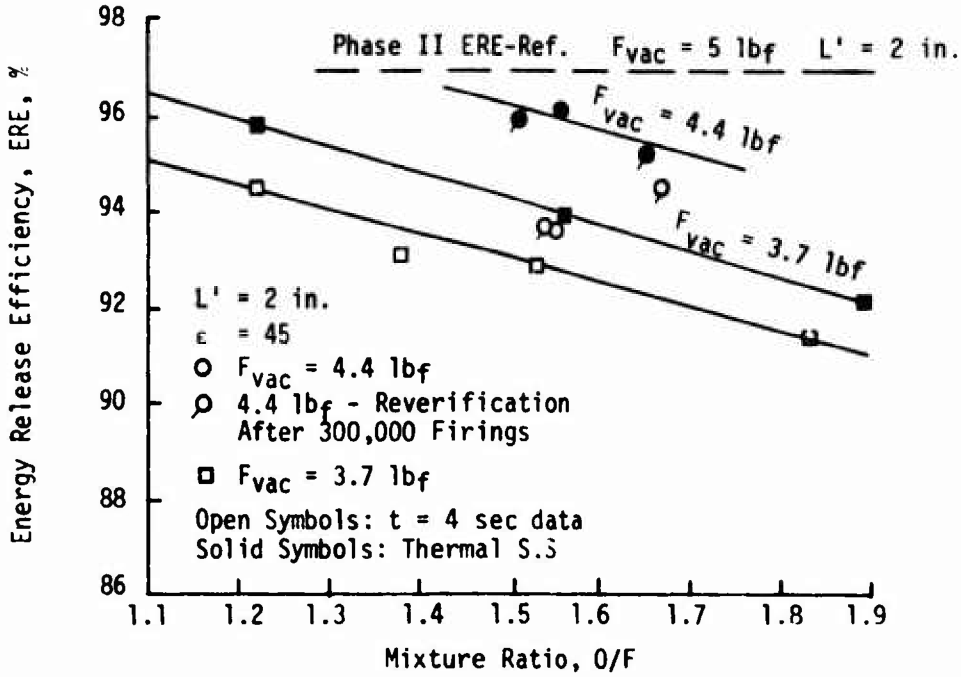

Figure 6.4-7. Mixture Ratio Effect on Injector 6-SP-45-C Steady State Energy Release Efficiency

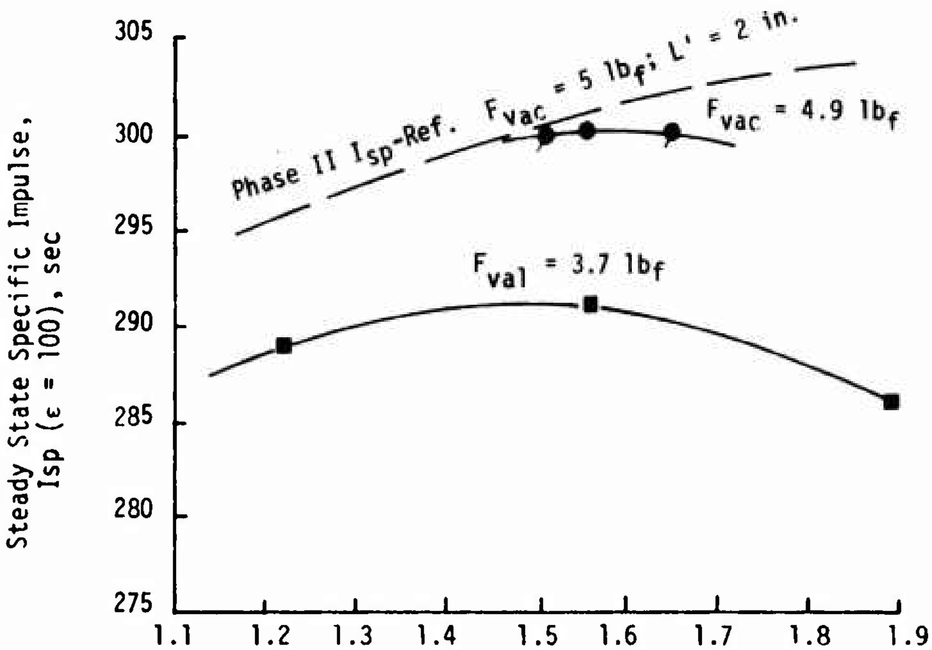

6.4-8

Mixture Ratio, O/F

Figure 6.4-8. Steady State Specific Impulse versus Mixture Ratio, Eng. SN-1, Injector 6-SP-45-C

6.4.3, Performance (cont.)

The mechanisms which account for the decrease in steady state performance at higher O/F's are: the decrease in oxidizer spray angle and increase in axial injection velocity. Both reduce the oxidizer droplet residence time available for vaporization within the chamber. The condition is aggravated at high O/F due to the increases in oxidizer injection velocity which also decreases oxidizer vaporization efficiency.

Engine SN 2 (6-SP-0-C injector) was selected for limited duration firings with an insulated chamber and tank blowdown pressurization system. Again, as a means of lowering chamber wall temperatures, the oxidizer spray fan had been modified to produce a more axial spray to minimize oxidizer impingement on the chamber wall. Figure 6.4-9 shows that the 6-SP-0-C ERE decreases sharply with increasing O/F compared to a slight ERE improvement with increasing O/F which was observed by Phase II data.

The physical mechanism for the decreasing ERE with increasing O/F is the same as previously explained for the 6-SP-45-C engine. Since the 6-SP-0-C injector results in less inter-element spray overlap/ interaction that the 6-SP-45-C injector, its striated mixture ratio performance is more sensitive to high O/F as indicated by Figure 6.4-10. The steady state performance of this design maximizes at $\approx$ 295 sec I_{sp} at engine O/F = 1.4. At nominal design O/F = 1.6, Phase III steady state performance between I_{sp} = 285 to 287 sec is indicated. No change in steady state performance was noted when comparing data obtained before and after the 50,000 pulse demonstration test firings.

Engine SN 3 (4-UD-28-S injector) is the most versatile design of all. The injector used in the Phase III testing is the same as employed on Phase II. It can be fired for unlimited durations (0.010 sec to 6300 sec demonstrated) with a radiation cooled adiabatic wall chamber and can operate with a blowdown feed pressurization system. Unlike Engines 1 and 2, the 4-UD-28-S injector has a constant ERE versus O/F. In a buried (adiabatic

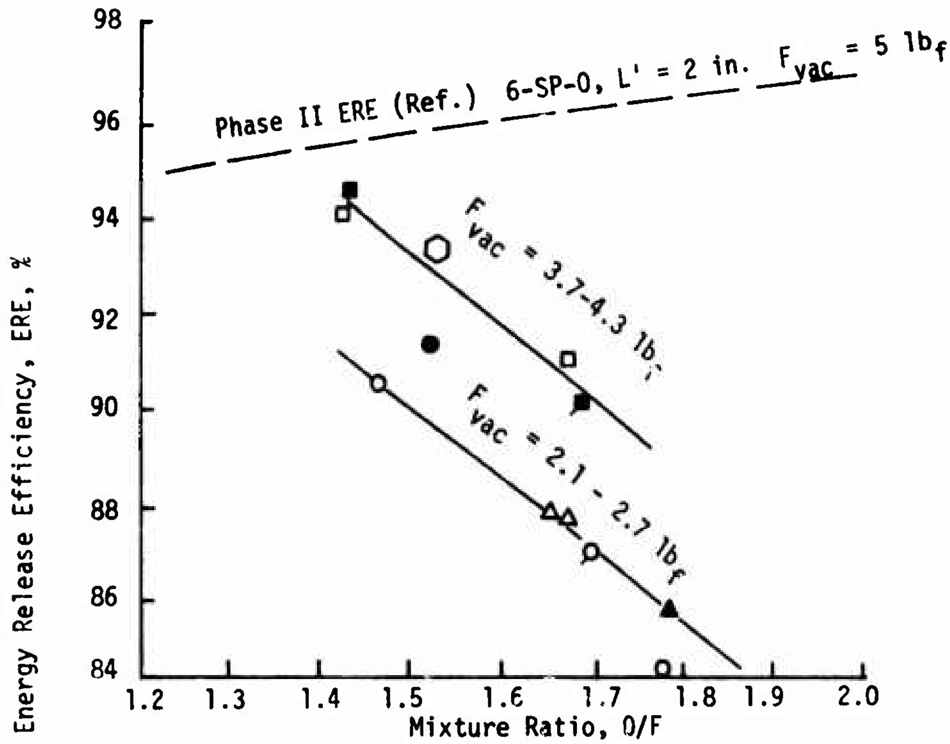

Figure 6.4-9. Mixture Ratio Effect on Injector 6-SP-O-C (Eng. SN 2) Energy Release Efficiency

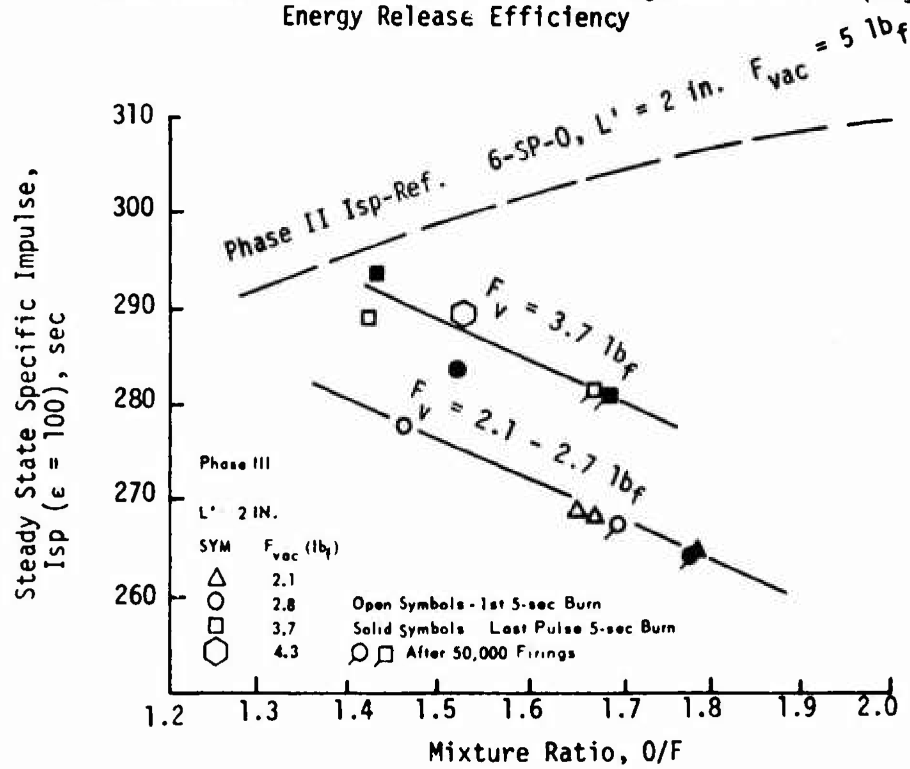

Figure 6.4-10. Steady State Specific Impulse versus Mixture Ratio, Injector 6-SP-O-C (Eng. SN 2)

6.4.3, Performance (cont.)

wall) condition, it could be fired up to a maximum F_{vac} = 4.2 lbf, at which point it delivered 283 sec steady state I_{sp} at a nominal O/F of 1.6.

Engines SN 1 and 3 required approximately 10 sec firing duration prior to achieving peak steady state performance; this compares to less than 5 sec for SN 2. For example, at 4 sec firing duration, transient I_{sp} performances were approximately 5 sec lower for the SN 1, 10 sec lower for the SN 3 and no different than steady state for SN 2. SN 2 Engine attains steady state performance more rapidly as a result of the rapid heating of the thin wall conical nozzle and throat; 0.75 sec to 1000°F vs ≈ 2 sec to 1000°F for SN 1. The transient performance loss is only partly attributable to the chamber and nozzle thermal heat loss. The remainder is attributable to a lower transient ERE which reflects unvaporized wall film at reduced chamber wall temperatures. This, in turn, implies higher wall film contamination during the thermal start transient of a given engine. Thin wall chamber designs are preferred where many short burns are required.

6.4.3.2 Blowdown

Although Engine SN 1 (6-SP-45-C injector) was primarily intended for a regulated pressurization feed system, it was tested at variable thrust levels during Phase III. The purpose of so doing was to obtain blowdown data considering possible use of this engine for a blowdown application and to determine the chamber wall operating temperature as a function of chamber pressure and engine thrust.

The ERE for SN 1 engine from 2.0 to 4.5 lbf thrust is shown on Figure 6.4-11. At the higher thrust levels, the Phase III ERE is ≈ 1% lower than the Phase II data which was obtained in a 2.75-in. length chamber. At minimum thrust, however, the Phase III ERE data is as much as 4% lower. The reduced Phase III efficiency can be attributed to a combination of shorter chamber length and modification of the oxidizer element spray to

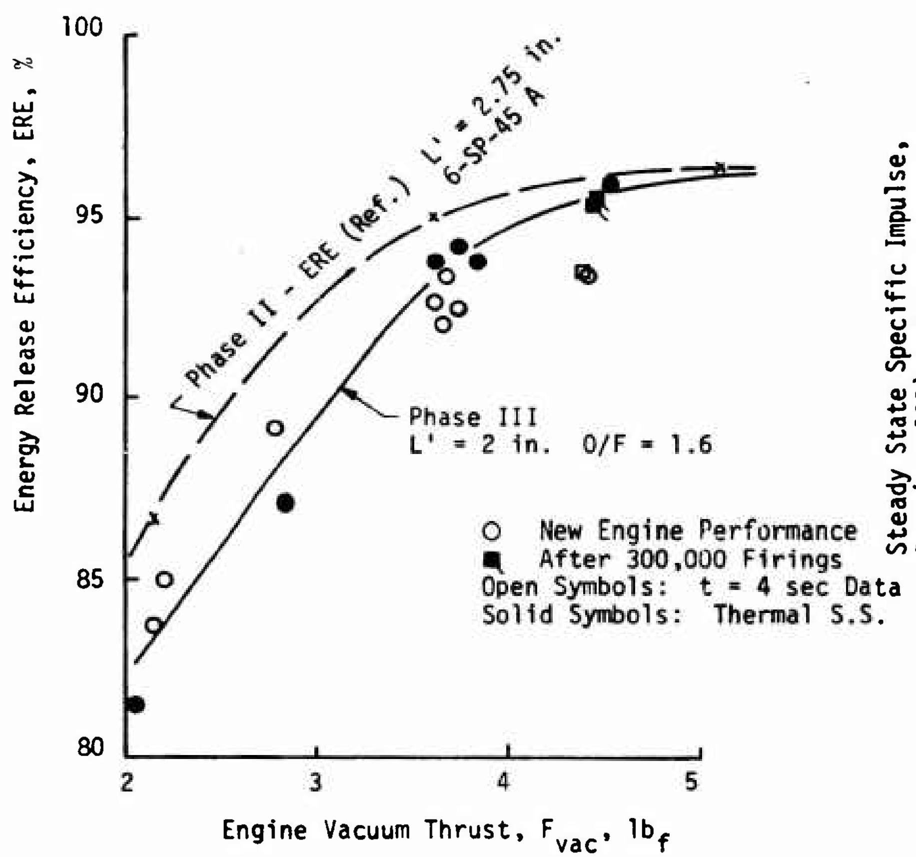

Figure 6.4-11. Steady State ERE, Simulated Blowdown Operation, Engine SN 1, Injector 6-SP-45-C

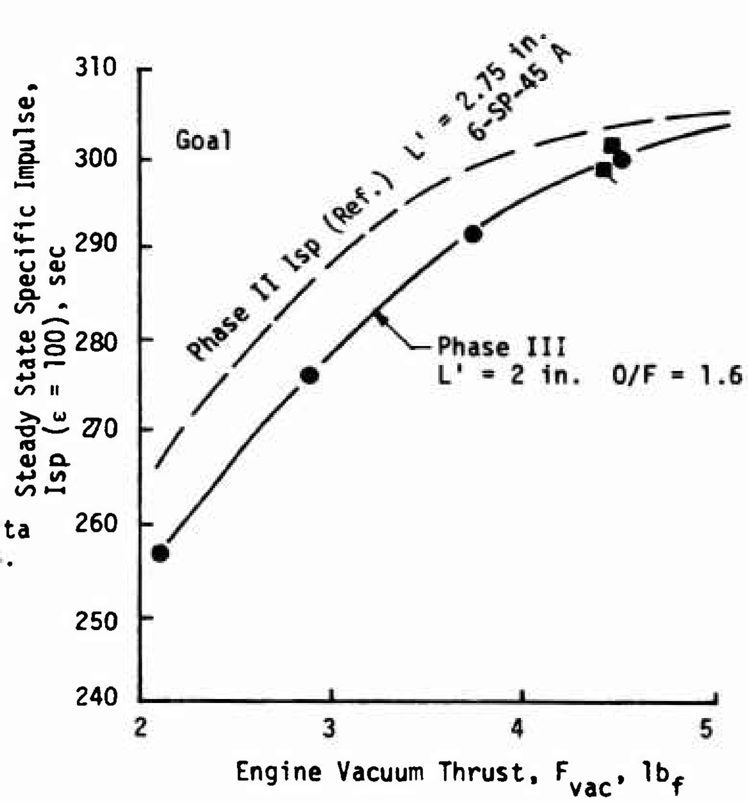

Figure 6.4-12. Steady State Specific Impulse versus Engine Vacuum Thrust, Engine SN 1, Injector 6-SP-45-C

6.4.3, Performance (cont.)

enhance chamber compatibility at higher thrust. The increased oxidizer injection velocity thus did not provide the anticipated improvement in blowdown performance forecasted in Phase II. The first 5 sec burn data at low thrust shows a higher ERE than the 4th burn. This is due to an O/F shift during the firing. The curve through these data represent an O/F = 1.6.

Figure 6.4-12 shows the steady state SN 1 engine specific impulse adjusted from the 45:1 area ratio nozzle tested to the nominal 100:1 area ratio. This correction involved adding 7.9 sec. This could be further increased by an additional 2 to 3 sec by use of a 150 or 200:1 expansion nozzle. The 300 sec I_{sp} goal was achieved at an engine thrust of 4.4 lbf (ϵ = 100:1). At the terminal blowdown state tested (F_{vac} = 2.1 lbf) the I_{sp} was 256 sec.

Blowdown ERE data for Engine SN 2 (6-SP-0-C injector, conical chamber) is given in Figure 6.4-13. This data appears consistent with the Phase II blowdown data with the 2-in. length chamber. Although the 6-SP-0-C injector has lower ERE and delivers lower steady state performance than the 6-SP-45-C at maximum thrust, its rate of degradation is significantly lower as engine thrust is reduced. At 2.1 lbf thrust, it still delivers 273 sec I_{sp} as shown in Figure 6.4-14, compared to only 256 sec for the 6-SP-45-C injector described previously. This difference is attributed to the high shear forces acting on the wall film in the long, low contraction ratio throat approach section of the conical chamber. This was verified at the conclusion of the durability testing by refiring the same injector in a cylindrical chamber. An 8 sec difference in specific impulse was noted at a thrust of 3 lbf. This type of design would be most useful for a 1 to 2 lbf thrust engine or one requiring extended blowdown capabilities.

Blowdown performance of Engine SN 3 (4-UD-28-S injector) is shown on Figure 6.4-15. The 4-UD-28-S injector is the same hardware which was tested in Phase II. For Phase III testing, the chamber length was

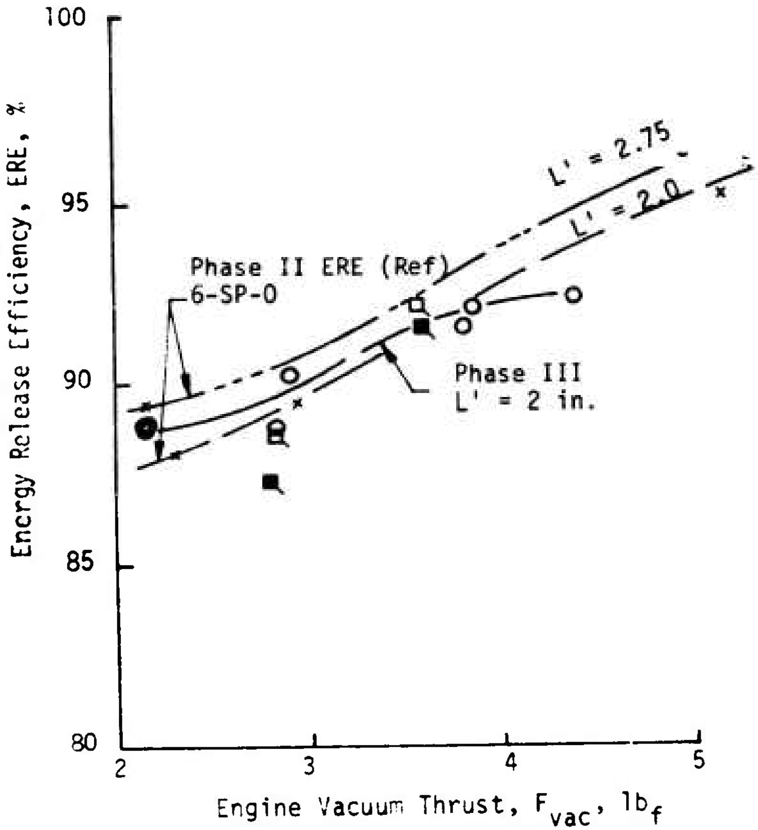

Figure 6.4-13. Energy Release Efficiency versus Engine Vacuum Thrust, Engine SN 2, Injector 6-SP-O-C Injector

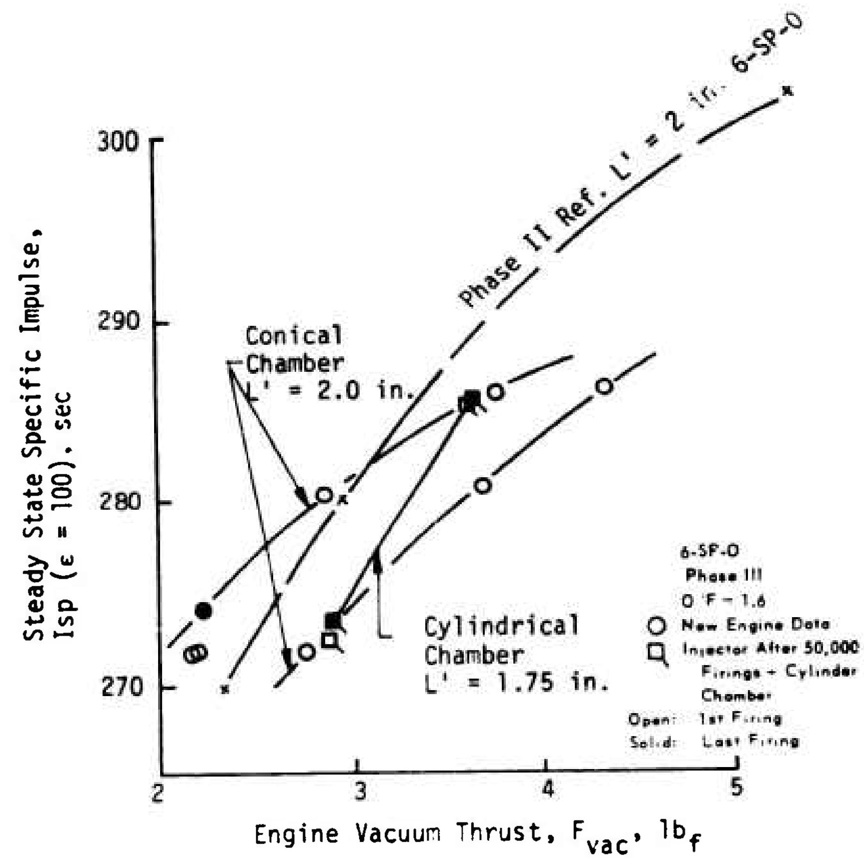

Figure 6.4-14. Steady State Specific Impulse versus Engine Vacuum Thrust, Engine SN 2, Injector 6-SP-O-C

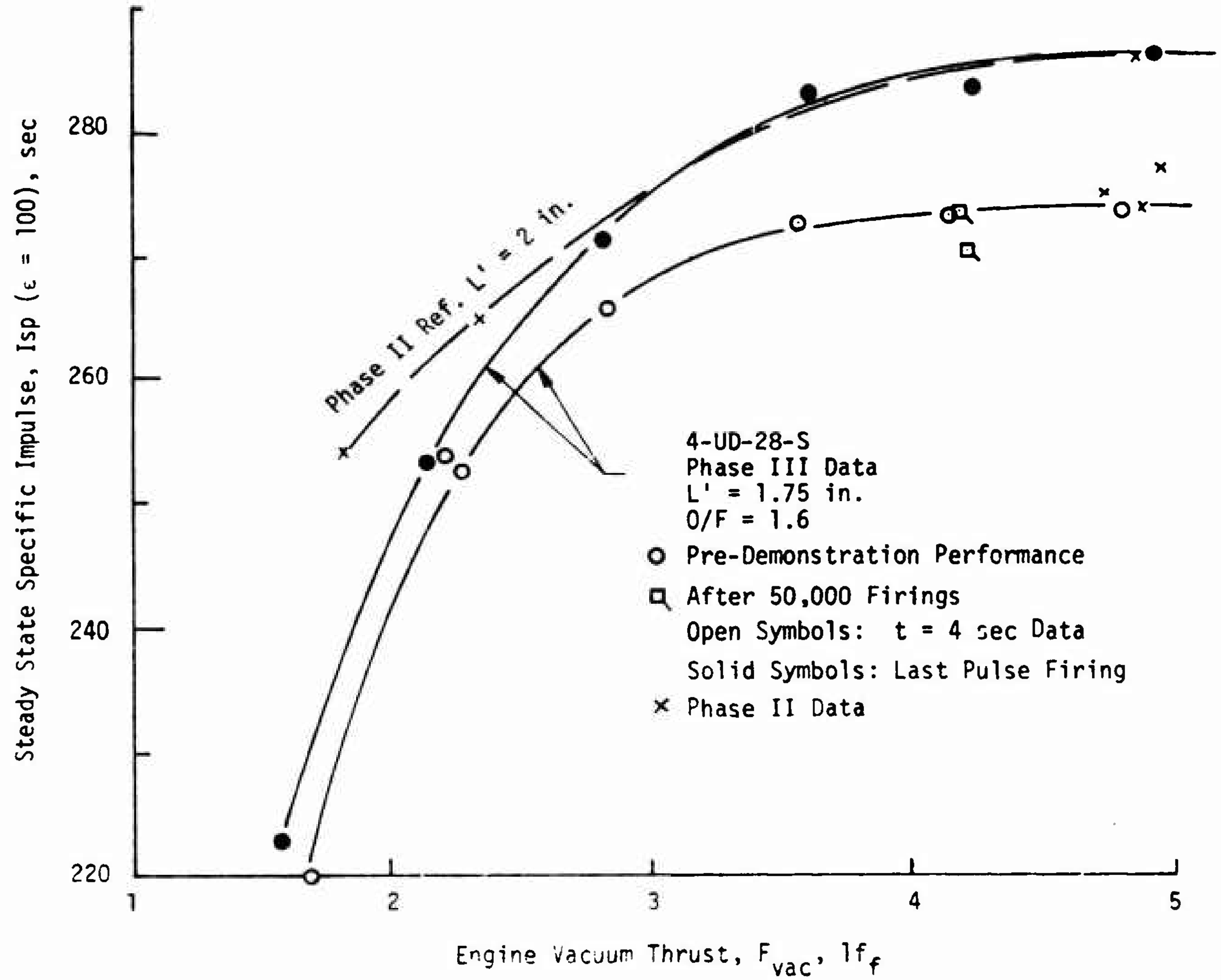

Figure 6.4-15. Engine SN 3 (Injector 4-UD-28-S) Simulated Blowdown Performance

6.4.3, Performance (cont.)

reduced from 2.0 in. to 1.75 in. and a chamber thermal liner added to reduce the chamber contraction ratio from 10.9 (Phase II) to 5.7. This reduced the heat soakback to the valve and the injector face temperature as shown in Figure 6.1-8.

The chamber length reduction did not affect performance over a blowdown range from 5 to 3 lbf thrust. A divergence in blowdown performance between the Phase II and Phase III data was noted below 3 lbf as shown in Figure 6.4-15. At the low thrust levels the performance reduction was accompanied by increased chugging. At the minimum thrust (F_{vac} = 1.6 lbf, P_c = 50 psia) the chugging pressure amplitude was 8 psi. The occurrence of chugging introduces a time varying engine O/F which reduces engine performance via a time variant mixture ratio maldistribution performance loss accounting for the teep performance drop off at low thrust. It is suspected that the difference between the Phase II and Phase III blowdown performance at low thrust is due primarily to this mechanism rather than a reduction in propellant vaporization efficiency in the shorter chamber.

As stated above, the Phase III chamber was shorter and had a lower chamber contraction ratio than the Phase II design. Both of these effects reduce chamber volume, gas residence time, and chamber L*. Since both test series were conducted with the same injector, no differences in injection mass distribution or atomized drop size distributions can be ascribed to the injector. It is concluded that the reduced chamber L* made the Phase III unit more susceptible to chugging at a higher thrust level causing the faster performance drop.

For practical considerations, the 4-UD-28-S engine probably should not be used below a minimum F_{vac} = 2.1 lbf. At that thrust level it delivers a 253 sec I_{sp}. The 1.6 lbf thrust test which provided the 223 sec I_{sp} was accomplished to evaluate extreme off-design conditions.

6.4.3, Performance (cont.)

Figure 6.4-16 compares the blowdown performance of the three Phase III engines over the thrust range from 2.1 to 5 lbf. Although SN 3's performance is at best barely equal to the performance of either the SN 1 or SN 2 engines its significant feature is an unlimited duty cycle capability coupled with the ability to operate in a fully insulated configuration. The SN 1 is best used for a pressure regulated system where very high performance is required. The SN 2 conical chamber configuration would be a candidate for an engine of the 1 to 2 lb thrust class where unlimited duty cycling capabilities are required. The 4-UD-0 injector design from Phase II which experienced thermal limitations at full thrust would also be a good candidate for a lower thrust design.

6.4.3.3 Pulse

Pulse performance data for the three engines are tabulated in Table 6.4-2 for nominal thrust pulses, blowdown thrust pulses where applicable, and minimum and maximum propellant inlet temperature tests. Electrical pulse widths (EPW) of 0.010, 0.025, 0.050, and 0.100 sec duration were tested. Pulsing performances are tabulated for both cold engine start and hot engine restarts. In addition, the 6-SP-45-C and 6-SP-0-C engines were pulsed through a special duty cycle described in Section 6.5. This pulse data are in Table 6.4-3.

All the pulse performance data summarized on Tables 6.4-2 and 6.4-3 and Figures 6.4-18 through 6.4-20 are averaged over a minimum of 4 or more consecutive pulses. This was necessary because it was difficult to accurately measure the minute flowrates associated with a single pulse. It was found that the cumulative flowrate of 4 or more pulses could be measured quite repeatably with the positive displacement flowmeters which were used.

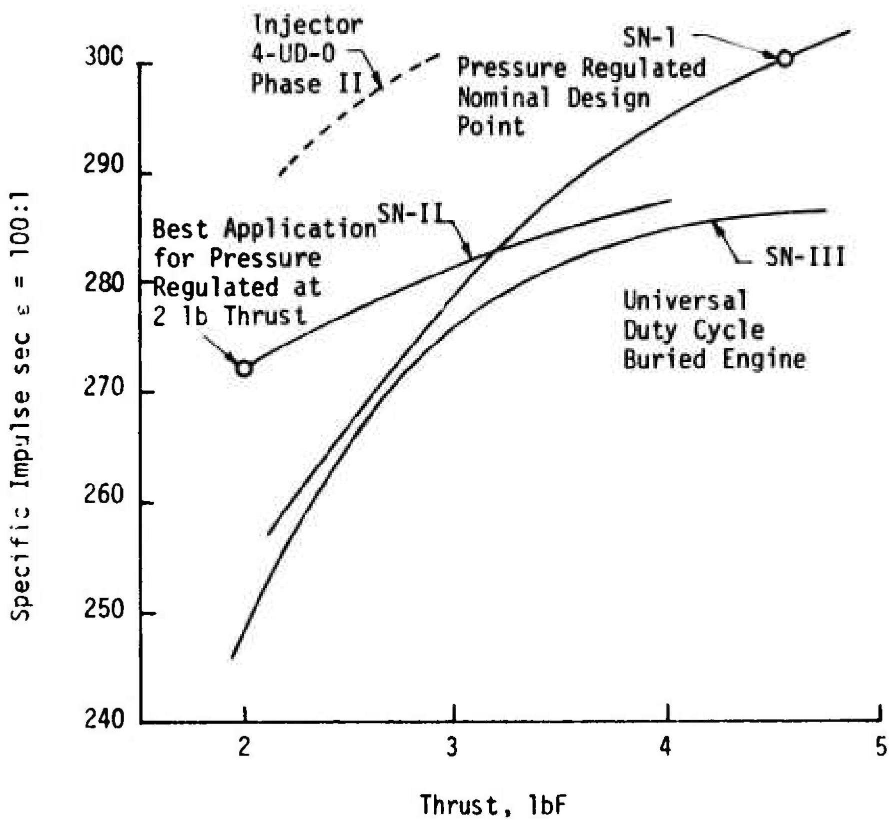

Figure 6.4-16. Comparison of Blowdown Performance Capability

TABLE 6.4-2

PULSE PERFORMANCE SUMMARY

Phase III Test Series QC-26-XXX

	Units																		
Test No.	-	196	195	192	194	193	200*	199*	206*	207*	216	215	214	217	228*	227*	226*	229*	225*
Injector	-	6-SP-45C, Engine SN 1 →									6-SP-OC, Engine SN 2 →								
L'	in.	2.0 →									2.0 →				1.75 →				
ϵ^{+}	-	45.3 →									43.6 →				50.6 →				
EPW	sec	0.010	0.010	0.025	0.050	0.100	0.025	0.100	0.025	0.025	0.010	0.010	0.025	0.100	0.010	0.025	0.100	0.010	0.100
Coast Time	sec	3.0	0.33	0.30	0.28	0.23	0.30	0.23	0.30	0.30	3.0	0.33	0.30	0.23	0.33	0.30	0.23	0.33	0.23
Steady State:																			
P_c	psia	150 →									125 →							75 →	
O/F	-	1.52	1.49	1.63	1.70	1.61	1.57	1.54	1.56	1.48	1.74	1.81	1.86	2.07	1.82	1.80	2.03	2.81	1.84
F_{vac} (ϵ)	lb_F	4.4 →									3.7 →								
T_{prop}	°F	Ambient →							19	123	Ambient →								
Cold Start:																			
Pulse Nos.	-	1-4	1-4	1-4	1-4	1-4	1-4	1-4	1-4	1-4	1-4	1-4	1-4	1-4	1-4	1-4	1-4	1-4	1-4
I_{Tot} (ϵ)$^{+}$	lb_F-sec	0.0383	0.0478	0.0851	0.2055	0.4222	0.103	0.3702	0.0851	0.1017	0.0303	0.0312	0.0852	0.3727	0.0299	0.0824	0.3611	0.0190	0.2024
I_{sp} (ϵ)	sec	184.1	191.1	226.5	249.0	267.4	239.2	260.9	214.3	245.8	167.3	167.4	209.1	260.0	164.6	212.5	253.9	153.6	204.2
I_{sp} (ϵ = 100)	sec	192.0	199.0	234.4	256.9	275.3	247.1	268.8	222.2	253.7	175.5	175.6	217.3	268.2	171.6	219.5	260.9	160.6	211.2
Hot Restart:																			
Pulse Nos	-	21-24	141-144	141-144	141-144	141-144	141-144	141-144	91-94	91-94	15-18	141-144	141-144	141-144	141-144	141-144	141-144	141-144	81-84
I_{Tot} (ϵ)	lb_F-sec	0.0424	0.0444	0.0947	0.2207	0.4408	0.1127	0.4429	0.1037	0.1077	0.0327	0.0381	0.0963	0.3956	0.0351	0.0907	0.3742	0.0200	0.2114
I_{sp} (ϵ)	sec	202.0	233.7	260.9	275.0	285.1	265.3	284.6	244.1	270.7	167.0	232.2	250.4	283.0	205.5	239.4	272.0	158.2	218.3
I_{sp} (ϵ = 100)	sec	209.9	241.6	268.8	282.9	293.0	274.1	292.5	252.0	278.6	175.2	240.4	258.6	291.2	212.5	246.4	279.0	165.2	225.3

*Post Demonstration Re-verification Tests.

$^{+}$(ϵ) Data at area ratio tested, as indicated [illegible] (Cont.)

	Units											
Test No.	-	173	172	171	170	[illegible]69	177*	175*	175*	174*	18[illegible]	183*
Injector	-	4-U[illegible]-28S, Engine SN 3 →										
L'	in.	1.7[illegible] →										
ε	-	51.3 →										
EPW	sec	0.010	0.010	0.025	0.050	0.100	0.010	0.025	0.050	0.0937	0.[illegible]25	0.025
Coast	sec	3.0	0.33	0.30	0.28	0.23	0.33	0.30	0.28	0.23	0.30	0.30
Steady State:												
P_c	psia	150 →										
O/F	-	1.59	1.53	1.63	1.65	1.62	1.47	1.55	1.59	1.58	1.57	1.58
F_{vac} (ε)	lb_F	4.4 →					4.2 →					
T_{prop}	°F	Ambient →									22	121
Cold Start:												
Pulse Nos.	-	1-4	1-4	1-4	1-4	2-5	2-5	2-5	2-5	2-5	2-5	1-4
I_{Tot} (ε)	lb_F-sec	0.0388	0.0385	0.0992	0.2025	0.4116	0.0394	0.1021	0.2055	0.4091	0.1012	0.1048
I_{sp} (ε)	sec	188.8	190.4	216.3	230.4	250.4	190.5	224.2	236.8	245.4	226.1	23[illegible].1
I_{sp} (100)	sec	195.8	197.4	223.3	237.4	257.4	197.5	231.2	243.8	252.4	233.1	24[illegible].1
Warm Restart:												
Pulse Nos.	-	15-18	110-113	101-104	119-123	108-111	133-142	133-142	133-142	133-142		
T_{wall}	°F	142	418	725	1300	1810	345	662	934	1190		
T_{inj}	°F	80	117	138	182	236	117	144	180	238		
I_{Tot} (ε)	lb_F-sec	0.0422	0.0413	0.1044	0.2100	0.4143	0.0423	0.1055	0.2103	0.4204		
I_{sp} (ε)	sec	203.6	207.2	242.1	251.7	262.6	206.3	2[illegible]7.2	249.5	260.6		
I_{sp} (100)	sec	210.6	2[illegible]4.2	249.1	258.[illegible]	269.[illegible]	21[illegible].3	2[illegible]4.2	256.5	267.6		
Hot Restart												
[illegible]ulse Nos.	-		133-142	133-142	13[illegible]	[illegible]33-[illegible]42	Post Demonstration Re-verification Tests conducted with Radiation Cooled Chamber as shown above.				97-100	97-100
T_{wall}	°F		433	890	14[illegible]0	1960						
T_{inj}	°F		[illegible]	[illegible]57	1[illegible]3						11[illegible]	200
I_{Tot} (ε)	lb_F-sec		[illegible]0414	0.[illegible]	0.[illegible]	[illegible]					0.[illegible]030	0.1082
I_{sp} (ε)	sec		[illegible]8	[illegible]	[illegible]	[illegible]					230.2	2[illegible]6.[illegible]
I_{sp} (100)	sec		[illegible]3	[illegible]	[illegible]	[illegible]					237.2	265.8

TABLE 6.4-3

PULSING PERFORMANCE, SPECIAL PMPM/CONTAM DUTY CYCLE

Phase III Test Series: PC-26-XXX

Test No.	-	201 →										213 →									
Injector	-	6-SP-45C Engine SN 1 →										6-SP-OC Engine SN 2 →									
L'	in.	2.0 →										2.0 →									
ε	-	45.3 →										43.6 →									
EPW	sec	.010	.010	.025	.050	.100	.100	.050	.025	.010	.010	.010	.010	.025	.050	.100	.100	.050	.025	.010	.010
Coast Time	sec	3.0	.33	.30	.28	.23	.23	.28	.30	.33	3.0	3.0	.33	.30	.28	.23	.23	.28	.30	.33	3.0
Steady State:																					
Pc	psia	125 →										125 →									
O/F	-	1.57 →										1.65 →									
F_{vac} (ε)	lb_f	4.4 →										3.7 →									
T_{prop}	°F	Ambient →										Ambient →									
Pulse Data:																					
Pulse Nos.	-	1-4	5-8	9-12	13-16	17-20	21-24	25-28	29-32	33-36	37-40	1-4	5-8	9-12	13-16	17-20	21-24	25-28	29-32	33-36	37-40
I_T (ε)	lb_f-sec	.0385	.0406	.1051	.2129	.4243	.4340	.2120	.1051	.0429	.0430	.0291	.0305	.0827	.1703	.3654	.3695	.1825	.0881	.0350	.0369
O/F_{Pulse}		1.29	1.34	1.42	1.42	1.43	1.46	1.42	1.45	1.38	1.22	1.48	1.62	1.63	1.64	1.66	1.66	1.66	1.65	1.69	1.42
Isp (ε)	sec	180.2	203.3	244.5	260.2	269.8	269.0	261.5	251.4	219.9	211.1	155.4	179.8	214.8	229.7	254.9	261.0	253.7	226.4	203.4	199.9
Isp (ε= 100)	sec	188.1	211.2	252.4	268.1	277.7	276.9	262.4	259.3	227.8	219.0	163.6	188.0	223.0	237.9	263.1	269.2	261.9	234.6	211.6	208.1
$T_{chamber}$	°F	80	130	180	280	450	730	925	920	940	940	-	-	-	-	-	-	-	-	-	-

6.4.3, Performance (cont.)

Figures 6.4-17 compares the specific impulse for the 3 engines as a function of pulse train length expressed as total impulse. The specific impulse in this figure is computed by dividing the total impulse for all pulses by the total propellant consumption. All performance values increase with pulse train length due to heating of the chamber which reduces losses caused by wall film at any total impulse value. The longer duration pulses provide higher performance due to a more favorable ratio of propellant through put to residual manifold volume. The longer burns also represent a higner percentage duty cycle which allows the chamber less time to cool down between pulses. This is illustrated by the 0.3 vs 3% duty cycle for 0.010 sec pulses.

The asympotic values of the specific impulse in long pulse trains rank in the same order as the steady state values: i.e., the highest performing steady state design is also the best pulsing design. The two engines containing the thin wall thermal liner (SN 1 and 3 approach their asympotic pulsing specific impulse much more rapidly than engines SN 2 which was tested without the liner. The thin liner allows the forward end to heat rapidly at first and suppresses the maximum temperature at later times by precluding axial conduction from the hot throat region. Thus, pulsing I_s for Engine SN 2 although rising slowly at first, eventually reaches a value closer to the steady firing condition.

Pulsing performance data for both cold start and hot restarts of Engine SN 1 (6-SP-45-C) are shown in Figure 6.4-18. For reference, the Phase II pulse data for the 6-SP-45-A engine is also indicated thereon. Phase III pulsing performance at minimum impulse is higher than the Phase II data and exceeds the goal of 240 sec at 0.05 lb-sec by a 6 sec margin. This is due to the reduced residual volumes which more than offsets the [illegible] reduction in chamber length. The slight reduction in performance ([illegible]) at larger impulse values reflects the reductions made at steady state to improve chamber wall cooling.

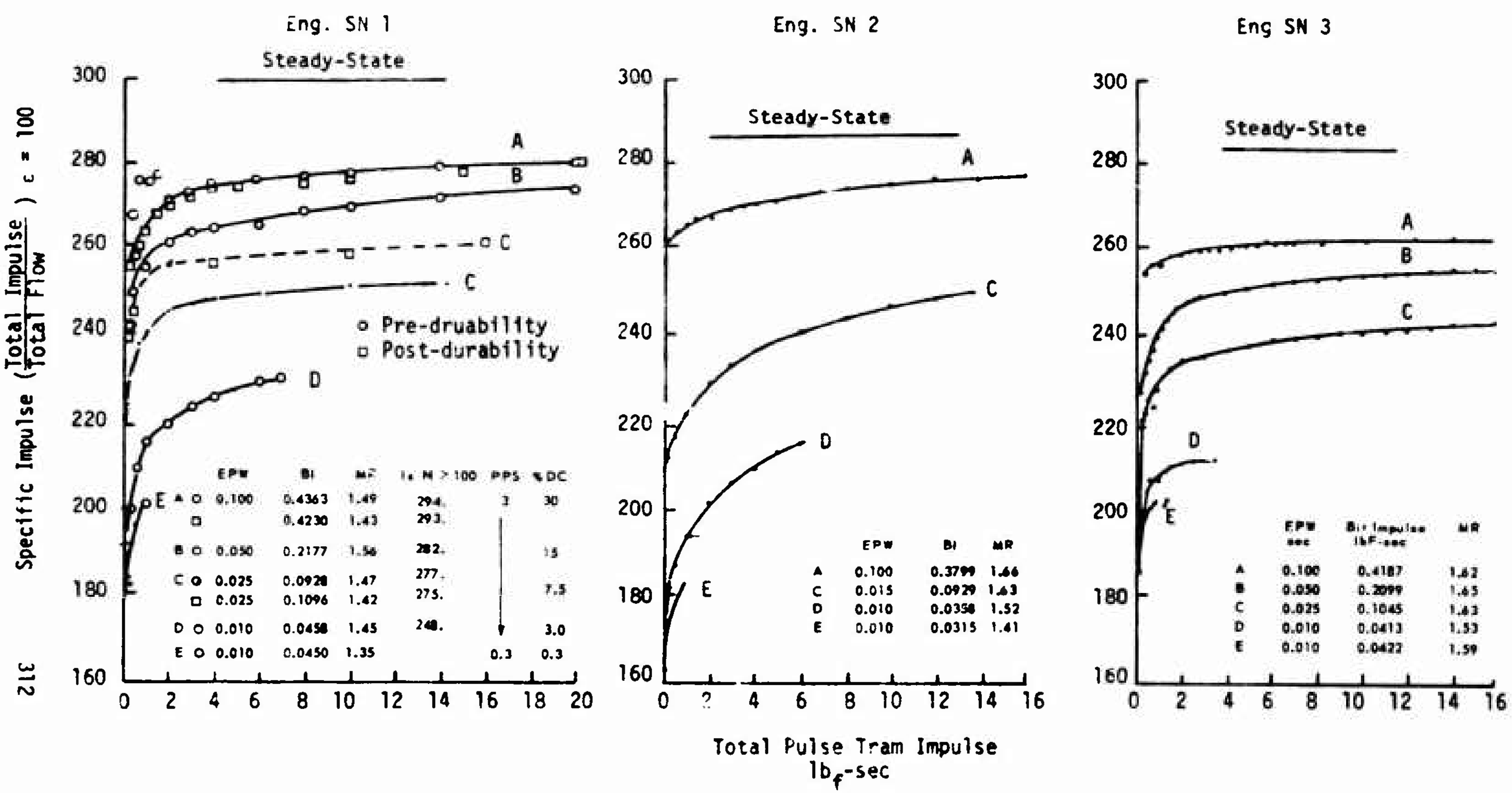

Figure 5.4-17. Short Pulse Train Performance

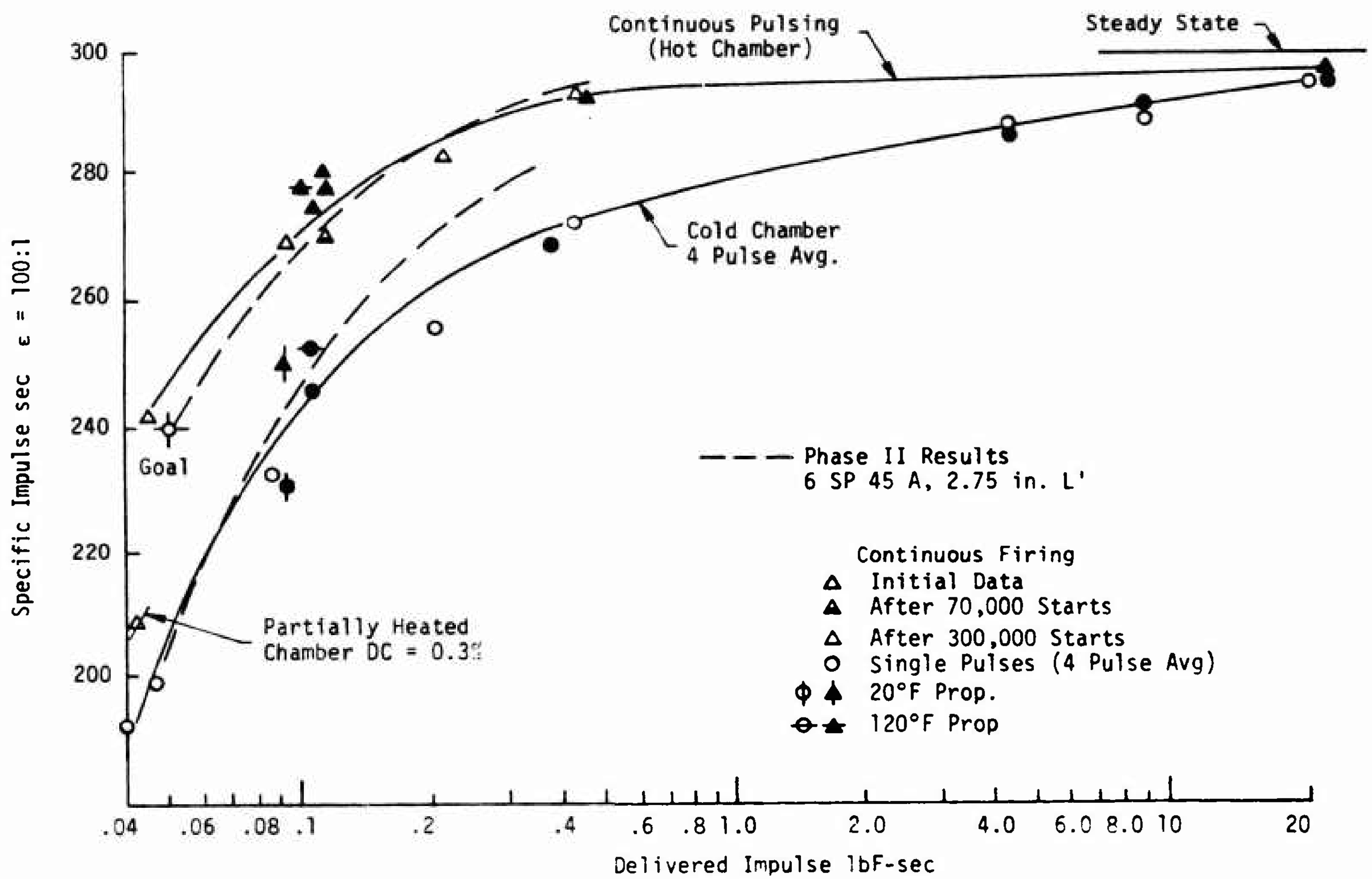

Figure 6.4-18. Engine SN 1 (Radiation Cooled-Regulated) Pulsing Performance Evaluation

6.4.3, Performance (cont.)

The single point at 0.043 lbf-sec bit-impulse and 209 sec pulse performance is an 0.3% duty cycle (0.010 sec on/ 3.0 sec coast) test which was summarized for pulse numbers 21-24 at which point the chamber wall was still cold. All other hot restart data points were summarized for pulse numbers 141-144 as indicated by Table 6.4-2. Thus, the limited pulses obtained at 0.3% duty cycle represent an intermediate wall temperature condition and its corresponding pulse performance is intermediate between the cold start and the hot equilibrium wall temperature condition. It was shown during Phase II testing (see Figure 5.3-20) that pulse performance is dependent upon wall temperature due to the wall film vaporization characteristics. For the 0.100 sec EPW (≈ 0.4 lbf-sec impulse), the cold restart data for pulse numbers 1-4 are ≈ 3% lower than the Phase II data. This difference is due to a combination of shorter chamber length, and the more compatible injector pattern of the 6-SP-45-C which results in lower chamber wall temperature rise rates.

Pulsing performance of Engine SN 2 is shown on Figure 6.4-19 at 3.8 lbf and at a blowdown thrust of 2.2 lbf. Both cold start and hot restart Phase III data are indicated thereon as well as the Phase II data at maximum (5.0 lbf) thrust. The lower Phase III pulsing performance can again be attributed to a reduction of chamber length from 2.75-in. to 2.0-in. There was no change in performance throughout the 50,000 firing qualification test series. This engine provides a 245 pulsing specific impulse at 0.05 lbF-sec which is 5 sec over the contract goal.

Engine SN 2 was re-evaluated in a 1.75-in. length chamber which showed a further pulsing performance reduction due to length change. At the minimum blowdown thrust, the 6-SP-0-C injector/1.75 in. cylindrical chamber was tested to a minimum bit impulse of 0.018 lbf-sec. This is significantly lower than the contract goal minimum bit impulse of 0.05 lbf-sec. At the 0.02 lbf-sec impulse level, the cold start and hot restart pulse

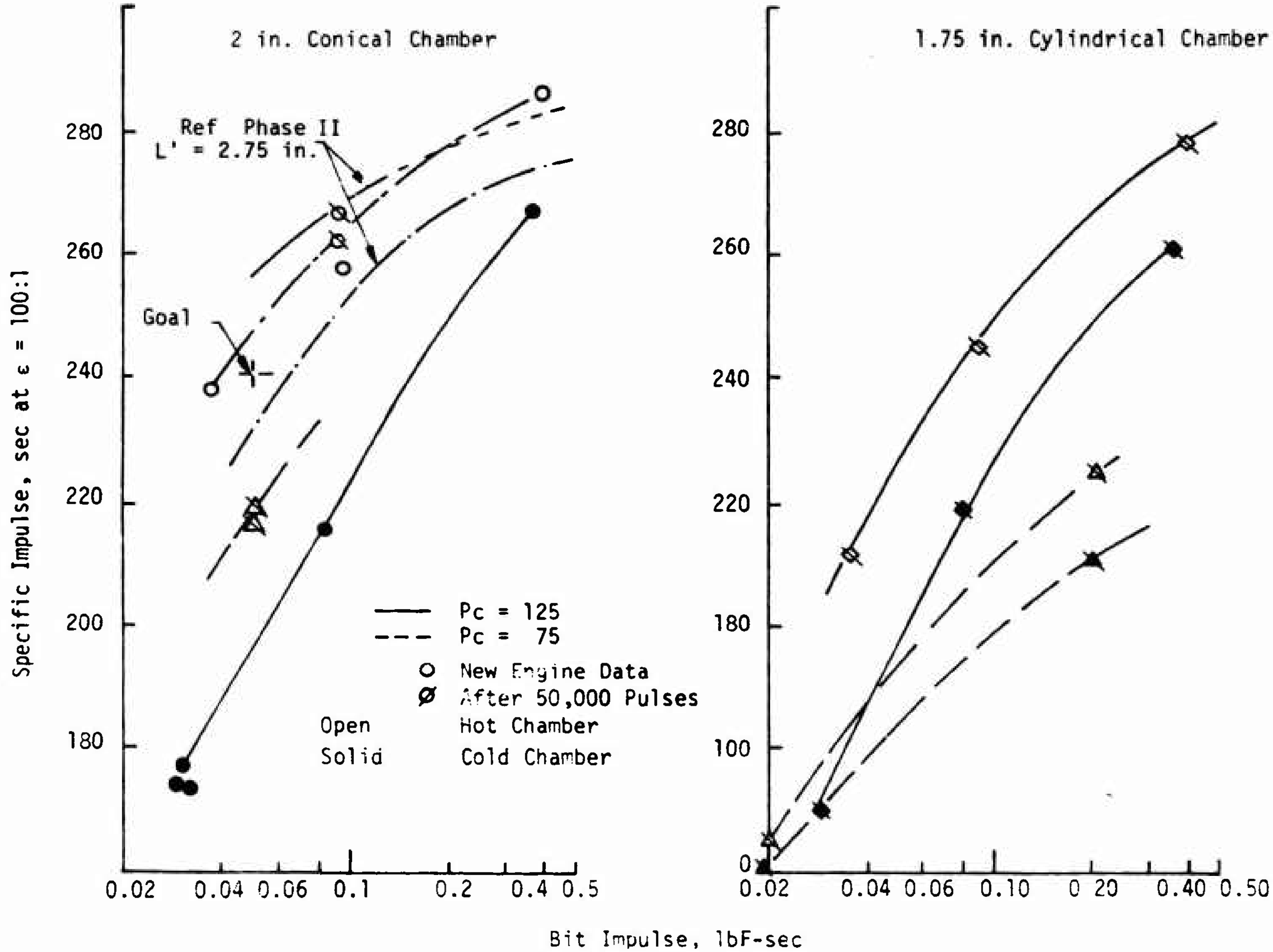

Figure 6.4-19. Engine SN 2 Pulsing Performance (Injector 6-SP-0-C)

6.4.3, Performance (cont.)

performances were 161 sec and 165 sec I_{sp}, respectively. The latter value corresponds to a chamber wall temperature of only 350°F and still rising with each pulse. Pulse trains longer than 150 pulses would result in improved performances. The use of the 2 in. conical chamber design would also be expected to result in an improvement in pulsing performance. At the longer EPW's the pulsing performance asympotically appears to be approaching the steady state blowdown I_{sp} = 274 sec.

The pulsing performance of Engine SN 3 (4-UD-28-S) is shown in Figure 6.4-20 at 4.4 lbf thrust. All data were obtained in the 1.75-in. length chamber. Prior to the engine life demonstration test series, the 4-UD-28-S engine was pulse tested in an insulated adiabatic chamber. After 50,000 demonstration firings, the insulation was removed for hardware inspection. The pulse verification tests were repeated with the chamber being radiation cooled. The radiation cooled chamber pulse performance was 1 to 2% lower in I_{sp} as noted in Figure 6.4-20 for the hot restarts. No change was evident for the cold starts. To verify that the pulse performance reduction was due to the cooler injector and chamber operating temperatures rather than due to an engine degradation resulting from the 50,000 firings, an earlier pulse sequence was evaluated in the predemonstration (adiabatic engine) tests when the injector and chamber wall temperatures were more nearly equal to the final radiation cooled temperatures. These data are provided in Table 6.4-2 under the designation "warm restarts". It can readily be seen that the pre-demonstration and post-demonstration pulse performances are equivalent when performance is evaluated at comparable temperatures. It was thus verified that the 50,000 demonstration firings produced no degradation upon engine performance. The buried design tested provided a 223 sec specific impulse at 0.05 lbf-sec. This could have been increased to 227 if the lower volume Phase III valve manifold plate had been employed. The difference between the insulated and exposed chamber is 4 sec.

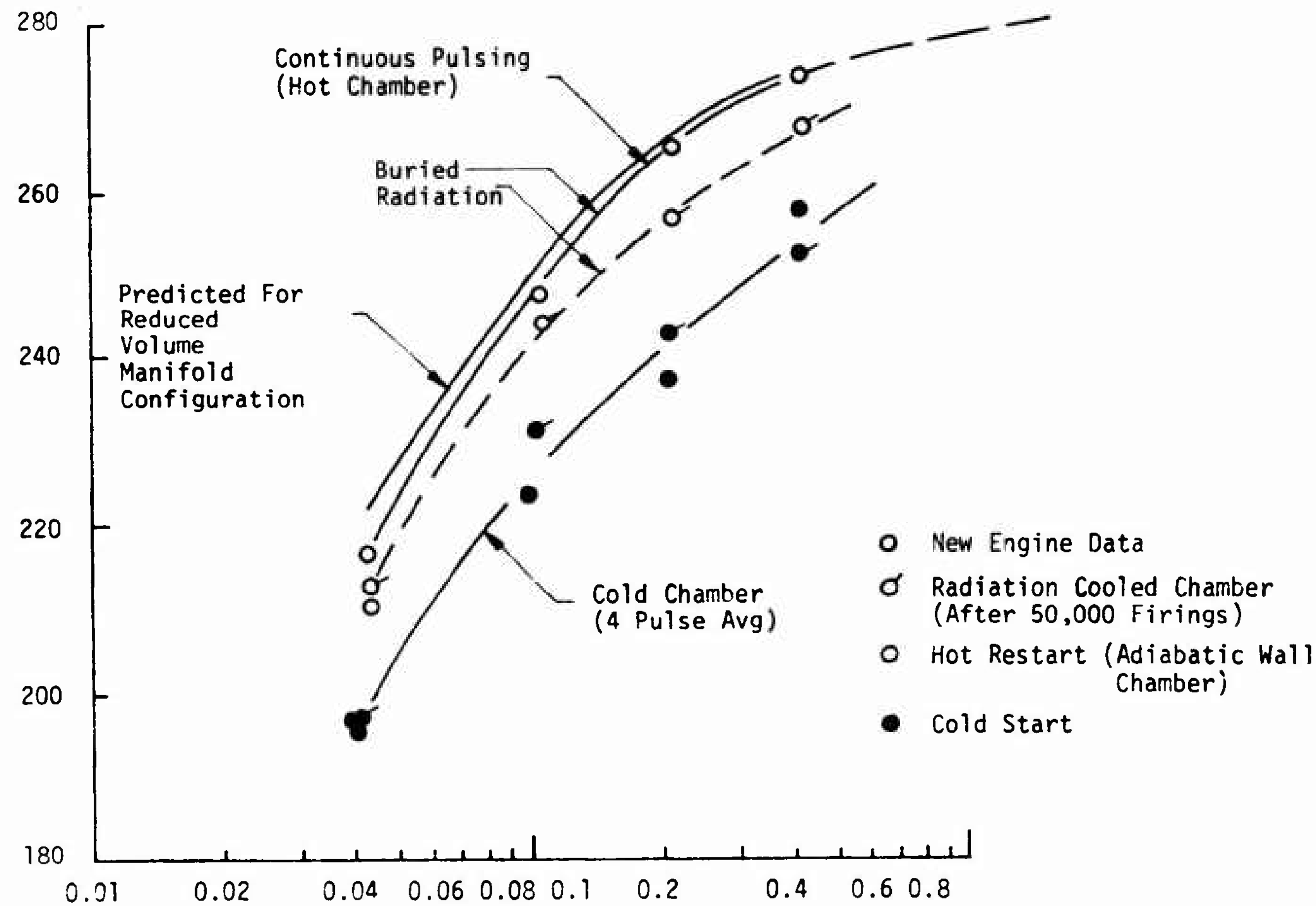

Figure 6.4-20. Engine SN 3 Pulsing Performance (Injector 4-UD-28-S)

6.4.3, Performance (cont.)

Pulsing performance results with the SN 1 (6-SP-45-C) and SN 2 (6-SP-0C) engines in the special duty cycle are described further in Section 6.5. Figure 6.4-21 provides a comparison of the 3 Phase III engines pulsed and the Phase II design having the highest pulsing performance but no capability for steady state firing at full thrust. The specific impulse at a bit impulse of 0.05 sec are summarized as follows:

	Injector	Hot Chamber	Cold Chamber
Engine SN 1	6-SP-45-C	246	205
2	6-SP-0-C	245	197
3	4-UD-28SC	227	209
Best of Phase II	4-UD-0	257	235

The contract specifications state that the 5-lbf bipropellant engine must be capable of operating over a 20 to 120°F propellant inlet temperature range. Verification testing was conducted throughout this operating range. The Phase I analytical study indicated that variable propellant inlet temperature would have little effect upon steady state operation, but a highly sensitive effect upon pulsing performance. Therefore, Engines SN 1 and 3 were tested at the extreme inlet temperatures at 0.025 sec EPW as shown in Figure 6.4-22. In general, pulsing performance increased linearly with hotter propellants. The magnitude of the performance increase was on the order of + 30 sec I_{sp} per 100°F at the 0.025 sec EPW.

The physical mechanism for the above temperature dependence can be explained by the CONTAM model. The postfire injector dribble volume expulsion rate is controlled by the propellant vapor pressure. Hotter propellants result in higher pressure which result in faster manifold expulsion and consequently higher combustion efficiency during the transient. Similarly, the hot restart performance is higher because hotter injector face/manifold temperatures increase propellant expulsion rate. Besides the injector temperature dependence, the chamber wall temperature is also affected by

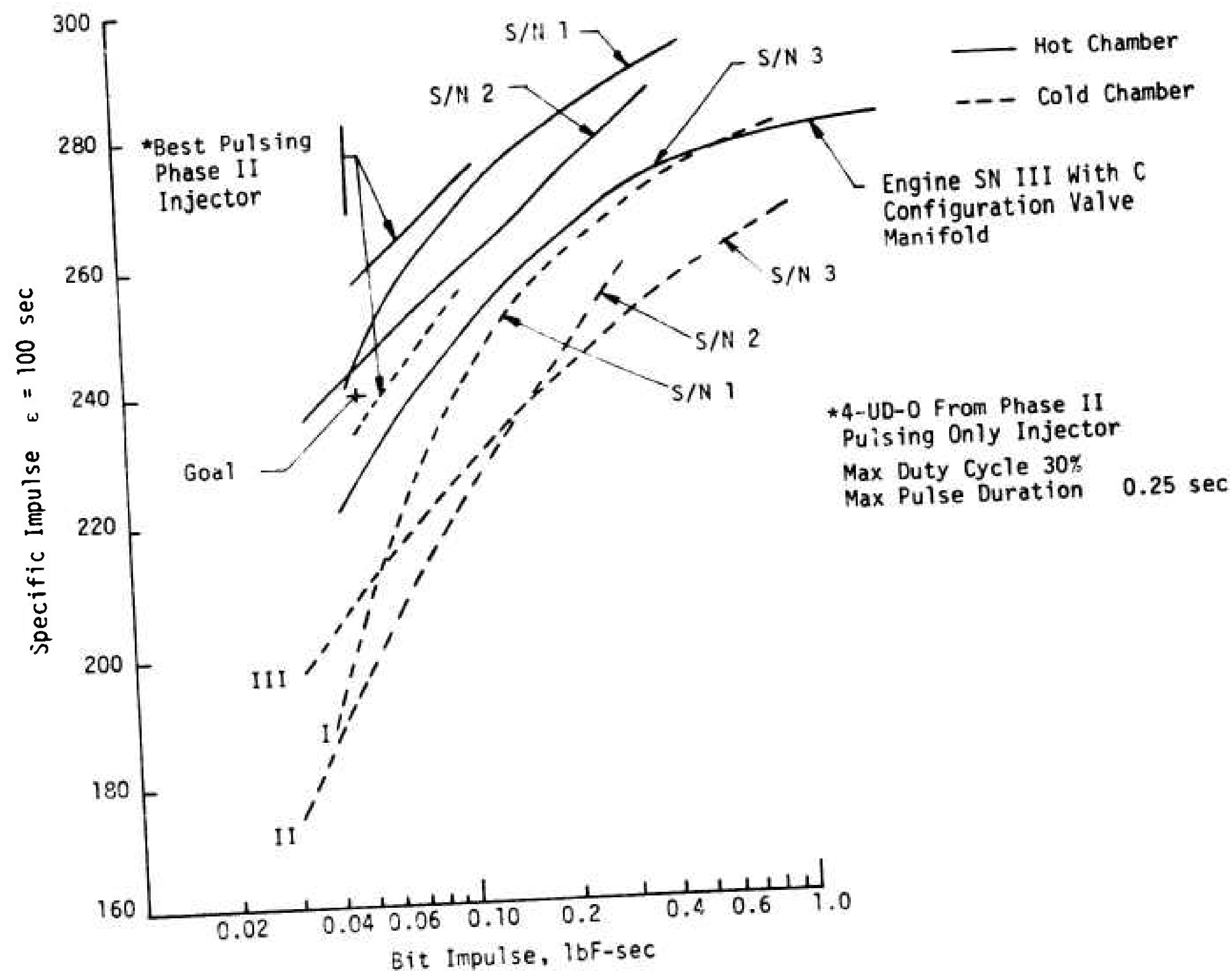

Figure 6.4-21. Comparison of Pulse Mode Specific Impulse

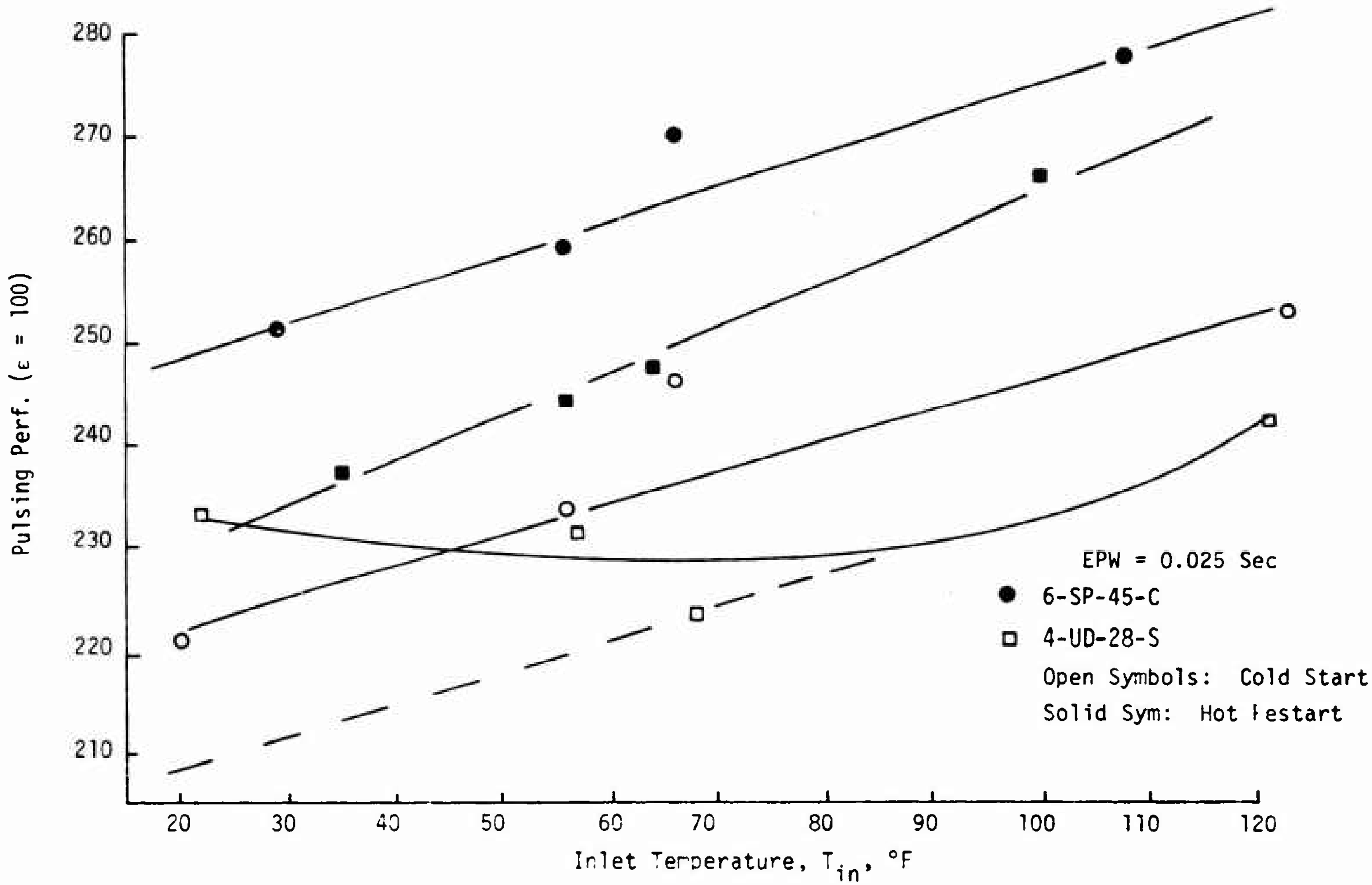

Figure 6.4-22. Propellant Inlet Temperature Effect on 0.025 sec Duration Pulse Pulse

the propellant inlet temperature because of the heat conduction in the small engine size. The chamber wall temperature has a first order effect upon the transient wall film vaporization efficiency.

To summarize, the pulsing performance is related to the following three inter-related parameters.

(1) Chamber pressure or engine thrust
(2) Electrical Pulse Width (EPW) or bit impulse
(3) Chamber wall, injector manifold, and propellant inlet temperature

Pulse performance is highest at high P_c or high engine thrust because this condition has the highest steady state performance.

Long EPW or large bit impulse improves pulsing performance because the low transient combustion performance associated with the injector manifold dribble volume is "amortized" by a more heavily weighted higher steady state performance.

Hotter temperatures result in more rapid postfire dribble volume expulsion and more efficient transient combustion.

6.4.3.4 Performance Summary and Conclusions

A significant advancement in the state-of-the-art has been demonstrated for 5 lbf-bipropellant engine technology. Prior small thruster engine development efforts have depended heavily upon trial and error techniques to arrive at an engine configuration. By comparison with the earlier bipropellant engines available within the industry[15], the engines developed on this contract have demonstrated higher steady state performance, higher transient pulse performance, repeatable small impulse bits. better chamber thermal compatibility, and extensive engine life cycle capability.

(15) Rollbuhler, R. J., Experimental Investigation of Reaction Control, Storable Bipropellant Thrusters NASA TN D 4416, April 1968

6.4.3, Performance (cont.)

The achievements on this contract were made possible by the judicious application of available analytical models throughout the Phase I analytical design study, Phase II verification testing, and Phase III demonstration testing. Primary engine operational and performance requirements were identified from the contract statement-of-work. These contract goals were then translated into the required engine design parameters.

The JANNAF performance methodology[16] had previously been applied only to larger thrust engines. It specifically absolved itself of applicability to engines of less than 100 lbf thrust. ALRC was aware of the stated model limitations but used them for lack of an alternative design criteria applicable to the 5 lbf bipropellant engine. It was understood in undertaking the Phase I design analysis, that the JANNAF models would be used for engine optimization and identification of design trends. These analyses were calibrated for numerical accuracy using the Phase II and Phase III test data at area ratios of 1.6:1 and 50:1 and found to be reasonably accurate (within $\approx$ 1%). The single parameter missing from the JANNAF methodology was the wall film losses. These were accommodated by including wall film as part of energy release efficiency.

The modified Priem propellant vaporization model was utilized extensively with the ALRC analytical/empirical drop size correlation extended to include micro-orifice platelet elements to analytically predict engine combustion efficiency. The number and type of injection elements, injector pattern layout, chamber length and diameter were analytically optimized to deliver the 300 sec I_{sp} steady state performance goal.

(16) J. L. Pieper, "ICRPG Liquid Propellant Thrust Chamber Performance Evaluation Manual", CPIA No. 178, September 1968.

6.4.3, Performance (cont.)

After having designed for steady state performance, the CONTAM (Reference 2) computer model was utilized to evaluate transient pulsing performance. Engine design parameters were selected to optimize transient performance as well as steady state performance within the extremes of the required engine operational specifications. Due to the diversity of specific requirements of various potential 5 lbf bipropellant engine users, three separate engine point designs were analytically synthesized for development from the engine requirements.

The Phase II verification test data verified the validity Phase I analyses by exceeding the performance goals. This was achieved, however, at the cost of chamber wall temperatures some what in excess of 3000°F implying limited life cycle capability for Phase III demonstration. Fortified by Phase II experimental performance and thermal test data, the analytical models were further calibrated and appropriate design modifications were incorporated to improve thermal compatibility necessary to achieve engine life cycle requirements with minimum sacrifice of engine performance.

Phase III testing has verified that the above objectives have been satisfied and all three engines have demonstrated their respective pulsing life cycle goals.

Near the end of this contract an add-on study was included to compare the Pulse Mode Performance Model (Reference 3) (PMPM) and CONTAM model against the engine pulse data to evaluate their applicability as transient engine performance models and analytical engine design tools. The results of this study are presented in Section 6.5.

6.4, Test Data Evaluation (cont.)

6.4.4 Thermal Data Evaluation

Extensive thermal instrumentation of critical engine components provided the means of predicting the duty cycle and ultimate life capabilities of those components normally subject to overheating or failure due to thermal cycling. Instrumentation available for this purpose includes the following:

Valve body temperature	TVB
Valve manifold temperature	TVM
Thermal shunt temperatures	TSH1, TSH2
4-10 chamber and nozzle	See Figure 6.2-3

Figure 6.2-2 shows a typical instrumented columbium chamber.

6.4.4.1 Steady State and Blowdown Thermal Characteristics

Engine temperatures at various operating pressures and mixture ratios were evaluated from direct measurements made in long duration firings such as the 6301 sec test shown in Figure 6.3-14, or by extrapolation of transient temperature measurements from 15 to 20 sec burns shown in Figures 6.4-23 and 6.4-24. Extrapolation of chamber/nozzle transient data are felt to be reasonably accurate since the engine temperatures are very close to the maximum values at the end of 15 sec and were confirmed by the longer duration tests. Figure 6.4-24 shows the valve body and thermal shunt temperatures to still be rising after 20 sec and thus steady state data for these components are quoted only from the very long duration tests when equilibrium conditions are reached.

The data, shown in Figure 6.4-23 are for the radiation cooled engine. The designations, L&R, are thermocouples located on the left (L) and right (R) side of the nozzle at the same axial station. All of the

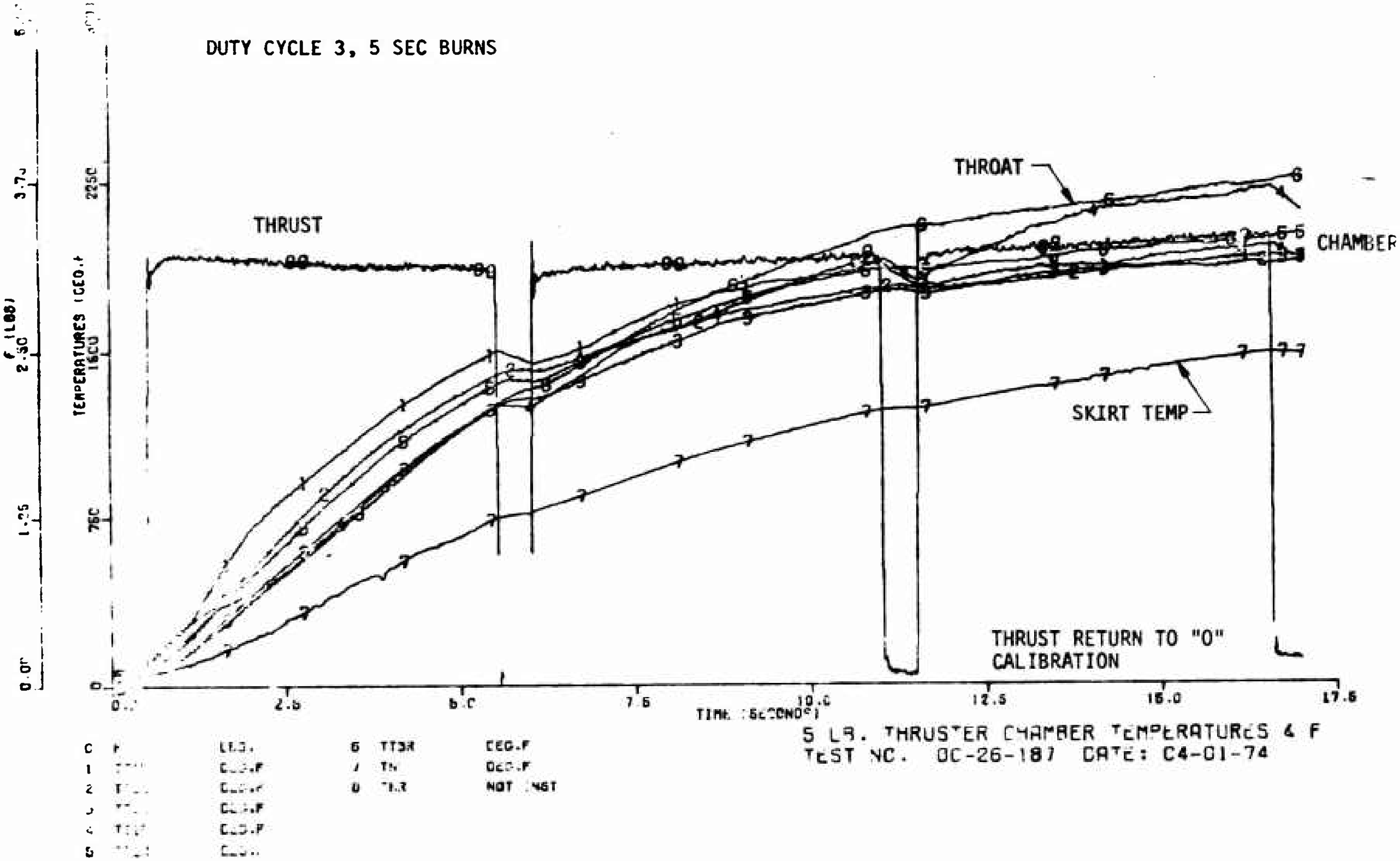

Figure 6.4-23. Typical Engine Temperatures, SN 1 Radiation Cooled (P_c = 115, MR = .155)

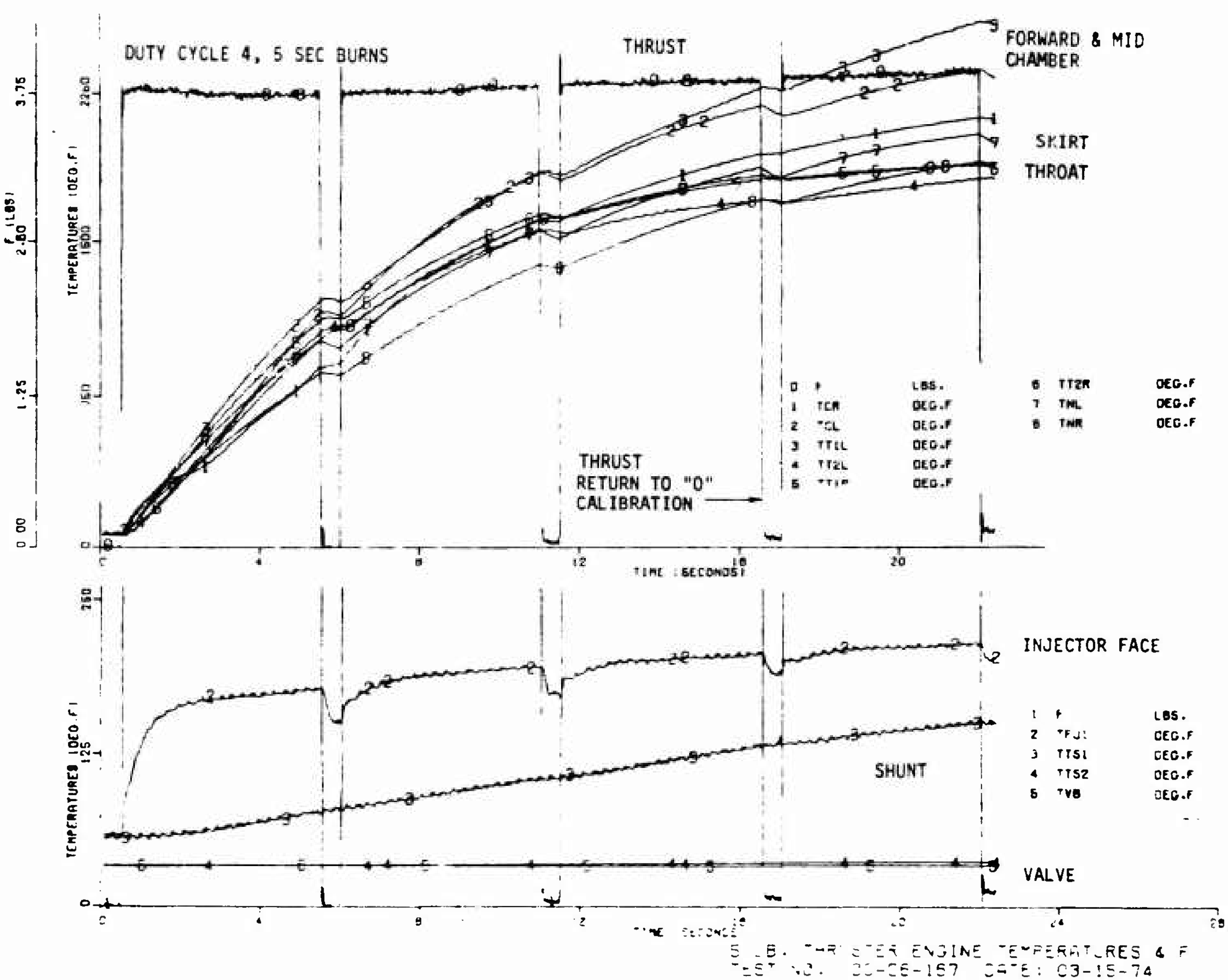

Figure 6.4-24. Typical Engine Temperatures, SN 3 Buried Nozzle (P_c = 150, MR = 1.61)

data for the chamber and throat region are noted to fall within a narrow band indicating a uniform thermal environment and reliable measurements. TNL is a single temperature at area ratio 30 in the skirt where radiation cooling is much more efficient. TNL and TNR, for the buried engine, are shown in Figure 6.4-24 and are seen to be much closer to the chamber temperature.

One phenomena noted in testing with the tungsten-rhenium type thermocouples is that as the junction starts to fail with age, temperatures tend to drift higher, often reaching fictiously high values (4000-5000°F) before opening completely. This tends to lead to conservatism in both testing and data evaluation and often to needless alarm. This could be typically represented by TT3R (Parameter 6) in Figure 6.4-23.

Figures 6.4-25, -26, and -27 provide the steady state axial temperature profiles over a range of chamber pressures for each of the engines tested. Valve body, manifold, flange and thermal shunt temperatures are provided where steady state was attained.

The large axial temperature gradients between the relatively cold flange and the hot first thermocouple station at 0.9 in. is developed by use of the chamber liner, thermal dam, and shunt as predicted in Figure 6.1-7. The temperatures of the shunt and valve manifold were obtained from the 283 sec firing at maximum chamber pressure. The maximum temperatures @ 3300°F, are found about 1-1/4 in. from the injector as determined by the chamber heat markings. These temperatures are about 300°F higher than predicted in the Phase I analyses for a 97% energy release efficiency engine with "0"% barrier cooling. These thermal conditions correspond to a specific impulse of 300 sec. A slight decrease in chamber pressure is noted to make a substantial difference in the thermal profiles. This dramatic difference is believed to result from a change in the bipropellant reaction mechanism from blow-apart at the 3 lower pressures to spray penetration at the 125 psia level. This is supported by the mixture ratio effects insert provided. Increasing MR

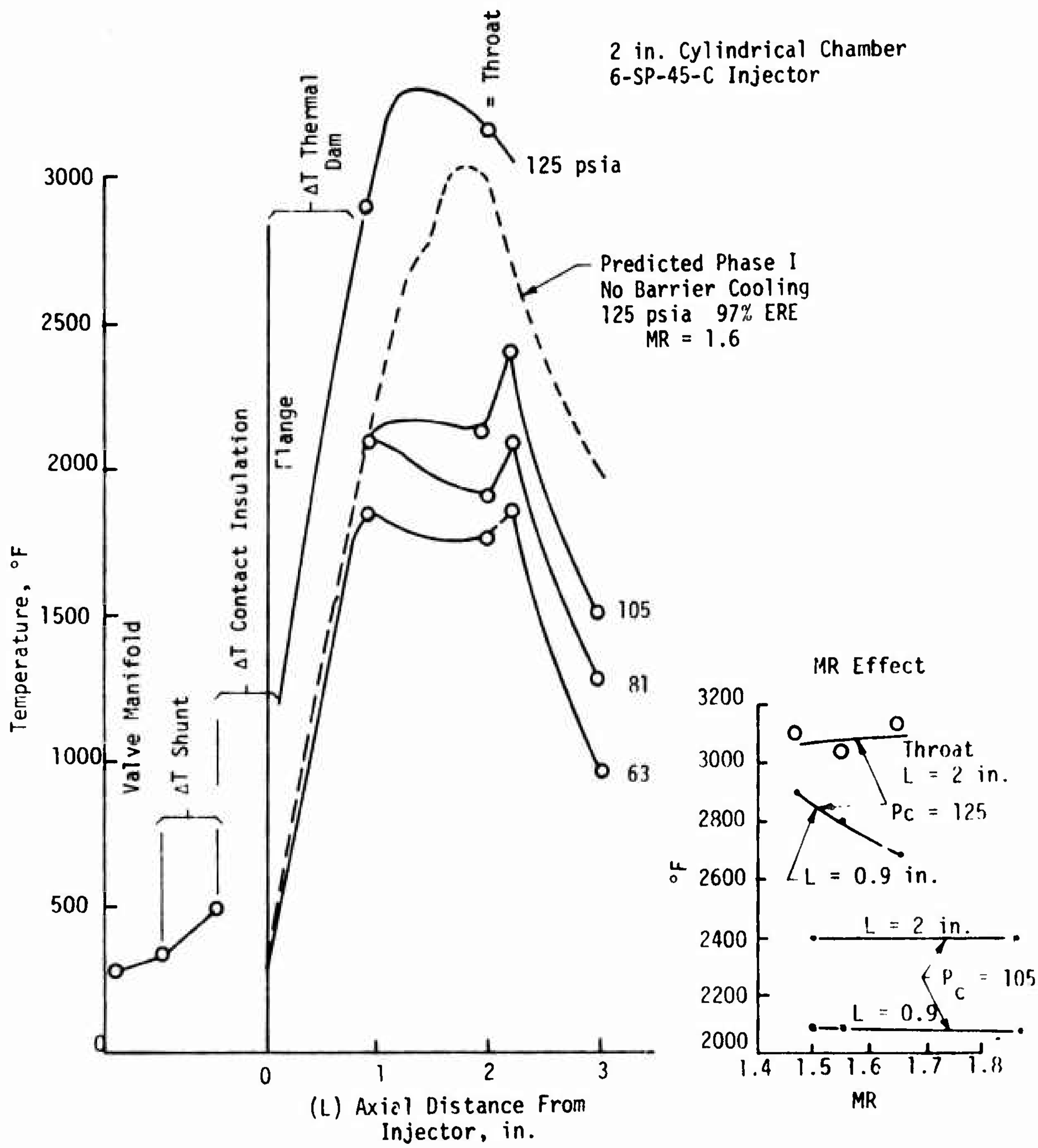

Figure 6.4-25. Axial Temperature Profile, Engine SN 1 Radiation Cooled

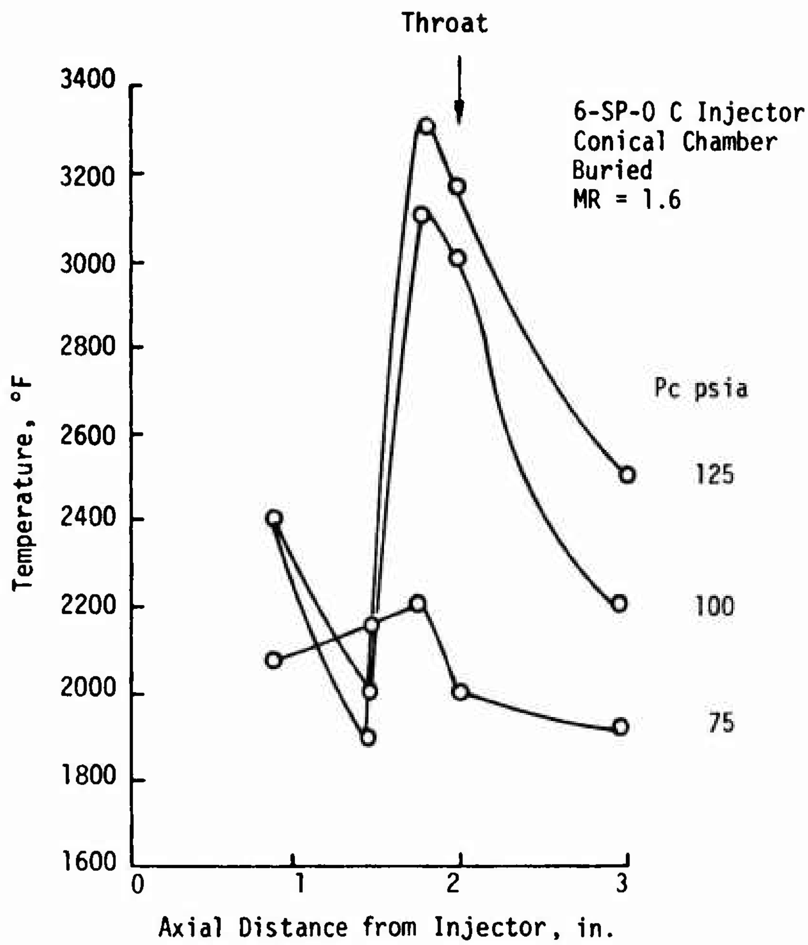

Figure 6.4-26. Axial Chamber Profiles, Engine SN 2

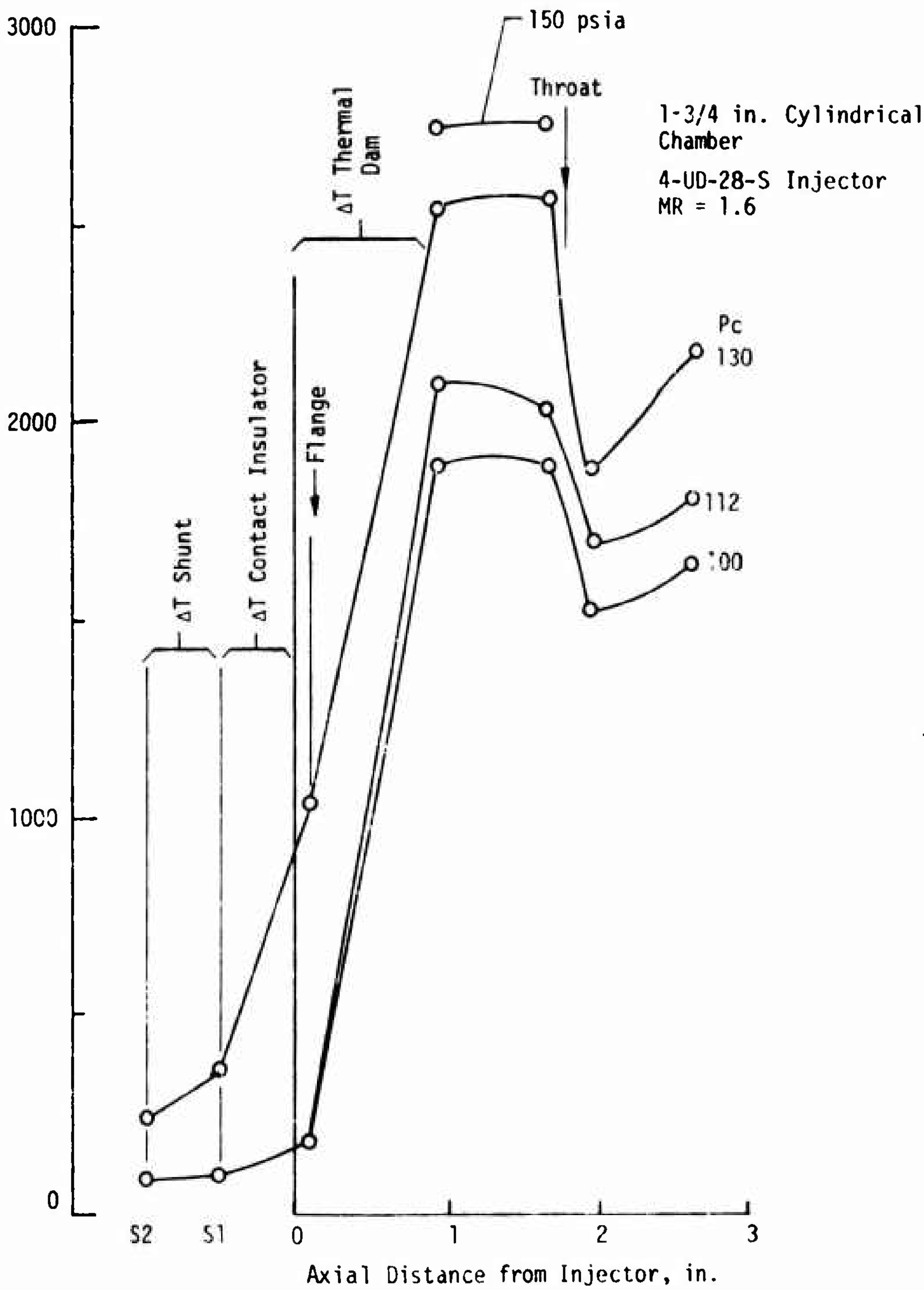

Figure 6.4-27. Axial Temperature Profiles, Engine SN 3
Buried Operation

at high pressure is noted to result in a reduction of temperature in the forward chamber region indicating the oxidizer to be passing through the fuel and cooling the wall. At lower pressures, the forward chamber region is at the fuel monopropellant temperature at all mixture ratios, indicating the fuel is being thrown back on the wall. This fuel then carries on out also cooling tne throat. The drop in temperature in the convergent nozzle (1.94 in., see Figure 6.2-3) is due to impingement of the nonvaporized portion of the fuel. The subsequent temperature rise is due to mixing and reaction of the vapors passing through the throat. This phenomenon is not noted at the high flow condition because of the oxidizer rich environment near the wall.

A similar effect is noted on Engine SN 2 in Figure 6.4-26. The latter skirt temperatures are hotter because the engine is buried and cannot radiate. This may be aggravated by a trip of the laminar boundary layer in the throat region.

The steady state temperature from the 6301 sec burn of Engine SN 3 (buried) are shown in Figure 6.3-14. The combustion mechanism is different for the SN 3 injector design in that a portion of the fuel from each injection orifice is impinged directly upon the wall and the oxidizer spray is axial rather than outboard toward the fuel. Thus, no marked change in compatability should be expected as a result of a change from blow apart to spray penetration. The rapid drop in temperature downstream of the throat on this design is believed to be the result of the sudden expansion and flow acceleration of fuel rich vapors near the chamber wall which would reduce the adiabatic wall temperature. The subsequent downstream temperature rise is a result of mixing of the hot core gas with the fuel rich barrier.

Figure 6.4-28 shows parametric plots of maximum wall temperature vs chamber pressure and maximum wall temperature vs steady state specific impulse for each of the three engines. The conclusions drawn from this figure are as follows:

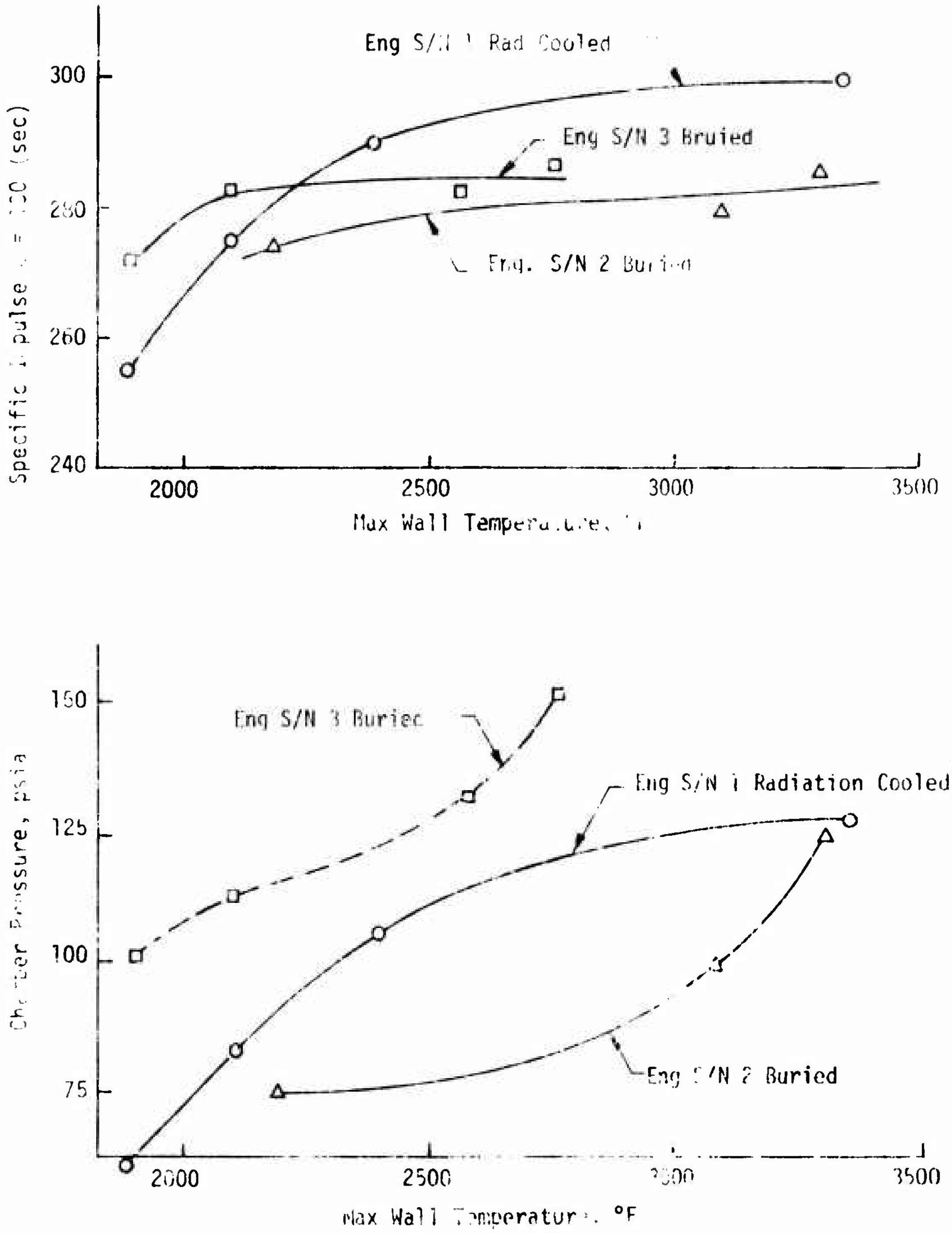

Figure 6.4-28. Maximum Nozzle Temperature Versus Specific Impulse and Chamber Pressure

6.4.4, Thermal Data Evaluation (cont.)

(1) An engine which provides a 300 sec specific impulse will require a chamber material which can operate at 3300°F if long duration firings are required. Multiple firings from 30-60 seconds can be attained when chambers operate as heat sink with sufficient cooldown periods between burns (Engine SN 1).

(2) A radiation cooled engine which operates at 2600°F and has no burn time or duty cycle limitations can provide a specific impulse of 295 sec (Engine SN 1).

(3) A buried engine which operates at 2600°F and has no burn time or duty cycle limitation can provide a specific impulse of 283 sec (Engine SN 3).

(4) The relationship between performance and wall temperature at a given thrust level is mainly a function of the injector design.

(5) The 4-UD-28-S injector design providing barrier cooling results in maximum chamber wall temperatures which are less sensitive to chamber pressure than the designs optimized for complete propellant reaction.

Figure 6.4-29 shows the injector face temperature for Engine SN 3 vs time and chamber pressure as parameters. Injector temperatures are noted to approach their steady state values within the first several seconds of firing, thus allowing an accurate assessment by direct measurement in firings lasting longer than ≈ 5 sec. A significant increase in face temperature is noted when chamber pressure is increased beyond 150 psia. The desire to limit heat input to the valve influenced the selection of 150 psia as the maximum chamber pressure for sustained firing for this engine. The resulting injector temperature of ≈ 250°F is compatible with virtually unlimited firing duration and thermal cycling. The injector temperature in

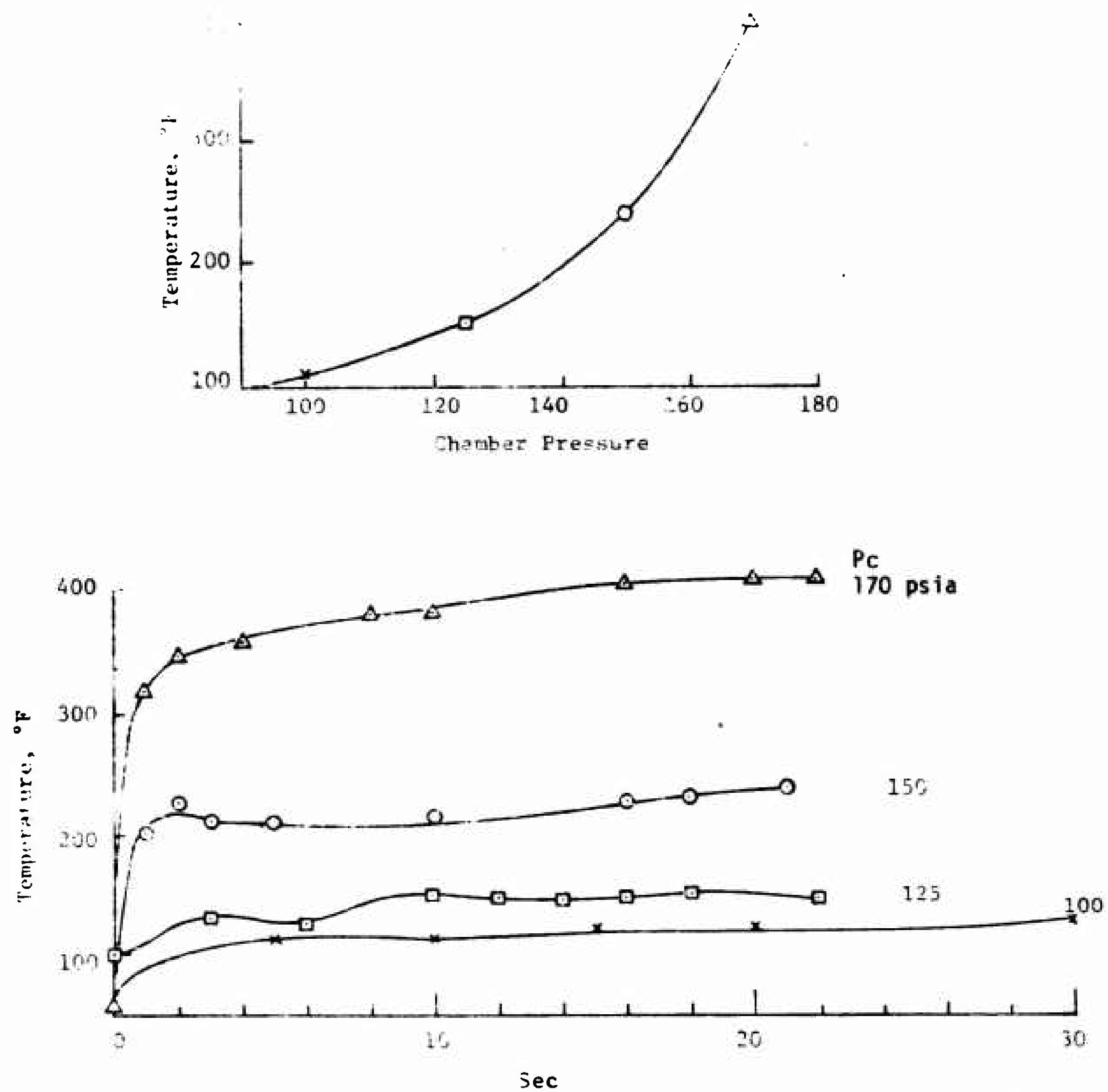

Figure 6.4-29. Injector Face Temperature, Engine S/N 3

6.4.4, Thermal Data Evaluation (cont.)

the 1 hour and 45 minute steady burn reached a maximum value of 270°F and 290°F in the 5 hour 50,000 pulse duty cycle.

The injectors of the SN 1 and 2 Phase III engines were not instrumented. Temperatures from these must be quoted from the Phase II measurements as follows:

Engine 1	6-SP-45	<220°F
Engine 2	6-SP-0	≈150°F

which indicates a very conservative design. The Phase III injectors actually should be slightly cooler than the above due to the smaller head end chamber diameter effect shown in Figure 6.1-8.

6.4.4.2 Thermal Characteristics - Pulsing

The pulsing thermal characteristics of each engine were evaluated by firing trains of pulses of sufficient length to allow all critical engine components to attain a condition of thermal equilibrium. These were conducted at the highest operating pressure which is the most adverse operating condition and over duty cycles (DC) ranging from 0.3 to 30% where

$$DC = \frac{\text{fire period}}{\text{fire period + coast period}} \times 100$$

Figure 6.4-30 through 6.4-33 provide representative data for the following measured parameters.

TfJ	Injector face temperature
TVM	Valve manifold temperature
TTS1 and 2	Thermal shunt temperatures
TVB	Valve body temperatures

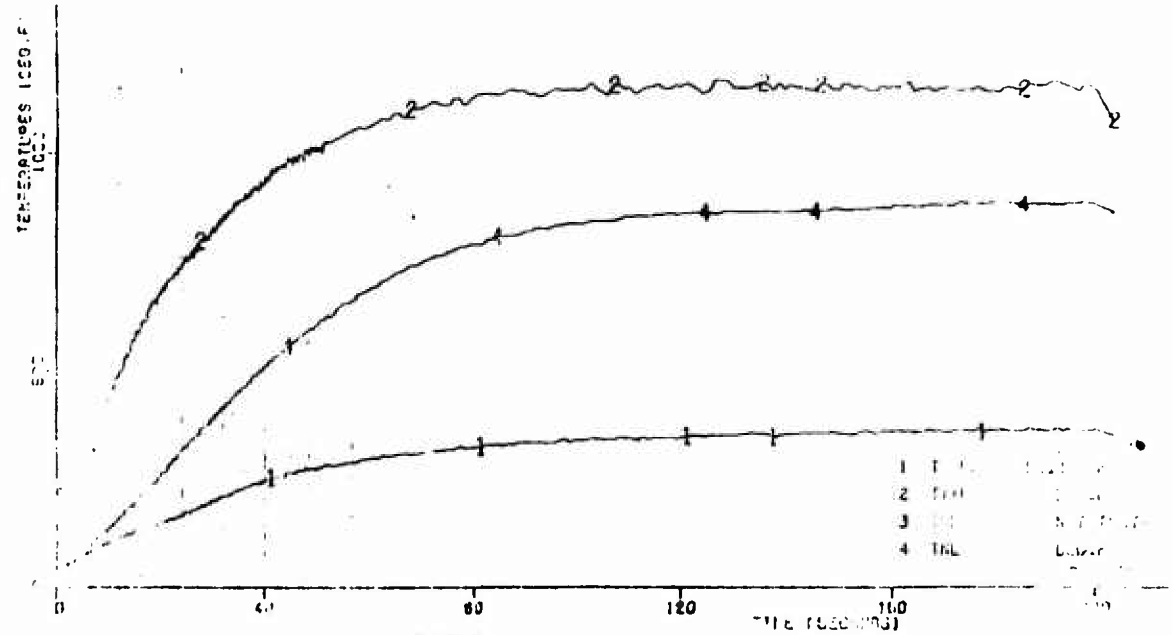

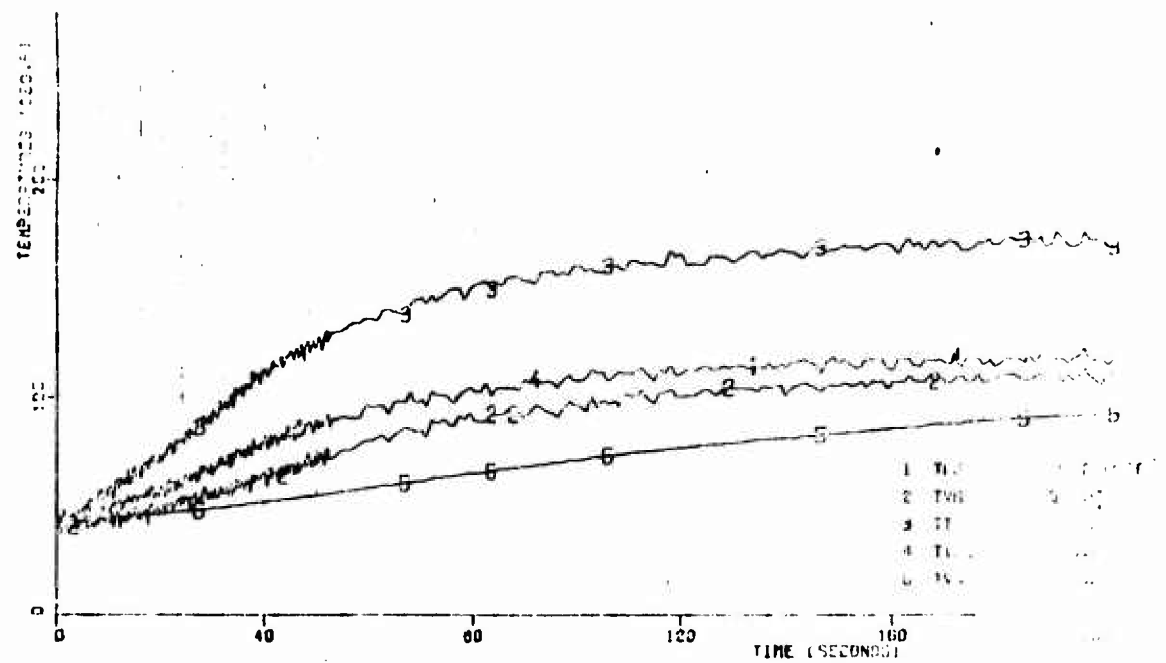

Figure 6.4-30. Radiation Cooled Engine Temperatures, 7.7% Duty Cycle, (S/N 1, P_c = 125 psia)

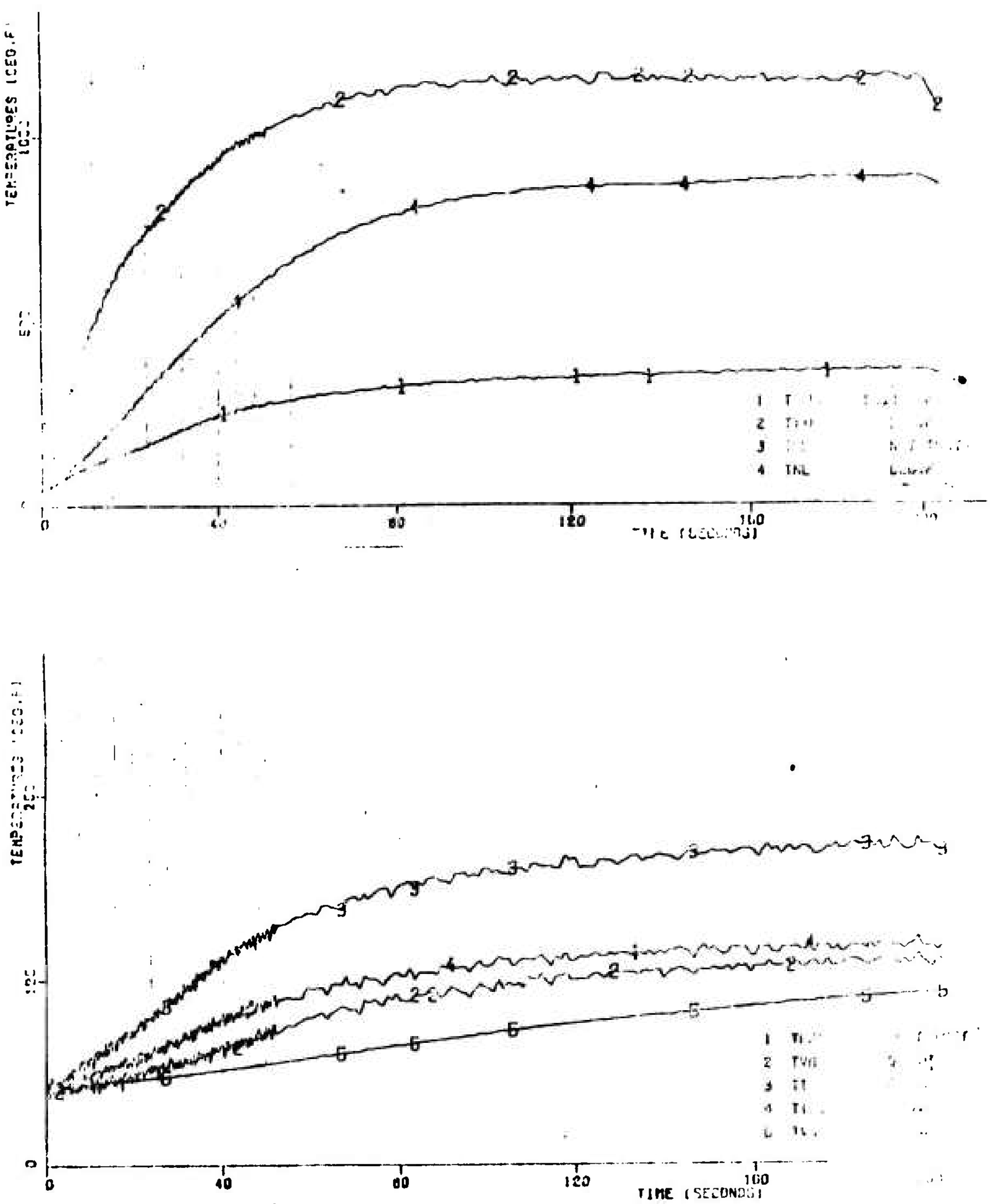

Figure 6.4-30. Radiation Cooled Engine Temperatures, 7.7% Duty Cycle, (S/N 1, P_c = 125 psia)

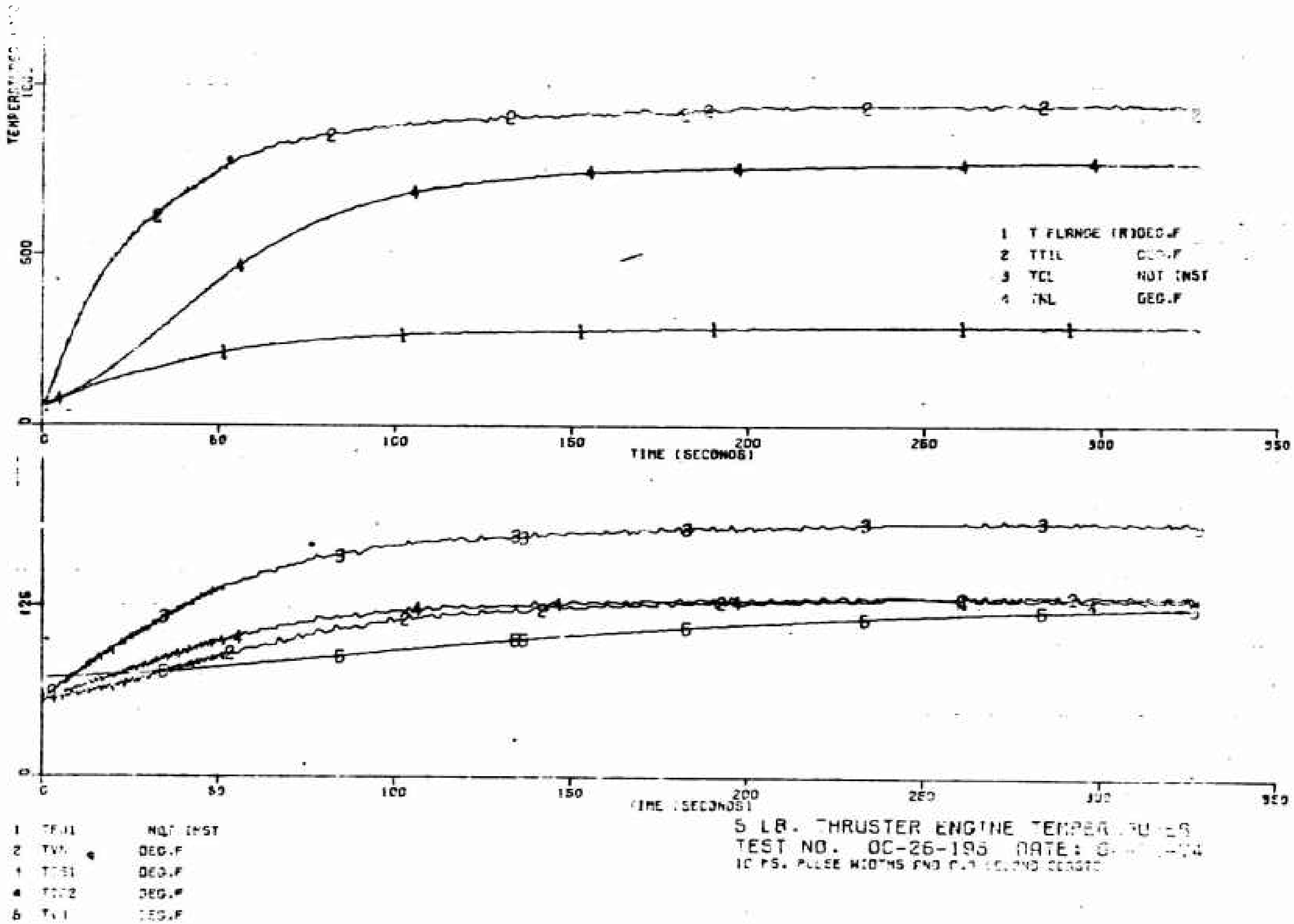

Figure 6.4-31. Radiation Cooled Engine Temperature, MIB Pulses, 3% Duty Cycle (S/N 1
P_c = 125 psia)

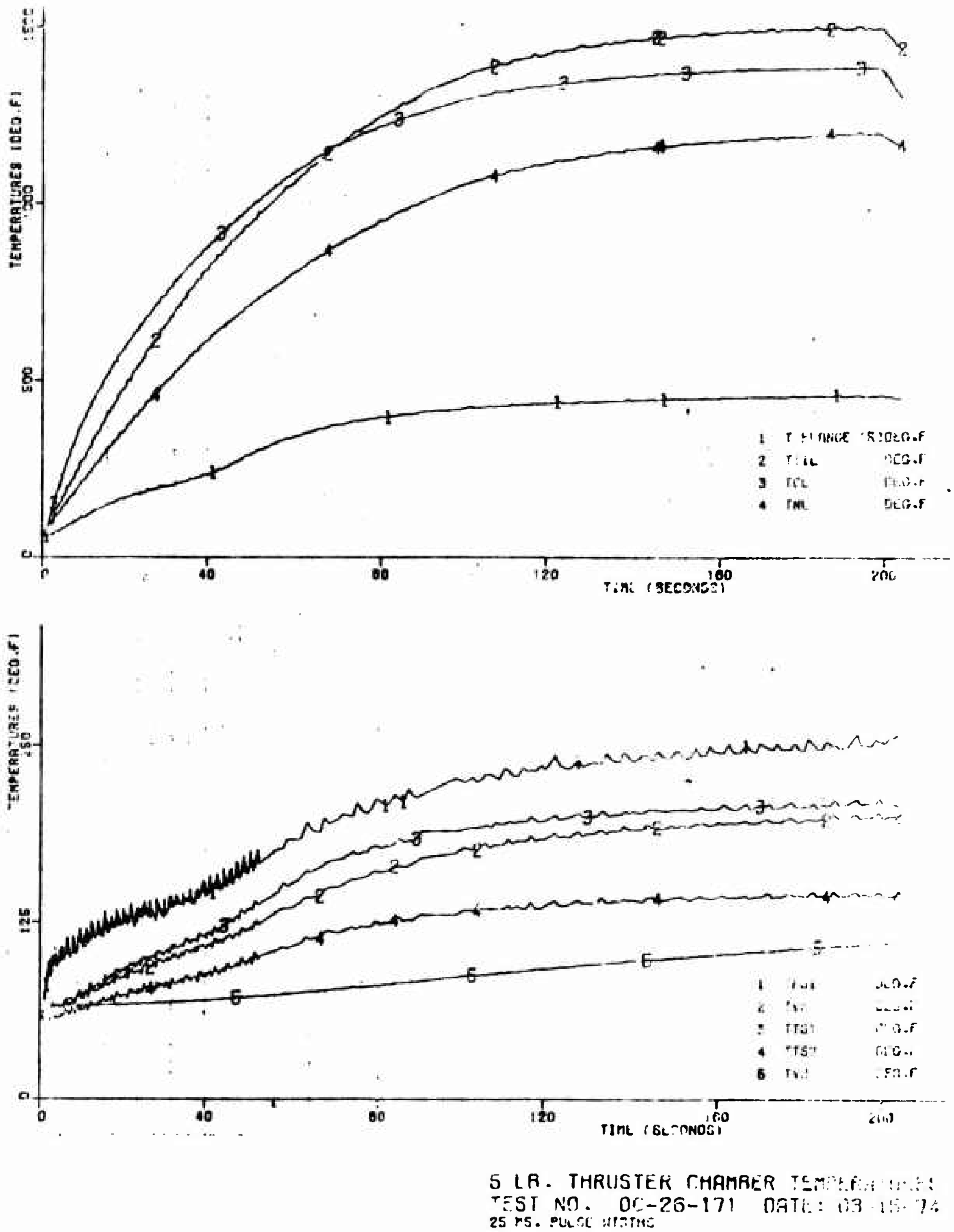

Figure 6.4-32. Buried Engine-Temperatures, 7.7% Duty Cycle (SN 3, P_c = 15[illegible] psia)

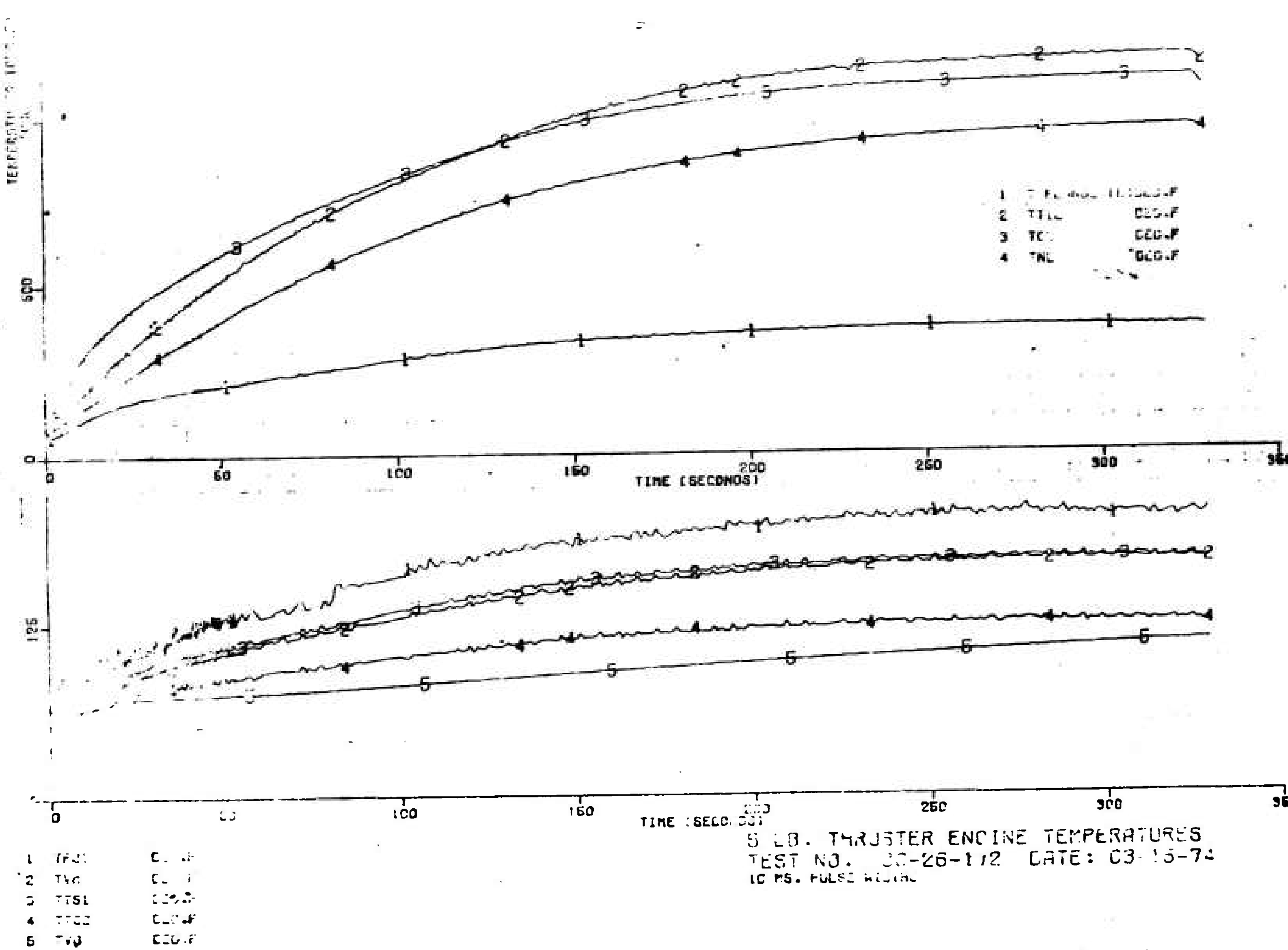

Figure 6.4-33. Buried Engine MIB Pulses, 3% Duty Cycle, (SN 3, P_c = 150 psia)

6.4.4, Thermal Data Evaluation (cont.)

F Flange	Chamber flange temperatures
TT 1L	Throat Temperature (left side)
TCL	Chamber Temperature (left side)
TNL	Nozzle temperature (left side)

The operating conditions for the 4 typical data plots shown are as follows:

Figure 6.4-30	Engine SN 1 Radiation cooled 7 7% DC, 0.025 sec EPW
6.4-31	Engine SN 1 Radiation cooled 0.3% DC, 0.010 sec EPW
6.4-32	Engine SN 3 Barrier cooled buried, 7.7% DC, 0.025 sec EPW
6.4-33	Engine SN 3 Barrier cooled buried, 3% DC, 0.010 sec EPW

The temperature cycling of parameters such as TfJ are a result of random temperature samples taken during burn and coast periods. The apparent change in cycling at 50 seconds is due to a reduction in digital data sampling rates at that time.

All temperature parameters except for TVR are noted to approach an equilibrium condition in these tests. The magnitude of the thermal cycling of each of the components is noted to be quite small. The thermal stresses due to pulsing are also very small and thus individual pulses represent only a pressure cycle applied to the cumulative damage relation for estimating engine life.

Figures 6.4-34 and 6.4-35 provide cross plots of the temperature parameters for each of the duty cycles evaluated. These data indicate that the most adverse thermal condition for the chamber and flange is the 100% duty cycle. No thermal pump up duty cycles were evident. The maximum injector temperature of the buried engine occurs between a 10 and 40% duty cycle $\approx$ 320°F or about 40°F higher than observed in continuous firing. No adverse effects were encountered in 5 hours of operation at a 10% DC or

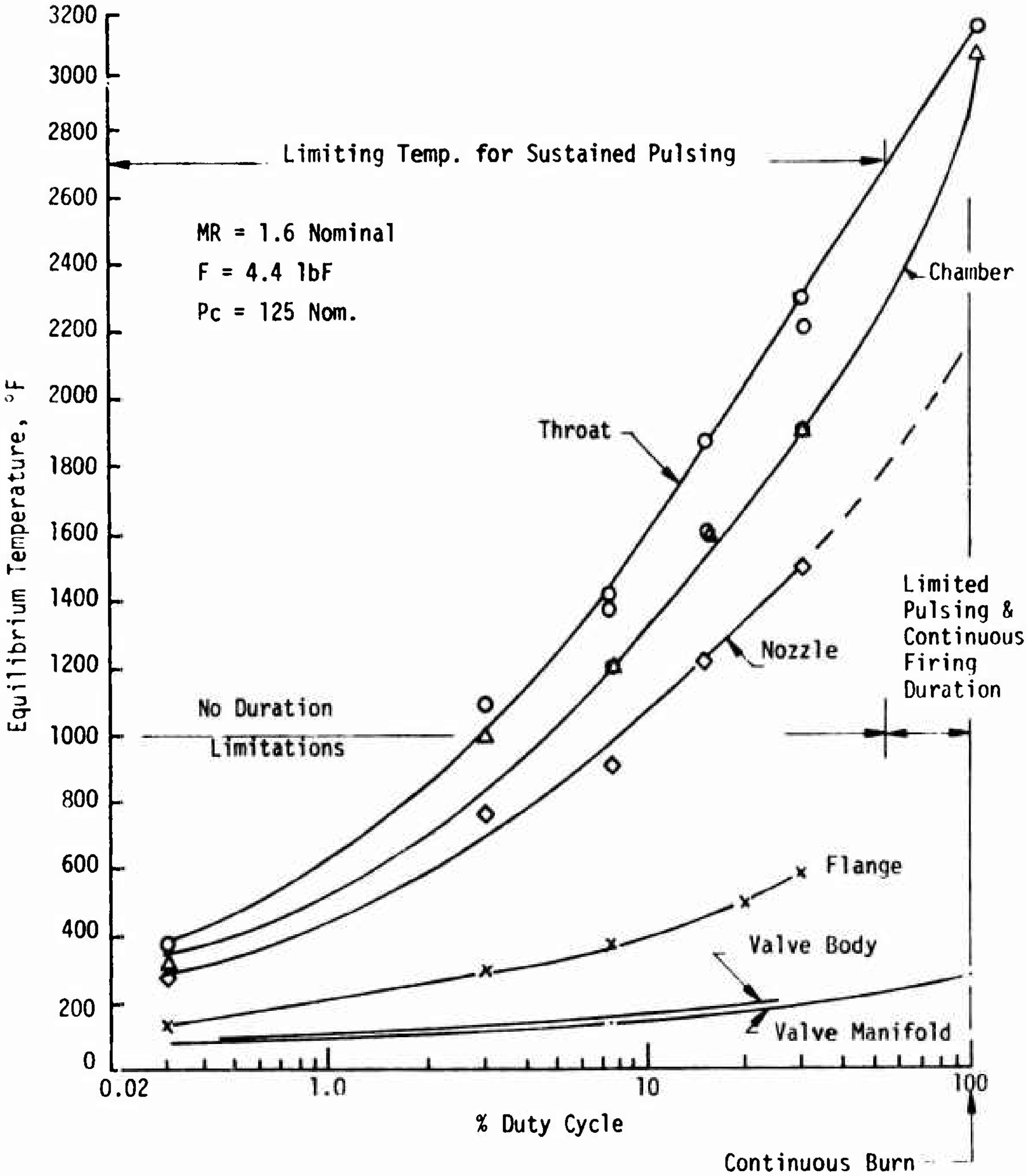

Figure 6.4-34. Continuous Pulsing Duty Cycle Thermal Characteristics, Regulated-Radiation Engine S/N 1

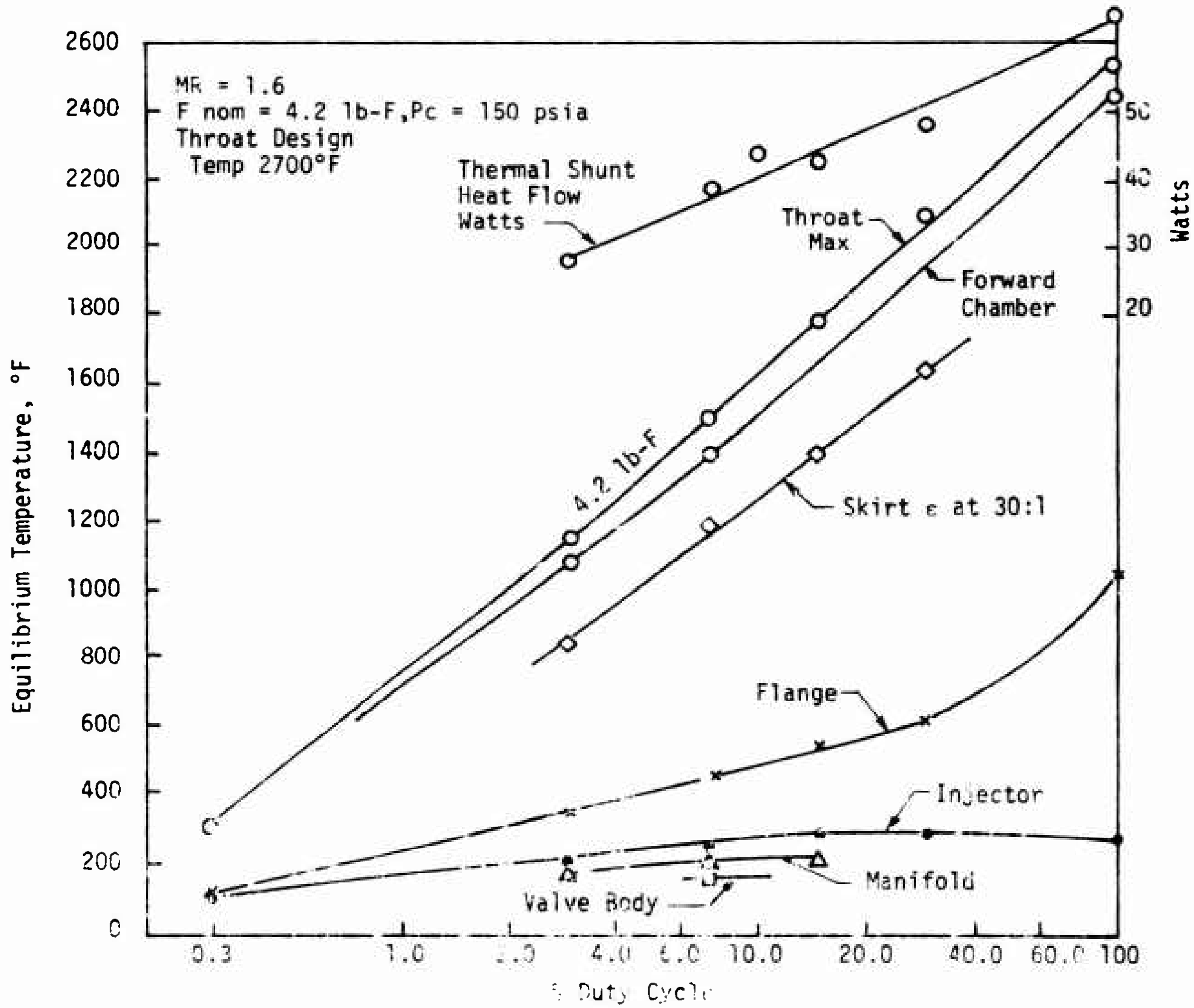

Figure 6.4-35. Continuous Pulsing Duty Cycle Thermal Characteristics, Buried Blowdown Engine S/N 3

1 hr 45 minutes at a 100% duty cycle. The equilibrium temperatures for the radiation cooled and buried engine designs are very similar for duty cycles from 0.3 to about 40%. In this operating range, the barrier cooling provides the same degree of heat regulation as does radiation cooling. At higher % duty cycles, the barrier cooling becomes much more effective in maintaining acceptable chamber wall temperatures than does radiation. The latter cooling process is less efficient due to the less favorable ratio of heat input to heat rejection time. The barrier cooled buried engine would be expected to operate at higher temperatures at very low duty cycles <0.3%. This has a favorable influence on pulsing performance.

The data of Figure 6.4-35 (Engine SN 3) indicate that all temperatures for all duty cycles 0-100% represent a safe operating condition at a chamber pressure of 150 psia. Operation at reduced pressures results in lower temperature and additional conservatism.

The data of Figure 6.4-34 (Engine SN 1) shows no duration limitations up to about a 50% duty cycle. Firing at duty cycles above 50% is limited to periods of 30 to 60 sec. This results from the inability to reject heat via chamber radiation at a fast enough rate at a chamber pressure of 125 psia. Multiple burns of duration from 30 to 60 seconds can be safely accomplished by employing the heat sink capabilities of the chamber and allowing sufficient cooldown time between burns. Unlimited firing durations at all duty cycles can be accommodated on this design by limiting the maximum chamber pressure to ≈ 115 psia as was indicated by the temperatures shown in Figures 6.4-25 and 6.4-28.

The maximum valve temperatures encountered in testing were approximately 230°F in pulsing and 300°F in steady state. This compares to an allowable value of 350°F for sustained operation.

6.4.4, Thermal Data Evaluation (cont.)

The heat rejection rate through the thermal shunt is maximum at 100% duty cycles. The heat flow in watts for the Phase III engines calculated by 0.55 (TTS1 - TTS2) are as follows:

	Max, P_c	Duty Cycle	
		100%	10%
Engine SN			
1	125	83	50
2	125	No data	38
3	150	66	44

These values also decrease as operating pressures are reduced. At 125 psia, engine SN 3 has a heat rejection ratio of 11 watts at the 100% duty cycle. Testing durations of Engine SN 2 at the 100% duty cycle and Engine SN 1 at reduced pressures were too short to allow engine heat rejection rates to attain an equilibrium value. The heat rejection rate of SN 1 at 110 psia was 27 watts after 15 sec of firing.

No specific goals on heat rejection rates were defined in the contract. Phase I mission studies identified typical limitations of 20 watts for small spacecraft and 40-60 watts for larger 3 axis stabilized systems. The measured heat rejection rates are compatible with acceptable values for larger spacecraft. Additional insulation between the chamber and valve manifold would be required for applications where a 25 watt limit is required.

6.5 PULSE PERFORMANCE MODELS EVALUATION

The JANNAF performance methodology provides analytical computer models for evaluating steady state performance. No standardized models are recommended by the JANNAF Performance Standardization Working Group, for predicting transient performance.

The CONTAM model had been initiated by McDonnell-Douglas Astronautics Company (MDAC) on company IR&D funds and further refined on AFRPL Contracts F04611-70-C-0076[17] and F04611-72-C-0037. The Transient Combustion Chamber (TCC) subprogram of the CONTAM computer model had been utilized during the Phase I analytical design study to optimize transient pulsing performance of the 5 lbf bipropellant engine. Results from this initial study are described in Sections 4.2.4 and 4.3. The effectiveness of the CONTAM analysis upon transient performance was evident by the excellent pulsing performances achieved during Phases II and III. While the correlations between prediction and experimental data were satisfactory, the model input required much detail and initial setup time and the computer run times were moderately long.

The AFRPL had also funded a second transient performance program through Rocketdyne designated as the Pulse Mode Performance Model (PMPM). Toward the end of the 5 lbf bipropellant engine contract, an add on study was funded to make an objective comparative evaluation of the two models. Both models were used in parallel to analyze one pulse duty cycle test of one engine during Phase III. "A priori" predictions of pulsing performance were made before the Phase III test using both models. The test results were then compared with both model predictions. Model input data were then adjusted to account for deviations between prediction vs actual data and the models were rerun. A final comparison was made between the test data and posttest analytical correlations.

The objectives of this study were as follows: (1) to determine the quantitative accuracy of the two models for usefulness as design prediction tools, (2) to compare the two models for ease of analysis in terms of

(17) R. J. Hoffman, et al., Plume Contamination Effects Prediction, The CONTAM Computer Program, Final Report and Program User's Manual, AFRPL-TR-71-109, December 1971.

model input complexity, model setup time, or performing analysis of a parametric nature, (3) to compare the cost of analysis in terms of computer run time for similar cases, (4) to identify the advantages and disadvantages of each model for particular types of analyses and identify significant shortcomings, if any of the models, (5) to make recommendations for using either model, (6) to recommend further model modifications, if any, to improve model accuracy or utility.

The first subtask of this study was to select an engine and duty cycle for analysis. Based upon Phase I design studies, the 6-SP-0 and 6-SP-45 injectors were analytically characterized in most detail. Although the 4-UD-28S injector is the most compatible, its design is more dependent upon intuition gained from a qualitative understanding of the injection mechanism which was derived from empirical observation of cold flow test data. Thus, to make a priori performance prediction, it was preferred to analyze either the 6-SP-0 or 6-SP-45 injectors. Both injectors use identical injection element designs. Their only differences are their element orientation which varies their amount of secondary spray overlap and mixing efficiency and minor differences in manifold dribble volumes.

Heretofore, to assure test data acquisition accuracy, all pulsing performance tests were limited to a single fixed pulse (FPW) width and coast time. This type of test duty cycle (although simple to analyze) would not have provided a basis for extensive checkout of the CONTAM and PMPM model capabilities. Therefore, a special duty cycle shown (schematically in Figure 6.5-1) was derived to provide EPW's between 0.010 to 0.100 sec over which range the bulk of the pulse performance variability was predicted to occur by their Phase I analysis. This was experimentally observed in Phase II test data. To assure experimental data accuracy the pulse widths were grouped in series of fours. The coast times between pulses and between pulse series were varied to obtain the widest possible range of engine operating temperatures which were shown to affect Phase II pulse performance shown in

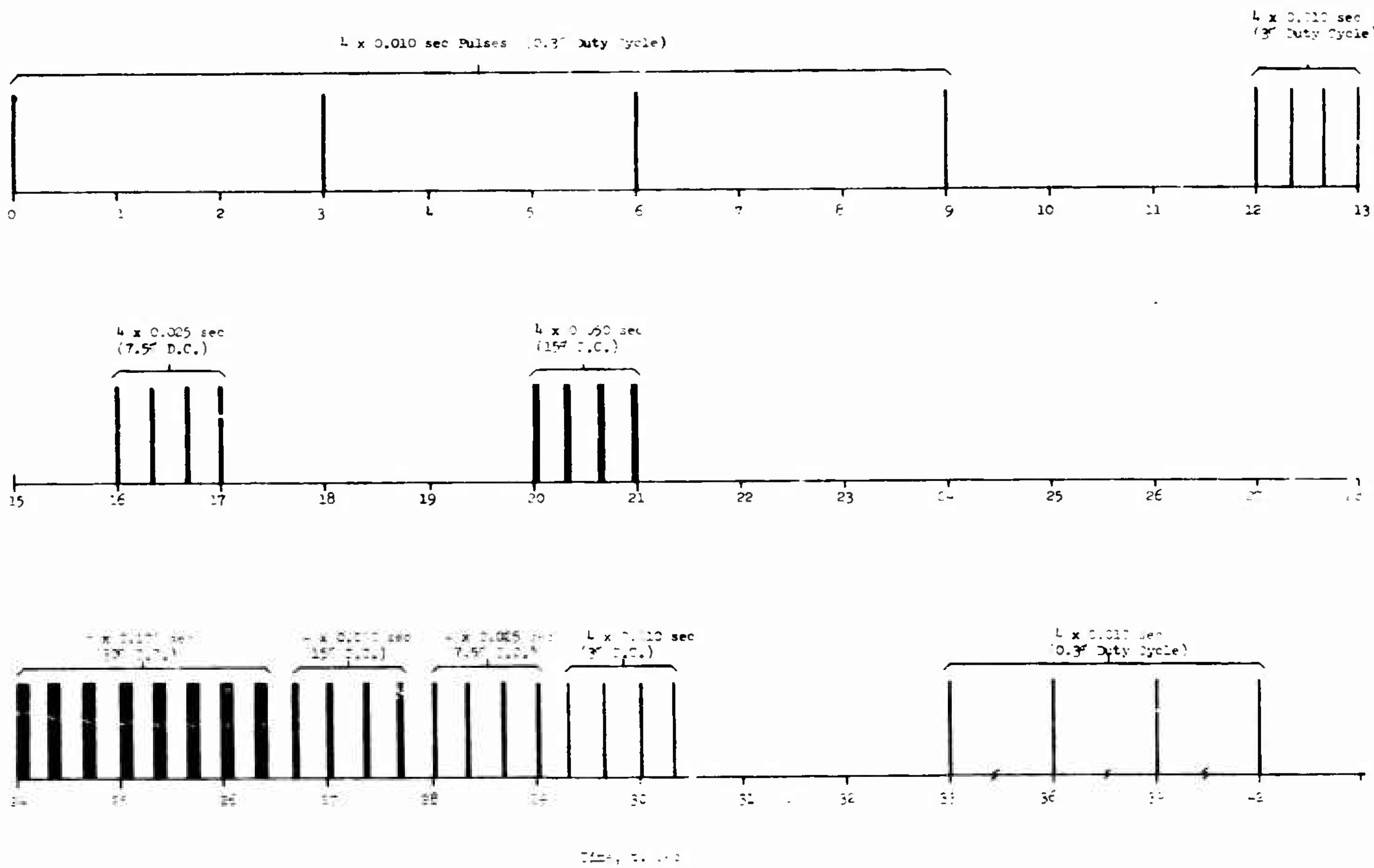

Figure 6.5-1. Special PMPM/CONTAM Duty Cycle Sequence

6.5, Pulse Performance Models Evaluation (cont.)

Figure 5.3-26. The pulse widths and duty cycle were designed to simulate the entire range of EPW for both cold start and hot restart pulsing performance. The experimental performance data for this special duty cycle is in Table 6.4-3 for both the 6-SP-0-C and 6-SP-45-C engines and are plotted vs bit impulse in Figure 6.5-2.

Since the objective was to evaluate differences between the two models rather than differences between the model inputs, an effort was made to insure model input similitude between the two models. Significant properties such as the mixture ratio dependence of gas temperature, molecular weight, characteristic exhaust velocity (C*), and nozzle thrust coefficient (C_F) were checked between the two models. Engine design parameters like injection orifice diameter, manifold dribble volumes, chamber length and diameter profile, and nozzle exit area ratio were also input identically. Engine operating conditions such as nozzle ambient pressure, propellant tank pressures, feed system design and resistance, maximum injector face and chamber wall operating temperatures as well as their thermal rise rates, chamber pressure, and mixture ratio were input identically. Thus, by assuring that both models used identical inputs, only differences between their internal computation techniques would be reflected in their respective solutions.

Coincidentally, both the CONTAM and PMPM sample cases contained in their respective users' manual were based upon properties for N_2O_4/MMH which is also the propellant combination used on the 5 lbf bipropellant engine. In many cases this simplified the model input and reduced the initial model input setup time. Critical properties were checked, however, against known ALRC gas properties. One significant deviation from the ALRC data was noted in high mixture ratio gas properties in both the sample case model inputs. Apparently both the CONTAM and PMPM high O/F gas properties were based upon chemical equilibrium properties assuming the excess N_2O_4 thermally decomposed into N_2 and O_2. In reality, in the 3 to 6 mixture ratio range the NO decomposition becomes kinetic rate limited and freezes at NO above O/F 6. At still higher O/F's, the decomposition products result in NO_2 and eventually

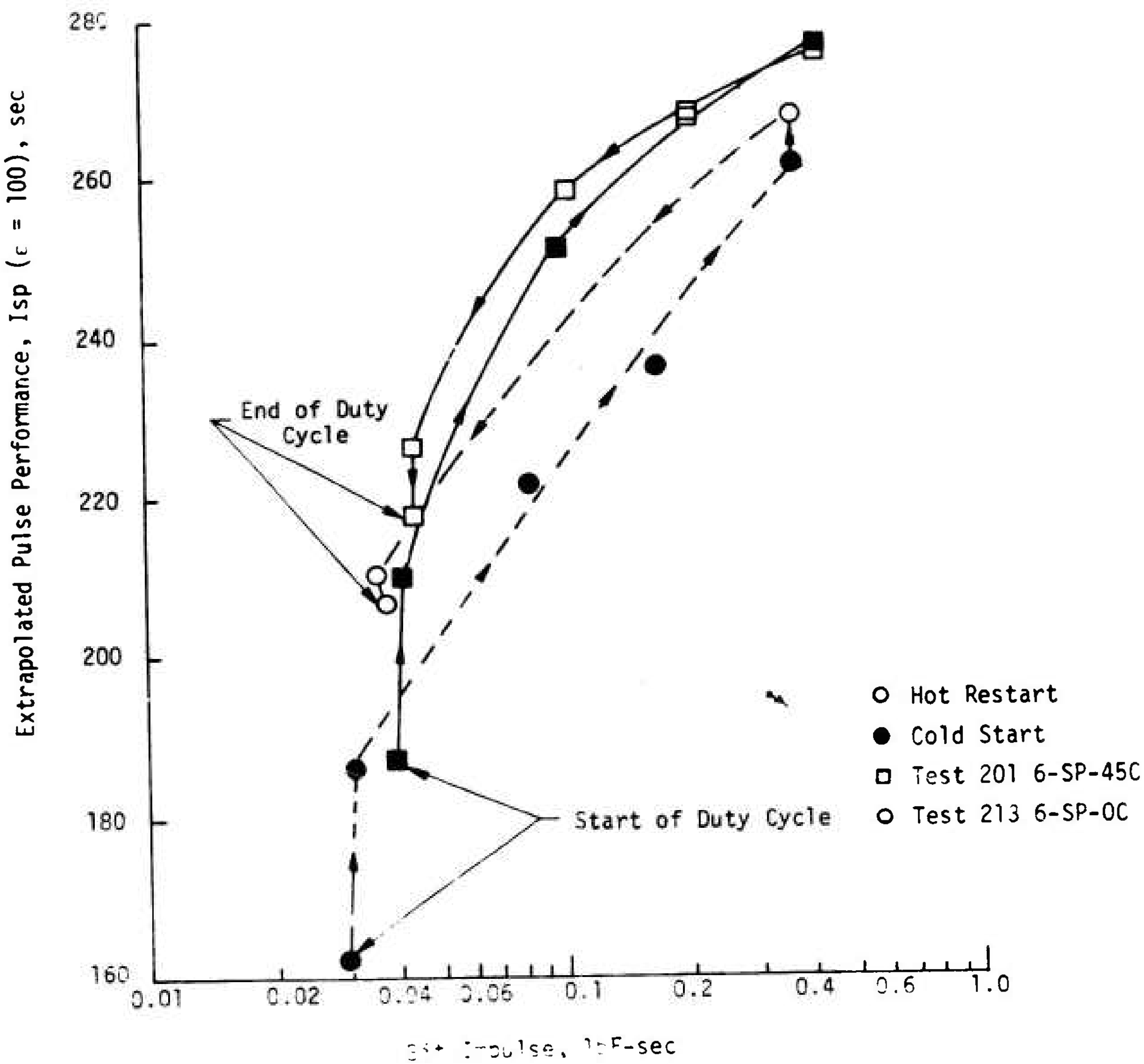

Figure 6.5-2. Special Duty Cycle Experimental Pulse Performance

N_2O_4 due to kinetic limitations at low gas temperatures. Since the NO decomposition reaction is exothermic, the real gas properties are significantly lower performing than assumed equilibrium gas properties. This is important to pulsing performance because the higher N_2O_4 vapor pressure results in very high O/F combustion of the oxidizer dribble volume after shutdown. This model input correction was made prior to making any analyses. It must be emphasized that the above error was only a shortcoming of the model input in the sample cases; it has no affect upon the integrity of the computer models themselves.

The PMPM analysis is described in Section 6.5.1; the CONTAM analysis is in Section 6.5.2. The transient models evaluation is summarized in Section 6.5.3.

6.5.1 Pulse Mode Performance Model (PMPM)

The transient pulsing performance analysis of the 5 lb_f bipropellant engine using the PMPM program is described herein.

6.5.1.1 Pre Test Performance Prediction

One of the first decisions which had to be made was to select either the 6-SP-45-C (Engine SN 1) or 6-SP-0-C (Engine SN 2) for analytical prediction/correlation. Based upon Phase I design studies and Phase II test results which were available prior to undertaking this task, it was known that many similarities exist between the two desiqns. Thus an analysis of either engine could be applied in many respects to the other with few modifications.

The 5 lb_f engines were designed using the modified Priem and CONTAM analytical models. The PMPM model is structured largely around the JANNAF steady state Distributed Energy Release[18] (DER) performance model.

(18) L. P. Combs, Liquid Rocket Performance Computer Model with Distributed Energy Release, Final Report, NASA CR-114462, Contract NAS 7-746, 10 June 1972.

6.5.1, Pulse Mode Performance Model (cont.)

Therefore, in addition to the special duty cycle performance prediction, some peripheral parametric analyses were added to evaluate the DER (designated as PMDER in PMPM portion of the model) as applicable to the steady state analysis of the various 5 lb_f engines and other operating characteristics. Although, it was obviously beyond the scope of the study to evaluate the engine performance characteristics in complete detail with PMDER to the depth of the modified Priem and CONTAM analyses, sufficient parameters were evaluated to gain insight into the DER/PMPM models.

Based upon the successful 300,000 test demonstration of the 6-SP-45-C engine, and its very high performance this design was selected for the baseline prediction. The Liquid Injector Spray Pattern (LISP) program is the first program run in the PMPM analysis. Since LISP is a straightforward computer program and is inexpensive to run ($\approx$ 15 sec on UNIVAC 1108 computer) parametric analyses of both the 6-SP-0-C and 6-SP-0 injectors were added. The splash plate elements produce spray patterns similar to an unlike doublet element. Therefore in the LISP analysis, the splash plate injectors were analyzed using the unlike doublet spray correlations. These micro-orifice injection elements were much smaller than the experimental injectors from which the empirical spray correlations were developed. Thus, it is not too surprising that the atomized drop size predictions from the LISP analysis are in considerable error as shown in Table 6.5-1, compared with the best estimates which were derived from the ALRC correlations. The latter are expected to be quite accurate since the Phases II and III engine performances have substantiated the Phase I performance predictions.

An important parameter in the PMDER analysis is the selection of the axial zone of mixing (ZOM) from the injector face at which the liquid spray distribution is supposed to characterize the gas mixing efficiency at the nozzle throat plane. The ZOM was parametrically varied at 0.2, 0.3, and 0.5 in. from the injector face for the 2.0 in. length chambers. The corresponding mixing efficiency, E_m, and characteristic exhaust velocity

TABLE 6.5-1

LISP ANALYSIS SUMMARY OF SPLASH PLATE INJECTORS

Engine:	6-SP-45-C	6-SP-OC	6-SP-0
Oxid Orifice dia, D_{ox}, (in.)	0.008	0.008	0.010
Fuel orifice dia, D_f (in.)	0.008	0.008	0.008
Oxid imp. angle, 0_{ox}, (degree)	40	40	60
Fuel Imp. angle, 0_f, (degree)	60	60	60
LISP Predictions:			
Oxid Drop dia, $\bar{D}_{ox}$, (in.)	0.0255	0.0255	0.0269
Fuel Drop dia, $\bar{D}_f$, (in.)	0.0080	0.0080	0.0085
(ZOM = 0.2 in.)			
Mixing Eff., % E_m	69.3	69.1	69.7
% C^*_{mix}	85.9	91.3	91.4
(ZOM = 0.3 in.)			
% E_m	63.4	69.2	67.9
% C^*_{mix}	81.5	89.2	89.5
(ZOM = 0.5 in.)			
% E_m	65.2	76.6	71.6
% C^*_{mix}	85.4	92.6	90.3
ALRC Drop Size Correlation:			
$\bar{D}_{ox}$, (in.)	0.0010	0.0010	0.0012
$\bar{D}_f$, (in.)	0.0014	0.0014	0.0014

mixing efficiency assuming complete droplet vaporization is shown for each engine at each of the three ZOM's in Table 6.5-1. Based upon the LISP predictions, C* mixing efficiency is not strongly influenced by the selection of ZOM. A ZOM = 0.5 in. was selected for the PMDER prediction but would not have altered the conclusions if either of the other two values had been used.

In the Stream Tube Combustion (PMSTC) portion of the PMDER, the ALRC drop size distributions were input by over-riding the LISP predicted values. The values of the fuel and oxidizer evaporation coefficients within ZOM were adjusted until the fuel and oxidizer vaporized fractions at ZOM appeared reasonable. A comparison of the PMSTC and modified Priem vaporization distributions are shown in Figure 6.5-3. PMDER does not allow for an MMH monopropellant vaporization option. The monopropellant vaporization transformation has been added into the modified Priem vaporization model at ALRC. The consequence of the monopropellant decomposition mechanism is to increase fuel vaporization rates near the injector face where the relative droplet/gas velocities are low.

After over-riding the LISP predicted drop sizes and inputting evaporation coefficients which gave reasonable vaporized fractions at ZOM, the propellant latent heats of vaporization had to be increased by some vapor superheat before the throat plane vaporization efficiencies could be made equal to the values predicted by the modified Priem analysis. If this was not done, virtually complete fuel and oxidizer vaporization efficiency was predicted at the throat and the only combustion inefficiency would have been due to mixing inefficiency. It is believed that the high predicted vaporization efficiencies were related to the high (6 to 10) chamber contraction ratios (CR) of these engines. The DER model consistently seems to overpredict vaporization efficiencies in high CR chambers and underpredict vaporization in low CR chambers.

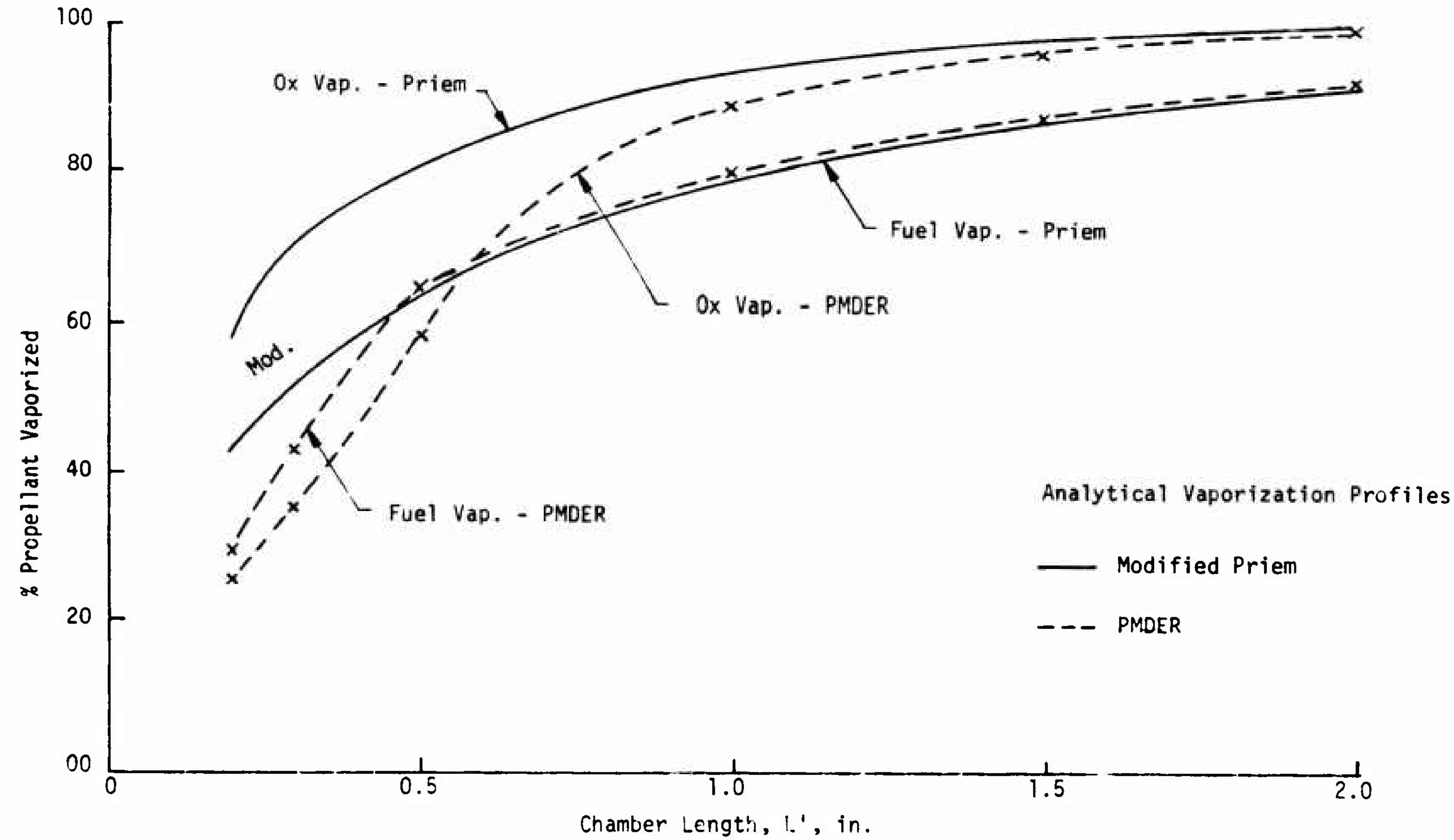

Figure 6.5-3. Comparison of Modified Priem and PMPM Vaporization Profiles

6.5.1, Pulse Mode Performance Model (cont.)

From Table 6.5-2 the LISP predictions indicated C* mixing efficiencies on the order of 85 to 90% even if both fuel and oxidizer are completely vaporized. These values are unrealistically low because the Phase II combined mixing and vaporization energy release efficiencies were ≈ 96%. Thus, higher mixing efficiencies can be predicted by using fewer stream tubes in the PMSTC analysis. The number of different radial and circumferential stream tubes was parametrically varied from 1-18 with results as shown in Table 6.5-2. From these results it is apparent that the C* mixing loss must be quite small to result in 300 sec delivered performance. Thus, it was concluded that a single stream tube analysis (or at most two stream tubes) describes the steady state performance best. It must be remembered that the DER model was initially developed for large diameter, high thrust liquid rocket engines. For the 5 lb_f bipropellant engine, the maximum chamber diameter ranges from 0.35 to 0.50 in. with the nozzle throat dia = 0.15 in. It is unrealistic to assume that large mixture ratio gradients can persist through a sonic throat which is only 0.15 in. diameter without mixing.

Due to the large computer core required by the entire PMPM program, the entire analysis from LISP to duty DCYCLE analysis was not analyzed in a single computer run. For simplicity the steady state analysis (LISP and PMSTC) was analyzed on one run using the PMDER portion of the computer program. From this steady state analysis the fuel and oxidizer spray depletion functions (vaporization rates) were transferred over as input into the remaining PULDC portion of the model which was used to predict transient performance.

The PULDC segment of the model consists primarily of the PULSE analysis and DCYCLE duty cycle analysis. PULSE includes IGN the Seamans' ignition model and BOIL the post shutdown manifold dribble volume expulsion subroutines. The IGN subroutine option was bypassed by using a constant ignition delay time as recommended in the PMPM final report. For the pretest prediction, an analytical ignition delay time of 0.2 millisecond was obtained from the CONTAM model and used for the PMPM input.

TABLE 6.5-2

MIXING PERFORMANCE SENSITIVITY TO STREAM TUBE QUANTITY

No. Radial Stream Tubes	x	No. Circum. Stream Tubes	=	Total No. Stream Tubes	% C^*_{mixing}	I_{sp} (ϵ = 100)
1		1		1	99.87	300.8
2		1		2	97.75	293.5
2		3		6	94.73	283.3
2		6		12	94.00	280.9
3		6		18	93.59	279.5

Repeated difficulties and frustrations were encountered in attempting to execute the BOIL subroutine because it improperly represented the engine in such fashion as to result in a program abort. Specifically within BOIL propellant temperatures are calculated vs time as the residual propellants in the manifold are expelled. BOIL predicted that the propellants were chilled below their freezing point which was not decernible in the experimental test data. Since the propellant temperature is used to enter an array to determine the propellant density and vapor pressure, this causes an error message to be printed each time subroutines YOF and LOCATE are called. After 50 such messages are printed the calculation is aborted. In order to minimize this inconvenience caused by BOIL, the PULSE analysis had to be run either at hot wall temperatures or limited to short expulsion intervals with ambient temperature walls which do not permit transient calculation for the complete manifold expulsion interval. In order to accurately characterize transient performance in DCYCLE, it is necessary to calculate shutdown characteristics over the entire range of coast times between pulses and the entire chamber wall temperature range encountered in the duty cycle. Thus numerous attempts had to be made to run BOIL before sufficient data was generated by PULSE to provide the range of input required by DCYCLE.

6.5.1.2 Data Comparison

Once the above input was generated the DCYCLE subprogram ran quickly and efficiently ($\approx$ 8 sec on UNIVAC 1108). An important input variable to DCYCLE is the empirical parameter, ECFQ, which correlates pulse performance with chamber wall temperature. This parameter is somewhat akin to an artificial increase in the chamber heat loss. Since no apparent physical mechanism exists to calculate this input analytically from engine design parameters, ECFQ = 1.00 was used for the pre-test pulse performance prediction. When ECFQ = 1.00, however, no influence of wall temperature upon pulse performance is predicted as shown in Figure 5.5-4, i.e., pulse I_{sp} is

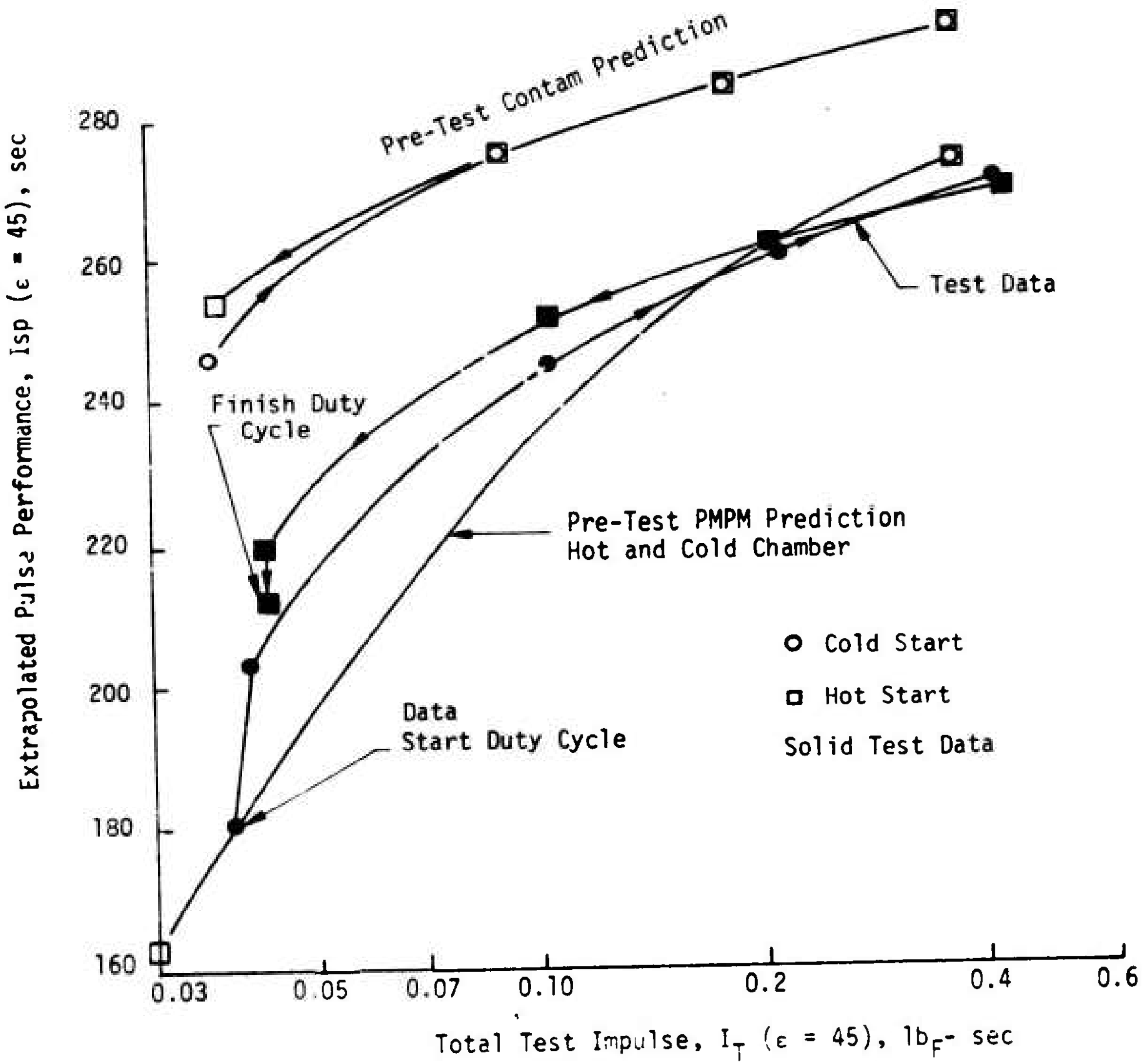

Figure 6.5-4. Pretest Model Predictions Compared Experimental Pulsing Data

only a function of EPW or total bit impulse. In reality, all Phase I and Phase II experimental data including the special duty cycle indicate a hysteresis effect yielding higher performance as the wall temperature increases. The CONTAM model predicts this effect and attributes it to the wall film vaporization mechanism which the PMPM model disregards. In general, the PMPM prediction shows a steeper slope in performance improvement with increase in bit impulse than the experimental data.

Chamber wall temperature rise rates and cooldown rates were obtained from the Phase II test data. These values were used as input into DCYCLE to predict wall temperature vs pulse duty cycle. A comparison between the pre-test PMPM wall temperature prediction and the experimental data is shown in Figure 6.5-5. DCYCLE correctly predicted the wall temperature trend vs pulse number but significantly under-predicted the maximum wall temperature.

6.5.1.3 Input Adjustment and Re-Analysis

Following the comparison of the pre-test PMPM prediction with the experimental data, the model input parameters were reviewed to determine if modified input parameters could improve the correlation with the experimental data.

All of the input parameters which were modified are summarized in Table 6.5-3. The fabrication inspection records were reviewed to determine the actual measured fuel and oxidizer injection orifice diameters instead of the nominal design values. Injector dribble volumes downstream of the valve seat were re-calculated for the Phase III hardware. Compared to the nominal Phase I design values the revised fuel dribble volume was $\approx$ 3% smaller and the oxidizer volume $\approx$ 15% larger.

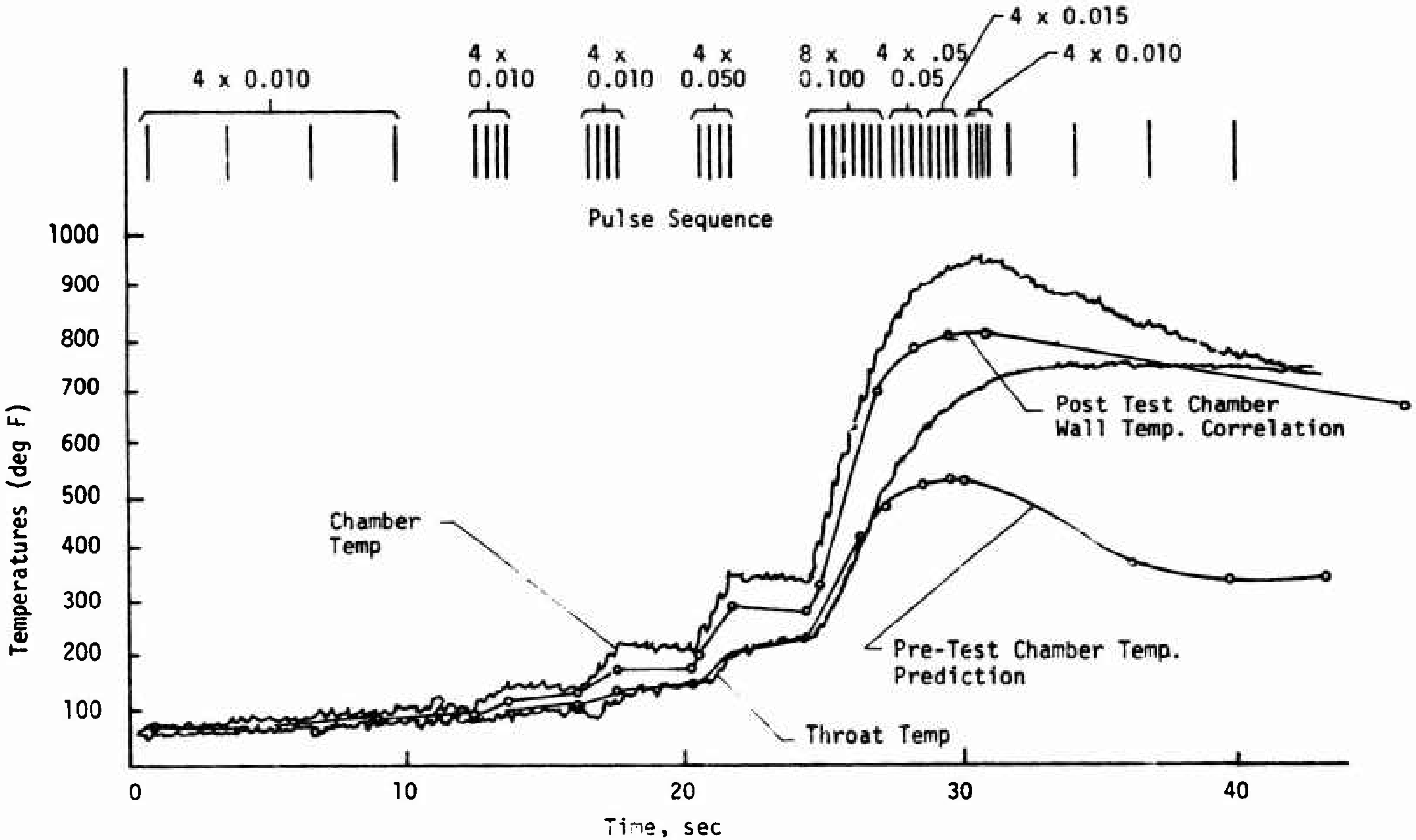

Figure 6.5-5. PVRM Wall Temperature Prediction/Correlation

TABLE 6.5-3

PMPM INPUT MODIFICATIONS

Parameter	Units	Pretest Prediction	Posttest Correlation
Injector Design:			
Oxid Orifice dia	in.	0.0080	0.0060
Fuel Orifice dia	in.	0.0080	0.0071
Oxid Dribble Volume	$in.^3$	0.000297	0.000344
Fuel Dribble Volume	$in.^3$	0.000314	0.000305
Chamber Design:			
Chamber dia at Injector	in.	0.355	0.500
Chamber Length	in.	2.0	2.0
Chamber Volume	$in.^3$	0.326	0.363
Chamber Surface Area	$in.^2$	2.88	3.04
Nozzle Exit Area Ratio	-	50:1	100:1
Valve Response, Electrical Signal to Start of Travel:			
Oxid	sec	0.0000	0.0025
Fuel	sec	0.0000	0.0025
Valve Inlet Pressure:			
Oxid	psia	330	360
Fuel	psia	188	270
Ignition Delay Time:	sec	0.0002	0.0010
Chamber Heating Coefficient (COEHTH)	$msec^{-1}$	0.000172	0.000230
Chamber Cooling Coefficient (COEHTC)	$msec^{-1}$	0.000046	0.000027
Thrust Correlation Coefficient (ECFQ)	-	1.00	0.88
Subroutine BOIL	-	Yes	No

6.5.1, Pulse Mode Performance Model (cont.)

Instead of assuming that the valve movement was initiated instantaneously with the valve actuation signal, a 2.5 millisecond delay on both opening and closing was introduced to more nearly duplicate actual test conditions listed previously in Table 2.1-1. This had no influence on pulse performance other than a constant time-shift in engine response relative to the electrical signal. The ignition delay time was increased from 0.2 millisec to 1.0 millisec to correspond with the observed delays and modification made to the CONTAM analysis described in subsection 6.5.2.3.

Fuel and oxidizer valve inlet pressures were adjusted to reflect actual pressures used in Test 201. Feed system resistances were altered correspondingly to duplicate the actual steady state engine balance mixture ratio and flowrates.

The use of a diverging conical chamber liner to reduce injector face operating temperature and heat soakback into the valves by preventing hot gas recirculation near the face provided an unusual combustion chamber contour which was assessed with difficulty. A modification to the chamber profile data input from the test hardware was required to enable more consistent performance prediction between PMDER and PULSE. The liner had a 0.355-in. diameter at the injector face tapering outward to the 0.500 in. diameter was held constant in a cylindrical section $\approx$ 1.0 in. long before convering into the nozzle throat. This chamber profile was initially input into PMDER to yield $\approx$ 97% vaporization efficiency at P_c = 125 psia and to generate the propellant spray depletion functions. When the corresponding chamber length, volume, and surface area were input together with the spray depletion functions into PULSE, however, the resultant steady state output P_c was only 87 psia and the corresponding performance was only $\approx$ 160 sec I_{sp} at ϵ = 50:1 (167 sec at ϵ = 100). This accounted for the low pulse performance efficiency predicted at the 0.010 sec EPW in Figure 6.5-4 in spite of zero thermal heat loss (ECFQ = 1.00). In the re-analysis, a 0.500 in. diameter cylindrical chamber was input from the injector face plane to the nozzle convergent section in PMDER. The propellant latent heats of formation were fictitiously altered slightly to force the same steady state vaporization rates in PMDER as achieved in the pre-test prediction. The new spray depletion functions were input into PULSE together with the corresponding chamber length, volume, and surface area. By thus assuming the test chamber profile with a cylindrical contour the PULSE P_c = 125 psia was in agreement with the PMDER analysis. No other options for attaining these results were apparent. The best post test pulse performance correlation was achieved by setting ECFQ = 0.88. The nozzle exit area ratio, ϵ = 100, was specified in the re-analysis to correspond to the nominal engine design extrapolated performance.

The chamber heating rate and cooling rate coefficients shown in Table 6.5-3 were input to provide a better correlation of wall temperature vs pulse number. Subroutine BOIL was bypassed in the re-analysis.

6.5.1.4 Final PMPM/Data Corrclation

Based upon the input modifications described above, the final posttest PMPM performance correlation is compared to the special duty cycle test data for Engine SN 1 (6-SP-45-C) in Figure 6.5-6. Several significant conclusions can be derived from this comparison as follows.

An empirical ECFQ = 0.88 factor provides the best data fit. It results in the best correlation of average pulse performance over the entire range from 0.010 to 0.100 sec EPW. Higher values of ECFQ will provide better correlation of the long (0.100 sec EPW) pulse data; lower ECFQ is needed to correlate the 0.010 sec EPW data. The value used does account for a differential performance between early and late pulses of the same pulse width, but grossly underestimates differences between the 0.3% duty cycle and 3% duty cycle firings at 0.010 sec EPW. This aspect requires further investigation.

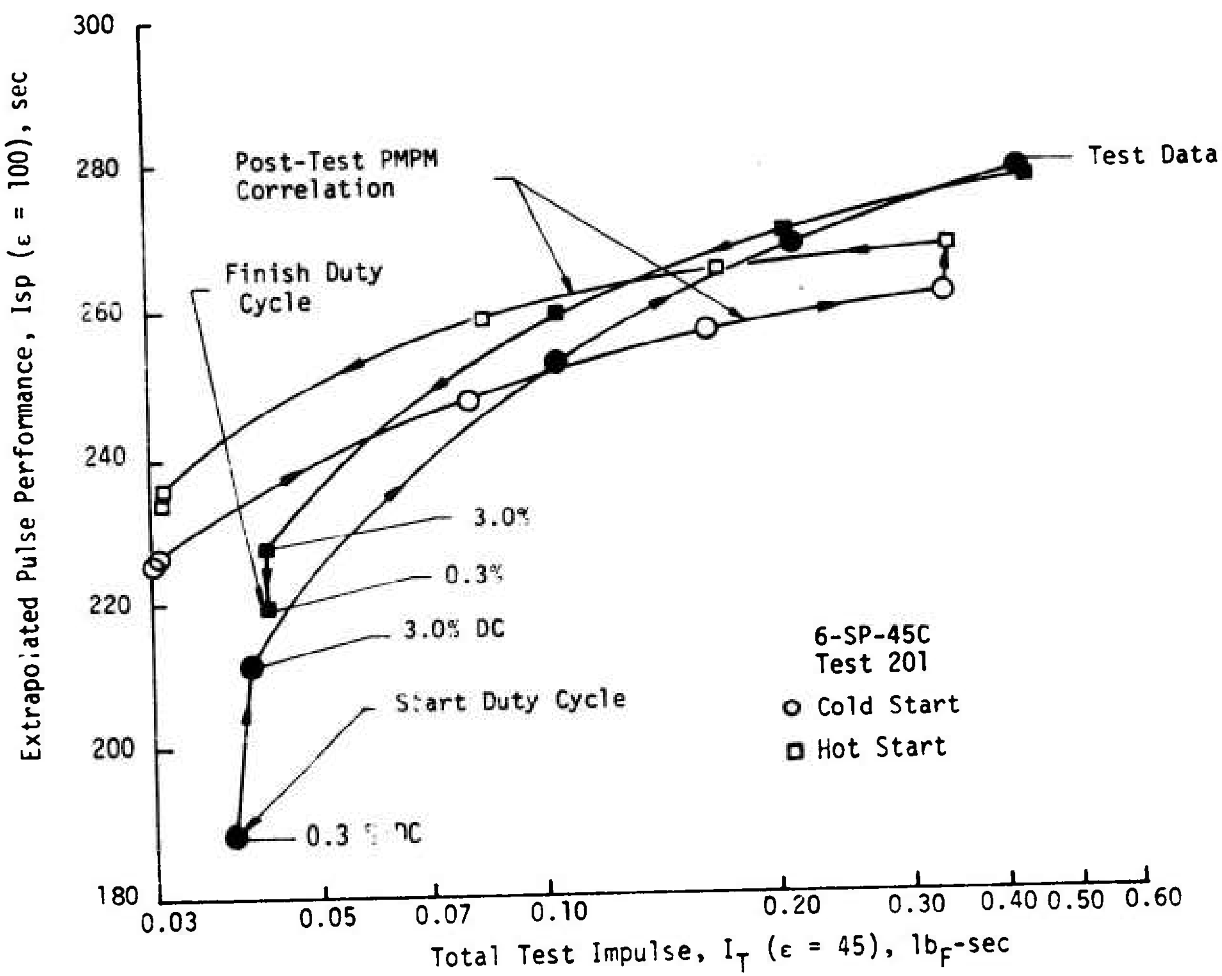

Figure 6.5-6. Final PMPM Performance Correlation

6.5.1, Pulse Mode Performance Model (cont.)

From the previous transient analysis of the 5 lb_f bipropellant engine using the CONTAM model, it is known that the above model inadequacy in PMPM is due to the total disregard of the wall film vaporization mechanism. The PMPM model was structured around the existing DER model. The DER in turn was developed to analyze large engines whose fraction of spray impingement upon the chamber wall can be neglected in comparison with the mass of free propellant droplets entrained by hot gases. Thus, the PMPM model did not treat wall film vaporization as an important consideration. The CONTAM model, on the other hand, recognized that small thrusters result in significant spray impingement upon the chamber walls and accounted for wall film vaporization rate as well as free droplet combustion.

The posttest correlation of chamber wall temperature with the revised model input vs the test data is shown in Figure 6.5-5. The posttest correlation provides an excellent mean value between the two chamber thermocouple measurements. Therefore, the performance deviation noted in Figure 6.5-6 cannot be attributed to mispredictions of chamber wall temperature or transient heat loss.

Figure 6.5-7 provides further proof that the pulse performance reduction at cold chamber wall temperatures is due to a chamber wall film vaporization mechanism rather than due to chamber heat loss. Figure 5.3-20 and Phase II data showed that pulse performance varied rapidly from ambient chamber wall temperature to the fuel saturation temperature but was essentially independent of wall temperature above that value. Insufficient ranges of chamber wall temperature for all pulse widths were available from the special duty cycle test alone. Therefore, long pulse train data from Table 6.4-2 were used to supplement the special duty cycle thermal data in Figure 6.5-7. The long pulse train test points are denoted by an "X". Again, Figure 6.5-7 reverifies the Phase II results. Strong pulse performance dependence upon wall temperature is shown below the fuel saturation temperature. The 0.050 and 0.100 sec EPW data show little differences between early

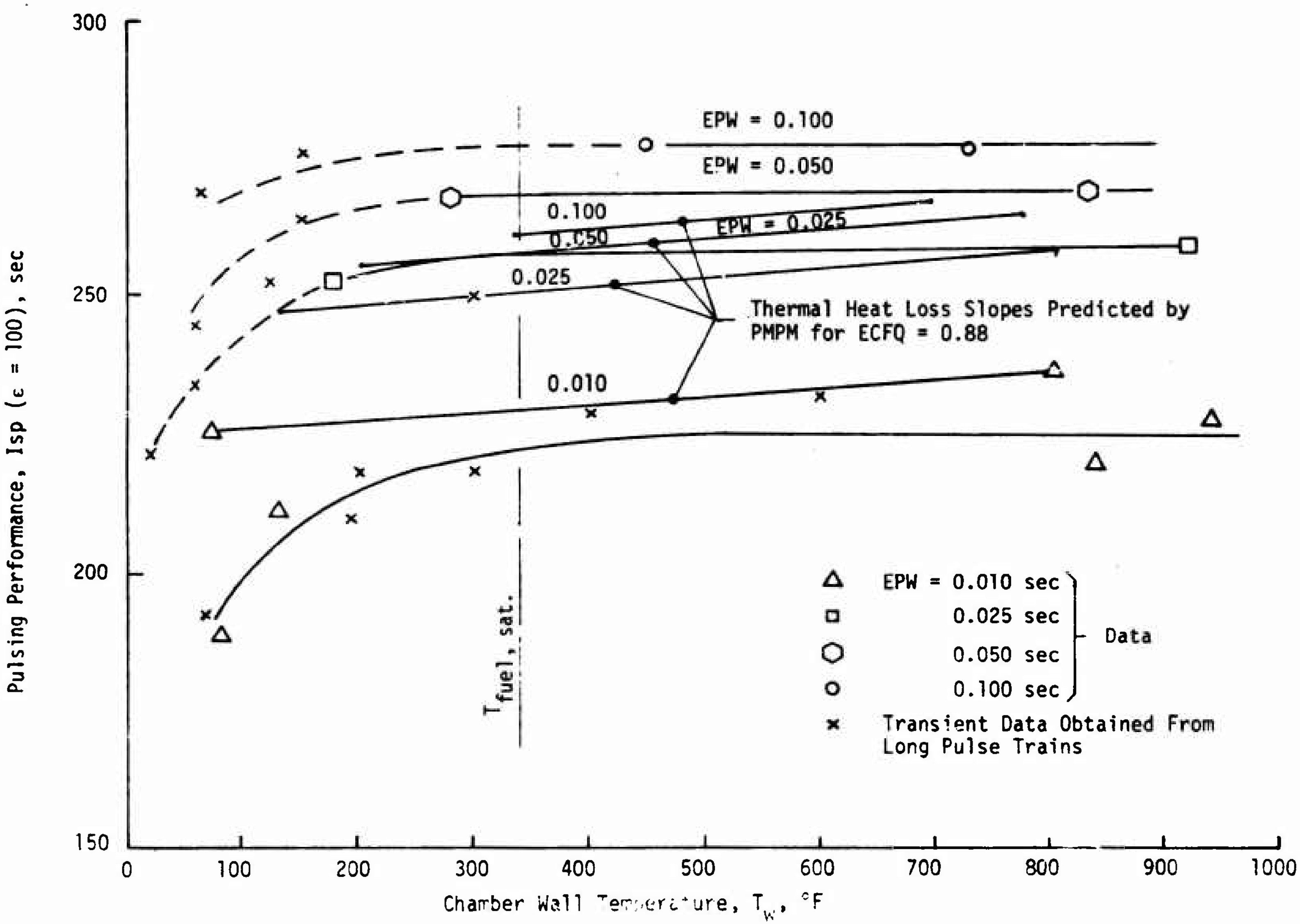

Figure 6.5-7. Wall Temperature Effect on Pulse Performance

(cooler) and late (warmer) wall temperature performance data. By comparison, the PMPM model would predict a linear performance increase between ambient temperature to the maximum chamber operating temperature. This assumption clearly is not supported by the experimental data.

The PMPM model was successful, however, in predicting the trend of pulse mixture ratio shift away from nominal O/F with decreasing EPW which was experimentally observed in Test 201 (see Table 6.4-2 and Figure 6.5-8). For constant tank pressure settings throughout the duty cycle, lower than nominal O/F's were consistently obtained at minimum EPW's. As EPW increased the pulse O/F asymptotically approached nominal O/F. The reason for this is as follows. At steady state flowrate the fuel feed system ΔP_f = PFTCV - P_c = 270-125 = 145 psia while the oxidizer feed system ΔP_o = POTCV-P_c = 360-125 = 235 psia. Prior to engine ignition, P_c = 0. Thus the steady state P_c = 125 psia is momentarily added to both feed system ΔP's upon valve opening. This identical incremental pressure has a greater relative impact on the feed system having the lower steady state ΔP (fuel). Thus the fuel overshoot prior to ignition exceeds the oxidizer overshoot resulting in lower than nominal O/F for the overall pulse. Figure 6.5-8 compares the PMPM predicted pulse mixture ratio vs the experimental data as a function of variable EPW. The PMPM model adequately predicts the pulse mixture ratio trend. The obvious implication is that if the feed system ΔP's between fuel and oxidizer are not equal for a pulse engine, a balance orifice should be installed on the lower resistance system to equalize steady state pressure drops and tank pressure settings. This was simulated on the PMPM model by pre-setting identical valve inlet pressures. For this condition, pulse mixture ratio remained nominal at all EPW's. The opposite was simulated by running PMPM with PFTCV = 360 psia and POTCV = 270 psia. At short EPW's the pulse mixture ratio progressively increased above nominal O/F. If a pulse engine is not balanced for equal feed pressures, it may deplete one propellant tank before the other and its total mission impulse can be reduced by operating off mixture ratio.

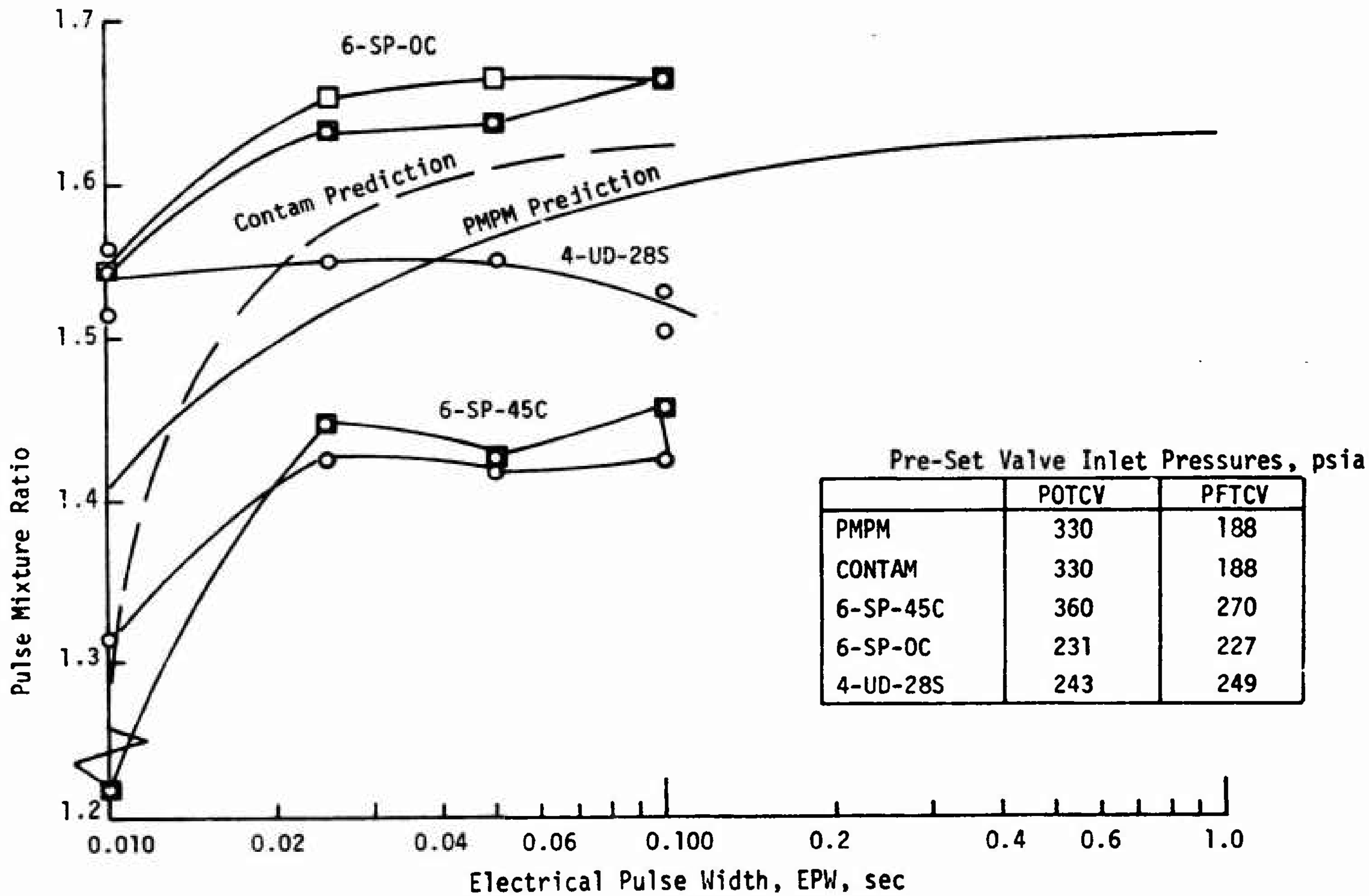

	POTCV	PFTCV
PMPM	330	188
CONTAM	330	188
6-SP-45C	360	270
6-SP-OC	231	227
4-UD-28S	243	249

Figure 6.5-3. Duration Effect on Pulse Mixture Ratio

6.5.1, Pulse Mode Performance Model (cont.)

It is still possible to improve the posttest PMPM correlation vs the experimental data shown in Figure 6.5-6 even without accounting for a wall film vaporization model. This might be accomplished by arbitrarily reducing the minimum bit impulse performance in PULSE by decreasing the input chamber length or volume below actual physical values. The input maximum chamber operating temperature has to be reduced to the fuel saturation temperature (350°F) and a value of ECFQ has to be selected to provide the overall best curve fit through the test data. Enough adjustment factors are available in PMPM to fit any desired test data. Such an accomplishment would prove nothing, however, because it is not physically realistic, it cannot be used as an a priori prediction tool, and it cannot be used to optimize performance based on physical engine design considerations. The model is however useful in predicting performance for a fully characterized design being subject to a new duty cycle. Additional program input expressing specific impulse as a function of chamber wall temperature would be required.

6.5.2 CONTAM Duty Cycle Analysis

The CONTAM model was utilized extensively in the Phase I design analysis to select the pertinent engine design parameters to achieve maximum transient performance and minimum contaminants. It was used to a lesser extent to correlate Phase II test results in order to implement engine design modification for Phase III. The fact that the CONTAM model adequately satisfied the above design objectives was demonstrated by the successful attainment of the 5 lb_f bipropellant engine contract goals during Phases II and III.

The objective of the add on study related to the CONTAM model was to evaluate the model as a duty cycle performance and contamination predictor as opposed to an engine point design analyzer. The results of that study are described herein.

6.5.2, CONTAM Duty Cycle Analysis (cont.)

6.5.2.1 Pretest Prediction

Unlike the PMPM analysis which evaluated all 40 pulses shown in the special duty cycle test of Figure 6.5-1, the CONTAM model only evaluated nine individual pulses within the duty cycle because of the long computer times required. These were pre-selected to be representative of transient performance trends. The nine particular pulses which were analyzed are listed in Table 6.5-4.

The CONTAM model predicts that for a given EPW, hardware temperature has the greatest impact upon pulse performance. This is because the shutdown injector manifold temperature directly influences the propellant vapor pressure of the residual propellants and the shutdown expulsion rate and combustion efficiency. The chamber temperature determines the wall film vaporization efficiency. The input chamber wall temperatures required by the CONTAM model were estimated from the Phase II data shown in Figure 5.3-19 as a function of its sequence within the special duty cycle. The pretest estimated wall temperatures which were used in the CONTAM predictions are in Table 6.5-4.

Whenever it was possible to do so, the identical input used in the PMPM analysis was also input into the CONTAM model. In this way, the performance comparison would be based on differences between the two models rather than differences between their input assumptions.

6.5.2.2 Data Comparison

A comparison of the pretest CONTAM performance predictions with the experimental pulse performance data is shown in Figure 6.5-4. This comparison shows that the CONTAM model consistently overpredicted performance. The predicted trend is correct and is roughly parallel to the hot chamber test data. The cold chamber test points, however, are significantly overpredicted. This is also shown in chronological pulse sequence between predicted and delivered performance in Figure 6.5-9. Pulse No. 1 with an ambient

TABLE 6.5-4

CONTAM PREDICTION SUMMARY

CONTAM Case No.	Duty Cycle Pulse No.	EPW sec	T_{cham}* °F	I_{sp}	T_{exp}**	T_J
1	1	0.010	70	160	60	70
2	8	0.010	165	210	120	100°F
3	40	0.010	1200	230	760	100°F
4	9	0.025	165	230	120	100°F
5	30	0.025	1600	270	790	100°F
6	13	0.050	370	270	170	100°F
7	28	0.050	1650	280	770	100°F
8	17	0.100	715	290	285	100°F
9	12	0.025	370	250	170	100°F

*CONTAM input temperature estimated from Phase II data (Figure 5.3-19)
**Experimental average wall temperature.

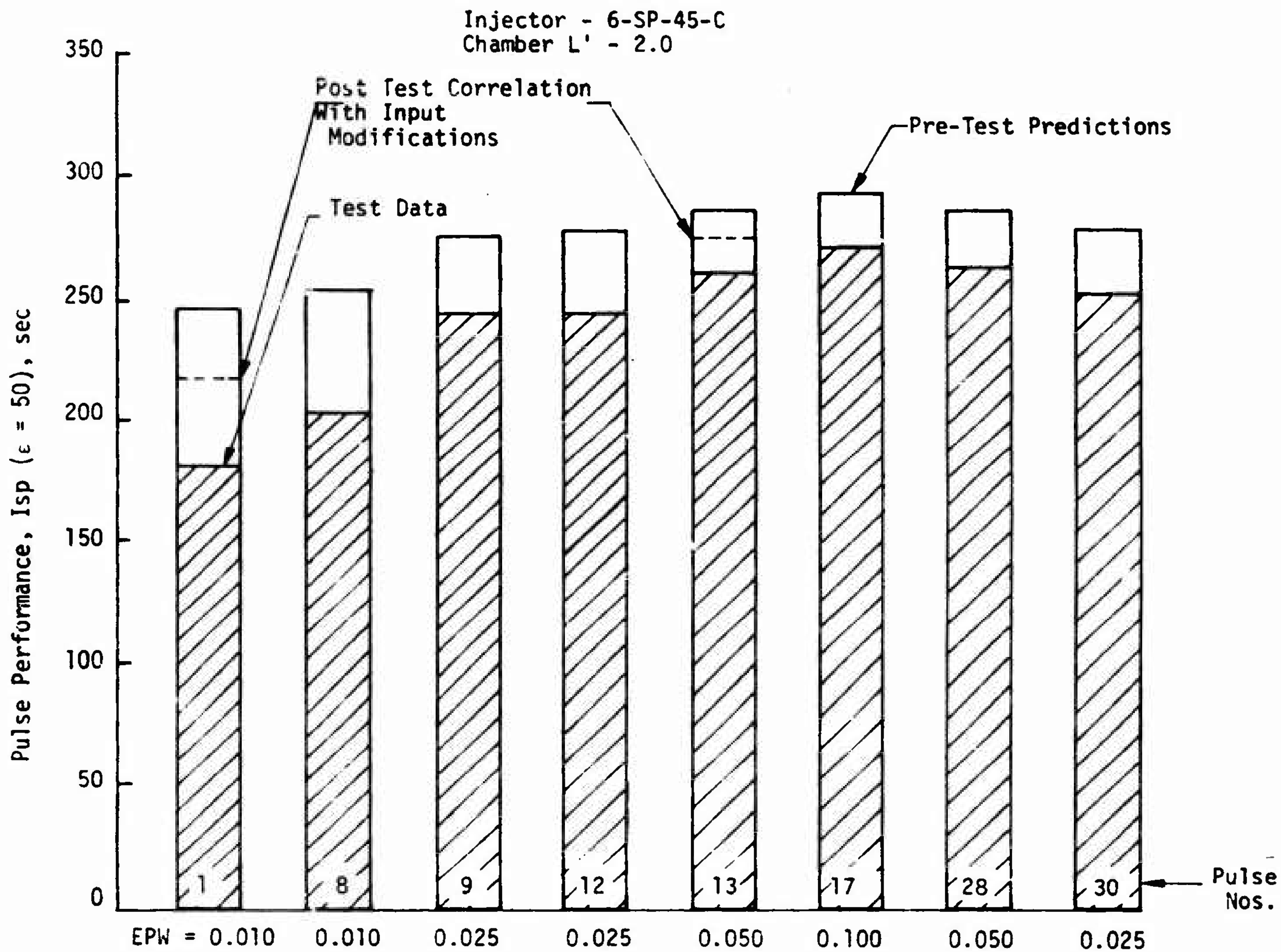

Figure 6.5-9. Comparison of Measured Performance to CONTAM Predicted Performance

chamber wall temperature start is overpredicted by $\approx$ 60 sec I_{sp}. Pulse Nos. 13 through 30 with wall temperatures ranging from 240°F to 900°F are consistently overpredicted by $\approx$ 22 sec I_{sp}.

A comparison between the CONTAM predicted and experimental pulse performance sensitivity to chamber wall temperature is shown in Figure 6.5-10. The CONTAM model, unlike PMPM, correctly predicts that the pulse performance is constant above the fuel saturation temperature. Below this temperature the model predicts a performance reduction trend with colder wall temperature but the magnitude of the drop off is underestimated.

6.5.2.3 Input Adjustment and Re-Analysis

The primary inaccuracy of the CONTAM model is in predicting engine shutdown characteristics. This is especially true for cold wall pulse firings. In a typical shutdown transient, CONTAM predicts the following sequence of events. Upon valve closure the residual droplets and chamber wall film continue burning even after the injection flowrate is terminated. As the residual propellants within the chamber are depleted, chamber pressure plummets from the steady state value to below the oxidizer vapor pressure. When this occurs oxidizer injection is initiated from the oxidizer manifold dribble volume into the chamber. The combustion gas mixture becomes oxidizer rich and eventually flames out (quenches). Cold flow expulsion of the oxidizer spray into the chamber continues until the oxidizer dribble volume is dry. When the chamber pressure falls below the fuel vapor pressure, fuel manifold expulsion into the chamber is initiated. When sufficient fuel is injected into the chamber, the CONTAM model currently predicts re-ignition with the oxidizer already in the chamber yielding bipropellant performance. Re-ignition causes P_c to rise above the fuel vapor pressure cutting off fuel injection. Intermittent combustion and injection is predicted by CONTAM until the fuel within the dribble volume is consumed. As long as active combustion is predicted by the CONTAM model, the predicted pulse

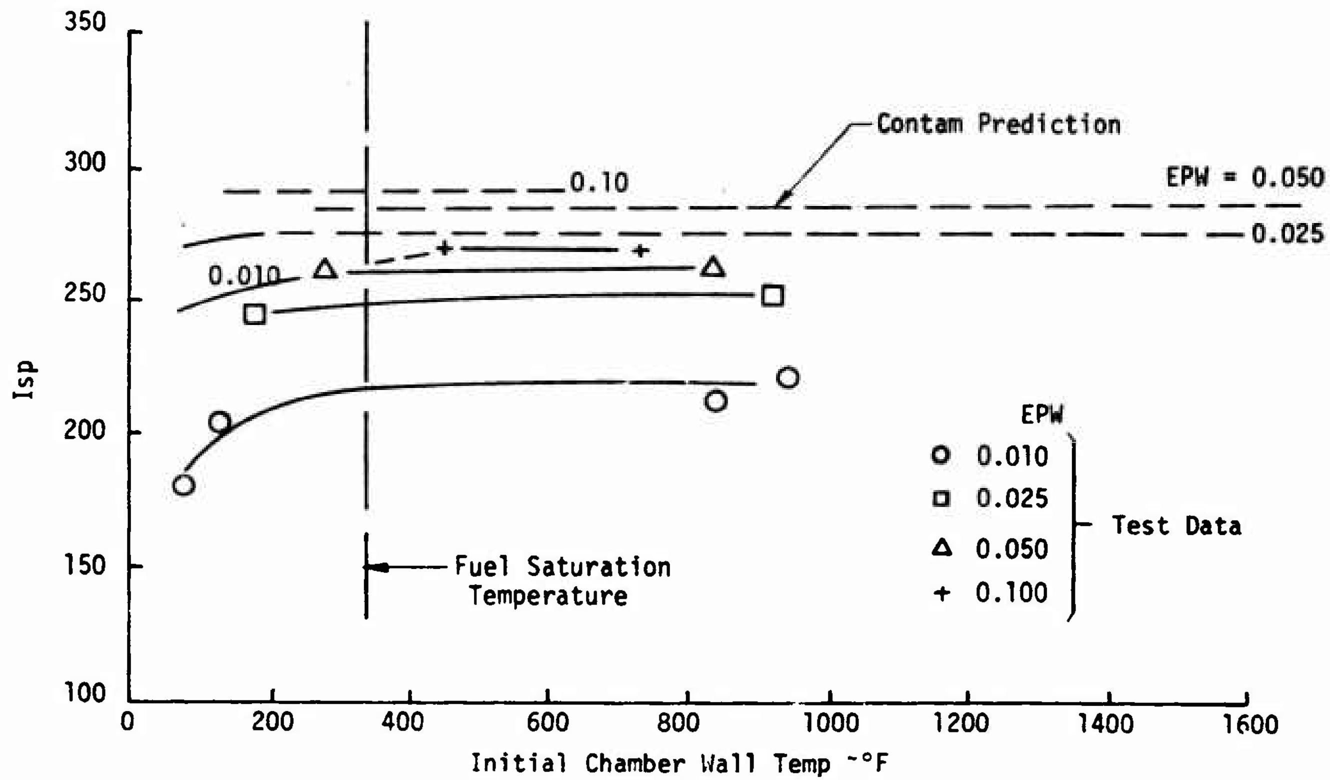

Figure 6.5-10. CONTAM Prediction of Wall Temperature Effect on Pulse Performance

performance stays relatively high. Currently, the only criteria for extinguishment is an adiabatic quenching distance criterion. Combustion is predicted to be sustained as long as the chamber diameter exceeds the adiabatic quenching distance which is a function of P_c and flame temperature corresponding to the gas mixture ratio. Under the current CONTAM mechanism the pulse performance loss is primarily predicted to be due to an injection mixture ratio maldistribution following shutdown which is initially oxidizer rich, followed by fuel rich combustion of the propellant residuals in the dribble volume. It appears from the foregoing comparison that combustion extinguishment is probably physically occurring earlier than is currently being predicted by CONTAM. Nor is there any perceptible evidence in measured P_c or thrust that re-ignition is occurring upon re-initiation of fuel expulsion, at least for cold chamber shutdowns. This can be analyzed by modifying the quenching distance criterion built into the model to be wall temperature dependent to account for earlier flame extinction which results from non-adiabatic heat losses from the combustion gas to cold chamber walls. Although the long term solution was identified, the model alteration was not actually incorporated during this study due to funding limitations and also because the objective of this study was to evaluate the present models as is. The only modifications made were in input data rather than program modifications.

The CONTAM model predicts thrust from a (C*) · (C_f) correlation. The C* is internally calculated within the model from input arrays of gas temperature, molecular weight, and specific heat ratio vs fuel fraction (mixture ratio). The nozzle C_F is also input vs fuel fraction. Although the C* (combustion) efficiency is internally calculated within the model based upon propellant vaporization considerations, no calculations are provided for C_F (nozzle) efficiency. Therefore throughout Phases I, II, and III including this study, the predicted C_F was input instead of the theoretical one-dimensional equilibrium C_F. The predicted C_F accounts for nozzle divergence losses, steady state boundary layer losses, and kinetic recombination performance losses in consonance with the recommended simplified JANNAF performance methodology. The kinetic loss, however, and to a lesser extent the

6.5.2, CONTAM Duty Cycle Analysis (cont.)

boundary layer loss is dependent upon engine thrust and P_c. Since C_F can only be input as a function of fuel fraction (O/F), the steady state C_F was used. During shutdown when P_c is on the order of 1 psia the kinetic loss increases significantly compared to the steady state input, and transient C_F at the same mixture ratio is much lower than the steady state input array. This was not incorporated into the analysis but the transient C_F can easily be reduced from the steady state value within the program.

The discussion at the beginning of Section 6.5 described the deviation in performance at oxidizer rich mixture ratios between assumed chemical equilibrium and actual kinetically limited N_2O_4 decomposition products. The CONTAM program uses fuel fraction as a parameter instead of mixture ratio ($\dot{W}_{ox}/\dot{W}_{fuel}$). The fuel fraction is input in 0.1 increments from 0 to 1 as shown below.

Fuel Fraction	0.0	0.1	0.2	0.3	0.4	0.5	0.6	0.7	0.8	0.9	1.0
O/F	∞	9	4	2.33	1.5	1.0	0.67	0.43	0.25	0.11	0

Therefore between stoichiometric O/F and infinity (pure oxidizer) only two oxidizer rich mixture ratio points are defined by the input. The shutdown transient O/F commonly exceeds 25:1. Thus long interpolations are required between O/F = 9 to ∞ and the oxidizer rich combustion products are poorly defined because of the coarse grid input data. Similarly only three data points define the entire steady state mixture ratio range. By comparison four intermediate fuel rich mixture ratio points are defined between 0 and 1.0. Some adjustment was made at the O/F = 4 and 9 input points to better define high O/F performance in the re-analysis.

Some of the test records, especially for the colder propellant inlet temperatures showed longer ignition delays than were predicted by CONTAM. Using the input activation energy, molar collision frequency and heat of reaction of the initiating reaction contained in the CONTAM sample

6.5.2, CONTAM Duty Cycle Analysis (cont.)

case, ignition was predicted ≈ 0.2 millisec from time of injection. In the posttest correlation, this was increased to a 1 millisec ignition delay time based on test data as discussed in the next section.

6.5.2.4 Final Correlation

Figure 6.5-11 compares the transient chamber pressure predictions using the 0.2 and 1.0 millisec ignition delay time for a cold wall start. The longer input ignition delay retards initial P_c response and causes a P_c overshoot. More wall film accumulation at start results in higher P_c after reaching steady state. Increasing the ignition delay reduced cold wall 0.010 sec pulse performance by 11 sec. The over pressure matches the observed data range.

Figure 6.5-11 also shows the difference in shutdown transient P_c due to kinetically limited high O/F gas properties. This modification decreased pulse performance by an additional 3 sec.

The re-calculated manifold dribble volumes for injector 6-SP-45-C reduced performance by 2 sec. An additional 2 sec pulse performance decrement was accounted for by transient chamber heat loss.

Although the flame quenching criteria was not modified in the computer model, the effect of earlier quenching was approximated by cutting off the pulse bit impulse integral at an earlier point in time, e.g., integration of the impulse for only 0.015 sec after shutdown compared to 0.035 sec reduced the bit impulse by 10 sec.

The effect of all of the above modifications upon the CONTAM posttest correlation for the first 0.010 sec EPW cold pulse is shown in Figure 6.5-12. The modifications incorporated thus far have reduced the initial deviation between pretest prediction and experimental data by ≈ 40%. The posttest correlation is already in close agreement (1%) with the experimental data for the 0.010 sec EPW hot pulse.

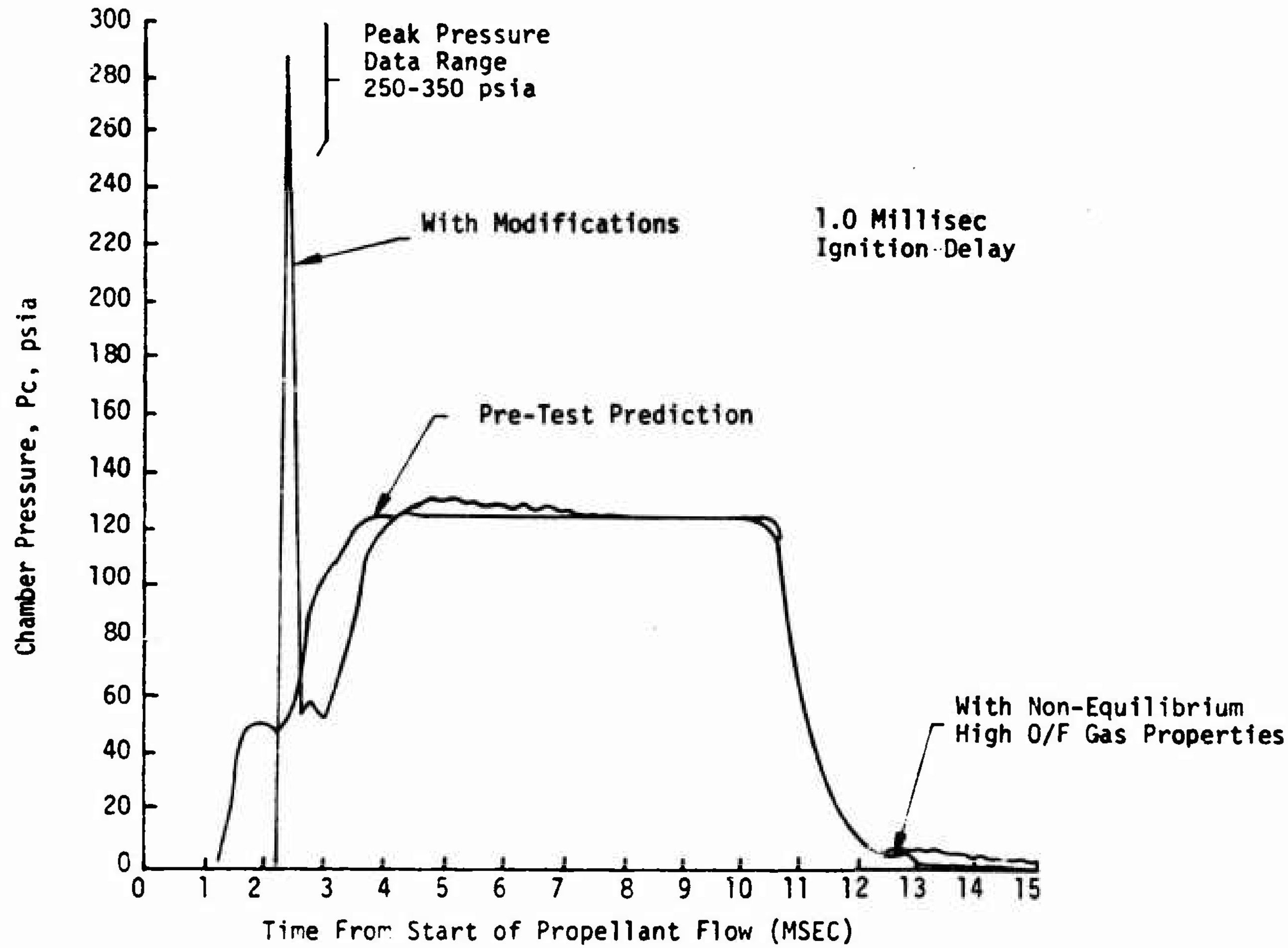

Figure 6.5-11. Predicted Chamber Pressure Characteristics for a Cold Wall Start

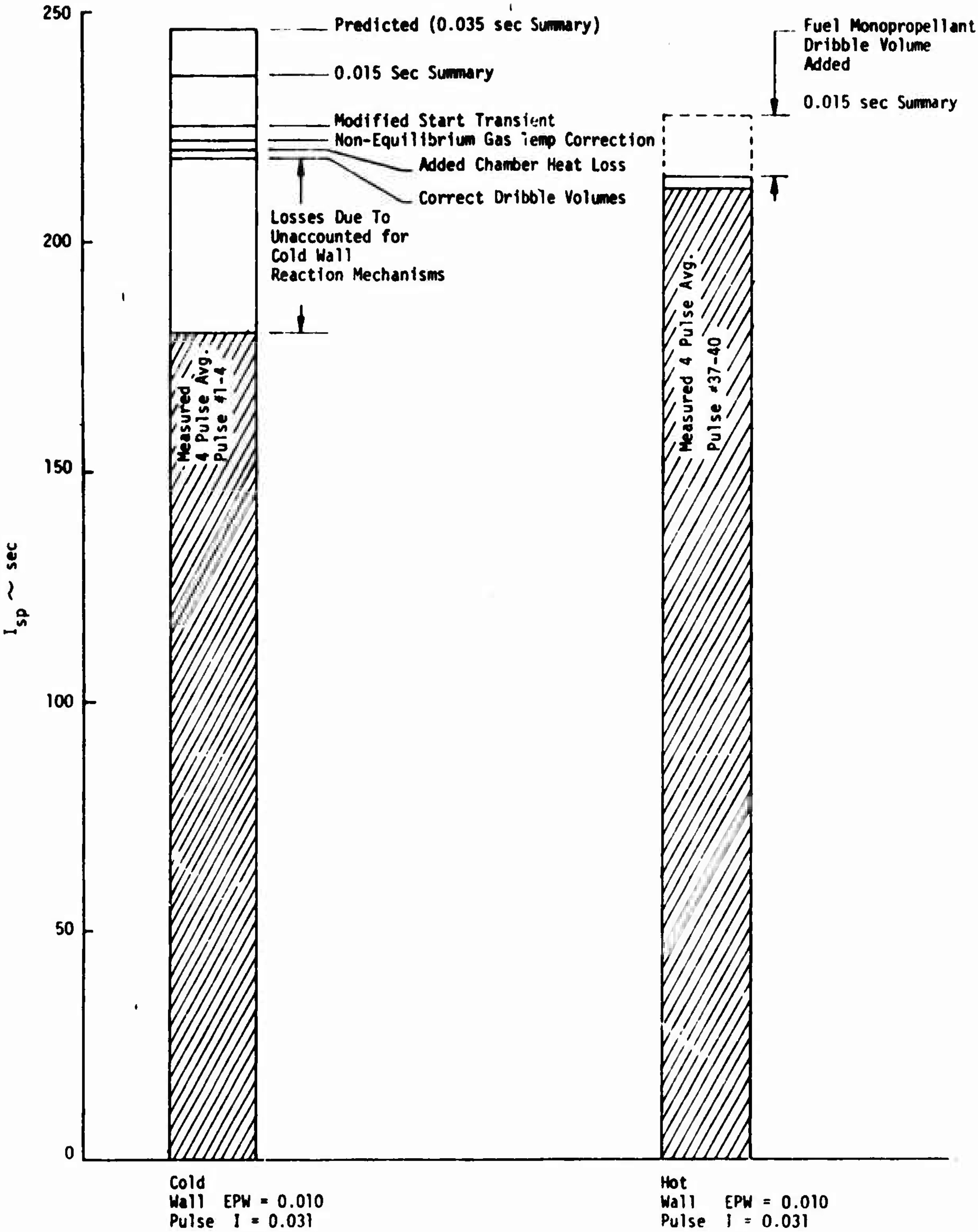

Figure 6.5-12. Effect of Modifications upon the CONTAM Posttest Correlation for the First 0.010 sec EPW Cold Pulse

6.5.2, CONTAM Duty Cycle Analysis (cont.)

Figure 6.5-9 shows how the input modifications could improve the CONTAM model correlations with the experimental data. Although not all test cases were rerun due to a limited computer budget, a typical cold short pulse and hot long pulse were re-analyzed. In both instances, the deviations between prediction and test were reduced by approximately one-half.

6.5.3 Comparative Model Evaluation

6.5.3.1 Summary

The philosophical approaches differ between the PMPM and CONTAM models. PMPM makes analytical simplifications to speed computation time, then depends upon empirical coefficients to match the experimental data. These parametric trends are then used as input to synthesize engine response for various complex duty cycles. CONTAM is the more physically mechanistic model between the two. It considers the details of each pulse and performs its calculations accordingly. In order to perform parametric analyses, however, it must "start from scratch" for each new case. Although it is more detailed in its considerations it is also the more expensive to operate.

The preferred transient model depends upon the type of problem and the objectives of the analyst. As a pretest analytical design tool, CONTAM is vastly superior because it is more physically mechanistic. CONTAM is more sophisticated in its treatment of the start transient, ignition model, and post-shutdown manifold expulsion characteristics. CONTAM is also more completely debugged and less problems were encountered in running the computer program.

6.5.3, Comparative Model Evaluation (cont.)

The LISP subprogram of PMPM should be used for injector spray pattern design analysis and injector pattern optimization. Provided that empirical single element spray correlations exist for the element type of interest. LISP provides an excellent means for assessing pattern design variations upon the injection mass and mixture ratio distributions. LISP predicts the relative mixing effect upon combustion efficiency and implicitely suggests chamber compatibility trends based on wall mixture ratio considerations. To perform a detailed compatibility prediction, the Injector Chamber Compatibility[19] (ICC) computer program should be used. ICC, like PMPM, is related to the basic JANNAF DER model. ICC was not used to predict 5 lbf bipropellant engine compatibility. The CONTAM model does not account for spray distribution effects upon steady state mixing efficiency and assumes the combustion products are well mixed. Although this was completely adequate for the 5 lbf engine (best PMPM correlation also assumed single streamtube), this may be unrealistic as engine size increases. CONTAM does not predict chamber compatibility effects.

PMPM has an advantage in predicting steady state vaporization efficiency. The vaporization rates in CONTAM must be specified by inputting an empirical K-prime vaporization rate coefficient for oxidizer and fuel. It is up to the analyst to select the appropriate K' for a particular drop size, chamber contraction ratio, and propellant volatility. The latter

(19) W. S. Hines, L. P. Combs, W. M. Ford, and R. Van Wyk; Development of Injector Chamber Compatibility Analysis, Final Report, Contract F04611-68-C-0043, AFRPL-TR-70-12, March 1970.

parameters are computed internally in PMDER. Neither model was capable of predicting acceptable atomized drop sizes for the 5 lbf micro-orifice injection elements. Drop size was obtained for input to both models from the ALRC analytical/empirical drop size correlation.

CONTAM has a capability to analyze the monopropellant decomposition-vaporization interaction which PMDER does not. Extensive analyses at ALRC indicate all hydrazine derivative fuels (including MMH) benefit from decomposition vaporization. For long chambers and high vaporization rates near the nozzle throat plane, neglecting monopropellant decomposition has only a small effect upon performance; but near the injector face plane where the droplet/gas relative velocities are low, the fuel vaporization rate with decomposition is significantly higher than predicted by PMDER. ALRC has always accounted for the monopropellant decomposition mechanism in its modification of the Priem vaporization model.

In the PMPM final report it was recommended that the ignition subroutine IGN be bypassed because of computational problems. The ignition model in CONTAM works perfectly. However, the input ignition data in the sample case should be reviewed and calibrated with the 5 lbf engine ignition test data. A constant ignition time delay can be specified by input to either model.

The primary advantage of the PMPM model over CONTAM is its faster computer run time and economy of analysis. This advantage is largely eliminated if subroutine BOIL must be run for long injector manifold expulsion times in subprogram PULSE. The BOIL subroutine is not completely debugged for cold pulses or low injector thermal soakback rates. Numerous computer case aborts occurred in running BOIL in the PULSE program. On the other hand if BOIL is bypassed, the effect of injector and chamber wall temperature at shutdown is not accounted for in the shutdown impulse. CONTAM treats the shutdown impulse calculation procedure more accurately and efficiently and is preferred since it can be executed for comparable computer run times. As discussed in Section 6.5.3, however, the CONTAM quenching distance criteria should be calibrated using the 5 lbf data to account for wall temperature effects. This modification would improve both cold wall pulse performance prediction accuracy and the engine contaminant production model accuracy.

The DCYCLE program using subroutine SYNTHE is an efficient program for economically evaluating various engine duty cycles provided that realistic parametric input data is available. This parametric input data can either by obtained from empirical engine test data if available, or obtained from analytical CONTAM model predictions. At the beginning of this study it was hoped that either one of these models would show a clear cut advantage so that it could be used exclusively for all analyses. As indicated above, however, the optimum analysis in terms of engine design analysis, pretest performance prediction capability, experimental test data correlation, and parametric engine operational or duty cycle evaluation should utilize parts of both the PMPM and CONTAM computer models.

If funding is insufficient to setup and utilize both models, the following is recommended. Use the CONTAM model exclusively when pretest design analysis, pretest performance prediction, or engine contamination analyses is the primary objective. Use the PMPM model exclusively when the engine has already been designed, fabricated, and tested and it is not intended to further optimize engine performance by design modification. The PMPM model is more economical if experimental data is already available and the primary objective is to correlate the test data or to extrapolate it to future duty cycles within the range of existing experimental parametric limits.

Table 6.5-5 summarizes the ALRC analysis experience in terms of initial model setup time, and subsequent typical UNIVAC 1108 computer run times to be expected in using the PMPM and CONTAM models. As shown, both models require extensive input data. Comparable total set up times on the

TABLE 6.5-5

APPROXIMATE COST SUMMARY OF COMPUTER ANALYSIS

	Time Unit	PMPM	CONTAM
MODEL SETUP TIME:			
First Case - Manpower			
N_2O_4/MMH	hr	40 - 60	40 - 60
Other Propellant Combinations	hr	80 - 100	80 - 100
COMPUTER RUN TIMES** (per case):			
CONTAM	sec	-	120 - 180
PMPM			
LISP	sec	15	-
PMSTC	sec	45	-
PULSE+/Without BOIL	sec	10	-
PULSE+/With BOIL	sec	40 - 80	-
DCYCLE	sec	8	-

*Estimated Setup Time
**On UNIVAC 1108
+Without ignition subroutine IGN

order of 1 to 1-1/2 man weeks should be anticipated for each model using the N_2O_4/MMH propellant combination. For other propellant combinations approximately one extra man week should be allowed for to generate and input the required propellant properties data.

If engine contamination is an important consideration PMPM in its present state is not capable of evaluating this parameter. This is due to its neglect of the wall film vaporization mechanism. It is expected, however, with very little modification that both the engine axis droplet contaminants and wall film contaminants can be modeled into the DCYCLE subroutine with little effort. With this modification, various duty cycles with variable EPW's and coast times can be evaluated to predict their influence upon engine contaminants. This can be input by specification of contaminants as a function of EPW and wall temperature. This data, however, must be derived experimentally from the test data or predicted as an output of the CONTAM program. To compute this parameter internally in PMDER or PULSE would probably be prohibitive.

Basically, the primary utility of the PMPM model is for its posttest data correlation capability. Its usefulness as a quantitative prediction tool is limited due to the number of empirical coefficients which are required which cannot be computed analytically from engine design parameters.

The CONTAM model appears to account for most of the important physical processes occurring within the 5 lbf bipropellant engine. However, it seems to over-estimate the persistence of combustion for cold chamber walls. With some further model calibration using the 5 lbf engine test data, it should provide an excellent prediction capability.

6.5.3, Comparative Model Evaluation (cont.)

6.5.3.2 Conclusions

1. A need has been established for both the PMPM and CONTAM computer models.

2. The PMPM model is more economical to operate for performing parametric analyses.

3. The CONTAM model is more physically mechanistic for evaluating engine design parameter and operating influences upon pulsing performance or contamination.

4. The simplified JANNAF performance methodology is adequate to predict 5 lbf bipropellant engine performance trends and the influence of engine design parameters on steady state performance.

5. Using the JANNAF methodology, accurate performance extrapolations were made from sea level (ϵ = 1.7) to vacuum (ϵ = 50) test conditions. From this, it was inferred that further extrapolation to the nominal engine design (ϵ = 100) condition could be accurately made. Extrapolation from ϵ = 1.7 to ϵ = 50 added $\approx$ 60 sec I_{sp}; extrapolation from ϵ = 50 to ϵ = 100 adds only 7 sec I_{sp}.

6.5.3.3 Recommendations

1. Calibrate the CONTAM flame quenching criterion on shutdown with the 5 lbf test data to account for cold wall effects.

2. Review the CONTAM N_2O_4/MMH ignition input data. Calibrate the input with experimental 5 lbf ignition delay test data.

6.5.3, Comparative Model Evaluation (cont.)

3. Add a contamination correlation subroutine to the DCYCLE subprogram of PMPM to evaluate engine contamination resulting from variable duty cycles.

4. Add a monopropellant fuel vaporization option to PMDER to account for hydrazine derivative decomposition reactions near the injector face plane.

5. Modify both PMPM and CONTAM to predict transient C_F's lower than steady state value by accounting for higher kinetic losses at low chamber pressure.

6. Modify CONTAM input to accept more detailed description of fuel fraction (mixture ratio) influence upon propellant gas properties (especially near stoichiometric and at high mixture ratio).

7. Generate empirical spray coefficients for micro-orifice injection elements so future 5 lbf engines can be accurately characterized in subprogram LISP of PMPM.

8. Input steady state kinetic rather than equilibrium performance data vs gas mixture ratio. This includes high O/F data for N_2O_4 rich decomposition reactions.

9. Modify the BOIL shutdown subroutine in subprogram PULSE in PMPM. The present BOIL model does not properly reflect the observed energy balance of the injector and propellants during propellant expulsion in cold chamber pulsing.

10. Update the IGN ignition subroutine in subprogram PULSE in PMPM to enable prediction of hypergolic ignition time delays.

6.6 OPTICAL CONTAMINATION MEASUREMENTS

Although not required by the contract, an effort was made to quantify changes in transparency of a view port located in the side of the vacuum test cell, parallel to the exhaust plume as shown in Figure 6.6-1.

6.6.1 MK I Optical Transmission and Measuring System Description

The optical system shown in Figure 6.6-2 consisted of a light source and two light paths (No. 1 = measuring, No. 2 = reference) to an optical detector. The two inputs to the detector (a photomultiplier) were scanned sequentially at an adjustable rate. The ratio between the detected measuring signal and the reference signal is a function of the optical transmission of the measuring path which includes the window downstream of the engine exhaust plume. This ratio was first found for a standard system (e.g., clean lucite window). Subsequent changes in transmission in the measuring path were determined by finding the new ratio between measuring path and reference path signals. Since the photomultiplier has a known sensitivity (milliamps output/radiant watt input), absolute transmission could also be determined. At present, however, the system was set up to make relative transmission measurements. That is, the end results were expressed in percent reduction to window transmission as a function of eng . . pulse quantity. A permanent record of the measuring and reference light intensity data was provided on the same direct write oscillograph as engine thrust, pressure and electrical parameters as shown in Figure 6.6-3.

6.6.2 Test Conditions

A series of 50,000 pulses were conducted using Engine SN 2 in the buried configuration. All tests involved 0.025 sec pulse duration at a rate of 4 pulses per sec as follows:

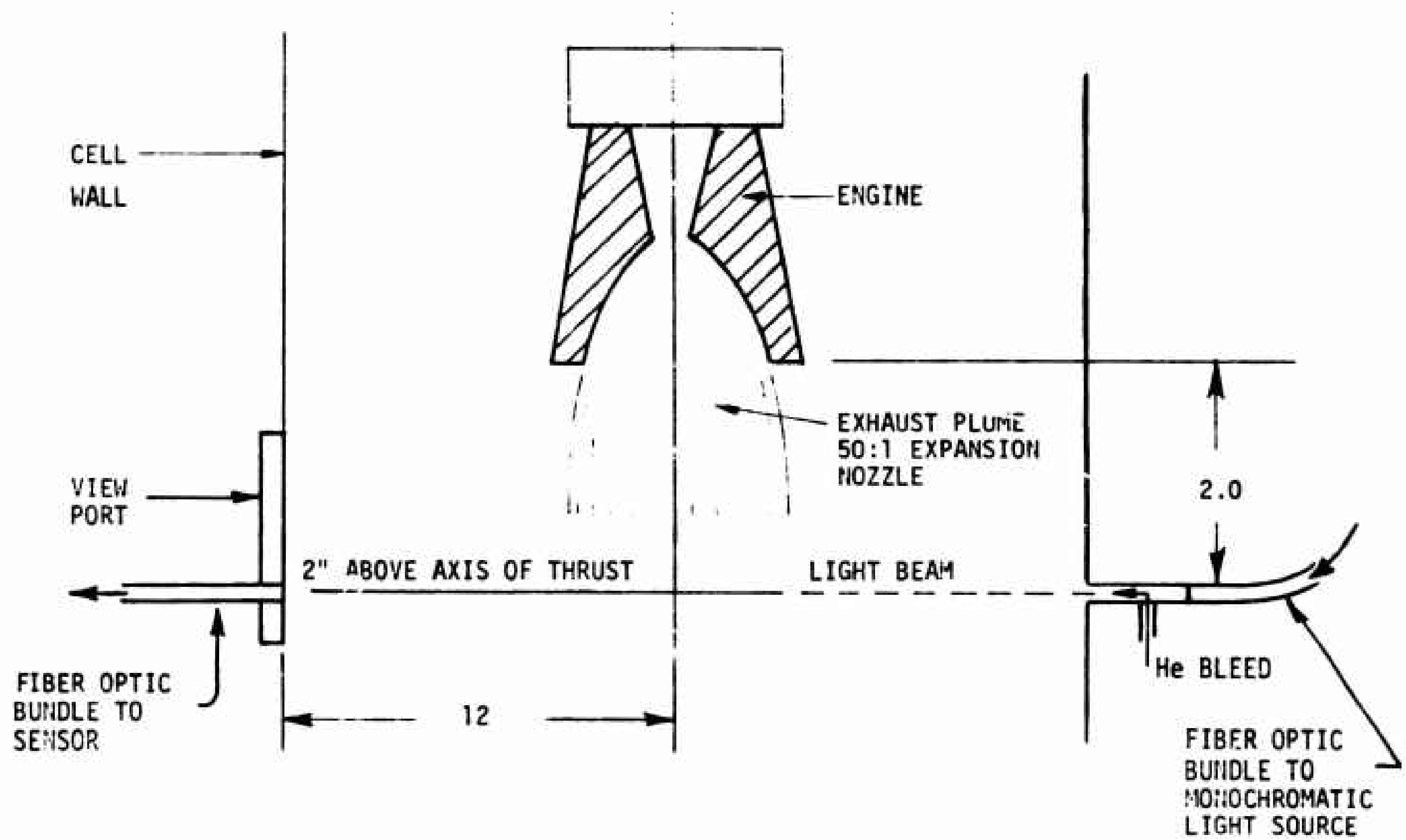

Figure 6.6-1. Exhaust Plume Contamination Test Configuration

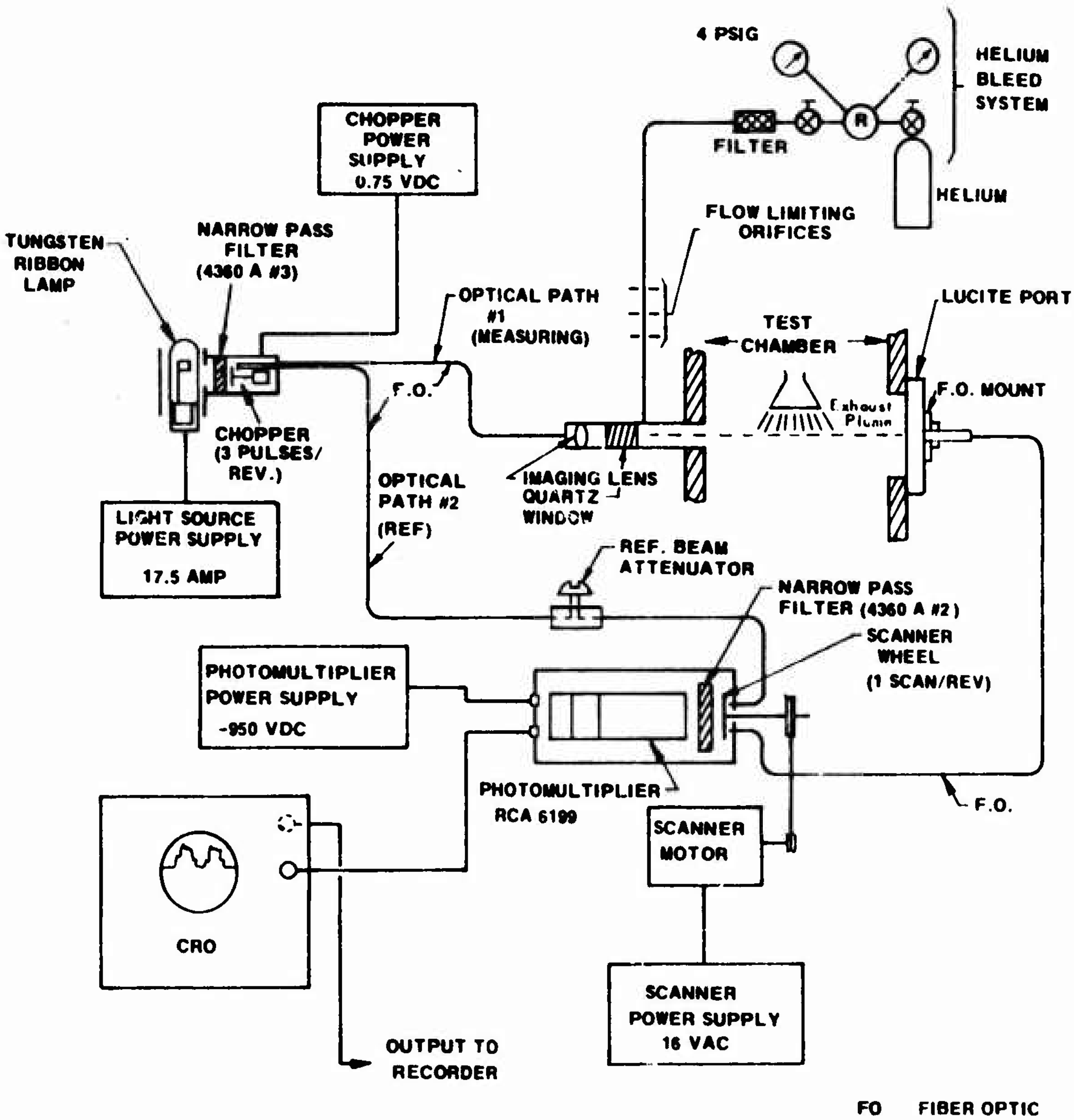

Figure 6.6-2. MK I Optical Transmission and Measuring System

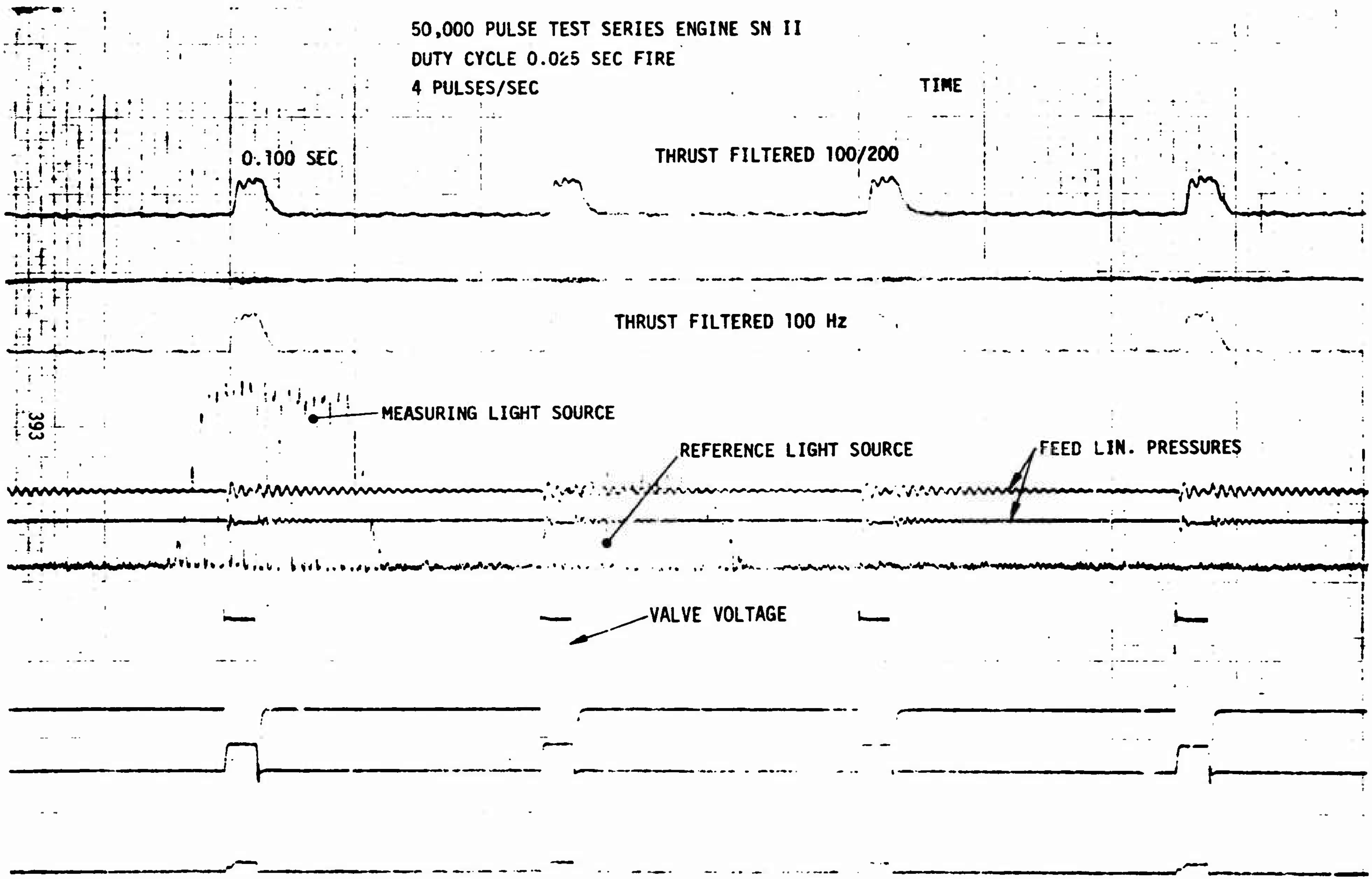

Figure 6.6-3. Optical Transmission Data

6.6.2, Test Conditions (cont.)

Test No.	Pulses	P_c	Notes
218	0-600	125	} ≈ 1/2 hour period between sequences
219	601-1200	75	
220	1201-8513	125	Continuous firing
221	8514-9114	125	} 2, 1/2 hour coasts in this interval
222	9115-9715	75	
220*	9716-48376	125	Continuous firing
223	48376-48979	125	} 2, 1/2 hour coast in this interval
224	49980-50000	75	

*Continuation of Run 220

The test cell was held at vacuum conditions of between 0.4 and 0.5 psia during the full 50,000 pulse duty cycle and no hardware or test parameters other than tank pressure were changed.

In the absence of specific requirements a 4360 A° No. 2 filter was arbitrarily selected to provide the reference illumination condition. The total impulse delivered during this test was approximately 5000 lbF-sec and the average specific impulse was 257 sec based on the 50:1 expansion ratio nozzle employed.

6.6.3 Results of Optical Contamination Tests

Figure 6.6.4 shows the intensity of light relative to the pretest value. The transmission efficiency over the first 8500 pulses averages about 97%. If deposition exists it would appear that an equilibrium state is achieved in which the rate of deposit equals the rate of sublimation. The transmission appears to be restored to 100% following a 1 hour coast. It is possible however that this entire 3% deviation is inherent within the measurement system.

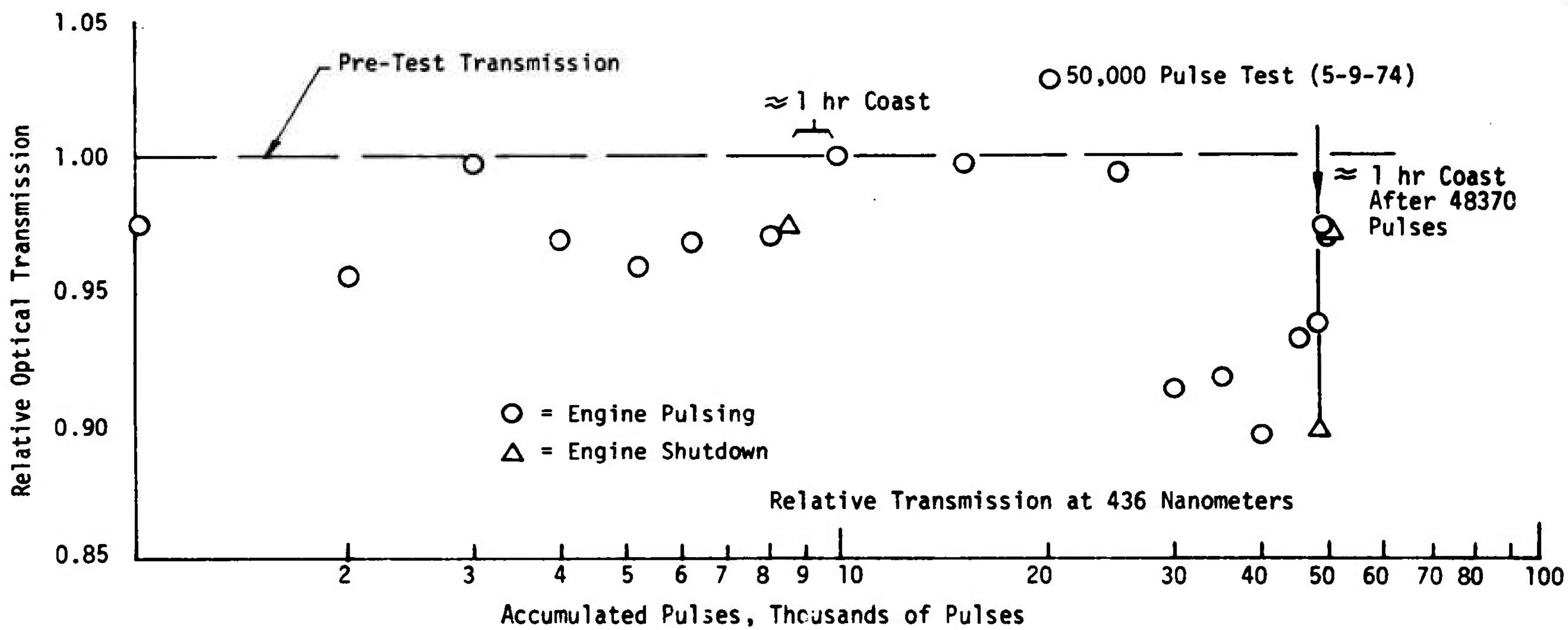

Figure 6.6-4. Five Pound Thruster Vacuum Window Optical Transmission versus Accumulated Engine Pulses

6.6.3, Results of Optical Contamination Tests (cont.)

No significant degradation was noted for approximately 25,000 pulses. A 7% shift in efficiency was recorded between 25,000 and 30,000 pulses. This was accompanied by a slight change in the fuel tank pressure from 205 to 200 psia and a increase in vacuum cell pressure from 0.4 to 0.5 psia. No other changes were observed in the operating parameters. The transmission efficiency stabilized at ≈ 93% between pulse No. 30,000 and 48,376. The efficiency of light transmission returned to the earlier value of 97.5% following two half hour coast periods, during which several short performance re-evaluation tests were conducted.

6.6.4 Conclusions and Recommendations

The conclusions drawn from this evaluation are that there was no significant accumulated plume contamination resulting from the ejection of wall film for the configuration tested. Minor changes in light transmission efficiency appear to be temporary and of an undefined nature due possibly to experimental techniques or a process of deposition and sublimation.

Additional experimental work involving multi sensor locations, variable duty cycles, mixture ratios, engine efficiencies and light frequencies could be useful in providing a greater understanding of the potential contamination mechanism.

6.7 RELIABILITY

6.7.1 Structural Analysis Update

The 3 dimensional finite element, plastic structural analyses conducted in Phase I (presented in Section 4.3.5) were updated to properly account for the final Phase III chamber designs and to incorporate the thermal data obtained in the Phase III testing. Each of the 5 thrust chamber structural failure modes presented on Page 77 were re-evaluated.

6.7.1, Structural Analysis Update (cont.)

The data provided in Table 6.7-1 summarize the effective stress, total strain and factor of safety at 6 axial positions. The steady state data are based on a 170 psia chamber pressure and maximum temperatures which allows an 11% thermal margin for the radiation cooled chamber and 15% margin for the buried engine. All stresses are noted to fall below the yield strength values.

The data in Table 6.7-2 provide the anticipated life for each of the potential structural failure modes. The indicated life includes margins for unanticipated over pressure and over temperature operation. The duration capability of the silicide chamber coating at an over temperature condition appears to be the limiting parameter.

The engine (exclusive of coating and valve) has the capability of providing:

(1) In excess of 10^7 cold starts

(2) 14 hours of long duration accumulated burn (equal to about 200,000 lbF-sec of impulse) while allowing for over 10^6 hot or cold starts during this period. Burn durations of 5 sec or less do not contribute to the 14 hour limit.

The coating life based on available exposure to air data at 1 ATM suggests a 22 hour capability at 2700°F and 4 hour exposure time at 3000°F. These times may be unduly conservative; a postfire metallurgical evaluation of the SN-1 chamber reveals that the internal chamber surface which was exposed to fuel rich combustion products degraded less than the external surface which was exposed to a mixture of air and engine exhaust products at 0.5 - 1.0 psia. Additional work to define coating life under rocket engine conditions are required.

The life capabilities of the valve and other components are discussed in the following section.

TABLE 6.7-1

THRUST CHAMBER STRUCTURAL ANALYSIS UPDATE POTENTIAL

Potential Failure Mode	Most Likely Failure Location	Firing Mode	Nominal Operating Condition -1 psia	Nominal Operating Condition -1 °F	Nominal Operating Condition -2 psia	Nominal Operating Condition -2 °F	Potential Max Pressure and Temp Employed in Analysis psia	Potential Max Pressure and Temp Employed in Analysis °F	Capabilities at Max Pressure and Temp Conditions Used in Analysis
Ignition Spikes	0.017 in. thick wall near forward flange	Cold starts	150	70	125	70	460	20	3500 psia required to yield
		Hot restarts	150	800	125	800	360	800	560 psia required to yield
		Duty cycle > 50%							
Creep to Rupture	Start of convergent nozzle	Steady firing No thermal cycles	150	2550	125	2700	170	3000	2400 hours at 3000°F
Coating Life	Combustion chamber	Time at temperature					170	3000	4 hours
					125	2700			22 hours
			150	2550					50 hours
Thermal cycling through the wall temp gradient	Throat	Pulses > 0.5, < 5.0 with or without complete cooling between pulses	150	500 -2000	125	500-2000	170	500 and 2000	$> 10^7$
Thermal cycling Axial temp gradient	Start of convergent nozzle	Burns > 5 sec with complete cooling between firings	150	2550		2700	170	3000	$1.5\ 10^6$ starts and 14 hours at max temperature
Pressure pulses		High % duty cycle					170	3000	8×10^6
		Low % duty cycle					170	<3000	$> 10^7$

TABLE 6.7-2

STEADY STATE RESULTS

Station	Time	(°F) $T_{W.G.}$	(psi) σ_{Eff} Stress	% ϵ_{Eff} Total Strain	ksi F_{ty}	ksi F_{tu}	$F.S._y$
1	RT	70	2780	0.012	60	80	21.6
	SS	800	16820	0.081	55	76	3.3
2	RT	70	1810	0.008	60	80	33.2
	SS	1550	4730	0.024	30	50	6.3
3	RT	70	750	0.003	60	80	-
	SS	2828	5460	0.044	11	13	2.0
4	RT	70	380	0.002	60	80	-
	SS	2957	9710	0.088	10	11	1.03
5	RT	70	220	0.001	60	80	-
	SS	2898	9110	0.078	11	12	1.2
6	RT	70	30	-	60	80	
	SS	2561	11610	0.077	13	16	1.12

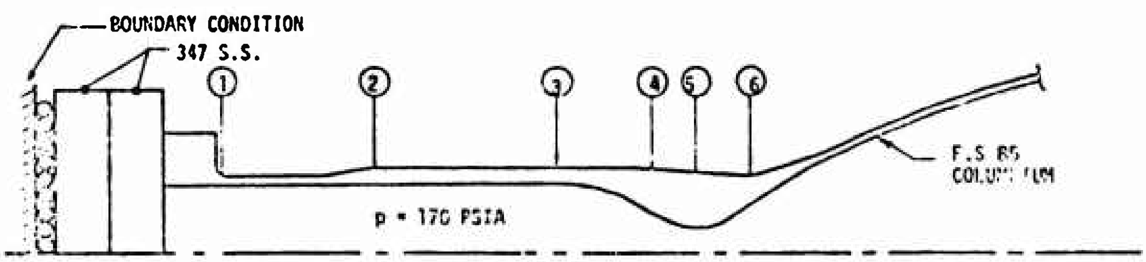

6.7, Reliability (cont.)

6.7.2 <u>Failure Mode and Effects</u>

6.7.2.1 Failure Mode Analyses, Definition of Terms Used

- Failure Mode - Generalized Description of the Manner of Failure
- Cause - Detailed Descriptions of the Mechanism by which Components could Fail Resulting in a Particular Mode
- Classification
  - Critical - Failure causing mission abort or safety hazard
  - Major - Failure degrading reliability or performance of the system
  - Minor - Failure having no significant effect on reliability or performance
- Symptoms - Information which indicates the Failure Occurrence which are Detectable in Flight
- Action - Reaction to Symptoms Required to Maximize Mission/Hardware Safety
- Effects - Description of the Manner in which the Failure Affects Engine/Flight Hardware and Mission
- Prevention - The Design Features and Acceptance Test Procedures used to Preclude the Failure

6.7.2.2 Failure Mode and Control Analysis-Engine

Failure Mode	Cause	Class	In-Flight Symptoms	Mission Action	Effect: Hardware	Effect: Mission	Prevention/Control: Design	Prevention/Control: Acceptance Test
External Leakage (Propellant)	Failure of one of the valve-to-injector static seals.	Major	A reduction in the engine's thrust. Vapors in engine compartment.	Shutdown and isolate engine.	An off-mixture ratio and reduced thrust will occur. Continued steady state operation could be detrimental.	Reduced ability to deliver specified total impulse. Possible termination of the engine's use due to improper operation. Increased contamination in vicinity of vehicle.	Double (redundant) seals are used in both the oxidizer and fuel inlets.	Leak checked at 1.6 times operating pressure. Proof pressure tested.
	Failure of both valve-to-injector static seals (oxidizer and fuel).	Critical	Reduced engine thrust; erratic chamber pressure; vapor and heat in engine compartment.	Isolate engine immediately upon detection.	Local hypergolic reaction may result in engine or system components damage. Continued operation likely to aggravate situation.	Reduced engine thrust. Termination of the engine use. Possible premature termination of the mission.	Double (redundant) seals are used in both the oxidizer and fuel manifolds.	Leak checked at 1.6 times operating pressure. Proof pressure tested.
Internal Leakage (Propellant)	Failure of a single valve seat insert-to-injector body weld.	Major	Possible improper engine ignition would occur when commanded. Outgassing thru nozzle with engine off; tank pressure decay.	Engine may be isolated.	Possible damage to injector due to improper ignition.	Increased contamination in vicinity of vehicle. Loss of propellant overboard.	Valve seat inserts are welded in place. Weld design proven in past experience and fully inspectable.	Welds are inspected. - Optical (at 20 x min). - X-ray. - Ultrasonic No cracks or porocity permitted.
Internal Leakage (Propellant)	Failure of both valve seat insert-to-injector body welds.	Critical	Impulse and chamber pressure when not commanded. Extraneous vehicle moments.	Isolate engine.	Further hardware damage not likely.	Increased contamination in vicinity of vehicle. Loss of propellant overboard. Engine's use would be terminated. Possible loss of spacecraft control and mission termination.	Valve seat inserts are welded in place. Weld design proven in past experience and fully inspectable.	Welds are inspected. - Optical (at 20 x min). - X-ray. - Ultrason[illegible] No crack[illegible] or po[illegible]ocity permitte[illegible].

Failure Mode	Cause	Class	In-Flight Symptoms	Mission Action	Effect: Hardware	Effect: Mission	Prevention/Control: Design	Prevention/Control: Acceptance Test
Internal Leakage (Propellant)	Failure of injector platelet stack to injector body braze joint.	Major	Erratic chamber pressure.	Shutdown/ Isolate Engine	Local hypergolic reaction may result in erratic engine operation and injector damage, continued operation may cause additional damage.	Reduced engine utility, possible termination of engine use.	Braze joint design proven in past experience and engine development. Fire testing of failed parts shows little adverse affect on operation.	Braze joint is gas pressure tested at 2 x operating pressure no leakage permitted.
Internal Leakage (Propellant)	Failure of one or more bonded interfaces in platelet stack.	Major	Erratic chamber pressure. Reduced thrust.	Shutdown/ Isolate Engine	Inter-manifold leakage will cause local hypergolic reaction resulting in erratic engine operation and possible local injector damage. External leakage will result in propellant flow into combustion chamber causing reduced engine thrust and possible locally increased combustion chamber wall temperatures.	Reduced engine utility, possible termination of engine use.	Bonded interface proven in past experience of engine development. Fire testing of failed parts shows little adverse effect on operation.	Bonded interfaces are gas pressure tested at 2 x operating pressure prior to platelet stack installation in body. Retested following installation.
External Leakage at Injector to Chamber Joint (Combustion products)	Failure of static seal at injector to chamber joint.	Critical	Reduced engine thrust. Erratic chamber pressure, vapors and heat in engine compartment	Isolate engine immediately upon detection.	Hot combustion gases escaping beyond engine shell may cause damage to system components. Continued operation highly detrimental.	Reduced engine thrust. Termination of the engine's use. Possible premature termination of the mission.	The metal V seal used has been proven in past experience on engine development. Seal surfaces are fully inspectable and are located in a very cool area.	Seal and seal surfaces are optically inspected at 20 x minimum. Surface imperfections are cause for rejection.

Failure Mode	Cause	Class	In-Flight Symptoms	Mission Action	Effect: Hardware	Effect: Missions	Prevention/Control: Design	Prevention/Control: Acceptance Test
Orifice Plugging	Internal contamination in the engine manifold or injector.	Major	Reduced or erratic thrust. Excessive skin temperature	Desirable to isolate or disable engine if detected.	May cause off mixture ratio operation with attendant thrust reduction.	Reduced ability to deliver specified impulse. Possible termination of the engine's use.	Filters are located at the inlets to the bipropellant valve to prevent downstream contamination.	Cleanliness controls will be used during engine and system buildup. Contamination check will be made.
					May cause partial or complete removal of outer fuel barrier for cooling resulting in excessive skin temperatures or combustion burnout.	Combustion zone wall burn out would result in termination of engine's use.	Initial tests show that contamination from nozzle end is not a problem.	
Excessive Skin Temperature	Improper operation of injection elements resulting in variation of barrier cooling.	Major	High engine skin temperature.	Desirable to isolate or disable engine if detected.	May cause partial or complete removal of outer fuel barrier for cooling which may result in excessive skin temperatures or combustion burnout.	Reduced engine life or possible termination of the engine's use due to overheating or wall burn out.	Discrete film coolant orifices are avoided. Use of main elements for barrier cooling has been demonstrated.	Proper cooling can be demonstrated during hot-fire acceptance test.
	Degradation of external insulation.	Minor	High engine compartment temperature.	Desirable to isolate or disable engine if detected.	Could result in damange or degradation to surrounding structure or equipment. No damage to engine.	Depends on engine location and proximity of heat affected system components.	Insulation design will be proven during development.	- Visual inspections to assure proper fabrication and installation. - Operating verified during fire test.
Combustion Instability (High Frequency)	Change in engine operating conditions or ignition delay.	Major	Erratic thrust, high engine wall temperature.	Shutdown engine immediately upon detection. Isolate and/or disable valve if incident is repeated.	May result in structural failure of the thrust chamber.	Inability to deliver specified total impulse in proper orientation. Possible termination of engine's use.	Engine design has demonstrated insensitivity to instability when tested at conditions to produce instability.	Off design operation could be verified during hot-fire acceptance tests.
Structural Failure of Thrust Chamber	Overstress of thrust chamber's metal wall.	Major	Sudden loss of thrust. Heat and vapor in engine compartment.	Shutdown and disable valve and/or isolate engine immediately upon detection	Destruction of thrust chamber. Damage to surrounding structure and equipment.	Termination of engine's use. Possible termination of mission.	Thrust chamber design is based on adequate safety margins for pressure and structural stress.	Proof pressure test. Hot fire test.

Failure Mode	Cause	Class	In-Flight Symptoms	Mission Action	Effect: Hardware	Effect: Missions	Prevention/Control: Design	Prevention/Control: Acceptance Test
Structural Failure of Engine Mount	Overstress of engine mount.	Critical	Change in engine thrust vector. Vapors and heat in engine compartment.	Shutdown and disable valve and/or isolate engine immediately upon detection.	Propellant inlet lines may be broken. Possible damage to surrounding structure equipment.	Inability to deliver specified total impulse in proper orientation. Termination of engine's use. Possible termination of mission.	The engine mount's design is based on adequate structural safety margin.	Nondestructive tests to assure integrity of mount.
Hot Gas Leakage at P_c Instrumentation Port	Insufficient or failed seal.	Major	Heat, vapors in engine compartment. Excessive local skin temperature. Erratic instrument reading.	Desirable to disable engine.	Dependent upon amount of hot gas leakage, possible damage to: - Instrument - Engine - Surrounding Structure	Possible termination of engine's use	Materials selection and mechanical design will minimize possibilities of leakage. Any welds involved will use proven designs and will be fully inspectable.	The engine is leak checked at 1.6 times operating pressure using N_2 gas. No leakage is allowed at the thrust chamber pressure pick off or pressure transducer. Welds will be inspected. - Visually - X-ray - Ultrasonic

6.7.2.3 Valve

Failure Mode	Cause	Class	In-Flight Symptoms	Mission Action	Effect: Hardware	Effect: Missions	Prevention/Control: Design	Prevention/Control: Acceptance Test
Internal Leakage Past the Valve Seat (Propellant)	Contamination	Major	Possible improper engine ignition (hard start). Propellant venting thru nozzle when engine is off.	If detected engine may be isolated.	Possible damage to injector due to pre-ignition back-flow of propellant.	Increased contamination in vicinity of vehicle. Loss of propellant. Extraneous impulse applied to vehicle. Possible termination of use of en^ir	Filter elements (20/35 micron) are located at the valve inlet ports. The metal valve seat and teflon flapper button arrangement compensates for minor contamination. Small contamination particles tend to become imbedded in the teflon with flapper actuation thus reducing the leakage path opening between flapper and seat.	Internal leakage tests using gas (N_2) are performed as part of the acceptance test. These tests require that the leakage (N_2 gas) at either valve outlet port shall not exceed 10 cc/hr when monitored for 5 minutes with 500 psig applied at both inlet ports. Additional leakage tests are performed at the thrust chamber acceptance test level.
External Leakage from Valve (Propellant)	Fracture of one flexure sle ve	Major	Reduced engine thrust. Abnormal valve electrical behavior. Vapors in engine compartment.	Desirable to isolate engine if detected.	Continued operation could aggrevate valve damage. Substantial external leakage of oxidizer or fuel could result in an off mixture ratio and reduction of the engine's thrust.	Loss of propellant overboard. Possible termination of the engine's used.	The valve armature, flexure tubes, and the flappers are a completely welded assembly. The flexure tube concept has been proven reliable from the results obtained from the manufacturer of bipropellant valves for the Minuteman program. External leakage would require failure of the torque motor cover seal.	An external leakage test is performed as part of the valve acceptance test. No visible indication of leakage is allowed when N_2 gas at 500 psig is applied simultaneously to the valve inlet and outlet ports. The proof pressure test is performed at 1.5 times the design operating pressure. Additional leakage tests are performed at the thrust chamber acceptance test level.

Failure Mode	Cause	Class	In-Flight Symptoms	Mission Action	Effect: Hardware	Effect: Missions	Prevention/Control: Design	Prevention/Control: Acceptance Test
	Fracture of both flexure sleeves.	Critical	Possible explosion. Reduced engine thrust. Vapors and heat in engine compartment. Possible extraneous thrust.	Isolate engine immediately upon detection.	Continued operation likely to aggravate situation. Leakage of both oxidizer and fuel would result in hypergolic reaction and valve damage.	Termination of engine's use. Possible mission termination. Increased contamination in vicinity of vehicle.	(See above)	
Failure of Valve to Open.	Valve torque motor failure, electrical connector or wire break.	Major	Engine will not fire when commanded. Abnormal valve electrical behavior.	Isolate engine.	No further hardware damage is likely.	Engine's use would be terminated.	The valve contains no sliding parts precluding material galling. The materials wetted by the propellants are 17.7 pH corrosion resistant steel and 304 L corrosion resistant steel chosen for their excellent compatibility with the propellants. The permanent magnets in the torque motor are Alinco. This material was selected to benefit from the high energy product. The torque motor coils use a high temperature ML and incapsulated with a resilient compound. This construction permits thermal expansion and provides a cushion for the coils during exposure to shock and vibration.	Tests to determine that the valve actuates properly are included in the valve acceptance test. The thrust chamber acceptance test includes valve cycling.

Failure Mode	Cause	Class	In-Flight Symptoms	Mission Action	Effect: Hardware	Effect: Missions	Prevention/Control: Design	Prevention/Control: Acceptance Test
Failure of Valve to Close	Contamination, flexure sleeve failure	Critical	Impulse and chamber pressure when not commanded. Extraneous vehicle moments. Abnormal valve electrical behavior.	Isolate engine.	Further hardware damage not likely.	Loss of propellant overboard. Increased contamination in vicinity of vehicle. Possible loss of spacecraft control. Engine's use would be terminated.	The valve is normally closed due to the magnetic bias of the torque motor and flexture tube loading so that interruption of electrical power will result in valve closure. Filter elements (20/35 micron) are located at the valve inlet ports to prevent contamination entry through the inlet ports and into the shutoff points. The valve contains no sliding parts precluding metal galling. The materials wetted by the propellants are 17.7 pH corrosion resistant steel and 304 L corrosion resistant steel chosen for their excellent propellant compatibility. The permanent magnets in the torque motor are Alinco. This material was selected to benefit from the high energy product. The torque motor coils are a high temperature ML and incapsulated with a resilient compound. This construction permits thermal expansions and provides a cushion for the coils during exposure to shock and vibration.	Tests to determine that the valve actuates properly are included in the valve acceptance test. The thrust chamber acceptance test includes valve cycling.

Failure Mode	Cause	Class	In-Flight Symptoms	Mission Action	Effect: Hardware	Effect: Missions	Prevention/Control: Design	Prevention/Control: Acceptance Test
Failure of Valve to Close Fully	Contamination	Major	Impulse and chamber pressure when not commanded. Abnormal valve electrical behavior.	Isolate engine.	Further hardware damage not likely.	Increased contamination in vicinity of vehicle. Loss of propellant overboard. Engine's use may be terminated.	(see above)	
Change in Propellant Pressure Drop Through Valve	Fuel and/or oxidizer flow path altered due to contamination or change in valve seat opening dimensions.	Minor	Slightly reduced engine thrust. Possible MR change.	None, isolate engine if severe loss of thrust occurs.	Slight flow reductions are nondetrimental.	Possible termination of engine use.	Very low ΔP results in injector manifold controlling flow rather than valve stroke. The valve flapper stops are individually adjusted during valve assembly to achieve the proper orifice opening required. The flapper stops, used for this adjustment, are welded in place.	The valve acceptance test includes functional testing, requiring not only cycling the valve, but also specific flow rates. The thrust chamber assembly acceptance test also requires valve cycling and specific pressure drops.
Delayed Valve Opening	Contamination or bent flexure sleeve.	Minor	Slightly impaired impulse response. Abnormal valve electrical behavior.	None, unless guidance requires.	No effect except valve will open slowly.	Delay in attaining rated thrust level. Reduced pulse mode performance. The navigation equipment may have to adjust the engine firing duration to allow for slow thrust buildup.	Filter elements (20/35 micron) are located at the valve inlet ports upstream from the opening shutoff ports. The valve design contains no sliding parts and all clearances are relatively large minimizing its susceptibility to contamination.	Valve response tests as part of the valve acceptance test require the valve to close fully in .005 sec or less. Valve response tests are also included in the thrust chamber assembly acceptanct test.

Failure Mode	Cause	Class	In-Flight Symptoms	Mission Action	Effect: Hardware	Effect: Missions	Prevention/Control: Design	Prevention/Control: Acceptance Test
Valve Restricted Flow (Filter Clogging)	Valve inlet filter clogged.	Minor	Reduced engine thrust.	If severe, disable engine.	An off mixture ratio and reduced thrust will occur. No damage likely.	Reduced ability of engine to deliver specified total impulse. Possible termination of the engine's use due to improper operation.	Valve filter element is oversize for total anticipated mission life to achieve nearly constant ΔP.	The valve acceptance test includes a flow and pressure drop test which requires the valve assembly to have specific flow rates (oxidizer and fuel) and pressure drops. Thrust chamber assembly acceptance tests require the complete assembly to have specific performance requirements for flow rate and mixture ratio.

6.7, Reliability (cont.)

6.7.3 Engine Reliability Assessment

In making an accurate assessment of the reliability of the bipropellant engine system (valve/injector/chamber), both active and passive time periods were considered. The active mode is critical from the standpoint of the large number of operating cycles and the passive mode is critical from the standpoint of the long time durations in orbit.

6.7.3.1 Reliability Mathematical Models

Overall mission reliability is the product of the active and passive reliabilities as follows:

R(mission) = R(active) x R(passive)

where the active reliability model is:

R(active) = R(structure) x R(leakage)

Due to minimal anticipated structural loads during the engine passive mode, the structural reliability was estimated to be 1.0. The passive model thus reduces to:

R(passive = R(leakage)

6.7.3.2 Failure Rates

The failure rate values used in performing the reliability calculations are primarily generic in nature, i.e., they are based on type of component rather than exact design/application. In selecting generic failure rates, consideration was given to stress analyses and Phase III demonstration testing performed on the actual components.

6.7.3, Engine Reliability Assessment (cont.)

6.7.3.2.1 Stress Analysis

The combustion chamber stress analysis provided in 6.6.1 indicated 10% life limits of 3400 hours for creep and 500,000 cycles for fatigue - both far in excess of the 10 hour and 300,000 cycle requirements.

The injector was designed for a thermal cycle life in ecess of 1,000,000 cycles.

Phase III testing subjected three different engines to 300K, 50K and 50K cycles respectively with no failures. The 300K cycle series corresponds to the maximum design goal.

Additional test data was obtained on the Moog bipropellant valve. This data includes one similar valve cycled 1,000,000 times on the Minuteman III program and additional vendor tests of 27,000 cycles on each of 75 valves. These tests, represent 3.425×10^6 cycles without failure. The upper 50% confidence limit estimate (binomial) on valve failure rate is 2×10^{-7} failures/cycle.

The data obtained from Phase III testing indicates that the overall performance reliability of the engine should approach 1.0 provided the engine "sees" the proper inputs and no structural degradation of injector or chamber occur. For example, data on minimum impulse bit testing indicates a three sigma spread of approximately $\pm$ 0.003 lbF sec compared to a goal of $\pm$ 0.005 lbF sec. This calculation was made on the 6th through 30th pulses in a series starting with ambient conditions. As detailed in Figure 6.4-5 the variability between pulses actually decreases as repeated pulses are applied. Similar statements of confidence could be made for the other performance parameters.

6.7.3, Engine Reliability Assessment (cont.)

6.7.3.3 Predictions

Individual component reliability values were computed using an exponential reliability model.

$$R = e^{-(\text{failure rate x duration})}$$

where failure rate (FR) is appropriately modified by environmental and criticality factors. The failure rates, factors, durations and resultant reliabilities are shown in Table 6.7-3.

Two worst-case operational profiles were selected for use in the computations. The results indicate that single-engine reliability values are expected to range from 0.994660 for the "short duration/regulated pressure" mission to 0.990334 for the "long duration/blowdown" mission.

Note that these numbers are limited only by the degree of test experience. If the test experience on the valves, for example, were increased from 3.4 x 10^6 cycles to 30 x 10^6 cycles, it is anticipated that a 0.999 engine system would be achieved.

6.7.3.4 Redundancy Considerations

As stated in the failure modes and effects analysis, an "engine-out-capability" is assumed for any system employing these engines. Active redundancy requirements for a system R of 0.999 in terms of the calculated single-engine R would be as follows:

TABLE 6.7-3

RELIABILITY COMPUTATIONS

Component	$\lambda \cdot Kop^{(1)}$	Mode(s)$^{(2)}$	$\alpha^{(3)}$	$\beta^{(4)}$	$FR^{(5)}$	Duration Short	Duration Long	(6) Short	(6) Long	Inactive $R^{(7)}$ Short Duration	Inactive $R^{(7)}$ Long Duration	Active $R^{(7)}$ Short Duration	Active $R^{(7)}$ Long Duration
Bipro Valve	0.2												
		Internal Leak	0.6	0.02	0.0024	30 days	10 yr	1.728	210	0.999998	0.999790	-	-
		Fail to Open	0.1	1.0	0.020	175 Kc	300 Kc	3500	6000	-	-	0.996506	0.994017
		Fail to Close	0.05	1.0	0.010	175 Kc	300 Kc	1750	3000	-	-	0.998251	0.997004
		External Leak	0.25	0.02	0.001	2 hr	10 hr	0.002	0.010	-	-	1.0	1.0
Valve Manifold Seal (Redundant)	20	External Leak	1.0	0.02	0.4	2 hr	10 hr	0.8	4.0	-	-	1.0	1.0
Injector	250	Low Performance	1.0	0.1	25	2 hr	10 hr	50	250	-	-	0.999950	0.999750
Metal Seal	20	External Leak	1.0	0.02	0.4	2 hr	10 hr	0.8	4.0	-	-	0.999999	0.999996
Chamber	250	Low Performance	1.0	0.1	25	2 hr	10 hr	50	250	-	-	0.999950	0.999750
						Product Component R's =				0.999998	0.999790	0.994662	0.990543

Short Duration Engine R = 0.994660

Long Duration Engine R = 0.990334

Notes:

(1) $\lambda \cdot Kop$ is the generic failure rate in failures per million hours or cycles times an environmental adjustment.
(2) Mode of failure.
(3) Frequency ratio of failure mode.
(4) Criticality factor - the conditional probability of engine failure given the occurrence of the component mode of failure.
(5) FR - the resultant failure rate = $\lambda \cdot Kop \cdot \alpha \cdot \beta$ in parts per million.
(6) Failure Rate x Duration in ppm.
(7) R = Reliability = $e^{-(FR \times Duration)}$

6.7.3, Engine Reliability Assessment (cont.)

Engine Out Allowance	System Reliability	
	Short Duration	Long Duration
One of Two	0.999971	0.999907
One of Four	0.999830	0.999447
One of Six	0.999579	0.998646*

*May be assumed to be equivalent to 0.999
(within data accuracy)

7.0 CONCLUSIONS AND RECOMMENDATIONS

7.1 CONCLUSIONS

A large improvement over the characteristics of current monopropellant and bipropellant engines in the 5-lbF thrust class has been demonstrated. This low dribble volume multielement injector bipropellant engine (see Figure 7.1-1) offers: (1) unlimited duty cycle capability and practically unlimited accumulated and steady state firing life (200 hours) without loss in performance; (2) rapid response, 0.0056 sec from signal to 90% thrust without need for thermal conditioning; (3) precise and highly repeatable impulse bits with nearly square wave thrust-time characteristics demonstrated to 0.018 lbF-sec repeatable within ± 3% and capabilities down to ≈ 0.005 lbF-sec; (4) a delivered specific impulse of 295 sec where the engine installation allows radiation cooling or 283 sec for a fully insulated buried configuration; (5) pulse mode specific impulse in excess of 240 sec at bit impulse values down to 0.05 sec and (6) very low plume contamination.

7.2 RECOMMENDATIONS

The technology demonstrated under this contract suggests several avenues for further development and test evaluation which should lead to low thrust bipropellant engines for Air Force RCS applications which have improved performance, life and operational flexibility.

Engine Durability Evaluation

The ultimate limitations of the 5-lbF thrust engine design developed and the materials utilized therein could be established in a fire-to-destruction effort. This would require in the order of 10^6 pulses and in the order of 200 hours of accumulated burn time. The data obtained demonstrating the durability of the coated columbium alone would be highly useful to any of the long lived columbium component engines now in development. The overall durability of the 5 lbF engine could show the engine to exceed the durability of other spacecraft

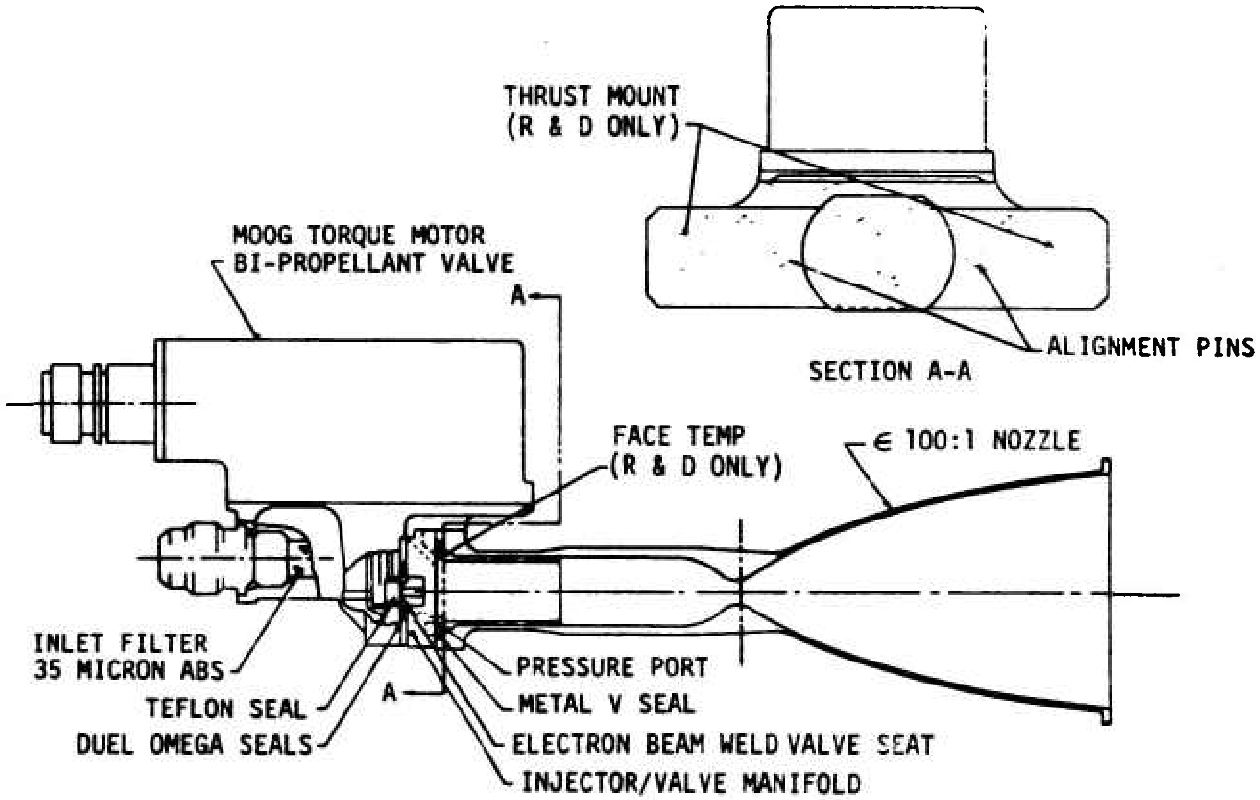

Figure 7.1-1. 5 lb Thrust Bipropellant Engine Thrust Chamber Assembly

components. This durability evaluation could be a portion of an overall program directed toward flight qualification of the engine.

Engine Scaling Demonstration

Data obtained in the course of testing showed the unique characteristics of certain 4-element injector designs resulted in the delivery of high performance down to the 2 lbF thrust level. It is anticipated that a 1 lbF thrust bipropellant engine which has nearly the same level of performance but a minimum impulse bit capability of 0.005 lb-sec could be developed using the technology obtained on this program. Conversely, preliminary design analysis shows that the same valve and injector integration approach can be employed on larger engines up to the 25 lbF thrust level. These larger engines would be higher performing than the 5 lbF unit but would be not significantly heavier.

Propellant Change Over

Conversation with spacecraft primes indicates that the adaption of this engine design to a N_2O_4/N_2H_4 propellant system would allow bipropellant engines in the 1.0 to 25.0 lbF range to be operated with very small (0.1 to 0.5 lbF) monopropellant engines which are fed from a common fuel system. The commonality of the fuel leads to improved spacecraft propellant utilization and system weight savings and simplification.

Improved Engine Thermal Isolation

The engine design developed cannot be divorced from the spacecraft heat balance. Depending upon installation and duty cycle, there can be a heat flow of 10 to 75 watts to the spacecraft. This could be substantially reduced or eliminated through an improvement in the chamber to valve interface design. A major advantage would result from the use of a more thermally resistive

7.2, Recommendations (cont.)

material, i.e., titanium, for the chamber forward end. The compatibility of titanium and combustion products was proved on this program. The durability and life cycle capability of titanium to columbium joins remains to be demonstrated.

Modular Propulsion System Design

The five pound thrust bipropellant engines developed could be sensitive to certain feed system configurations which effect transitory flow conditions during the start up process. This can be evaluated by the operation of an array of engines which are fed from a common feed system. The engine feed system module demonstrated could be palletized for application to various spacecraft and designed with the potential for flight evaluation.